Contents

CONTRIBUTORS vii

Metal Complexes of Monocarbon Carboranes: A Neglected Area of Study?

THOMAS D. MCGRATH and F. GORDON A. STONE

I. Introduction 1
II. Synthesis. 3
III. Reactions 7
IV. Monocarbollide–Metal Complexes with Non-Icosahedral Core Frameworks. . 28
Acknowledgements 38
References 38

Synthesis of Novel Silicon-Containing Compounds via Lewis Acid-Catalyzed Reactions

IL NAM JUNG and BOK RYUL YOO

I. Introduction 41
II. Allylsilylation Reactions with Allyltriorganosilanes 42
III. Intramolecular Alkenyl-Migration Reaction of Alkenylchlorosilanes 49
IV. Friedel–Crafts Alkylation Reaction with Organosilicon Compounds 50
V. Hydrosilylation Reaction with Triorganosilanes. 57
Acknowledgments 58
References 58

Bidentate Group 13 Lewis Acids with *ortho*-Phenylene and *peri*-Naphthalenediyl Backbones

MOHAND MELAIMI and FRANÇOIS P. GABBAÏ

I. Introduction 61
II. Synthesis. 62
III. Interaction with Lewis Basic Substrates 85
IV. Conclusion 97

Acknowledgments 98
References 98

Metallasilsesquioxanes

VOLKER LORENZ and FRANK T. EDELMANN

I. Introduction 101
II. Silsesquioxane Precursors 105
III. Metallasilsesquioxanes 106
IV. Future Outlook 148
Acknowledgments 150
References 150

Cations of Group 14 Organometallics

THOMAS MÜLLER

I. Introduction 155
II. Synthetic Approaches to R_3E^+ Ions 156
III. Structure and Properties of R_3E^+ Cations 165
IV. A chemistry of R_3E^+ cations 206
Acknowledgements 210
References 210

Recent Advances in Nonclassical Interligand Si···H Interactions

GEORGII I. NIKONOV

I. Introduction 217
II. Silane σ-Complexes and Si–H···M Agostic Complexes 219
III. Silylhydride Complexes with Interligand Hypervalent Interactions M–H···SiX 270
IV. Multicenter H···Si Interactions in Polyhydridesilyl Complexes 291
V. Conclusions and Outlook 303
Acknowledgments 304
References 304

INDEX 311
CUMULATIVE LIST OF CONTRIBUTORS FOR VOLUME 1-36 317
CUMULATIVE INDEX FOR VOLUMES 37–53 321

Contributors

Numbers in parentheses indicated the pages on which the authors' contributions begin.

FRANK T. EDELMANN (101), Chemisches Institut der Otto-von-Guericke-Universität, Magdeburg, Universitätsplatz 2, D-39106 Magdeburg, Germany

FRANÇOIS P. GABBAI (61), Department of Chemistry, Texas A&M University, College Station, TX 77843, USA

IL NAM JUNG (41), Organosilicon Chemistry Laboratory, Korea Institute of Science and Technology, P.O. Box 131, Cheongryang, Seoul 130-650, Korea

VOLKER LORENZ (101), Chemisches Institut der Otto-von-Guericke-Universität, Magdeburg, Universitätsplatz 2, D-39106 Magdeburg, Germany

THOMAS D. MCGRATH (1), Department of Chemistry and Biochemistry, Baylor University, Waco, TX 76798-7348, USA

MOHAND MELAIMI (61), Department of Chemistry, Texas A&M University, College Station, TX 77843, USA

THOMAS MÜLLER (155), Institut für Anorganische und Analytische Chemie, Johann Wolfgang Goethe Universität, Frankfurt, Marie Curie-Str. 11, D 60439, Frankfurt/Main, Germany

GEORGII I. NIKONOV (211), Chemistry Department, Moscow State University, Vorob'evy Gory, 119992 Moscow, Russia

F. GORDON A. STONE (1), Department of Chemistry and Biochemistry, Baylor University, Waco, TX 76798-7348, USA

BOK RYUL YOO (41), Organosilicon Chemistry Laboratory, Korea Institute of Science and Technology, P.O. Box 131, Cheongryang, Seoul 130-650, Korea

Metal Complexes of Monocarbon Carboranes: A Neglected Area of Study?

THOMAS D. MCGRATH and
F. GORDON A. STONE[a,*]

[a]Department of Chemistry and Biochemistry, Baylor University, Waco, TX 76798-7348, USA

I. Introduction 1
II. Synthesis 3
A. Triruthenium and Triosmium Complexes 3
B. Mononuclear Compounds of Iron, Molybdenum, Tungsten, Rhenium, Platinum, Nickel and Cobalt 5
III. Reactions 7
A. Ruthenium and Osmium Cluster Compounds 7
B. Mononuclear Metal Compounds 9
C. Zwitterionic Bimetallic Compounds 22
IV. Monocarbollide–Metal Complexes with Non-Icosahedral Core Frameworks 28
A. Chemistry of the 11-Vertex Dianions $[1,1,1\text{-}(CO)_3\text{-}2\text{-}Ph\text{-}closo\text{-}1,2\text{-}MCB_9H_9]^{2-}$ (M = Mn, Re) 29
B. Chemistry of the 11-Vertex Trianions $[1,3,6\text{-}\{M(CO)_3\}\text{-}3,6\text{-}(\mu\text{-}H)_2\text{-}1,1,1\text{-}(CO)_3\text{-}2\text{-}Ph\text{-}closo\text{-}1,2\text{-}MCB_9H_7]^{3-}$ (M = Mo, W) 36
Acknowledgements 38
References 38

I
INTRODUCTION

The first metallacarboranes were isolated in M. F. Hawthorne's laboratory and contained a metal ion, two carbon and nine boron atoms forming an icosahedral $\{closo\text{-}MC_2B_9\}$ cage structure.[1,2] It was immediately recognized that these species may be viewed as having metal ions coordinated in a pentahapto manner by the open face of a $[nido\text{-}7,8\text{-}C_2B_9H_{11}]^{2-}$ dianion. This was a useful formalism since it emphasized an isolobal relationship between the carborane dianion and the ubiquitous $[C_5H_5]^-$ ligand. Following isolation of metal dicarbollides from reactions between metal salts and salts of $[nido\text{-}7,8\text{-}C_2B_9H_{11}]^{2-}$, it was logical that the monocarbon trianion $[nido\text{-}7\text{-}CB_{10}H_{11}]^{3-}$ would react in a similar way to afford monocarbon metallacarboranes also with icosahedral frameworks. Indeed, a few complexes of this kind were isolated[3] soon after the first dicarbon analogues were discovered. Importantly in the early work, two types of monocarbollide metal compound were characterized. In the first a metal ion is sandwiched between $[nido\text{-}7\text{-}CB_{10}H_{11}]^{3-}$ ligands, as in the Fe^{III} complex $[commo\text{-}2,2'\text{-}Fe\text{-}(closo\text{-}2,1\text{-}FeCB_{10}H_{11})_2]^{3-}$ (**1**) (Chart 1). In the second the cage-carbon atom carries an NR_3 or an NR_2 group, with the metal ion sandwiched between $[7\text{-}NR_3\text{-}nido\text{-}7\text{-}CB_{10}H_{10}]^{2-}$ groups, as in the Fe^{III} complex $[commo\text{-}2,2'\text{-}Fe\text{-}(1\text{-}NH_3\text{-}closo\text{-}2,1\text{-}FeCB_{10}H_{10})_2]^-$ (**2**), or $[7\text{-}NR_2\text{-}nido\text{-}7\text{-}CB_{10}H_{10}]^{3-}$

*Corresponding author.
E-mail: gordon_stone@baylor.edu (F.G.A. Stone).

ADVANCES IN ORGANOMETALLIC CHEMISTRY
VOLUME 53 ISSN 0065-3055/DOI 10.1016/S0065-3055(05)53001-6

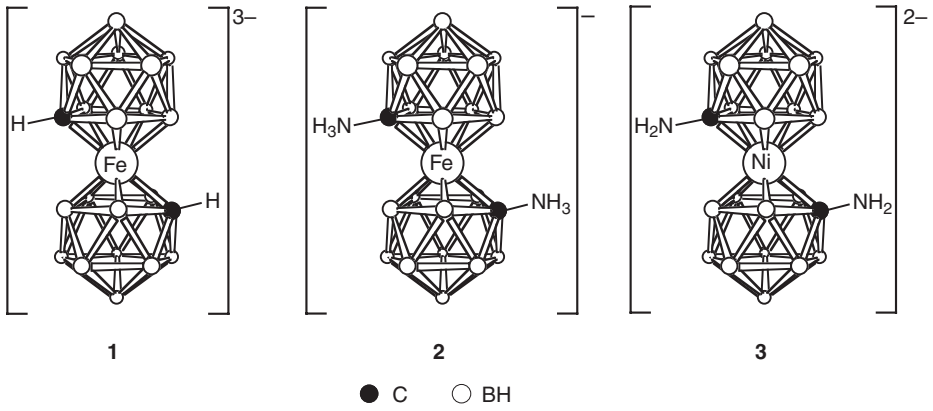

CHART 1.

groups as in [*commo*-2,2′-Ni-(1-NH_2-*closo*-2,1-$NiCB_{10}H_{10})_2]^{2-}$ (**3**). The zwitterionic ligands [7-NR_3-*nido*-7-$CB_{10}H_{10}]^{2-}$ are isolobal with the dicarbollide anion [*nido*-7,8-$C_2B_9H_{11}]^{2-}$, whereas the trianions [7-NR_2-*nido*-7-$CB_{10}H_{10}]^{3-}$ are isolobal with [*nido*-7-$CB_{10}H_{11}]^{3-}$.

In what has become a very large field of study during the past 40 years, metallacarborane chemistry has primarily focused on species with cages containing two or more carbon atoms,[4,5] whereas monocarbollide metal complexes have received very little attention.[4,6,7] The neglect of this area is somewhat surprising because monocarbollide metal complexes having [*nido*-7-$CB_{10}H_{11}]^{3-}$, [7-NR_3-*nido*-7-$CB_{10}H_{10}]^{2-}$, or [7-NR_2-*nido*-7-$CB_{10}H_{10}]^{3-}$ groups would be expected to display reactivity patterns different from those of the corresponding dicarbollide species. In particular, the higher formal negative charge associated with the trianions [*nido*-7-$CB_{10}H_{11}]^{3-}$ and [7-NR_2-*nido*-7-$CB_{10}H_{10}]^{3-}$, compared with the dianion [*nido*-7,8-$C_2B_9H_{11}]^{2-}$, renders metal complexes of the trianions more reactive towards electrophiles. As will be described later this feature provides avenues for introducing functional groups into a carborane cage, a topic of growing interest.

In metallacarborane chemistry it can be argued that it is more profitable to study molecules having half-sandwich 'piano-stool' structures than those with 'full-sandwich' structures. This is because in the piano-stool complexes the metal is ligated on one side by the carborane cage systems [{7,8-R_2-*nido*-7,8-$C_2B_9H_9$} (R = H or Me), {*nido*-7-$CB_{10}H_{11}$}, {7-NR_2-*nido*-7-$CB_{10}H_{10}$}, or {7-NR_3-*nido*-7-$CB_{10}H_{10}$}] and on the other side by the conventional ligands (CO, PR_3, CNR, alkynes, etc.) of coordination chemistry. With a combination of different coordinated groups within the coordination sphere of the metal there is the probability of reactions occurring between the ligands and other substrate molecules, and also with the carborane cage itself, with the latter thus adopting a non-spectator role in the chemistry derived.[8] Both mono- and di-carbollide metal carbonyl half-sandwich complexes are especially desirable as synthons. They have isolobal relationships with cyclopentadienide metal carbonyls that are known to function as precursors to numerous other species through the lability of their carbonyl groups. Dicarbollide metal

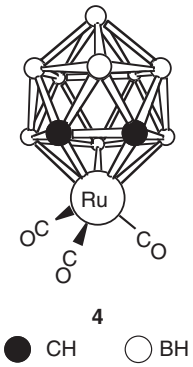

CHART 2.

carbonyls display a very extensive chemistry, as shown by [3,3,3-$(CO)_3$-*closo*-3,1,2-$RuC_2B_9H_{11}$] (**4**),[9] thereby pointing to the desirability of obtaining related monocarbollide metal carbonyl species for use in synthesis (Chart 2).

In an attempt to redress the imbalance between studies on the dicarbollide and monocarbollide metal compounds we began a comprehensive study of the latter, concentrating our studies on the piano-stool-type complexes for the reasons given above. Our progress to date in this area will be the subject of this review. So far, most of the work has involved compounds in which the metal is one of the 12 vertexes in a {*closo*-2,1-MCB_{10}} cage system, thereby complementing the host of studies made on their {*closo*-3,1,2-MC_2B_9} counterparts. However, as will also be described, preliminary investigation of 11-vertex {*closo*-1,2-MCB_9} systems is revealing the existence of unprecedented molecular structures in the metallacarborane field. We do not review in this chapter recent developments in the chemistry of monocarbollide–metal complexes in which the cage-carbon carries an NR_3 or NR_2 group because we have recently given an account of such species.[10]

II
SYNTHESIS

A. *Triruthenium and Triosmium Complexes*

The methodologies used to prepare monocarbollide metal carbonyls resemble those used to obtain cyclopentadienide metal carbonyls. The latter are generally obtained by one of two methods: heating cyclopentadiene or a substituted cyclopentadiene with a metal carbonyl or a metal carbonyl anion, or treating the carbonyl or a halo derivative of it with a salt of the cyclopentadienide ion. Similarly, procedures involving either heating a *nido*-carborane with a metal carbonyl or treating a metal carbonyl or a carbonyl-metal halide with the salt obtained by deprotonating a *nido*-carborane have afforded monocarbollide metal carbonyl complexes.

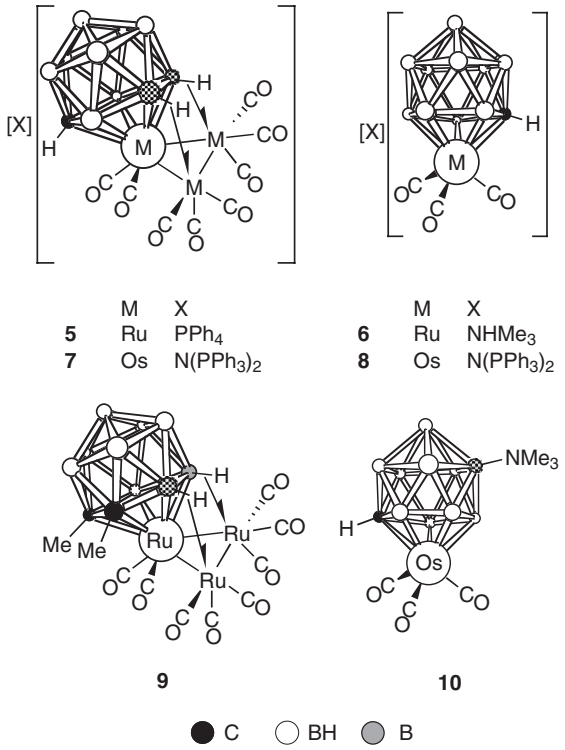

CHART 3.

Thus, in tetrahydrofuran (THF) at reflux temperatures $[Ru_3(CO)_{12}]$ and $[NHMe_3][nido\text{-}7\text{-}CB_{10}H_{13}]$ react to give an anionic trinuclear ruthenium complex $[PPh_4][2,2\text{-}(CO)_2\text{-}7,11\text{-}(\mu\text{-}H)_2\text{-}2,7,11\text{-}\{Ru_2(CO)_6\}\text{-}closo\text{-}2,1\text{-}RuCB_{10}H_9]$ (**5**)* (Chart 3) following the addition of $[PPh_4]Cl$.[11] Subsequent analysis of this system revealed evidence for traces of the mononuclear species $[NHMe_3][2,2,2\text{-}(CO)_3\text{-}closo\text{-}2,1\text{-}RuCB_{10}H_{11}]$ (**6**) in the initial product mixture, but its isolation in a pure form proved impossible.[12] In contrast, the corresponding reaction between $[Os_3(CO)_{12}]$ and $[N(PPh_3)_2][nido\text{-}7\text{-}CB_{10}H_{13}]$ in refluxing bromobenzene affords an approximately equimolar mixture of the analogous triosmium cluster $[N(PPh_3)_2][2,2\text{-}(CO)_2\text{-}7,11\text{-}(\mu\text{-}H)_2\text{-}2,7,11\text{-}\{Os_2(CO)_6\}\text{-}closo\text{-}2,1\text{-}OsCB_{10}H_9]$ (**7**) and the monoosmium complex $[N(PPh_3)_2][2,2,2\text{-}(CO)_3\text{-}closo\text{-}2,1\text{-}OsCB_{10}H_{11}]$ (**8**).[12] The structures of the anions of **5** and **7** are similar to that of neutral $[3,3\text{-}(CO)_2\text{-}1,2\text{-}Me_2\text{-}4,8\text{-}(\mu\text{-}H)_2\text{-}3,4,8\text{-}\{Ru_2(CO)_6\}\text{-}closo\text{-}3,1,2\text{-}RuC_2B_9H_7]$ (**9**) obtained from the reaction between

*The compounds described in Sections II and III are based upon *closo*-1-carba-2-metalladodecaborane fragments, with many bearing exo-polyhedral substituents. It should be noted that, although many contain chiral centers, the species are formed as racemates. Substituted boron atoms at positions 3, 7, 11, or 6 could equally be labeled 6, 11, 7, and 3, respectively. In each case the former is used, in accordance with IUPAC convention. Likewise, compounds in Section IV are based upon *closo*-1-metalla-2-carbaundecaborane fragments and several are chiral. Boron atoms bearing substituents at the 4, 5, 6, or 7 positions could equally be labeled 5, 4, 7, and 6, respectively, but again the former is used by convention.

$[Ru_3(CO)_{12}]$ and 7,8-Me_2-*nido*-7,8-$C_2B_9H_{11}$.[13] In all the trimetal species a {*nido*-CB_{10}} or {*nido*-C_2B_9} framework bridges a triangular arrangement of ruthenium or osmium atoms with the open $\overline{CBBBB}$ or $\overline{CCBBB}$ faces, respectively, coordinated in a pentahapto fashion to one metal atom while the carborane cage forms two exopolyhedral B–H→M bonds with the other two metal atoms.

Surprisingly, instead of affording a mixture containing the anions of the cluster compound **7** and the mononuclear species **8**, the complex [12-NMe_3-2,2,2-$(CO)_3$-*closo*-2,1-$OsCB_{10}H_{10}$] (**10**) is obtained by heating $[Os_3(CO)_{12}]$ with $[NHMe_3]$[*nido*-7-$CB_{10}H_{13}$] in refluxing bromobenzene. The NMe_3 group is attached to a boron atom in the pentagonal belt lying above that of the $\overline{CBBBB}$ ring η^5-coordinated to the metal.[12] The source of the trimethylamine group must be the cation $[NHMe_3]^+$, but the pathway by which its NMe_3 fragment migrates to the cage is not clear.

B. *Mononuclear Compounds of Iron, Molybdenum, Tungsten, Rhenium, Platinum, Nickel and Cobalt*

Reactions between salts of [*nido*-7-$CB_{10}H_{13}]^-$ and $[Fe_3(CO)_{12}]$ afford the mononuclear anionic iron compound [2,2,2-$(CO)_3$-*closo*-2,1-$FeCB_{10}H_{11}]^-$, typically isolated as its $[N(PPh_3)_2]^+$ salt (**11**) (Chart 4).[14] No anionic triiron complex analogous to **5** and **7** is formed in this reaction. The anionic mononuclear iron, ruthenium and osmium complexes and the previously mentioned neutral mononuclear ruthenium dicarbollide complex **4**, obtained from $[Ru_3(CO)_{12}]$ and *nido*-7,8-$C_2B_9H_{13}$, are isolobal with the cyclopentadienide species $[Mn(CO)_3(\eta\text{-}C_5H_5)]$ and $[Fe(CO)_3(\eta\text{-}C_5H_5)]^+$.

In an attempt to prepare a molybdenum complex related to compound **11**, $[Mo(NCMe)_3(CO)_3]$ was treated with $[NHMe_3]$[*nido*-7-$CB_{10}H_{13}$] followed by $[N(PPh_3)_2]Cl$ but the desired complex $[N(PPh_3)_2]$[2,2,2,2-$(CO)_4$-*closo*-2,1-$MoCB_{10}H_{10}$] (**12**) was obtained only in poor yield.[14] This complex was also formed in the reaction between Na_3[*nido*-7-$CB_{10}H_{11}$] and $[Mo(NCMe)_3(CO)_3]$ presumably *via* an intermediate species [2,2,2-$(CO)_3$-*closo*-2,1-$MoCB_{10}H_{11}]^{3-}$, isolobal with the long-known [3,3,3-$(CO)_3$-*closo*-3,1,2-$MoC_2B_9H_{11}]^{2-}$ dianion.[2] Evidently any salt of [2,2,2-$(CO)_3$-*closo*-2,1-$MoCB_{10}H_{11}]^{3-}$ is readily oxidized, scavenging a CO molecule to afford the final product. It was possible to prepare **12** by adding $[Mo(NCMe)_3(CO)_3]$ in NCMe to a THF suspension of Na_3[*nido*-7-$CB_{10}H_{11}$] at low temperatures while bubbling CO through the mixture, followed by addition of $H[BF_4]\cdot OEt_2$ and $[N(PPh_3)_2]Cl$.[14] It seems likely that in this reaction sequence, **12** is formed *via* a pathway involving the unstable hydrido species [2,2,2-$(CO)_3$-2-H-*closo*-2,1-$MoCB_{10}H_{11}]^{2-}$ and [2,2,2-$(CO)_3$-2,2-$(H)_2$-*closo*-2,1-$MoCB_{10}H_{11}]^-$ with the latter eliminating hydrogen and capturing a CO molecule to yield the observed product. The tungsten compound **13**, an analogue of **12**, can be prepared similarly using $[W(NCEt)_3(CO)_3]$ as the tungsten source.[15a]

Salts of [*nido*-7-$CB_{10}H_{11}]^{3-}$ have not been extensively employed as yet to obtain half-sandwich compounds {2-(ligand)$_n$-*closo*-2,1-$MCB_{10}H_{11}$}, but their potential as precursors is demonstrated in the synthesis of rhenium and platinum compounds. Thus salts of the dianion [2,2,2-$(CO)_3$-*closo*-2,1-$ReCB_{10}H_{11}]^{2-}$ have been prepared by

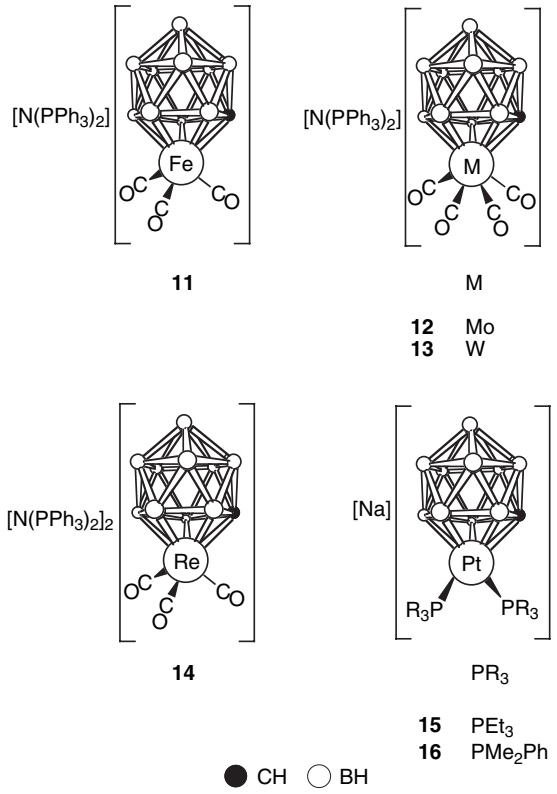

CHART 4.

treating $[ReBr(THF)_2(CO)_3]$ with $Na_3[nido\text{-}7\text{-}CB_{10}H_{11}]$ followed by addition of the appropriate cation, with the bis-$[N(PPh_3)_2]^+$ salt **14** typically isolated.[16] The dianion of **14** is isolobal with the long-known species $[3,3,3\text{-}(CO)_3\text{-}closo\text{-}3,1,2\text{-}ReC_2B_9H_{11}]^-$ and $[Re(CO)_3(\eta\text{-}C_5H_5)]$, and displays an extensive chemistry discussed further below. Interestingly, mention was made of a species $[2,2,2\text{-}(CO)_3\text{-}closo\text{-}2,1\text{-}MnCB_{10}H_{11}]^{2-}$, a manganese analogue of the dianion of **14**, in the original report of monocarbollide metal complexes, but without information on its properties.[3a]

Monocarbollide platinum complexes have also been prepared from $Na_3[nido\text{-}7\text{-}CB_{10}H_{11}]$. The latter in THF with $[PtCl_2(PR_3)_2]$ affords $Na[2,2\text{-}(PR_3)_2\text{-}closo\text{-}2,1\text{-}PtCB_{10}H_{11}]$ [$PR_3 = PEt_3$ (**15**),[17] PMe_2Ph (**16**)[18]], species which as described later provide entry into a range of other compounds with similar $\{closo\text{-}2,1\text{-}PtCB_{10}\}$ frameworks.[17–19] The $[NMe_4]^+$ salt of the platinacarborane anion in **15** had been prepared much earlier by a 'polyhedral expansion' reaction involving treatment of $[NMe_4][closo\text{-}2\text{-}CB_{10}H_{11}]$ with $[Pt(trans\text{-stilbene})(PEt_3)_2]$.[7a] Several related complexes were similarly obtained by treating this carborane anion with Ni^0, Pd^0 or Pt^0 reagents, and as such rank among the earliest of monocarbollide metal complexes to be described.

Contemporary studies with the nickel system have extended the series of known nickel-monocarbollide anions (Chart 5). The salt $[NMe_4][2,2\text{-}(CNBu^t)_2\text{-}closo\text{-}2,1\text{-}NiCB_{10}H_{11}]$ (**17a**) was prepared in the original study, using $[Ni(CNBu^t)_2(cod)]$

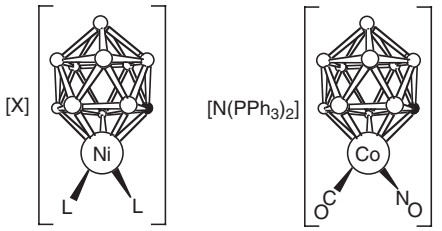

	X	L_2
17a	NMe_4	$(CNBu^t)_2$
17b	$N(PPh_3)_2$	$(CNBu^t)_2$
18	$N(PPh_3)_2$	$(CO)_2$
19	$N(PPh_3)_2$	$(CNXyl)_2$
20	$N(PPh_3)_2$	cod

21

● CH ○ BH

CHART 5.

(cod = 1,5-cyclooctadiene) as the Ni^0 reagent.[7a] Use of $[Ni(CO)_4]$, $[Ni(CNXyl)_2(cod)]$ (Xyl = $C_6H_3Me_2$-2,6), or $[Ni(cod)_2]$ as the nickel source afforded the corresponding $\{NiCB_{10}\}$ species, isolated as the salts $[N(PPh_3)_2][2,2\text{-}L_2\text{-}closo\text{-}2,1\text{-}NiCB_{10}H_{11}]$ [L = CO (**18**), CNXyl (**19**); L_2 = cod (**20**)] following addition of $[N(PPh_3)_2]Cl$.[20] Indeed, this polyhedral expansion route remains an attractive possibility for preparing other monocarbollide metal compounds, as demonstrated by the recent synthesis of the cobalt compound $[N(PPh_3)_2][2\text{-}CO\text{-}2\text{-}NO\text{-}closo\text{-}2,1\text{-}CoCB_{10}H_{11}]$ (**21**), formally isoelectronic with **18**, by reacting $[closo\text{-}2\text{-}CB_{10}H_{11}]^-$ with $[Co(CO)_3(NO)]$ in THF, followed by addition of $[N(PPh_3)_2]Cl$.[21] Complex **21** belongs to a rare class of nitrosyl substituted metallacarboranes and as far as we are aware is the first involving a monocarbollide metal species.[22]

As has been described, the 'parent' monocarbollide-metal carbonyl piano-stool species $[2\text{-}(CO)_n\text{-}closo\text{-}2,1\text{-}MCB_{10}H_{11}]^{x-}$ are now known for all of the metals M = Mo (**12**), W (**13**), Re (**14**), Fe (**11**), Ru (**6**), Os (**8**), and Ni (**18**). Evidence also exists for a dicarbonyl-platinum analogue of compound **18**,[20] and as mentioned earlier, the manganese analogue of **14** has also briefly been reported.[3a] A notable absence from this list, however, is any representative of the Group 9 metals. The carbonyl nitrosyl-cobalt complex **21** is very closely related to the hitherto unknown dicarbonyl-cobalt dianion $[2,2\text{-}(CO)_2\text{-}closo\text{-}2,1\text{-}CoCB_{10}H_{11}]^{2-}$ and this species remains an attractive synthetic target.

III
REACTIONS

A. *Ruthenium and Osmium Cluster Compounds*

On protonation with $H[BF_4]\cdot OEt_2$ in THF the anionic trinuclear metal complexes **5** and **7** afford the neutral hydrido compounds $[2,2\text{-}(CO)_2\text{-}7,11\text{-}(\mu\text{-}H)_2\text{-}2,7,$

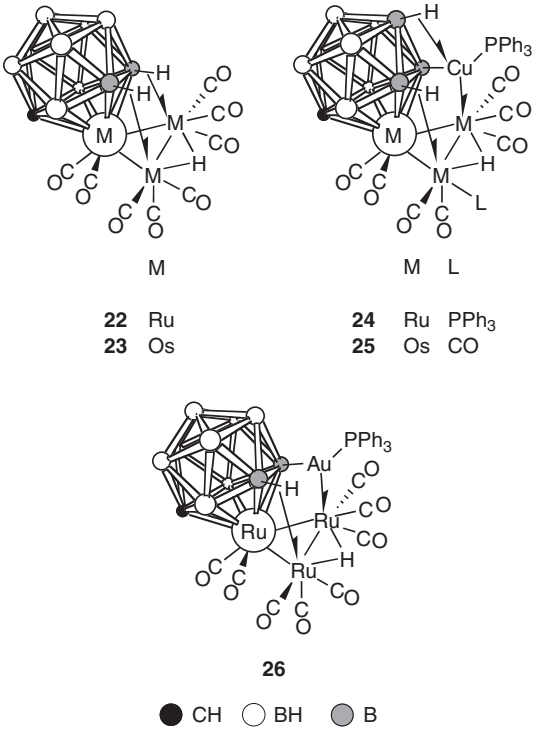

CHART 6.

11-{$M_2(\mu\text{-H})(CO)_6$}-*closo*-2,1-$MCB_{10}H_9$] [M = Ru (**22**) and Os (**23**)], respectively (Chart 6).[11,12] An X-ray diffraction study upon **22** revealed that in these species the hydrido ligand bridges the M–M bonding unit that is attached to the cage *via* the two B–H→M bonds. The bridging hydride reveals itself in the ^{1}H NMR spectrum with diagnostic peaks at δ –19.03 (**22**) and δ –18.65 (**23**). The B–H→M linkages are also readily identified from the NMR spectra, in the ^{1}H spectra by quartet resonances at δ –10.31 [J(BH) = 56 Hz] (**22**) and δ –13.50 [J(BH) = 45 Hz] (**23**), and in their fully coupled ^{11}B spectra with doublets at δ 23.4 [J(BH) = 52 Hz] (**22**) and at δ 13.1 [J(BH) = 45 Hz] (**23**).

Both **5** and **7** undergo an interesting reaction in THF with [$CuCl(PPh_3)_3$] or [$CuCl(PPh_3)]_4$, respectively, in the presence of Tl[PF_6], affording the neutral cluster compounds **24** and **25**, respectively. In the formation of these species one of the hydrides of a B–H→M bond (M = Ru, Os) has migrated to a bridging M(μ-H)M site, being replaced by an isolobal $\{Cu(PPh_3)\}^+$ fragment. A B–H→Cu bond, involving a BH unit in the B_5 pentagonal belt lying above the $\overline{CBBBB}$ ring pentahapto coordinated to the metal vertex, further attaches the copper to the cage. In the ruthenium compound a PPh_3 molecule derived from the copper reagent substitutes for one of the CO ligands on the Ru_3 triangle. Salts of the anion **5** react with [$AuCl(PPh_3)$] to yield **26** which has structural features similar to **24**, except that the gold atom has only a single B–Au σ-bonding attachment to the cage. The difference

in the bonding of Cu and Au atoms to the cage in **24** and **26** no doubt relates to the tendency of copper to seek a higher coordination number than gold, as discussed further below.

B. *Mononuclear Metal Compounds*

1. Formation of Charge-Compensated Complexes with Donor Ligands

a. Complexes of Iron

Salts of the mononuclear iron anion of **11** undergo a variety of reactions (Chart 7).[14,23] The CO groups in **11** are not readily substituted by donor ligands. However, in the presence of Me_3NO, one CO group is readily replaced by donor molecules to yield $[N(PPh_3)_2][2,2\text{-}(CO)_2\text{-}2\text{-L-}closo\text{-}2,1\text{-}FeCB_{10}H_{11}]$ [L = PPh_3 (**27**), $CNBu^t$ (**28**), SMe_2 (**29**)]. More interestingly, **11** reacts with electrophiles (NO^+, Ph_3C^+, H^+) in the presence of certain solvents L to give the species $[2,2,2\text{-}(CO)_3\text{-}7\text{-L-}closo\text{-}2,$

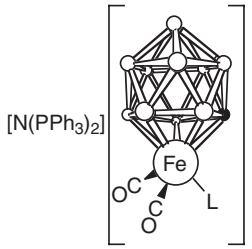

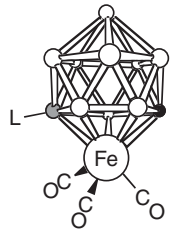

L		L	
27	PPh_3	**30**	$O(CH_2)_4$
28	$CNBu^t$	**31**	OEt_2
29	SMe_2	**32**	SMe_2
		34	*E*-N(Me)=C(H)Me
		36	NH_2Me
		37	NH(Me)Et

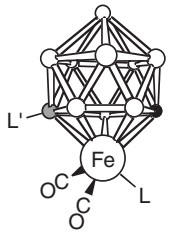

L	L'	
33	SMe_2	SMe_2
35	PPh_3	$NCBu^t$

● CH ○ BH ● B

CHART 7.

1-$FeCB_{10}H_{10}$] [L = $O(CH_2)_4$ (**30**), OEt_2 (**31**), SMe_2 (**32**)], in which a donor molecule L is bonded to a boron atom that is in a β site with respect to the carbon in the $\overline{CBBBB}$ ring coordinated to the iron atom.[14] Apart from the use of X-ray crystallography to confirm the structures, NMR spectra leave no doubt about the presence of the {B–L^+} groups in these charge-compensated products. Thus, for example, in the $^{11}B\{^1H\}$ NMR spectrum of **30** there is a resonance at δ 20.4 which remains a singlet in a fully coupled ^{11}B spectrum while the other peaks, corresponding in total intensity to nine boron nuclei, display ^{11}B–^1H coupling (ca. 130 Hz).

If compound **29** is treated with SMe_2 and H_2SO_4 the zwitterionic complex [2,2-$(CO)_2$-2,7-$(SMe_2)_2$-*closo*-2,1-$FeCB_{10}H_{10}$] (**33**) is obtained in which an SMe_2 group is attached both to the metal vertex and to a boron atom situated in one of the β sites in the $\overline{CBBBB}$ ring coordinated to the iron, a result confirmed by X-ray diffraction.[23] In reactions of this kind the β rather than the α sites are favored for substitution by a donor molecule because the H atoms of their BH groups are the more hydridic and therefore are more susceptible to attack by electrophiles.

When complex **11** in NCMe is treated with CF_3SO_3Me, the product obtained is [2,2,2-$(CO)_3$-7-{(*E*)-N(Me)═C(H)Me}-*closo*-2,1-$FeCB_{10}H_{10}$] (**34**) in which an iminium group {*E*-N(Me)═C(H)Me} is attached to a β-boron in the pentagonal $\overline{CBBBB}$ ring ligating the iron.[23] The mode of formation of the iminium group present in **34**, and related complexes derived from other nitriles, involves CF_3SO_3Me reacting with NCMe to give an *N*-methylnitrilium cation $[MeN{\equiv}CMe]^+$ which itself then abstracts H^- from the cage BH vertex to give an imine molecule. This then coordinates *via* the nitrogen atom to the naked site created at the boron vertex. The *E*-forms of imines are more stable than the *Z*-configurations and this must favor a facile rearrangement of initially formed *Z*–N(Me)═C(H)Me into *E*–N(Me)═C(H)Me in the reaction.[23] It is interesting that if a similar reaction is carried out with compound **27** as substrate, and employing the more bulky $NCBu^t$ instead of NCMe, a typical charge-compensated product [2,2-$(CO)_2$-2-PPh_3-7-$NCBu^t$-*closo*-2,1-$FeCB_{10}H_{10}$] (**35**) is formed.

Introducing a functional imine group into the cage system in this manner opens the possibility of further syntheses with the substituent group. Several reactions have been studied.[23] Formally, the β-boron appended $\{N(Me){=}C(H)Me\}^+$ group in **34** carries a positive charge, with two canonical forms for the fragment, one with the charge residing on the N atom and the other with the charge residing on the C atom of the *C*(H)Me terminus. The former is favored and thus it would be anticipated that the imine group would react with nucleophiles such as OH^- or H^-. Accordingly, treatment of **34** in THF with water yields the complex [2,2,2-$(CO)_3$-7-NH_2Me-*closo*-2,1-$FeCB_{10}H_{10}$] (**36**), a process catalyzed by PMe_3. The $\{N(Me) = C(H)Me\}^+$ group may also be reduced by $Na[BH_3CN]$ to give [2,2,2-$(CO)_3$-7-NH(Me)Et-*closo*-2,1-$FeCB_{10}H_{10}$] (**37**).

Treatment of **11** in THF with $Bu^tC{\equiv}CH$ in the presence of Me_3NO, to facilitate removal of CO, yielded a single isomer of a species $[N(PPh_3)_2][2,2\text{-}(CO)_2\text{-}2,3\text{-}\eta^2{:}\sigma\text{-}\{(E)\text{-}CH{=}C(H)Bu^t\}\text{-}closo\text{-}2,1\text{-}FeCB_{10}H_{10}]$ (**38**), resulting from insertion of an alkyne molecule into a cage B–H bond (Chart 8). While the gross features of the molecular structure could be deduced from NMR data, the site of attachment of the

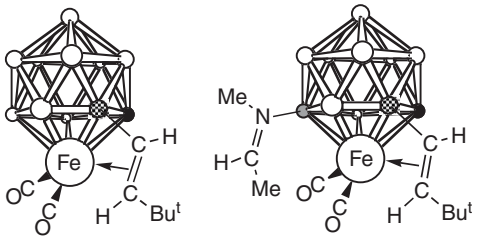

38 **39**

CH BH B

CHART 8.

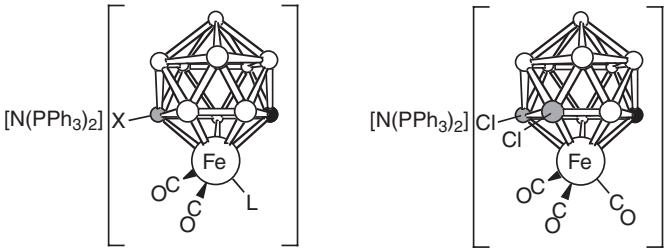

	L	X
40	CO	Cl
41	CO	I
43	$CNBu^t$	I
44	CO	C_6H_4Me-4

42

CH BH B

CHART 9.

E-C(H)═C(H)Bu^t moiety to the cage could not be resolved with certainty. Crystals suitable for an X-ray diffraction study could not be obtained so **38** was reacted in NCMe with CF_3SO_3Me to give the imine derivative [2,2-$(CO)_2$-2,3-η^2:σ-{(*E*)-CH═C(H)Bu^t}-11-{(*E*)-N(Me)═C(H)Me}-*closo*-2,1-$FeCB_{10}H_9$] (**39**). The latter did provide good quality crystals and its structure was fully resolved by X-ray diffraction. The {(*E*)-C(H)═C(H)Bu^t} group is attached to a boron atom α to the carbon in the $\overline{CBBBB}$ ring bonded to the iron while the C(H)═C(H) double bond is η^2 coordinated to the metal atom. The {N(Me)═C(H)Me} group occupies the site on the $\overline{CBBBB}$ ring which is β with respect to the carbon atom and is more remote from the α-bound vinyl group.

Treatment of complex **11** in NCMe with H_2SO_4 and dihalogen equivalents results in hydride abstraction and formation of *B*-halogenated anions (Chart 9).[24] Thus, with *N*-chlorosuccinimide (2 equiv) or iodine (1 equiv), the species $[N(PPh_3)_2][7\text{-}X\text{-}2,2,2\text{-}(CO)_3\text{-}closo\text{-}2,1\text{-}FeCB_{10}H_{10}]$ [X = Cl (**40**), I (**41**)] are formed. Use of 4 equiv of

N-chlorosuccinimide yields dichloro-substituted $[N(PPh_3)_2][7,11\text{-}Cl_2\text{-}2,2,2\text{-}(CO)_3\text{-}closo\text{-}2,1\text{-}FeCB_{10}H_9]$ (**42**). In each of these products, hydride replacement again occurs at boron atoms that are β with respect to the carbon atom in the iron-bound $\overline{CBBBB}$ face, a feature confirmed by an X-ray diffraction study upon complex **42**. This site of substitution was also verified by treatment of **41** with $Ag[BF_4]$ in the presence of THF, which afforded compound **30** *via* AgI elimination.

The potential of complexes **40**–**42** as precursors to further iron-monocarbollide species is also demonstrated[24] by the conversion of **41** to $[N(PPh_3)_2][7\text{-}I\text{-}2,2\text{-}(CO)_2\text{-}2\text{-}CNBu^t\text{-}closo\text{-}2,1\text{-}FeCB_{10}H_{10}]$ (**43**), parallel to the synthesis of **28** from **11**. Moreover, the utility of species such as **41** for the introduction of cluster organyl substituents was shown by its reaction with $[MgBr(C_6H_4Me\text{-}4)]$ in THF, which gave $[N(PPh_3)_2][7\text{-}(C_6H_4Me\text{-}4')\text{-}2,2,2\text{-}(CO)_3\text{-}closo\text{-}2,1\text{-}FeCB_{10}H_{10}]$ (**44**) *via* a cross-coupling reaction. Derivatives of the manganese dicarbollide anion $[3,3,3\text{-}(CO)_3\text{-}closo\text{-}3,1,2\text{-}MnC_2B_9H_{11}]^-$, isolobal with the anion of **11**, have recently also been demonstrated to possess an extensive cage substitution chemistry,[22e] with many parallels evident between the two systems. Compounds such as **40**–**44** would be expected to undergo many of the reactions observed for the corresponding $\{MnC_2B_9\}$ species, leading to complexes bearing multiple cage-boron substituents.

b. Complexes of Molybdenum and Tungsten

The monocarbollide-molybdenum and -tungsten carbonyl complexes **12** and **13** in many ways show a similar chemistry to that of **11** (Chart 10). Because the earlier mentioned molybdenum salt **12** in solution is somewhat unstable, the derivatives $[N(PPh_3)_2][2,2,2\text{-}(CO)_3\text{-}2\text{-}PPh_3\text{-}closo\text{-}2,1\text{-}MCB_{10}H_{11}]$ [M = Mo (**45**), W (**46**)] were usually employed in further synthesis.[14,15a] These reagents, along with other M-substituted species $[N(PPh_3)_2][2,2,2\text{-}(CO)_3\text{-}2\text{-}CNBu^t\text{-}closo\text{-}2,1\text{-}MCB_{10}H_{11}]$ [M = Mo (**47**), W (**48**)], were prepared by reaction of **12** or **13** with the donor ligand in the presence of Me_3NO. When $Bu^tC{\equiv}CH$ is the added ligand in the latter reaction, two carbonyl molecules are substituted and the alkyne behaves as a four-electron donor in the products $[N(PPh_3)_2][2,2\text{-}(CO)_2\text{-}2\text{-}(Bu^tC{\equiv}CH)\text{-}closo\text{-}2,1\text{-}MCB_{10}H_{11}]$ [M = Mo (**49**), W (**50**)].[14,15a] A series of charge-compensated complexes $[2,2,2\text{-}(CO)_3\text{-}2\text{-}PPh_3\text{-}7\text{-}L\text{-}closo\text{-}2,1\text{-}MCB_{10}H_{10}]$ has been prepared by treating mixtures of either the molybdenum **45** or the tungsten **46** precursors with a donor molecule L and either CF_3SO_3Me or concentrated H_2SO_4 [L = OEt_2, M = Mo (**51**), M = W (**52**); L = $O(CH_2)_4$, M = Mo (**53**), M = W (**54**); L = SMe_2, M = Mo (**55**); L = $S(CH_2)_4$, M = Mo (**56**), M = W (**57**); L = $CNBu^t$, M = Mo (**58**), M = W (**59**); L = CNXyl, M = Mo (**60**), M = W (**61**)].[14,15a]

As noted earlier, reactivity at the exo-polyhedral groups L without degradation of the cage system is of interest because functionalization of cage boron atoms opens the way to further new chemistry. If the donor atom is the oxygen of an ether molecule it carries a formal positive charge rendering an adjacent atom susceptible to attack by nucleophiles. Thus, treatment of **52** in THF with Me_3NO, followed by addition of $[PPh_4]Br$, affords $[PPh_4][2,2,2\text{-}(CO)_3\text{-}2\text{-}PPh_3\text{-}7\text{-}OEt\text{-}closo\text{-}WCB_{10}H_{10}]$ (**62**), resulting from cleavage of an Et group from the precursor. The potential of

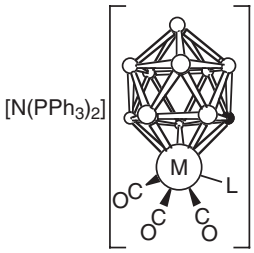

	M	L
45	Mo	PPh_3
46	W	PPh_3
47	Mo	$CNBu^t$
48	W	$CNBu^t$

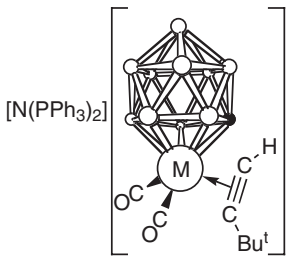

	M
49	Mo
50	W

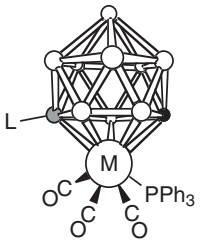

	M	L
51	Mo	OEt_2
52	W	OEt_2
53	Mo	$O(CH_2)_4$
54	W	$O(CH_2)_4$
55	Mo	SMe_2
56	Mo	$S(CH_2)_4$
57	W	$S(CH_2)_4$
58	Mo	$CNBu^t$
59	W	$CNBu^t$
60	Mo	CNXyl
61	W	CNXyl

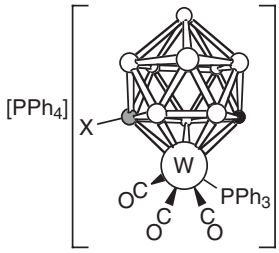

	X
62	OEt
63	$O(CH_2)_3C(H)O$

● CH ○ BH ● B

Chart 10.

this methodology to introduce functional groups on the cage is well illustrated by a similar reaction with **54**. In the latter, the CH_2 group to be displaced is anchored to the boron-bound oxygen by the CH_2 chain. Treatment with Me_3NO followed by $[PPh_4]Br$ allowed the isolation of the compound $[PPh_4][2,2,2\text{-}(CO)_3\text{-}2\text{-}PPh_3\text{-}7\text{-}\{O(CH_2)_3C(H)O\}\text{-}closo\text{-}2,1\text{-}WCB_{10}H_{10}]$ (**63**) with a pendant aldehyde group attached to the cage.[15a]

The high anionic charge of the ligand $[nido\text{-}7\text{-}CB_{10}H_{11}]^{3-}$ is capable of stabilizing metals in higher oxidation states than the formal +II state of the molybdenum and

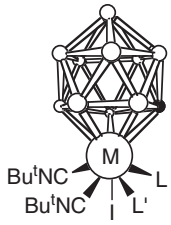

	M	L	L'
64	Mo	CNBu^t	CNBu^t
65	W	CNBu^t	CO
66	W	CO	CO

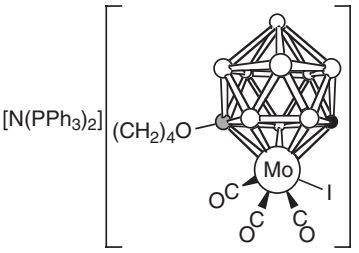

67

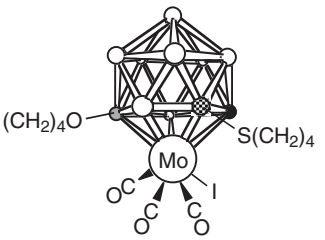

68

CH BH B

Chart 11.

tungsten found in the complexes discussed above. Since these two metals are capable of having oxidation states above M^{II}, oxidation rather than cage substitution can occur when the species **12** and **13** are treated with some reagents.[15b] However, there was a perceived need in such reactions for donors other than CO to be present, since in the higher oxidation state stabilization by the π bonding of CO molecules to the metal would be less effective. Thus when **12** in CH_2Cl_2 is treated with iodine in the presence of excess CNBu^t the neutral Mo^{IV} compound [2,2,2,2-(CNBu^t)$_4$-2-I-*closo*-2,1-$MoCB_{10}H_{11}$] (**64**) is produced in high yield (Chart 11). A similar reaction with **13** affords a mixture of the tungsten compounds [2,2,2-(CNBu^t)$_3$-2-CO-2-I-*closo*-2,1-$WCB_{10}H_{11}$] (**65**) and [2,2-(CNBu^t)$_2$-2,2-(CO)$_2$-2-I-*closo*-2,1-$WCB_{10}H_{11}$] (**66**).

Compound **12** displays an altogether different reactivity pattern upon treatment with iodine in the presence of an ether or a thioether.[15b] Thus, the sole product of the reaction of **12** in THF with iodine was the anionic Mo^{II} complex [N(PPh$_3$)$_2$][2,2,2-(CO)$_3$-2-I-7-O(CH$_2$)$_4$-*closo*-2,1-$MoCB_{10}H_{10}$] (**67**), with the carborane cage having undergone a substitution at a boron vertex. The substitution occurs at a β boron atom in the $\overline{CBBBB}$ face that ligates the molybdenum atom. When **67** is treated with further iodine in THF no reaction occurs. However, treatment with iodine using

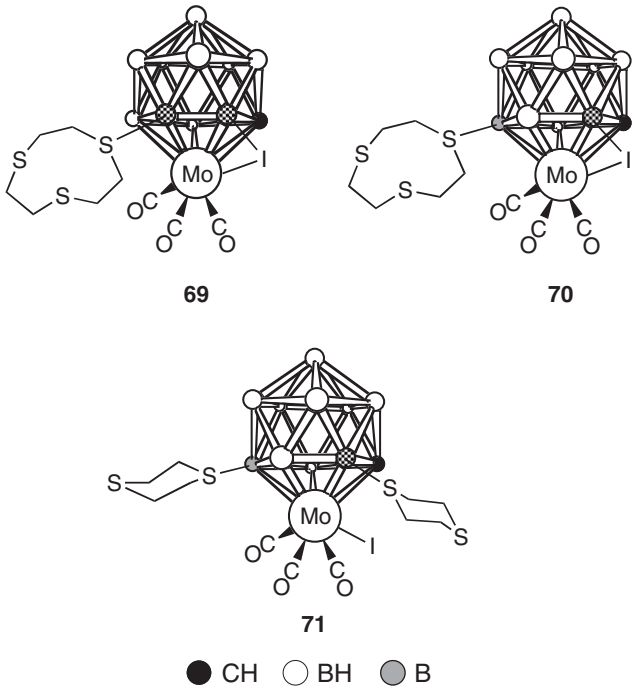

Chart 12.

$S(CH_2)_4$ as solvent results in a second cage substitution to give [2,2,2-$(CO)_3$-2-I-3-$S(CH_2)_4$-11-$O(CH_2)_4$-*closo*-2,1-$MoCB_{10}H_9$] (**68**), suggesting that iodine is more reactive in this medium. Notably, this second boron-bound substituent becomes attached to a boron atom in an α site in the molybdenum-coordinated $\overline{CBBBB}$ face.

With thioether ligands and iodine, compound **12** also reacts to yield cage-substituted species, but the situation is more complicated than that with THF.[15b] With equimolar amounts of iodine and thioethers L [L = $S(CH_2)_4$, *cyclo*-1,4-$S_2(CH_2)_4$, *cyclo*-1,4,7-$S_3(CH_2)_6$, *cyclo*-1,4,7,10-$S_4(CH_2)_8$] two distinct product types are formed (Chart 12). The members of the first series have the general formulation [2,2,2-$(CO)_3$-2,3-(μ-I)-*n*-L-*closo*-2,1-$MoCB_{10}H_9$] and for each L they are formed as a mixture of two isomers ($n = 7$ or 11). An X-ray crystallographic study on one isomer of the species [2,2,2-$(CO)_3$-2,3-(μ-I)-*n*-{*cyclo*-1,4,7-$S_3(CH_2)_6$}-*closo*-2,1-$MoCB_{10}H_9$] established that the iodide ligand bridges between the metal atom and an α boron atom in the coordinating $\overline{CBBB}$*B* face of the carborane cage. The trithiacyclononane ligand is bonded to a boron atom in a site that is β with respect to the cage-carbon atom in the open $\overline{CBB}$*B*$\overline{B}$ face of the cage. This isomer is thus formulated as [2,2,2-$(CO)_3$-2,3-(μ-I)-7-{*cyclo*-1,4,7-$S_3(CH_2)_6$}-*closo*-2,1-$MoCB_{10}H_9$] (**69**) with the iodine atom and the thioether attached to adjacent sites, α and β respectively, in the pentahapto $\overline{CBBBB}$ face. The other isomer is of formulation [2,2,2-$(CO)_3$-2,3-(μ-I)-11-{*cyclo*-1,4,7-$S_3(CH_2)_6$}-*closo*-2,1-$MoCB_{10}H_9$] (**70**) with the two substituents located at non-adjacent α and β′ boron atoms of the $\overline{CBBB}$*B*$\overline{B}$ belt. The iodine-promoted replacement of boron-bound hydrides

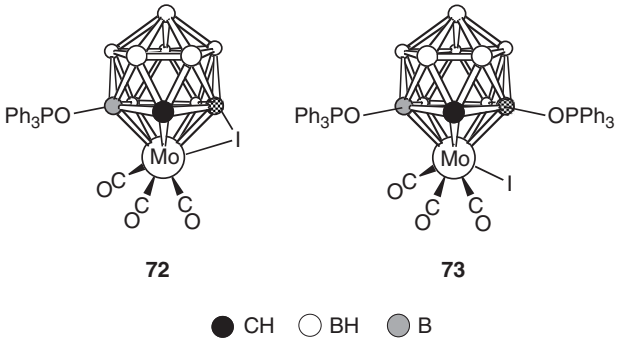

CHART 13.

by the two electron donor thioether molecules may formally be regarded as an oxidative-substitution reaction, as discussed in more detail elsewhere.[15b]

In the second series of compounds formed in the reaction between **12** and I_2 and thioethers, two thiane molecules are attached to the cage in non-adjacent α and β′ sites with respect to the carbon in the $\overline{CBBBB}$ ring. These products are formed as single isomers and the structure of [2,2,2-$(CO)_3$-2-I-3,11-{*cyclo*-1,4-$S_2(CH_2)_4$}$_2$-*closo*-2,1-$MoCB_{10}H_9$] (**71**) was confirmed by X-ray diffraction.

In contrast to the above reactions of **12** with I_2, compound **45** in CH_2Cl_2 with the interhalogen ICl (1 equiv) gave a mixture of [2,2,2-$(CO)_3$-2,3-(μ-I)-6-$OPPh_3$-*closo*-2,1-$MoCB_{10}H_9$] (**72**) and [2,2,2-$(CO)_3$-2-I-3,6-$(OPPh_3)_2$-*closo*-2,1-$MoCB_{10}H_9$] (**73**), both identified with the aid of X-ray diffraction studies (Chart 13).[25] The bridging iodide in **72** is similar to that found in compounds **69** and **70** and related species, and is bonded to both the molybdenum vertex and an α boron atom in the Mo-bound $\overline{CBBBB}$ belt; the second boron-bound substituent, an $OPPh_3$ molecule, is bonded to the other α boron atom. In **73** there are two $OPPh_3$ substituents, both of which are bound to α boron atoms in the $\overline{CBBB}B$ ring; the iodide is terminal to the molybdenum. Arguably, complexes **72** and **73** could both be formed from a common intermediate, similarly to the scheme proposed for the formation of compounds **69**–**71**.[15b] However, the reaction here must be considerably more complex: although the $OPPh_3$ molecules are believed to originate from the Mo-bound PPh_3 ligand of the precursor **45**, it is not clear how they are oxidized and then become attached to the cluster.

c. Complexes of Nickel and Cobalt

In common with the molybdenum (**12**) and tungsten (**13**) species discussed earlier, the nickel-bound CO ligands in **18** are somewhat labile and hence phosphine-substituted derivatives [$N(PPh_3)_2$][2-CO-2-PR_3-*closo*-2,1-$NiCB_{10}H_{11}$] [R = Et (**74**), Ph (**75**)] were again prepared and used in further studies (Chart 14).[20] Protonation of **74** or **75** with H[BF_4] OEt_2 in CH_2Cl_2–OEt_2 then afforded zwitterionic species, with **74** giving as expected [7-OEt_2-2-CO-2-PEt_3-*closo*-2,1-$NiCB_{10}H_{10}$] (**76**).[20] However,

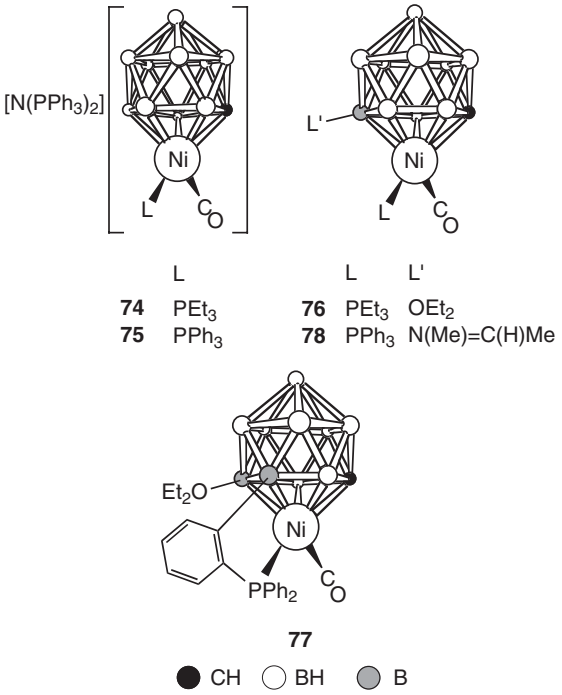

	L		L	L'
74	PEt_3	**76**	PEt_3	OEt_2
75	PPh_3	**78**	PPh_3	N(Me)=C(H)Me

77

CH BH B

Chart 14.

the analogous product was not obtained from **75**, which instead yielded [7-OEt_2-2-CO-2,11-PPh_2(C_6H_4-2′-*B*)-*closo*-2,1-$NiCB_{10}H_9$] (**77**) in which an additional *ortho*-cycloboronation of a phosphine phenyl ring has occurred. Compound **75**, like complexes **11** and **38** (and **45** and **46**[15a]), also reacts with NCMe and CF_3SO_3Me to afford a product, [7-{N(Me)═C(H)Me}-2-CO-2-PPh_3-*closo*-2,1-$NiCB_{10}H_{10}$] (**78**), with a boron-bound iminium group. However, **78** is formed as a mixture of both *E* and *Z* isomers, a feature confirmed by NMR spectroscopy and X-ray diffraction analyses.[20]

Treatment of the cobalt complex **21** with PEt_3 or $CNBu^t$, or with PPh_3 in the presence of Me_3NO, affords $[N(PPh_3)_2][2\text{-NO-2-L-}closo\text{-2,1-}CoCB_{10}H_{11}]$ [L = PEt_3 (**79**), $CNBu^t$ (**80**), PPh_3 (**81**)] (Chart 15).[21] Surprisingly, with an excess of $CNBu^t$ compound **21** reacts to give the Co^{III} species [2,2,2-$(CNBu^t)_3$-2,1-*closo*-$CoCB_{10}H_{11}$] (**82**).

Compound **79** reacts with $O(CH_2)_4$ and NCMe in the presence of CF_3SO_3Me, like the iron complex **11** and the molybdenum and tungsten complexes **45** and **46**, to give zwitterionic compounds [2-NO-2-PEt_3-7-L-*closo*-2,1-$CoCB_{10}H_{10}$] [L = $O(CH_2)_4$ (**83**), NCMe (**84**)].[21] Interestingly, the acetonitrile reaction gave in addition to **84** small amounts of the imine complex [7-{N(Me) = C(H)Me}-2-NO-2-PEt_3-*closo*-2,1-$CoCB_{10}H_{10}$] (**85**), a product related to the iron and nickel compounds **34** and **78**, respectively. The latter pair were the only products when **11** and **75**, respectively, were

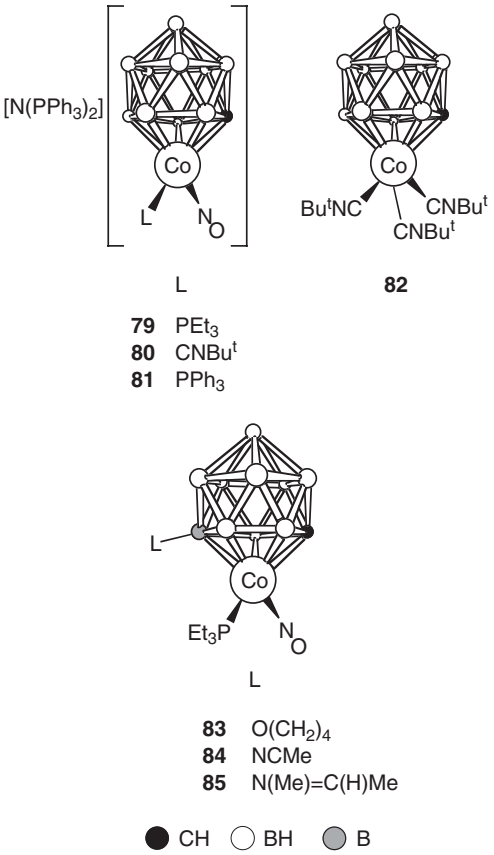

CHART 15.

treated with NCMe in the presence of CF_3SO_3Me. It was thought that in the reaction with the iron and nickel compounds the acetonitrile was preferentially methylated to give $[MeC{\equiv}NMe]^+$, and that this species then reacts with hydridic hydride from a cage $B–H^{\delta-}$ to yield the $B–N(Me){=}C(H)Me$ group. That the same reaction with the cobalt complex **74** proceeds to give only small amounts of **85**, with **84** as the major product, is probably due to the β-$B–H^{\delta-}$ group in the Co^I compound having enhanced hydridic character due to the presence of the PEt_3 ligand contributing electron density to the cage system. Hence, the electrophile Me^+ preferentially reacts with the β-B–H group, rather than the nitrogen of the :NCMe reagent.

2. Protonation and Related Reactions of Platinum Complexes

It is apparent from the reactions described above that in the anionic monocarbollide metal carbonyls the negative charge is delocalized over the icosahedral framework and not localized on the metal center. Thus protonation of **11** in THF

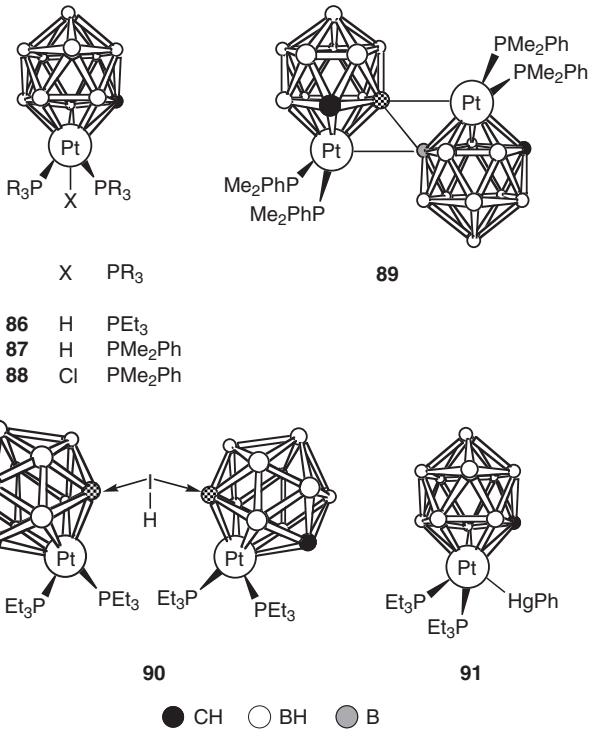

Chart 16.

affords the zwitterionic complex **30** rather than an Fe^{IV} hydrido complex [2,2,2-$(CO)_3$-2-H-*closo*-2,1-$FeCB_{10}H_{11}$]. Several attempts to protonate the rhenium complex **14** were also unsuccessful, and ZINDO (Zerner's Intermediate Neglect of Differential Overlap) and EHMO (Extended Hückel Molecular Orbital) calculations indicated that the negative charge in the rhenium dianion was very diffuse and highly delocalized about the *closo*-icosahedral framework.[16] The net result is that the exo-polyhedral cage B–H units have enhanced hydridic character and thus have a propensity to be removed on treatment with electrophiles such as H^+, Me^+, Ph_3C^+, or NO^+.

The platinum complex **15** is an exception to the behavior of the anionic mononuclear monocarbollide complexes **11**–**14**, **45**, **46**, **74**, **75**, and **79**, in that on protonation with $H[BF_4] \cdot OEt_2$ in THF it forms a neutral stable hydrido compound [2,2-$(PEt_3)_2$-2-H-*closo*-2,1-$PtCB_{10}H_{11}$] (**86**) (Chart 16) rather than a zwitterionic species [7-$O(CH_2)_4$-2,2-$(PEt_3)_2$-*closo*-2,1-$PtCB_{10}H_{10}$].[17] Probably in **15** the nucleophilicity of the metal center is sufficiently enhanced by the two strongly donating PEt_3 groups ligating the platinum that the proton attacks the metal rather than a hydride of a B_β–$H^{\delta-}$ group in the metal coordinating $\overline{CBBBB}$ ring system. However, the products obtained by protonating **15** and similar platinum complexes depend on the acid used and the nature of the phosphine ligands.

Protonation of compound **16** with HCl in Et_2O afforded three products. The anticipated hydrido species [2,2-$(PMe_2Ph)_2$-2-H-*closo*-2,1-$PtCB_{10}H_{11}$] (**87**) was formed in about 15% yield, along with the chloride complex [2,2-$(PMe_2Ph)_2$-2-Cl-*closo*-2,1-$PtCB_{10}H_{11}$] (**88**) in yields of about 10%.[18] Formation of the latter is understandable because it is a characteristic of transition metal hydrides such as **87** to react with Cl^- to give chloro complexes. The reaction product formed in highest yield (ca. 20%), however, was the diplatinum species **89**. An X-ray diffraction study showed the molecule to consist of two {*closo*-2,1-$PtCB_{10}$} cage frameworks, conjoined by a B–B connectivity [1.726(8) Å] and by two relatively long Pt–B connectivities [2.660(6) and 2.632(6) Å]. The B–B link is formed between a boron atom that is in a β site in the platinum-bound $\overline{CBBBB}$ ring of one sub-cluster and one in an α site in the other $\overline{CBBBB}$ ring. Each of these two boron atoms is also involved in a B–Pt linkage to the adjacent {$PtCB_{10}$} moiety. Thus the PtBPtB unit forms a 'butterfly' arrangement, with the platinum atoms at the wing-tips, similar to the four boron atoms which join together two {*nido*-7,8-$C_2B_9H_{11}$} cage systems in the 'macropolyhedral' carborane $C_4B_{18}H_{22}$.[26]

The pathway by which **89** is formed is not known but appears to involve oxidation of the anion in **16** followed by a combination of two {2,2-$(PMe_2Ph)_2$-*closo*-2,1-$PtCB_{10}H_{11}$} fragments with loss of molecular hydrogen. Interestingly, $C_4B_{18}H_{22}$ is also formed by loss of hydrogen upon oxidation of the anion [*nido*-7,8-$C_2B_9H_{12}]^-$.

The results obtained by protonating **16** with HCl in Et_2O prompted an investigation of products formed by treating **15** with the same acid. The reaction afforded a complex mixture among which was the hydrido complex **86** formed in only ca. 10–15% yield. The carborane anion [*nido*-7-$CB_{10}H_{13}]^-$ was detected by $^{11}B\{^1H\}$ NMR spectroscopy among the products and this led to the addition of $[NEt_4]I$ to the mixture in an attempt to obtain anions of any other carborane species present. This permitted the isolation of the very unusual green crystalline compound [7,7′-μ-{I(H)}-{2,2-$(PEt_3)_2$-*closo*-2,1-$PtCB_{10}H_{10}$}$_2$] (**90**). An X-ray diffraction study revealed that the molecule has two {2,2-$(PEt_3)_2$-*closo*-2,1-$PtCB_{10}H_{10}$} units bridged by an iodine atom. Although the H atom of the HI group was not unambiguously located, a weak residual peak was found in the final electron density map. Thus formally the compound results from replacement of a cage hydride in each of two anions of **15** by iodine. Moreover, in both halves of the molecule the boron atoms linked to the iodine are in a β site with respect to the carbons in the $\overline{CBBBB}$ rings ligating the metal atoms. There is precedent for a structure in which two carborane cages are joined by a halide bridge. Thus in the compound [9,9′-(μ-Br)-(*closo*-1,7-$C_2B_{10}H_{11})_2][BF_4]$, two {*closo*-1,7-$C_2B_{10}H_{11}$} cages are linked by a bridging Br ligand.[27] Moreover, the B–Br–B angle therein (111.7°) is remarkably similar to the B–I–B angle [112.1(3)°] in **90**. The attachment of the H atom to the iodine in the latter allows a satisfactory explanation for the valence electron count in **90** that would not be possible if it were absent. The HI group *via* its iodine atom can be regarded as formally donating an electron pair to each {*closo*-2,1-$PtCB_{10}H_{10}$} unit. In this manner, the icosahedral {$PtCB_{10}H_{10}I$} moieties each attain the necessary 13 skeletal electron pairs for a filled orbital description, it being noted that a {$Pt(PEt_3)_2$} group is isolobal with a BH vertex contributing two electrons for

cluster bonding, and an {I:→B} vertex would contribute three electrons behaving like a CH unit.

During the course of studies with compound **15** reactions with PhSeCl and PhTeI were investigated to determine if simple metathetical reactions would occur to give species [2,2-$(PEt_3)_2$-2-XPh-*closo*-2,1-$PtCB_{10}H_{11}$] (X = Se, Te). It had previously been shown that a mercury compound [2,2-$(PEt_3)_2$-2-HgPh-*closo*-2,1-$PtCB_{10}H_{11}$] (**91**) can be prepared by treating **15** with PhHgCl.[17] With the selenium and tellurium reagents in THF, however, complex mixtures of products were obtained *via* pathways not established.[19] From PhSeCl the compounds [2-PEt_3-2,*n*-$(SePh)_2$-*closo*-2,1-$PtCB_{10}H_{10}$] [*n* = 3 (**92**) or 7 (**93**)] and [2-PEt_3-2-SePh-3-{$O(CH_2)_4Cl$}-*closo*-2,1-$PtCB_{10}H_{10}$] (**94**) were characterized (Chart 17). From reactions described earlier in this chapter, it seems very likely that **94** results from nucleophilic attack of Cl^- on an intermediate having an $O(CH_2)_4$ molecule coordinated to a boron located in an α site in the metal-ligating $\overline{CBBBB}$ ring. With PhTeI, a product of formulation [2,2-$(PEt_3)_2$-7-{$Te(Ph)CH_2Cl$}-*closo*-2,1-$PtCB_{10}H_{10}$] (**95**) was obtained, along with the poly-tellurium species **96**. The {CH_2Cl} moiety in **95** was presumably derived from dichloromethane used in workup procedures.

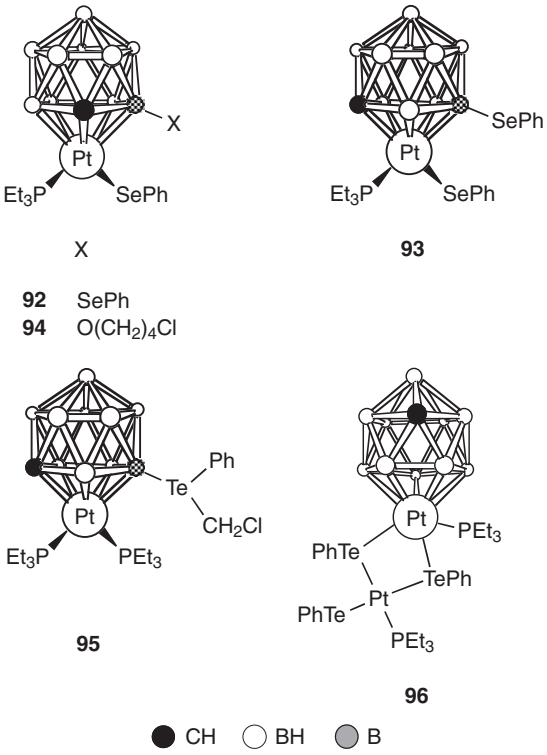

X

92 SePh
94 $O(CH_2)_4Cl$

93

95

96

Chart 17.

C. *Zwitterionic Bimetallic Compounds*[†]

Although the monocarbollide metal carbonyl complexes do not yield neutral hydrido compounds when they are protonated they do, in common with the platinum (**15**), cobalt (**81**) and nickel (**17**, **19**, **20**, **75**) monocarbollide compounds, often afford stable bimetal complexes on reaction with sources of the fragments $\{M(PPh_3)\}^+$ (M = Cu, Ag, Au) which are isolobal with the proton. Thus, the platinum compound **15** reacts with the reagents $[CuCl(PPh_3)]_4$ and $[AuCl(PPh_3)]$ to give [2,7,11-{Cu(PPh_3)}-7,11-(μ-H)$_2$-2,2-(PEt_3)$_2$-*closo*-2,1-$PtCB_{10}H_9$] (**97**) and [2-{Au(PPh_3)}-2,2-(PEt_3)$_2$-*closo*-2,1-$PtCB_{10}H_{11}$] (**98**), respectively (Chart 18).[17] The cobalt compound **81** also reacts with $[CuCl(PPh_3)]_4$ and $[AuCl(PPh_3)]$, in the presence of Tl[PF_6], to form [2,7,11-{Cu(PPh_3)}-7,11-(μ-H)$_2$-2-NO-2-PPh_3-*closo*-2,1-$CoB_{10}H_9$] (**99**) and [2-{Au(PPh_3)}-2-NO-2-PPh_3-*closo*-2,1-$CoCB_{10}H_{11}$] (**100**), and with Ag[BF_4] and PPh_3 to yield [2,7-{Ag(PPh_3)}-7-(μ-H)-2-NO-2-PPh_3-*closo*-2,1-$CoCB_{10}H_{10}$] (**101**).[21] It should be noted that in the copper and silver complexes the direct metal–metal bond is supported by agostic B–H⟶M (M = Cu or Ag) interactions whereas in the gold species it is believed that only a direct metal–metal bond is present.

Similarly to the platinum and cobalt systems, treatment of the nickel complexes **17b**, **19**, and **75** with $[CuCl(PPh_3)]_4$ and Tl[PF_6] affords the respective bimetallic species[28] [2,7,11-{Cu(PPh_3)}-7,11-(μ-H)$_2$-2-L-2-L′-*closo*-2,1-$NiCB_{10}H_9$] [L = L′ = $CNBu^t$ (**102**); L = L′ = CNXyl (**103**); L = CO, L′ = PPh_3 (**104**)]. In addition, a species with L = $CNBu^t$ and L′ = PPh_3 (**105**) was surprisingly formed along with **102**. With Ag[BF_4] and PPh_3, complex **75** gave [2,7-{Ag(PPh_3)}-7-(μ-H)-2-CO-2-PPh_3-*closo*-2,1-$NiCB_{10}H_{10}$] (**106**), directly analogous to **101**. However, when **75** was treated with Ag[BF_4] alone, the same Ni–Ag species **106** was also obtained in modest yields *via* PPh_3 scavenging, and was accompanied by small quantities of the full-sandwich species [Ag(PPh_3)$_3$][*commo*-2,2′-Ni-{*closo*-2,1-$NiCB_{10}H_{11}$}{7′-O(CH_2)$_4$-*closo*-2′,1′-$NiCB_{10}H_{10}$}] (**107**).[28] Formation of the latter may be rationalized in terms of a coming together of {*closo*-2,1-$NiCB_{10}$} and {*nido*-7-CB_{10}} fragments that are formed when PPh_3 is scavenged from the precursor. An Ag^+-promoted oxidative substitution[15b] of a boron-bound hydride by a THF molecule has also occurred during the reaction. Treatment of compounds **19** and **75** with [AuCl(PPh_3)] in the presence of Tl[PF_6] also gave bimetallic species [2,7-{Au(PPh_3)}-7-(μ-H)-2-L-2-L′-*closo*-2,1-$NiCB_{10}H_{10}$] [L = L′ = CNXyl (**108**); L = CO, L′ = PPh_3 (**109**)]. Of these, an X-ray diffraction study upon **108** showed the presence of an Ni–Au bond that was supplemented by a B–H⟶Au agostic-type interaction, so that the structure is similar to **106**, rather than **98**.

In contrast with the bimetallic nickel-monocarbollide derivatives **102**–**106**, **108**, and **109**, the $\{Cu(PPh_3)\}^+$ adduct [7,8,12-{Cu(PPh_3)}-7,8,12-(μ-H)$_3$-2,2-(cod)-*closo*-2,1-$NiCB_{10}H_8$] (**110**) formed from **20** lacks an Ni–Cu bond and the exo-polyhedral

[†]In structural formulae, metal–metal bonds are drawn for simplicity as a single line, but this need not imply a conventional single bond. This depiction is only used to indicate the presence of a connectivity between the two atoms, and does not necessarily denote a particular distribution of electrons in these zwitterionic compounds.

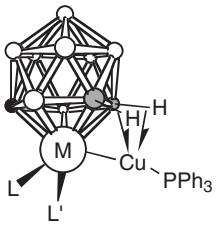

	M	L	L'
97	Pt	PEt_3	PEt_3
99	Co	PPh_3	NO
102	Ni	$CNBu^t$	$CNBu^t$
103	Ni	CNXyl	CNXyl
104	Ni	CO	PPh_3
105	Ni	$CNBu^t$	PPh_3

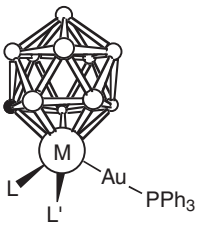

	M	L	L'
98	Pt	PEt_3	PEt_3
100	Co	PPh_3	NO

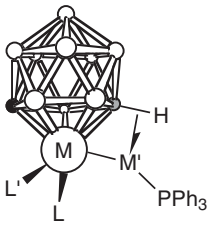

	M	M'	L	L'
101	Co	Ag	NO	PPh_3
106	Ni	Ag	CO	PPh_3
108	Ni	Au	CNXyl	CNXyl
109	Ni	Au	CO	PPh_3

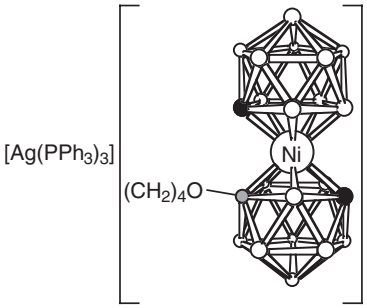

107

● CH ○ BH ● B

Chart 18.

metal fragment is supported only by three B–H→Cu interactions (Chart 19).[28] The reasons for this preference are not clear, but might be related to the differing donor properties of the nickel-bound ligands and the consequent effect on charge distribution within the cluster.

Several other species are also known where there are no metal–metal bonds and $\{M(PPh_3)\}^+$ (M = Cu or Ag) fragments are attached to the cage in an exo-polyhedral manner, namely [7,8,12-$\{Cu(PPh_3)\}$-7,8,12-(μ-H)$_3$-2,2,2-(CO)$_3$-*closo*-2,1-$FeCB_{10}H_8$] (**111**), [7,12-$\{Ag(PPh_3)\}$-7,12-(μ-H)$_2$-2,2,2-(CO)$_3$-*closo*-2,1-$FeCB_{10}H_9$] (**112**), [7,8,12-$\{Cu(PPh_3)\}$-7,8,12-(μ-H)$_3$-2,2,2-(CO)$_3$-2-PPh_3-*closo*-2,1-$MoCB_{10}H_8$] (**113**) and [7,12-$\{Ag(PPh_3)\}$-7,12-(μ-H)$_2$-2,2,2-(CO)$_3$-2-PPh_3-*closo*-2,1-$MoCB_{10}H_9$] (**114**).[29] These charge-compensated products are formed in reactions between **11** and **45**, respectively, with $\{M(PPh_3)\}^+$. It is noteworthy that the $\{Au(PPh_3)\}^+$ moiety does not bond with either **11** or **45** perhaps because it is less electrophilic

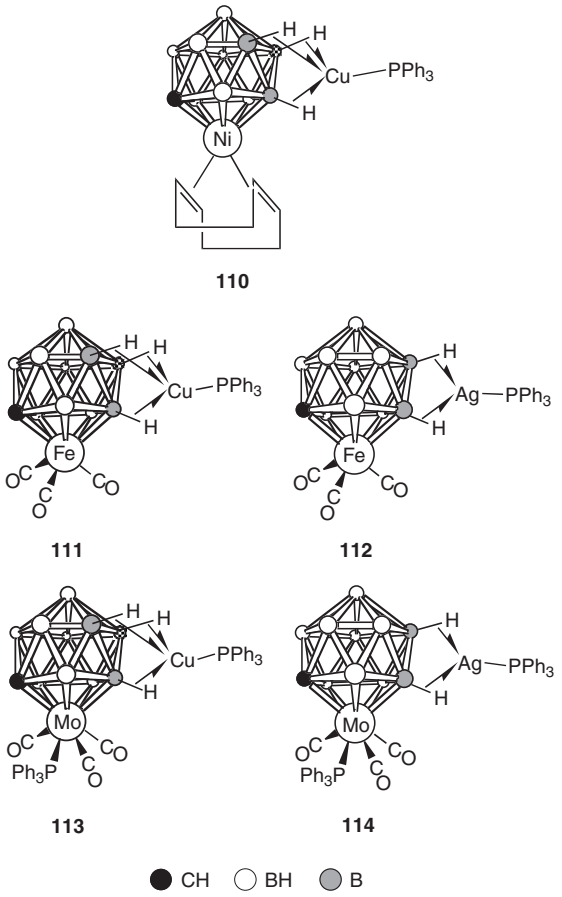

CHART 19.

than the copper and silver fragments and is not stabilized by a single B–H→Au bond. Moreover, the negative charges associated with the anions of **11** and **45** are evidently insufficiently metal centered for direct Fe–Au and Mo–Au bonds to be formed as occurs in the corresponding reactions with the reagents **15**, **19**, **75**, and **81**. An interesting feature of the complexes formed by $\{Cu(PPh_3)\}^+$ is the propensity for copper to use four valence orbitals in bonding so that there are three attachments to the cage system, as shown by the X-ray diffraction studies upon **97**, **99**, **104**, **110**, and **113**. The difference in geometries in bonding of the $\{M(PPh_3)\}^+$ (M = Cu or Au) group may be the consequence of the valence hybrid sp_z and the degenerate pair of p_x and p_y orbitals for copper being sufficiently close to make all three orbitals valence orbitals, whereas with gold the p_x and p_y orbitals are of much higher energy and therefore less accessible for bonding.[30]

The mode of attachment of the $\{M(PPh_3)\}^+$ fragments (M = Cu, Ag) to the cage via only B–H→M bonds is not limited to the complexes **110**–**114**, as evidenced by the structures of [12-{$Fe(CO)_2(\eta$-$C_5Me_5)$}-12-(μ-H)-2,2,2-$(CO)_3$-2-PPh_3-*closo*-2,1-$MoCB_{10}H_{10}$] (**115**) and [7,8,12-{$RuCl(PPh_3)_2$}-7,8,12-(μ-H)$_3$-2,2,2-$(CO)_3$-2-PPh_3-

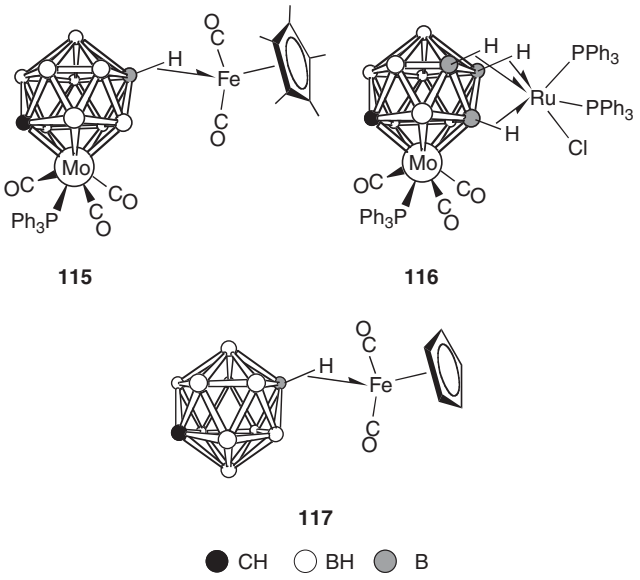

CHART 20.

closo-2,1-$MoCB_{10}H_8$] (**116**) in which the electrophilic metal–ligand groups are bonded to the cage frameworks *via* one and three agostic B–H→ML_n bonds, respectively (Chart 20).[29] The various bimetal compounds formed from **11** and **45** illustrate the ability of the mononuclear iron and molybdenum anions to function as mono-, bi-, or tri-dentate ligands to the transition metal–ligand fragments. It is noteworthy that in the adduct **115** formed with the iron moiety $\{Fe(CO)_2(\eta\text{-}C_5Me_5)\}^+$ the latter group is coordinated by a single agostic-type B–H→Fe bond involving a boron atom that is situated in the B_5 belt above the metal ligating $\overline{CBBBB}$ ring and which is antipodal to the cage carbon atom. There is a striking similarity between the structure of compound **115** and that of [12-$\{Fe(CO)_2(\eta\text{-}C_5H_5)\}$-12-(μ-H)-*closo*-1-$CB_{11}H_{11}$] (**117**). The latter complex was prepared as part of a study using carborane anions as weakly coordinating anions.[31] The $\{Mo(CO)_3(PPh_3)\}$ vertex in **115** is notionally replaced by the isolobal BH vertex in **117**.

It has been determined for the anion [*closo*-$CB_{11}H_{12}]^-$ that the B–H vertex antipodal to the cage carbon atom is the most electron-rich site, thus rationalizing the location of the *exo*-$\{Fe(CO)_2(\eta\text{-}C_5H_5)\}^+$ fragment in compound **117**. For metallacarboranes there is an accumulation of extra electron density at sites adjacent to the metal. Indeed, for dicarbollide complexes {3-L_n-1,2-R_2-*closo*-3,1,2-$MC_2B_9H_9$} (R = H or Me) activation of vertexes not in the coordinating $\overline{CCBBB}$ ring is quite rare. It might seem plausible that in **115**, with a bulky PPh_3 ligand and an $\{Fe(CO)_2(\eta\text{-}C_5Me_5)\}$ group in play, the $\overline{CBBBB}$ sites in the metallacarborane fragment are not as readily accessible. However, the species [*n*-$\{Fe(CO)_2(\eta\text{-}C_5Me_5)\}$-*n*-(μ-H)-3,3,3-$(CO)_3$-*closo*-3,1,2-$ReC_2B_9H_{10}$], derived from [3,3,3-$(CO)_3$-*closo*-3,1,2-$ReC_2B_9H_{11}]^-$ and $\{Fe(CO)_2(\eta\text{-}C_5Me_5)\}^+$, is formed as an equimolar mixture of two

isomers ($n = 4$ and 8), with the *exo* group attached to the α or β boron atoms in the coordinating $\overline{CCBBB}$ ring.[32] This suggests that steric effects are not dominant in **115** and that the antipodal B–H vertex is the most electronically favorable site for coordinating an *exo*-ML_n moiety.

The rhenium reagent **14** reacts with the complexes $[PtCl_2L_2]$ in the presence of $Tl[PF_6]$ to give the compounds [2,7-{PtL_2}-7-(μ-H)-2,2,2-$(CO)_3$-*closo*-2,1-$ReCB_{10}H_{10}$] [L = PPh_3 (**118**), PEt_3 (**119**); L_2 = dppe (**120**; dppe = $Ph_2PCH_2CH_2PPh_2$)] (Chart 21).[16] An X-ray diffraction study established that the B–H→Pt bond involves a BH group in a β position in the $\overline{CBBBB}$ ring pentahapto coordinated to the rhenium. There was no evidence for isomers in which there was a B_α–H→Pt bridge bond, in accord with the β-BH groups being the more hydridic in character than the α-BH groups in the $\overline{CBBBB}$ ring. An analogous palladium compound **121** has been prepared in a similar manner from $[PdCl_2(dppe)]$. This product displays dynamic behavior on the NMR time scale in accord with an exchange between the two equivalent B_β–H bonds in the $\overline{CBBBB}$ coordinating face which form the B–H→Pd linkage, thus generating a pseudo plane of symmetry within the molecule.

Compound **14** also reacts with the group 9 transition metal complexes $[M(NCMe)_3(\eta\text{-}C_5Me_5)][BF_4]_2$ to form the binuclear metal compounds [2,3,7-{$M(\eta\text{-}C_5Me_5)$}-3,7-(μ-H)$_2$-2,2,2-$(CO)_3$-*closo*-2,1-$ReCB_{10}H_9$] [M = Rh (**122**), Ir (**123**)].[33] An X-ray diffraction study revealed that in **122** the {$Rh(\eta\text{-}C_5Me_5)$}

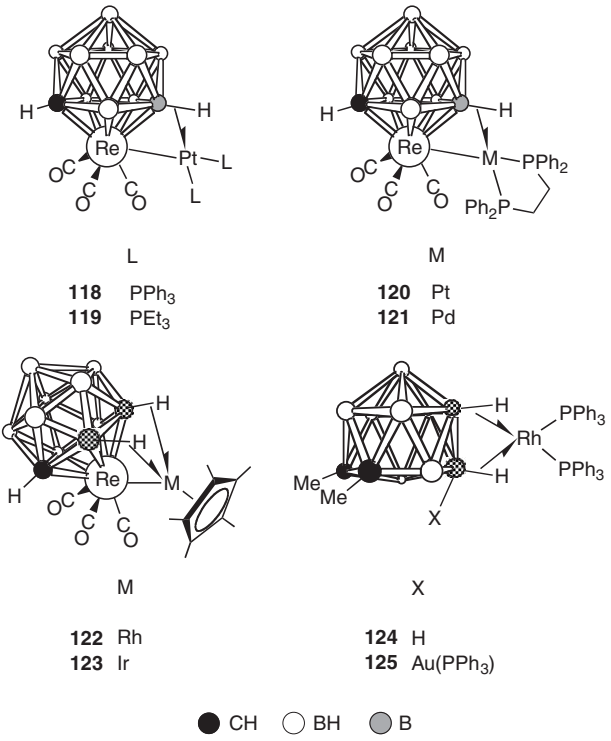

CHART 21.

fragment is attached to the {*closo*-2,1-$ReCB_{10}$} framework by an Re–Rh bond and two B–H→Rh linkages. The latter involve boron atoms in α and β sites with respect to the carbon atom of the $\overline{CBBBB}$ face of the cage ligating the rhenium atom. The complex is highly dynamic in solution with different processes in play. One involves heterolytic fission of the Re–Rh bond and migration of the {$Rh(\eta\text{-}C_5Me_5)$} fragment about the polyhedral {*closo*-2,1-$ReCB_{10}$} framework. This occurs *via* multiple exchanges of B–H bonds, employing a maximum of three B–H→Rh bonds and involving BH vertexes in both the Re-coordinating lower CB_4 and the upper B_5 pentagonal belts. A very similar dynamic exchange process, in which a {$Rh(PPh_3)_2$} fragment traverses the B–H vertexes in an exo-polyhedral manner, occurs for the complexes [*exo*-5,10-{$Rh(PPh_3)_2$}-5,10-$(\mu\text{-}H)_2$-*endo*-10-X-7,8-Me_2-*nido*-7,8-$C_2B_9H_7$] [X = H (**124**),[34] Au(PPh_3) (**125**)[35]] and [8,9-{$Rh(PPh_3)_2$}-8,9-$(\mu\text{-}H)_2$-3,3,3-$(CO)_3$-*closo*-3,1,2-$ReC_2B_9H_9$]. The latter forms by treating Cs[3,3,3-$(CO)_3$-*closo*-3,1,2-$ReC_2B_9H_{11}$] with [$RhCl(PPh_3)_3$], and indeed the dicarbollide anion [3,3,3-$(CO)_3$-*closo*-3,1,2-$ReC_2B_9H_{11}$]$^-$, like **14**, affords a range of zwitterionic complexes on treatment with electrophilic metal-ligand fragments.[32]

Compounds **122** and **123** react with phosphines PR_3 to give species in which one of the B–H→M interactions in the precursors (M = Rh, Ir) is replaced by an M–PR_3 bond. These species are often formed as mixtures of isomers, of which the structural types are exemplified by the complexes [2,3-*anti*-{$Rh(PMe_2Ph)(\eta\text{-}C_5Me_5)$}-3-$(\mu\text{-}H)$-2,2,2-$(CO)_3$-*closo*-2,1-$ReCB_{10}H_{10}$] (**126**) and [2,7-*syn*-{$Ir(PMe_2Ph)(\eta\text{-}C_5Me_5)$}-7-$(\mu\text{-}H)$-2,2,2-$(CO)_3$-*closo*-2,1-$ReCB_{10}H_{10}$] (**127**) which were characterized by X-ray diffraction (Chart 22).[33] The nature of the isomerism derives from whether the B–H→M bridge involves an α-BH (as in **126**) or a β-BH (as in **127**) in the rhenium-bonded $\overline{CBBBB}$ face, in combination with the relative disposition (*anti* or *syn*) of the phosphine with respect to this hydride. A more detailed discussion of this system is presented elsewhere.[33]

The formation of the bimetallic complexes **118**–**123** involves combination of dicationic transition metal fragments with the dianion of compound **14**. A further possibility exists, scarcely studied for 12-vertex {*closo*-2,1-$ReCB_{10}$} species but more extensively exploited in the analogous 11-vertex {*closo*-1,2-MCB_9} system (M = Mn, Re) discussed in Section IV. Treatment of the dianion of **14** with two

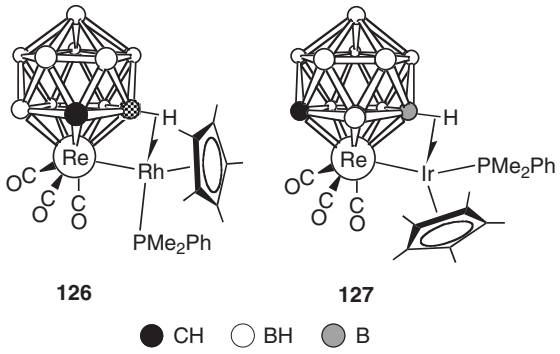

CHART 22.

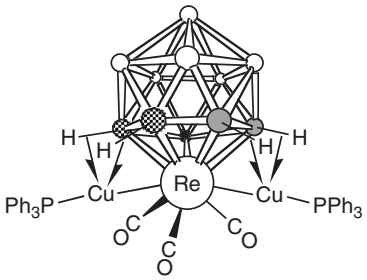

128

● CH ○ BH ● B

CHART 23.

equivalents of suitable monocationic fragments should give access to trimetallic species. Thus, **14** with $[CuCl(PPh_3)]_4$ and $Tl[PF_6]$ gave [2,3,7-{$Cu(PPh_3)$}-2,6,11-{$Cu(PPh_3)$}-3,6,7,11-(μ-H)$_4$-2,2,2-$(CO)_3$-*closo*-2,1-$ReCB_{10}H_7$] (**128**) (Chart 23).[36] An X-ray diffraction experiment upon **128** revealed a V-shaped Cu–Re–Cu unit [Cu–Re = 2.6500(11), 2.6658(12) Å; Cu–Re–Cu = 124.65(4)°], with each {$Cu(PPh_3)$} fragment attached *via* an Re–Cu bond and two B–H⇀Cu agostic-type linkages. Each pair of B–H⇀Cu interactions uses one α-B–H and one β-B–H in the Re-bound $\overline{CBBBB}$ face.

IV
MONOCARBOLLIDE–METAL COMPLEXES WITH NON-ICOSAHEDRAL CORE FRAMEWORKS

The material reviewed in this Chapter hitherto has focused on metallacarboranes in which the metal atom is a vertex in an icosahedral cage framework. Until recently, monocarbollide metal compounds with core structures other than 12 vertexes were very rare since suitable carborane precursors were not readily available.[4] However, Brellochs' recent development of the reaction of decaborane with aldehydes to give 10-vertex monocarboranes[37] permits a considerable expansion in this area of boron cluster chemistry. As a consequence, several intermediate-sized monocarboranes are now easily accessible and we have recently begun to exploit the opportunities that these present. In particular, we have focused thus far on complexes derived from the *C*-phenyl-substituted species [6-Ph-*nido*-6-CB_9H_{11}]$^-$.[38] It is clear from these initial studies that a wealth of new chemistry remains to be discovered in this area, not only from among the metal derivatives of {$PhCB_9$} carboranes such as those discussed in this section, but also in the metal complexes of other newly available carboranes.

A. *Chemistry of the 11-Vertex Dianions [1,1,1-(CO)$_3$-2-Ph-closo-1,2-MCB$_9$H$_9$]$^{2-}$ (M = Mn, Re)*

Treatment of [NEt$_4$][6-Ph-*nido*-6-CB$_9$H$_{11}$] in THF with Bu^{n}Li (2 equiv) followed by [Mn(NCMe)$_3$(CO)$_3$][PF$_6$] or [ReBr(THF)$_2$(CO)$_3$] gives the respective metallacarborane dianions, isolated as the mixed salts [NEt$_4$][N(PPh$_3$)$_2$][1,1,1-(CO)$_3$-2-Ph-*closo*-1,2-MCB$_9$H$_9$] [M = Mn (**129**),[39] Re (**130**)[40]], after addition of [N(PPh$_3$)$_2$]Cl (Chart 24). The actual existence during the synthesis of the trianion [6-Ph-*nido*-6-CB$_9$H$_9$]$^{3-}$ can only be inferred. X-ray diffraction studies of both salts confirmed that in their dianions the {M(CO)$_3$} group is η^6-coordinated by the $\overline{\text{CBBBBB}}$ face of the {6-Ph-*nido*-6-CB$_9$H$_9$} ligand, the metal vertex being closer to the two 'prow' atoms of the boat-shaped ligating face [Mn–C 2.125(7) and Mn–B 2.118(8) Å in **129**; Re–C 2.226(8) and Re–B 2.210(12) Å in **130**] than to the other four coordinating boron atoms [2.354(8)–2.424(9) Å in **129**; 2.477(11)–2.525(10) Å in **130**], a feature typical of such *closo*-11-vertex 1-metalla(hetero)boranes.[4,41]

The dianions of **129** and **130** show contrasting behavior upon treatment with oxidizing agents. Thus, complex **129** in CH$_2$Cl$_2$ with HgCl$_2$ gives [N(PPh$_3$)$_2$][1,1,1-(CO)$_3$-2-Ph-*closo*-1,2-MnCB$_9$H$_9$] (**131**) by a one-electron oxidation process.[39] Conversely, solutions of **130** in CH$_2$Cl$_2$ with HgCl$_2$ or I$_2$ give monoanionic complexes [N(PPh$_3$)$_2$][1,1-(CO)$_2$-1-X-2-Ph-*hypercloso*-1,2-ReCB$_9$H$_9$] [X = Cl (**132**), I (**133**)], respectively,[‡] that formally are products of two-electron oxidation reactions. The latter oxidations appear reversible, as treatment of **132** with Na[C$_{10}$H$_8$] (2 equiv) and CO at low temperatures regenerated the dianion of **130**.[42]

The anion of **131** is paramagnetic, formally Mn^{II}, and is surprisingly stable. A room temperature EPR (Electron Paramagnetic Resonance) study showed a six line pattern characteristic for a paramagnetic Mn^{II} complex with coupling to the ^{55}Mn nucleus, indicating significant localization of the unpaired electron onto the manganese. Additional coupling to the cage hydrogen and boron atoms observed at low temperature provided evidence that the radical center is also distributed over the whole cluster, a conclusion supported by DFT (Density Functional Theory) calculations. This delocalization is likely a contributor to the stability of **131**.

Unlike those in **130**, the CO groups in **132** and **133** are readily substituted by donor ligands and treatment with, for example, PEt$_3$ gave near-quantitative conversion to [N(PPh$_3$)$_2$][1-CO-1-PEt$_3$-1-X-2-Ph-*hypercloso*-1,2-ReCB$_9$H$_9$] [X = Cl (**134**), I (**135**)]. The rhenium-bound halide in these products may also be replaced upon reaction with donors L (1 equiv) in the presence of Tl[PF$_6$]. Thus, compound **134** with L = PEt$_3$ gave [1-CO-1,1-(PEt$_3$)$_2$-2-Ph-*hypercloso*-1,2-ReCB$_9$H$_9$] (**136**); while with L = CNBu^t it gave a mixture containing the species [1-L-1-L′-1-PEt$_3$-2-Ph-*hypercloso*-1,2-ReCB$_9$H$_9$] [L = CO, L′ = CNBu^t (**137**); L = L′ = CNBu^t (**138**)], along with small quantities of **136**, and with **138** being the major product.[42]

As with the icosahedral monocarbollide-metal species reviewed in the preceding sections, the boron-bound hydrides of **129** and **130** may be abstracted by Me$^+$ and

[‡]The descriptor *hypercloso* is used here for clusters whose shapes are closed triangulated polyhedra, but which have one less electron pair available for skeletal bonding than do conventional closo species, according to traditional electron counting methods.

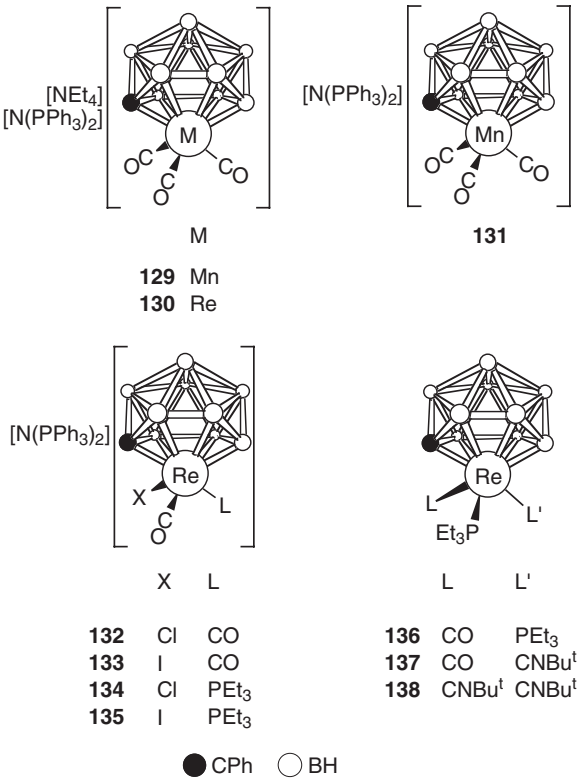

Chart 24.

replaced by donor ligands L.[42] Thus, treatment of **129** or **130** with CF_3SO_3Me in the presence of OEt_2 or NCMe gave, respectively, [6,7-L_2-1,1,1-$(CO)_3$-2-Ph-*closo*-1,2-MCB_9H_7] [M = Mn, L = OEt_2 (**139**); M = Mn, L = NCMe (**140**); M = Re, L = OEt_2 (**141**); M = Re, L = NCMe (**142**)] (Chart 25). The dianionic nature of the metallacarboranes in the precursors **129** and **130** allows for double hydride replacement to give neutral species, with both ligands L becoming bound to β boron atoms in the metal-bound $\overline{CBBBB}$ face. It is notable that in the formation of **140** and **142** boron-bound hydrides are replaced by NCMe molecules, similar to that in compound **84**, rather than imine moieties as was generally observed in other monoanionic icosahedral metallacarboranes such as **38** and **78**.

The neutral double zwitterions **139**–**142** are also susceptible to oxidation and treatment of **141** with I_2 (1 equiv) gave a surprising result.[42] In the product, [3,4-$(OEt)_2$-1,1,1-$(CO)_3$-2-Ph-*hypercloso*-1,2-$ReCB_8H_6$] (**143**), the rhenium center may be considered to be in the +III oxidation state, as in **132**–**138**, but the cluster in **143** has also lost one {BH} vertex. It is known[43] that oxidation of [6-Ph-*nido*-6-$CB_9H_{11}]^-$, the 10-vertex carborane parent of **129** and **130**, with $FeCl_3$ affords 9-vertex [4-Ph-*arachno*-4-CB_8H_{13}] and indeed the carborane subunit of **143** also has the {*arachno*-4-CB_8} geometry. In addition, two I^- ions would be liberated following the oxidation reaction and nucleophilic attack of these upon the positively

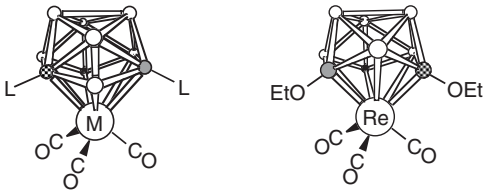

	M	L
139	Mn	OEt_2
140	Mn	NCMe
141	Re	OEt_2
142	Re	NCMe

143

● CPh ○ BH ● B

Chart 25.

charged B–OEt_2 moieties would remove one Et group from each – akin to the conversion of **52** to **62** – and yield the observed B–OEt substituents.

As does the dianion of **14**, the *closo*-11-vertex manganese- and rhenium-carborane dianions **129** and **130** react readily with cationic transition metal–ligand fragments, affording bimetallic products with novel structures in which the electrophilic metal–ligand groups $\{M'L_n\}$ are attached exo-polyhedrally to the $\{closo\text{-}1,2\text{-}MCB_9\}$ cage framework by rhenium–metal bonds supported by three-center two-electron B–H→M′ linkages.[40,44] Thus treatment of **129** or **130** with $[M'Cl_2(dppe)]$ (M′ = Ni, Pd or Pt), in the presence of $Tl[PF_6]$, gives the neutral complexes [1,3-{M′(dppe)}-3-μ-H-1,1,1-$(CO)_3$-2-Ph-*closo*-1,2-MCB_9H_8] [M = Mn, M′ = Ni (**144**); M = Mn, M′ = Pd (**145**); M = Mn, M′ = Pt (**146**); M = Re, M′ = Ni (**147**); M = Re, M′ = Pd (**148**); M = Re, M′ = Pt (**149**)] (Chart 26).[40,44] An X-ray diffraction study for **149** established that a {Pt(dppe)} fragment is located at a site exo-polyhedral to the rhenacarborane cluster, and is bonded *via* a Re–Pt linkage and a three-center two-electron B–H→Pt bond. The latter involves the boron at the γ-BH vertex in the six-membered ring ligating the rhenium.[40] In contrast, in the solid-state structure determined for **146** by X-ray diffraction there was no Mn–Pt bond present and the exo-polyhedral {Pt(dppe)} fragment was instead anchored only by two B–H→Pt linkages (structure **146a**).[44] In solution, however, it is thought that these species are fluxional between the two structural types observed crystallographically.

More remarkably, the reaction forming the Mn–Pt species is unique among the compounds **144**–**149** in that three other metallacarborane products were also isolated from this system alone. These are two 12-vertex species, [1-Ph-2,2,2-$(CO)_3$-7-X-8,8-dppe-*hypercloso*-8,2,1-$PtMnCB_9H_8$] [X = H (**150**), OEt (**151**)], and the complex [3,6,7-{$Mn(CO)_3$}-3,7-(μ-H)$_2$-1-Ph-6,6-dppe-*closo*-6,1-$PtCB_8H_6$] (**152**) formed by cluster contraction. Subsequent studies confirmed that the ethoxylated compound **151** is formed by reaction of **146** with adventitious EtOH present in the precursor **129**. Indeed, treatment of **146** with other alcohols ROH afforded similar species [1-Ph-2,2,2-$(CO)_3$-7-OR-8,8-dppe-*hypercloso*-8,2,1-$PtMnCB_9H_8$] [R = Me (**153**), $(CH_2)_2OH$ (**154**), $(CH_2)_4OH$ (**155**)] with, surprisingly, only mono-cage products observed when diols were used as substrates. All of the alkoxy-substituted compounds **151** and **153**–**155** are relatively stable and do not react further, whereas

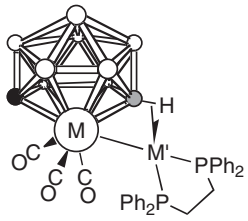

M M'

144 Mn Ni
145 Mn Pd
146 Mn Pt
147 Re Ni
148 Re Pd
149 Re Pt

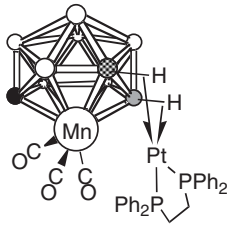

146a

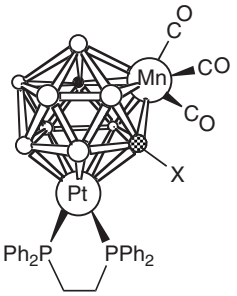

X

150 H
151 OEt
153 OMe
154 $O(CH_2)_2OH$
155 $O(CH_2)_4OH$

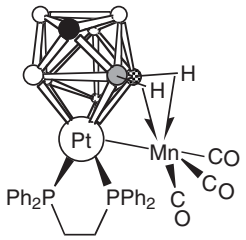

152

● CPh ○ BH ● B

Chart 26.

unsubstituted **150** appears to slowly decompose to form **152** *via* extrusion of the manganese vertex that becomes anchored in an exo-polyhedral site, and of a boron vertex, which is lost. The mechanisms by which all these transformations occur remain unclear.

Although stable and neutral bimetallic complexes were obtained from the dicationic fragments and **129** or **130** there was the possibility that reactions with two molar equivalents of a metal–ligand monocation should give rise to trimetallic species. However, reactions of **130** with sources of the cations $\{M'(CO)_3\}^+$ ($M' = Mn$, Re), namely $[Mn(NCMe)_3(CO)_3][PF_6]$ and $[ReBr(THF)_2(CO)_3]$, yielded as products $[N(PPh_3)_2][1,3,6\text{-}\{M'(CO)_3\}\text{-}3,6\text{-}(\mu\text{-}H)_2\text{-}1,1,1\text{-}(CO)_3\text{-}2\text{-Ph-}closo\text{-}1,2\text{-}ReCB_9H_7]$ [$M' = Mn$ (**156**), Re (**157**)], respectively (Chart 27).[40] In these molecules, the exo-polyhedral $\{M'(CO)_3\}$ moiety is almost certainly bonded to the cluster *via* two non-equivalent B–H⇀M′ interactions with an Re–M′ bond completing

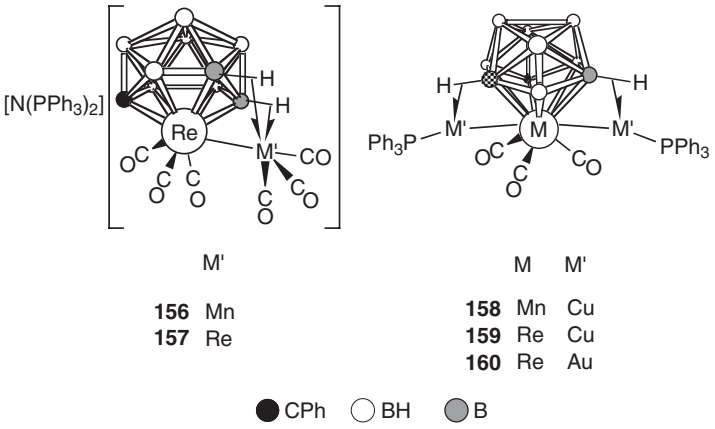

M'

156 Mn
157 Re

M M'

158 Mn Cu
159 Re Cu
160 Re Au

Chart 27.

the coordination sphere. Although an X-ray diffraction study was not possible to establish unambiguously the molecular structures, the ^{1}H NMR spectra revealed signals for the B–H⇀M′ groups, for **156** at δ –5.2 and –9.6, and for **157** at δ –3.5 and –7.9. The molecular asymmetry is evidenced by signals for nine non-equivalent boron atoms in each of the $^{11}B\{^{1}H\}$ NMR spectra and six separate resonances for the six CO ligands in their respective $^{13}C\{^{1}H\}$ NMR spectra.

Interestingly, treatment of **130** with an excess of the manganese and rhenium reagents did not afford neutral trimetallic species and only **156** and **157** were isolated.[40] Moreover, neither **156** or **157** reacted with the cations $\{M'(PPh_3)\}^+$ (M′ = Cu, Au). However, these same cations did react with **129** and **130**. When the two latter species are treated with 1 equivalent of an $\{M'(PPh_3)\}^+$ cation {from $[CuCl(PPh_3)]_4$ or $[AuCl(PPh_3)]$, respectively, in the presence of $Tl[PF_6]$}, the sole products isolated were the neutral trimetal compounds [1,6-$\{M'(PPh_3)\}$-1,7-$\{M'(PPh_3)\}$-6,7-$(\mu\text{-H})_2$-1,1,1-$(CO)_3$-2-Ph-*closo*-1,2-MCB_9H_7] [M = Mn, M′ = Cu (**158**); M = Re, M′ = Cu (**159**); M = Re, M′ = Au (**160**)], respectively. The corresponding $MnAu_2$ derivative has hitherto proved elusive. These products were obtained in higher yield when two equivalents of the copper or gold fragments were supplied. An X-ray diffraction study of **159** showed the molecule to consist of a central rhenacarborane moiety, with two $\{Cu(PPh_3)\}$ groups each attached to the cluster surface *via* an Re–Cu bond and a B–H⇀Cu interaction, the latter involving a β-boron atom in the rhenium-ligating $\overline{CBBBBB}$ face. Importantly, the two copper atoms are too far apart (~4 Å) to form a Cu–Cu bond so the trimetallic unit is V-shaped [Cu–Re–Cu = 93.89(2)°]. The structure of complex **159** resembles that of compound **128**, although in the latter species each Re–Cu bond is augmented by two B–H⇀Cu linkages. Moreover, the different geometric demands of the rhenacarborane in **128** force the Cu–Re–Cu angle to be some 30° larger than in **159**. Whereas the trimetal unit in **158**–**160** is not a closed triangle in the solid state, such an arrangement may occur in solution during the fluxional behavior observed in the NMR data for these complexes.[40]

In seeking further to add two different monocationic metal fragments to the dianion of **130** in a stepwise fashion, the latter was treated with [IrCl$(CO)_2(NH_2C_6H_4Me$-1,4)] and Tl[PF_6], in the hope of appending an $\{Ir(CO)_2\}^+$ fragment to the cluster. An anionic rhenium–iridium complex was indeed formed with its anion initially formulated[45] as an [*exo*-$\{Ir(CO)_3\}$-*endo*-$\{Re(CO)_2\}$-$\{CB_9H_9Ph\}]^-$ species on the basis of spectroscopic data and X-ray structural analysis of several derivatives. Subsequent studies, however, revealed the true identity of the product to be [$N(PPh_3)_2$][1,3,6-$\{Re(CO)_3\}$-3,6-$(\mu$-H$)_2$-1,1-$(CO)_2$-2-Ph-*closo*-1,2-$IrCB_9H_7$] (**161**) (Chart 28).[46,§] The original incorrect formulation arose from the difficulty of distinguishing between Re and Ir in X-ray diffraction studies of derivatives of **161**, and it was thought that one CO ligand had simply been transferred from the supposed endo-polyhedral Re vertex to the exo-polyhedral Ir center. No such ambiguity arises, however, when the two metal centers are from different rows of the Periodic Table. Thus, treatment of **130** with [Rh$(\mu$-Cl$)(CO)_2]_2$ and Tl[PF_6] afforded the Re–Rh analogue (**162**) of complex **161**, of which an X-ray diffraction analysis confirmed the anion to contain a rhodacarborane cluster with an exo-polyhedral rhenium fragment.[46] The Mn–Ir (**163**) and Mn–Rh (**164**) analogues were prepared similarly from **129**.

It is not clear how the anions of **161**–**164** are formed, although it seems reasonable that the $\{M'(CO)_2\}^+$ fragments (M′ = Rh, Ir) do initially become attached in exo-polyhedral sites prior to internal reorganization. In this connection the conversion of **146** to **152** might be relevant, as that process also involves assimilation of an $\{M'L_2\}$ fragment as a cluster vertex and extrusion of $\{Mn(CO)_3\}$, albeit with concomitant loss of a boron vertex. That the formation of **152** appears to proceed *via* a 12-vertex $\{PtMnCB_9\}$ intermediate might point to similar $\{MM'CB_9\}$ intermediates (M = Mn, Re; M′ = Rh, Ir) being involved in the pathway leading to **161**–**164**. All of compounds **161**–**164** are somewhat unstable in solution, and the manganese species particularly so. They undergo mutual CO scavenging to give, respectively, the complexes [$N(PPh_3)_2$][1,3-$\{M(CO)_4\}$-3-μ-H-1,1-$(CO)_2$-2-Ph-*closo*-1,2-M′CB_9H_8] [M = Re, M′ = Ir (**165**); M = Re, M′ = Rh (**166**); M = Mn, M′ = Ir (**167**); M = Mn, M′ = Rh (**168**)], with no other metallacarborane products formed.[46]

The single negative charge retained by **161**–**164** makes them attractive substrates to which a further different cationic metal fragment could be added. In the case of the manganese species **163** and **164**, their rather facile conversion to **167** and **168**, respectively, appeared to compromise their ability to accommodate a second exo-polyhedral moiety. However, this was not the case for the rhenium species **161** and **162** which, upon treatment with [$CuCl(PPh_3)]_4$ or [$AuCl(PPh_3)$] in the presence of Tl[PF_6], each unexpectedly give rise to two products.[45,46]

In the copper system, trimetallic Re–M′–Cu species [1,4,7-$\{Cu(PPh_3)\}$-1,5,6-$\{Re(CO)_3\}$-4,5,6,7-$(\mu$-H$)_4$-1,1-$(CO)_2$-2-Ph-*closo*-1,2-M′CB_9H_5] [M′ = Ir (**169**), Rh

[§]Note that in all of the compounds (**161**, **169**, **171**, **173**, **175**) reported in the initial communication in this area,[45] the endo-polyhedral iridium vertex was erroneously assigned as being rhenium whilst the exo-polyhedral $\{Re(CO)_3\}$ fragment in complexes **161**, **169**, and **175** was wrongly identified as $\{Ir(CO)_3\}$. The assignments herein are correct.

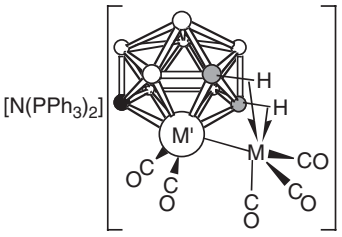

M M'

161 Re Ir
162 Re Rh
163 Mn Ir
164 Mn Rh

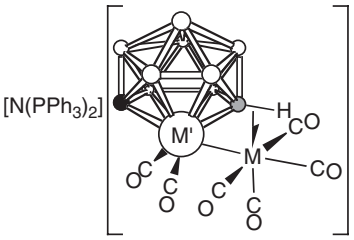

M M'

165 Re Ir
166 Re Rh
167 Mn Ir
168 Mn Rh

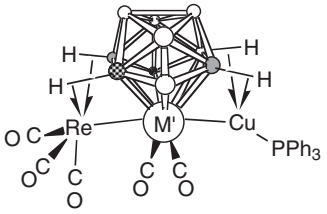

M'

169 Ir
170 Rh

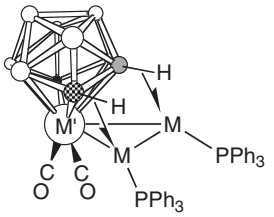

M M'

171 Cu Ir
172 Cu Rh
173 Au Ir
174 Au Rh

CHART 28.

(**170**)] were indeed obtained, as anticipated. The exo-polyhedral {$Cu(PPh_3)$} and {$Re(CO)_3$} units therein are bonded to the cluster surface by Cu–M′ and Re–M′ bonds, respectively, each of which is supplemented by two agostic-type interactions that employ α- and β-B–H units in the $\overline{CBBBBB}$ face ligating the cluster vertex M′. The major products in this system, however, were $M'Cu_2$ species [1,3-{$Cu(PPh_3)$}-1,6-{$Cu(PPh_3)$}(*Cu–Cu*)-3,6-(μ-H)$_2$-1,1-(CO)$_2$-2-Ph-*closo*-1,2-M′CB_9H_7] [M′ = Ir (**171**), Rh (**172**)]. These species merit comparison to the rhenium- and manganese-dicopper species **158** and **159**, which have molecular mirror symmetry and a V-shaped trimetal unit that lacks a Cu–Cu bond. Although **171** and **172** appear symmetric in solution on the NMR time scale due to fluxional processes, in the solid state the two copper centers are clearly inequivalent and a Cu–Cu bond is present. The metal triangle is supported by two B–H⇀Cu linkages, one to each Cu center, involving β- and γ-B–H vertexes in the M′-bound $\overline{CBBBBB}$ belt.

With a source of $\{Au(PPh_3)\}^+$ the complexes **161** and **162** also give two products, but no Re–M′–Au analogues of compounds **169** and **170** were observed. The major

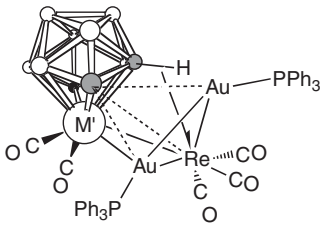

M'

175 Ir
176 Rh

CPh BH B

CHART 29.

products are the $M'Au_2$ derivatives [1,3-{$Au(PPh_3)$}-1,6-{$Au(PPh_3)$}(*Au–Au*)-3,6-(μ-H)$_2$-1,1-$(CO)_2$-2-Ph-*closo*-1,2-$M'CB_9H_7$] [M′ = Ir (**173**), Rh (**174**)], analogous to **171** and **172** described above.

The second product type in the gold system, although isolated in lesser amounts, is of great interest. In these species, compounds **175** and **176**, {$Re(CO)_3$} and {$Au(PPh_3)$} moieties are bonded to the cluster {$M'(CO)_2$} vertex (M′ = Ir, Rh) and to each other (Chart 29). The Au–Re vector is bridged by a second {$Au(PPh_3)$} fragment, so that overall {$M'ReAu_2$} 'butterflies' have been assembled starting from the rhenacarborane **130**. The rhenium center further interacts with the carborane *via* an additional B–H→Re linkage and one boron vertex lacks a terminal hydrogen atom. It is notable that this naked boron vertex [B(3)] is in contact with all four metal centers, so that the M_4B core resembles that in transition-metal boride clusters. Despite this, this boron atom resonates at δ 37.9 in its $^{11}B\{^1H\}$ NMR spectrum, substantially to higher field than in genuine borides. The mechanism by which the butterfly species **175** and **176** are formed is not clear, although it may reasonably be speculated that they are formed from Re–M′–Au species akin to **169** and **170**.

B. *Chemistry of the 11-Vertex Trianions [1,3,6-{M(CO)$_3$}-3,6-(μ-H)$_2$-1,1,1-(CO)$_3$-2-Ph-closo-1,2-MCB$_9$H$_7$]$^{3-}$ (M = Mo, W)*

Treatment of [NEt_4][6-Ph-*nido*-6-CB_9H_{11}] in THF with Bu^nLi (2 equiv), followed by 2 equivalents of [$Mo(NCMe)_3(CO)_3$] or [$W(NCEt)_3(CO)_3$], and then [NEt_4]I gives the salts [NEt_4]$_3$[1,3,6-{$M(CO)_3$}-3,6-(μ-H)$_2$-1,1,1-$(CO)_3$-2-Ph-*closo*-1,2-MCB_9H_7] [M = Mo (**177**), W (**178**)] (Chart 30).[47] An X-ray diffraction study of the dimolybdenum species showed that in these trianions one {$M(CO)_3$} group is bonded exo-polyhedrally to a {*closo*-1,2-MCB_9} cage system by a dative M→M bond supported by two three-center two-electron B–H→M linkages. These two species can be compared with the rhenium–manganese and dirhenium species **156** and **157** discussed earlier.

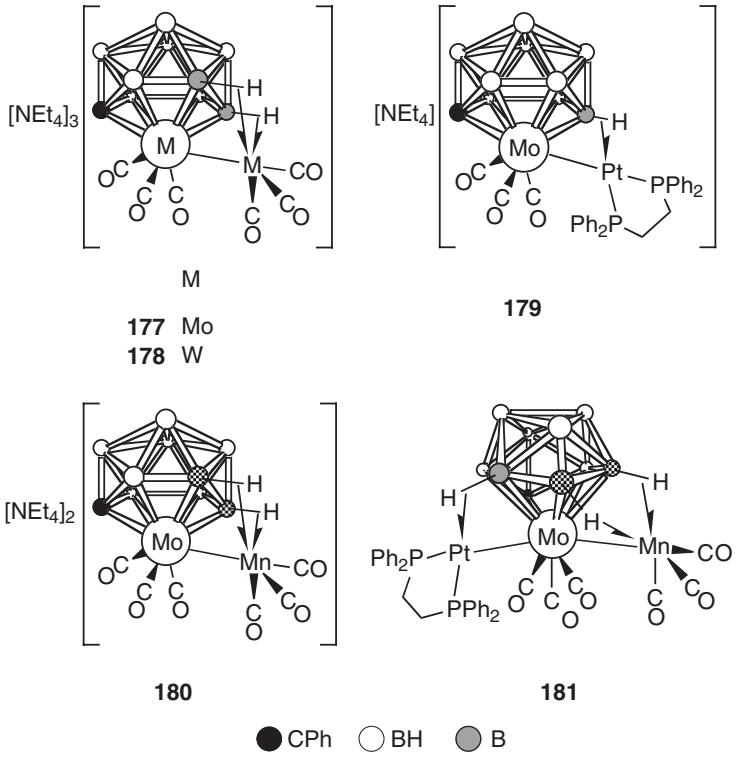

Chart 30.

Salts of the dimolybdenum trianion react[47a] readily with several cationic transition metal–ligand fragments with substitution of the exo-polyhedrally bonded $\{Mo(CO)_3\}$ group by a cationic fragment. Species prepared include $[NEt_4][1,3\text{-}\{Pt(dppe)\}\text{-}3\text{-}\mu\text{-}H\text{-}1,1,1\text{-}(CO)_3\text{-}2\text{-}Ph\text{-}closo\text{-}1,2\text{-}MoCB_9H_8]$ (**179**) by the reaction of **177** with $[PtCl_2(dppe)]$ and $Tl[PF_6]$, and $[NEt_4]_2[1,3,6\text{-}\{Mn(CO)_3\}\text{-}3,6\text{-}(\mu\text{-}H)_2\text{-}1,1,1\text{-}(CO)_3\text{-}2\text{-}Ph\text{-}closo\text{-}1,2\text{-}MoCB_9H_7]$ (**180**) by reaction with $[Mn(NCMe)_3(CO)_3][PF_6]$, respectively. Structural studies reveal the anion of **179** to be essentially isostructural with the corresponding $\{ReCB_9\}$ cluster **149**. The structure of complex **180** may also be compared with that of **177** and **178**, and with the $ReCB_9$ species **156** and **157**. However, unlike the two latter compounds, it was shown that a further metal fragment could be added to compound **180**. Thus, treatment with $[PtCl_2(dppe)]$ and $Tl[PF_6]$ gave a species that was characterized as $[1,3,7\text{-}\{Mn(CO)_3\}\text{-}1,6\text{-}\{Pt(dppe)\}\text{-}3,6,7\text{-}(\mu\text{-}H)_3\text{-}1,1,1\text{-}(CO)_3\text{-}2\text{-}Ph\text{-}closo\text{-}1,2\text{-}MoCB_9H_6]$ (**181**) by a preliminary X-ray diffraction study.

Compound **177** reacts with $H[BF_4]\cdot OEt_2$ (2 equiv) in the presence of CO and $[NEt_4]I$ with oxidation of the metal center and formation of an unusual cage expansion species, $[NEt_4][2,2,2\text{-}(CO)_3\text{-}2\text{-}I\text{-}1\text{-}Ph\text{-}8\text{-}OH\text{-}closo\text{-}2,1,8\text{-}MoC_2B_9H_9]$ (**182**) (Chart 31).[47b] With Ph_2S_2 as oxidizing agent, the dimolybdenum species $[N(PPh_3)_2][1\text{-}\{Mo(\mu\text{-}SPh)_2(CO)_4\}\text{-}2\text{-}Ph\text{-}hypercloso\text{-}1,2\text{-}MoCB_9H_9(Mo\text{–}Mo)]$ (**183**) was isolated following addition of $[N(PPh_3)_2]Cl$. Reaction of **177** with excess

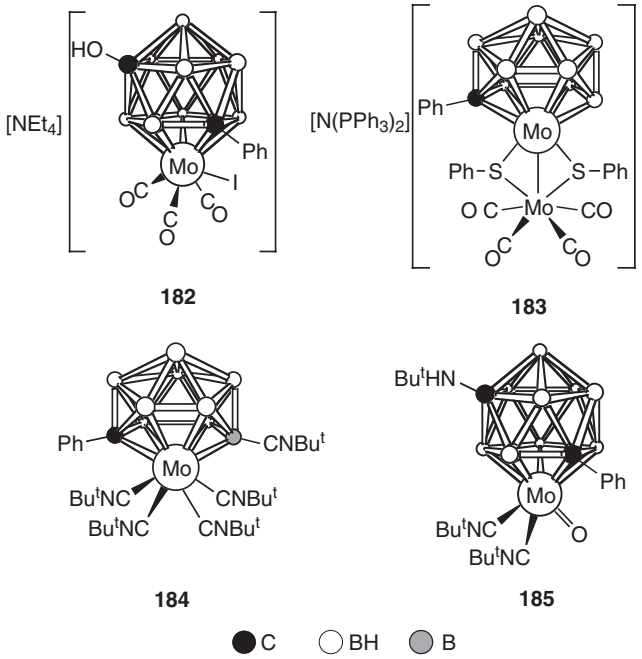

CHART 31.

$CNBu^t$ and $Ag[PF_6]$ (4 equiv) in MeCN gives the zwitterionic monomeric Mo^{II} complex [1,1,1,1,3-$(CNBu^t)_5$-2-Ph-*closo*-1,2-$MoCB_9H_8$] (**184**), along with another cage expansion product, [2,2-$(CNBu^t)_2$-2-(=O)-1-Ph-8-$NHBu^t$-*closo*-2,1,8-$MoC_2B_9H_9$] (**185**). It is notable that in both **182** and **185** the 'additional' {CX} vertex (X = OH, $NHBu^t$) has inserted at the same site with respect to the {CPh} vertex from the precursor **177** and, moreover, that this site is the same as that occupied by the platinum vertex in the 12-vertex cluster-expanded species **150**, **151** and **153**–**155** derived from **146**. These {CX} vertexes may formally be considered as being formed by cage-promoted hydroboration of CO and $CNBu^t$ groups.

ACKNOWLEDGEMENTS

The dedication and expertise of the coworkers cited in the references is gratefully acknowledged. We thank the Robert A. Welch Foundation for support of the research and Dr. Bruce E. Hodson for helpful comments during the preparation of this Chapter.

REFERENCES

(1) Hawthorne, M. F.; Young, D. C.; Wegner, P. A. *J. Am. Chem. Soc.* **1965**, *87*, 1818.
(2) Hawthorne, M. F.; Young, D. C.; Andrews, T. D.; Howe, D. V.; Pilling, R. L.; Pitts, A. D.; Reintjes, M.; Warren, L. F.; Wegner, P. A. *J. Am. Chem. Soc.* **1968**, *90*, 879.
(3) (a) Hyatt, D. E.; Little, J. L.; Moran, J. T.; Scholer, F. R.; Todd, L. J. *J. Am. Chem. Soc.* **1967**, *89*, 3342. (b) Knoth, W. H. *J. Am. Chem. Soc.* **1967**, *89*, 3342. (c) Knoth, W. H. *Inorg. Chem.* **1971**, *10*, 598. (d) Hyatt, D. E.; Scholer, F. R.; Todd, L. J.; Warner, J. L. *Inorg. Chem.* **1967**, *6*, 2229. (e) Knoth, W. H.; Little, J. L.; Todd, L. J. *Inorg. Synth.* **1968**, *11*, 41.

(4) (a) Grimes, R. N. (G. Wilkinson; E. W. Abel; F. G. A. Stone, Eds.), *Comprehensive Organometallic Chemistry*, **1982**, Vol. 1, Pergamon Press, Oxford, Section 5.5. (b) Grimes, R. N. (E. W. Abel; F. G. A. Stone; G. Wilkinson, Eds.), *Comprehensive Organometallic Chemistry II*, **1995**, Vol. 1, Pergamon Press, Oxford, (C. E. Housecroft, Ed.), Chapter 9. (c) Grimes, R. N. *Coord. Chem. Rev.* **2000**, *200–202*, 773.
(5) Saxena, A. K.; Hosmane, N. S. *Chem. Rev.* **1993**, *93*, 1081.
(6) (a) Wegner, P. A.; Guggenberger, L. J.; Muetterties, E. L. *J. Am. Chem. Soc.* **1970**, *92*, 3473. (b) Rietz, R. R.; Dustin, D. F.; Hawthorne, M. F. *Inorg. Chem.* **1974**, *13*, 1580. (c) Salentine, C. G.; Hawthorne, M. F. *J. Am. Chem. Soc.* **1975**, *97*, 6382. (d) Alcock, N. W.; Taylor, J. G.; Wallbridge, M. G. H. *J. Chem. Soc., Chem. Commun.* **1983**, 1168. (e) Stíbr, B.; Janousek, Z.; Base, K.; Plesek, J.; Solntsev, K. A.; Butman, L. A.; Kuznetsov, I. I.; Kuznetsov, N. T. *Collect. Czech. Chem. Commun.* **1984**, *49*, 1660. (f) Fontaine, X. L. R.; Greenwood, N. N.; Kennedy, J. D.; MacKinnon, P. I.; Macpherson, I. *J. Chem. Soc., Dalton Trans.* **1987**, 2385. (g) Alcock, N. W.; Jasztal, M. J.; Wallbridge, M. G. H. *J. Chem. Soc., Dalton Trans.* **1987**, 2793. (h) Fontaine, X. L. R.; Kennedy, J. D.; Thornton-Pett, M.; Nestor, K.; Stíbr, B.; Jelínek, T.; Base, K. *J. Chem. Soc., Dalton Trans.* **1990**, 2887. (i) Stíbr, B.; Jelínek, T.; Kennedy, J. D.; Fontaine, X. L. R.; Thornton-Pett, M. *J. Chem. Soc., Dalton Trans.* **1993**, 1261. (j) Jones, J. H.; Stíbr, B.; Kennedy, J. D.; Lawrence, A. D.; Thornton-Pett, M. *J. Chem. Soc., Dalton Trans.* **1993**, 1269. (k) Pisareva, I. V.; Chizhevsky, I. T.; Petrovskii, P. V.; Bregadze, V. I.; Dolgushin, F. M.; Yanovsky, A. I. *Organometallics* **1997**, *16*, 5598. (l) Pisareva, I. V.; Dolgushin, F. M.; Yanovsky, A. I.; Balagurova, E. V.; Petrovskii, P. V.; Chizhevsky, I. T. *Inorg. Chem.* **2001**, *40*, 5318. (m) Konoplev, V. E.; Pisareva, I. V.; Vorontsov, E. V.; Dolgushin, F. M.; Franken, A.; Kennedy, J. D.; Chizhevsky, I. T. *Inorg. Chem. Commun.* **2003**, *6*, 1454.
(7) (a) Carroll, W. E.; Green, M.; Stone, F. G. A.; Welch, A. J. *J. Chem. Soc., Dalton Trans.* **1975**, 2263. (b) Stone, F. G. A. *J. Organomet. Chem.* **1975**, *100*, 257.
(8) Jelliss, P. A.; Stone, F. G. A. *J. Organomet. Chem.* **1995**, *500*, 307.
(9) (a) Anderson, S.; Mullica, D. F.; Sappenfield, E. L.; Stone, F. G. A. *Organometallics* **1995**, *14*, 3516. (b) Anderson, S.; Mullica, D. F.; Sappenfield, E. L.; Stone, F. G. A. *Organometallics* **1996**, *15*, 1676. (c) Anderson, S.; Jeffery, J. C.; Liao, Y.-H.; Mullica, D. F.; Sappenfield, E. L.; Stone, F. G. A. *Organometallics* **1997**, *16*, 958. (d) Jeffery, J. C.; Jelliss, P. A.; Rudd, G. E. A.; Sakanishi, S.; Stone, F. G. A.; Whitehead, J. *J. Organomet. Chem.* **1999**, *582*, 90.
(10) McGrath, T. D.; Stone, F. G. A. *J. Organomet. Chem*. **2004**, *689*, 3891.
(11) Ellis, D. D.; Franken, A.; Stone, F. G. A. *Organometallics* **1999**, *18*, 2362.
(12) Ellis, D. D.; Franken, A.; McGrath, T. D.; Stone, F. G. A. *J. Organomet. Chem.* **2000**, *614–615*, 208.
(13) Liao, Y.-H.; Mullica, D. F.; Sappenfield, E. L.; Stone, F. G. A. *Organometallics* **1996**, *15*, 5103.
(14) Ellis, D. D.; Franken, A.; Jelliss, P. A.; Stone, F. G. A.; Yu, P.-Y. *Organometallics* **2000**, *19*, 1993.
(15) (a) Du, S.; Franken, A.; Jelliss, P. A.; Kautz, J. A.; Stone, F. G. A.; Yu, P.-Y. *J. Chem. Soc., Dalton Trans.* **2001**, 1846. (b) Du, S.; Kautz, J. A.; McGrath, T. D.; Stone, F. G. A. *J. Chem. Soc., Dalton Trans.* **2001**, 2791.
(16) Blandford, I.; Jeffery, J. C.; Jelliss, P. A.; Stone, F. G. A. *Organometallics* **1998**, *17*, 1402.
(17) Batten, S. A.; Jeffery, J. C.; Jones, P. L.; Mullica, D. F.; Rudd, M. D.; Sappenfield, E. L.; Stone, F. G. A.; Wolf, A. *Inorg. Chem.* **1997**, *36*, 2570.
(18) Blandford, I.; Jeffery, J. C.; Redfearn, H.; Rees, L. H.; Rudd, M. D.; Stone, F. G. A. *J. Chem. Soc., Dalton Trans.* **1998**, 1669.
(19) Batten, S. A.; Jeffery, J. C.; Rees, L. H.; Rudd, M. D.; Stone, F. G. A. *J. Chem. Soc., Dalton Trans.* **1998**, 2839.
(20) Franken, A.; Kautz, J. A.; McGrath, T. D.; Stone, F. G. A. Unpublished results.
(21) Kautz, J. A.; McGrath, T. D.; Stone, F. G. A. *Polyhedron* **2003**, *22*, 109.
(22) (a) Jeffery, J. C.; Stone, F. G. A.; Topaloglu, I. *J. Organomet. Chem.* **1993**, *451*, 205. (b) Dossett, S. J.; Li, S.; Stone, F. G. A. *Polyhedron* **1994**, *13*, 1773. (c) Ellis, D. D.; Jelliss, P. A.; Stone, F. G. A. *Chem. Commun.* **1999**, 2385. (d) Bitterwolf, T. E.; Scallorn, W. B.; Weiss, C. A.; Jelliss, P. A. *Organometallics* **2002**, *21*, 1856. (e) Hata, M.; Kautz, J. A.; Lu, X. L.; McGrath, T. D.; Stone, F. G. A. *Organometallics* **2004**, *23*, 3590.
(23) Franken, A.; Du, S.; Jelliss, P. A.; Kautz, J. A.; Stone, F. G. A. *Organometallics* **2001**, *20*, 1597.
(24) Ellis, D. D.; Franken, A.; Stone, F. G. A. Unpublished results.

(25) Kautz, J. A.; Stone, F. G. A.; Yu, P.-Y. Unpublished results.
(26) Janousek, Z.; Stíbr, B.; Fontaine, X. L. R.; Kennedy, J. D.; Thornton-Pett, M. *J. Chem. Soc., Dalton Trans.* **1996**, 3813.
(27) Yanovskii, A. I.; Struchkov, Yu. T.; Grushin, V. V.; Tolstaya, T. P.; Demkina, I. I. *Zh. Strukt. Khim.* **1988**, *29*, 89.
(28) Kautz, J. A.; McGrath, T. D.; Stone, F. G. A. Unpublished results.
(29) Ellis, D. D.; Franken, A.; Jelliss, P. A.; Kautz, J. A.; Stone, F. G. A.; Yu, P.-Y. *J. Chem. Soc., Dalton Trans.* **2000**, 2509.
(30) Hamilton, E. J. M.; Welch, A. J. *Polyhedron* **1990**, *9*, 2407.
(31) Liston, D. J.; Lee, Y. J.; Scheidt, W. R.; Reed, C. A. *Inorg. Chem.* **1987**, *26*, 2739.
(32) Ellis, D. D.; Jelliss, P. A.; Stone, F. G. A. *Organometallics* **1999**, *18*, 4982.
(33) Jeffery, J. C.; Jelliss, P. A.; Rees, L. H.; Stone, F. G. A. *Organometallics* **1998**, *17*, 2258.
(34) Long, J. A.; Marder, T. B.; Behnken, P. E.; Hawthorne, M. F. *J. Am. Chem. Soc.* **1984**, *106*, 2979.
(35) Jeffery, J. C.; Jelliss, P. A.; Stone, F. G. A. *J. Chem. Soc., Dalton Trans.* **1993**, 1073.
(36) Hodson, B. E.; Kautz, J. A.; McGrath, T. D.; Stone, F. G. A. Unpublished work.
(37) Brellochs, B. (M. G. Davidson, A. K. Hughes, T. B. Marder, K. Wade, Eds.), *Contemporary Boron Chemistry*, Royal Society of Chemistry, Cambridge, UK, **2000**, pp. 212–214.
(38) (a) Jelínek, T.; Kilner, C. A.; Thornton-Pett, M.; Kennedy, J. D. *Chem. Commun.* **2001**, 1790. (b) Jelínek, T.; Thornton-Pett, M.; Kennedy, J. D. *Collect. Czech. Chem. Commun.* **2002**, *67*, 1035.
(39) Du, S.; Farley, R. D.; Harvey, J. N.; Jeffery, J. C.; Kautz, J. A.; Maher, J. P.; McGrath, T. D.; Murphy, D. M.; Riis-Johannessen, T.; Stone, F. G. A. *Chem. Commun.* **2003**, 1846.
(40) Du, S.; Kautz, J. A.; McGrath, T. D.; Stone, F. G. A. *Organometallics* **2003**, *22*, 2842.
(41) (a) Kennedy, J. D. *Prog. Inorg. Chem.* **1986**, *34*, 211. (b) Barton, L.; Srivastava, D. K. (E. W. Abel; F. G. A. Stone; G. Wilkinson, Eds.), *Comprehensive Organometallic Chemistry II*, **1995**, Vol. 1, Pergamon Press, Oxford, UK, (C. E. Housecroft, Ed.), Chapter 8.
(42) Du, S.; Kautz, J. A.; McGrath, T. D.; Stone, F. G. A. Unpublished work.
(43) Franken, A.; Kilner, C. A.; Thornton-Pett, M.; Kennedy, J. D. *Collect. Czech. Chem. Commun.* **2002**, *67*, 869.
(44) Du, S.; Jeffery, J. C.; Kautz, J. A.; Lu, X. L.; McGrath, T. D.; Miller T.A.; Riis-Johannessen, T.; Stone, F. G. A. *Inorg. Chem.* **2005**, *44*, 2815.
(45) Du, S.; Kautz, J. A.; McGrath, T. D.; Stone, F. G. A. *Angew. Chem. Int. Ed.* **2003**, *42*, 5728.
(46) Du, S.; Hodson, B. E.; Kautz, J. A.; Lu, X. L.; McGrath, T. D.; Stone, F. G. A. Unpublished work.
(47) (a) Lei, P.; McGrath, T. D.; Stone, F. G. A. *Chem. Commun.* **2005**, 3706. (b) Lei, P.; McGrath, T.D.; Stone, F.G.A. unpublished work.

Synthesis of Novel Silicon-Containing Compounds via Lewis Acid-Catalyzed Reactions

IL NAM JUNG* and BOK RYUL YOO

Organosilicon Chemistry Laboratory, Korea Institute of Science and Technology, P.O. Box 131, Cheongryang, Seoul 130-650, Korea

I. Introduction . . . 41
II. Allylsilylation Reactions with Allyltriorganosilanes . . . 42
A. Allylsilylation of Alkenes . . . 42
B. Allylsilylation of Alkynes . . . 48
III. Intramolecular Alkenyl-Migration Reaction of Alkenylchlorosilanes . . . 49
IV. Friedel–Crafts Alkylation Reaction with Organosilicon Compounds . . . 50
A. Alkylation with Allylchlorosilanes . . . 50
B. Alkylation with Vinylchlorosilanes . . . 53
C. Alkylation with (ω-Chloroalkyl)chlorosilanes . . . 55
D. Alkylation with (Polychloroalkyl)chlorosilanes . . . 56
V. Hydrosilylation Reaction with Triorganosilanes . . . 57
Acknowledgments . . . 58
References . . . 58

I
INTRODUCTION

This review will describe Lewis acid-catalyzed reactions such as allylsilylation, intramolecular allyl-migration, Friedel–Crafts alkylation, and hydrosilylation reactions commonly used in organosilicon chemistry. The carbenium and silylenium ion intermediates are generated by the interactions of organosilicon compounds such as allyltriorganosilanes,[1a,2] alkenylchlorosilanes,[1b,3] (chloroalkyl)silanes,[1b,4] and triorganohydrosilanes[5] with Lewis acid catalysts, which then react with simple unsaturated electrophilic organic compounds.[1] The isolation and properties of silylenium ions is discussed by Müller in this volume (p. 155). This review will particularly focus on the Lewis acid-catalyzed reactions with unsaturated hydrocarbon compounds. It is well recognized that the reactivity of such electrophiles varies depending upon the electronic nature of substituents and the cation position in the organosilicon compounds.[1b,3,4]

It is useful to compare the reactivity and reaction patterns of various cationic organosilicon species in the Lewis acid-catalyzed reactions with those of their organic analogs. Positive charges on the carbon β to silicon are stabilized by the electron-donating silyl group through σ–π conjugation, commonly known as β-stabilization.[6–8] The reactivity and reaction modes of allylsilanes are different from one another, depending on the number (n) of chlorine substituent on the silicon atom of allylchlorosilanes ($CH_2{=}CHCH_2SiMe_{3-n}Cl_n$). Allylsilanes containing two

*Corresponding author. Tel.: +82-31-498-4304; fax: +82-31-498-4305.
E-mail: injung@jsisilicone.com (I.N. Jung).

ADVANCES IN ORGANOMETALLIC CHEMISTRY
VOLUME 53 ISSN 0065-3055/DOI 10.1016/S0065-3055(05)53002-8

or more chlorine substituents on silicon react readily with aromatic compounds to give alkylation products, 2-aryl-1-silylpropanes [Eq. (1)].[3] However, allyltrimethylsilane, having three methyl groups on the silicon (**1a**), in benzene solvent is dimerized to give the allylsilylation product 5-(trimethylsilyl)-4-(trimethylsilylmethyl)-1-pentene without any alkylation products [Eq. (2)].[2]

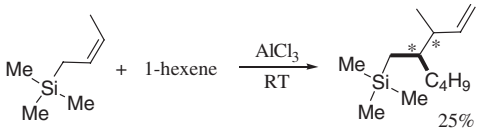

(1)

(2)

In aluminum chloride-catalyzed reactions, a small amount of hydrogen chloride, resulting from the reaction of anhydrous aluminum chloride with moisture inevitably present in the reactants, initiates the reaction.[9] The proton from the hydrogen chloride interacts with the π-bond of allylsilanes to give a carbenium ion on the carbon β to silicon, because the secondary silylpropyl cation can be stabilized by the electron-donating silyl group through β-stabilization as described above.[1b,3] The stabilization effects can be more significant for allyltrimethylsilane than for allylchlorosilanes because of the electron-donating effects from the methyl groups on silicon.[1b,2] This facilitates the protodesilylation[1a,2,10] of allyltrimethylsilane by hydrogen chloride in the presence of aluminum chloride, which gives propene and a Me_3SiCl–$AlCl_3$ complex. Me_3SiCl has been reported to be an excellent promoter of allylsilylation reactions.[1a,11–13] In contrast, the collapse of the β-silyl cation intermediates of allylchlorosilanes is largely retarded, primarily due to less effective σ–π conjugation brought on by the presence of the electronegative chlorine atom(s) on silicon.[1b,3] The cation intermediates undergo alkylation reactions with electron-rich aromatic systems faster than protodesilylation.[1b,3]

II
ALLYLSILYLATION REACTIONS WITH ALLYLTRIORGANOSILANES

A. *Allylsilylation of Alkenes*

Allylsilylation is an addition reaction of allylorganosilanes to carbon–carbon multiple bonds of unsaturated hydrocarbons in the presence of Lewis acids.[1a] Common examples of unsaturated hydrocarbons for allylsilylations include alkenes,[2] cycloalkenes,[1a,2] allyltriorganosilanes,[1a,2,11–13] 5-(trimethylsilyl)-1-pentenes,[13] diallylsilanes,[12,16] conjugated dienes,[13] and alkynes.[19–21]

1. Allylsilylation of Linear Alkenes

The addition reaction of allyltriorganosilanes to 1-alkenes in the presence of anhydrous aluminum chloride as catalyst at room temperature gives regiospecific allylsilylated products, in which the silyl group adds to the terminal carbon and the allyl group adds to the inner carbon of the double bond [Eq. (3)].[2] Compared with the starting alkenes, the products of the allylsilylation reaction possess two additional carbon atoms in addition to a (triorganosilyl)methyl branch at the carbon β to the double bond.

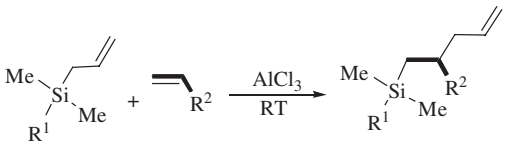

R^1=Me, R^2=CH_3 (61%)
R^1=Me, R^2=C_4H_9 (78%)
R^1=Me, R^2=C_6H_{13} (60%)
R^1=Ph, R^2=C_4H_9 (42%)
R^1=CH_2Ph, R^2=C_4H_9 (47%) (3)

The stereohomogeneous (*Z*)-crotyltrimethylsilane reacts with 1-hexene to give 3-methyl-4-(trimethylsilyl)methyl-1-octene as a mixture of two diastereomers in 25% yield [Eq. (4)].[2] The diastereomeric products possess a methyl group at the carbon α to the double bond, indicating that an allylic inversion occurs during the allylsilylation.[13,17]

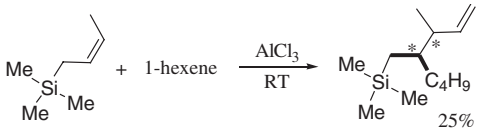

(4)

2. Allylsilylation of 4-(Trimethylsilylmethyl)-1-Alkenes

As described above, the allylsilylation of terminal alkenes with **1a** affords 4-(silylmethyl)-1-alkenes. Since these products possess a vinyl group at the terminal position, they can be allylsilylated again with **1a**. Additional reaction in the presence of anhydrous aluminum chloride and trimethylchlorosilane activator[11,12] in organic solvents or neat at ~40 °C gives the double allylsilylation products, 2-alkyl-8,8-dimethyl-4-(trimethylsilylmethyl)-8-silanon-1-enes[13] as the major products. These products are unusual and different from the previously reported normal allylsilylation products,[2,11,12] because they have a double bond on the carbon with the R^2 group but not on the carbon with R^1 [Eq. (5)]. These results suggest that isomerization of the normal allylsilylation products to the unusual products occurs through a 1,5-hydride shift. Polymeric materials are also obtained due to additional allylsilylations.

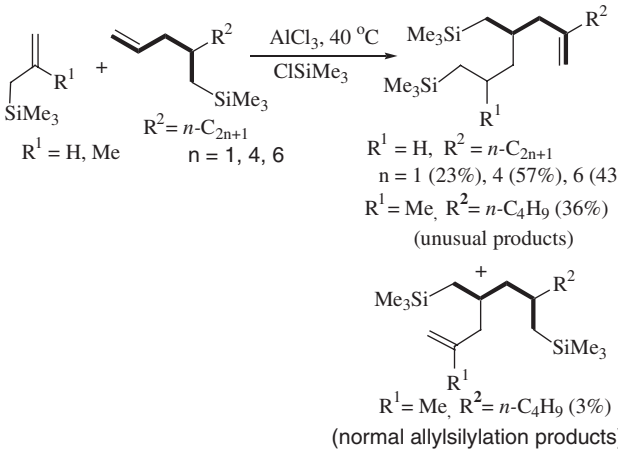

(5)

3. Allylsilylation of Cycloalkenes

Allyltrimethylsilane (**1a**) reacts with cycloalkenes such as cyclohexene and cyclopentene at room temperature to give stereospecifically *trans*-1-trimethylsilyl-2-allylcycloalkanes.[1a,2] These products are formed through *trans* addition and an allylic inversion.

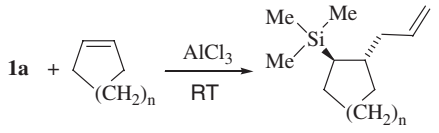

(6)

On the basis of the above results, a possible mechanism for the allylsilylation of cyclohexene with **1a** has been proposed as illustrated in Scheme 1. A silyl cation or a complex intermediate **I** is directly formed at the beginning stages of the reaction

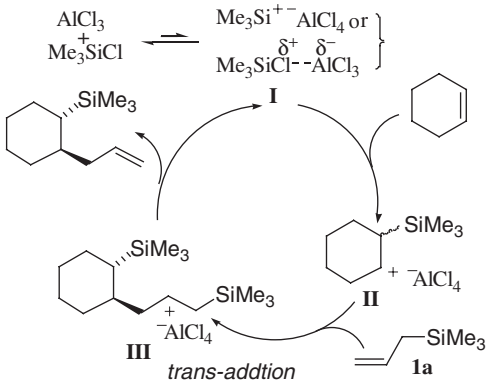

Scheme 1. Catalytic cycle of allylsilylation.

from aluminum chloride and trimethylchlorosilane,[1a,2,11–13] or from the protodesilylation of **1a** by acids resulting from the reaction of anhydrous aluminum chloride with adventitious water in the reaction mixture.[2,18,19] Intermediate **I** interacts with the carbon–carbon double bond of cyclohexene to generate the secondary carbenium ion intermediate **II**, which is stabilized by the silyl group β-stabilization effect.[11–13,20–22] Intermediate **II** then interacts with the double bond of **1a** in *trans*-fashion to avoid steric interactions between the bulky trimethylsilyl group and incoming **1a**. A new carbon–carbon bond is formed and a carbenium ion at the carbon β to silicon is generated, leading to **III**, which undergoes a desilylation reaction to give *trans*-allylsilylated products and to regenerate intermediate **I**.

4. Allylsilylation of 1-Allyl-2-(Trimethylsilyl)Cycloalkenes

Trans-1-allyl-2-(trimethylsilyl)cyclopentane and *trans*-1-allyl-2-(trimethylsilyl)-cyclohexane are formed from the reaction of **1a** with cyclopentene and cyclohexene, respectively. A second allylsilylation reaction of these compounds with **1a** also gives unusual allylsilylation products, 7-cyclopent-1-enyl-2,2-dimethyl-4-(trimethylsilylmethyl)-2-silaheptane (30%) and 4-((cyclohex-1-enyl)methyl)-2,2,8,8-tetramethyl-2,8-disilanonane (39%). As observed in the allylsilylation of 4-(trimethylsilylmethyl)-1-alkenes, these products are likely formed *via* intramolecular silyl rearrangements. In this case, the results strongly suggest that a 1,5-silyl shift and 1,5-hydride shift have occurred. Under the same reaction conditions, *trans*-1-allyl-2-(trimethylsilyl)cycloalkenes are isomerized to 3-[3-(trimethylsilyl)propyl]-cycloalkenes. Thus, both starting *trans*-1-allyl-2-(trimethylsilyl)cyclopentene and -hexene are isomerized to 3-(3-(trimethylsilyl)propyl)cyclopentene (24%) and 3-(3-(trimethylsilyl)propyl)cyclohexene (15%), respectively [Eq. (7)]. It seems reasonable that the first step in the isomerization is the addition of a silyl cation to the carbon–carbon double bond of the *trans*-1-allyl-2-(trimethylsilyl)cycloalkanes followed by a 1,5-hydride shift to give a carbocation on a ring carbon β to the silyl group. This is followed by regeneration of a silyl cation from the ring to form a double bond.[11,12]

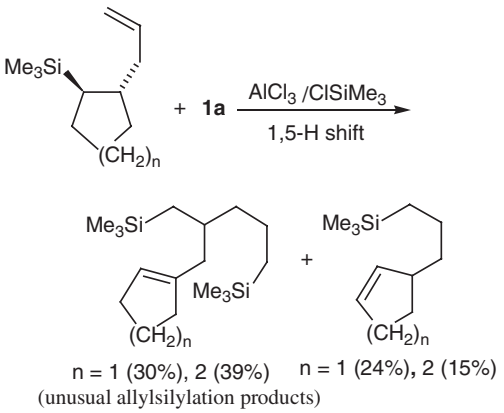

(7)

5. Allylsilylation of Diallylsilanes

Diallyldimethylsilanes undergo intramolecular allylsilylation to give cyclic polymer products in the presence of aluminum chloride.[12] When **1a** is used as a chain-terminating reagent, the formation of polymers is reduced and intramolecularly cyclized allylsilylation products are produced. Thus, a 1:3 reaction of diallylsilanes and monoallylsilanes at $-10\,^{\circ}C$ gives the monomeric cyclized allylsilylation products, isomeric *trans*- and *cis*-3-allyl-1,1-dimethyl-5-trialkylsilylmethyl-1-silacyclohexanes, in 45–76% yields [Eq. (8)]. In this reaction, trimethylchlorosilane is a good activator[12,16] for the aluminum chloride-catalyzed allylsilylation reaction.

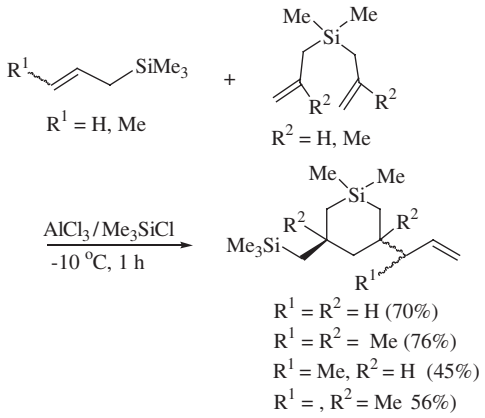

(8)

6. Allylsilylation of Conjugated Dienes

Reaction of linear conjugated dienes with **1a** at $-10\,^{\circ}C$ in hydrocarbon solvent in the presence of $Me_3SiCl/AlCl_3$ affords stereospecific *trans*-1-silyl-3-vinylcyclopentanes, indicating a [3 + 2] cycloaddition of the allyl group of **1a** with a carbon–carbon double bond of the diene [Eq. (9)].[13] In the [3 + 2] annulation reaction, of greater significance is the *trans* conformation of the trimethylsilyl group and vinyl groups.

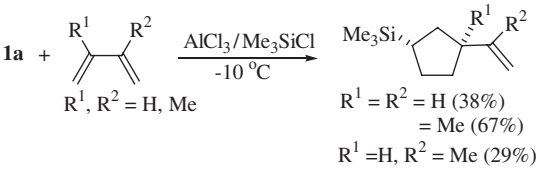

(9)

The reaction of cyclic conjugated dienes with **1a** in hydrocarbon solvent also gives stereospecific *trans*-1-silyl-3-vinylcyclopentanes as the major products.

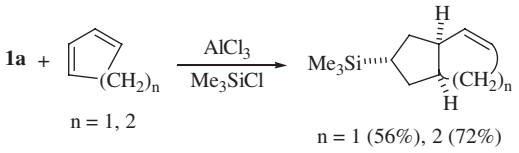

(10)

The reaction of 1,3-cyclohexadiene with **1a** at a temperature of −50 °C gives a 97:3 mixture of 1,4-allylsilylated product, *trans*-3-allyl-6-(trimethylsilyl)cyclohexene and 1,2-allylsilylated product, *trans*-3-allyl-4-(trimethylsilyl)cyclohexene, in quantitative yield. At the same temperature, the [3 + 2] cycloaddition product is detected only in trace amounts after 1 h. As the reaction mixture is warmed to −10 °C, the allylsilylated compounds are converted to the [3 + 2] cycloaddition product (72%). When purified *trans*-3-allyl-6-(trimethylsilyl)cyclohexene and *trans*-3-allyl-4-(trimethylsilyl)cyclohexene are treated separately under the same reaction conditions, the former compound is converted to the [3 + 2] cycloaddition product (major) and 3-(trimethylsilyl)propylbenzene [Eq. (11)], while the latter compound is converted to polymeric materials without giving any [3 + 2] cycloaddition product. The reaction rates of allylsilylation and [3 + 2] annulation are also accelerated by the addition of trimethylchlorosilane to aluminum chloride, as observed in other allylsilylation reactions.[14,15]

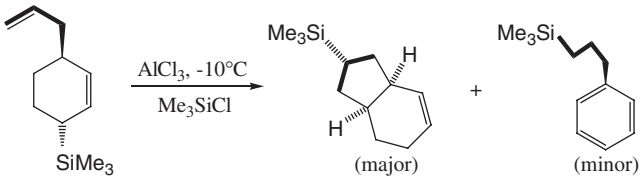

(11)

(2-Methyl-2-propenyl)trimethylsilane reacts with cyclohexene at −10 °C for 25 min to give *trans*-allylsilylated products, *trans*-3-(2-methyl-2-propenyl)-6-trimethylsilylcyclohexene (15%), and *trans*-3-(2-methyl-2-propenyl)-4-trimethylsilylcyclohexene (3%), but no [3 + 2] cycloaddition product. This result suggests that a methyl substituent on the middle carbon of the allyl group prevents the [3 + 2] cycloaddition reaction.

The probable mechanism for the allylsilylation and [3 + 2] cycloaddition is illustrated in Scheme 2, using the reaction of butadiene with **1a** as a representative example. Intermediate **I**, generated as described in Scheme 1, adds to a terminal carbon of butadiene to generate a new intermediate **IV**. This intermediate then interacts with the double bond of **1a** to give **V**, containing a new carbon–carbon bond. In the allylic cationic intermediate **IV**, 1,2-allylsilylation is not favored because of steric repulsion between the bulky trimethylsilyl group of intermediate **IV** and incoming **1a**. Intermediate **V** can undergo a 1,2-silyl shift[17,18] to intermediate **VI** at higher reaction temperatures, even though this is thermodynamically less favorable. Finally, the [3 + 2] cycloaddition product is formed by the cyclization of **VI** to give a five-membered ring through the intramolecular nucleophilic attack by the carbon–carbon double bond on the carbocation of **VI**, followed by the elimination of a silyl cation.

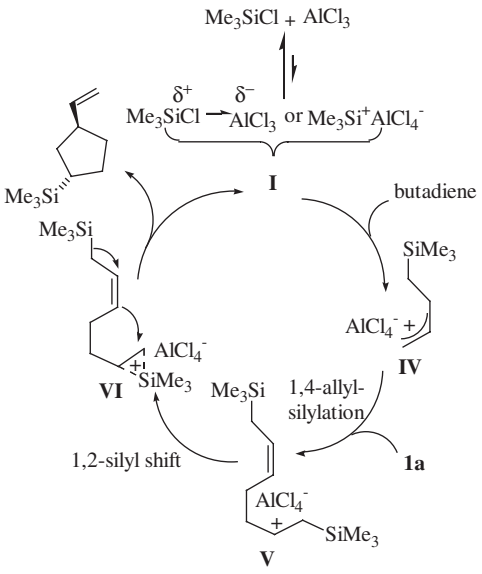

SCHEME 2.

B. *Allylsilylation of Alkynes*

The reaction of terminal alkynes with **1a** in the presence of Lewis acid catalyst at room temperature gives regio- and stereospecific *trans*-allylsilylation products (26–66%) from the addition of silyl and allyl groups to the terminal and inner carbon atoms, respectively, of the carbon–carbon triple bond [Eq. (12)].[19,20] The yields of these products are much improved by using trimethylchlorosilane as an activator.[28] In allylsilylations of 1-hexyne, the catalytic activity of Lewis acids decreases in the following order: $HfCl_4 > AlBr_3 > AlCl_3 > EtAlCl_2$.[21] Stereohomogeneous *Z*-crotyltrimethylsilane reacts with alkyne to afford the expected regiospecific allylsilylation product with allylic inversion.[1a,2,11–13] This implies that allylsilylation is not a concerted reaction but occurs stepwise, as observed in the allylsilylation of alkenes.[1a,2,11–13]

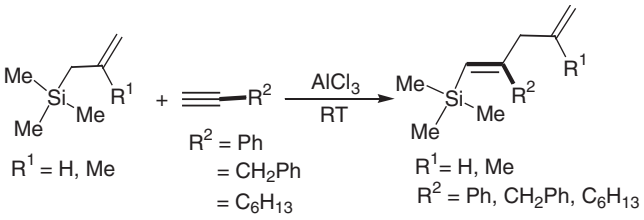

(12)

In the presence of hafnium tetrachloride/trimethylchlorosilane catalyst, alkynyl allylsilane compounds undergo an intramolecular allylsilylation reaction to give cyclic alkenylsilanes in good yields.[22]

III
INTRAMOLECULAR ALKENYL-MIGRATION REACTION OF ALKENYLCHLOROSILANES

The chemistry of alkenyl(ω-chloroalkyl)silanes containing both reactive chloroalkyl and alkenyl groups bonded to silicon, in the presence of Lewis acid catalysts is of interest. Simple alkenyl(chloromethyl)silanes [ω-(C_nRH_{2n-2})($ClCH_2$)$SiMe_2$, $n = 2, 3$] undergo intramolecular alkenyl-migration in the presence of Lewis acid catalyst to give C_1-increased alkenylchlorosilanes.[23,24] Thus, the reaction of (2-alkylvinyl)(chloromethyl)dimethylsilanes in the presence of aluminum chloride catalyst gives (3-alkylallyl)(dimethyl)chlorosilanes as the major products and (2-alkylcyclopropanyl)chlorosilanes as minor products [Eq. (13)].[23] In this reaction, the yield of vinyl-migration product decreases as the bulk of the alkyl substituent in the (2-alkylvinyl)silanes increases. The reaction of (1-hexylvinyl)(chloromethyl)dimethylsilane gives only (2-hexylcyclopropyl)dimethylsilane.

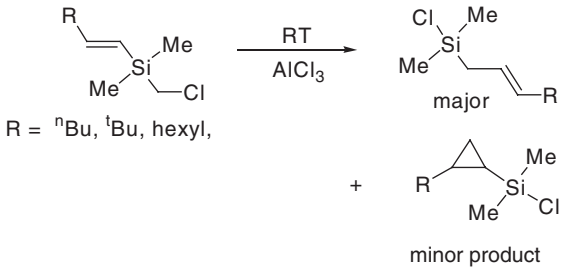

(13)

Allyl(chloromethyl)silanes also undergo intramolecular allyl-migration reactions analogous to that observed for (2-alkylvinyl)(chloromethyl)dimethylsilanes. When **1a** is used as a trapping agent, the carbocation formed at the carbon of the chloromethyl group interacts with the allyl group to form an intramolecularly cyclized silacyclopentanyl cation. The silacyclopentanyl cation is then trapped by **1a** to give the intramolecularly cyclized allylsilylation product [Eq. (14)].[24] The reaction of allyl(chloromethyl)dimethylsilane with **1a** in the presence of aluminum chloride catalyst at room temperature affords an isomeric mixture of 2-(2-allyl-4,4-dimethyl-4-silapentyl)-1,1-dimethylsilanes as trapped products in 40% yield and 3-butenyldimethylchlorosilanes as the allyl migration products in 18% yield [Eq. (14)]. However, the same reaction using allyl(chloromethyl)organochlorosilanes or allyl(chloromethyl)dichlorosilanes in the presence of aluminum chloride does not proceed, indicating that the reactions are sensitive to the electronic nature of the substituents on silicon. Generally, the chloromethyl group of allyl(chloromethyl) silanes is activated by alkyl groups bonded to silicon, while deactivated by chloro group(s) due to the decreased stabilizing ability of α-carbocations by the silyl group.[4] Allyl(chloromethyl)diorganosilanes ($CH_2{=}CH{-}CH_2SiR^1R^2CH_2Cl$; $R^1,R^2 = Me$ or Ph) undergo intramolecular allyl-migration reactions in the presence of aluminum chloride to give 3-butenyldiorganochlorosilanes ($CH_2{=}CH{-}CH_2{-}CH_2SiClR^1R^2$) in 40–75% yields.

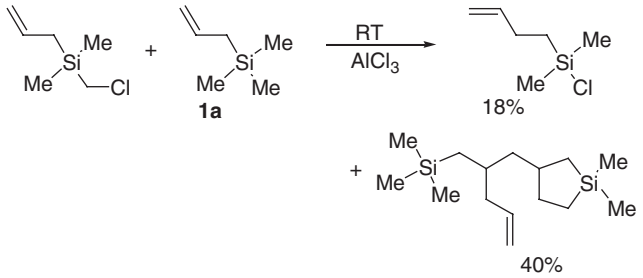

(14)

IV
FRIEDEL–CRAFTS ALKYLATION REACTION WITH ORGANOSILICON COMPOUNDS

Organosilicon compounds such as alkenylchlorosilanes and (chloroalkyl)chlorosilanes (alkyl = methyl, ethyl, propyl)[1b,4,14] react with aromatic compounds in the presence of Lewis acid catalysts to give Friedel–Crafts alkylation products. Common examples of alkenylchlorosilanes for the alkylations of aromatic compounds include vinylchlorosilanes and allylchlorosilanes.[1b,3] Aluminum chloride is a very effective catalyst for the reaction. In alkylation reactions with alkenylchlorosilanes, the reactivity of allylchlorosilanes is higher than that of vinylchlorosilanes. Triorganoalkenylsilanes such as vinyltrimethylsilane and allyltrimethylsilane do not react with benzene to give alkylated products.[2] In the aluminum chloride-catalyzed alkylation reactions, allylchlorosilanes or vinylchlorosilanes should have one or more chlorine atoms bonded to silicon.

A. *Alkylation with Allylchlorosilanes*

Allylchlorosilanes undergo Friedel–Crafts alkylation with aromatic compounds such as benzene derivatives[3] and ferrocene[25] to give [β-(chlorosilyl)alkyl]arene compounds in the presence of Lewis acid catalyst.[1b] Allylsilanes containing two or more chlorine atoms on silicon react smoothly with benzene under mild conditions to give alkylation products in good yields [Eq. (15)]. In alkylations of benzene, the reactivity of the allylsilanes increases as the number of chlorine atoms on the silicon increases, but decreases as the number of methyl groups increases. Because the reactivity of allylsilanes is sensitive to the electronic nature of the substituents on the silicon atom, allylsilane selection is an important factor for alkylation reactions.

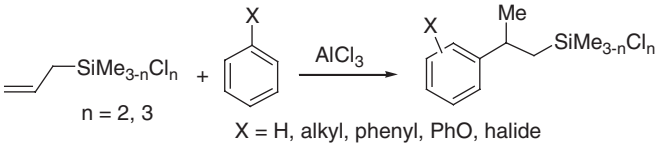

(15)

In the Friedel–Crafts alkylation of benzene derivatives (Ph–R: R = Me, Et, *i*-Pr, Ph, OPh, F, Cl, Br) with allyldichlorosilane (**1b**) in the presence of aluminum chloride catalyst,[3] monoalkylation products, 3-aryl-1,1-dichloro-1-silabutanes, are obtained in 60–83% isolated yields along with small amounts of dialkylation products. The *ortho*-, *meta*-, and *para*-isomeric monoalkylation products can all be formed, but the amount of *ortho*-isomer produced decreases as the steric bulk of the substituent on the benzene ring increases. For example, no *ortho*-alkylation product is found in the case of *i*-propylbenzene. The yield of *meta*-isomer increases as the reaction time increases or at higher temperatures, indicating that it is the thermodynamic product. The alkylation of halogen-substituted benzenes (R = F, Cl, Br) with **1b** gives *ortho*- and *para*-adducts predominantly (91–98%), indicating that halogen atoms are *ortho*- and *para*-directing groups in this reaction.

The effects of ring constituents in the alkylation of benzene derivatives (Ph–R) with **1a** are summarized in Table I.

According to Table I, the reactivity of substituted benzenes (Ph–R) decreases in the following order: R = Ph > PhO > *i*-Pr > Et > Me > H > F > Cl > Br.[3] The alkylation of alkylbenzenes is faster than that of halogen-substituted benzenes. Among the halogen-substituted benzenes, the fastest rate is observed for fluorobenzene and the slowest for bromobenzene, an observation which is not consistent with their relative electronegativities.[26–28] These results indicate that the resonance effect of halogen substituents upon the benzene ring should be considered in addition to electronic effects in order to explain the reaction rates.[26] Stronger resonance effects compared to electronic effects are apparently responsible for the *ortho*- and *para*-directing properties of the halogen atoms. The relative reaction rates for the alkylation of substituted benzenes with respect to benzene ($\log k_R/k_H$) can be plotted against substituent coefficients (σ)[26] for alkyl, aryl, and halogen groups. According to the Hammet equation,[29] $\log k_R/k_H = \rho\sigma$, where σ is a Hammet constant, ρ is found to be 3.1 from the relationship between the substituent coefficients (σ) and

TABLE I
RELATIVE ALKYLATION RATES[a] AND SUBSTITUENT CONSTANTS[42] (S) FOR SUBSTITUTED BENZENES (Ph–R)

	Relative rates		Substituent constants		
Ph–R	(k_R/k_H)	($\log k_R/k_H$)	σ_R	σ_I	σ
H	1.00	0.00	0.00	0.00	0.00
F	0.081	−1.04	0.74	−0.60	0.14
Cl	0.016	−1.44	0.72	−0.24	0.48
Br	0.011	−1.96	0.72	−2.52	0.54
Me	3.89	0.59	−0.01	−0.41	−0.42
Et	4.10	0.61	−0.02	−0.44	−0.46
i-Pr	5.65	0.72	–	–	–
Ph	10.27	1.01	0.25	−0.37	−0.12
PhO	9.42	0.97	0.76	−1.29	−0.53

Definitions: σ_R, resonance constant; σ_I, field constant; $\sigma = \sigma_R + \sigma_I$.
[a]Reaction mole ratio of **1b**/Ph–R/aluminum chloride = 1:20:0.1.

the relative reaction rates for the alkylation of substituted benzenes with respect to benzene ($\log k_R/k_H$).[3]

Allylchlorosilanes also react with naphthalene to give isomeric mixtures of polyalkylated products. However, it is difficult to isolate and purify the products for characterization because the products possess similar boiling points. The alkylation of anthracene with allylchlorosilanes or vinylchlorosilanes is not possible because of the deactivation of aluminum chloride catalyst by complex formation with anthracene.

In the polyalkylation reaction of benzene with allylchlorosilanes, trialkylated compounds are the most substituted products obtained in appreciable amount due to increased steric interactions with additional allyltrichlorosilane. This is the case even when more than a four-fold excess of allyltrichlorosilane is used. In addition, multi-step alkylation reactions give the trialkylated products in higher yields than the one-step reaction.

In the reaction with ferrocene,[30] allyldimethylchlorosilane reacts at 0 °C, allyl(methyl)dichlorosilane reacts at the reflux temperature of methylene chloride, but allylsilanes containing two or more chlorine substituents at the silicon do not give alkylation products. In alkylations of ferrocene, allyldimethylchlorosilane shows the highest activity, allyl(methyl)dichlorosilane is less reactive, and allylsilanes containing two or more chlorine-substituents at the silicon have no activity.[25] Allyltrimethylsilane reacts with both benzene and ferrocene to give allylsilylation products but no alkylation product.[1b,2,25]

The reaction of ferrocene with allylchlorosilanes in the presence of Lewis acid in methylene chloride solvent affords alkylated ferrocenes bearing chlorosilyl groups at the carbon β to the ferrocene ring [Eq. (16)].[25]

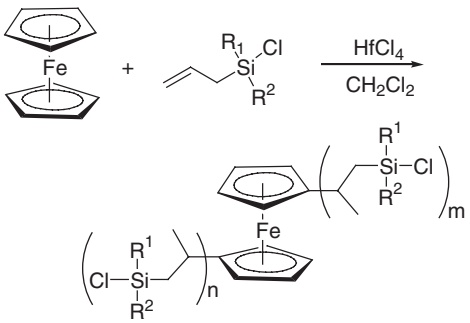

(16)

$R^1 = R^2 = Me$: n = 1 (76%), 2 (4%), m = 0

R^1 = Me, R^2 = Cl : n = 1 (82%), m = 0

R^1 = *i*-Pr, R^2 = Cl : n = 1 (84%), m = 0

R^1 = *n*-Hx, R^2 = Cl : n = 1 (90%), m = 0

R^1 = Cl, R^2 = H or Cl : n = 1 (trace), m = 0

The reactivity of allylchlorosilanes for the alkylation of ferrocene varies depending upon the substituents on the silicon atom. Generally, the reactivity increases as the number of alkyl groups on the silicon of allylsilanes increases.[4] Allyl(dialkyl)chlorosilanes react with ferrocene in the presence of $HfCl_4$ under mild reaction

conditions to give alkylated products, (2-silyl-1-methylethyl)ferrocenes, in good yields, while allyl(alkyl)dichlorosilanes give alkylated products at slightly higher temperatures. Allylsilanes fully substituted with alkyl groups on silicon undergo decomposition reactions rather than alkylation in the presence of hafnium chloride catalyst, while allyltrichlorosilane and allyldichlorosilane exhibit little reactivity. The reactivity of allylsilanes for the alkylation of ferrocene decreases in the following order: allyldialkylchlorosilane > allyl(alkyl)dichlorosilane ≫ allyldichlorosilane ≈ allyltrichlorosilane.[25] The catalytic efficiency of Lewis acids for the alkylation decreases in the following order: hafnium chloride > zirconium chloride > aluminum chloride > aluminum bromide.[25] Titanium(IV) chloride shows no catalytic activity for the alkylation of ferrocene. In the alkylation of ferrocene, the catalytic activity of aluminum chloride decreases, accompanied with a coloration to green-blue as the reaction proceeds. Eventually the alkylation reaction stops, with a deep-blue color present when high reaction temperatures are used. Complex formation of aluminum chloride with ferrocene is responsible for the deactivation of catalytic activity.[30] Generally, the abilities of Lewis acids to form complexes with ferrocene increase as the acidity of the Lewis acid increases. It is well documented that ferrocene can be oxidized and converted by most common electrophiles into a ferrocenium cation, which is reluctant to undergo electrophilic substitution.[31] These results indicate that both Friedel–Crafts alkylation with allylchlorosilanes and complexation with Lewis acids are competing reactions in the aluminum chloride-catalyzed alkylation of ferrocene.[31]

B. *Alkylation with Vinylchlorosilanes*

Vinylchlorosilanes undergo Friedel–Crafts alkylation with aromatic compounds in the presence of Lewis acids to give 2-(chlorosilyl)ethylarenes [Eq. (17)].[1b,32,33] The reactivity of vinylchlorosilanes for the alkylation of aromatic compounds is slightly lower than that of allylchlorosilanes.[1b,3,32] The reactivity of vinylsilanes for alkylation depends on the substituents on the silicon of the vinylsilane. The reactivity of vinylchlorosilanes decreases in the following order: dichloro(methyl)vinylsilane > trichlorovinylsilane > chloro(dimethyl)vinylsilane. The alkylation of monosubstituted benzenes such as toluene, chlorobenzene, and biphenyl with dichloro(methyl)vinylsilane (**1c**) at 75–80 °C for 2 h affords alkylated products in 50–63% yields.[32]

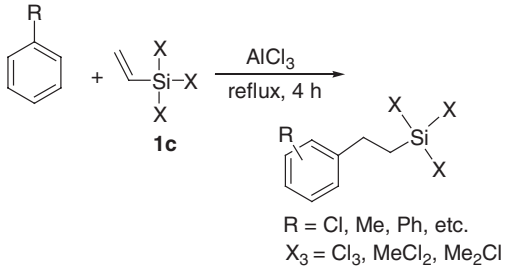

(17)

When benzene reacts with a six-fold excess of **1c** in the presence of aluminum chloride at room temperature, the peralkylated product,[34] hexakis[2-(dichloromethylsilyl)ethyl]benzene is obtained as the major component along with other lower polyalkylated products: pentakis-, tetrakis-, tris-, and bis[2-(dichloromethylsilyl)ethyl]benzene.

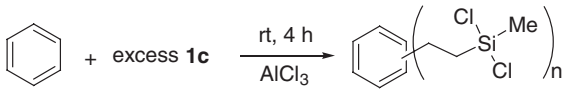

n = 6 (56%), 5 (21%), 4 (9%), 3 (9%), 2 (4%) (18)

In the peralkylation of alkylbenzenes with **1c** in the presence of aluminum chloride catalyst,[35] both polyalkylation and transalkylation reactions occur in competition. Peralkylation product yields decrease as the chain length of the alkyl substituent on the benzene ring increases. Toluene reacts with five equivalents of **1c** in the presence of aluminum chloride at room temperature for 2 h to give pentakis[2-(dichloromethylsilyl)ethyl]toluene as the major product in addition to less alkylated products: tetrakis-, tris-, bis-, and mono[2-(dichloromethylsilyl)ethyl]toluene. The peralkylation of alkylbenzenes having longer alkyl groups such as ethyl, *n*-propyl, and *n*-butyl, with **1c** gives the peralkylated products in low yields (about 25%) in addition to transalkylation products.

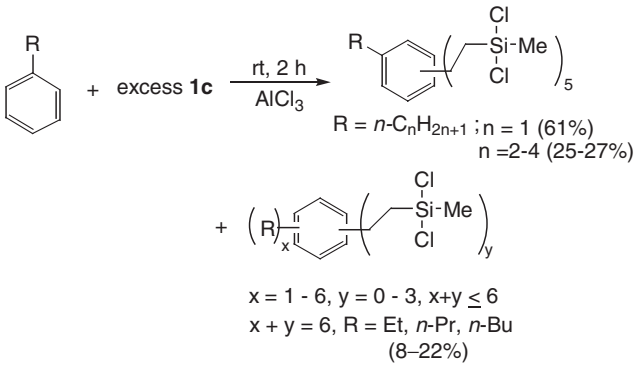

(19)

The reaction of ethylbenzene with five equivalents of **1c** under the same alkylation conditions used for toluene, gives pentakis- (25%), tetrakis- (9%), tris- (4%), and bis[2-(dichloromethylsilyl)ethyl]ethylbenzene (1%) as well as a mixture of many transalkylated products (44%). It is of interest that longer alkyl-substituted benzenes exhibited different behavior in peralkylations with **1c**. The transalkylation of ethylbenzene is responsible for the significantly low yield (25%) of peralkylation product in comparison with yields obtained from the alkylation of benzene[34] or toluene. Peralkylation of *n*-propylbenzene and *n*-butylbenzene gives similar results to those of ethylbenzene.

The reaction of *o*-, *m*-, or *p*-xylene with four equivalents of **1c** affords an isomeric mixture of peralkylated xylenes consisting of tetrakis[(dichloromethylsilyl)ethyl]-xylenes and isomeric transalkylation products. With longer reaction times and

higher temperatures, the formation of tetrakis[(dichloromethylsilyl)ethyl]-*p*-xylene is favored due to less steric hindrance between the substituents on benzene.

Peralkylation of mesitylene with **1c** gives only rearranged products without transalkylated products. The undesirable isomerization of 2,4,6-tris(dichloromethylsilylethyl)mesitylene to the 3,5,6- or 4,5,6-isomers can be avoided by carrying out the reaction in hexane at room temperature. In this case, the peralkylated product, 2,4,6-tris[2-(dichloromethylsilyl)ethyl]mesitylene, is obtained in 38% yield along with mono- and bis-alkylated mesitylenes in 7% and 37% yields, respectively. No rearranged products are formed.

Friedel–Crafts-type polyalkylations of alkyl-substituted benzenes with **1c** become less difficult as the number of electron-donating methyl groups on the benzene ring increases. This is consistent with the fact that the alkylation occurs via an electrophilic substitution. The tendency of starting methylbenzenes to form rearranged products also increases in the same order from toluene to mesitylene.

The alkylation of substituted benzenes possessing electron-withdrawing groups, such as chlorobenzene and anisole, with **1c** gives only mono-, bis-, and trisalkylated compounds. No peralkylated products are obtained even when heating the reaction mixtures for long periods. These results can be explained by the deactivation effects of the electron-withdrawing substituents and the complexation between $AlCl_3$ catalyst and the lone pairs of electrons of the substituents.

C. *Alkylation with (ω-Chloroalkyl)chlorosilanes*

The Friedel–Crafts alkylation of benzene with (ω-chloroalkyl)chlorosilanes ($Cl_mMe_{3-m}Si(CH_2)_n$-Cl, $m = 0$–3; $n = 1$–3) in the presence of aluminum chloride gives ω-(chlorosilyl)alkylbenzenes.[1b,4] The reactivities of (chloroalkyl)silanes depends on the substituents on silicon and the alkyl chain length between C–Cl and silicon. In the case of (chloromethyl)silanes ($Cl_mMe_{3-m}SiCH_2Cl$), the reactivity decreases as the number (m) of chlorine substituent(s) on the silicon atom increases. (Chloromethyl)trichlorosilane ($m = 3$) requires a reaction temperature of 200 °C for the alkylation of benzene in a sealed tube. Alkylation with (chloromethyl)methyldichlorosilane ($m = 2$) or (chloromethyl)dimethylchlorosilane ($m = 1$) at 80 °C affords benzyl(methyl)dichlorosilane in 71% yield and a 1:1 mixture of benzyl(methyl)dichlorosilane (demethylation product) and benzyldimethylchlorosilane in 41% yield. In the case of (chloromethyl)trimethylsilane ($m = 0$), reaction proceeds at room temperature to give trimethylchlorosilane and toluene, derived from the protodesilylation of the benzyltrimethylsilane product by hydrogen chloride.[4] Generally, electron-withdrawing chlorine substituent on the silicon atom of (chloromethyl)silanes deactivate the alkylation, while methyl groups facilitate the alkylation[3,4] and the subsequent decomposition of products. In the alkylation of benzene with (ω-chloroalkyl)trichlorosilanes in the presence of aluminum chloride, the spacer length between C–Cl and the silyl group plays an important role. Alkylation proceeds under milder conditions as the spacer length increases. Thus, reaction temperatures decrease from 200 °C for (chloromethyl)silane to room temperature for (β-chloroethyl)silane and (γ-chloropropyl)silane.[4]

D. *Alkylation with (Polychloroalkyl)chlorosilanes*

(Polychloromethyl)silanes ($Cl_mMe_{3-m}SiCH_{3-n}Cl_n$, $m = 0$–3; $n = 2$, 3) react with excess benzene in the presence of aluminum chloride to give (polyphenylmethyl)-silanes [Eq. (20)].[14] Such reactions occur at temperatures ranging from room temperature ($m = 0$, 1; $n = 2$) to 80 °C ($m = 2$, 3; $n = 2$, 3), indicating that the reactivity increases as the number (m) of electron-donating chlorine groups on silicon decreases. In particular, (dichloromethyl)silanes having two or three methyl groups at the silicon ($m = 0$ or 1; $n = 2$) undergo alkylation and decomposition reactions of their products at room temperature. Alkylation with (dichloromethyl)trimethylsilane ($m = 0$) occurs immediately at room temperature to give diphenylmethane and trimethylchlorosilane, but not (diphenylmethyl)trimethylsilane due to decomposition of the alkylation product. (Trichloromethyl)silanes ($m = 2$, 3; $n = 3$) react with excess benzene to give (triphenylmethyl)silanes as major products and the unexpected (diphenylmethyl)silanes as minor products. The (diphenylmethyl)silanes are formed by the decomposition of (triphenylmethyl)silanes under the reaction conditions. In the alkylation of benzene, the reactivity of (polychloromethyl)silanes ($Cl_mMe_{3m}SiCH_{3n}Cl_n$: $m = 0$–3; $n = 2$, 3) decreases in the following order: $m = 0 > 1 > 2 > 3$; $n = 3 > 2$.[14]

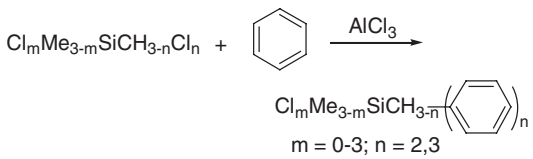

(20)

Friedel–Crafts alkylation reactions of biphenyl with (dichloroalkyl)chlorosilanes [$Cl_mMe_{3-m}Si(C_nH_{2n-1}Cl_2)$, $m = 0$–3, $n = 2$, 3] at temperatures ranging from 120 to 160 °C in the presence of Lewis acid catalyst give cyclized products, fluorenyl-substituted chlorosilanes, in 47–94% yields [Eq. (21)].[36] When (dichloromethyl)trichlorosilane reacts with a two-fold excess of biphenyl in the presence of aluminum chloride catalyst at 160 °C for 1 h, 9-(trichlorosilyl)fluorene is obtained in 91% yield. Reaction with (dichloromethyl)trichlorosilane at 120 °C for 1 h gives the cycloalkylation product in 94% yield. Under similar reaction conditions, (1,2-dichloroethyl)chlorosilanes afford 9-(chlorosilylmethyl)fluorenes in 35–47% yields and (2,3-dichloropropyl)dichlorosilane gives 9-(2-(trichlorosilyl)ethyl)fluorene in 48% yield. These results can be rationalized in terms of the stability,[4] ease of 1,2-migration, and electrophilic addition to biphenyl of the carbocation intermediates generated by the complexation of (dichloroalkyl)chlorosilanes (alkyl = ethyl and propyl) with aluminum chloride. In these reactions, the reactivities of (dichloroalkyl)silanes generally increase as the number of methyl groups on the silicon atom and the alkyl chain lengths increase. However, desilylation of the alkylated products and starting chlorosilanes is observed in the case of (dichloroalkyl)silanes having two or more methyl groups on silicon. Alkylation with (dichloromethyl)dimethylchlorosilane proceeds at 120 °C but gives fluorene and dimethyldichlorosilane, resulting from desilylation of the products. The reactivities of (dichloroalkyl)silanes decrease in the following order: $m = 0 > 1 > 2$; $n = 2 > 1$.

The catalytic efficiencies of Lewis acids for the cycloalkylation reactions decrease in the following order: $AlCl_3 > AlBr_3 > HfCl_4 > ZrCl_4 \gg TiCl_4$.[36]

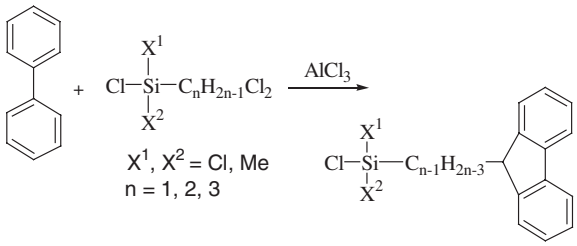

(21)

Known alkylation reactions of aromatic compounds with organosilicon compounds have been summarized in this review. A variety of chlorosilanes containing alkenyl and chloroalkyl groups can be used for the alkylation of aromatic compounds to afford the corresponding chlorosilyl-containing aromatic compounds. Such organosilicon compounds containing Si–Cl functionality are useful starting materials for the silicone industry.

V
HYDROSILYLATION REACTION WITH TRIORGANOSILANES

Triorganosilanes (R_3SiH) undergo hydrosilylation with unsaturated hydrocarbons in the presence of Lewis acids. The $AlCl_3$-catalyzed reaction[37,38] has received relatively little attention due to the strong catalytic activity of $AlCl_3$ for the polymerization of unsaturated hydrocarbons.[39,40] Hydrosilylations of alkenes and alkynes with chlorodialkylsilanes in the presence of $AlCl_3$ were first reported by Finke and Moretto[37a] in 1979, and later by Oertle and Wetter.[37b] In 1990, Yamamoto and Takemae studied the reaction of 1-methylcyclohexene with chlorodimethylsilane in the presence of $AlCl_3$ catalyst and found that hydrosilylation proceeded stereoselectively in a *trans*-addition manner.[38] Voronkov and co-workers[41] reported the hydrosilylation of alkynes and olefins with triethylsilane in the presence of a mixed catalytic system consisting of H_2PtCl_6 and $AlCl_3$.

The hydrosilylation of alkenes with trialkylsilanes in the presence of Lewis acid catalysts under mild conditions gives the corresponding (trialkylsilyl)alkanes [Eq. (22)]. Reaction with terminal alkenes such as 1-hexene and 1-dodecene at room temperature gives hydrosilylation products in 57 and 58% yields, respectively. Reactions with activated styrene derivatives such as styrene, *p*-chlorostyrene, and α-methylstyrene at −20 °C afford hydrosilylated products in 55–61% yields.[36]

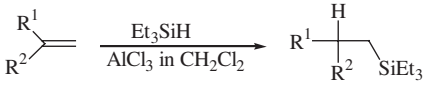

R^1 = H, R^2 = Me, ^{n}Bu, *n*-octyl, Ph, *p*-ClPh,
R^1 = Me, R^2 = Ph

(22)

Cycloalkenes such as cyclohexene, 1-methylcyclohexene, cyclopentene, and norbornene are hydrosilylated with triethylsilane in the presence of aluminum chloride catalyst in methylene chloride at 0 °C or below to afford the corresponding hydrosilylated (triethylsilyl)cycloalkanes in 65–82% yields [Eq. (23)]. The reaction of 1-methylcyclohexene with triethylsilane at −20 °C occurs regio- and stereoselectively to give *cis*-1-triethylsilyl-2-methylcyclohexane *via* a *trans*-hydrosilylation pathway. Cycloalkenes having an alkyl group at the double-bonded carbon are more reactive than non-substituted compounds in Lewis acid-catalyzed hydrosilylations.[36]

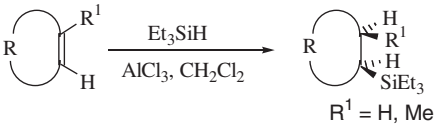

(23)

In these hydrosilylation reactions, the reactivity and product yields decrease as the bulk of the triorganosilane increases. The catalytic reactivity of Lewis acids decreases in the following order: $AlBr_3 > AlCl_3 > HfCl_4 > EtAlCl_2 > ZrCl_4 > TiCl_4$.[36] When triorganochlorosilane is used as an activator in the aluminum chloride-catalyzed reaction, the hydrosilylation rate drastically increases. The results are consistent with a stepwise reaction proceeding *via* the formation of a trialkylsilylenium ion intermediate.

Other Lewis acid-catalyzed hydrosilylations of alkenes and alkynes on hydride-terminated silicon surfaces result in a surface modified with alkyl and alkenyl functionalities.[42]

Acknowledgments

We thank the co-workers listed in the references for their enthusiasm, valuable contributions, and efforts. We also thank Prof. D. Son of Southern Methodist University, Dallas, Texas for his help and discussions in the preparation of this account.

References

(1) For reviews, see: (a) Jung, I. N.; Yoo, B. R. *Synlett* **1999**, 519. (b) Jung, I. N.; Yoo, B. R. *Adv. Organomet. Chem.* **2001**, *46*, 145.
(2) Yeon, S. H.; Lee, B. W.; Yoo, B. R.; Suk, M.-Y.; Jung, I. N. *Organometallics* **1995**, *14*, 2361.
(3) Lee, B. W.; Yoo, B. R.; Kim, S.-I.; Jung, I. N. *Organometallics* **1994**, *13*, 1312.
(4) Yoo, B. R.; Kim, J. H.; Lee, H.-J.; Lee, K.-B.; Jung, I. N. *J. Organometal. Chem.* **2000**, *605*, 239.
(5) Song, Y.-S.; Yoo, B. R.; Lee, G.-H.; Jung, I. N. *Organometallics* **1999**, *18*, 3109.
(6) Wierschke, S. G.; Chandrasekhar, J.; Jorgensen, W. L. *J. Am. Chem. Soc.* **1985**, *107*, 1496.
(7) Kresge, A. J.; Tobin, J. B. *Angew. Chem. Int. Ed. Engl.* **1993**, *32*, 721.
(8) Eabon, C.; Bott, R. W. (A. G. MacDiarmid, Ed.), *Organometallic Compounds of the Group IV Elements*, Vol. 1, Dekker, New York, 1968, Part 1, pp. 359–437.
(9) Thomas, C. A. *Anhydrous Aluminum Chloride in Organic Chemistry*, Reinhold, New York, 1941.
(10) Jenkins, P. R.; Gut, R.; Wetter, H.; Eschenmoser, A. *Helv. Chim. Acta* **1979**, *62*, 1922.
(11) Cho, B. G.; Choi, G. M.; Jin, J. I.; Yoo, B. R.; Suk, M. Y.; Jung, I. N. *Organometallics* **1997**, *16*, 3576.
(12) Choi, G. M.; Yeon, S. H.; Jin, J. I.; Yoo, B. R.; Jung, I. N. *Organometallics* **1997**, *16*, 5158.
(13) Choi, G. M.; Yoo, B. R.; Lee, H.-J.; Lee, K. B.; Jung, I. N. *Organometallics* **1998**, *17*, 2409.
(14) Yoo, B. R.; Kim, J. H.; Cho, B. G.; Jung, I. N. *J. Organomet. Chem.* **2001**, *631*, 36.
(15) Yeon, S. H.; Lee, B. W.; Kim, S.-I.; Jung, I. N. *Organometallics* **1993**, *12*, 4887.

(16) Kamigaito, M.; Sawamoto, M.; Hiagshimura, T. J. *Polym. Sci. Polym. Chem.* **1991**, *29*, 1909.
(17) Knölker, H.-J.; Jones, P. G.; Pannek, J.-B.; Weinkauf, A. *Synlett* **1991**, *2*, 147. Knölker, H.-J.; Foitzik, N.; Goesmann, H.; Graf, R.; Jones, P. G.; Wanzl, G. *Chem. Eur. J.* **1997**, *3*, 538. Knölker, H.-J.; Jones, P. G.; Pannek, J.-B. *Synlett* **1994**, *2*, 131.
(18) Danheiser, R. L.; Dixon, B.-R.; Gleason, R.-W. *J. Org. Chem.* **1992**, *57*, 6094.
(19) Yeon, S. H.; Han, J. S.; Hong, E.; Do, Y.; Jung, I. N. *J. Organomet. Chem.* **1995**, *499*, 159. In this paper, we made a mistake in assigning the stereochemistry of the allylsilylation product obtained from the reaction of phenylacetylene with allyltrimethylsilane. It was not *cis*-product but *trans*-product. We thank Prof. Y. Yamamoto of Tohoku University for the correction.[20]
(20) Asao, N.; Yoshikawa, E.; Yamamoto, Y. *J. Org. Chem.* **1996**, *61*, 4974.
(21) Yoshikawa, E.; Gevorgyan, V.; Asao, N.; Yamamoto, Y. *J. Am. Chem. Soc.* **1997**, *119*, 6781.
(22) Imamura, K. I.; Yoshikawa, E.; Gevorgyan, V.; Yamamoto, Y. *J. Am. Chem. Soc.* **1998**, *120*, 5339.
(23) Tamao, K.; Nakajima, T.; Kumada, K. *Organometallics* **1984**, *3*, 1655.
(24) Jung, H. Y.; Park, Y.-A.; Yoo, B. R.; Tamao, K.; Jung, I. N. *Organometallics* **2004**, *23*, 4910.
(25) Ahn, S.; Song, Y. S.; Yoo, B. R.; Jung, I. N. *Organometallics* **2000**, *19*, 2777.
(26) Swain, C. G.; Unger, S. H.; Rosenquist, N. R.; Swain, M. S. *J. Am. Chem. Soc.* **1983**, *105*, 492.
(27) Hansch, C.; Leo, A.; Taft, R. W. *Chem. Rev.* **1991**, *91*, 165.
(28) Brown, H.; Okamoto, Y. *J. Am. Chem. Soc.* **1958**, *80*, 4979.
(29) Hammet, L. P. *Physical Organic Chemistry*, McGraw-Hill, New York, **1940** p. 40.
(30) Olah, G. A.; Bach, T.; Prakash, G. K. S. *New J. Chem.* **1991**, *15*, 571.
(31) Herberhold, M. (A. Togni, T. Hayashi, Eds.), *Ferrocenes*, VCH, New York, **1995**, p. 219.
(32) Andrianov, K. A.; Zhdanov, A. A.; Odinnets, V. A. *Zh. Obshch. Khim.* **1961**, *31*, 4033. *Chem. Abstr.* **1962**, *57*, 9874a.
(33) Nametkin, N. S.; Vdovin, V. M.; Findel-Shtein, E. S.; Oppengeim, V. D.; Chekalina, N. A. *Isv. Akad. Nauk. SSSR., Ser. Khim.* **1966**, *11*, 1998.
(34) Cho, E. J.; Yoo, B. R.; Jung, I. N.; Sohn, H.; Powell, D. R.; West, R. *Organometallics* **1997**, *16*, 4200.
(35) Cho, E. J.; Lee, V.; Yoo, B. R.; Jung, I. N. *J. Organomet. Chem.* **1997**, *548*, 237.
(36) Song, Y.-S.; Kong, S. D.; Khan, S. A.; Yoo, B. R.; Jung, I. N. *Organometallics* **2001**, *20*, 5586.
(37) (a) Finke, U.; Moretto, H. Ger. Patent **1979**, 2804204; *Chem. Abstr.* **1979**, *91*, 193413x. (b) Oertle, K.; Wetter, H. F. *Tetrahedron Lett.* **1985**, *26*, 5511.
(38) Yamamoto, K.; Takemae, M. *Synlett* **1990**, 259.
(39) Olah, G. A. *Friedel–Crafts and Related Reactions*, Vol. 2, Wiley, New York, 1963, pp. 1301–1304.
(40) Kennedy, J. P.; Marechal, E. *Carbocationic Polymerization*, Wiley-Interscience, New York, **1982** pp. 95–100.
(41) Voronkov, M. G.; Sushchinskaya, S. P.; Pukhnarevich, V. B. *Zh. Obshch. Khim.* **1981**, *51*, 242. *Chem. Abstr.* **1981**, *95*, 25190m.
(42) Buriak, J. M.; Stewart, M. P.; Geders, T. W.; Allen, M. J.; Choi, H. C.; Smith, J.; Raftery, D.; Canham, L. T. *J. Am. Chem. Soc.* **1999**, *121*, 11491.

Bidentate Group 13 Lewis Acids with ortho*-Phenylene and* peri*-Naphthalenediyl Backbones*

MOHAND MELAIMI and FRANÇOIS P. GABBAÏ*

Department of Chemistry, Texas A&M University, College Station, TX 77843, USA

I. Introduction 61
II. Synthesis 62
A. Boron Polydentate Lewis Acids 62
B. Aluminum, Gallium and Indium Polydentate Lewis Acids 73
III. Interaction with Lewis Basic Substrates 85
A. Complexation of Organic Substrates 85
B. Complexation of Anions 89
IV. Conclusion 97
Acknowledgments 98
References 98

I
INTRODUCTION

The chemistry of polydentate Lewis acids[1–3] is still in its infancy but is rapidly expanding to a number of areas including molecular and anion recognition, catalysis and crystal engineering. Conceptually, polydentate Lewis acids are often regarded as the charge reverse analogs of polydentate Lewis bases and are thus expected to act as polydentate ligands for electron-rich substrates.[4] This analogy was recognized almost four decades ago by Shriver and Biallas who showed that methoxide anions are effectively chelated by 1,2-bis(difluoroboryl)ethane (**1**), a charge reverse analog of ethylenediamine (Scheme 1).[5] Following this seminal contribution, a great deal of effort has been devoted to the synthesis and study of such polydentate Lewis acids. An important part of the compounds that have been investigated consists of polyfunctional organostannanes[1] and organomercurials.[6–11] Despite the soft Lewis acidity of tin and mercury, these compounds exhibit remarkable properties and have been used as receptors for anions as well as for small electron-rich molecules. For example, while the 1,2-distannylbenzene **2**[12] or the mercuraborand **3**[13] readily complex chloride anions, trinuclear mercury derivatives such as trimeric perfluoro-*ortho*-phenylene **4** can be used as receptors for organic substrates including acetone (Scheme 2).[14] Aiming at more powerful Lewis acids, a great deal of effort has been devoted to the preparation of polydentate Lewis acids that contain hard Lewis acidic elements of group 13.[15,16] Despite their greater sensitivity toward hydrolysis and oxidation, several polydentate group 13 derivatives have been successfully synthesized and investigated.

An important aspect of this research resides in the choice of the backbone that serves to hold the Lewis acidic site. In order to insure that the Lewis acidic sites

*Corresponding author.
E-mail: francois@tamu.edu (F.P. Gabbaï).

ADVANCES IN ORGANOMETALLIC CHEMISTRY
VOLUME 53 ISSN 0065-3055/DOI 10.1016/S0065-3055(05)53003-X

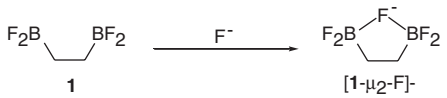

SCHEME 1.

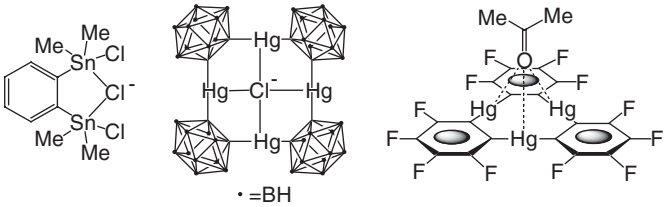

SCHEME 2.

remain available, it is important to choose a backbone that does not contain accessible Lewis basic sites such as oxygen or nitrogen atoms which could neutralize the Lewis acidic centers by intramolecular Lewis adduct formation or by through-bond π-electron donation. Moreover, as in the chemistry of polydentate Lewis bases, the structure of the backbone should serve to dictate the spatial orientation of the Lewis acidic centers as well as the overall rigidity or flexibility of the target polydentate Lewis acid. Since the occurrence of cooperative effects is entropically impaired with flexible systems, the preorganization of the Lewis acidic sites in a rigid molecular edifice is often preferred. Recent achievements in this area have centered on derivatives of *ortho*-substituted benzenes and *peri*-substituted naphthalenes. In this chapter, we will review the chemistry of bidentate Lewis acids containing two group 13 elements linked by an *ortho*-phenylene[15,16] or a *peri*-naphthalenediyl backbone. This contribution follows an earlier review concerned with *peri*-naphthalenediyl group 13 derivatives.[17]

II
SYNTHESIS

A. *Boron Polydentate Lewis Acids*

1. *Ortho*-Phenylene Boron Derivatives

Bidentate boranes with an *o*-phenylene backbone constitute some of the simplest examples of polydentate Lewis acids with rigid backbones. They can be prepared by the reaction of boron halides with a 1,2-dimetallated benzene derivative. Thus, the reaction of 1,2-bis(chloromercurio)benzene (**5**) with boron trichloride affords 1,2-bis(dichloroboryl)benzene (**6**, Scheme 3).[18]

This compound (**6**) can also be obtained in one step by the reaction of 1,2-bis(trimethylstannyl)benzene (**7**) with an excess of boron trichloride at −78 °C in dichlormethane.[19] It can also be prepared by the reaction of 1,2-bis(trimethylsilyl)benzene (**8**) with boron trichloride. In the latter, the reaction proceeds *via* the monoborylated intermediate **9** (Scheme 4).

When the distannyl reagent **7** is employed, the fate of the reaction apparently depends on the reaction conditions. Indeed, Eisch observed that the reaction of **7** with boron trichloride at −40 °C in hydrocarbon solvent is not always selective and leads to the formation of both a monoborylated intermediate (**10**) that slowly converts into **6** (Scheme 5).[20] The outcome of these reactions is apparently further complicated by a fast methyl group transfer from the tin to the boron centers yielding the undesired monoborylated derivative **11**. Eisch also found that such reactions are not limited to the case of boron trialide but can be performed with dialkyl boron halide starting materials. For example, the reaction of the distannane

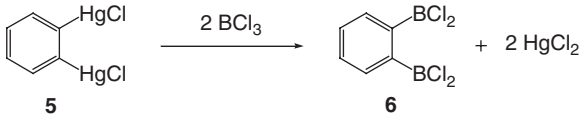

Scheme 3.

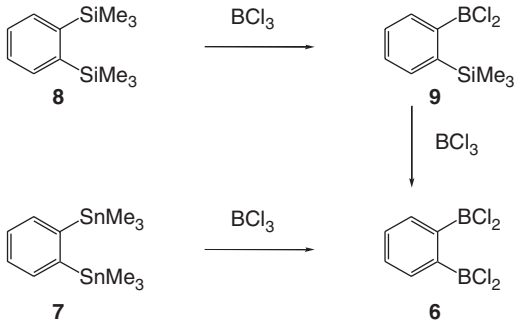

Scheme 4.

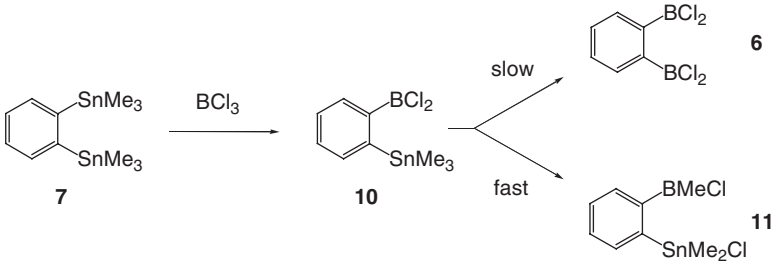

Scheme 5.

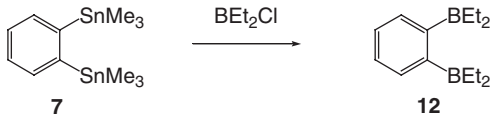

SCHEME 6.

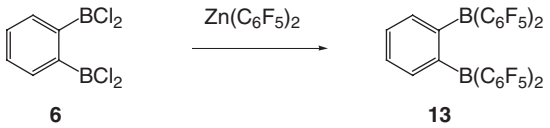

SCHEME 7.

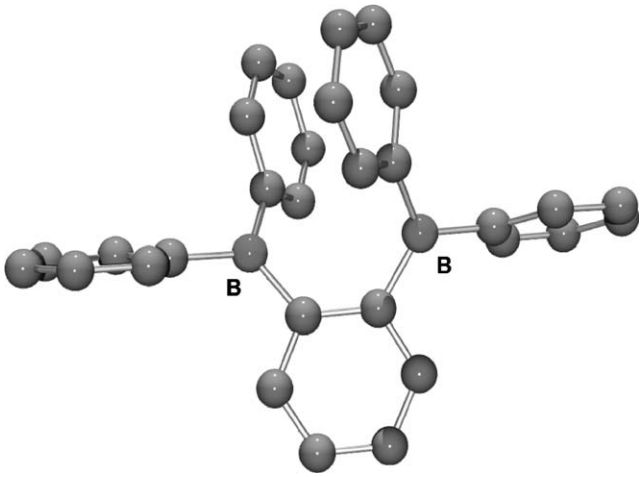

FIG. 1. Compound **13**. F-atoms from C_6F_5 groups omitted for clarity.

7 with diethylboron chloride is clean and affords high yields of 1,2-bis(diethylboryl)benzene (**12**, Scheme 6).

1,2-Bis(dichloroboryl)benzene (**6**) is an important starting material which lends itself to facile derivatization. As shown by Piers, it cleanly reacts with bis(pentafluorophenyl)zinc to afford the corresponding bidentate Lewis acid **13** (Scheme 7).[21] The molecular structure of diborane **13** has been determined and is shown in Fig. 1. In this structure, the vicinal boron atoms are held at 3.26 Å and from one another and seem to be ideally positioned to cooperatively interact with monoatomic anions. The fully fluorinated version of this bidentate Lewis acid has also been prepared.[21] Original efforts focused on the use of 1,2-bis(dichloroboryl)tetrafluorobenzene **14** as a starting material (Scheme 8). This compound could be observed in the early stage of the reaction of trimeric perfluoro-*o*-phenylenemercury (**4**) with boron trichloride, but was found to be unstable toward condensation into 9,10-dichloro-9,10-dihydro-9,10-diboraoctafluoroanthracene **15**. The successful synthesis of the fully fluorinated

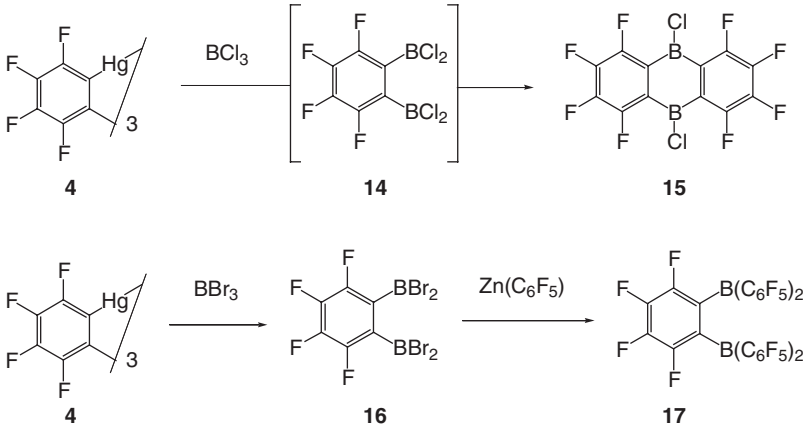

Scheme 8.

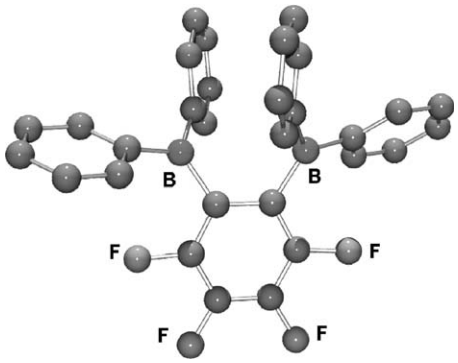

Fig. 2. Compound **17**. F-atoms from C_6F_5 groups omitted for clarity.

derivative employed the more stable 1,2-bis(dibromoboryl)tetrafluorobenzene **16**. This derivative was obtained from the reaction of the trinuclear organomercurial **4** with BBr_3 and was converted into **17** by treatment with bis(pentafluorophenyl)zinc. The structure of **17** (Fig. 2) has also been determined and closely resembles that of **13** (Fig. 1). However, this structure displays a significantly shorter distance of 3.14 Å between the two boron centers.

Distannyl derivatives have also been used as starting materials for the synthesis of fluorinated *ortho*-phenylene diboranes. The reaction of 1,2-bis(trimethylstannyl)tetrafluorobenzene (**18**)[22] with BCl_3 affords 9,10-dichloro-9,10-dihydro-9,10-diboraoctafluoroanthracene (**15**) (Scheme 9).[23,24] This compound can be further derivatized by treatment with bis(pentafluorophenyl)dimethyltin which affords the fully fluorinated 9,10-bis(pentafluorophenyl)-9,10-dihydro-9,10-diboraoctafluoroanthracene (**19**). This conversion can also be effected by the reaction of **15** with bis(pentafluorophenyl)zinc.[21]

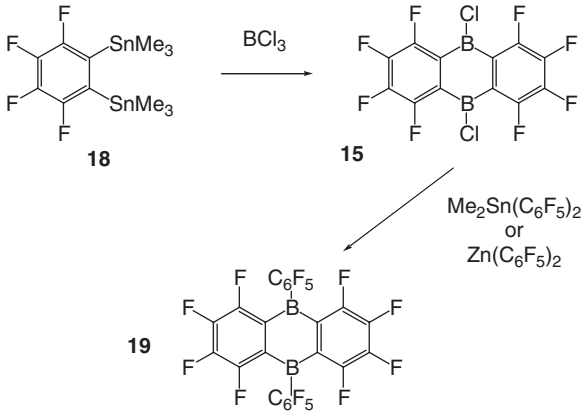

SCHEME 9.

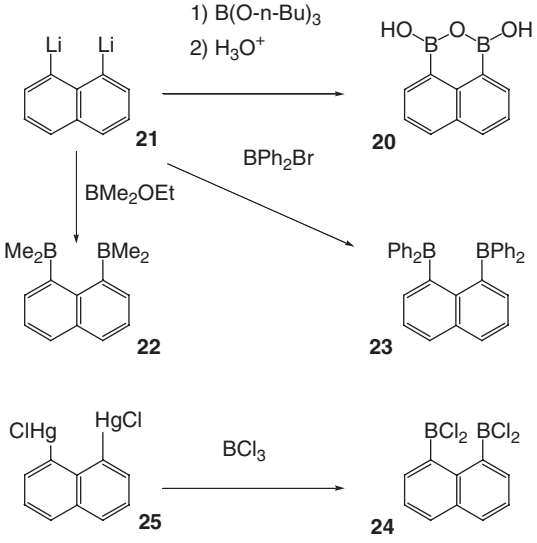

SCHEME 10.

2. 1,8-Naphthalenediyl Boron Derivatives

1,8-Diborylnaphthalenes constitute another class of rigid bidentate boranes. The first example of such derivatives were reported by Letsinger who prepared 1,8-naphthalenediboronic anhydride (**20**) from 1,8-dilithionaphthalene (**21**) and tris-*n*-butylborate followed by hydrolysis (Scheme 10).[25] While a variety of 1,8-diborylnaphthalenes are known,[17,26] only a few of them have been investigated as bidentate Lewis acids. Symmetrical examples of such compounds include 1,8-bis(dimethylboryl)naphthalene **22**,[27–29] 1,8-bis(diphenylboryl)naphthalene **23**[30] and 1,8-bis(dichloroboryl)naphthalene **24**.[31] Compounds **22** and **23** have been prepared

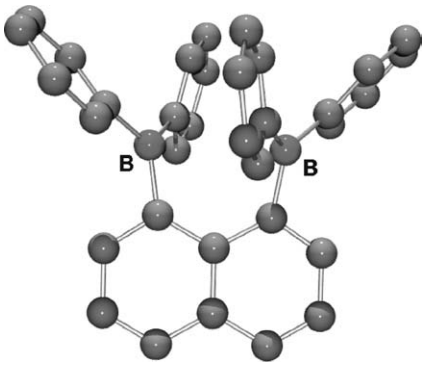

FIG. 3. Structure of the diborane **23**.

by reacting the 1,8-dilithionaphthalene with an excess of the appropriate electrophile, while the tetrachloride **24** has been synthesized by the reaction of 1,8-bis(chloromercurio)naphthalene (**25**) with BCl_3.[31]

Compound **24** is very sensitive to hydrolysis and affords the 1,8-naphthalenediboronic anhydride **20** when exposed to moisture. Compound **22**, also referred to as hydride sponge, was prepared by the reaction of 1,8-dilithionaphthalene with dimethylboron ethoxide and isolated as a pale yellow oil.[27] A metathesis reaction involving the 1,8-dilithionaphthalene and diphenylboron bromide procedure was also used to generate 1,8-bis(diphenylboryl)-naphthalene **23**.[32] The structure of this compound has been determined by X-ray diffraction (Fig. 3). As often encountered in the structure of *peri*-substituted naphthalene derivatives, the naphthalene backbone of this derivative is subjected to distortions, which result from steric repulsions occurring between the proximal boryl moieties. The non-bonding boron–boron distances are close to 3 Å, thus allowing for the occurrence of cooperative effects. The structure of this diborane has been computationally optimized using Density Functional Theory (DFT) methods (B3LYP, 6-31 + G* for the boron centers, 6-31G for all other atoms). The optimized geometry is close to that observed in the crystal. It is interesting to note that the Lowest Unoccupied Molecular Orbital (LUMO) bears strong contribution from the boron p_z orbitals which point toward one another (Fig. 4).

Unsymmetrically *peri*-substituted 1,8-diborylnaphthalenes have also been prepared and investigated as bidentate Lewis acids. The synthesis of such derivatives is non-trivial because it necessitates the sequential introduction of boryl moieties at the *peri*-positions of the naphthalene backbone. Thus far, this strategy has only been applied successfully on few occasions. The reaction of 1,8-dilithionaphthalene-tmeda with one equivalent of dimesitylboronfluoride results in the formation of dimesityl-1,8-naphthalenediylborate **26** as a monoborylated naphthalene product (Scheme 11).[32] This derivative is the only example of an anionic 1,8-boron-bridged naphthalene derivative. However, it is important to note that Siebert has reported the synthesis and structure of a neutral 1,8-boron-bridged naphthalene derivative which features a (di-*iso*-propylamino)boron moiety bridging the two naphthalene *peri*-carbon atoms.[33] A single-crystal analysis carried out on **26**-$Li(py)_4$ confirmed

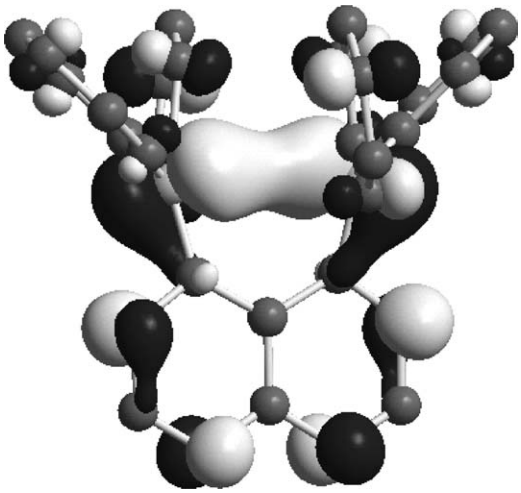

FIG. 4. LUMO of diborane **23** obtained by DFT calculation.

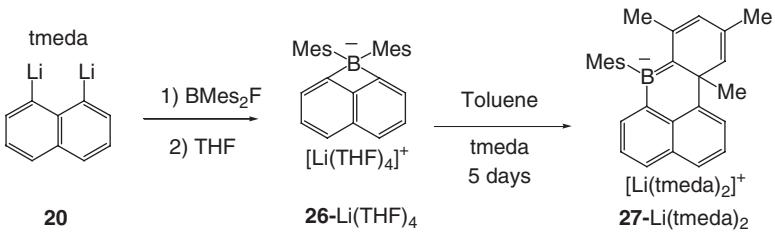

SCHEME 11.

the existence of a strained boracycle as indicated by the values of the endocyclic angles that show considerable contractions (C–B–C = 80.5°, C–C–C = 103.3°) (Fig. 5).[32] Upon standing at room temperature in toluene for an extended period of time, **26** undergoes a ring expansion reaction to afford 8,10,11a-trimethyl-7-mesityl-11a*H*-7-borata-benzo[de]anthracene (**27**).[34] This isomerization reaction allows for a relief of the ring strain present in **26** at the expense of the aromaticity of one of the mesityl substituents. As shown by its crystal structure, compound **27** constitutes a rare example of a bora-alkene and features a carbon–boron double bond of 1.475(6) Å incorporated in a conjugated hexa-1-boratriene system (Fig. 6).

26-Li(THF)$_4$ undergoes ring opening reactions in the presence of various electrophiles including trimethylstannyl chloride[35] and diorganylboronhalides.[32,34] Thus, reactions with dimethylboron bromide, diphenylboron bromide and trimethylstannyl chloride lead to high yields of 1-(dimesitylboryl)-8-(dimethylboryl)naphthalene (**28**),[35] 1-(dimesitylboryl)-8-(diphenylboryl)naphthalene (**29**),[32] and 1-(dimesitylboryl)-8-(trimethylstannyl)naphthalene (**30**),[32] respectively (Scheme 12). By contrast, reaction of **26** with dimesitylboronfluoride does not lead to the formation of 1,8-bis(dimesitylboryl)naphthalene, which likely results from the high steric demand of the mesityl substituents. Both **28** and **29** have been fully

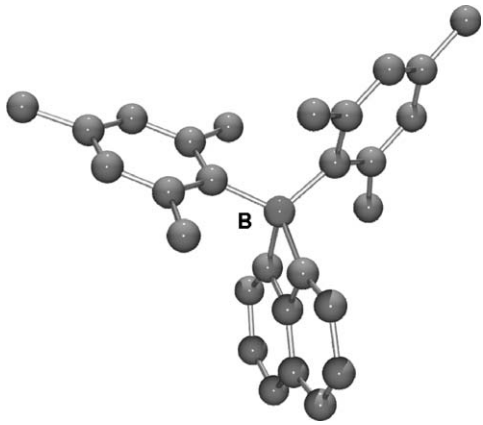

FIG. 5. Structure of the borate anion **26**.

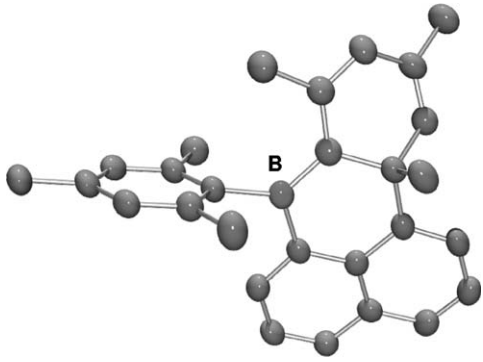

FIG. 6. Structure of the borataalkene anion **27**.

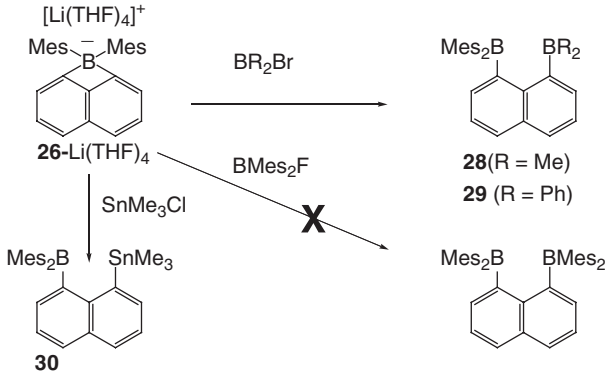

SCHEME 12.

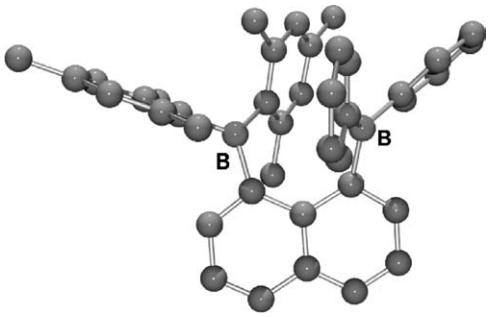

FIG. 7. Structure of the diborane **29**.

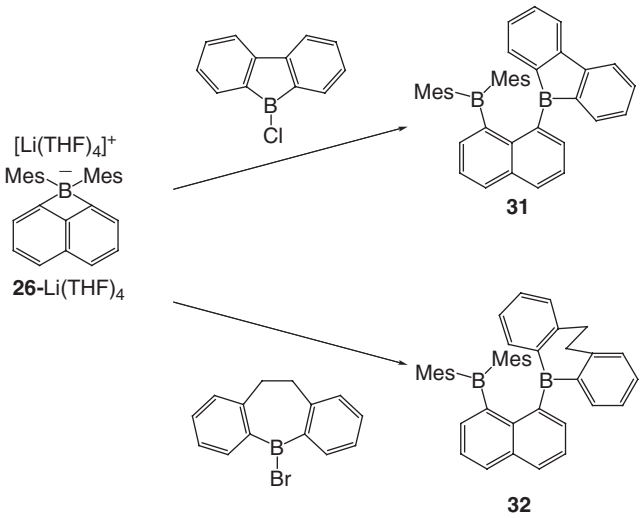

SCHEME 13.

characterized. The crystal structure of **29** indicates that the boron centers are separated by 3.35 Å (Fig. 7). This separation is greater than that observed in **23** and results from the increased steric demand of the boron substituents.

In order to allow for a closer approach of the boron centers, the introduction of flat cyclic boryl moieties with reduced steric hindrance has also been pursued. Thus, the reaction of **26** with 9-chloro-9-borafluorene and 5-bromo-10,11-dihydrodibenzo[b,f]borepin resulted in the formation of diboranes **31** and **32** which bear two different boryl moieties at the *peri*-positions of naphthalene (Scheme 13).[34] These diboranes have been characterized by multinuclear NMR spectroscopy and X-ray single-crystal analysis. In **31**, the boron center of the borafluorenyl moiety is π-coordinated by the *ipso*-carbon of a mesityl group with which it forms a contact of 2.730(3) Å (Fig. 8). As a result of this interaction, the boron center involved in this contact is slightly pyramidalized ($\Sigma_{angle} = 355.7^{\circ}$). In the case of **32** (Fig. 9), the distance between the boron center of the boracylic moiety and the *ipso*-carbon of

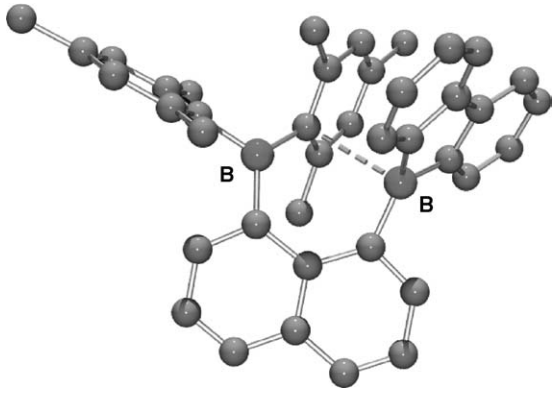

FIG. 8. Structure of the diborane **31** showing the short C_{ipso}–B interaction.

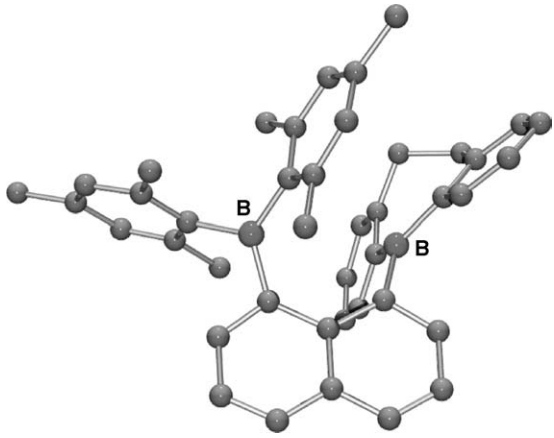

FIG. 9. Structure of the diborane **32**.

the mesityl group is much longer (3.15 Å) indicating a weaker interaction. The differences observed in the structures of **31** and **32** substantiate the increased Lewis acidity of the boron center of **31**. This increased acidity results from the anti-aromatic character of the 9-borafluorenyl moiety, which favors coordination events that remove the boron p-orbital from conjugation.[36,37] The relief of strain energy in the borole ring upon boron pyramidalization also contributes to the increased acidity of the B(2) boron center.[37]

In an effort to prepare bidentate boranes as colorimetric anion sensors, the incorporation of chromophoric boron moieties has also received attention. Reaction of 10-bromo-9-thia-10-boranthracene **33** with dimesityl-1,8-naphthalenediylborate **26** affords diborane **34** (Scheme 14).[38] This bright yellow diborane is soluble in chloroform, THF and pyridine. It has been fully characterized but its X-ray crystal structure could not be determined experimentally. Its structure was computationally optimized using DFT methods (B3LYP, 6-31 + G* for the boron and sulfur

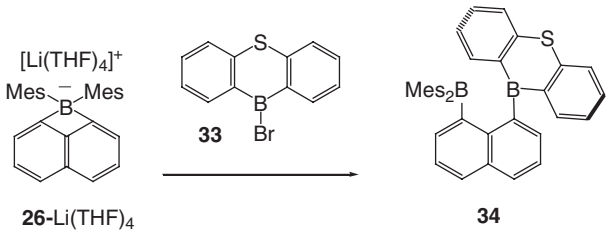

SCHEME 14.

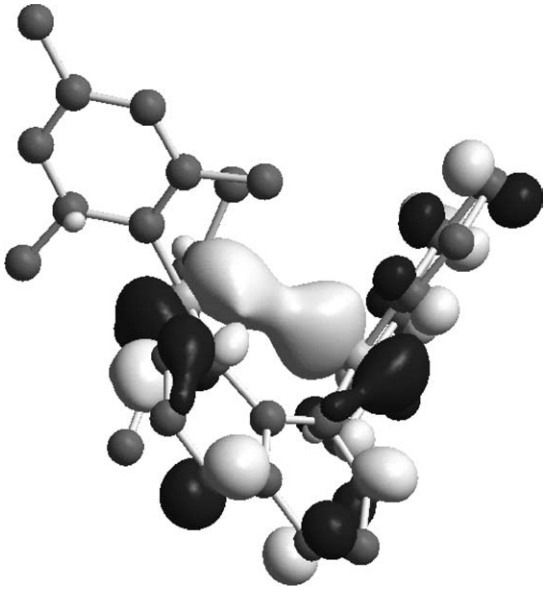

FIG. 10. DFT orbital picture showing the in-phase interaction of boron's empty p AO in the LUMO of **34**.

centers and 6-31G for all other atoms, Fig. 10). The optimized geometry is close to that observed for other diboranes bearing a dimesitylboryl group.[32,34] Most importantly, examination of the DFT orbitals reveals that the boron p_z orbitals contribute to the LUMO and are oriented toward one another in a transannular fashion as observed for 1,8-bis(diphenylboryl)naphthalene.

The UV–Vis spectrum of **34** features a broad band centered at 363 nm, $\varepsilon = 17{,}400\,\mathrm{mol^{-1}\,cm^{-1}}$. As indicated by a time-dependent DFT calculation, electronic excitations from the Highest Occupied Molecular Orbital (HOMO), HOMO-1 and HOMO-2 to the LUMO are the major contributors to this broad band.

Naphthalene-based bifunctional Lewis acids that involve boron and a heavier group 13 element have also been prepared starting from the boron/tin derivative **30** (Scheme 15).[35] Thus, the transmetalation reaction of **30** with gallium trichloride or indium trichloride in tetrahydrofuran (THF) results in high yields of 1-(dichlorogallium)-8-(dimesitylboron)naphthalenediyl **35** and 1-(dichloroindium)-8-(dimesitylboron)

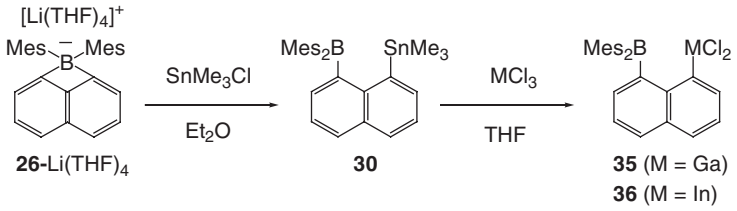

SCHEME 15.

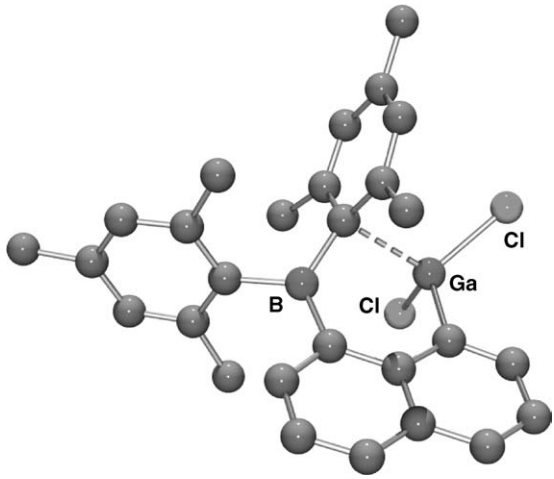

FIG. 11. Structure of **35** showing the short C_{ipso}–Ga interaction.

naphthalenediyl **36**. These boron/gallium and boron/indium heteronuclear bidentate Lewis acids have been characterized by multinuclear NMR, elemental analysis, and X-ray single-crystal analysis. Owing to the presence of a short contact between the *ipso*-carbon of a mesityl group and the heavy group 13 element (C_{ipso}–Ga = 2.28 Å, C_{ipso}–In = 2.44 Å), compounds **35** and **36** are best described as intramolecular π-arene complexes and were the first example of such complexes (Fig. 11).[39] As shown by ^{1}H and ^{13}C NMR spectroscopy, this π-interaction subsists in solution. For example, the methyl groups of the mesityl substituents give rise to six distinct resonances. Moreover, the ^{13}C NMR of the mesityl *ipso*-carbon atom coordinated to the heavy group 13 element (δ = 120.0 for **35** and 125.2 for **36**) is shifted to high field when compared to trimesitylboron (δ = 144.8 ppm) providing further proof for the existence of the π-interaction in solution.

B. *Aluminum, Gallium and Indium Polydentate Lewis Acids*

In comparison to their boron analogs, polydentate Lewis acids containing the heavier main group elements are generally scarce. This state of affairs certainly

reflects the synthetic difficulties that might be encountered in the design and preparation of such systems which typically exhibit high air and moisture sensitivity.

1. *Ortho*-Phenylene Aluminum, Gallium and Indium Derivatives

We note that while tin reagents have often been employed for the organoboron halides,[19,20,23,24] the use of organostannanes as starting materials can also be applied to the synthesis of heavier group 13 derivatives. In the context of polyfunctional Lewis acid chemistry, this type of reaction has been employed for the preparation of *ortho*-phenylene aluminum derivatives. Thus, the reaction of 1,2-bis(trimethylstannyl)benzene **7** with dimethylaluminum chloride, methylaluminum dichloride or aluminum trichloride affords 1,2-bis(dimethylaluminum)phenylene **37**, 1,2-bis(chloro(methyl)aluminum)phenylene **38** and 1,2-bis(dichloroaluminum)phenylene **39**, respectively (Scheme 16).[40] Unfortunately, these compounds could not be crystallized and their identities have been inferred from NMR data only. In the case of **39**, the aluminum derivative could not be separated from trimethyltin chloride with which it reportedly forms a polymeric ion pair consisting of trimethylstannyl cations and bis(trichloroaluminate) anions **40**.

9,10-Dihydro-9,10-dialaanthracene derivatives have also been reported. As shown by Bickelhaupt, the reaction of *ortho*-phenylenemagnesium **41** with $MeAlCl_2$ leads to the formation of 9,10-dimethyl-9,10-dihydro-9,10-dialaanthracene as a bis(THF) adduct (**42**, Scheme 17).[41] When taken out of solution, crystals of this adduct proved unstable toward THF loss so that the crystal structure could not be determined.

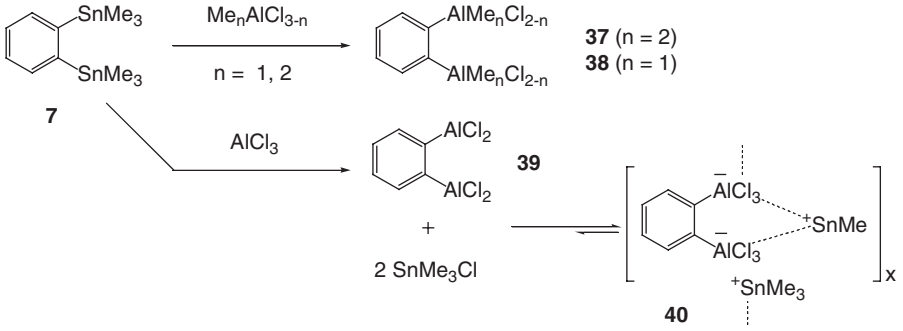

SCHEME 16.

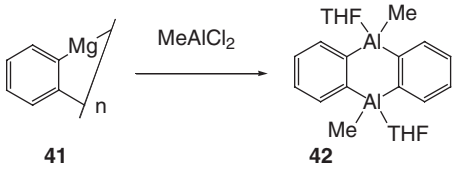

SCHEME 17.

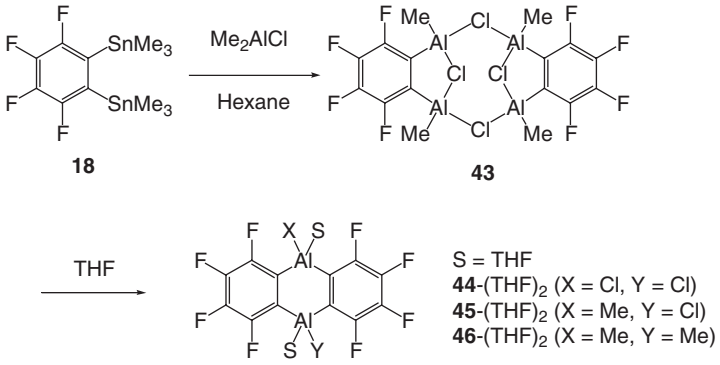

SCHEME 18.

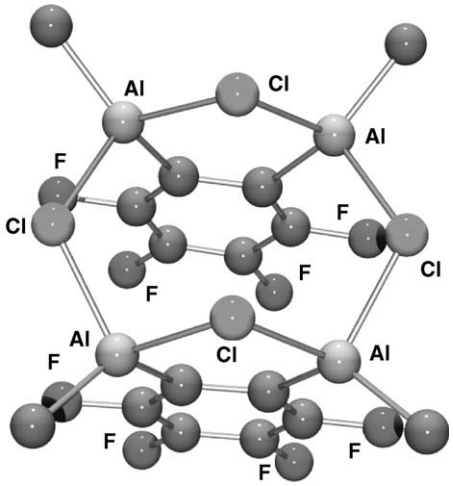

FIG. 12. Structure of **43**.

Efforts to prepare fluorinated analogs of these derivatives have also been made. When 1,2-bis(trimethylstannyl)tetrafluorobenzene (**18**) is allowed to react with dimethylaluminum chloride in hexane, the reaction follows a slightly different course than that observed in the case of 1,2-bis(trimethylstannyl)benzene (**18**) and affords 1,2-bis(chloromethylalumino)tetrafluorobenzene (**43**, Scheme 18). As indicated by X-ray analysis, the molecule has two 1,2-bis(alumino)tetrafluorobenzene units which are connected through an eight-membered $(AlCl)_4$ ring (Fig. 12).[42] This compound is not stable when exposed to polar solvents such as THF which induces a ring closure reaction to produce a mixture of 9(X),10(Y)-9,10-dialaoctafluoroanthracene species as bis(THF) adducts (X = Y = Cl (**44**), X = Cl, Y = CH_3 (**45**), X = Y = CH_3 (**46**)) as indicated by X-ray crystallography (Fig. 13) and ^{19}F NMR spectroscopy carried out on the co-crystal of the three derivatives.[43] This cyclization reaction is similar to that observed in the case of 1,2-bis

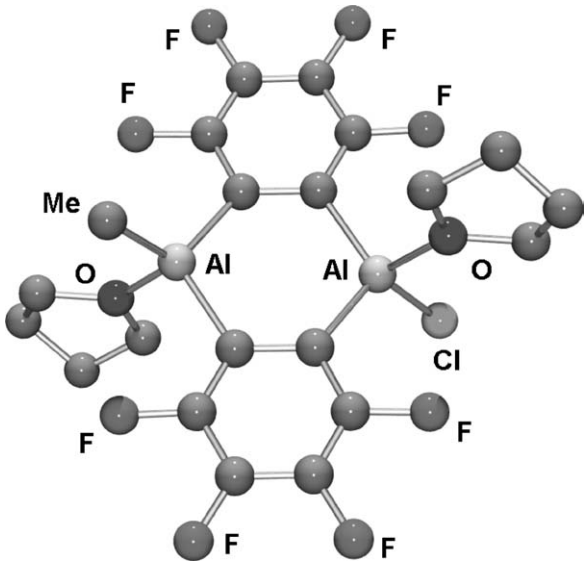

FIG. 13. Structure of the dialuminum derivative **45**-$(THF)_2$.

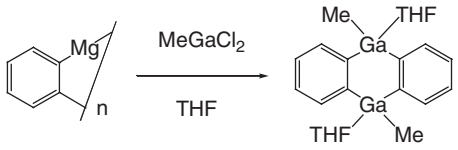

41 **47**-$(THF)_2$

SCHEME 19.

(dichloroboryl)tetrafluorobenzene (**14**) which promptly converts into 9,10-dichloro-9,10-dihydro-9,10-diboraoctafluoroanthracene (**15**). Both aluminum atoms of **44**–**46** are in a distorted tetrahedral environment composed of the *ipso*-carbon atoms of the perfluorinated aromatic ring, the oxygen atom of a THF molecule and the disordered methyl group/chloride ion.

The same strategy has also been applied to the preparation of the corresponding digallium system.[41] Reaction of *o*-phenylene magnesium (**41**) and $MeGaCl_2$ in THF affords 9,10-dimethyl-9,10-dihydro-9,10-digallaanthracene (**47**) as a bis(THF) adduct (Scheme 19, Fig. 14). The THF ligands could be readily displaced by pyridine to afford the corresponding bis(pyridine) adduct. The latter has been fully characterized. Its structure indicates the presence of two tetrahedrally coordinated gallium centers.[41] In this regard, its structure is comparable to that of the 9,10-dialaanthracene-bis(THF) adducts **44**–**46**.

Ortho-phenylene-diindium complexes constitute a well-developed class of derivatives. The indium analog of **42** and **47** has been prepared by the reaction of *o*-phenylene magnesium with methyl indium dichloride.[43] The same reaction carried

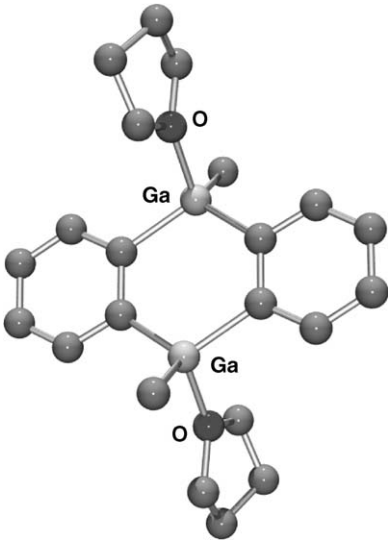

FIG. 14. Structure of **47**-$(THF)_2$.

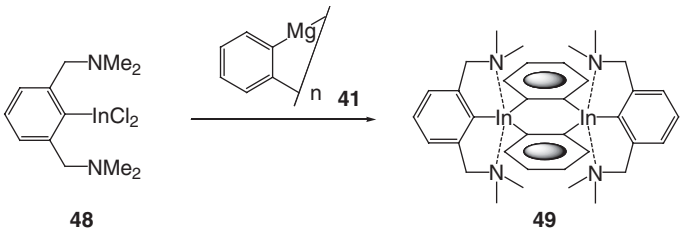

48 **49**

SCHEME 20.

out with 2,6-bis(dimethylaminomethyl)phenylindium dichloride (**48**) instead of methyl indium dichloride also affords the corresponding bimetallic complex **49** which could be isolated in fairly high yield (Scheme 20).[44] Its crystal structure confirms that each indium center is pentacoordinated (Fig. 15). Because of the constraints imposed by the ligand structure, the coordination geometry of each indium center deviates from an ideal trigonal pyramidal arrangement. The most noticeable distortion affects the N-In-N angle [143.5(2)°] which is much smaller than the expected 180°.

A series of *ortho*-phenylene-diindium complexes have also been prepared by transmetalation of the corresponding poly-mercury derivatives with indium(I) halides. Such transmetalation reactions are very advantageous; they proceed smoothly and yield mercury metal as a sole byproduct, which greatly facilitates the isolation of the target molecule.[45,46] Trimeric *ortho*-phenylene-mercury (**50**)[47] is well-known to undergo such transmetalation. The preparation of *ortho*-dilithiobenzene, tetrameric *ortho*-phenylenemagnesium[48] and dimeric *ortho*-phenylenezinc[49] are representative examples that demonstrate the importance of this synthetic method. In

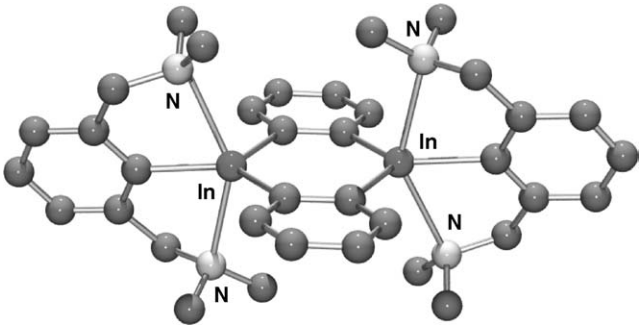

FIG. 15. Structure of **49**.

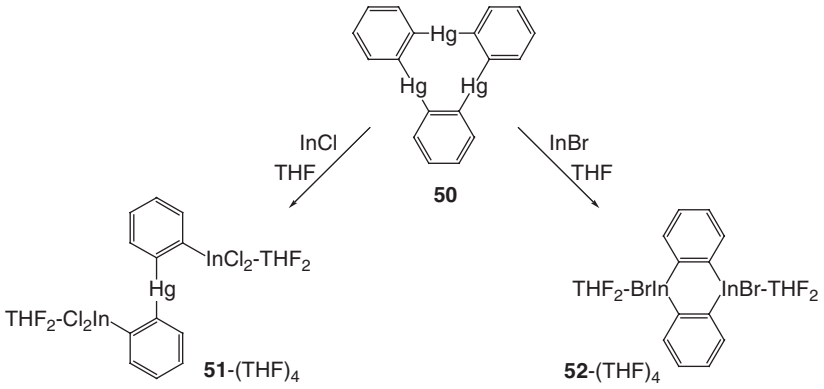

SCHEME 21.

contrast to those clean transmetalations, the equimolar reaction of InCl with **50** takes an unexpected course and yields the heteronuclear trifunctional Lewis-acid **51** which has been isolated as a *tetrakis*(THF) adduct (Scheme 21).[50]

The structure of **51**-$(THF)_4$ consists of two *ortho*-phenylene indium dichloride moieties linked through a central Hg atom, giving rise to a pseudo-centric core (Fig. 16). The mercury atom is, as expected, linearly coordinated. Each indium atom is penta-coordinated in a trigonal–bipyramidal fashion with two THF molecules at the axial positions and two chloride ligands as well as a phenylene ring at the equatorial sites.

Unlike InCl, InBr reacts cleanly with **50** in THF to afford the *tetrakis*(THF) adducts of 9,10-dibromo-9,10-dihydro-9,10-diindaanthracene **52** in high yield (Scheme 21).[51] Compound **52** crystallizes as a *tetrakis*(THF) adduct with two independent molecules in the unit cell. Both molecules are centrosymmetric (Fig. 17). Each indium atom is pentacoordinated in a trigonal–bipyramidal fashion, with two molecules of THF at the axial positions. Upon standing in a dry inert atmosphere, **52**-$(THF)_4$ readily loses two equivalents of THF to afford **52**-$(THF)_2$ as indicated by elemental analysis.

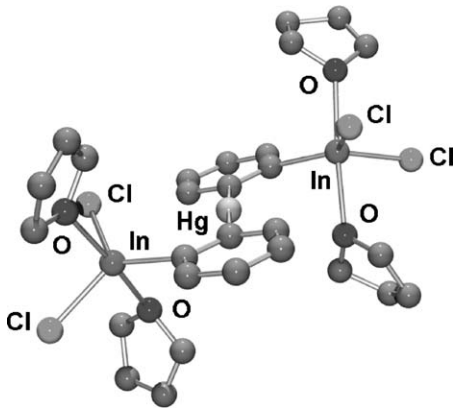

FIG. 16. Structure of **52**-$(THF)_4$.

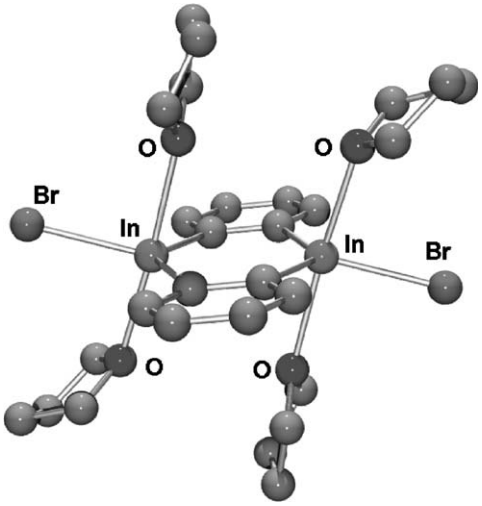

FIG. 17. Structure of **53**-$(THF)_4$.

In order to increase the Lewis acidity of the indium centers in compounds such as **52**, the preparation of derivatives that incorporate a tetrafluorophenylene backbone has also been pursued. 1,2-Bis(halomercurio)tetrafluorobenzene (halide = chloride (**53**) or bromide (**54**)) reacts with two equivalents of the corresponding indium(I) halide in THF at 25 °C to afford the *tetrakis*(THF) adduct of the respective 9,10-dihalo-9,10-dihydro-9,10-diinda-octafluoroanthracene (halide = chloride (**55**) or bromide (**56**)) (Scheme 22).[52] Compound **56** is also prepared by the reaction of $(o\text{-}C_6F_4Hg)_3$ (**4**) with InBr in refluxing toluene followed by treatment with THF. The formation of the diindacycles **55** and **56** in the reaction of **53** and **54** with two equivalents of the corresponding indium(I) halide is surprising since, in principle, bis(indiumdihalide) complexes would be the expected products. This cyclization

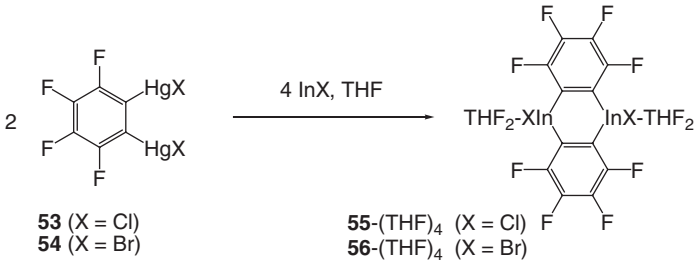

SCHEME 22.

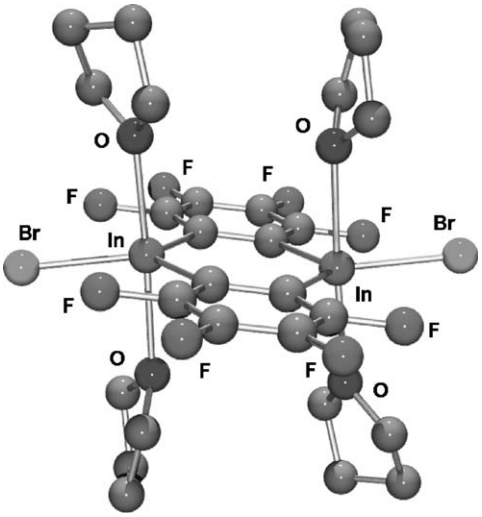

FIG. 18. Structure of **56**-$(THF)_4$.

reaction is reminiscent of that encountered in the case of the tetrafluorophenylene dialuminum complex **43** which also undergoes a ring closure reaction in the presence of donor solvents.[43] Compounds **55** and **56** form stable *tetrakis*(THF) adducts which do not lose THF under normal conditions. Thus, their behavior is different from that of **52**-$(THF)_4$, which was found to spontaneously lose two THF molecules at room temperature in an inert atmosphere. This reflects an increase in the Lewis acidity of the indium centers which can be associated with the presence of perfluorinated ligands. Structural studies have been undertaken on several adducts of these diindacycles (Fig. 18). While the structures resemble that of the perprotio-analog, the In–O bonds of **56**-$(THF)_4$ are shorter by 0.08 Å than those of **52**-$(THF)_4$ thus also reflecting the increased Lewis acidity of the indium centers.

2. 1,8-Naphthalenediyl Gallium and Indium Derivatives

While no aluminum derivatives featuring the 1,8-naphthalenediyl backbone have ever been isolated, several gallium species have been successfully prepared. With the

exception of the mixed boron/gallium derivative **35** motioned above,[35] 1,8-naphthalenediyl gallium derivatives have been prepared by transmetallation of 1,8-bis(trimethylstannyl)naphthalene **57** with $GaCl_3$.[53,54] Under strictly anhydrous conditions and upon heating for 6 h at 65 °C, the reaction of **57** with $GaCl_3$ in toluene leads to high yields of bis(μ-1,8-naphthalenediyl)(μ-chloride)methyltin(IV)chlorogallium(III) (**58**) (Scheme 23).[53] Compound **58** adopts an unusual structure in that it features a folded eight-membered dimetallacycle in which the two metals are bridged by a chloride ligand (Fig. 19). Lowering the reaction temperature to −25 °C, leads to a decrease in the yield of **58** and the appearance of a new product which has been identified as an adduct formed between bis(μ-1,8-naphthalenediyl)bis(gallium(III)chloride) and trimethyltin chloride [**59**-$Me_3SnCl]_2$.[54] The presence of a digallacycle unit in **59** indicates that the complete

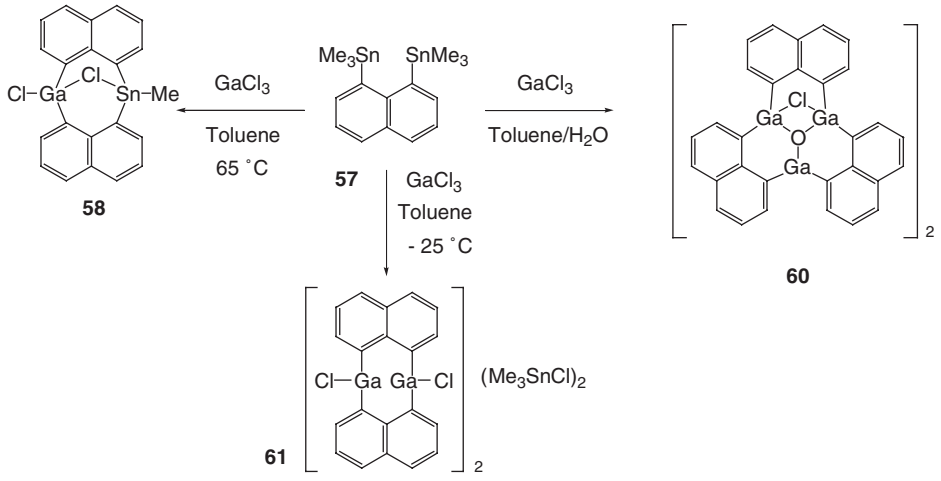

Scheme 23.

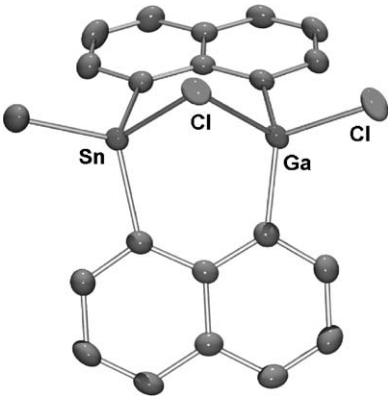

Fig. 19. Structure of **59**.

substitution of the stannyl groups of **57** is possible. As shown by ^{1}H NMR spectroscopy, [**59**-$Me_3SnCl]_2$ does not retain its structure in pyridine solutions but rather dissociates to give Me_3SnCl-py and solvent-stabilized molecules of the digallacyle. In the presence of traces of water, the room temperature transmetallation reaction leads to a low yield of a third derivative **60** which consists of a 12-membered macrocycle containing three gallium atoms linked by 1,8-naphthalenediyl ligands and arranged about a central oxygen atom. The charge balance of **60** is achieved by the presence of a chloride atom that bridges two of the gallium centers. In the crystal, **60** exists as a dimer wherein the monomers are bridged *via* a Ga–O–Ga–O four-membered ring (Fig. 20). The three gallium atoms are separated by approximately 3 Å and form a nearly equilateral triangle.

In an effort to extend the use of organostannanes as starting materials for organoindium species, the reaction of **57** with $InCl_3$ in acetonitrile has been investigated (Scheme 24).[55] Remarkably, this reaction leads to the formation of the diindacycle bis(μ-1,8-naphthalenediyl)bis(chloroindium(III)) (**61**) which could be isolated as a *tetrakis*(pyridine) adduct by subsequent addition of pyridine. It is interesting to note that the *tetrakis*(THF) adduct of this diindacycle has been isolated in trace amounts in the reaction between InCl and 1,8-bis(chloromercurio)naphthalene (*vide infra*). The synthesis that uses the distannyl derivative **57** as a starting material appears to be a worthy alternative since it affords **61** in a 65% yield. Attempts to prepare a non-cyclic 1,8-(diindium)naphthalenediyl complex

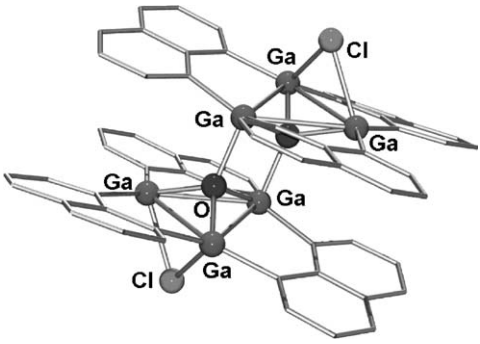

FIG. 20. Structure of **60**.

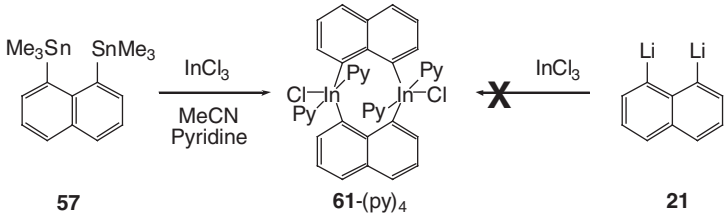

SCHEME 24.

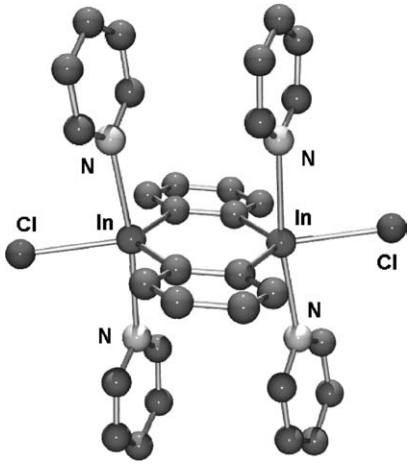

FIG. 21. Structure of **60**-$(py)_4$.

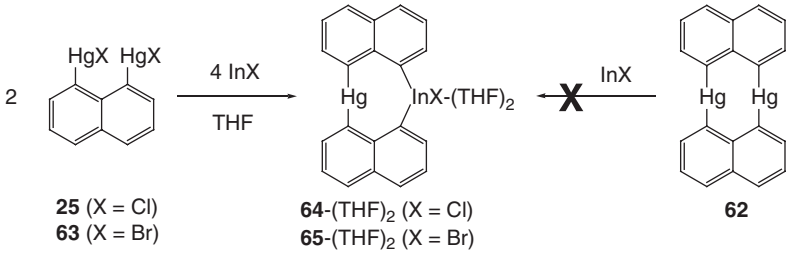

SCHEME 25.

have not been successful. Even in the presence of an excess of $InCl_3$, the reaction depicted in Scheme 24 always affords **61** as the only identifiable product. Attempts to prepare **61** by metathesis have also been pursued. As shown by ^1H NMR spectroscopy, treatment of $InCl_3$ with an equimolar amount of the 1,8-dilithionaphthalene in Et_2O affords a 25% yield of the diindacycle. The indium centers of **61** are pentacoordinated in an approximate trigonal–bipyramidal fashion with pyridine ligands occupying the axial sites (Fig. 21). The indium coordination sphere undergoes strong distortions as shown by the value of the C–In–C angle (153.3°).

As for the synthesis of *ortho*-phenylene indium complexes, the transmetallation reactions of organomercurials with indium(I) halides have also been considered for the preparation of 1,8-naphthalenediyl diindium complexes. While the dimercuracycle **62** fails to react with InBr, 1,8-bis(chloromercurio)naphthalene (**25**) and 1,8-bis(bromomercurio)naphthalene (**63**) react with their respective indium(I) halides to yield the mercura-indacycles **64** and **65** (Scheme 25) which have been isolated as bis(THF) adducts.[56] The indium center of **65**-$(THF)_2$ is penta-coordinated and

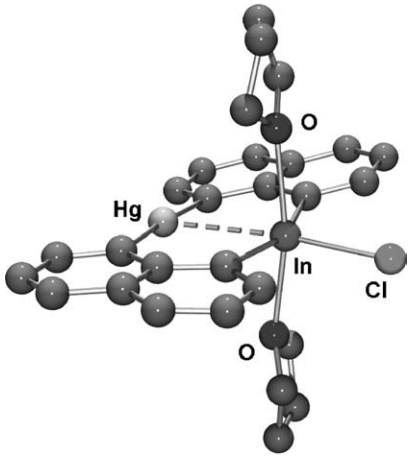

FIG. 22. Structure of **64**-$(THF)_2$.

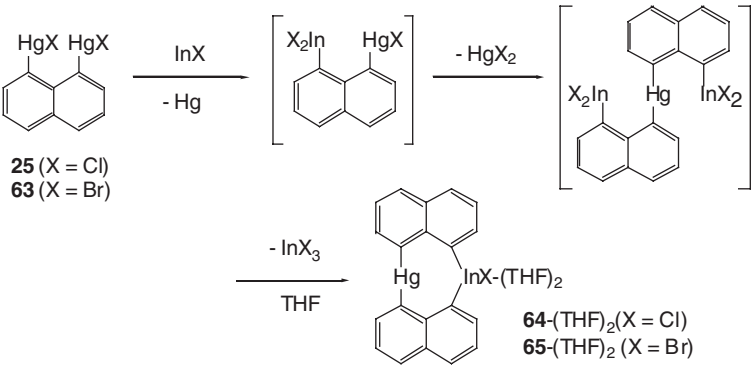

SCHEME 26.

adopts a distorted trigonal–bipyramidal coordination sphere (Fig. 22). The main deviation from an ideal geometry occurs in the equatorial plane as indicated by the large C–In–C angles (150.9°). The most noticeable feature in the structure of **65**-$(THF)_2$ is the very short transannular Hg···In distance of 3.03 Å. There are no data available for Hg–In bonds. However, this distance is shorter than the sum of the van-der-Waals radii of the two metals (3.6 Å),[57] close to the sum of the metallic radii (3.12 Å) and just slightly greater than the sum of the Pauling covalent radii (2.94 Å).

The formation of **64** and **65** most probably involves transmetallation of only one mercury center followed by a series of ligand exchange processes leading to a ring closure as shown in Scheme 26. Considering the steric and geometrical constraints in **64** and **65**, such ring closure reactions are remarkable and seem to parallel those involved in the formation of the gallium/tin derivative **58**.[53]

III
INTERACTION WITH LEWIS BASIC SUBSTRATES

A. *Complexation of Organic Substrates*

1. Complexation of Organic Carbonyls

Several reports demonstrate that polyfunctional Lewis acids are valuable catalysts for reactions involving organic carbonyls such as aldehydes and ketones.[58,59] It has been suggested that the high catalytic activity observed in these reactions is a result of the ability of the bifunctional Lewis acid to chelate the carbonyl oxygen atom. While the double coordination of formamides has been investigated in detail,[8,10] the knowledge gathered on the chelation of ketones or aldehydes is somewhat limited.[60–62] The Lewis acidic properties of the tetrachlorodiborane **24** have been investigated in solution. In addition to catalyzing Diels–Alder reactions,[63] this derivative forms identifiable complexes with dimethylpyranone (Scheme 27).[64] Thus, upon addition of one equivalent of dimethylpyranone, formation of the 1:1 complex **24**-(μ_2-dimethylpyranone) (**66**) is observed. The identity of this complex has been confirmed by IR and ^{1}H NMR spectroscopies, which are in agreement with the simultaneous coordination of the carbonyl functionality to both boron centers. Comparison of the IR stretching frequencies and ^{1}H NMR chemical shifts suggest that the Lewis-acidic strength of **24** is close to that of BCl_3. The addition of one more equivalent of dimethylpyranone leads to the formation of a 2:1 complex in which there is coordination of one ketone per boron center (**67**).

2. Complexation of Diazines

9,10-Dibromo-9,10-dihydro-9,10-diindaanthracene (**52**) contains two electrophilic indium centers positioned at the opposite apexes of a flat six-membered ring (Scheme 28). The specific arrangement of the two indium centers in this molecule indicates that the cooperative binding of bifunctional bases with adjacent basic sites might be attainable.

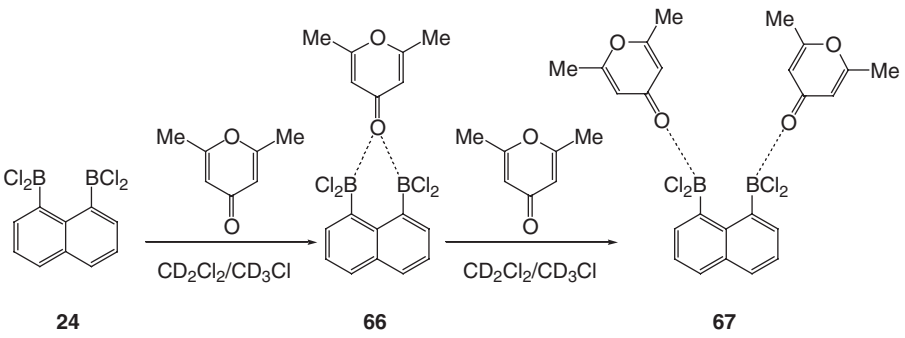

Scheme 27.

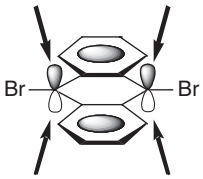

52

SCHEME 28.

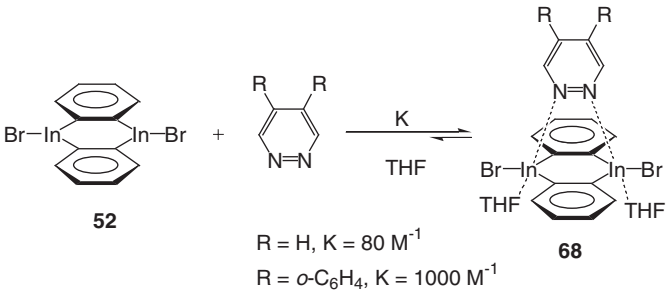

52 **68**

SCHEME 29.

With this in mind, the coordination chemistry of **52** with different diazine structural isomers was investigated.[65] There were no detectable changes in the ^{1}H NMR spectrum of **52** in a THF-d_8 solution when either pyrazine or pyrimidine were added in 1:1 or 1:2 molar ratios, which suggested that only weak interactions might occur between **52** and these bases. In contrast, incremental addition of pyridazine or phthalazine to a THF-d_8 solution of **52** at 25 °C resulted in an upfield shift of the aromatic ^{1}H NMR resonances of the diindacycle **52** thus reflecting the formation of complexes between **52** and the 1,2-diazines. Analysis of the tritration data clearly indicated the formation of 1:1 Lewis acid–diazine complexes **52**-pyridazine-$(THF)_2$ and **52**-phthalazine-$(THF)_2$ whose stability constants are equal to 80 ($\pm$10) and 1000 ($\pm$150) M^{-1}, respectively (Scheme 29). These data, as a whole, indicate that **52** is a selective receptor for 1,2-diazines.

While the 1:1 complex **52**-phthalazine-$(THF)_2$ seems to be the preferred species in solution, pale yellow crystals of the less soluble 1:2 complex **52**-$(phthalazine)_2$-(THF) (**68**) spontaneously formed from a saturated THF solution containing equimolar amounts of **52** and phthalazine. As shown in Fig. 23, the diindacycle acts as a ditopic receptor for one phthalazine molecule. Each indium atom adopts a trigonal–bipyramidal coordination geometry. The two nitrogen atoms of the chelated phthalazine molecule occupy one of the axial sites of each indium center. The coordination sphere of the indium atoms is completed by axial ligation of a THF or phthalazine molecule. These results indicate that, as a result of subtle structural variations, the indium p-orbitals of **52** can be brought to converge thus allowing chelation of bifunctional bases with adjacent electrophilic centers.

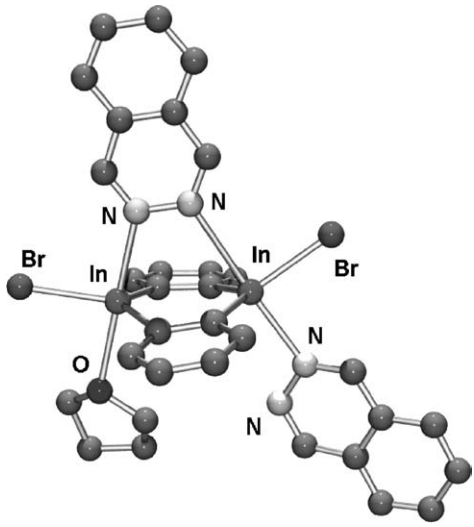

FIG. 23. Structure of **68**.

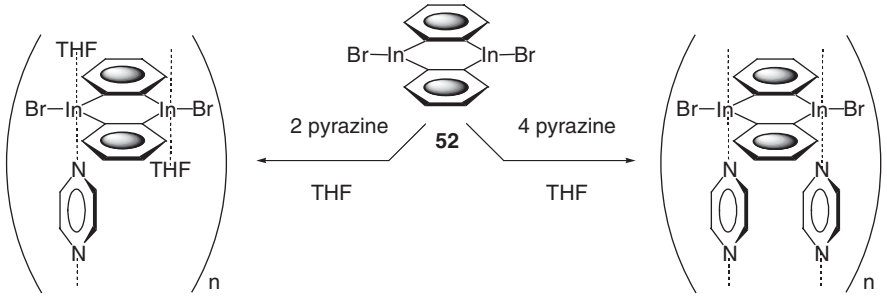

69 **70**

SCHEME 30.

Although only weak association takes place between compound **52** and pyrazine in solution, slow cooling of a THF solution of **52** containing one or two equivalents of pyrazine results in the crystallization of polymeric [**52**-$(THF)_2$-pyrazine]$_n$ (**69**) and [**52**-pyrazine$_2$]$_n$ (**70**) (Scheme 30).[66] In **69**, the diindacyclic part of the complex is planar within experimental error (Fig. 24). Each indium atom is in a trigonal–bipyramidal coordination geometry. The axial positions are unsymmetrically occupied by one THF and one pyrazine molecule, respectively. The infinite chains run parallel to one another and do not form any short inter-chain contacts. The monomeric units [**52**-$(THF)_2$-pyrazine] are linked through a single In–N linkage. All diindacycles are parallel to one another. In turn, chains of **69** are reminiscent of stairs in which the diindacycles would constitute the steps.

The stoichiometry of the assembly of **52** with pyrazine can be conveniently controlled. When the ratio of pyrazine:**52** was increased to four, crystals of a novel

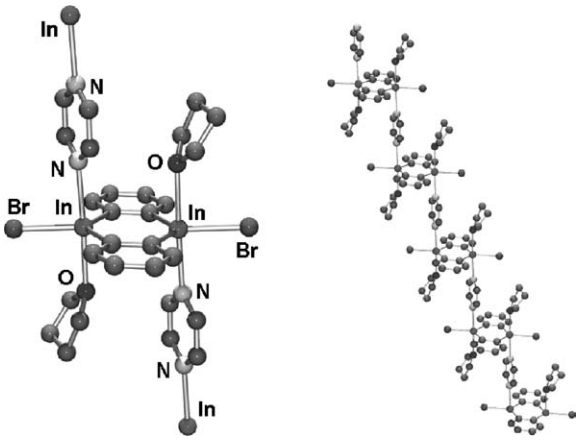

FIG. 24. Structure of **70**. Environment of a diindacyclic unit (left) and view of a portion of the coordination polymer (right).

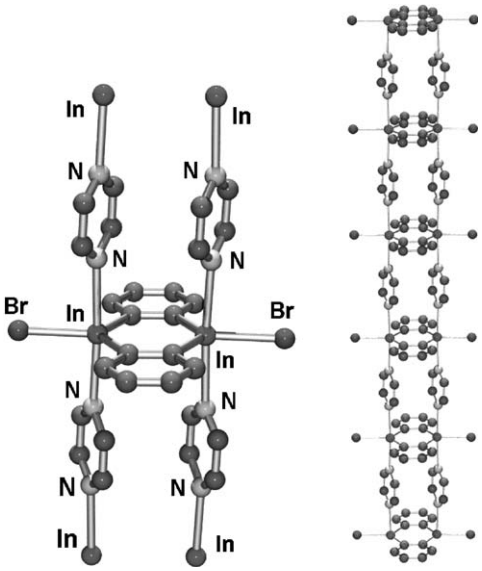

FIG. 25. Structure of **71**. Environment of a diindacyclic unit (left) and view of a portion of the coordination polymer (right). The interstitial THF molecules are not shown.

compound (**70**) spontaneously precipitated (Scheme 30). The ^{1}H NMR spectrum revealed the presence of two molecules of pyrazine and two molecules of THF per molecule of **52**. Compound **70** crystallizes with two interstitial THF molecules and consists of polymeric [**52**-(pyrazine)$_2$]$_n$ (Fig. 25). Unlike in **69**, the monomeric units of **70** are assembled through two In–N linkages. Thus, chains of **70** resemble a ladder in which the diindacycles would constitute the rungs, while the [In-pyrazine$_2$]$_n$ sequences would constitute the parallel side-pieces (Fig. 25). The space

generated between each step of the ladder approaches closely the shape of a rectangle of 7.8×3.6 Å. The interstitial THF molecules are positioned half-way between the steps and do not penetrate the cavity deeply enough to be involved in short intermolecular contacts.

B. *Complexation of Anions*

1. 1,8-Naphthalenediyl-diboranes

The strong basicity of 1,8-bis(dimethylamino)naphthalene ("proton sponge") results from the ability of this base to form a very stable conjugate acid in which the proton is simultaneously bonded to each nitrogen atom. Based on the expectation that the reverse-charge analogue of this species might exhibit unusual acidity, 1,8-bis(dimethylboryl)naphthalene (**22**) has been investigated as an anion receptor.[27,28] In the presence of potassium hydride in THF, **22** forms a kinetically and thermodynamically stable 1:1 borohydride complex ($[\mathbf{22}\text{-}\mu_2\text{-H}]^-$) which fails to reduce benzaldehyde (Fig. 26, Scheme 31). In the crystal, both boron centers participate in a 3c–2e bond with the hydride anion, this situation being responsible for the unusual Lewis acidity of **22**. It is noteworthy that the presence of a hydride bridge allows for tetrahedralization of the boron centers, which are only separated by 2.54 Å. In addition to abstracting hydrides from a variety of substrates such as monofunctional borohydride or zirconocene chloride hydride, **22** readily chelates fluoride and hydroxide anions when treated with $[Me_3SiF_2]^-[S(NMe_2)_3]^+$ and $NEt_3/H_2O/PPh_4Cl$, respectively. While complexation of small anions appears quantitative, **8** does not interact strongly with larger anions such as chloride and bromide.

By contrast, addition of PPNCl (PPN = bis(triphenylphosphineiminium)) to **24** leads to the formation of the chloride chelate complex $[\mathbf{24}\text{-}\mu_2\text{-Cl}]^-$ (Scheme 32).[31]

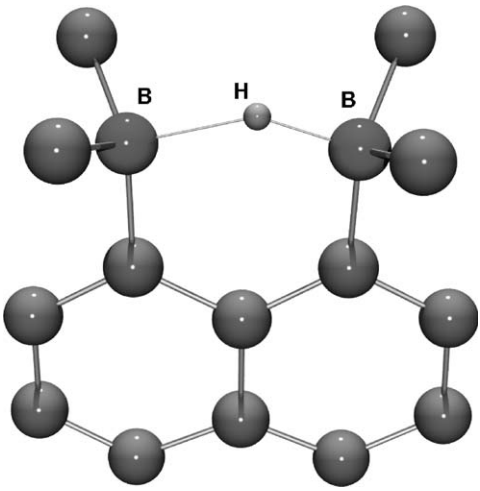

FIG. 26. Structure of $[\mathbf{22}\text{-}\mu_2\text{-H}]^-$.

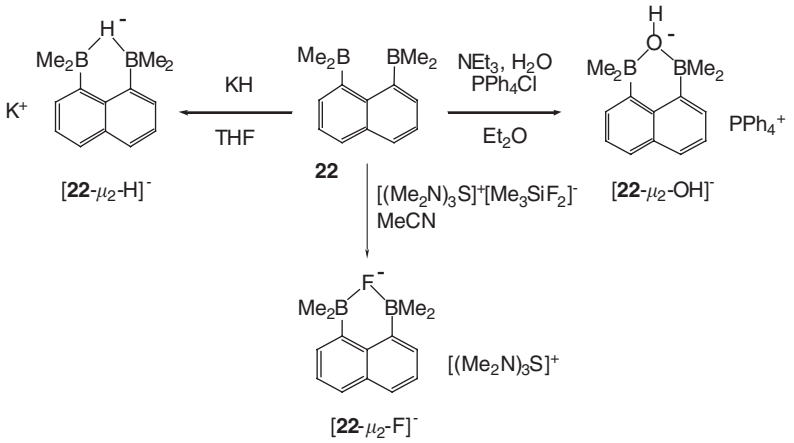

SCHEME 31.

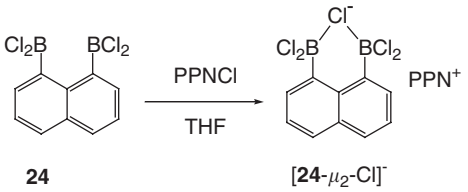

SCHEME 32.

The ^{11}B NMR spectrum of this complex exhibits a peak at 13 ppm which is not affected by the addition of 10 equivalents of $PhBCl_2$. This observation points to the greater thermodynamical stability of [**24**-μ_2-Cl]$^-$ when compared to $[PhBCl_3]^-$. The crystal structure of the $[Ph_3PNPPh_3]^+$(PPN) salt of [**24**-μ_2-Cl]$^-$ has been determined and was found to be slightly disordered (Fig. 27). The chloride anion is coordinated to both boron centers with which it forms B–Cl bonds of av. 1.92(1) Å with a B–Cl–B angle of av. 105.8°. As shown by the puckered structure of the resulting chelate six-membered ring, the small space generated between the two boron centers is at the lower limit for accepting a large anion such as a chloride.

Taking into account the importance of the fluoride anion in the treatment of osteoporosis[67] and in dental care,[68] a great deal of effort is currently devoted to the design of selective fluoride sensors.[69,70] Since 1,8-diborylnaphthalene species constitute ideal molecular recognition unit for fluoride, the bright yellow diborane **34** has been investigated as a colorimetric fluoride sensor.[38] In **34**, the boron center is incorporated in a chromophore so that its empty p-orbital strongly contributes to the LUMO of the molecule. Since the LUMO acts as the electron-accepting orbital in the transitions responsible for the yellow color of this molecule, any events leading to the disruption of the LUMO should greatly affect the absorption spectrum of compound **34** and should produce a colorimetric response. In the presence

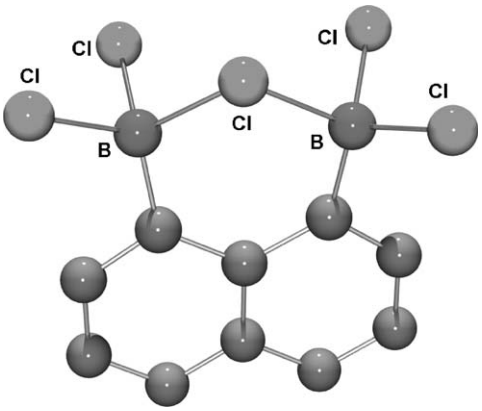

FIG. 27. Structure of [**24**-μ_2-Cl]$^-$.

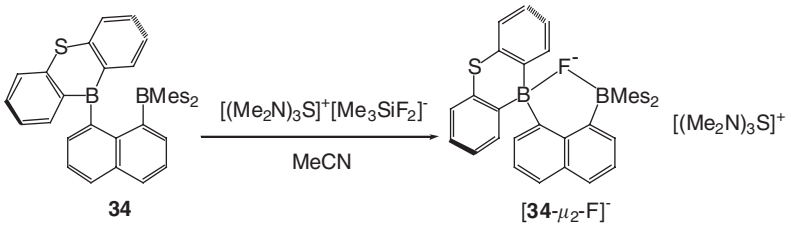

SCHEME 33.

of $[Me_3SiF_2]^-[S(NMe_2)_3]^+$ in THF, compound **34** readily complexes fluoride anions (Scheme 33). This reaction is accompanied by a rapid loss of the yellow color and affords the anionic chelate complex [**34**-μ_2-F]$^-$ which has been fully characterized. The ^{19}F NMR resonance of the bridging fluoride appears at -188 ppm. As confirmed by single-crystal X-ray analysis (Fig. 28), the fluorine atom is bound to both boron centers and forms B–F bonds of comparable lengths (F–B(1) 1.633(5) Å, F–B(2) 1.585(5) Å). The sum of the coordination angles ($\sum_{(C-B1-C)} = 347.8^o, \sum_{(C-B1-C)} = 341.2^o$) indicates that both boron centers are substantially pyramidalized.

As predicted, fluoride complexation leads to population of the LUMO of **34** and is logically accompanied by an instantaneous loss of the yellow color. Remarkably, no changes in the color of the solution or in the NMR of diborane **34** are observed in the presence of chloride, bromide or iodide anions indicating that the larger halides are not complexed. This finding corroborates earlier observations made by Katz on 1,8-bis(dimethylboryl)naphthalene (**22**).[28] Presumably, the size of the binding pocket provided by this bidentate borane can be held responsible for this selectivity. As determined by a UV–Vis titration experiment, **34** complexes fluoride anions with a binding constant of at least $5 \times 10^9\ M^{-1}$ which exceeds that observed for monofunctional borane receptors by 3–4 orders of magnitude.[70] The addition of water does not lead to decomplexation of the fluoride anion as typically observed

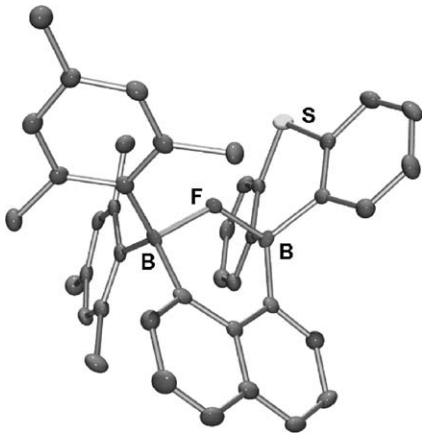

FIG. 28. Structure of [**34**-μ_2-F]$^-$.

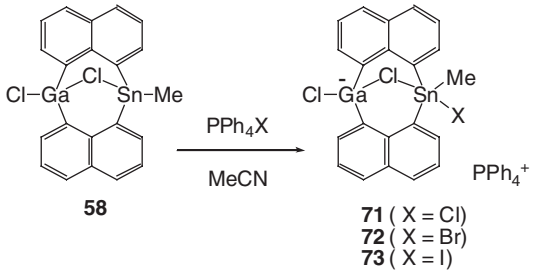

SCHEME 34.

for fluoride adducts of monofunctional boranes.[71] These differences substantiate the chelating ability of **34** which leads to the formation of a thermodynamically more stable fluoride complex.

2. 1,8-Naphthalenediyl Gallium Species

The ability of 1,8-naphthalenediyl gallium derivatives to complex anions has also been studied.[72] Treatment of bis(μ-1,8-naphthalenediyl)(μ-chloride)methyltin-chlorogallium **58** with one equivalent of tetraphenylphosphonium chloride, bromide and iodide in hot acetonitrile results, upon cooling, in the crystallization of the corresponding anionic adduct [**58**–X] $[PPh_4]^+$ (**71**, $X = Cl^-$; **72**, $X = Br^-$; **73**, $X = I^-$) (Scheme 34). The composition and structures of **71**–**73** have been confirmed by elemental analysis and single-crystal X-ray diffraction (Fig. 29). In all cases, the added halide coordinates to the tin center. Thus, unlike in **58**, the tin atom is surrounded by five ligands and adopts a distorted trigonal–bipyramidal geometry. Inspection of the structure of **71** indicates that the bridging chloride ligand (Cl(1)) shifts toward the gallium center upon coordination of an extra halide ligand

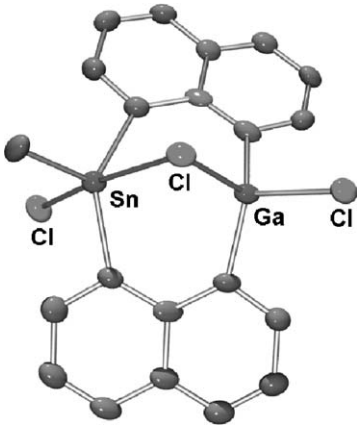

FIG. 29. Solid-state molecular structure of the anionic component of **71**.

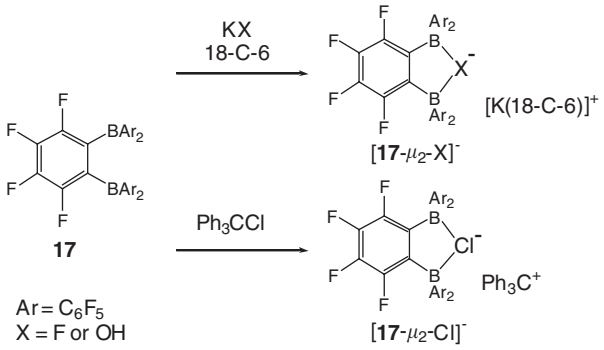

SCHEME 35.

at tin. A similar effect is observed in **72** and **73**. These results indicate that the Lewis-acidic gallium and tin centers of **58** cooperate in the binding of anionic substrates. This synergy arises from the presence of a bridging chloride atom by which the gallium center transfers its Lewis acidity to the four-coordinate tin center. In other words, the primary Lewis-acidic site of **58** is the triorganotin chloride moiety whose electron deficiency is enhanced through partial abstraction of its chloride ligand by the neighboring gallium center.

3. *Ortho*-Phenylene Diboranes and Dialanes

Ortho-phenylene diboranes constitute another important class of polydentate Lewis acids which have been considered for the complexation of anions.[16,15] In this context, most efforts have centered on the study of the ligative behavior of 1,2-bis(bis(pentafluorophenyl)boryl)tetrafluorobenzene (**17**). Similar to **22**, compound **17** forms chelate fluoride ([**17**-μ_2-F]$^-$) and hydroxide ([**17**-μ_2-OH]$^-$) complexes when treated with KF/18-C-6 and KOH/18-C-6, respectively (18-C-6 = 18-crown-6) (Scheme 35).[21] The crystal structure of these anionic complexes has not been

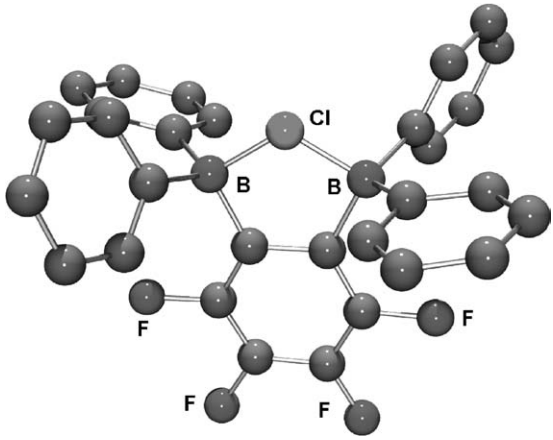

FIG. 30. Structure of [**17**-μ_2-Cl]$^-$. F-atoms from C_6F_5 groups omitted for clarity.

determined. However, NMR data unambiguously support the existence of symmetrical bridged structures. In the case of the fluoride complex [**17**-μ_2-F]$^-$, the bridging fluoride atom gives rise to a ^{19}F NMR resonance at −167.2 ppm. This chemical shift is similar to that observed for the bridging fluoride in the 1,8-diborylnaphthalenes [**22**-μ_2-F]$^-$ and [**34**-μ_2-F]$^-$.[27,38]

This anionic complex ([**17**-μ_2-F]$^-$) has also been generated as a tritylium salt by the reaction of diborane **17** with $[Ph_3C]^+[BF_4]^-$.[73] The ability of **17** to abstract a fluoride from $[BF_4]^-$ is noteworthy and provides a measure of its Lewis acidic strength. The complexation of chloride has also been examined. Thus, reaction of **17** with Ph_3CCl leads to the formation of [**17**-μ_2-Cl]$^-$ which has been isolated as the trityl salt.[74] The structure of this salt has been determined by single-crystal X-ray diffraction (Fig. 30). The chloride anion is essentially symmetrically coordinated to both boron centers with which it forms B–Cl bonds of 2.033(2) and 2.040(2) Å. The B–Cl–B angle of 94.34(6)° is somewhat acute which suggests that chloride anion might be too large to comfortably sit in the bite provided by **14**. This angle is also more acute than that of 105.8° observed within the six-membered chelate ring of [**24**-μ_2-Cl]$^-$. Bidentate **14** also abstracts chloride from $PhMe_2CCl$. Although no details are available, it has been reported that dialuminum complexes such as **37**, **38** and **39** are able to abstract the chloride ligand from $Cp_2TiMeCl$ to afford the corresponding metallocenium salt which readily polymerizes ethylene.[40]

In an effort to generate weakly coordinating anions for application in olefin polymerization catalysis, the complexation of alkoxide and phenoxide anion by **17** has also been studied.[73] Thus, the reaction of **17** with Ph_3COMe and $Ph_3COC_6F_5$ affords the corresponding complexes [**17**-μ_2-OMe]$^-$ and [**17**-μ_2-O(C_6F_5)]$^-$ which have been isolated as trityl salts (Scheme 36). In both cases, the ^{19}F NMR spectra are consistent with C_{2v} symmetry, therefore indicating that their chelate structures persist in solution. Both of these salts have been structurally characterized (Fig. 31). The bridging oxygen atom is trigonal planar in both complexes which contrast with the pyramidal structure of isoelectronic alkyloxonium $[R_3O]^+$ salts. The same

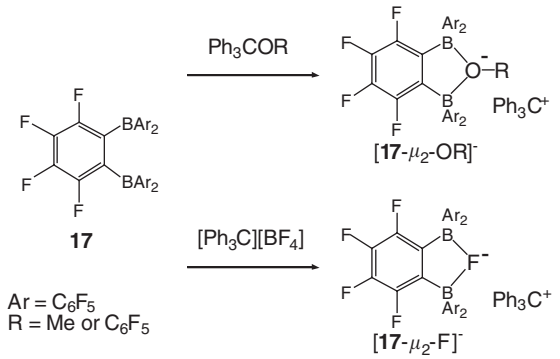

SCHEME 36.

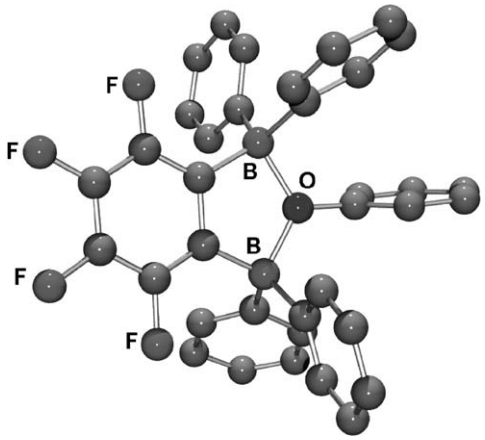

FIG. 31. Structure of $[\mathbf{17}\text{-}\mu_2\text{-}O(C_6F_5)]^-$. F-atoms from C_6F_5 groups omitted for clarity.

strategy has also been applied to the synthesis of the azide and dimethylamide[16] chelate complexes (Scheme 37). The latter salt is not stable and undergoes elimination of triphenylmethane to produce a $H_2C = NMe$ adduct of **17**. In this adduct, the imine interacts only with one boron center.

Some of the aforementioned tritylium salts have been used as methide abstractors for the generation of zirconocenium olefin polymerization catalysts. The reaction of $[\mathbf{17}\text{-}\mu_2\text{-}F]^-[Ph_3C]^+$ and $[\mathbf{17}\text{-}\mu_2\text{-}N_3]^-[Ph_3C]^+$ with Cp_2ZrMe_2 does not lead to stable zirconocenium species.[16] Instead, the azide or the fluoride anion undergoes rapid transfer to the zirconium center. Anion transfer to the zirconium center is not observed when these reactions are carried out with the methoxide and the pentafluorophenoxide containing anions $[\mathbf{17}\text{-}\mu_2\text{-}OMe]^-$ and $[\mathbf{17}\text{-}\mu_2\text{-}O(C_6F_5)]^-$ indicating that they are much more robust.[73] The catalytic activity of the metallocenium salt $[Cp_2ZrMe]^+$ $[\mathbf{17}\text{-}\mu_2\text{-}O(C_6F_5)]^-$ in the polymerization of ethylene is remarkably high, which can be correlated to the non-coordinating nature of the sterically hindered and fluorinated anionic chelate $[\mathbf{17}\text{-}\mu_2\text{-}O(C_6F_5)]^-$.

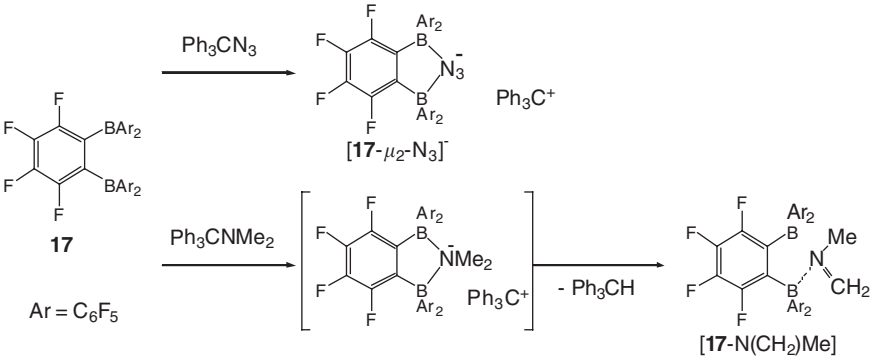

SCHEME 37.

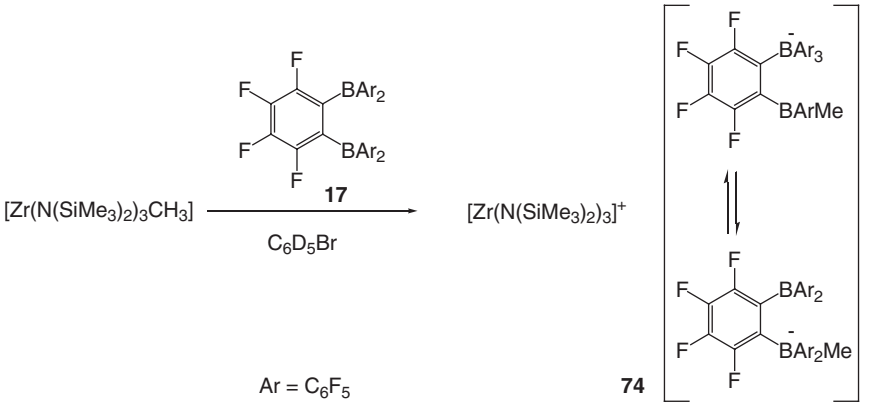

SCHEME 38.

Fluorinated *ortho*-phenylene diboranes have also been considered as neutral methide abstractors. The reaction of **17** with $[Zr(N(SiMe_3)_2)_3CH_3]$ in C_6D_5Br results in methide abstraction and formation of an ion pair containing the $[Zr(N(SiMe_3)_2)_3]^+$ cation (Scheme 38).[75] By contrast with the anionic chelate complexes of **17** which all feature a bridged structure, methide complexation to **17** triggers a ligand redistribution reaction and subsequent formation of a non-bridged borate anion (**74**) as depicted in Scheme 38. In solution, anion **74** exists as a mixture of two structural isomers as indicated by NMR spectroscopy. Diborane **17** also reacts with Cp_2ZrMe_2 to afford the expected metallocenium which, however, slowly decomposes when kept for several days at room temperature in C_6D_5Br.

The fluorinated diboraanthracene **19** has also been investigated as a neutral methide abstractor for Cp_2ZrMe_2.[23,24,75] Marks investigated the Lewis acidity of this bifunctional borane toward acetonitrile and demonstrated that this derivative is a stronger Lewis acid than $B(C_6F_5)_3$. Some of the factors contributing to the unusually high Lewis activity of this diborane include the nearly perpendicular conformation of the two C_6F_5 rings which prevents significant π-electron donation to

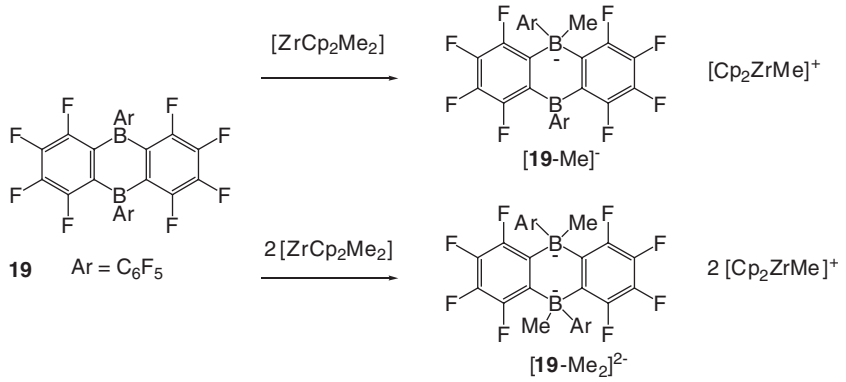

SCHEME 39.

the boron centers and, possibly, the antiaromatic character of the diboranthracene ring system which will favor any event leading to the removal of the boron empty orbital from conjugation with the *ortho*-phenylene π-electrons. In the presence of one or two equivalents of Cp_2ZrMe_2, this diborane is able to abstract not only one but also two methide groups to form the corresponding anions (Scheme 39).[23,24,75] The resulting anions have been characterized by NMR in CD_2Cl_2. Both anions appear to have static structures on the NMR timescale.

IV
CONCLUSION

As presented in this review, a variety of synthetic strategies are now available for the synthesis of *ortho*-phenylene and *peri*-naphthalenediyl group 13 derivatives. Owing to the development of reliable synthetic strategies, bidentate boranes can be conveniently prepared with a relatively high degree of predictability. Moreover, these boron derivatives can be prepared with various substituents which can be used to control the Lewis acidic or chromophoric properties of the bifunctional boranes. By contrast, the composition and structure of the heavier group 13 *ortho*-phenylene and *peri*-naphthalenediyl derivatives have proved much harder to master. Many reactions are accompanied by unpredicted events such as spontaneous ring closure as in the case of the diindacycles **55**, **56** and **61**. Further complications sometimes result from incomplete substitutions as encountered in the gallium/tin derivative **58** and the mercuraindacycles **64** and **65**. The most attractive sets of properties so far discovered concerned that ability of the diboranes to complex small anions. The bright yellow diborane **34** serves as a sensor for fluoride anions. The charge neutrality of this sensor as well as the short space available between the boron centers makes this sensor highly selective for fluoride. It is also important to note that by virtue of its bidentate nature, the fluoride association constant is remarkably high and by far exceeds that measured for monofunctional borane receptors. The fluorinated diboranes also show a high affinity for anions. For example, the fully

fluorinated bidentate Lewis acid **17** forms extremely stable anionic complexes with pentafluorophenoxide. The resulting anion is remarkably robust and by virtue of its large size, weakly coordinating, a set of properties which makes it useful in olefin polymerization catalysis.

Acknowledgments

We would like to thank the National Science Foundation (CAREER CHE-0094264), the Welch Foundation (Grant A-1423) and the Lavoisier from the French Ministry of Foreign Affairs (grant to M.M.).

References

(1) Kaufmann, D. E.; Otten, A. *Angew. Chem. Int. Ed. Engl.* **1994**, *33*, 1832.
(2) Schmidtchen, F. P.; Berger, M. *Chem. Rev.* **1997**, *97*, 1609.
(3) Dietrich, B. *Pure Appl. Chem.* **1993**, *65*, 1457.
(4) Gabbaï, F. P. *Angew. Chem. Int. Ed. Engl.* **2003**, *42*, 2218.
(5) Schriver, D. F.; Biallas, M. J. *J. Am. Chem. Soc.* **1967**, *89*, 1078.
(6) Hawthorne, M. F. *Pure Appl. Chem.* **1994**, *66*, 245.
(7) Hawthorne, M. F.; Zheng, Z. *Acc. Chem. Res.* **1997**, *30*, 267.
(8) Wedge, T. J.; Hawthorne, M. F. *Coord. Chem. Rev.* **2003**, *240*, 111.
(9) Vaugeois, J.; Simard, M.; Wuest, J. D. *Coord. Chem. Rev.* **1995**, *145*, 55.
(10) Wuest, J. D. *Acc. Chem. Res.* **1999**, *32*, 81.
(11) Haneline, M. R.; Taylor, R. E.; Gabbaï, F. P. *Chem. Eur. J.* **2003**, *9*, 5188.
(12) Altmann, R.; Jurkschat, K.; Schurmann, M.; Dakternieks, D.; Duthie, A. *Organometallics* **1998**, *17*, 5858.
(13) Yang, X.; Knobler, C. B.; Hawthorne, M. F. *Angew. Chem. Int. Ed. Engl.* **1991**, *30*, 1507.
(14) Beckwith King, J. D.; Haneline, M. R.; Tsunoda, M.; Gabbaï, F. P. *J. Am. Chem. Soc.* **2002**, *124*, 9350.
(15) Chen, E. Y.-X.; Marks, T. *J. Chem. Rev.* **2000**, *100*, 1391.
(16) Piers, W. E.; Irvine, G. J.; Williams, V. C. *Eur. J. Inorg. Chem.* **2000**, 2131.
(17) Hoefelmeyer, J. D.; Schulte, M.; Tschinkl, M.; Gabbaï, F. P. *Coord. Chem. Rev.* **2002**, *235*, 93.
(18) Clement, R. *C. R. Acad. Sci. Paris* **1966**, *263*, 1398.
(19) Kaufmann, D. E. *Chem. Ber.* **1987**, *120*, 901.
(20) Eisch, J. J.; Kotowicz, B. W. *Eur. J. Inorg. Chem.* **1998**, 761.
(21) Williams, V. C.; Piers, W. E.; Clegg, W.; Elsegood, M. R. J.; Collins, S.; Marder, T. B. *J. Am. Chem. Soc.* **1999**, *121*, 3244.
(22) Chivers, T. *J. Organomet. Chem.* **1969**, *19*, 75.
(23) Metz, M. V.; Schwartz, D. J.; Stern, C. L.; Marks, T. J.; Nickias, P. N. *Organometallics* **2002**, *21*, 4159.
(24) Metz, M. V.; Schwartz, D. J.; Stern, C. L.; Nickias, P. N.; Marks, T. J. *Angew. Chem. Int. Ed. Engl.* **2000**, *112*, 1368.
(25) Letsinger, R. L.; Smith, J. M.; Gilpin, J.; MacLean, D. B. *J. Org. Chem.* **1965**, *30*, 807.
(26) Weinman, W.; Hergel, A.; Deforth, T.; Krämer, A.; Pritzkow, H.; Siebert, W. *Z. Naturforsch., B* **1996**, *51b*, 1104.
(27) Katz, H. E. *J. Am. Chem. Soc.* **1985**, *107*, 1420.
(28) Katz, H. E. *J. Org. Chem.* **1985**, *50*, 5027.
(29) For 1-dimethylboryl-8-silyl-naphthalene complexes see: Katz, H. E. *Organometallics* **1986**, *5*, 2308–2311; Katz, H. E. *J. Am. Chem. Soc*. **1986**, *108*, 7640.
(30) Hoefelmeyer, J. D.; Gabbaï, F. P. *J. Am. Chem. Soc.* **2000**, *122*, 9054.
(31) Katz, H. E. *Organometallics* **1987**, *6*, 1134.
(32) Hoefelmeyer, J. D.; Gabbaï, F. P. *Organometallics* **2002**, *21*, 982.
(33) Hergel, A.; Pritzkow, H.; Siebert, W. *Angew. Chem. Int. Ed. Engl.* **1994**, *33*, 1247.
(34) Hoefelmeyer, J. D.; Solé, S.; Gabbaï, F. P. *Dalton Trans.* **2004**, 1254.
(35) Schulte, M.; Gabbaï, F. P. *Chem. Eur. J.* **2002**, *8*, 3802.

(36) Eisch, J. J.; Galle, J. E.; Kozima, S. *J. Am. Chem. Soc.* **1986**, *108*, 379. Herberich, G. E.; Buller, G.; Hessner, B.; Oschmann, W. *J. Organomet. Chem.* **1980**, *195*, 253.
(37) Chase, P. A.; Piers, W. E.; Patrick, B. O. *J. Am. Chem. Soc.* **2000**, *122*, 12911.
(38) Solé, S.; Gabbaï, F. P. *Chem. Commun.* **2004**, 1284.
(39) For a recent example see: Sirimanne, C. T.; Knox, J. E.; Heeg, M. J.; Schlegel, H. B.; Winter, C. H. *J. Am. Chem. Soc*. **2003**, *125*, 11152.
(40) Eisch, J. J.; Mackenzie, K.; Windisch, H.; Krüger, C. *Eur. J. Inorg. Chem.* **1999**, 153.
(41) Dam, M. A.; Nijbacker, T.; de Kanter, F. J. J.; Akkerman, O. S.; Bickelhaupt, F.; Spek, A. L. *Organometallics* **1999**, *18*, 1706.
(42) Tschinkl, M.; Bachman, R. E.; Gabbaï, F. P. *Chem. Commun.* **1999**, 1367.
(43) Tschinkl, M.; Cocker, T. M.; Bachman, R. E.; Taylor, R. E.; Gabbaï, F. P. *J. Organomet. Chem.* **2000**, *604*, 132.
(44) Dam, M. A.; Nijbacker, T.; de Pater, B. T.; de Kanter, F. J. J.; Akkerman, O. S.; Bickelhaupt, F.; Smeets, W. J. J.; Spek, A. L. *Organometallics* **1997**, *16*, 511.
(45) Tschinkl, M.; Schier, A.; Riede, J.; Schmidt, E.; Gabbaï, F. P. *Organometallics* **1997**, *16*, 4759.
(46) Tschinkl, M.; Schier, A.; Riede, J.; Gabbaï, F. P. *Inorg. Chem.* **1997**, *36*, 5706.
(47) Wittig, G.; Bickelhaupt, F. *Chem. Ber.* **1958**, *91*, 883.
(48) Tinga, M. A. G. M.; Schat, G.; Akkerman, O. S.; Bickelhaupt, F.; Horn, E.; Kooijman, H.; Smeets, W. J. J.; Spek, A. L. *J. Am. Chem. Soc.* **1993**, *115*, 2808.
(49) Schreuder Goedheijt, M.; Nijbacker, T.; Akkerman, O. S.; Bickelhaupt, F.; Veldman, N.; Spek, A. L. *Angew. Chem. Int. Ed. Engl.* **1996**, *35*, 1550.
(50) Gabbaï, F. P.; Schier, A.; Riede, J. *Chem. Commun.* **1996**, 1121.
(51) Gabbaï, F. P.; Schier, A.; Riede, J.; Schichl, D. *Organometallics* **1996**, *15*, 4119.
(52) Tschinkl, M.; Schier, A.; Riede, J.; Gabbaï, F. P. *Inorg. Chem.* **1998**, *37*, 5097.
(53) Tschinkl, M.; Hoefelmeyer, J. D.; Cocker, T. M.; Bachman, R. E.; Gabbaï, F. P. *Organometallics* **2000**, *19*, 1826.
(54) Hoefelmeyer, J. D.; Brode, D. L.; Gabbaï, F. P. *Organometallics* **2001**, *20*, 5653.
(55) Hoefelmeyer, J. D.; Schulte, M.; Gabbaï, F. P. *Inorg. Chem.* **2001**, *40*, 3833.
(56) Gabbaï, F. P.; Schier, A.; Riede, J.; Sladek, A.; Görlitzer, H. W. *Inorg. Chem.* **1997**, *36*, 5694.
(57) Pyykkö, P.; Straka, M. *Phys. Chem. Chem. Phys.* **2000**, *2*, 2489. Bondi, A. *J. Phys. Chem.* **1964**, *68*, 441.
(58) Ooi, T.; Takahashi, M.; Yamada, M.; Tayama, E.; Omoto, K.; Maruoka, K. *J. Am. Chem. Soc.* **2004**, *126*, 1150.
(59) Maruoka, K. *Organomet. News* **1995**, *2*, 29.
(60) Sharma, V.; Simard, M.; Wuest, J. D. *J. Am. Chem. Soc.* **1992**, *114*, 7931.
(61) Koehler, K.; Piers, W. E. *Can. J. Chem.* **1998**, *76*, 1249.
(62) Tschinkl, M.; Schier, A.; Riede, J.; Gabbaï, F. P. *Organometallics* **1999**, *18*, 1747.
(63) Reilly, M.; Oh, T. *Tetrahedron Lett.* **1995**, *36*, 221.
(64) Reilly, M.; Oh, T. *Tetrahedron Lett.* **1995**, *36*, 217.
(65) Gabbaï, F. P.; Schier, A.; Riede, M.; Hynes, J. *Chem. Commun.* **1998**, 897.
(66) Gabbaï, F. P.; Schier, A.; Riede, J. *Angew. Chem. Int. Ed. Engl.* **1998**, *37*, 622.
(67) Briancon, D. *Rev. Rheum.* **1997**, *64*, 78.
(68) Matuso, S.; Kiyomiya, K.; Kurebe, M. *Arch. Toxicol.* **1998**, *72*, 798.
(69) Martínez-Máñez, R.; Sancenón, F. *Chem. Rev.* **2003**, *103*, 4419.
(70) Yamaguchi, S.; Akiyama, S.; Tamao, K. *J. Am. Chem. Soc.* **2000**, *122*, 6335.
(71) Yamaguchi, S.; Akiyama, S.; Tamao, K. *J. Am. Chem. Soc.* **2001**, *123*, 11372.
(72) Hoefelmeyer, J. D.; Gabbaï, F. P. *Chem. Commun.* **2003**, 712.
(73) Williams, V. C.; Irvine, G. J.; Piers, W. E.; Li, Z.; Collins, S.; Clegg, W.; Elsegood, M. R. J.; Marder, T. B. *Organometallics* **2000**, *19*, 1619. Henderson, L. D.; Piers, W. E.; Irvine, G. J.; McDonald, R. *Organometallics* **2002**, *21*, 340.
(74) Lewis, S. P.; Taylor, N. J.; Piers, W. E.; Collins, S. *J. Am. Chem. Soc.* **2003**, *125*, 14686.
(75) Williams, V. C.; Dai, C.; Li, Z.; Collins, S.; Piers, W. E.; Clegg, W.; Elsegood, M. R. J.; Marder, T. B. *Angew. Chem. Int. Ed. Engl.* **1999**, *38*, 3695.

Metallasilsesquioxanes

VOLKER LORENZ and FRANK T. EDELMANN*

Chemisches Institut der Otto-von-Guericke-Universität, Magdeburg, Universitätsplatz 2, D-39106 Magdeburg, Germany

I. Introduction 101
II. Silsesquioxane Precursors 105
III. Metallasilsesquioxanes 106
A. Metallasilsesquioxanes of Main-Group Metals 106
B. Metallasilsesquioxanes of the Early Transition Metals 120
C. Metallasilsesquioxanes of the Middle and Late Transition Metals 140
IV. Future Outlook 148
Acknowledgments 150
References 150

Dedicated to Professor Karl-Heinz Thiele on the occasion of his 75th birthday

I
INTRODUCTION

Polyhedral oligosilsesquioxanes having the general formula $(RSiO_{1.5})_n$ form an unusual and interesting class of organosilicon compounds, which currently have a tremendous impact on both catalysis research[1,2] and materials science.[3] Due to their chemical composition they can be viewed as intermediates between silica, (SiO_2), on one side and the silicones, $(R_2SiO)_n$, on the other (the Latin word *sesqui* translates as one and a half). In accordance with several unique properties, the polyhedral silsesquioxanes have been termed the "smallest particles of silica possible"[4] or "small soluble chunks of silica".[2] In general, one can distinguish between completely condensed polyhedral silsesquioxanes and incompletely condensed molecules.

The first report on silsesquioxanes ever in the literature was published in 1946 by Scott.[5] Thermal rearrangement of the cohydrolysis product of dichlorodimethylsilane and trichloromethylsilane afforded six different methypolysiloxanes. One of them was a sublimable material, which was assigned the formula $[CH_3SiO_{3/2}]_{2n}$. The first structural investigations on crystalline organosilsesquioxanes were carried out by Barry and co-workers in 1955.[6] These authors prepared a series of organosilsesquioxanes and were the first to demonstrate that these materials have cage-like oligomeric structures. Crystalline cubic octamers were isolated in the case of the methyl, ethyl, *n*-propyl, *n*-butyl and cyclohexyl derivatives, while in the case of methyl substituents a hexagonal prismatic dodecamer was also obtained and characterized. A trigonal prismatic structure was proposed for a phenylsilsesquioxane derivative. The polycondensation of phenylsilanetriol leading to 8- to 12-unit cage-like oligophenylsilsesquioxanes was later investigated in detail by Brown.[7] Among the

*Corresponding author.
E-mail: frank.edelmann@vst.uni-magdeburg.de (F.T. Edelmann).

ADVANCES IN ORGANOMETALLIC CHEMISTRY
VOLUME 53 ISSN 0065-3055/DOI 10.1016/S0065-3055(05)53004-1

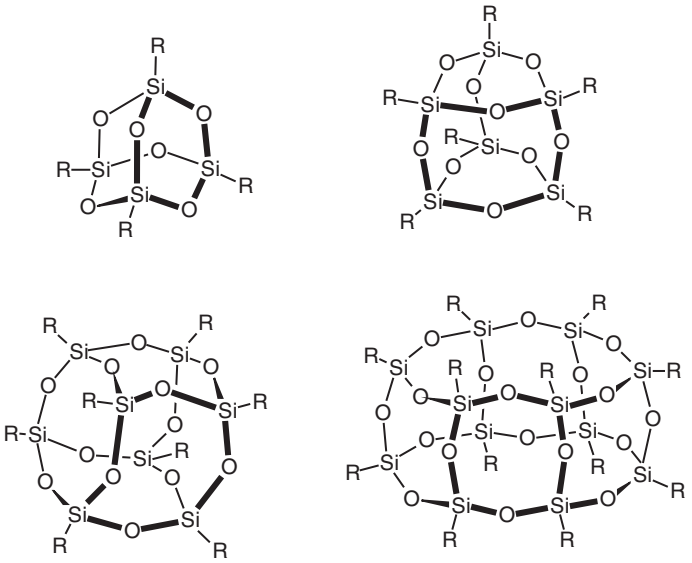

Scheme 1. Completely condensed oligomeric silsesquioxanes (R = H, alkyl, cycloalkyl, aryl).

simplest members of this class, the silsesquioxane cage molecules $(HSiO_{3/2})_n$ with $n = 8$, 10, 12, 14 and 16 have been reported.[8,9] Scheme 1 gives an overview of such *closo*-silsesquioxane cages known to date.

Much more interesting with respect to various promising applications are incompletely condensed silsesquioxanes retaining reactive Si–OH functional groups. Compounds of this type range from simple disiloxanediols, $[RSi(OH)_2]_2O$, to 12-membered-ring tetrasilanols and incompletely condensed cubic cage compounds. Scheme 2 depicts the most prominent examples of incompletely condensed silsesquioxanes. Among these, the cage-like derivatives can be regarded as small, soluble, three-dimensional fragments of certain silica structures such as β-tridymite and β-crystobalite. Feher and co-workers[10] were the first to point out this structural relationship. This important finding was the starting point for numerous studies in the area of incompletely condensed silsesquioxanes and metallasilsesquioxanes derived from them.

The first report on such compounds dates back to 1965, when Brown and Vogt first described the polycondensation of trichlorocyclohexylsilane, $CySiCl_3$ (**1**, Cy = *cyclo*-C_6H_{11}), in acetone/water mixtures.[11] Thus given the right reaction conditions, incompletely condensed silsesquioxanes can be isolated from the same reaction mixtures as their *closo*-counterparts. Until now the main synthetic access to incompletely condensed polyhedral silsesquioxanes involves hydrolysis of organotrichlorosilanes followed by polycondensation. In recent years several synthetic methods have also been developed to open the closed-cage structures depicted in Scheme 1 in order to convert these rather unreactive materials into synthetically more useful oligosilanol derivatives.[12–17]

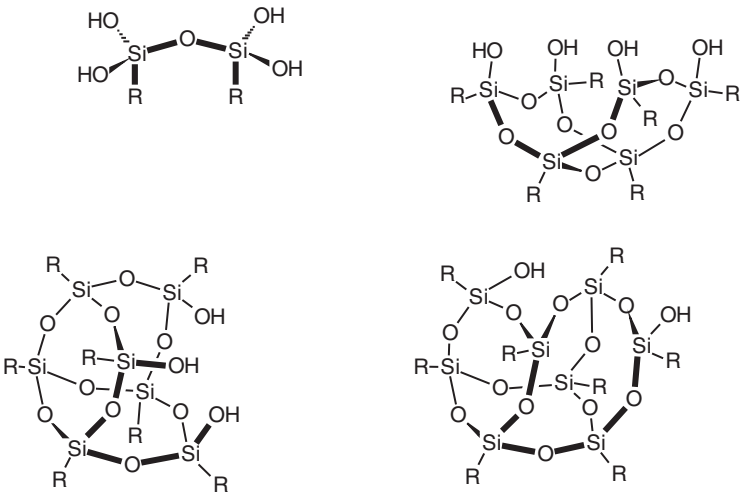

Scheme 2. Incompletely condensed oligomeric silsesquioxanes (R = alkyl, cycloalkyl, aryl).

The formation of incompletely condensed polyhedral silsesquioxanes involves hydrolysis of the starting monoorganosilanes $RSiX_3$ (X = Cl, OR) followed by a multistep hydrolysis process as illustrated in Scheme 3. In the first step the organotrichlorosilane (or organotrialkoxysilane) is attacked by water to form an organo silanetriol intermediate, which under these conditions is generally unstable with respect to subsequent condensation reactions. Among open-chain condensation products which can be found in these reaction mixtures are tetraorganodisiloxanediols and hexaorganotrisiloxanetriols. Other intermediates can be cyclic oligosilanols. Finally, completely and incompletely condensed oligomeric silsesquioxanes are formed. The relative amounts of individual compounds in the resulting reaction mixtures depend on several factors such as the nature of the R group, the pH as well as the concentration of water and solvents.[18–20]

By far the most important and most thoroughly investigated representatives among the incompletely condensed polyhedral silsesquioxanes are the heptameric trisilanols $R_7Si_7O_9(OH)_3$ (Scheme 4).

The fact that silsesquioxane molecules like **2**–**7** contain covalently bonded reactive functionalities make them promising monomers for polymerization reactions or for grafting these monomers to polymer chains. In recent years this has been the basis for the development of novel hybrid materials, which offer a variety of useful properties.[3,4] This area of applied silsesquioxane chemistry has been largely developed by Lichtenhan *et al.*[4] With respect to catalysis research, the chemistry of metallasilsesquioxanes also receives considerable current interest.[1,2,10,21] As mentioned above, incompletely condensed silsesquioxanes of the type $R_7Si_7O_9(OH)_3$ (**2**–**7**, Scheme 4) share astonishing structural similarities with β-tridymite and β-cristobalite and are thus quite realistic models for the silanol sites on silica surfaces.[1,2,21–26] Metal complexes derived from **2**–**7** are therefore commonly regarded as ''realistic'' models for industrially important metal catalysts immobilized on silica surfaces.[1,2,22] It is

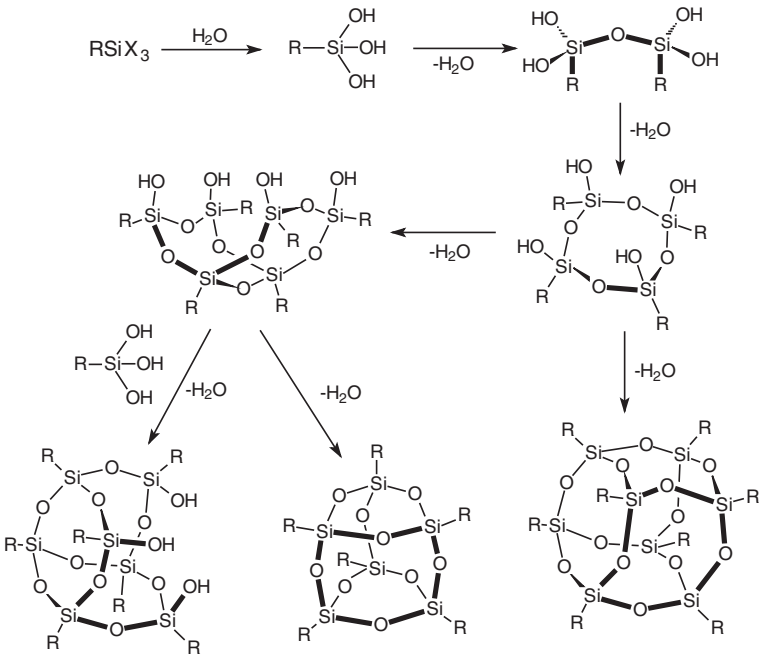

SCHEME 3. Formation of completely and incompletely condensed silsesquioxanes upon hydrolysis of $RSiX_3$ (X = Cl, OR) followed by condensation steps.

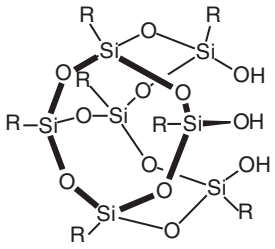

2: R = *cyclo*-C_5H_9

3: R = *cyclo*-C_6H_{11}

4: R = *cyclo*-C_7H_{13}

5: R = norbornyl

6: R = *i*-butyl

7: R = *i*-octyl

SCHEME 4. Schematic representation of heptameric trisilanols $R_7Si_7O_9(OH)_3$.

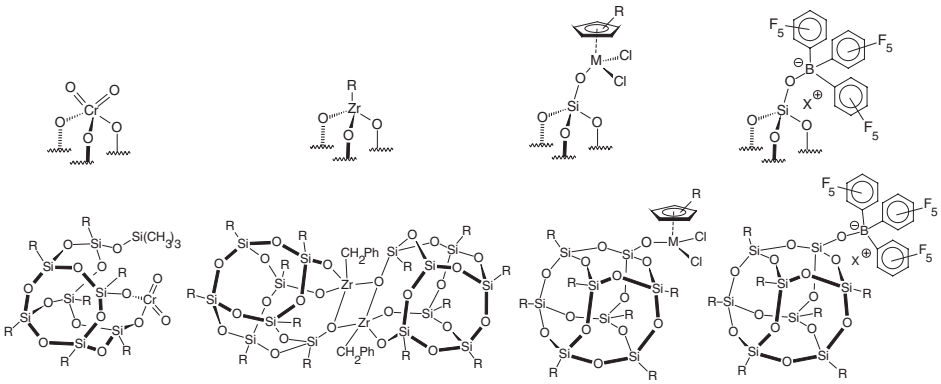

SCHEME 5. Silica-supported species, which have been successfully modeled with the use of silsesquioxanes.

mainly the latter aspect, i.e. the mimicking of heterogeneous metal catalysts with the use of soluble compounds, that currently attracts various research groups to the chemistry of incompletely condensed silsesquioxanes. Examples of silica-supported species, which have been successfully modeled with the use of silsesquioxanes are e.g., Phillips- and Ziegler-Natta-type olefin polymerization catalysts as well as silica-supported perfluoroborato co-catalysts (Scheme 5).[27]

II
SILSESQUIOXANE PRECURSORS

Preparation and derivative chemistry of **3** have been mainly developed by Feher and co-workers.[10] The preparation of the cyclohexyl-substituted derivative **3** is simple and straightforward, though time-consuming. The synthetic procedure involves the controlled hydrolysis of **1** in an acetone/water mixture. Separation of **3** from two other silsesquioxane derivatives (the fully condensed prismatic hexamer and a disilanol tetramer) formed in this reaction can be accomplished by a simple extraction procedure. A certain disadvantage of this synthesis is that the kinetically controlled formation of the incompletely condensed silsesquioxane cage by condensation of the *in situ* formed cyclohexylsilanetriol, $CySi(OH)_3$ (**8**), requires reaction times of up to 3 years (!) to proceed to completion. In the case of R = cyclohexyl, the process cannot be accelerated significantly by means of stirring, heating, ultrasound etc.[10] However, synthetically useful quantities of **3** can be ''harvested'' already after a few months.

The hydrolysis/condensation process takes a somewhat different course when cyclopentyl and cycloheptyl substituents are employed instead of cyclohexyl. In 1991 Feher *et al.*[28] reported the preparation of **2** and **4** *via* hydrolytic condensation reactions of *c*-$C_5H_9SiCl_3$ (**9**) and *c*-$C_7H_{13}SiCl_3$ (**10**), respectively. It was reported that these straightforward syntheses produce multigram quantities of incompletely condensed silsesquioxanes within a few days. In these two cases no completely condensed silsesquioxane derivatives were formed. While **2** was obtained as the sole

product, a mixture of **4** and the tetrasilanol (c-$C_7H_{13})_6Si_6O_7(OH)_4$ (**11**) was obtained with R = cycloheptyl. The cyclopentyl derivative **2** has been frequently employed in the synthesis of metallasilsesquioxanes, whereas **4** did not receive much attention as a possible starting material. Thus far, the majority of metallasilsesquioxanes have been synthesized starting with the cyclohexyl-substituted species **3**. In our laboratory, we found over the years that crystallinity and/or solubility of metallasilsesquioxanes are generally most favorable when **3** is used as starting material. These practical reasons justify the greater efforts put into the time-consuming and more tedious preparation of **3** as compared to **2** and **4**.

The preparation of the heptanorbornyl silsesquioxane trisilanol **5** has been reported by Maschmeyer *et al.*[29] It is formed in admixture with the corresponding tetrasilanol. The norbornyl-substituted species still await further exploration as precursors in metallasilsesquioxane chemistry. The same applies for the isobutyl and isooctyl derivatives **6** and **7**, respectively, which have been propagated in the patent literature by Lichtenhan and Abbenhuis.[1] The application of high-speed experimentation techniques to optimize the preparation of silsesquioxanes as precursors for Ti catalysts has been reported by Maschmeyer *et al.*[30]

Various synthetic routes are available to introduce metal atoms into the cage systems of **2**–**7**. The most straightforward route involves protonation of suitable metal precursors such as alkoxides, amides or organometallic compounds by the free trisilanols **2**–**7**.[1–3] For example, as shown by Feher *et al.*, the reactivity of **3** can be modified and tuned by silylation of the Si–OH functions using Me_3SiCl/NEt_3 in different stoichiometric amounts.[10,31] This way the silylated derivatives $Cy_7Si_7O_9(OH)_2(OSiMe_3)$ (**12**), $Cy_7Si_7O_9(OH)(OSiMe_3)_2$ (**13**) and $Cy_7Si_7O_9(OSiMe_3)_3$ (**14**) can be selectively prepared starting from **3**. Another possibility of modifying the reactivity of **3**, **12** and **14** is to prepare the corresponding thallium silanolates by treatment of the free silanols with thallium ethoxide (*vide infra*).[32] Both the silyl derivatives and the thallium salts have been successfully employed in the preparation of metallasilsesquioxanes, especially *via* reactions with high-oxidation state transition metal halides.[1–3]

III
METALLASILSESQUIOXANES

A. *Metallasilsesquioxanes of Main-Group Metals*

1. Group 1 Metal Derivatives (Li, Na, K): Useful Starting Materials

Fully metalated silsesquioxane derivatives of the type $Cy_7Si_7O_9(OM)_3$ (M = Li, Na, K) would constitute highly desirable precursors for the construction of "realistic" catalyst model compounds, including novel heterobimetallic species. However, such alkali metal derivatives of **2**–**7** were unknown until recently, and structural information on such materials was lacking. There have also been contrasting reports in the literature concerning the metalation of **3** by alkali metal

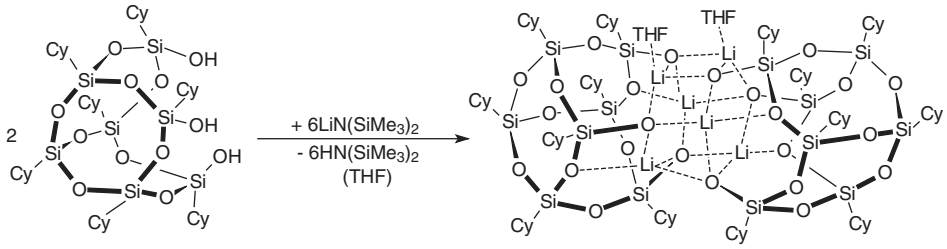

SCHEME 6. Synthesis of $[(Cy_7Si_7O_{12})_2Li_6(THF)_2]$ THF (**16**).

reagents. It was reported by Feher *et al.* that treatment of **3** with three equivalents of NaO*t*Bu resulted in complete breakdown of the silsesquioxane cage.[23] In contrast, Aspinall *et al.* more recently succeeded in synthesizing $Cy_7Si_7O_9(OLi)_3$ (**15**) by the reaction of **3** with *n*-butyllithium.[33] $Cy_7Si_7O_9(OLi)_3$ (**15**) was isolated in virtually quantitative yield as an amorphous, air-stable (!) solid of unknown structure. We found in our laboratory that with the proper choice of deprotonating agents well-defined, crystalline alkali metal silsesquioxanes are readily available. These are excellent precursors for the preparation of unprecedented catalyst model compounds.

Alkali metal bis(trimethylsilyl)amides are the reagents of choice for achieving smooth and high-yield deprotonation of the incompletely condensed silsesquioxane **3**.[34] Treatment of **3** with $LiN(SiMe_3)_2$ in diethyl ether/THF (tetrahydrofuran) according to Scheme 6 afforded the crystalline lithium silsesquioxane dimer $[(Cy_7Si_7O_{12})_2Li_6(THF)_2] \cdot THF$ (**16**) in 93% yield. This reaction is not limited to the THF-adduct **16**. The corresponding acetone solvate $[(Cy_7Si_7O_{12})_2Li_6(Me_2CO)_3]$ (**17**) as well as the dimeric potassium derivative $[(Cy_7Si_7O_{12})_2K_6(DME)_4]$ (**18**) have been isolated in a similar manner.[34,35]

An X-ray diffraction study revealed a dimeric molecular structure of **16** (Scheme 6). The central structural unit of **16** consists of a box-shaped Li_6O_6 polyhedron. THF ligands are coordinated to two lithium ions, while the other four interact with framework oxygen atoms of the silsesquioxane cages. This bonding situation results in tetracoordination around each lithium. Structurally related box-shaped Li_6O_6 or Li_6S_6 polyhedra have previously been reported for some hexameric lithium phenoxides or arenethiolates,[36] but are unprecedented in silsesquioxane chemistry. The same structural motif has been established for the closely related molecular structure of $[(Cy_7Si_7O_{12})_2Li_6(Me_2CO)_3]$ (**17**).[34,35]

The use of $KN(SiMe_3)_2$ as metalating reagent enabled us to prepare the dimeric potassium derivative $[(Cy_7Si_7O_{12})_2K_6(DME)_4]$ (**18**) as a crystalline solid, which was structurally characterized by X-ray diffraction (Scheme 7). Here again a box-shaped K_6O_6 polyhedron forms the central structural unit. Four potassium ions are coordinated by DME (1,2-dimethoxyethane) ligands.[35]

The lithiated species **15** and **16** represent highly valuable intermediates in the synthesis of novel metallasilsesquioxanes. For this purpose it is not essential to isolate these lithium derivatives as crystalline solids. It has been found a convenient synthetic route to prepare **15** *in situ* by metalation of **3** with three equivalents of $LiN(SiMe_3)_2$

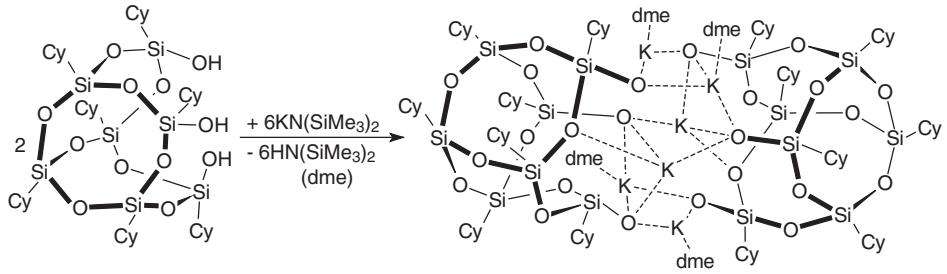

SCHEME 7. Synthesis of $[(Cy_7Si_7O_{12})_2K_6(DME)_4]$ (**18**).

and to use the resulting solution for subsequent reactions. *In situ* prepared **15** has already been successfully employed for the synthesis of novel heterobimetallic metallasilsesquioxanes containing lithium and beryllium,[37] boron,[38] zirconium,[34] lanthanide elements[33,34] and chromium.[35] They can be expected to play an increasing role as highly useful building blocks in metallasilsesquioxane chemistry.

2. Group 2 Metal Derivatives (Be, Mg)

Metallasilsesquioxanes containing alkaline earth elements remain a little investigated class of compounds. Until now, beryllium and magnesium are the only elements of Group 2 which have been successfully incorporated into silsesquioxane cages. The compound $[Cy_7Si_7O_{12}BeLi]_2 \cdot 2THF$ (**19**) was prepared in high yield by reacting *in situ* prepared $Cy_7Si_7O_9(OLi)_3$ (**15**) with anhydrous $BeCl_2$ in THF at 20 °C (Scheme 8).[37] The molecular structure of **19** has been determined by X-ray diffraction and was the first structurally characterized silsesquioxane derivative of beryllium. Self-assembly under formation of a dimer occurs in a rather unsymmetrical manner. Two lithium and two beryllium ions are bridged by the deprotonated silsesquioxane ligands in such a way that a different coordination environment results for each metal ion. THF ligands are coordinated to one lithium and one beryllium, while the other two metal ions are connected only to siloxide oxygens. Both Li ions are tetracoordinate. In contrast, the coordination geometry around one beryllium is distorted tetrahedral, while its counterpart is coordinated in an exactly trigonal planar fashion (angle sum 359.8°).

The only other alkaline earth metal for which metallasilsesquioxanes have been reported is magnesium. The first magnesium derivative was reported by Liu in 1996.[39,40] Butylethylmagnesium reacts with **3** to give $[Cy_7Si_7O_9(OH)O_2Mg]_n$ (**20**, $n = 1, 2$). Treatment of **20** with $TiCl_4$ afforded the novel heterobimetallic Mg/Ti metallasilsesquioxane $[Cy_7Si_7O_{12}MgTiCl_3]_n$ (**21**, $n = 1, 2$), which shows a high-catalytic activity for ethylene polymerization. A polymeric magnesasilsesquioxane material was made by Lichtenhan *et al.* from a silsesquioxane disilanol and dialkylmagnesium,[41] and another magnesium silsesquioxane has been used as an intermediate in reactions with epoxides.[42] The reaction of **2** with methylmagnesium chloride leads to the unprecedented tetranuclear magnesium silsesquioxane complex **22** in high yield (87%) as large, colorless, cube-like crystals (Scheme 9).[43] The crystal structure shows an unusually short Mg–Cl bond (2.255 Å), indicative of an

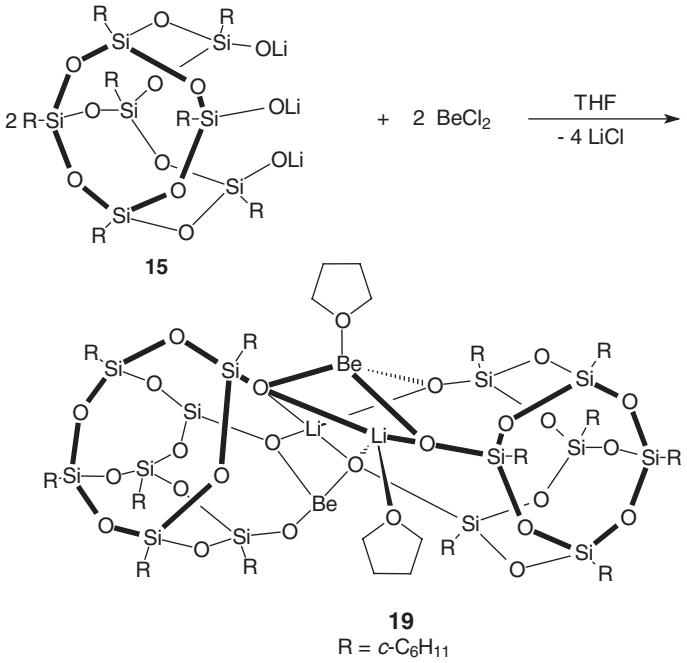

SCHEME 8. Synthesis of $[Cy_7Si_7O_{12}BeLi]_2\,2THF$ (**19**).

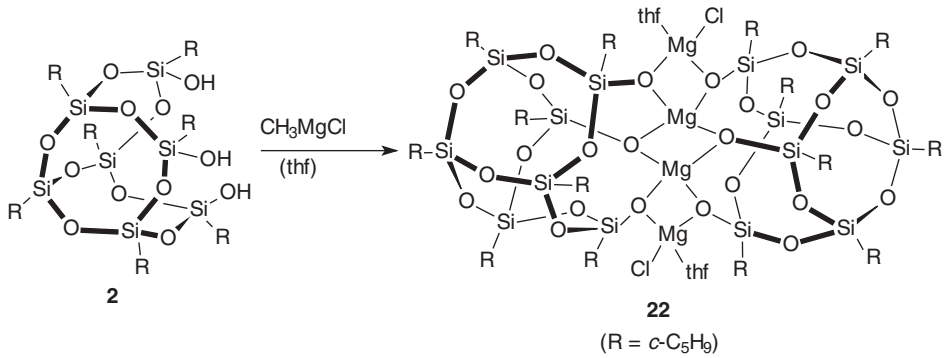

SCHEME 9. Synthesis of $[(c\text{-}C_5H_9)_7Si_7O_{12}]_2Mg_4Cl_2(THF)_2$ (**22**).

electron-deficient magnesium atom. Compound **22** has been used as transmetalation reagent for the synthesis of other metallasilsesquioxanes (Si, Ti), but transmetalation activity was found to be low.

Microporous, amorphous Mg–Si–O metallosilicates with a very narrow pore size distribution around 6 Å diameter and a typical surface area of ca 350 m^2/g were obtained from the controlled calcination of compound **22**.[44] The resulting Mg–Si–O material was found to be very active in 1-butanol conversion even at 200 °C giving both dehydrogenation and dehydration.

3. Group 13 Metal Derivatives (B, Al, Ga, In, Tl)

Group 13 metallasilsesquioxane chemistry is well developed. All elements from boron to thallium have been successfully incorporated into silsesquioxane cages. The first boron-containing silsesquioxane species, $[Cy_7Si_7O_{12}B]_2$ (**23**), was reported by Feher *et al.* in 1992.[45] The analogous cyclopentyl-substituted derivative was described by Duchateau *et al.*[38] Dimeric **24** was prepared as colorless crystals in 64% yield upon treatment of **2** with BI_3 in the presence of triethylamine according to Scheme 10. Compound **24** was also obtained when **2** was reacted with $LiBH_4$, eliminating LiH.[38]

When the monosilylated precursor **26** was reacted in a similar manner with $LiBH_4$ according to Scheme 11, the resulting product was the solvent-free lithium borate salt **27** (74% yield). This compound could be recrystallized from *n*-hexane.

In addition, several silsesquioxane–borato complexes have been described and their reactivity investigated.[46] Treatment of $B(C_6F_5)_3$ with the *closo*-silsesquioxane monosilanol (c-$C_5H_9)_7Si_8O_{12}(OH)$ (**28**) or **2** in the presence of a Brønsted base afforded the silsesquioxane–borates $X^+[(c\text{-}C_5H_9)_7Si_8O_{13}B(C_6F_5)_3]^-$ (**29**, $X^+ = PhN(H)Me_2^+$; **30**, $X^+ = Et_3NH^+$) and $X^+[(c\text{-}C_5H_9)_7Si_7(OH)_2O_{10}B(C_6F_5)_3]^-$ (**31**, $X^+ = PhN(H)Me_2^+$; **32**, $X^+ = Et_3NH^+$), respectively (cf. Scheme 5). When the stronger nucleophilic base pyridine is used, only $(C_6F_5)_3B \cdot (NC_5H_5)$ is formed instead, demonstrating the competition between $B(C_6F_5)_3$ and H^+ to react with the

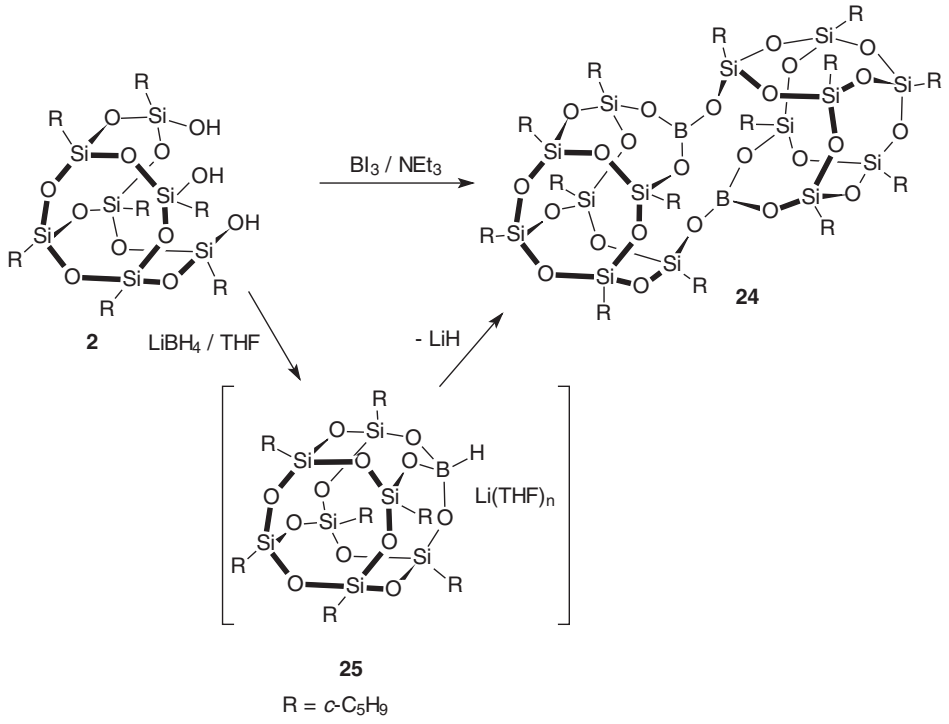

SCHEME 10. Alternative preparations of the dimeric boron silsesquioxane **24**.

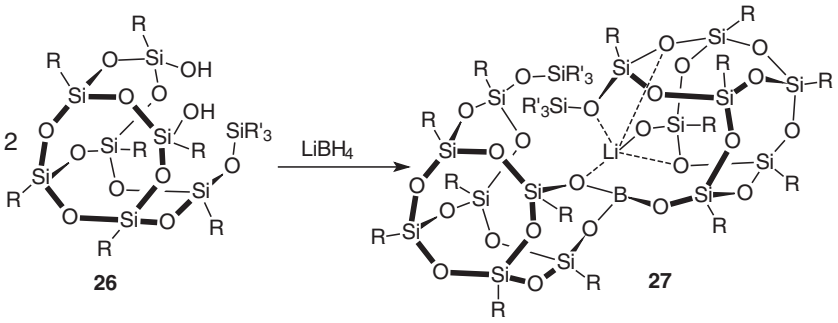

SCHEME 11. Synthesis of $Li[B\{(c\text{-}C_5H_9)_7Si_7O_{11}(OSiMePh_2)\}_2]$ (**27**).

added amine. The dimethylaniline in **29** and **31** is readily exchanged by NEt_3 to form **30** and **32**. With the more nucleophilic base pyridine the B–O bond in **29** and **30** is split, yielding $(C_6F_5)_3B \cdot (NC_5H_5)$ and the free silsesquioxane silanol **28**. Initial reactivity studies showed that complexes **29**–**32** readily undergo hydrolysis under formation of the hydroxyborato complexes $X^+[(C_6F_5)_3BOH]^-$ ($X^+ = PhN(H)Me_2^+$, Et_3NH^+), while alcoholysis of **29** and **31** with *i*-PrOH gave the alkoxide $[PhN(H)Me_2]^+[(C_6F_5)_3BOiPr]^-$.[46]

The first aluminasilsesquioxane derivative was made by Feher and co-workers in 1989.[47] The reaction of a benzene solution of **3** with $AlMe_3$ afforded in virtually quantitative yield the dimeric aluminasilsesquioxane $[Cy_7Si_7O_{12}Al]_2$ (**33**), i.e. the aluminum analog of $[Cy_7Si_7O_{12}B]_2$ (**23**). A similar reaction of **3** with $(i\text{-}PrO)_3Al$ also produced **33** in nearly quantitative yield, although only after prolonged heating to 65–110 °C. No monomeric intermediates could be observed in these reactions. However, the monomeric adducts $Cy_7Si_7O_{12}Al(ONMe_3)$ (**34**) and $Cy_7Si_7O_{12}Al(OPPh_3)$ (**35**) were readily obtained by cleavage of the dimer in the presence of Me_3NO or Ph_3PO, respectively.[47] The triphenylphosphine oxide adduct **35** was structurally characterized by X-ray diffraction.

In striking contrast to the formation of dimeric **33** from **3** and $AlMe_3$ as reported by Feher *et al.*,[47] the analogous reaction between the cyclopentyl-substituted silsesquioxane precursor **2** and $AlEt_3$ according to Scheme 12 afforded polymeric $[(c\text{-}C_5H_9)_7Si_7O_{12}Al]_n$ (**36**), which was found to be insoluble in most common organic solvents (hexane, toluene, THF).[48] Monomeric $[(c\text{-}C_5H_9)_7Si_7O_{11}(OSiMe_3)]AlEt \cdot NEt_3$ (**37**) was obtained when the monosilylated precursor $(c\text{-}C_5H_9)_7Si_7O_9(OSiMe_3)(OH)_2$ (**38**) was treated with one equivalent of $AlEt_3$ in the presence of triethylamine. By allowing $AlEt_3$ to react with two equivalents of **38**, the Brønsted acidic aluminasilsesquioxane $[(c\text{-}C_5H_9)_7Si_7O_{11}(OSiMe_3)]Al[(c\text{-}C_5H_9)_7Si_7O_{10}(OSiMe_3)(OH)]$ (**39**) was selectively formed, which contains a strong intramolecular hydrogen bond. Although the high strength of this hydrogen bond reduces the Brønsted acidity of **39** substantially, the compound can be easily deprotonated by amines to yield the corresponding ammonium salts $X^+[\{(c\text{-}C_5H_9)_7Si_7O_{11}(OSiMe_3)\}_2Al]^-$ (**40**–**42**, $X^+ = Et_3NH^+$, $PhN(H)Me_2^+$, $C_5H_5NH^+$).

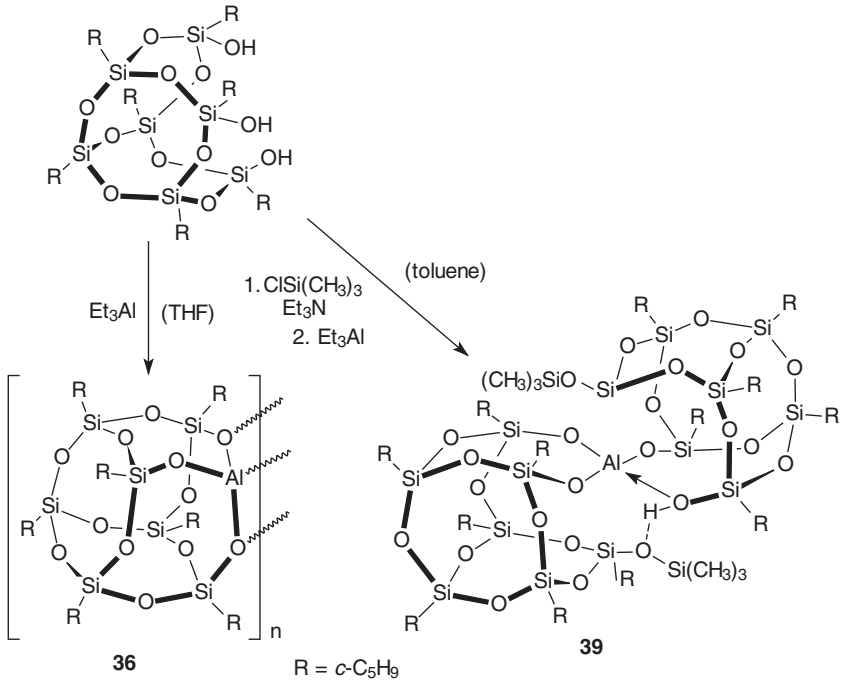

SCHEME 12. Synthesis of the aluminasilsesquioxanes **36** and **39**.

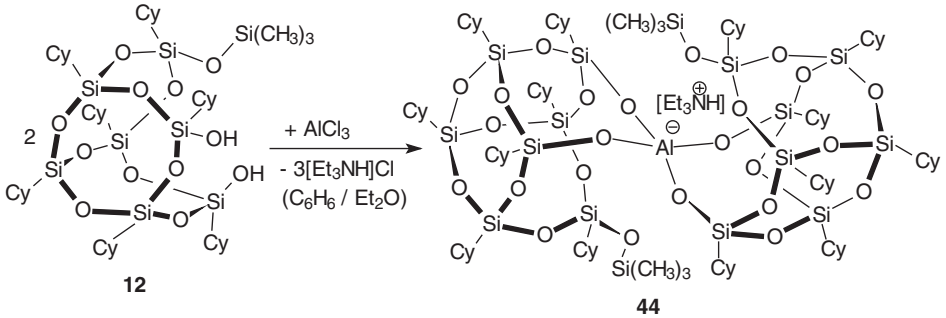

SCHEME 13. Synthesis of $[Et_3NH]^+[\{Cy_7Si_7O_{11}(OSiMe_3)\}_2Al]^-$ (**44**).

An X-ray crystal structure of **40** revealed that the ammonium cation is bonded to the aluminasilsesquioxane anion by a hydrogen bond. The corresponding lithium salt $[Li(THF)_2]^+[\{(c\text{-}C_5H_9)_7Si_7O_{11}(OSiMe_3)\}_2Al]^-$ (**43**) could best be prepared by protonolysis of $(c\text{-}C_5H_9)_7Si_7O_9(OSiMe_3)(OH)_2$ (**38**) with half an equivalent of $LiAlH_4$.[48]

The cyclohexyl-substituted analog of **40**, $[Et_3NH]^+[\{(c\text{-}C_6H_{11})_7Si_7O_{11}(OSiMe_3)\}_2Al]^-$ (**44**), was synthesized independently in our laboratory by dehydrochlorination of the monosilylated precursor **12** with anhydrous $AlCl_3$ in the presence of triethylamine (Scheme 13).[49] A comparison of the X-ray crystal structures of

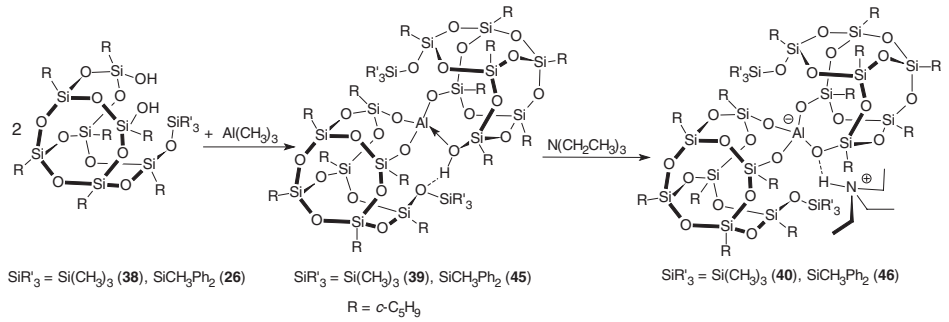

SCHEME 14. Formation of aluminasilicates **40** and **46**.

40 and **44** clearly revealed the difference in steric congestion between cyclopentyl and cyclohexyl-substituted aluminasilsesquioxanes. Whereas in the latter structure the aluminasilicate anion and the triethylammonium cation form a separated ion pair,[49] less steric crowding in **40** allows the formation of a contact ion pair in which the ammonium proton forms a hydrogen bond with one of the Al–O–Si oxygen atoms in the aluminasilicate anion.[48]

The steric factors affecting the Brønsted acidity of these aluminasilsesquioxanes have been studied in great detail by Duchateau *et al.* (Scheme 14).[50] By reacting $AlMe_3$ with two equivalents of the monosilylated precursors **38** and **26**, the corresponding Brønsted acidic aluminasilsesquioxanes **39** and **45** were prepared. These complexes react readily with triethylamine to yield the corresponding triethylammonium salts **40** and **46**. Hydrogen bonding between the acidic SiO(H)→Al proton and the pendant silylether function is effectively reduced by increasing the steric bulk of the silyl ether substituents, resulting in a higher acidity for **45** compared to that of **39**.[50]

With the rarely used octameric silsesquioxane ligand $(c\text{-}C_5H_9)_8Si_8O_{11}(OH)_2$ (**47**), which lacks pendant silylether functions, the acidic proton cannot satisfactorily be stabilized. This renders the putative Brønsted acid $[(c\text{-}C_5H_9)_8Si_8O_{13}]Al[(c\text{-}C_5H_9)_8Si_8O_{12}(OH)]$ (**48**) unstable. In the absence of proton acceptors, the disproportionation product $[(c\text{-}C_5H_9)_8Si_8O_{13}]_3Al_2$ (**49**) is formed instead of **48**. However, in the presence of triethylamine the initially formed Brønsted acid **48** readily transfers its proton to the amine, affording the triethylammonium salt **50** (Scheme 15).[50]

Several other aluminasilsesquioxanes have been studied in detail by Duchateau *et al.* as model supports for silica-grafted aluminum alkyl species.[51] Upon treatment with $AlMe_3$ the *closo*-silsesquioxane monosilanol $(c\text{-}C_5H_9)_7Si_8O_{12}(OH)$ (**28**) afforded polymeric $[\{(c\text{-}C_5H_9)_7Si_8O_{13}\}AlMe_2]_n$ (**51**), which is readily transformed into the corresponding monomeric pyridine adduct, $[(c\text{-}C_5H_9)_7Si_8O_{13}]AlMe_2(py)$ (**52**) (Scheme 16).

When the monosilylated precursor $(c\text{-}C_5H_9)_7Si_7O_9(OSiMePh_2)(OH)_2$ (**26**) was analogously reacted with $AlMe_3$, noticeable amounts of the 1:2 product $[\{(c\text{-}C_5H_9)_7Si_7O_{11}(OSiMePh_2)\}(AlMe_2)_2]_2$ (**53**) and the Brønsted acidic 2:1 product **45** were formed besides the main product of the reaction, $[\{(c\text{-}C_5H_9)_7Si_7O_{11}(OSiMePh_2)\}AlMe]_2$ (**54**) (Scheme 17). The latter is a mixture of three dimeric

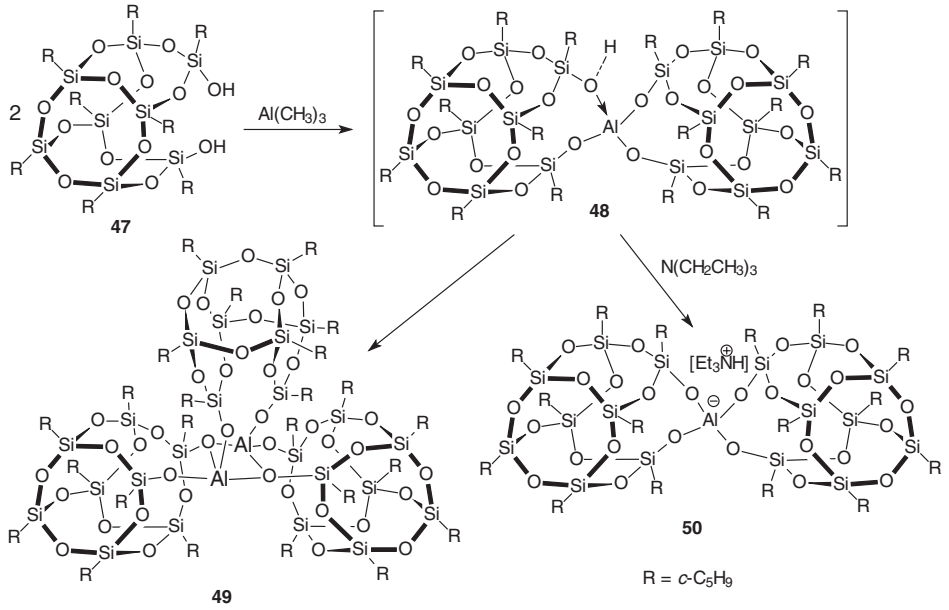

SCHEME 15. Formation of aluminasilsesquioxanes **49** and **50**.

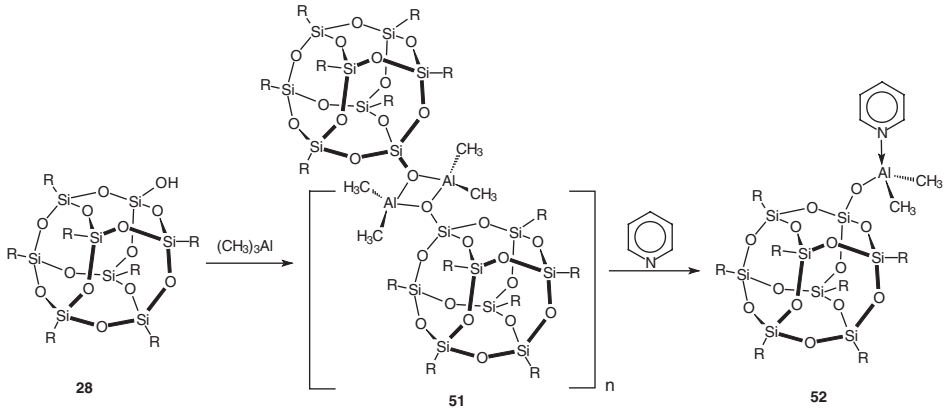

SCHEME 16. Synthesis of aluminasilsesquioxanes **51** and **52**.

conformational isomers, all with the aluminum methyls *trans* to each other. The difference of the conformers originates from the different orientation of the silsesquioxane ligands.[51]

The first and thus far only indasilsesquioxane derivative was synthesized in our laboratory. The compound $[Cy_7Si_7O_{12}InMe(OH)]_2$ (**55**) was prepared in high yield (84%) by reacting trisilanol **3** with trimethylindium in toluene solution at 20 °C (Scheme 18). The molecular structure of **55** has been determined by X-ray diffraction. Self-assembly under formation of a centrosymmetric dimer occurs through

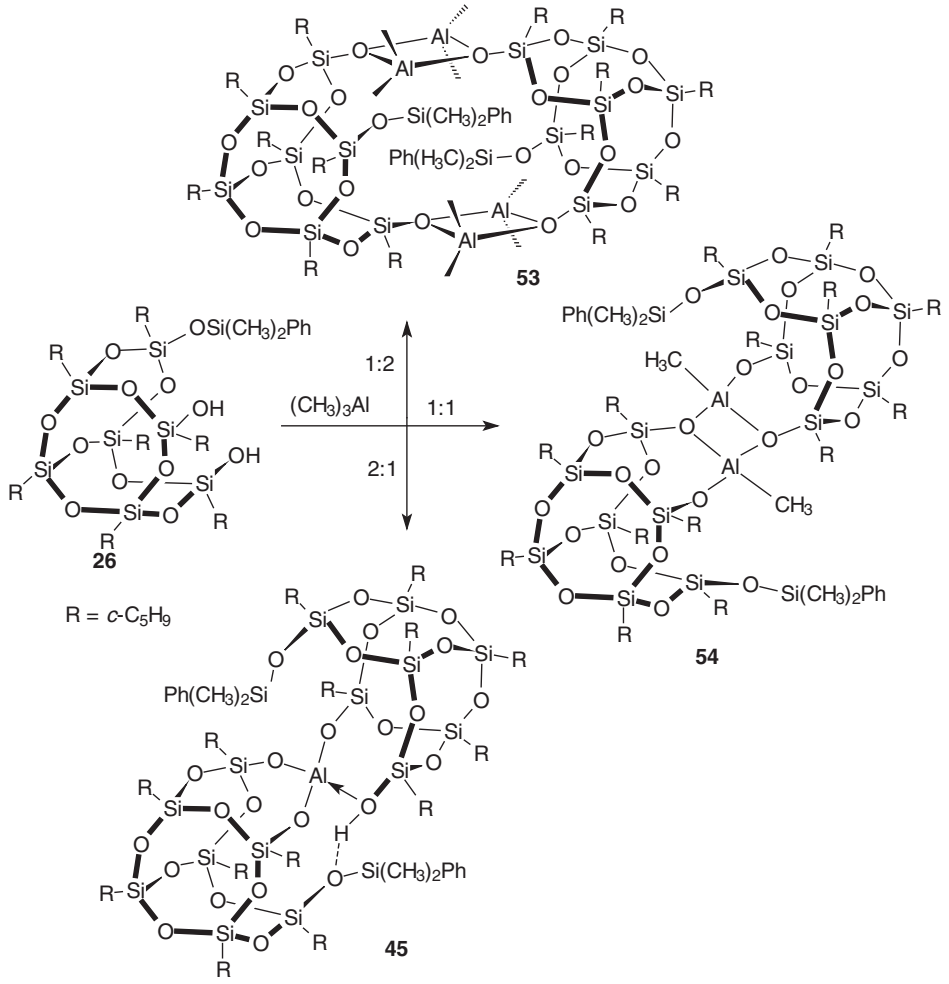

SCHEME 17. Reactions of $(c\text{-}C_5H_9)_7Si_7O_9(OSiMePh_2)(OH)_2$ (**26**) with $AlMe_3$.

cage oxygen atoms, which act as bridging ligands between the two indium atoms. The central four-membered In_2O_2 ring forms a rectangular plane with In–O–In and O–In–O bond angles of 101.0(1) and 79.0(1), respectively, and an average In–O distance of 2.123 Å. Certainly, the most striking structural feature of **55** is the presence of two Si–OH groups in close proximity to the methylindium centers. However, no further protonation of the methyl groups at indium can occur, because the silanol functions are both engaged in hydrogen bonding to oxygen atoms of the silsesquioxane cages.[52]

Several gallium-containing metallasilsesquioxanes have been reported, although their chemistry is still less developed than that of their aluminum congeners. According to a report by Feher *et al.*, **3** reacts with $GaCl_3$ in the presence of "proton sponge" to form the ionic complex $[C_{14}H_{19}N_2]^+[Cy_7Si_7O_{12}GaCl]^-$ (**56**)

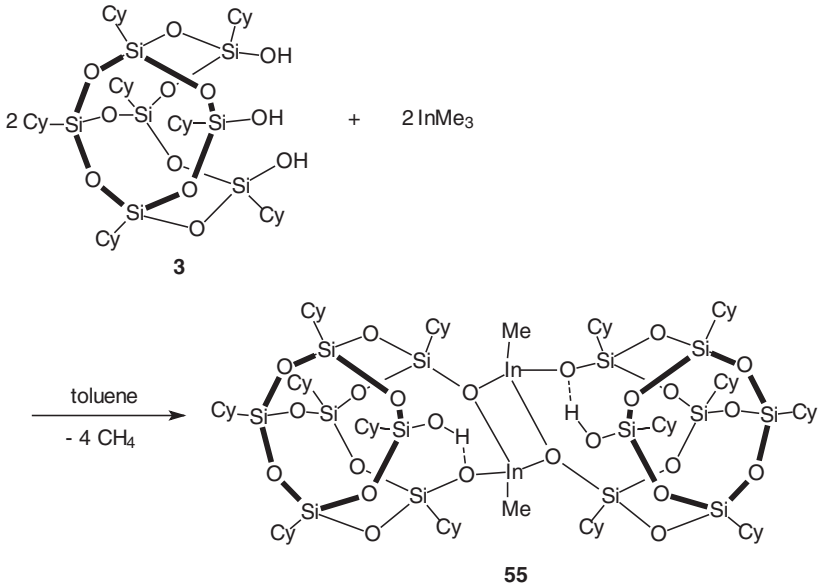

SCHEME 18. Synthesis of $[Cy_7Si_7O_{12}InMe(OH)]_2$ (**55**).

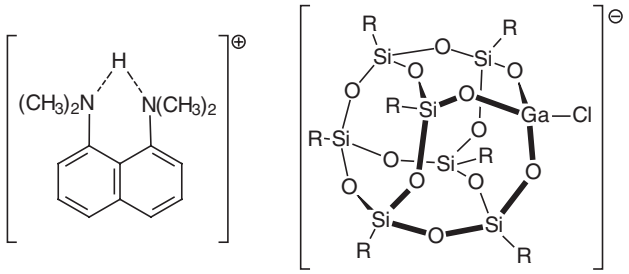

56 (R = *c*-C_6H_{11})

SCHEME 19. Structure of $[C_{14}H_{19}N_2]^+[Cy_7Si_7O_{12}GaCl]^-$ (**56**).

(Scheme 19).[53] Refluxing of **56** in THF led to the formation of dimeric $[Cy_7Si_7O_{12}Ga]_2$ (**57**) as a structural analog of the corresponding boron and aluminum dimers **23** and **33**, respectively. The reactivity of **58** also resembles that of the aluminum species **33** in that the dimeric structure could readily be split by triphenylphosphine oxide to form the neutral Lewis base adduct $Cy_7Si_7O_{12}Ga(OPPh_3)$ (**58**).

More recently the chemistry of gallium-containing metallasilsesquioxanes has been studied in greater detail by Duchateau and co-workers (Scheme 20).[38] Using similar conditions Feher *et al.* reported for the synthesis of **56** and the dimer $[Cy_7Si_7O_{12}Ga]_2$ (**57**),[53] the reaction of **3** with $GaCl_3$ in the presence of triethylamine gave moderate yields (38%) of the monomeric gallasilsesquioxane **59**. The bulky

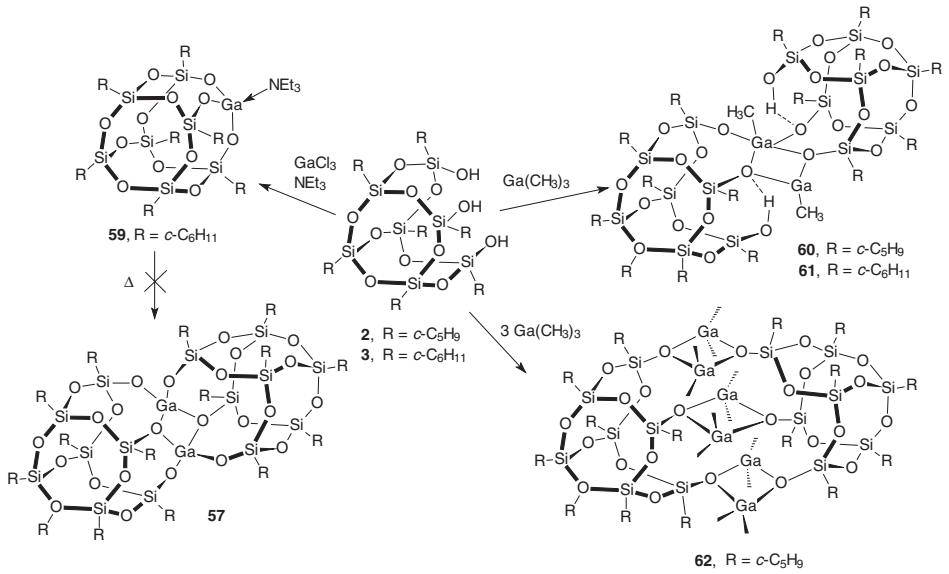

SCHEME 20. Synthesis of gallasilsesquioxanes derived from **2** and **3**.

triethylamine in **59** binds surprisingly strongly to the gallium center, as attempts to form $[Cy_7Si_7O_{12}Ga]_2$ (**57**) by heating **59** in toluene failed.

A second series of gallasilsesquioxanes was prepared using the monosilylated derivative **26** as precursor.[38] Salt metathesis between **26** and 0.5 equivalents of gallium trichloride in the presence of triethylamine yielded the triethylammonium gallate $[Et_3NH]^+[\{(c\text{-}C_5H_9)_7Si_7O_{11}(OSiMePh_2)\}_2Ga]^-$ (**63**), similar to the aluminate complex $[Et_3NH]^+[\{(c\text{-}C_5H_9)_7Si_7O_{11}(OSiMePh_2)\}_2Al]^-$ (**46**), which was obtained when **26** was reacted with $AlCl_3$ in the presence of NEt_3. An X-ray crystal structure determination of **63** revealed a contact ion pair in the solid state in which the ammonium ion is hydrogen bonded to one of the Ga–O–Si oxygens.

Upon treatment with another equivalent of trimethylgallium, **63** is readily deprotonated with liberation of triethylamine and formation of the dimethylgallium gallate **64**. When, instead of **2**, the monosilylated disilanol **26** was treated with an equimolar amount of $GaMe_3$, the dimeric monomethylgallium silsesquioxane complex **65** was formed. A similar reaction with two equivalents of trimethylgallium afforded the tetranuclear gallium complex **66** in good yields (72%) in the form of an air-stable white solid (Scheme 21).[38] Controlled calcination of certain gallium silsesquioxane precursors has been shown by Wada *et al.*[54] to afford microporous gallium silicate materials.

Several thallium silsesquioxane complexes have been reported by Feher *et al.*[23,32] These include the compounds $R_7Si_7O_9(OTl)_3$ (**67**, R = *c*-C_5H_9; **68**, R = *c*-C_6H_{11}), $R_7Si_7O_9(OSiMe_3)(OTl)_2$ (**69**, R = *c*-C_5H_9; **70**, R = *c*-C_6H_{11}) and $R_7Si_7O_9(OSiMe_3)_2(OTl)$ (**71**, R = *c*-C_5H_9; **72**, R = *c*-C_6H_{11}). These thallasilsesquioxanes are not prone to cycloelimination reactions or the formation of "ate" complexes. Thus they are versatile anionic equivalents of the incompletely condensed silsesquioxane

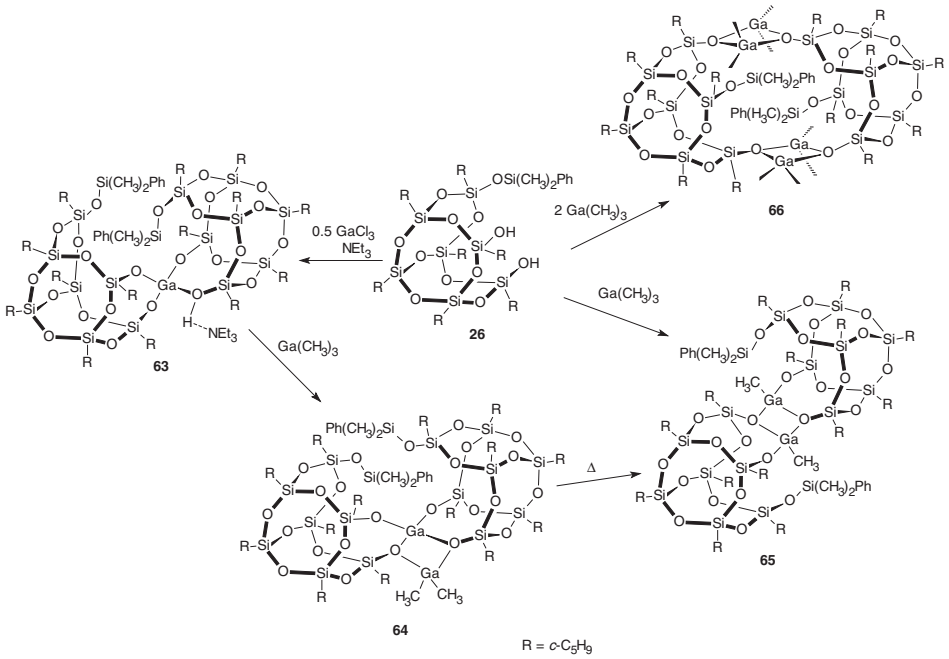

SCHEME 21. Synthesis of gallasilsesquioxanes derived from **26**.

systems, which react with a variety of metal and non-metal halides to afford high yields of the corresponding metallasilsesquioxanes. They are especially useful for reactions with high-valent transition metal halides where dehydration reactions of the silsesquioxane framework is a frequently encountered problem. However, their overall synthetic value is limited due to the high toxicity of thallium reagents.

4. Group 14 Metal Derivatives (Ge, Sn)

Silylated derivatives of incompletely condensed silsesquioxanes are often used as starting materials for the synthesis of metallasilsesquioxanes. However, their chemistry is not considered to fall within the scope of this review article. Thus, only germanium and tin derivatives will be mentioned. Apparently, lead-containing metallasilsesquioxanes have not yet been reported in the literature. The first report on a germanium silsesquioxane complex dates back to 1989, when Feher *et al.*[10] described the synthesis of $Cy_7Si_7O_{12}GeMe$ (**73**) from **3** and methyl trichlorogermane in the presence of triethylamine. Colorless crystals of **73** were isolated in 92% yield. In the same paper, the synthesis of the first tin(IV) silsesquioxane derivative was reported. Treatment of **3** with $MeSnCl_3/NEt_3$ afforded $Cy_7Si_7O_{12}SnMe$ (**74**) in 96% yield. A series of di- and triorganotin(IV) silsesquioxane complexes has been prepared in our laboratory in 1999.[55] These include the diorganotin(IV)-capped silsesquioxanes $Cy_7Si_7O_9(OSiMe_3)(O_2SnR_2)$ (**75**, R = Me; **76**, R = *n*-Bu) and the triorganotin(IV) derivatives $Cy_7Si_7O_9(OSiMe_3)_2(OSnR_3)$ (**77**, R = Me; **78**,

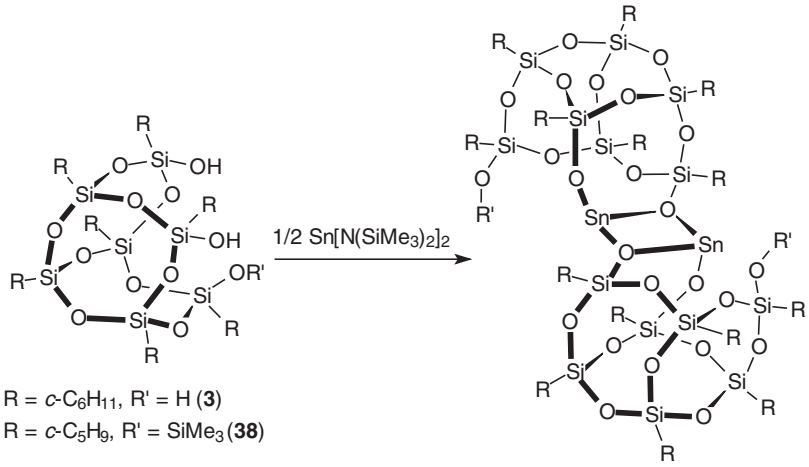

SCHEME 22. Preparation of stannasilsesquioxanes **79** and **80**.

R = CH_2Ph). All these compounds have been made by reacting **3** with the corresponding organotin(IV) chlorides in the presence of appropriate amounts of triethylamine. Recently various other stannasilsesquioxanes have been reported, including the first tin(II) species.[56] Protonolysis of tin(II) amides was found to be an effective route to prepare tin(II) silsesquioxanes. For example, the reaction of $Sn[N(SiMe_3)_2]_2$ with trisilanol **3** or disilanol **38** afforded the stannasilsesquioxanes $[Cy_7Si_7O_{11}(OH)Sn^{II}]_2$ (**79**) and $[(c\text{-}C_5H_9)_7Si_7O_{11}(OSiMe_3)Sn^{II}]_2$ (**80**) (Scheme 22). Both are dimers with three-coordinated tin centers. Taking the lone pair into account, the tin atoms are distorted-tetrahedrally surrounded. The central four-membered Sn_2O_2 ring is planar.

Similar to the longer known diorganotin(IV)-capped silsesquioxanes $Cy_7Si_7O_9(OSiMe_3)(O_2SnR_2)$ (**75**, R = Me; **76**, R = *n*-Bu), two stannasilsesquioxanes have been prepared in which two silanol oxygens are bridged by a $Sn(acac)_2$ moiety. The compounds **81** and **82** were made in good yields according to Scheme 23 by reaction of the precursors **2** and **38**, respectively, with $Cl_2Sn(acac)_2$ in the presence of NEt_3.[56]

Unexpectedly, the reaction of $SnCl_4$ with **38** was sluggish and produced ill-defined products.[56] Treatment of **2** with an equimolar amount of $SnCl_4$ in toluene in the presence of NEt_3 afforded the ionic trimer **83** instead of the expected monomeric $(c\text{-}C_5H_9)_7Si_7O_{12}SnCl$ (Scheme 24). In this chloride-bridged cluster each tin atom is connected to two different silsesquioxane cages. Three chlorides are μ_2-bridging, while one is μ_3-bridging between all three tin centers. The chloro complex **83** is moisture sensitive and gradually hydrolyses to the corresponding hydroxide species **84**. When for example, a bromoform solution of **83** was layered with water and left at ambient temperature, large colorless crystals of **84** suitable for X-ray analysis formed overnight. Complex **84** is isostructural to **83** and consists of an

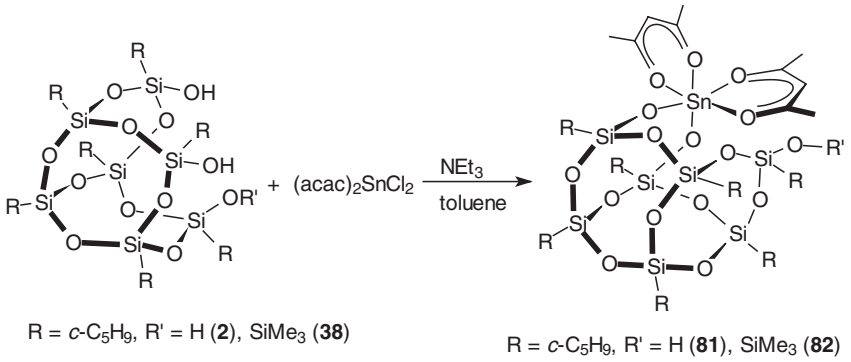

SCHEME 23. Preparation of stannasilsesquioxanes **81** and **82**.

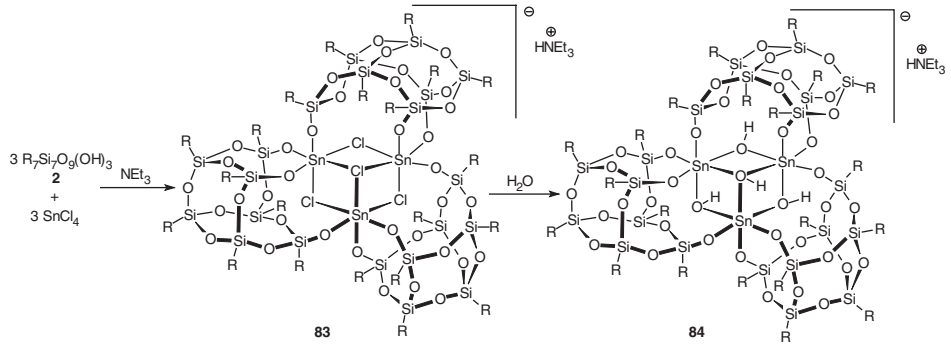

SCHEME 24. Preparation of the trinuclear tin silsesquioxane clusters **83** and **84**.

anionic cluster in which three silsesquioxane cages are held together by three tin atoms with bridging hydroxyl groups.

B. *Metallasilsesquioxanes of the Early Transition Metals*

1. Group 3 Metal Derivatives (Sc, Y, La, and the Lanthanides and Actinides)

Metallasilsesquioxanes of rare earth metals could be very important as homogeneous analogs of rare earth metal silica-supported catalysts and rare earth silicates, which are potential materials for optoelectronics. Thus this area of research is of considerable interest for several fields of chemistry including catalysis and materials science. However, investigations in the area of metallasilsesquioxanes of rare earth metals are often hampered by difficulties with crystallization and characterization of these compounds. The first metallasilsesquioxanes incorporating lanthanide elements have been described in 1994 by Herrmann *et al.*[57] These materials were obtained by reacting **3** with the tris(silylamides) $Ln[N(SiMe_3)_2]_3$ of Y and Nd. Due to their very high solubility no structural characterization of the initially formed products was possible. However, with the use of triphenylphosphine oxide

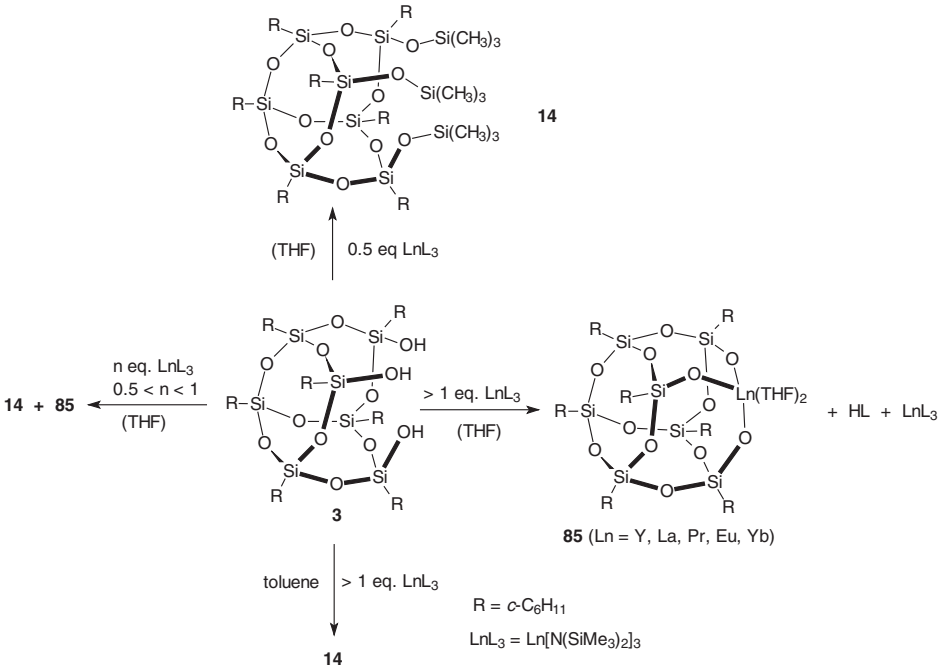

SCHEME 25. Reactions of **3** with $Ln[N(SiMe_3)_2]_3$ (Ln = Y, La, Pr, Eu, Yb).

as supporting ligand X-ray quality single crystals could be obtained, and a dimeric structure was established for the Y and Nd silsesquioxane complexes.

More recently, Aspinall *et al.* reported the synthesis of a series of lanthanide silsesquioxanes resulting from reactions of **3** with lanthanide tris(silylamides) $Ln[N(SiMe_3)_2]_3$ (Ln = Y, La, Pr, Eu, Yb).[58] However, single crystals of these materials suitable for X-ray diffraction could not be obtained. The somewhat complicated situation is illustrated in Scheme 25. The lanthanide tris(silylamides) reacted with two-third equivalents of the trisilanol **3** in THF to give the lanthanide silsesquioxanes **85**, which are dimeric in solution at 233 K. Reaction of $Ln[N(SiMe_3)_2]_3$ with one equivalent of **3** in THF resulted in complete conversion of **3** to the trisilylated compound **14**, as did the reaction of $Ln[N(SiMe_3)_2]_3$ with two-third equivalents of **3** in toluene.

Variable temperature ^{13}C NMR data of the Y derivative were consistent with a monomer/dimer equilibrium for compounds **85** in solution as depicted in Scheme 26.[58]

The chloro-functionalized lanthanide silsesquioxane complexes **86** (Ln = Y, La) are accessible by the reaction of **85** with one equivalent of Me_3SiCl according to Scheme 27.[58]

Well-defined monomeric derivatives could be obtained by reacting **85** (Ln = Y, La, Yb) with $(Me_2NCH_2CH_2)_2NMe$ (PMDTA) (PMDTA = N,N,N′,N″,N″-pentamethyldiethylenetriamine) in a 1:1 molar ratio in THF solution. The products

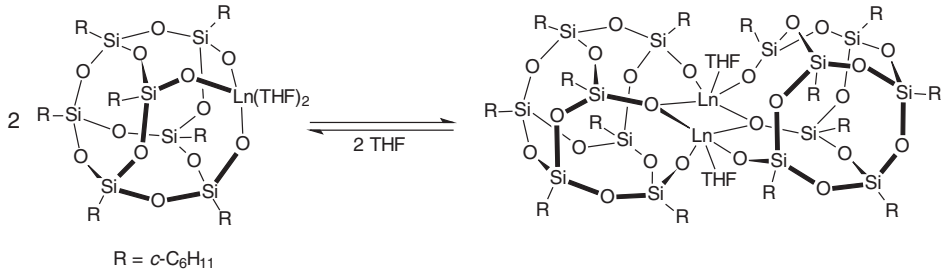

SCHEME 26. Proposed monomer/dimer equilibrium for compounds **85**.

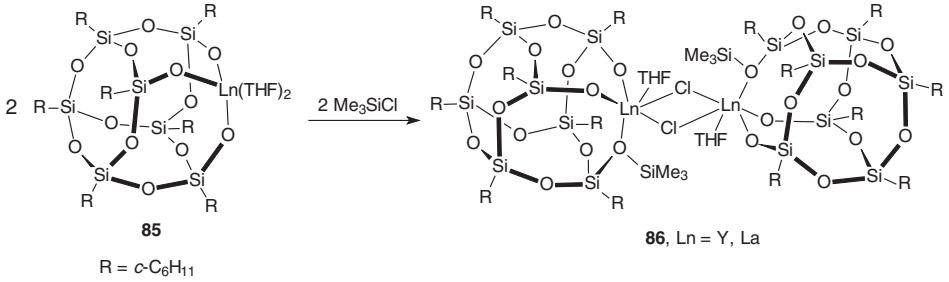

SCHEME 27. Preparation of functionalized lanthanide silsesquioxanes **86**.

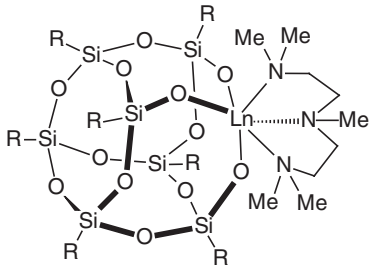

SCHEME 28. Structure of $Cy_7Si_7O_{12}Ln(PMDTA)$ (**87**, Ln = Y, La, Yb).

$Cy_7Si_7O_{12}Ln(PMDTA)$ (**87**, Ln = Y, La, Yb) are depicted in Scheme 28. In all these cases severe disorder problems prevented a structural characterization of the lanthanide silsesquioxanes by X-ray diffraction.[58]

The ytterbium derivative $Cy_7Si_7O_{12}Yb(PMDTA)$ (**87**, Ln = Yb) was also obtained directly by reacting $Yb[N(SiMe_3)_2]_3$ with the trisilanol **3** in the presence of PMDTA.[59] Attempts to grow single crystals of $Cy_7Si_7O_{12}Yb(PMDTA)$ resulted in a small number of good-quality prisms, which were shown by X-ray diffraction to be the heterobimetallic Li/Yb silsesquioxane complex $[(Cy_7Si_7O_{12})\{Cy_7Si_7O_{11}$

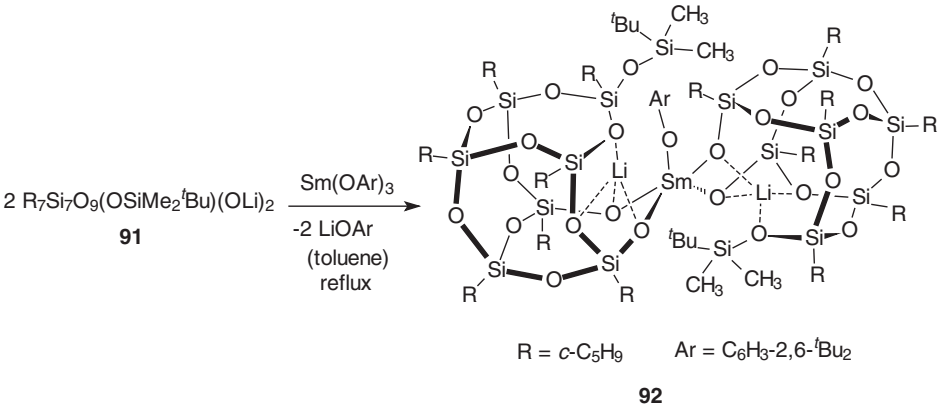

SCHEME 29. Synthesis of the heterobimetallic Li/Sm silsesquioxane complex **92**.

$(OSiMe_3)\}YbLi_2(THF)_2(MeCN)] \cdot 2.5THF$ (**88**). Its formation can be ascribed to the presence of a very small impurity of $LiN(SiMe_3)_2$ in the $Yb[N(SiMe_3)_2]_3$ starting material. Although $HN(SiMe_3)_2$ does not react directly with **3** on standing at room temperature overnight, small quantities of $Cy_7Si_7O_9(OH)_2(OSiMe_3)$ (**12**) were probably formed under the catalytic influence of a Lewis acidic lanthanide species, thus accounting for the monosilylated silsesquioxane ligand in **88**. Compound **88** could be more rationally prepared by lithiation of **12** with *n*-BuLi and reaction of the resulting $Cy_7Si_7O_9(OLi)_2(OSiMe_3)$ (**89**) with $Cy_7Si_7O_{12}Yb(THF)_2$ (**85**, Ln = Yb). The yttrium analog of **88** was prepared in a similar manner.

Arnold *et al.*[60] reported the synthesis and structural characterization of an aryloxide-functionalized samarium silsesquioxane complex. Steric protection of **2** by one $SiMe_2tBu$ group generated a new disilanol ligand, $(c\text{-}C_5H_9)_7Si_7O_9(OH)_2(OSiMe_2tBu)$ (**90**), that allows only restricted access to a coordinated metal. Lithiation of **90** with *t*BuLi afforded the stable dilithium intermediate $(c\text{-}C_5H_9)_7Si_7O_9(OLi)_2(OSiMe_2tBu)$ (**91**). Subsequent reaction of **91** with the homoleptic samarium aryloxide $Sm(OC_6H_3tBu_2\text{-}2,6)_3$ according to Scheme 29 gave the novel heterobimetallic Li/Sm silsesquioxane complex **92**, which was structurally characterized by X-ray diffraction.

Our own efforts in this field resulted in the isolation of an unprecedented cerium(IV) silsesquioxane complex[61] as well as the structural characterization of a bimetallic ytterbium derivative.[34] Treatment of $Ce[N(SiMe_3)_2]_3$ with two equivalents of the disilanol $Cy_8Si_8O_{11}(OH)_2$ (**93**) (the cyclohexyl-substituted analog of **47**) in diethyl ether in the presence of an excess of pyridine exclusively afforded the diamagnetic complex $(Cy_8Si_8O_{13})_2Ce(py)_3$ (**94**). The same compound **94**, albeit in somewhat lower yield, could also be prepared by direct reaction of anhydrous $CeCl_3$ with two equivalents of **93** in THF/pyridine mixture (Scheme 30). Quite surprisingly in both cases cerium was oxidized to the tetravalent oxidation state. The compound gave satisfactory C-, H-, N-analysis and was fully characterized by IR and ^1H, ^{13}C and ^{29}Si NMR spectra as well as X-ray single crystal diffraction.

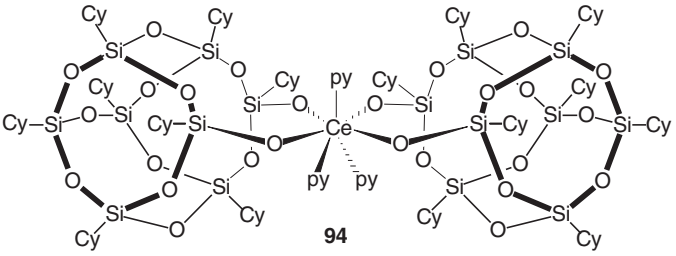

SCHEME 30. Schematic representation of the cerium(IV) silsesquioxane **94**.

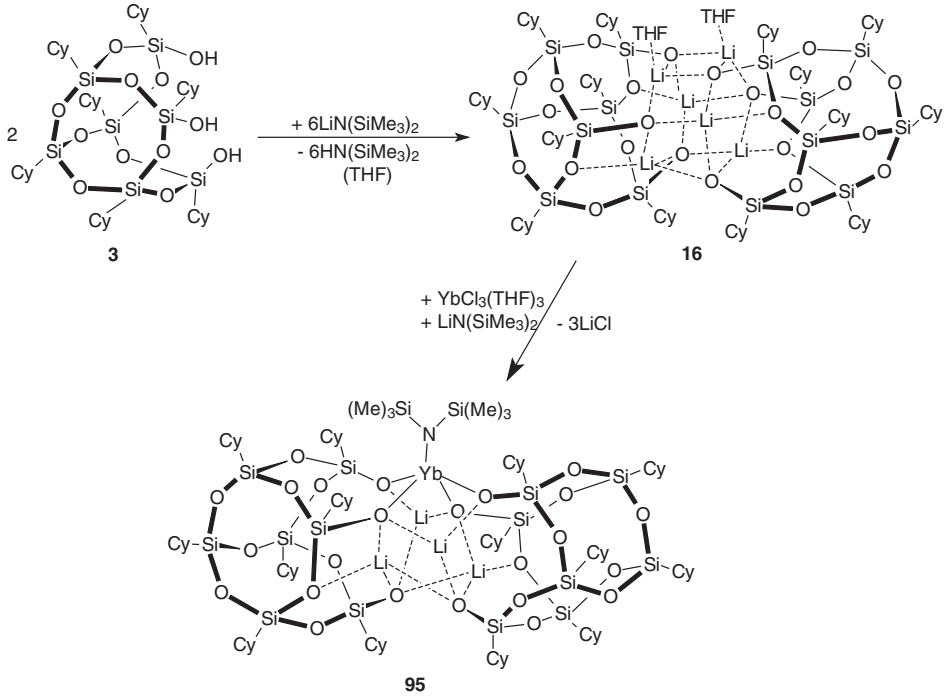

SCHEME 31. Preparation of the amidoytterbium silsesquioxane **95**.

Compound **94** represents the first example of a metallasilsesquioxane derived from the octameric disilanol ligand $[(c\text{-}C_6H_{11})_8Si_8O_{13}]^{2-}$.[14,17,62] The central Ce atom is coordinated by four oxygen atoms of two siloxane ligands and three nitrogens of three pyridine molecules resulting in a distorted pentagonal bipyramidal arrangement.

Finally, an unprecedented functionalized ytterbium silsesquioxane was obtained as outlined in Scheme 31. Trisilanol **3** was lithiated *in situ* using an excess of $LiN(SiMe_3)_2$, followed by treatment of the reaction mixture with anhydrous ytterbium trichloride.[34] The resulting colorless crystals of **95** were fully characterized by spectroscopic and analytical methods as well as an X-ray crystal structure

determination. In this molecule a reactive ytterbium bis(trimethylsilyl)amide unit resides on a model silica surface formed by two lithium-linked silsesquioxane cages. Thus **95** represents the first example of a monofunctional lanthanide silsesquioxane, which could be of interest for catalytic applications (Scheme 31).[34]

Two novel complexes of samarium and scandium containing silsesquioxane silanolate ligands have been synthesized with the use of the *closo*-silsesquioxane silanolate ligand $Cy_7Si_8O_{12}O^-$ and structurally characterized by X-ray diffraction.[63] Yellow $(C_5Me_5)_2Sm[\mu\text{-}Cy_7Si_8O_{12}O]_2Li(THF)$ (**98**), the first *organo*lanthanide silsesquioxane complex reported in the literature, has been obtained by treatment of the "ate"-complex $(C_5Me_5)_2Sm(\mu\text{-}Cl)_2Li(THF)_2$ with $Cy_7Si_8O_{12}OLi$ (**97**) in a molar ratio of 1:2 (Scheme 32). The starting material $Cy_7Si_8O_{12}OH$ (**96**) was prepared in close analogy to a published procedure[64] in two steps by treatment of $Cy_7Si_7O_9(OH)_3$ (**3**) with $SiCl_4$ in the presence of triethylamine, followed by hydrolysis of the intermediate chlorosilane $Cy_7Si_7O_{12}Cl$. Metalation of $Cy_7Si_8O_{12}OH$ with methyllithium in diethylether proceeded smoothly at room temperature to afford $Cy_7Si_8O_{12}OLi$ (**97**), which was used *in situ* for further reactions. The ^{29}Si NMR spectrum of **98** shows eight resonances of the same intensity, indicating that all silicon atoms of the $Cy_7Si_8O_{12}$ cages are chemically non-equivalent despite the C_{3v} symmetry of the ligand. This was confirmed by an X-ray diffraction study, which revealed the presence of a heterobimetallic complex in which samarium and lithium are bridged by two silsesquioxane silanolate ligands.

A different synthetic approach was chosen to synthesize a related scandium silsesquioxane complex.[63] Treatment of $(C_5Me_5)Sc(acac)_2$[65] with the free silanol $Cy_7Si_8O_{12}OH$ (**96**) in refluxing toluene (molar ratio 1:1) resulted in elimination of pentamethylcyclopentadiene and formation of the novel binuclear scandium complex $[Sc(acac)_2(\mu\text{-}Cy_7Si_8O_{12}O)]_2$ (**99**) (Scheme 32). Colorless single crystals of **99** suitable for X-ray diffraction were obtained by fractional crystallization from pentane. The crystal structure consists of dimeric molecules in which two $Sc(acac)_2$ units are symmetrically bridged by the monoanionic silsesquioxane silanolate ligands. Compound **99** represents the first example of a scandium complex containing silsesquioxane derivatives as ligands. The only closely related compound is the trinuclear scandium disiloxanediolate complex $[(Ph_2Si_2O)_2O]_2Sc_3(acac)_5$, which has been prepared in a similar manner by treatment of $(C_5Me_5)Sc(acac)_2$ with 1,1,3,3-tetraphenyldisiloxanediol.[66]

The first and thus far only silsesquioxane complex of an actinide element is $[Cy_7Si_7O_{12}]_2U$ (**100**).[35] This colorless, nicely crystalline uranium(VI) compound is formed upon reaction of **3** with any uranium precursor, e.g., UCl_4 in the presence of NEt_3. In all cases oxidation of uranium to the hexavalent oxidation state is observed. The best synthetic route leading to **100** in ca. 80% yield is the reaction of **3** with uranocene as outlined in Scheme 33.

2. Group 4 Metal Derivatives (Ti, Zr, Hf)

Apparently, the most thoroughly investigated class of complexes in this area are Ti complexes because of their promising catalytic applications.[1–3] The first Ti derivatives were made by Feher *et al.* and include Ti(III)[67,68] and Ti(IV) silsesquioxanes.[69,70] The former have been prepared by reacting **3** with either

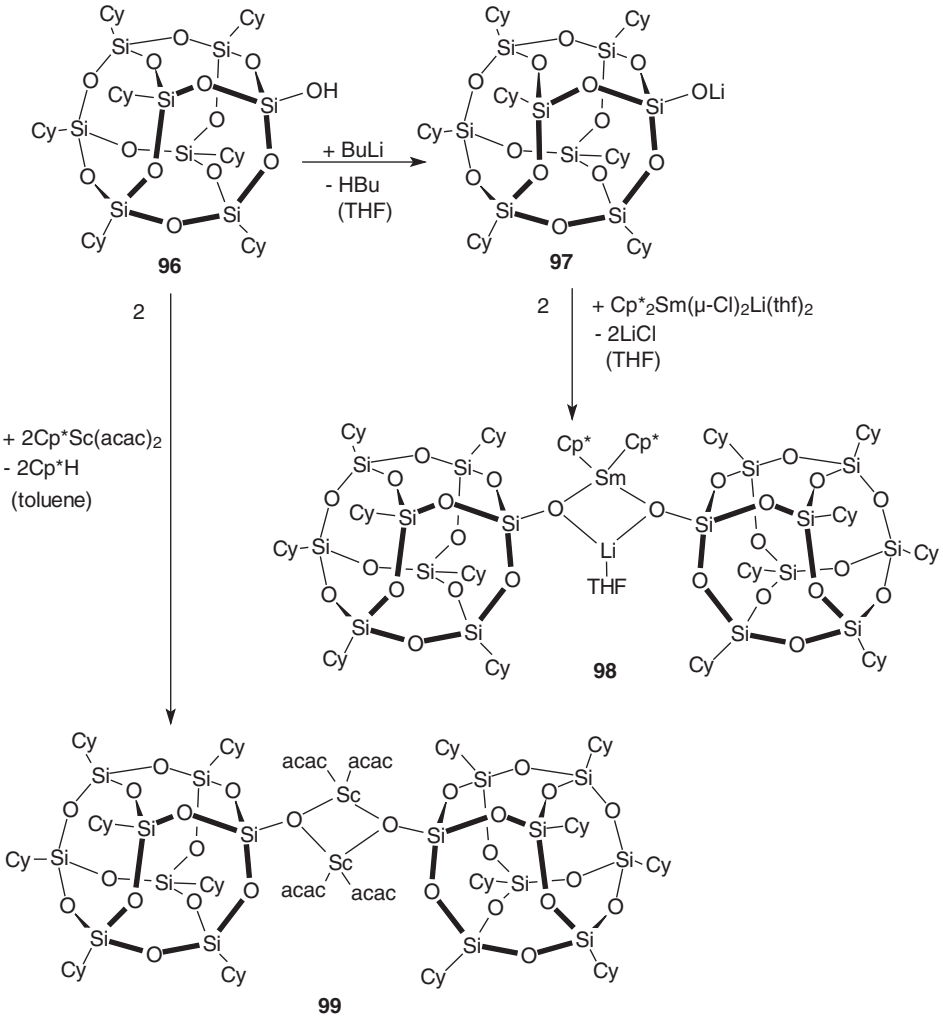

SCHEME 32. Synthesis of the Sm and Sc silsesquioxane complexes **98** and **99**.

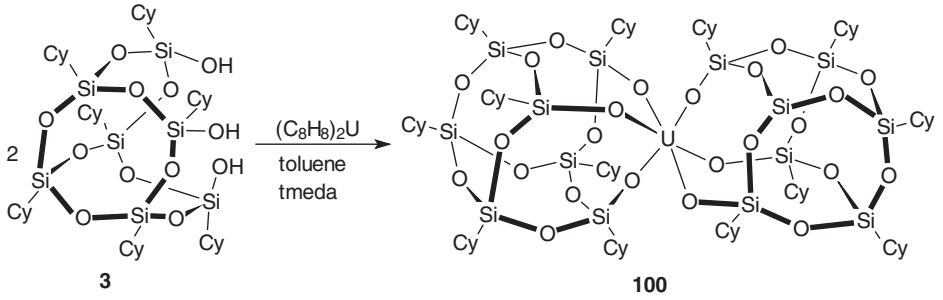

SCHEME 33. Preparation of the uranium(VI) silsesquioxane complex **100**.

$Ti[N(SiMe_3)_2]_3$ or $TiCl_3(NMe_3)_2$. Blue dimeric $[Cy_7Si_7O_{12}Ti]_2$ (**101**) is the initial product in these reactions. Treatment of **101** with pyridine affords the bis-adduct $[Cy_7Si_7O_{12}Ti(py)]_2$ (**102**).[67,68] Corner-capping of the silsesquoxane framework with a TiCp unit is also readily achieved yielding monomeric $Cy_7Si_7O_{12}TiCp$ (**103**).[69,70] Other titanasilsesquioxanes have been designed as model compounds for titanosilicates, which are industrially important as oxidation catalysts.[71] Examples of such realistic models include $(MeC_5H_4)_4Ti_4(Si\mathit{t}Bu)_4O_{12}$ (**104**),[72] $[2,6\text{-}\mathit{i}Pr_2C_6H_3NH_3][(RSiO_3)_3Ti_4Cl_4(\mu_3\text{-}O)]$ [**105**, R = 2, 6-$\mathit{i}Pr_2C_6H_3N(SiMe_3)$],[73] $[Cy_7Si_7O_{12}MgTiCl_3]_n$ (**21**, $n = 1, 2$),[39,40] $[(c\text{-}C_5H_9)_7Si_7O_{12}(SiMe_2R)]_2Ti$ (**106**, R = vinyl, allyl) and $[R_7Si_7O_{12}TiO\mathit{i}Pr]_n$ (**107**, R = c-C_5H_9; **108**, c-C_6H_{11}; $n = 1, 2$).[74] It is widely accepted that various titanasilsesquioxanes are versatile catalysts themselves, e.g., in olefin polymerizations and epoxidation reactions.[1–3]

A series of titanasilsesquioxane alkoxides, including $[R_7Si_7O_{12}TiO\mathit{i}Pr]_n$ (**107**, R = c-C_5H_9; **108**, c-C_6H_{11}; $n = 1, 2$) and $[Cy_7Si_7O_{12}Ti(\mu\text{-}OMe)(MeOH)]_2$ (**109**) were published by Crocker and co-workers.[74,75] Treatment of $Cy_7Si_7O_{12}Ti(O^{\mathit{i}}Pr)$ (**108**) with methanol affords the six-coordinate titanasilsesquioxane dimer $[Cy_7Si_7O_{12}Ti(\mu\text{-}OMe)(MeOH)]_2$ (**109**), which was structurally characterized. The monomer/dimer equilibrium of **108** and the formation of **109** are depicted in Scheme 34.[74–77]

The dimeric ethoxide derivative **113** was prepared in our laboratory according to Scheme 35 directly by treatment of **3** with an equimolar amount of titanium tetraethoxide.[78] In this case the formation of a monomeric intermediate was not observed. Related complexes, although monomeric, have also been isolated from reactions of **3** with $Ti(CH_2Ph)_4$, $Ti(NMe_2)_4$ or $Ti(OSiMe_3)_4$ yielding $Cy_7Si_7O_{12}TiCH_2Ph$ (**110**), $Cy_7Si_7O_{12}TiNMe_2$ (**111**) and $Cy_7Si_7O_{12}TiOSiMe_3$ (**112**), respectively.[74,75]

Compound **113** was isolated in 81% yield as a moisture-sensitive, colorless crystalline solid, which is thermally quite robust (m.p. 263–265 °C). High-thermal stability is quite characteristic for the majority of the metallasilsesquioxanes reported so far. An X-ray crystal structure determination revealed the presence of a dimeric compound with bridging alkoxide ligands and coordinated ethanol molecules in analogy with the structure of the corresponding methoxide derivative $[Cy_7Si_7O_{12}Ti(\mu\text{-}OMe)(MeOH)]_2$ (**109**).[76] In dimeric **113** the Ti atoms are hexacoordinated with the silsesquioxane cages acting as tridentate ligands. The complex comprises two bridging ethoxide ligands as well as two terminal ethanol molecules coordinated to titanium. Hydrogen bridges connect the OH group of each ethanol ligand with a silsesquioxane oxygen, which is coordinated to the opposite titanium center.[78]

Crocker and co-workers[77] reported the use of **108** as starting material in the preparation of monomeric titanasilsesquioxane phenoxide derivatives. Heating of the isopropoxide precursor with phenols resulted in elimination of *i*-PrOH and formation of the corresponding titanium phenoxide complexes (Scheme 36).

It was also shown by Crocker *et al.*[77] that treatment of the monosilylated precursor $Cy_7Si_7O_9(OH)_2(OSiMe_3)$ (**12**) with one equivalent of $Ti(O\mathit{i}Pr)_4$ produced monomeric $[Cy_7Si_7O_{11}(OSiMe_3)]Ti(O\mathit{i}Pr)_2$ (**117**) as the sole product. A homoleptic bis(silsesquioxane) titanium complex, $[Cy_7Si_7O_{11}(OSiMe_3)]_2Ti$ (**118**), was prepared by reacting **12** with tetrabenzyltitanium, $Ti(CH_2Ph)_4$. Independently it was found in our laboratory that compound **118** is also readily accessible by reacting $Ti(OEt)_4$ or

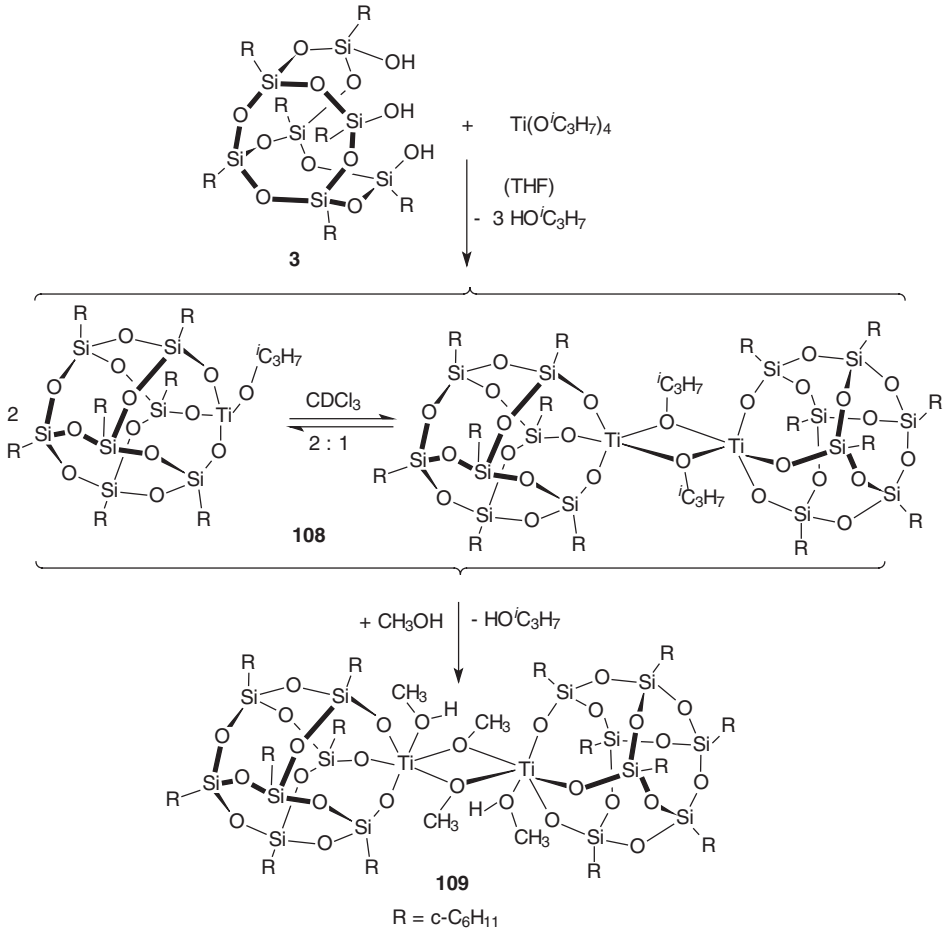

SCHEME 34. Monomer/dimer equilibrium of **108** and formation of **109**.

Ti(O*i*Pr)$_4$ with **12** according to Scheme 37.[78] Both reactions afford white crystalline **118** in almost quantitative yield (96–97%) while employing commercially available reagents. An X-ray diffraction study published by Crocker *et al.*,[77] revealed that the central Ti atom in **118** is tetrahedrally coordinated by the two dianionic silsesquioxane cages.

The preparation and characterization of analogous homoleptic titanasilsesquioxane complexes containing vinylic substituents was reported by Wada *et al.* (Scheme 38).[75]

Several titanocene derivatives containing silsesquioxane ligands have also been prepared and characterized.[78] It soon turned out that reactions of **3** or its monosilylated derivative **12** with titanocene dihalides are not straightforward and usually lead to the formation of product mixtures. A common feature appears to be the formation of μ-oxo species despite the use of carefully dried solvents. Although at this stage the occurrence of partial hydrolysis cannot completely be ruled out, we

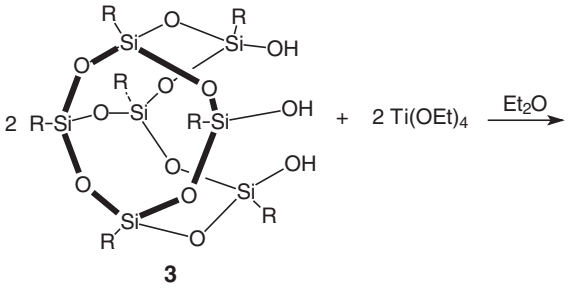

3

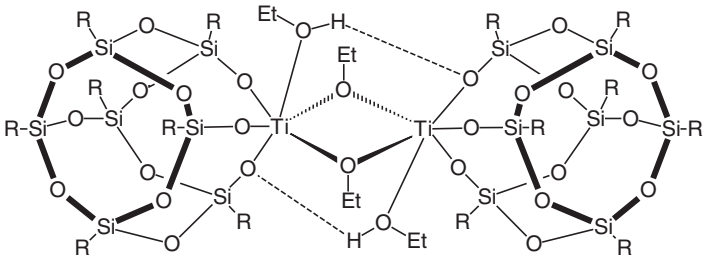

113

R = *c*-C_6H_{11}

SCHEME 35. Preparation of $[Cy_7Si_7O_{12}Ti(\mu\text{-OEt})(EtOH)]_2$ (**113**).

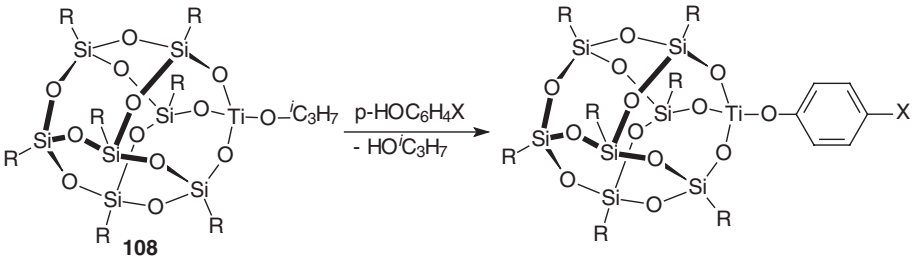

108

R = *c*-C_6H_{11}

114-116, X = H, F, NO_2

SCHEME 36. Formation of titanasilsesquioxane phenoxides **114**–**116**.

assume that the oxygen bridges in these complexes result from degradation of the silsesquioxane frameworks. A typical example is the reaction of **12** with Cp_2TiCl_2 in toluene solution in the presence of triethylamine. In this case the μ-oxo-dititanium complex (μ-O)$[Cy_7Si_7O_{11}(OSiMe_3)Ti]_2$ (**123**) has been isolated in ca. 70% yield in the form of orange crystals (Scheme 39).

The molecular structure of **123** has been established by an X-ray diffraction analysis, which revealed the presence of a dinuclear metallasilsesquioxane with a central Ti–O–Ti unit. During the course of the reaction one Cp ligand per Ti atom is eliminated upon protonolysis to give the observed mono(cyclopentadienyl) titanium(IV) derivative.

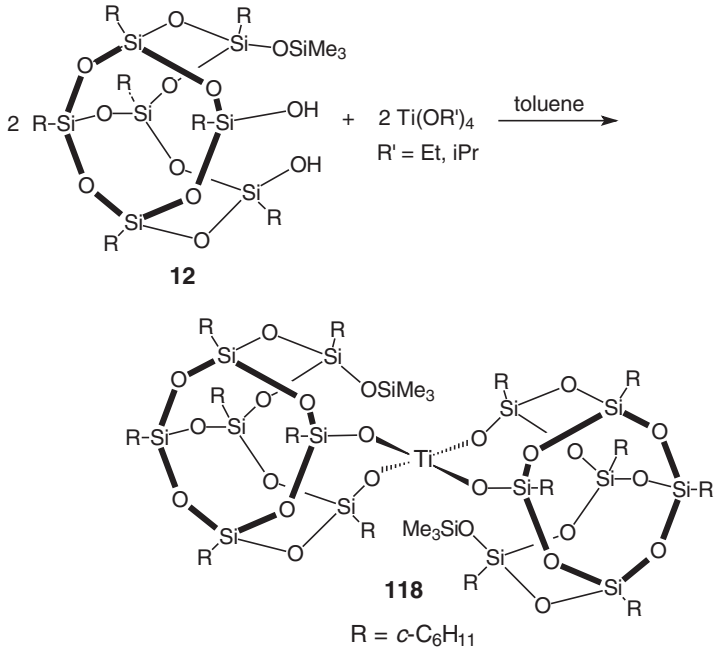

SCHEME 37. Preparation of $[Cy_7Si_7O_{11}(OSiMe_3)]_2Ti$ (**118**).

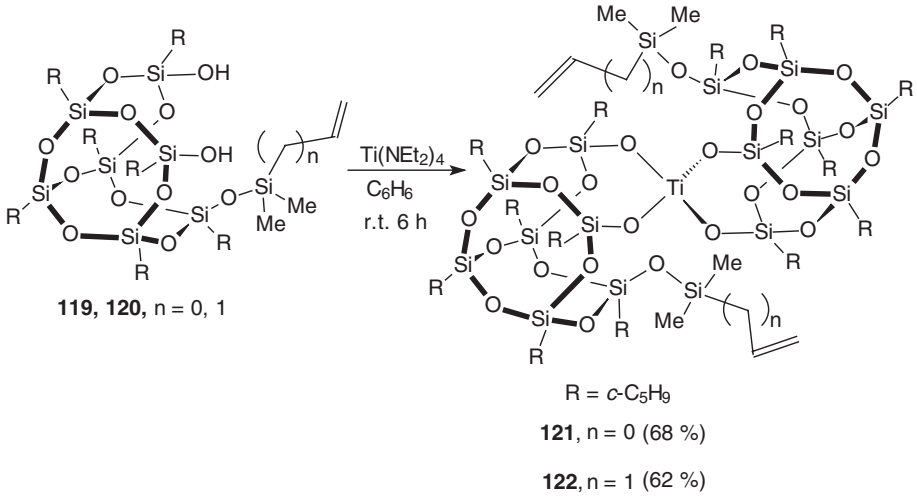

SCHEME 38. Preparation of vinylic titanasilsesquioxanes **121** and **122**.

Apparently, at least two different products are formed when **12** is reacted with the corresponding pentamethylcyclopentadienyl complex $Cp^*_2TiCl_2$ in the presence of triethylamine.[78] While a yellow component has not yet been identified, it was possible to isolate and fully characterize the red crystalline trinuclear 1,3,5-trititana-2,4,6-trioxane derivative $Cp^*_2Ti_3O_3[Cy_7Si_7O_{11}(OSiMe_3)]_2$ (**124**) (Scheme 40).

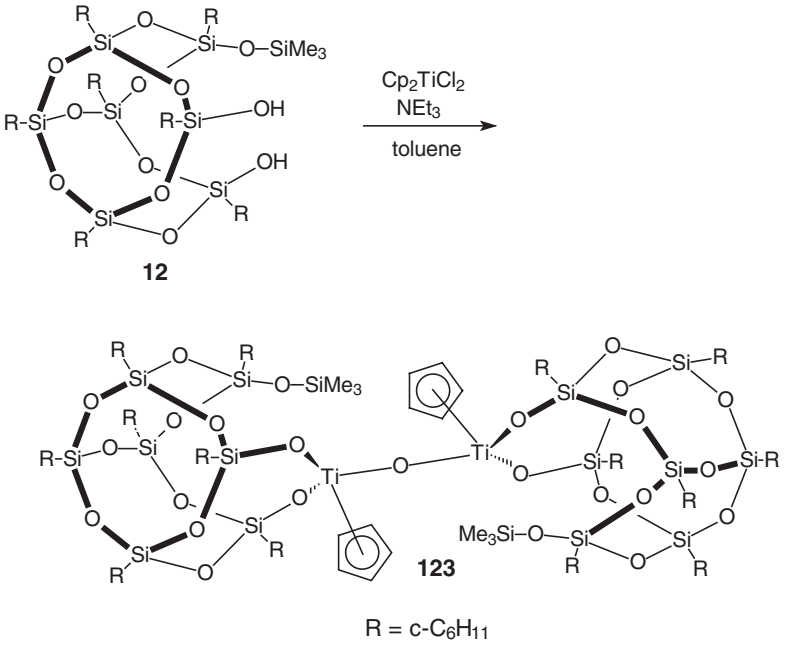

SCHEME 39. Formation of (μ-O)[$Cy_7Si_7O_{11}(OSiMe_3)Ti]_2$ (**123**).

The molecular structure of **124** has been elucidated by an X-ray structural analysis. The central structural motif of **124** is an unsymmetrically substituted six-membered Ti_3O_3 ring. Two pentamethylcyclopentadienyl ligands are coordinated to one titanium atom, while the other two are free of Cp^*. They are both part of eight-membered $TiSi_3O_4$ ring systems within the silsesquioxane frameworks. This results in an unusual bis(spirocyclic) inorganic ring system in the molecular structure of **124**.

In a more straightforward manner a bis(pentamethylcyclopentadienyl) titanium(III) silsesquioxane complex is formed according to Scheme 40.[78,79] This synthesis has been developed as a new preparative route leading to model compounds for titanium catalysts immobilized on silica surfaces. It involves addition of the silsesquioxane precursors across the Ti–C bond of the ''tucked in'' fulvene titanium complex $Cp^*Ti(C_5Me_4CH_2)$.[80–82] The main advantage of this ''fulvene route'' is that it is a salt-free method by which bis(pentamethylcyclopentadienyl) titanium complexes can be obtained without the need of separating any by-products. The method has been first successfully employed by Teuben *et al.*, who prepared various new Cp^*_2Ti derivatives by reacting $Cp^*Ti(C_5Me_4CH_2)$ with protic reagents such as alcohols, thiols etc.[81,82] We found that the fulvene complex $Cp^*Ti(C_5Me_4CH_2)$ is also the reagent of choice to make novel titanium silsesquioxanes. For example, treatment of $Cp^*Ti(C_5Me_4CH_2)$ with one equivalent of the disilylated silsesquioxane precursor **13** resulted in clean formation of the Ti(III) silsesquioxane complex **125** (Scheme 41).

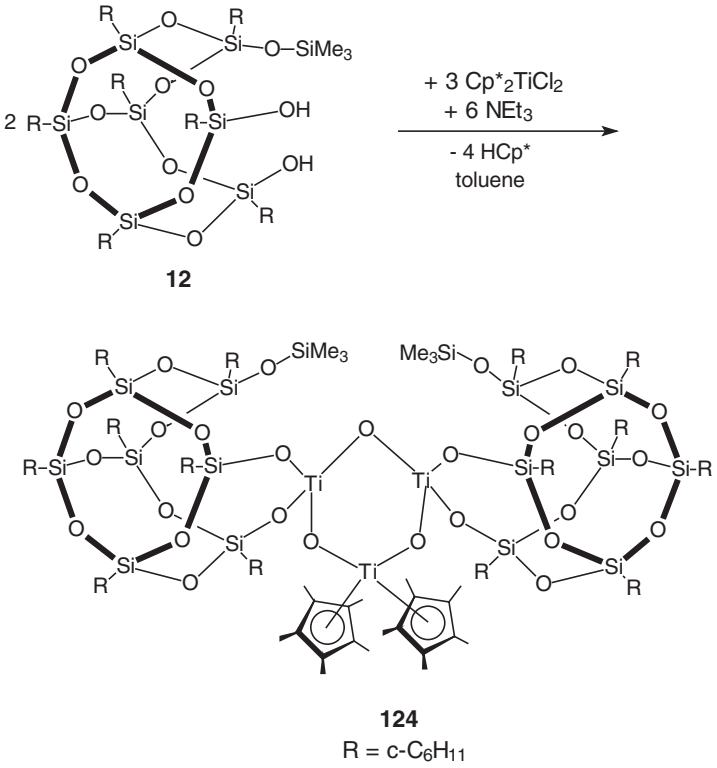

SCHEME 40. Formation of $Cp^*_2Ti_3O_3[Cy_7Si_7O_{11}(OSiMe_3)]_2$ (**124**).

Simple crystallization from the concentrated reaction mixture afforded **125** in the form of air-sensitive, dark-green crystals. The low isolated yield (16%) can be traced back to the very high solubility of **125** even in non-polar organic solvents, which makes it somewhat difficult to recover the material from concentrated solutions in toluene or hexane. The novel titanium(III) silanolate derivative **125** has been fully characterized. An X-ray diffraction study revealed that a Cp^*_2Ti unit has been generated upon protonation of the coordinated tetramethylfulvene ligand. The resulting deprotonated silsesquioxane is coordinated to titanium as a bulky monodentate silanolate ligand. The Ti–O bond length in **125** is 1.927(2) Å.

The ''fulvene route'' was also successfully employed in the preparation of a compound, which can be regarded as one of the most advanced molecular models for a catalytically active titanium center on a silica surface.[78,79] When $Cp^*Ti(C_5Me_4CH_2)$ was reacted with the monosilylated silsesquioxane precursor **12** in refluxing toluene a color change from deep purple to amber was observed. Crystallization afforded a bright-yellow material, which was subsequently shown to be the novel *mono*(pentamethylcyclopentadienyl) titanium(IV) silsesquioxane complex **126** (69% yield). Its formation is illustrated schematically in Scheme 42.

The surprising outcome of this reaction is the exclusive formation of a Cp^*Ti^{IV} complex in which two silsesquioxanes are bonded in different ways to a single Ti

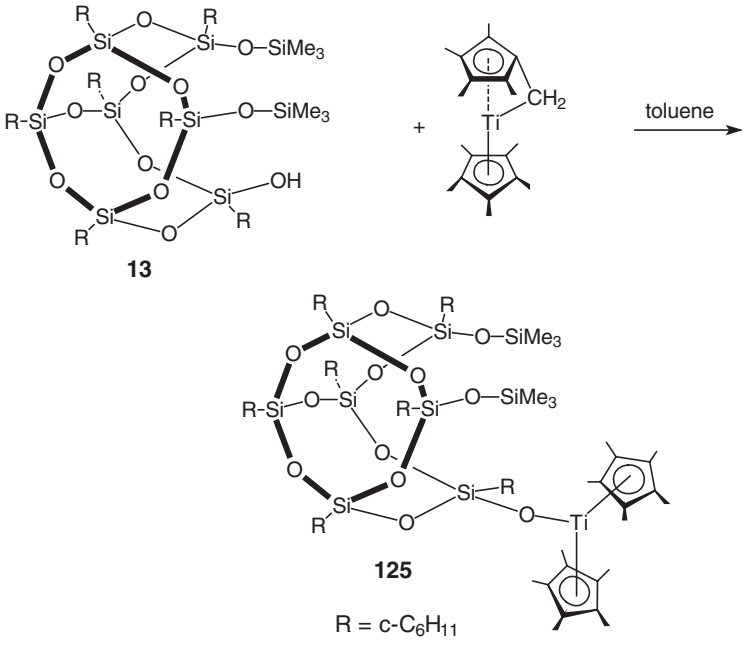

SCHEME 41. Synthesis of **125** *via* the fulvene route.

center. In the course of the reaction one equivalent of pentamethylcyclopentadiene is eliminated. According to an X-ray diffraction analysis a mono(pentamethylclopentadienyl) titanium unit resides on a ''model silica surface'' formed by one chelating and one monodentate silsesquioxane ligand. With an average of 1.796(3) Å the three Ti–O bond lengths are practically identical. A unique feature of **126**, which makes this compound a particularly ''realistic'' model system is a silanol function in close proximity to the titanium center. Very weak hydrogen bonding interaction of this silanol group with a cage oxygen atom apparently prevents the molecule from intermolecular protonation of the remaining Cp^* ligand, thus ''taming'' the reactivity of the Si–OH function.

A series of half-sandwich titanium complexes has been prepared with the use of the *closo*-silsesquioxane monosilanol ligand (c-$C_5H_9)_7Si_8O_{12}$(OH) (**28**) (Schemes 42 and 43).[64] For example, the reaction of [1,3-$C_5H_3(SiMe_3)_2$]Ti($CH_2Ph)_3$ with one equivalent of silanol **28** resulted in selective substitution of one benzyl group, affording the mono(silsesquioxane) complex **127** in moderate yield (Scheme 43). Introduction of a second bulky silsesquioxane failed.

Deprotonation of **28** with *n*-BuLi in hexane solution at 25 °C readily affords the stable silsesquioxane lithium salt (c-$C_5H_9)_7Si_8O_{13}Li$ (**128**).[64] The room temperature reaction of **128** with [1,3-$C_5H_3(SiMe_3)_2$]$TiCl_3$ in hexane according to Scheme 44 yielded [1,3-$C_5H_3(SiMe_3)_2$][(c-$C_5H_9)_7Si_8O_{13}$]$TiCl_2$ (**129**). The bis(silsesquioxane) product **130** could be selectively prepared by salt metathesis between [1,3-$C_5H_3(SiMe_3)_2$]$TiCl_3$ and two-equivalents of **128** in hexane at 25 °C.

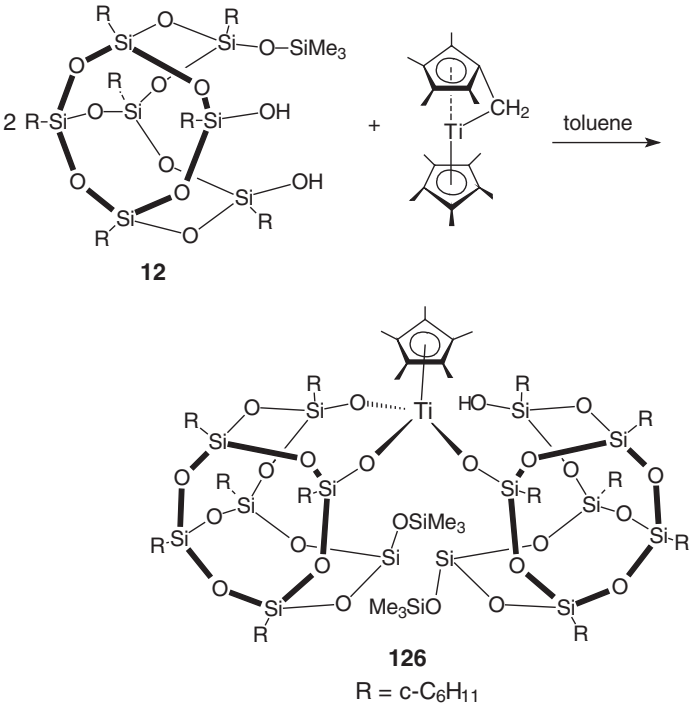

SCHEME 42. Preparation of **126** *via* the fulvene route.

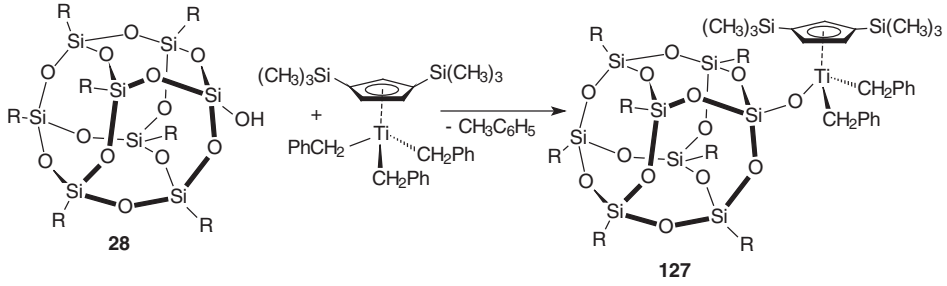

SCHEME 43. Synthesis of **127**.

Zirconium silsesquioxane complexes, which have been reported in the literature include the species $Cy_7Si_7O_{12}ZrCp^*$ (**131**),[83] $[(c\text{-}C_5H_9)_7Si_7O_{11}(OSiMe_3)]_2Zr(THF)_2$ (**132**),[84] and $[\{(c\text{-}C_5H_9)_7Si_7O_{12}\}Zr(CH_2Ph)]_2$ (**133**),[84] which have all been synthesized by synthetic routes well-established for the corresponding titanium derivatives. The zirconocene complex $[(c\text{-}C_5H_9)_7Si_7O_{11}(OSiMePh_2)]ZrCp_2$ (**134**) was obtained by treatment of Cp_2ZrMe_2 with an aluminosilsesquioxane.[51] The availability of permetalated $Cy_7Si_7O_9(OLi)_3$ (**15**) enabled us to prepare the

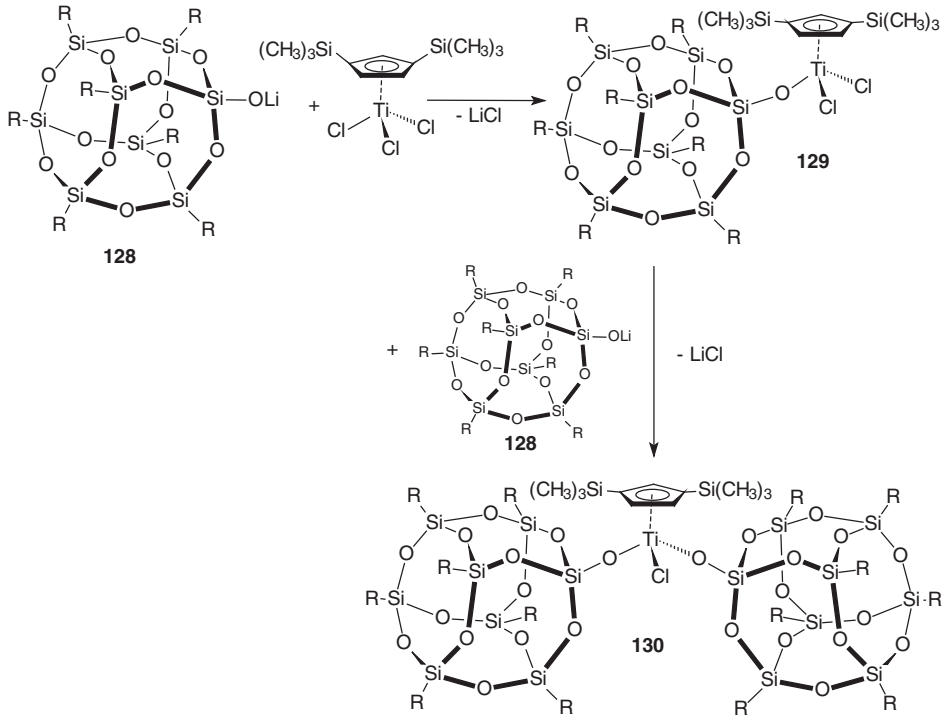

SCHEME 44. Synthesis of the silsesquioxane titanium half-sandwich complexes **129** and **130**.

first heterobimetallic zirconium silsesquioxane complex. The compound $(Cy_7Si_7O_{12})_2Zr[Li(O{=}CMe_2)]_2$ (**135**) was prepared according to Scheme 45 and structurally characterized by X-ray diffraction.[34]

Collins *et al*. reported the use of the borylated silsesquioxane intermediate **136** for the synthesis of the zirconocene derivative **137** according to Scheme 46.[85]

Hafnium-containing metallasilsesquioxanes reported in the literature include the species $Cy_7Si_7O_{12}HfCp^*$ (**138**)[55] and $[(c\text{-}C_5H_9)_7Si_7O_{12}HfCH_2Ph]_2$ (**139**).[84]

A new development in silsesquioxane chemistry is the combination of silsesquioxanes with cyclopentadienyl-type ligands. Recently, several synthetic routes leading to silsesquioxane-tethered fluorene ligands have been developed.[86,87] The scenario is illustrated in Scheme 47. A straightforward access to the new ligand **140** involves the 1:1 reaction of **2** with 9-triethoxysilylmethylfluorene. Alternatively, the chloromethyl-substituted *closo*-silsesquioxane derivative **141** can be prepared first and treated subsequently with lithium fluorenide to afford **140**. Compound **141** has been used as starting material for the preparation of the trimethylsilyl and trimethylstannyl derivatives **142** and **143**, respectively, as well as the novel zirconocene complex **144**. When activated with MAO (methylalumoxane), **144** yields an active ethylene polymerization system.

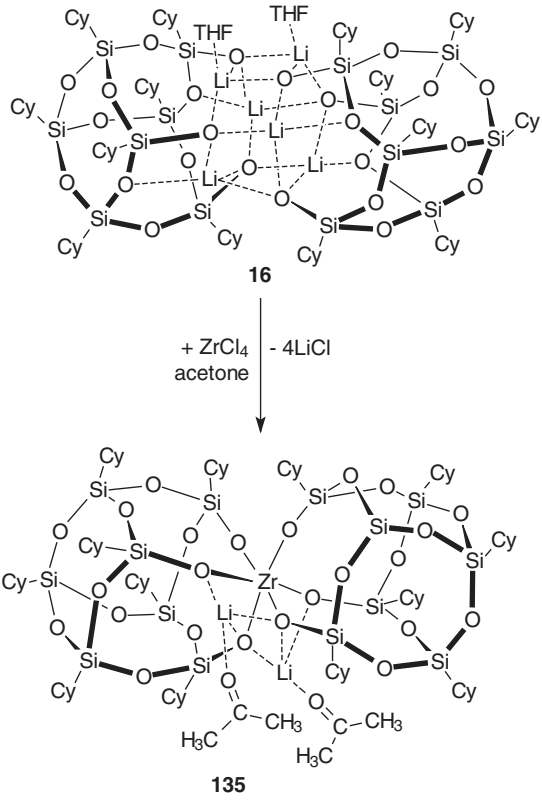

SCHEME 45. Synthesis of $(Cy_7Si_7O_{12})_2Zr[Li(O{=}CMe_2)]_2$ (**135**).

In a recent paper, Duchateau *et al.* have extended this synthetic approach to a series of silsesquioxane-tethered fluorene ligands and the corresponding zirconocenes with various cyclopentadienyl ligands at Zr. The various possibilities are illustrated in Scheme 48.[87]

Yet another interesting variety is the incorporation of functional side-groups in metallasilsesquioxanes of zirconium and hafnium. Mitsudo *et al.* reported the synthesis and structural characterization of novel zirconocene or hafnocene-containing metallasilsesquioxanes with a vinyl group, $Cp_2M[(vinyl)Me_2Si](c\text{-}C_5H_9)_7Si_7O_{12}$ (**145**, M = Zr; **146**, M = Hf).[88] Hydrosilylation of the vinyl group in **145** with $Me_3SiH(OEt)$ in the presence of a $Pt_2(dvs)_3$ catalyst(1 mol% as Pt, dvs = divinyltetramethyldisiloxene) in toluene at 30 °C for 72 h cleanly occurred with excellent regioselectivity to give $Cp_2Zr[Me_2(EtO)SiCH_2CH_2SiMe_2](c\text{-}C_5H_9)_7Si_7O_{12}$ (**147**).

A major part of the work described in this section has been carried out with the aim of applying these silsesquioxane complexes of Ti, Zr and Hf in catalytic processes such as ethylene polymerization, olefin epoxidation and Oppenauer oxidation. These catalytic aspects have been highlighted in several recent review articles.[1,2]

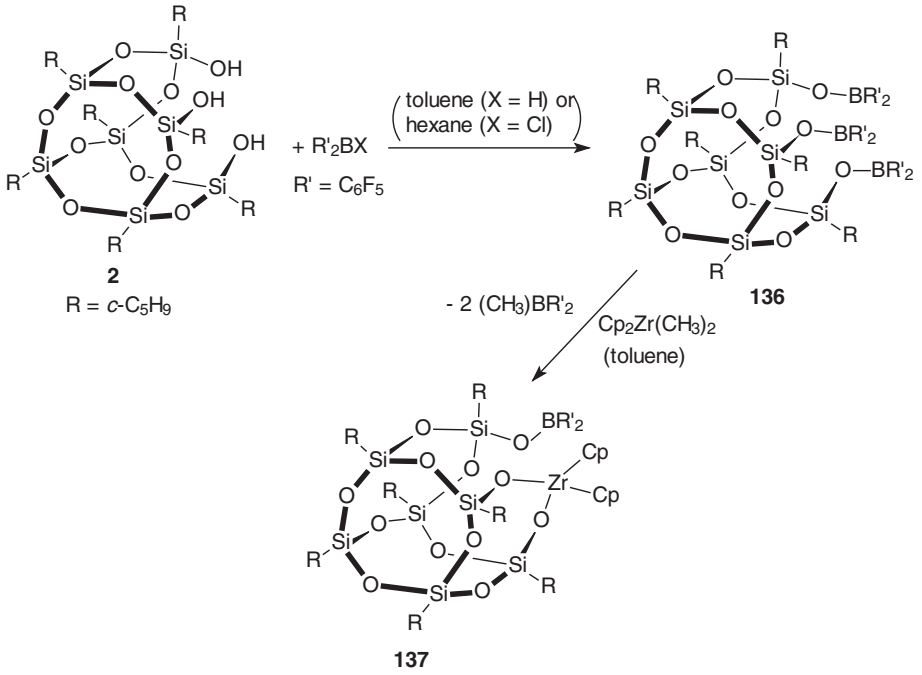

SCHEME 46. Synthesis of the zirconasilsesquioxane **137**.

3. Group 5 Metal Derivatives (V, Nb, Ta)

Significantly less is known about metallasilsesquioxanes incorporating Group 5 metals. The vanadyl silsesquioxane $Cy_7Si_7O_{12}V{=}O$ (**148**) was reported by Feher *et al*. more than 10 years ago and has been shown to be a single-site catalyst for olefin polymerization.[68,89–91] In 1990 Feher and co-workers reported the preparation of the dark-blue dimeric vanadium(III) complex $[Cy_7Si_7O_{12}V(py)_2][Cy_7Si_7O_{12}V]$ (**149**), in which two pyridine ligands are added to one of the vanadium centers.[68] Thus it was surprising that until recently no metallasilsesquioxane had been described for the heavier Group 5 metals, which was presumably due to the lack of suitable synthetic procedures.

Recently, we succeeded in the synthesis and structural characterization of first niobium-containing metallasilsesquioxane complex.[35] In analogy to the corresponding reactions with titanium tetraalkoxides, niobium pentaethoxide cleanly reacts with **3** in a 1:1 molar ratio to give high yields of dimeric $[Cy_7Si_7O_{12}NbOEt(\mu\text{-}OEt)]_2$ (**149**) as a colorless, crystalline solid (Scheme 49).

During the course of our investigations we found that various tantalum silsesquioxanes are readily accessible *via* a versatile amide route.[92] Commercially available tantalum diethylamide, $Ta(NMe_2)_5$, was chosen as the key starting material for the development of a salt-free route leading to tantalum silsesquioxane derivatives. Clean protonation and liberation of three equivalents of dimethylamine took place upon reaction of $Ta(NMe_2)_5$ with **3** in a 1:1 molar ratio. Pale yellow

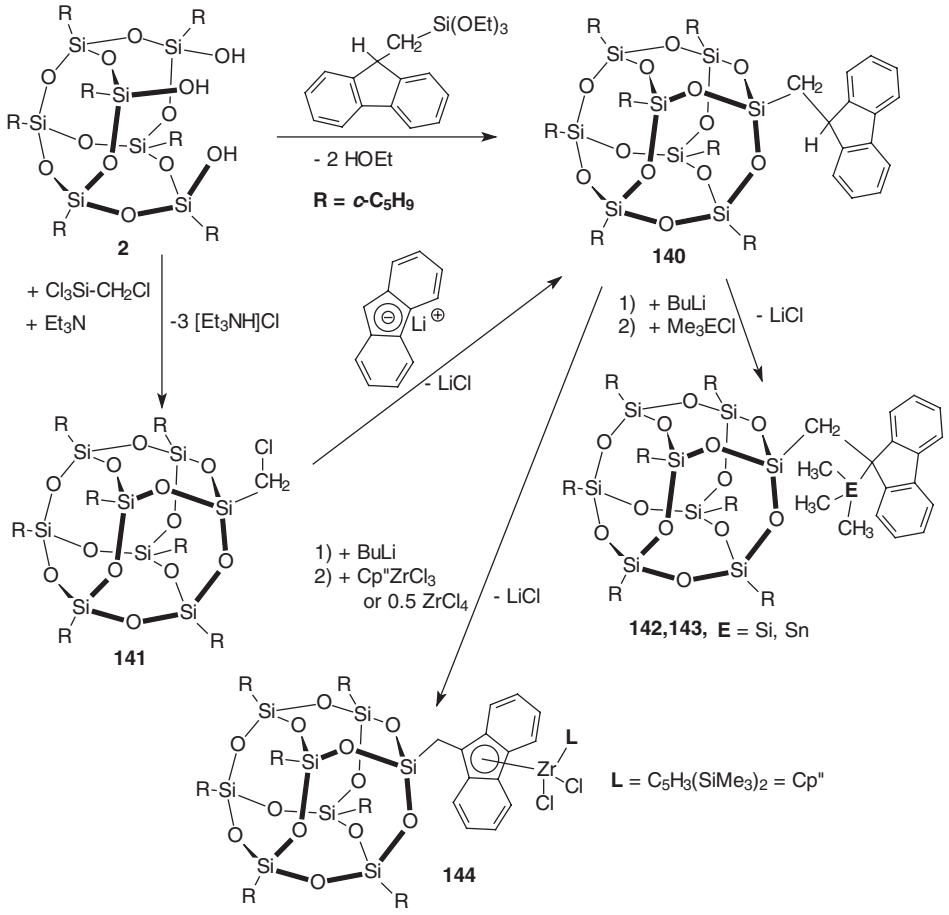

SCHEME 47. Synthesis and reactivity of silsesquioxane-tethered fluorene ligands.

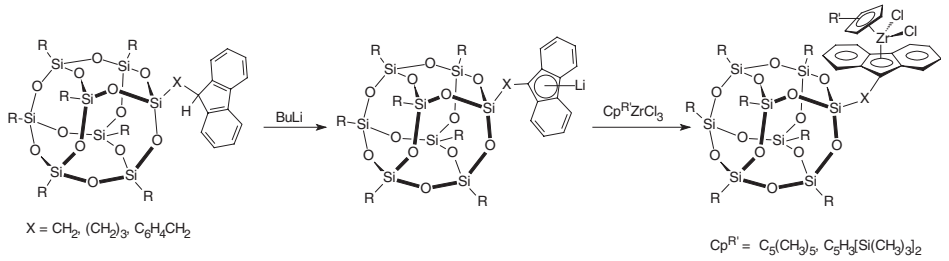

SCHEME 48. Synthesis of silsesquioxane-tethered zirconocenes.

$Cy_7Si_7O_{12}Ta(NMe_2)_2$ (**150**) was isolated in 92% yield. Somewhat surprisingly, similar treatment of $Ta(NMe_2)_5$ with **1** in a 1:2 molar ratio did not lead to the formation of the neutral tantalum(V) species $Cy_7Si_7O_{12}Ta[Cy_7Si_7O_{11}(OH)]$ with one Si–OH

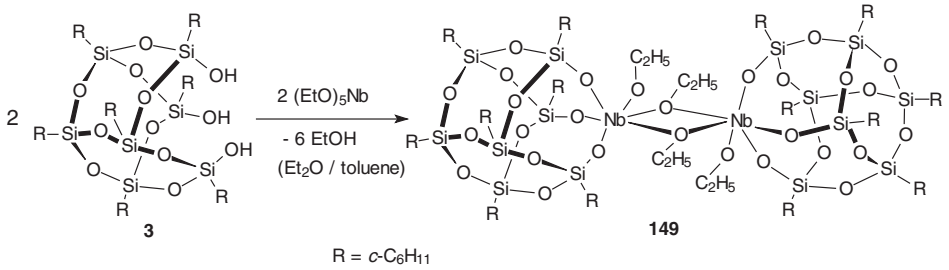

SCHEME 49. Synthesis of $[Cy_7Si_7O_{12}NbOEt(\mu\text{-}OEt)]_2$ (**149**).

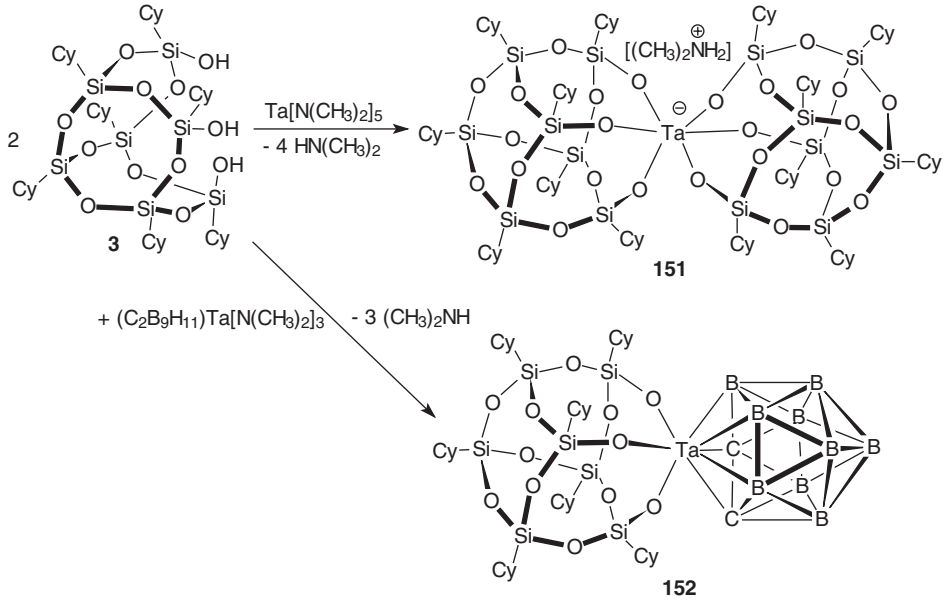

SCHEME 50. Preparation of tantalasilsesquioxanes.

function remaining intact. Instead, liberation of only four equivalents of dimethylamine occurred and the anionic bis(silsesquioxane) "sandwich" complex $[Ta(Cy_7Si_7O_{12})_2]^-$ was obtained in the form of its colorless dimethylammonium salt **151** (89% yield) (Scheme 50). In the resulting anion, the central Ta atom is encapsulated between two silsesquioxane frameworks in a similar manner as in the neutral uranium(VI) species $U(Cy_7Si_7O_{12})_2$ (**100**).[35] We then investigated the possibility of adapting the amide route to more complex systems. Indeed, the amido tantalacarborane species $(C_2B_9H_{11})Ta(NMe_2)_3$ was found to react cleanly with one equivalent of **3** to afford the novel "mixed-sandwich" complex $Cy_7Si_7O_{12}$-$Ta(C_2B_9H_{11})$ (**152**), which was isolated in 82% yield as an orange, crystalline solid. Compound **152** is the first representative of a novel class of inorganic cage compounds in which a carborane and a silsesquioxane framework are linked

through a single metal center. Further examples of such hybrid complexes should be accessible by varying either the central atom or using different carborane and silsesquioxane ligands.

These results clearly demonstrate that the amide route is a versatile synthetic pathway to novel tantalasilsesquioxanes, each of them representing a novel type of metallasilsesquioxane. Suitable tantalum dimethylamides are readily protonated in the presence of silsesquioxanes bearing Si–OH functional groups to form either ''half-sandwich'' or ''sandwich'' complexes depending on the stoichiometry. This salt-free method is likely to work equally well with the corresponding Nb derivatives as well as with other Si–OH-functionalized silsesquioxanes. The ''mixed-sandwich'' complex $Cy_7Si_7O_{12}Ta(C_2B_9H_{11})$ (**152**) is just the first example of an unusual new class of hybrid compounds combining carborane and silsesquioxane chemistry. Tantalum silsesquioxanes have also been investigated by Basset *et al.* as model compounds for the formation of alkylidenetantalum species on silica surfaces.[93]

The dimer of the vanadyl silsesquioxane complex **148** was used by Mitsudo *et al.* to prepare catalysts with a characteristic pore structure and excellent activity toward the selective photoassisted catalytic oxidation of methane into methanal.[94]

C. *Metallasilsesquioxanes of the Middle and Late Transition Metals*

1. Group 6 Metal Derivatives (Cr, Mo, W)

Several Group 6 metallasilsesquioxanes have been reported in the literature and investigated with respect to catalytic applications. However, their number is still scarce, and further exploration of this class of metallasilsesquioxanes is warranted. The disilanol derivative $Cy_7Si_7O_9(OH)_2(OSiMe_3)$ (**12**) reacts with chromium trioxide in CCl_4 in the presence of anhydrous $MgSO_4$ to give the chromate ester $Cy_7Si_7O_9(OSiMe_3)CrO_4$ (**153**), which has been tested as an ethylene polymerization catalyst.[95,96] The chromium(VI) derivative **153** can be regarded as a molecular model of the chromium-based Phillips catalyst. This and related chromium silsesquioxanes have also been demonstrated to be active catalysts for the epoxidation of olefins with *t*-butylhydroperoxide.[97] The chromate ester **153** has also been employed as the starting material for the synthesis of microporous chromium silicate materials (Scheme 51), which catalyze the oxidation of ammonia.[98]

While previously reported Cr silsesquioxane complexes contained chromium in the hexavalent oxidation state, the recently synthesized lithium silsesquioxane precursors such as **15**–**17** enabled the synthesis of an unprecedented heterobimetallic chromium species.[35] Treatment of **16** with anhydrous $CrCl_3$ in THF resulted in formation of green crystalline **154**, which was structurally characterized by X-ray diffraction (Scheme 52).

The molybdate ester $Cy_7Si_7O_9(OSiMe_3)MoO_4$ (**155**) was made by Feher *et al.*,[32] in 1995 by reacting the thallium intermediate $Cy_7Si_7O_9(OSiMe_3)(OTl)_2$ (**70**) with MoO_2Cl_2. As mentioned earlier, it is one of the advantages of the thallium silsesquioxane reagents that they can be used as precursors in reactions with high-valent

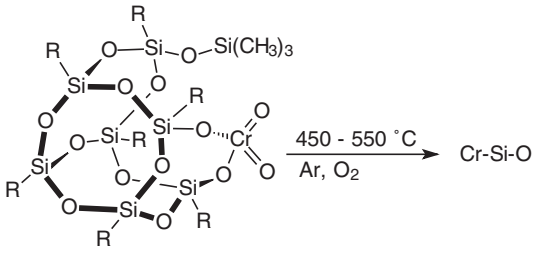

153, R = *c*-C_6H_{11}

SCHEME 51. Synthesis of microporous chromium silicate materials from **153**.

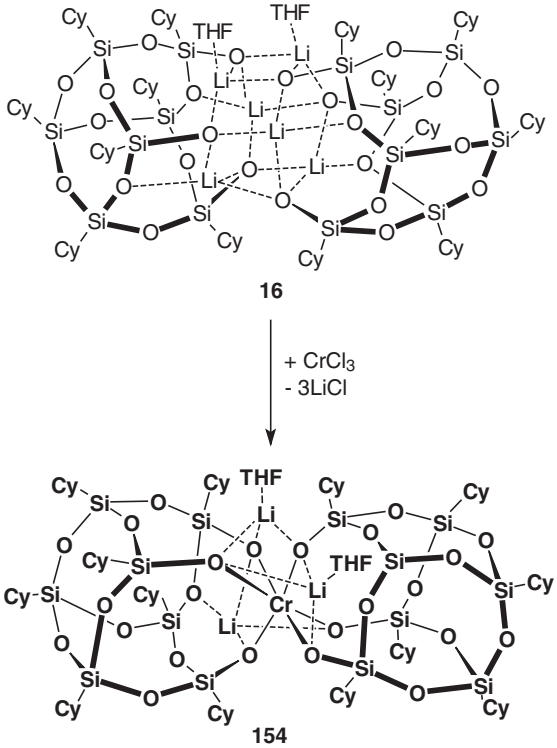

SCHEME 52. Synthesis of the LiCr silsesquioxane complex **154**.

metal halides. Feher *et al.*[99] also reported the prepartion of the Schrock-type molybdenum carbene complex **156** (Scheme 53).

The first metallasilsesquioxanes containing metal–metal triple bonds have been reported by Chisholm and Feher *et al.*[100] The reaction between two equivalents of **3** and $Mo_2(OtBu)_6$ in benzene or toluene at room temperature (Scheme 54) led to rapid replacement of all six alkoxide ligands and formation of orange, crystalline

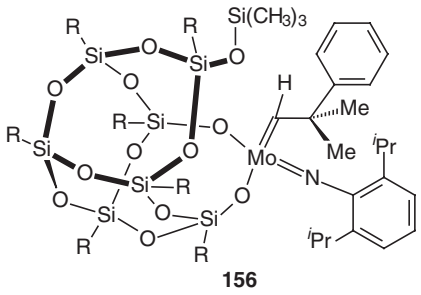

SCHEME 53. Structure of **156**.

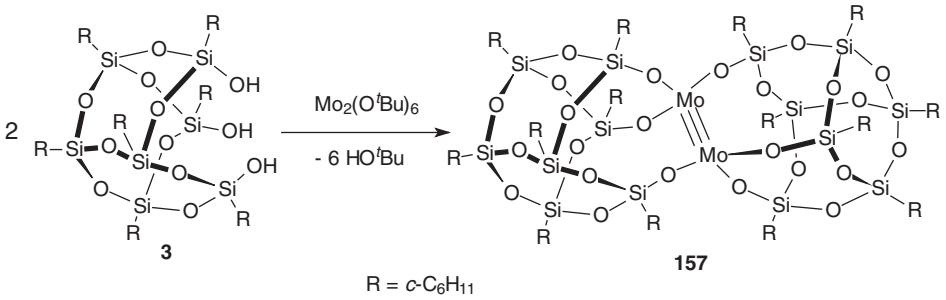

SCHEME 54. Synthesis of the dimeric molybdenum silsesquioxane complex **157**.

157 in 80% yield. The dimeric structure with a Mo≡Mo triple bond as depicted in Scheme 54 was established by a single-crystal X-ray diffraction study.

The analogous reaction of **3** with $W_2(OtBu)_6$ gave a brown solution, from which a yellow, microcrystalline material could be isolated.[100] Based on spectroscopic data the latter was formulated as $[Cy_7Si_7O_{12}]_2W_2(\mu\text{-}H)(OtBu)$ (**158**). Cleavage of the Mo≡Mo triple bond in **157** occurred upon treatment of this compound with NO (two equivalents) to afford the dimeric nitrosyl molybdenum silsesquioxane complex $[Cy_7Si_7O_{12}]_2Mo_2(NO)_2$ (**159**).[100]

A metallasilsesquioxane derivative of tungsten(VI), which is an analog of the uranium(VI) complex (**100**) was prepared by Smet *et al.*[101] Quite remarkably the compound $[Cy_7Si_7O_{12}]_2W$ (**160**) was formed directly by reaction WCl_6 with two equivalents of **3** even without the presence of a base to facilitate the elimination of HCl. According to a single crystal X-ray structure analysis, the tungsten atom in monomeric neutral **160** is encapsulated between the two bulky silsesquioxane cages (Scheme 55).

2. Group 7 Metal Derivatives

No fully characterized metallasilsesquioxane derivatives of Mn, Tc or Re have been reported until now. It has been reported that reactions of **2** or **3** with rhenium(VII) precursors are complicated and often result in dehydration of the silsesquioxane cage without incorporation of rhenium.[1,35] Recently it has been found

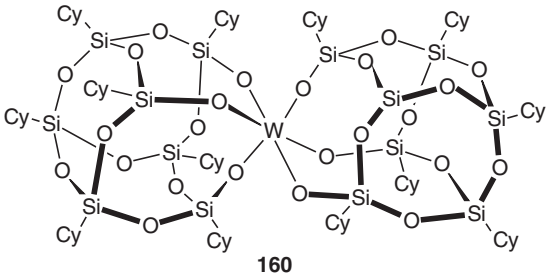

160

SCHEME 55. Structure of $[Cy_7Si_7O_{12}]_2W$ (**160**).

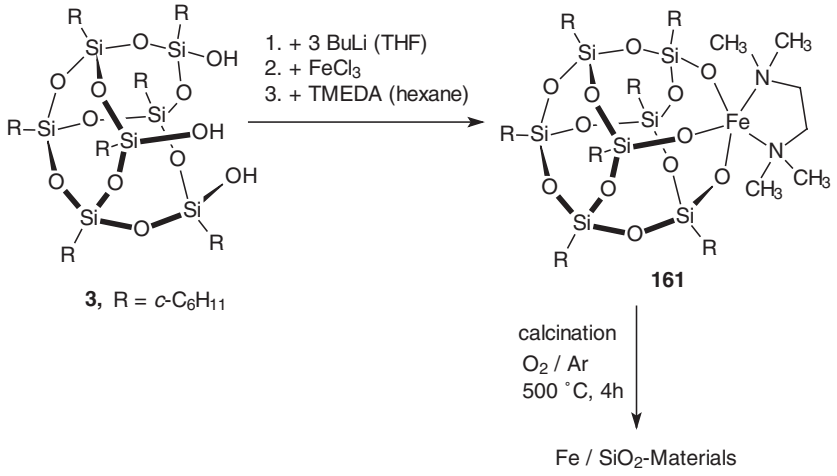

SCHEME 56. Preparation of the ferrasilsesquioxane complex **161** and its conversion into iron on microporous silica.

that the reaction of **16** with anhydrous $MnCl_2$ in THF affords a colorless heterobimetallic Li/Mn silsesquioxane complex of unknown structure.[35]

3. Group 8 Metal Derivatives (Fe, Ru, Os)

The first iron-containing silsesquioxanes which appeared in the literature were compounds containing ferrocenyl units as side-groups.[102–104] However, these are not within the scope of this review as iron is not part of the metallasilsesquioxane skeleton. Meanwhile, several ferrasilsesquioxane complexes have been synthesized. The first iron(III) compound of this type was prepared in our laboratory according to Scheme 56.[105] In **161**, the coordination sphere of iron is completed by TMEDA (N,N,N′,N′-tetramethylethylenediamine) as a chelating amine ligand. Pale yellow, crystalline **161** was isolated in 80% yield and structurally characterized by X-ray diffraction. This compound was later used by Maxim *et al.*[106,107] to prepare iron particles dispersed on microporous silica *via* controlled calcination of the ferrasilsesquioxane precursor as depicted in Scheme 56.

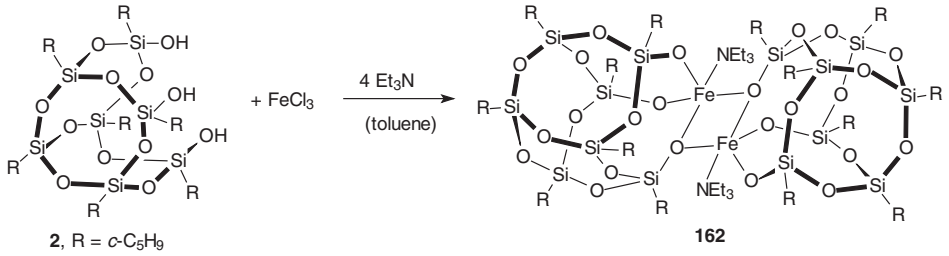

2, R = *c*-C_5H_9 **162**

SCHEME 57. Synthesis of the dimeric ferrasilsesquioxane **162**.

More recently Shapley *et al.*[108] carried out a reaction of the cyclopentyl-substituted precursor **2** with $FeCl_3$ in the presence of NEt_3 in toluene solution (Scheme 57). In contrast to the formation of **161**[105] this reaction afforded brown, dimeric [(*c*-$C_5H_9)_7Si_7O_{12}Fe(NEt_3)]_2$ (**162**) in 73% yield.

A series of ferrasilsesquioxanes stabilized by phosphine ligands has been prepared and characterized by Baker *et al.*[109] Reactions of the iron(II) precursor $FeCl_2$(dcpe) (dcpe = bis(dicyclohexylphosphino)ethane) with **2** or the monosilylated precursor (*c*-$C_5H_9)_7Si_7O_9(OSiMe_3)(OH)_2$ (**38**) afforded the (dcpe)iron(II)-silsesquioxane complexes (*c*-$C_5H_9)_7Si_7O_9(OH)[O_2Fe(dcpe)]$ (**163**, 91% yield) and (*c*-$C_5H_9)_7Si_7O_9(OSiMe_3)[O_2Fe(dcpe)]$ (**164**, 89% yield), respectively, in the form of colorless crystals. The iron(III) analog (*c*-$C_5H_9)_7Si_7O_{12}Fe(PCy_3)$ (**165**, colorless crystals, 91% yield) was prepared and isolated in a similar manner from the reaction of **2** with $FeCl_3(PCy_3)$ in the presence of triethylamine. Compound **165** exhibits some interesting reaction chemistry with water. Treatment of solutions of **165** in benzene with a slight stoichiometric excess of water in the presence of NEt_3 leads to formation of the μ-oxo-bridged dianionic complex **166**. The same compound could also be prepared directly in 92% yield by reacting **2** with $FeCl_3(PCy_3)$ in the presence of water and triethylamine as illustrated in Scheme 58.

Several anionic ferrasilsesquioxane complexes have also been isolated by Shapley *et al.*[108] The high-spin iron(III) silsesquioxane complexes [N(*n*Bu)$_4$][(*c*-$C_5H_9)_7Si_7O_{12}FeCl$] (**167**) and [N(*n*Bu)$_4$][(*c*-$C_5H_9)_7Si_7O_{12}FeOSiMe_3$] (**168**) were obtained from reactions of **2** with either [N(*n*Bu)$_4$][$FeCl_4$] or [N(*n*Bu)$_4$][$Fe(OSiMe_3)_4$]. Substitution of the terminal chloride or trimethylsilanolate ligands with *t*-butoxide afforded [N(*n*Bu)$_4$][(*c*-$C_5H_9)_7Si_7O_{12}FeO$*t*Bu] (**169**), while a similar substitution reaction with the methyl ester of *N*-acetylcysteine produced the unusual anionic ferrasilsesquioxane complex [N(*n*Bu)$_4$][(*c*-$C_5H_9)_7Si_7O_{12}Fe\{SCH_2CH(NHCOMe)$-$CO_2Me\}$] (**170**). The latter reactions show that complexes **167** and **168** are excellent precursors for the synthesis of other iron(III) silsesquioxanes.

Ruthenium and osmium complexes containing silsesquioxane ligands have also been reported in the literature.[99,108,110–113] A Schrock-type ruthenium carbene complex, $Cy_7Si_8O_{12}CH{=}RuCl_2(PCy_3)_2$ (**171**) was made by Feher *et al.* in a similar manner as the molybdenum carbene complex **156**.[108] Other silsesquioxane complexes of Ru and Os contain metal complex fragments bonded to side chains of specially designed silsesquioxane ligands. For example, Braunstein *et al.*[110] used

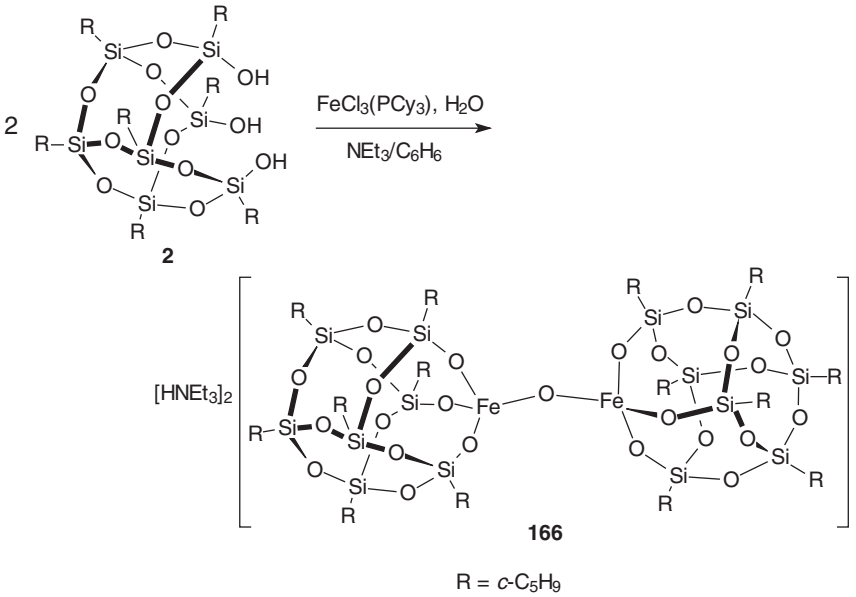

Scheme 58. Direct preparation of **166**.

thiol-functionalized silsesquioxane derivatives such as **172** and **175** to synthesize coordination compounds with ruthenium and osmium clusters as outlined in Scheme 59. All cluster complexes shown in Scheme 59 have been isolated in the form of yellow, crystalline solids.

Ruthenium complexes of a novel silsesquioxane-based tridentate phosphine ligand have been prepared and characterized by Mitsudo *et al.*[111] The synthesis of the ligand **178** is depicted in Scheme 60. Reactions of **178** with several late transition metal complexes were examined. A typical example is the reaction with three equivalents of $[RuCl_2(cymene)]_2$, which produced the red triruthenium complex $(c\text{-}C_5H_9)_7Si_7O_9[OSiMe_2CH_2CH_2PPh_2RuCl_2(cymene)]_3$ (**179**) in almost quantitative yield.

An osmium cluster complex involving direct bonding of a silanol oxygen atom was reported already in 1990 by Shapley and Feher *et al.*[112] The reaction shown in Scheme 61 was conducted in cyclooctene at 130 °C for 24 h. The product **180** was isolated as a stable, yellow solid in 13% yield following chromatography. The most striking feature of the molecular structure of **180** is the formation of a siloxane linkage by the cyclodehydration of two silanol groups of **3**.

Several multifunctional donor ligands based on the *closo*-Si_8O_{12} silsesquioxane cage have also been reported in the literature, including complexes containing $Ru(terpy)_3$ units.[113] Finally, an unusual anionic osmasilsesquioxane complex containing a nitrido function has recently been described by Shapley *et al.*[108] The tetraphenylphosphonium salt $[PPh_4][(c\text{-}C_5H_9)_7Si_7O_{11}(OSiMe_3)Os(N)Cl_2]$ (**181**) was isolated as a diamagnetic, air-stable, purple crystalline solid (Scheme 62).

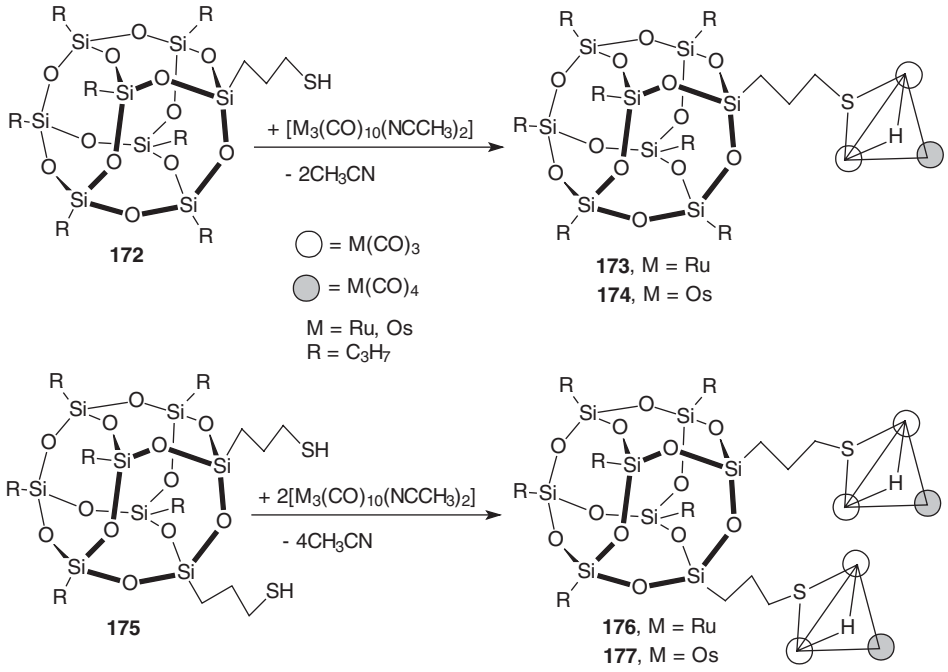

SCHEME 59. Synthesis of silsesquioxane thiol-coordinated ruthenium and osmium clusters.

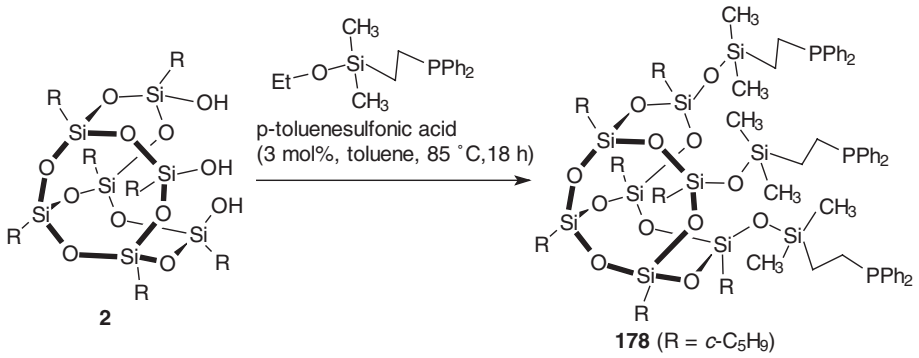

SCHEME 60. Synthesis of the silsesquioxane-based tridentate phosphine ligand **178**.

4. Group 9 Metal Derivatives (Co, Rh)

Apparently "real" metallasilsesquioxanes of cobalt, rhodium or iridium have thus far not been reported in the literature. However, several silsesquioxane ligands containing donor-substituted side chains as well as related silsesquioxane dendrimers have been found to form complexes with cobalt and rhodium complex fragments.[103,114–118]

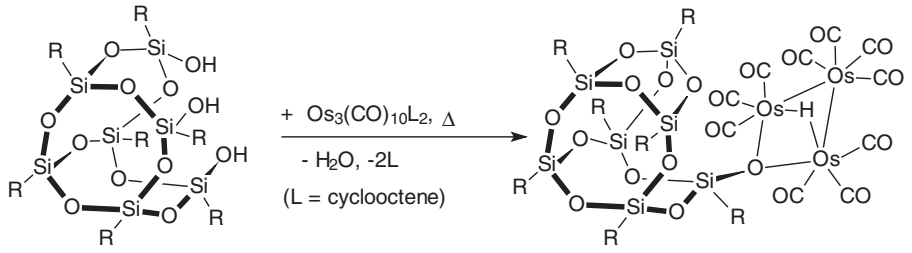

3 **180**, R = *c*-C_6H_{11}

SCHEME 61. Synthesis of the silsesquioxane triosmium cluster compound **180**.

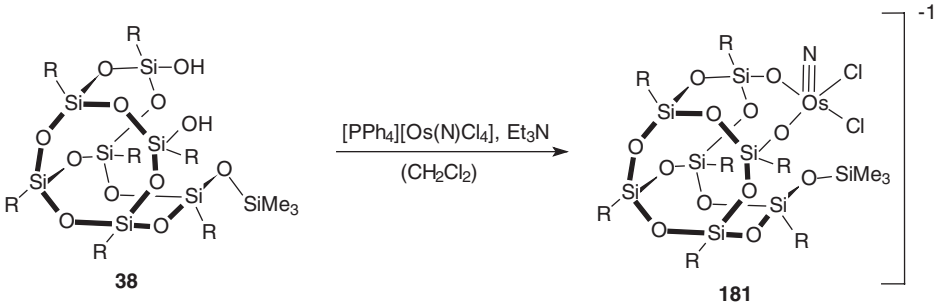

38 **181**

SCHEME 62. Synthesis of the nitrido-osmasilsesquioxane complex **181**.

5. Group 10 Metal Derivatives (Pt)

While apparently no metallasilsesquioxane complexes of nickel and palladium have yet been prepared, several literature reports have appeared on platinum compounds containing silsesquioxane ligands. Abbenhuis reported the synthesis and characterization of three platinum(II) complexes stabilized by the chelating diphosphine ligand dppe (= 1, 2-bis(diphenylphosphino)ethane) as outlined in Scheme 63.[119,120]

After prolonged reaction times (typically 7 days) all three compounds were isolated in good yields (90%) in the form of colorless crystals. The crystal structure of **182** was determined by X-ray diffraction. In other cases reactions of silsesquioxane precursors with platinum complexes have been found to be far less straightforward. Upon treatment of two equivalents of the dithallium intermediate **69** with the square planar platinum(II) complex $PtCl_2$(COD), small amounts of the highly unusual heterobimetallic Pt/Tl silsesquioxane complex **185** were formed (pale yellow needles, 6% yield). A single crystal X-ray diffraction study revealed as the most striking structural feature of **185** the presence of a σ-bond between the silsesquioxane frame and the metal-coordinated cyclooctenyl ligand. A 1:1 reaction of the same reactants also afforded moderate yields of the expected platinasilsesquioxane derivative **186** (Scheme 64).

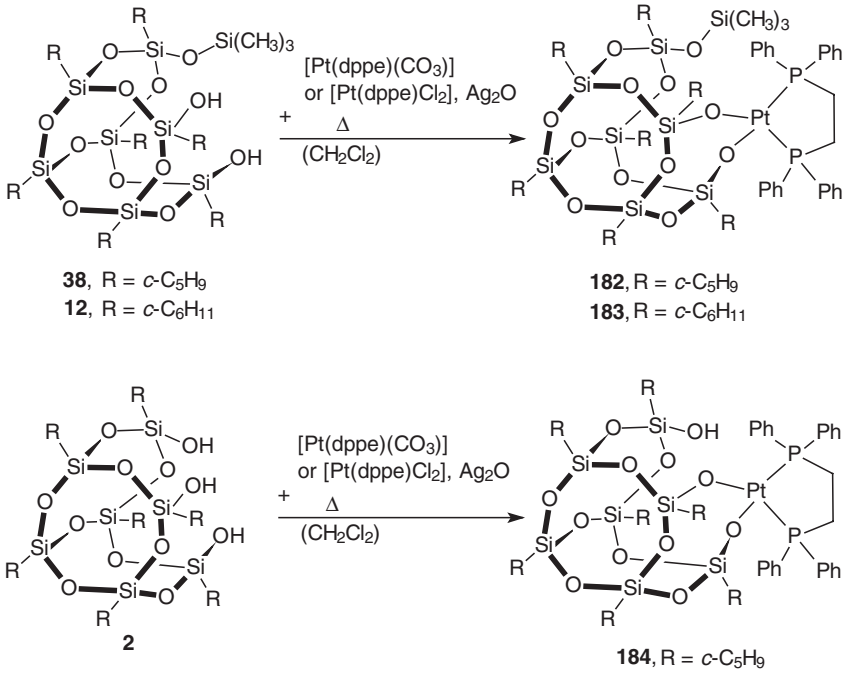

SCHEME 63. Synthesis of the platinum silsesquioxane complexes **182**–**184**.

6. Group 11 Metal Derivatives (Cu, Au)

The first silsesquioxane derivative of copper was made in our laboratory according to Scheme 65.[121] The reaction of the monosilylated disilanol precursor **12** with tetrameric copper(I)-*t*-butoxide in a molar ratio of 2:1 afforded the colorless copper(I) silsesquioxane complex **187**, in which the Cu_4O_4 core of copper(I)-*t*-butoxide is retained.

Thiol-functionalized silsesquioxane ligands such as $(c\text{-}C_5H_9)_7Si_7O_{12}CH_2CH_2CH_2SH$ (**188**) have been successfully employed by Schmid *et al.*[122] in the synthesis of gold complexes, especially Au_{55} clusters. More simple gold(I) silsesquioxane derivatives include the complexes $(c\text{-}C_5H_9)_7Si_7O_9(OH)(OAuPPh_3)_2$ (**189**) and $(c\text{-}C_5H_9)_7Si_7O_9(OAuPPh_3)_3$ (**190**).[123] They are readily accessible by reacting the corresponding silanol precursors with appropriate amounts of $Au(O_2CNEt_2)(PPh_3)$.

IV
FUTURE OUTLOOK

During the past 15 years metallasilsesquioxanes have emerged from the status of mere laboratory curiosities and have become a well-investigated and highly valuable

186.

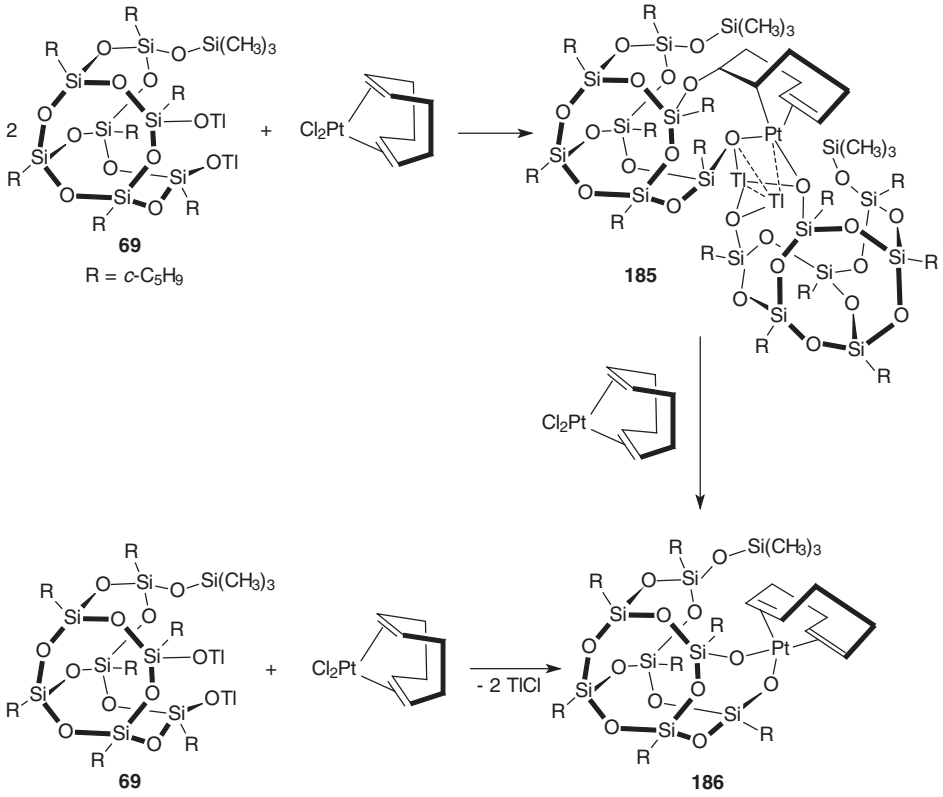

SCHEME 64. Synthesis of the platinum silsesquioxane complexes **185** and **186**.

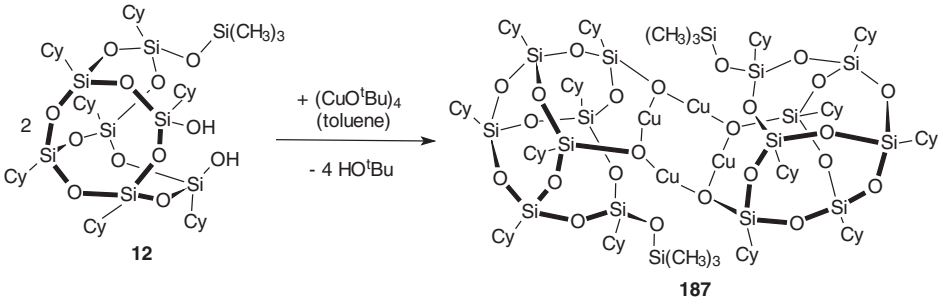

SCHEME 65. Synthesis of the copper(I) silsesquioxane complex **187**.

class of compounds. They are of fundamental interest as "realistic" molecular models of silica-supported metal catalysts. Various metallasilsesquioxanes have meanwhile turned out to be promising catalysts by in their own right. Novel aspects include the tethering of silsesquioxane cages to cyclopentadienyl-type ligands

(cf. Section III.B.2), the copolymerization and cross-linking of vinyl-substituted silsesquioxane titanium complexes with siloxane oligomers[124] and the preparation of metal oxide particles on microporous silica by controlled calcination of suitable metallasilsesquioxanes (cf. Sections III.C.1 and III.C.3). These aspects are expected to play an increasing role in future metallasilsesquioxane chemistry. Certainly, the recently discovered alkali metal silsesquioxane reagents such as **15–17** will become key intermediates in the synthesis of complex heterobimetallic metallasilsesquioxanes, which in turn could be promising precursors for multi-metallic silicate materials. Clearly, more work needs to be done to extend the "Periodic Table of metallasilsesquioxanes." Various metals (e.g., the heavier alkali and alkaline earth metals, Mn, Re, Ir, Ni, Ag etc.) have not yet been successfully incorporated into silsesquioxane derivatives. Strikingly, the vast majority of metallasilsesquioxanes reported thus far are derived from the incompletely condensed trisilanols $R_7Si_7O_9(OH)_3$ (**2–7**). Extension of this chemistry to other silsesquioxane cage compounds remains a largely open field, where many exciting results can be expected for years to come.

Acknowledgments

Our own work described in this report was generously supported by the Deutsche Forschungsgemeinschaft within the Schwerpunktprogramm "Spezifische Phänomene in der Silicium-Chemie." This support is most gratefully acknowledged. Special thanks are also due to my co-workers whose names appear in the list of references and to the Otto-von-Guericke-Universität and the Fonds der Chemischen Industrie for financial support.

References

(1) Most recent review articles: Lorenz, V.; Fischer, A.; Gießmann, S.; Gilje, J. W.; Gun'ko, Yu.; Jacob, K.; Edelmann, F. T. *Coord. Chem. Rev.* **2000**, *206–207*, 321; Duchateau, R. *Chem. Rev.* **2002**, *102*, 3525; Hanssen, R. W. J. M.; van Santen, R. A.; Abbenhuis, H. C. L. *Eur. J. Inorg. Chem.* **2004**, 675.
(2) Abbenhuis, H. C. L. *Chem. Eur. J.* **2000**, *6*, 25.
(3) Harrison, P. G. *J. Organomet. Chem.* **1997**, *542*, 141.
(4) Lichtenhan, J. D. *Comments Inorg. Chem.* **1995**, *17*, 115.
(5) Scott, D. W. *J. Am. Chem. Soc.* **1946**, *68*, 356.
(6) Barry, A. J.; Daud, W. H.; Domicone, J. J.; Gilkey, J. W. *J. Am. Chem. Soc.* **1955**, *77*, 4248.
(7) Brown, J. F. Jr. *J. Am. Chem. Soc.* **1965**, *87*, 4317.
(8) Müller, R.; Köhne, R.; Sliwinski, S. *J. Pr. Chem.* **1959**, *9*(4), 71.
(9) Frye, C. L.; Collins, W. T. *J. Am. Chem. Soc.* **1970**, *92*, 5586.
(10) Feher, F. J.; Newman, D. A.; Walzer, J. F. *J. Am. Chem. Soc.* **1989**, *111*, 1741.
(11) Brown, J. F.; Vogt, L. H. *J. Am. Chem. Soc.* **1965**, *87*, 4313.
(12) Feher, F. J.; Phillips, S. H.; Ziller, J. W. *J. Am. Chem. Soc.* **1997**, *119*, 3397.
(13) Feher, F. J.; Soulivong, D.; Lewis, G. T. *J. Am. Chem. Soc.* **1997**, *119*, 11323.
(14) Feher, F. J.; Soulivong, D.; Eklund, A. G. *Chem. Commun.* **1998**, 399.
(15) Feher, F. J.; Nguyen, F.; Soulivong, D.; Ziller, J. W. *Chem. Commun.* **1999**, 1705.
(16) Feher, F. J.; Terroba, R.; Ziller, J. W. *Chem. Commun.* **1999**, 2153.
(17) Feher, F. J.; Terroba, R.; Ziller, J. W. *Chem. Commun.* **1999**, 2309.
(18) Kudo, T.; Gordon, M. S. *J. Am. Chem. Soc.* **1998**, *120*, 11432.
(19) Kudo, T.; Gordon, M. S. *J. Phys. Chem. A* **2000**, *104*, 4058.
(20) Jug, K.; Wichmann, D. *J. Comp. Chem.* **2000**, *21*, 1549.
(21) Voronkov, M. G.; Lavrentyev, V. L. *Top. Curr. Chem.* **1982**, *102*, 199.

(22) Feher, F. J.; Budzichowski, T. A.; Blanski, R. L.; Keller, K. J.; Ziller, J. W. *Organometallics* **1991**, *10*, 2526.
(23) Feher, F. J.; Budzichowski, T. A. *Polyhedron* **1995**, *14*, 3239.
(24) Harrison, P. G. *J. Organomet. Chem.* **1997**, *542*, 141.
(25) Murugavel, R.; Voigt, A.; Walawalkar, M. G.; Roesky, H. W. *Chem. Rev.* **1996**, *96*, 2205.
(26) Hambley, T. W.; Maschmeyer, T.; Masters, A. F. *Appl. Organomet. Chem.* **1992**, *6*, 253.
(27) Severn, J. R.; Duchateau, R.; van Santen, R. A.; Ellis, D. D.; Spek, A. L.; Yap, G. P. A. *Dalton Trans.* **2003**, 2293.
(28) Feher, F. J.; Budzichowski, T. A.; Blanski, R. L.; Weller, K. J.; Ziller, J. W. *Organometallics* **1991**, *10*, 2526.
(29) Hambley, T. W.; Maschmeyer, T.; Masters, A. F. *Appl. Organomet. Chem.* **1992**, *6*, 253.
(30) Pescarmona, P. P.; van der Waal, J. C.; Maxwell, I. E.; Maschmeyer, T. *Angew. Chem.* **2001**, *113*, 762; *Angew. Chem. Int. Ed.* **2001**, 40, 740.
(31) Feher, F. J.; Newman, D. A. *J. Am. Chem. Soc.* **1990**, *112*, 1931.
(32) Feher, F. J.; Rahimian, K.; Budzichowski, T. A.; Ziller, J. W. *Organometallics* **1995**, *14*, 3920.
(33) Annand, J.; Aspinall, H. C.; Steiner, A. *Inorg. Chem.* **1999**, *38*, 3941.
(34) Lorenz, V.; Gießmann, S.; Gun'ko, Y. K.; Fischer, A. K.; Gilje, J. W.; Edelmann, F. T. *Angew. Chem.*, **2004**, *116*, 4703; *Angew. Chem. Int. Ed.* **2004**, *43*, 4603.
(35) Lorenz, V.; Gießmann, S.; Gun'ko, Y. K.; Fischer, A. K.; Gilje, J. W.; Edelmann, F. T. *Unpublished results*.
(36) Haiduc, I.; Edelmann, F. T. *Supramolecular Organometallic Chemistry*, Wiley-VCH, Weinheim, 1999.
(37) Lorenz, V.; Fischer, A.; Edelmann, F. T. *Inorg. Chem. Commun.* **2000**, *3*, 292.
(38) Gerritsen, G.; Duchateau, R.; van Santen, R. A.; Yap, G. P. *Organometallics* **2003**, *22*, 100.
(39) Liu, J.-C. *Chem. Commun.* **1996**, 1109.
(40) Liu, J. C. *Appl. Organomet. Chem.* **1999**, *13*, 295.
(41) Haddad, T. S.; Lichtenhan, J. D. *J. Inorg. Organomet. Polym.* **1995**, *5*, 237.
(42) Smet, P.; Riondato, J.; Pauwels, T.; Moens, L.; Verdonck, L. *Inorg. Chem. Commun.* **2000**, *3*, 557.
(43) Hanssen, R. W. J. M.; Meetsma, A.; van Santen, R. A.; Abbenhuis, H. C. L. *Inorg. Chem.* **2001**, *40*, 4049.
(44) Maxim, N.; Magusin, P. C. M. M.; Kooyman, P. J.; van Wolput, J. H. M. C.; van Santen, R. A.; Abbenhuis, H. C. L. *Chem. Mater.* **2001**, *13*, 2958.
(45) Feher, F. J.; Budzichowski, T. A.; Ziller, J. W. *Inorg. Chem.* **1992**, *31*, 5100.
(46) Duchateau, R.; van Santen, R. A.; Yap, G. P. A. *Organometallics* **2000**, *19*, 809.
(47) Feher, F. J.; Budzichowski, T. A.; Weller, K. J. *J. Am. Chem. Soc.* **1989**, *111*, 7288.
(48) Duchateau, R.; Harmsen, R. J.; Abbenhuis, H. C. L.; van Santen, R. A.; Meetsma, A.; Thiele, S. K.-H.; Kranenburg, M. *Chem. Eur. J.* **1999**, *5*, 3130.
(49) Edelmann, F. T.; Gun'ko, Y. K.; Giessmann, S.; Olbrich, F.; Jacob, K. *Inorg. Chem.* **1999**, *38*, 210.
(50) Skowronska-Ptasinska, M. D.; Duchateau, R.; van Santen, R. A.; Yap, G. P. A. *Eur. J. Inorg. Chem.* **2001**, 133.
(51) Skowronska-Ptasinska, M. D.; Duchateau, R.; van Santen, R. A.; Yap, G. P. A. *Organometallics* **2001**, *20*, 3519.
(52) Lorenz, V.; Fischer, A.; Jacob, K.; Edelmann, F. T. *Inorg. Chem. Commun.* **2003**, *6/7*, 795.
(53) Feher, F. J.; Budzichowski, T. A.; Ziller, J. W. *Inorg. Chem.* **1997**, *36*, 4082.
(54) Wada, K.; Yamada, K.; Kondo, T.; Mitsudo, T. *Chem. Lett.* **2001**, 12.
(55) Gun'ko, Y. K.; Nagy, L.; Brüser, W.; Lorenz, V.; Fischer, A.; Gießmann, S.; Edelmann, F. T.; Jacob, K.; Vértes, A. *Monatsh. Chem.* **1999**, *130*, 45.
(56) Duchateau, R.; Dijkstra, T. W.; Severn, J. R.; van Santen, R. A.; Korobkov, I. V. *Dalton Trans.* **2004**, 2677.
(57) Herrmann, W. A.; Anwander, R.; Dufaud, V.; Scherer, W. *Angew. Chem.* **1994**, *106*, 1338; *Angew. Chem. Int. Ed. Engl.* **1994**, *33*, 1285.
(58) Annand, J.; Aspinall, H. C. *J. Chem. Soc., Dalton Trans.* **2000**, 1867.
(59) Annand, J.; Aspinall, H. C.; Steiner, A. *Inorg. Chem.* **1999**, *38*, 3941.
(60) Arnold, P. L.; Blake, A. J.; Hall, S. N.; Ward, B. D.; Wilson, C. *Dalton Trans.* **2001**, 488.

(61) Gun'ko, Yu. K.; Reilly, R.; Edelmann, F. T.; Stalke, D. *Angew. Chem.* **2001**, *113*, 1319; *Angew. Chem. Int. Ed.* **2001**, *40*, 1279.
(62) Feher, F. J.; Soulivong, D.; Nguyen, A. G. *Chem. Commun.* **1998**, 1279.
(63) Lorenz, V.; Fischer, A.; Edelmann, F. T. *J. Organomet. Chem.* **2002**, *647*, 245.
(64) Duchateau, R.; Abbenhuis, H. C. L.; van Santen, R. A.; Thiele, S. K.-H.; van Tol, M. F. H. *Organometallics* **1998**, *17*, 5222.
(65) Piers, W. E.; Bunel, E. E.; Bercaw, J. E. *J. Organomet. Chem.* **1991**, *407*, 51.
(66) Lorenz, V.; Fischer, A.; Jacob, K.; Brüser, W.; Edelmann, F. T. *Chem. Eur. J.* **2001**, *7*, 848.
(67) Feher, F. J.; Gonzales, S. L.; Ziller, J. W. *Inorg. Chem.* **1988**, *27*, 3440.
(68) Feher, F. J.; Walzer, J. F. *Inorg. Chem.* **1990**, *29*, 1604.
(69) Feher, F. J.; Budzichowski, T. A.; Rahimian, K.; Ziller, J. W. *J. Am. Chem. Soc.* **1992**, *114*, 3859.
(70) Field, L. D.; Lindall, C. M.; Maschmeyer, T.; Masters, A. F. *Aust. J. Chem.* **1994**, *47*, 1127.
(71) Murugavel, R.; Roesky, H. W. *Angew. Chem.* **1997**, *109*, 491; *Angew. Chem. Int. Ed. Engl.* **1997**, *36*, 476.
(72) Winkhofer, N.; Voigt, A.; Dorn, H.; Roesky, H. W.; Steiner, A.; Stalke, D.; Reller, A. *Angew. Chem.* 1994, *106*, 1414; Angew. Chem. Int. Ed. Engl. **1994**, *33*, 1352.
(73) Voigt, A.; Murugavel, R.; Montero, M. L.; Wessel, H.; Liu, F.-Q.; Roesky, H. W.; Usón I.; Albers, T.; Parisini, E. *Angew. Chem.* **1997**, *109*, 1020; *Angew. Chem. Int. Ed. Engl.* **1997**, *36*, 1001.
(74) Maschmeyer, T.; Klunduk, M. C.; Martin, C. M.; Shephard, D. S.; Thomas, J. M.; Johnson, B. F. G. *Chem. Commun.* **1997**, 1847.
(75) Wada, K.; Yamada, K.; Izuhara, D.; Kondo, T.; Mitsudo, T. *Chem. Lett.* **2000**, 1332.
(76) Crocker, M.; Herold, R. H. M.; Orpen, A. G. *Chem. Commun.* **1997**, 2411.
(77) Crocker, M.; Herold, R. H. M.; Orpen, A. G.; Overgaag, M. T. A. *J. Chem. Soc., Dalton Trans.* **1999**, 3791.
(78) Edelmann, F. T.; Gießmann, S.; Fischer, A. *J. Organomet. Chem.* **2001**, *620*, 80.
(79) Gießmann, S.; Fischer, A.; Edelmann, F. T. *Chem. Commun.* **2000**, 2153.
(80) Bercaw, J. E. *J. Am. Chem. Soc.* **1974**, *96*, 5087.
(81) Pattiasina, J. W.; Hissink, C. E.; de Boer, J. L.; Meetsma, A.; Teuben, J. H. *J. Am. Chem. Soc.* **1985**, *107*, 7785.
(82) Pattiasina, J. W. Ph.D. Thesis, Rijksuniversiteit Groningen, **1988**.
(83) Feher, F. J. *J. Am. Chem. Soc.* **1986**, *108*, 3850.
(84) Duchateau, R.; Abbenhuis, H. C. L.; van Santen, R. A.; Meetsma, A.; Thiele, S. K.-H.; van Tol, M. F. H. *Organometallics* **1998**, *17*, 5663.
(85) Metcalfe, R. A.; Kreller, D. I.; Tian, J.; Kim, H.; Taylor, N. J.; Corrigan, J. F.; Collins, S. *Organometallics* **2002**, *21*, 1719.
(86) Severn, J. R.; Duchateau, R.; van Santen, R. A.; Ellis, D. D.; Spek, A. L. *Organometallics* **2002**, *21*, 4.
(87) Severn, J. R.; Duchateau, R.; van Santen, R. A.; Ellis, D. D.; Spek, A. L.; Yap, G. P. A. *Dalton Trans.* **2003**, 2293.
(88) Wada, K.; Bundo, M.; Nakabayashi, D.; Itayama, N.; Kondo, T.; Mitsudo, T. *Chem. Lett.* **2000**, 628.
(89) Feher, F. J.; Walzer, J. F. *Inorg. Chem.* **1991**, *30*, 1689.
(90) Feher, F. J.; Walzer, J. F.; Blanski, R. L. *J. Am. Chem. Soc.* **1991**, *113*, 3618.
(91) Feher, F. J.; Blanski, R. L. *J. Am. Chem. Soc.* **1992**, *114*, 5886.
(92) Fei, Z.; Busse, S.; Edelmann, F. T. *Chem. Commun.* **2002**, 2587.
(93) Chabanas, M.; Quadrelli, E.A.; Fenet, B.; Coperet, C.; Thivolle-Cazat, J.; Basset, J.M.; Lesage, A.; Emsley, L. *Angew. Chem.* **2001**; *Angew. Chem. Int. Ed.* **2001**, *40*, 4493.
(94) Wada, K.; Nakashita, M.; Yamamoto, A.; Mitsudo, T. *Chem. Commun.* **1998**, 133.
(95) Feher, F. J.; Blanski, R. L. *J. Chem. Soc., Chem. Commun.* **1990**, 1614.
(96) Feher, F. J.; Blanski, R. L. *Makromol. Chem., Macromol. Symp.* **1993**, *66*, 95.
(97) Vorstenbosch, M. L. W. *Alkene Epoxidation with Silsesquioxane-Based Chromium and Titanium Complexes*, Schuit Institute of Catalysis, Eindhoven, **2002**.
(98) Maxim, N.; Abbenhuis, H. C. L.; Stobbelaar, P. J.; Mojet, B. L.; van Santen, R. A. *Phys. Chem. Chem. Phys.* **1999**, *1*, 4473.
(99) Feher, F. J.; Soulivong, D.; Eklund, A. G.; Wyndham, K. D. *Chem. Commun.* **1997**, 1185.

(100) Budzichowski, T. A.; Chacon, S. T.; Chisholm, M. H.; Feher, F. J.; Streib, W. *J. Am. Chem. Soc.* **1991**, *113*, 689.
(101) Smet, P.; Devreese, B.; Verport, F.; Pauwels, T.; Svoboda, I.; Foro, S.; van Beeumen, J.; Verdonck, L. *Inorg. Chem.* **1998**, *37*, 6583.
(102) Morán, M.; Casado, C. M.; Cuadrado, I. *Organometallics* **1993**, *12*, 4327.
(103) Marcolli, C.; Calzaferri, G. *Appl. Organomet. Chem.* **1999**, *13*, 213.
(104) Casado, C. M.; Cuadrado, I.; Morádo, M.; Alonso, B.; Barranco, M.; Losada, J. *Appl. Organomet. Chem.* **1999**, *13*, 245.
(105) Edelmann, F. T.; Lorenz, V.; Fischer, A. *Z. Anorg. Allg. Chem.* **2000**, *626*, 1728.
(106) Maxim, N.; Overweg, A.; Kooyman, P. J.; van Wolput, J. H. M. C.; Hanssen, R. W. J. M.; van Santen, R. A.; Abbenhuis, H. C. L. *J. Phys. Chem. B* **2002**, *106*, 2203.
(107) Maxim, N.; Overweg, A.; Kooyman, P. J.; van Santen, R. A.; Abbenhuis, H. C. L. *J. Mater. Chem.* **2002**, 3792.
(108) Shapley, P. A.; Bigham, W. S.; Hay, M. T. *Inorg. Chim. Acta* **2003**, *345*, 255.
(109) Baker, R. T.; Ott, K. C.; Tumas, W.; Liu, F.; John, K. D.; Scott, B. L. *Angew. Chem*. **2000**, *112*, 3257; *Angew. Chem. Int. Ed*. **2000**, *39*, 3127.
(110) Braunstein, P.; Galsworthy, J. R.; Hendan, B. J.; Marsmann, H. C. *J. Organomet. Chem.* **1998**, *551*, 125.
(111) Wada, K.; Izuhara, D.; Shiotsuki, M.; Kondo, T.; Mitsudo, T. *Chem. Lett.* **2001**, 734.
(112) Liu, J.; Wilson, S. R.; Shapley, J. R.; Feher, F. J. *Inorg. Chem.* **1990**, *29*, 5138.
(113) Murfee, H. J.; Thomas, J. P.; Greaves, J.; Hong, B. *Inorg. Chem.* **2000**, *39*, 5209.
(114) Rattay, M.; Fenske, D.; Jutzi, P. *Organometallics* **1998**, *17*, 2930.
(115) Harrison, P. G.; Hall, C. H. *J. Sol–gel. Sci. Tech.* **1998**, *13*, 391.
(116) Ropartz, L.; Morris, R. E.; Schwarz, G. P.; Foster, D. F.; Cole-Hamilton, D. J. *Inorg. Chem. Commun.* **2000**, *3*, 714.
(117) Ropartz, L.; Morris, R. E.; Schwarz, G. P.; Foster, D. F.; Cole-Hamilton, D. J. *J. Mol. Catal. A* **2002**, *182–183*, 99.
(118) Lücke, S.; Stoppek-Langner, K.; Kuchinke, J.; Krebs, B. *J. Organomet. Chem.* **1999**, *584*, 11.
(119) Abbenhuis, H. C. L.; Burrows, A. D.; Kooijman, H.; Lutz, M.; Palmer, M. T.; van Santen, R. A.; Spek, A. L. *Chem. Commun.* **1998**, 2627.
(120) Quadrelli, E. A.; Davies, J. E.; Johnson, B. F. G.; Feeder, N. *Chem. Commun.* **2000**, 1031.
(121) Edelmann, F. T.; Gießmann, S.; Fischer, A. *Inorg. Chem. Commun.* **2000**, *3*, 658.
(122) Schmid, G.; Pugin, R.; Malm, J. O.; Bovin, J. *Eur. J. Inorg. Chem.* **1998**, 813.
(123) Abis, L.; Armelao, L.; Belli Dell'Amico, D.; Calderazzo, F.; Garbassi, F.; Merigo, A.; Quadrelli, E. A. *J. Chem. Soc., Dalton Trans.* **2001**, 2704.
(124) Skowronska-Ptasinska, M. D.; Vorstenbosch, M. L. W.; van Santen, R. A.; Abbenhuis, H. C. L. *Angew. Chem*. **2002**, *114*, 659; *Angew. Chem. Int. Ed*. **2002**, *41*, 637.

Cations of Group 14 Organometallics

THOMAS MÜLLER*

Institut für Anorganische und Analytische Chemie, Johann Wolfgang Goethe Universität, Frankfurt, Marie Curie-Str. 11, D 60439 Frankfurt/Main, Germany

I. Introduction . . . 155
II. Synthetic Approaches to R_3E^+ Ions . . . 156
A. Heterolytic Cleavage of E–X Bonds . . . 156
B. Hydride Transfer Reaction . . . 157
C. Electrophilic Cleavage of E-Alkyl and E-Silyl Bonds . . . 159
D. Oxidative Cleavage of E–E and E–C Bonds . . . 160
E. Addition of Electrophiles to Heavy Carbenes . . . 164
III. Structure and Properties of R_3E^+ Cations . . . 165
A. Theoretical Considerations . . . 165
B. NMR Spectroscopic Properties of R_3E^+ Cations . . . 169
C. Miscellaneous Spectroscopic Data of R_3E^+ Cations . . . 189
D. Solid State Structure of R_3E^+ Cations and Related Species . . . 190
IV. A chemistry of R_3E^+ cations . . . 206
Acknowledgements . . . 210
References . . . 210

Dedicated to the memory of Dr. Uwe Herzog

I
INTRODUCTION

There is a fundamental interest in understanding similarities and differences between carbon and heavier group 14 elements. Many theoretical and experimental studies were carried out in order to ascertain whether the organic compounds of heavier group 14 elements could be demonstrated to exhibit similar chemical properties to their carbon analogues. Such studies have, for example, recently led to the successful isolation of compounds containing formal E≡E triple bonds.[1] One of the most demanding and difficult challenges to chemists was to demonstrate the existence of, and to isolate and characterize, the heavier congeners of carbonium ions R_3E^+ (E = Si, Ge, Sn, Pb). In particular, the silylium ions, R_3Si^+, have received much attention and the debate on their existence was controversial, lively and sometimes overemphasized. Even in 2001, the year of the 100th anniversary of the discovery of the trityl cation,[2,3] no direct structural proof for the existence of analogous three-coordinate, trivalent cationic species R_3E^+ was provided. NMR[4,5] and computational evidence[6,7] for the existence of trimesitylsilylium Mes_3Si^+, **1**, was given, but the only crystallographically characterized tricoordinated cations of the elements silicon[8] and germanium[9] were the cyclic cations **2** and **3**, which are stabilized either by conjugation or homoconjugation.

*Corresponding author. Tel.: +49-69-79829166; fax: +49-69-79829188.
E-mail: dr.thomas.mueller@chemie.uni-frankfurt.de (T. Müller).

ADVANCES IN ORGANOMETALLIC CHEMISTRY
VOLUME 53 ISSN 0065-3055/DOI 10.1016/S0065-3055(05)53005-3

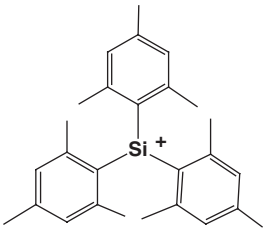

1

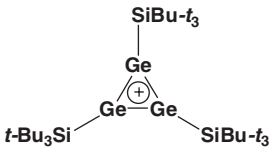

2

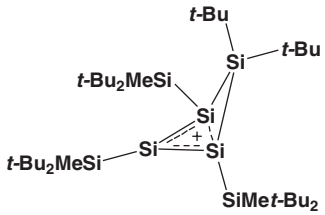

3

The major obstacle for the synthesis of R_3E^+ ions is their inherent high electrophilicity and high reactivity, which leads such species to interact in solution and solid state with solvents and/or counteranions that are found to be innocent in other areas of chemistry. In addition, the tendency of the higher congeners of carbon to extend their coordination sphere, their inherent reluctance towards π-conjugation and to hyperconjugative effects due to less-effective orbital overlap and, finally, the larger size of the electron-deficient center, which is harder to protect sterically, are factors, which complicate the isolation and characterization of organometallic cations of group 14 elements. Since the mid 1990s significant breakthroughs in synthetic methodology have been achieved and at the time this review was finalized (Autumn 2004) for all group 14 elements but lead, examples of strictly three-coordinated, trivalent organometallic R_3E^+ cations have been synthesized, isolated and fully characterized including by crystallography. Moreover, several group 14 element cations having novel bonding features or unusual structures were identified. It is worth mentioning that this progress was facilitated by major advances in computational chemistry, which critically attended the experimental achievements and supported greatly the identification of the synthesized species.

Several reviews appeared on the heavier congeners of the carbenium ions. Clearly, the silylium ion problem has received the most attention, and both theoretical as well as experimental aspects have been reviewed.[10–16] The chemistry of cationic germanium, tin and lead is covered by a recent review by Zharov and Michl.[17] We will concentrate in this review on the description of the progress made during the last 4 years and will try to give an account on the synthesis, the properties and the structure of organosubstituted three-coordinated, trivalent group 14 element cations and closely related species in the condensed phase.

II
SYNTHETIC APPROACHES TO R_3E^+ IONS

A. *Heterolytic Cleavage of E–X Bonds*

The heterolytic cleavage of a C(sp^3)–X bond (X: good leaving group e.g. halide, sulfonates and perchlorate) is the first step in a typical S_N1 reaction and it is the most popular synthetic approach to persistent carbocations.[18] The high bond energy

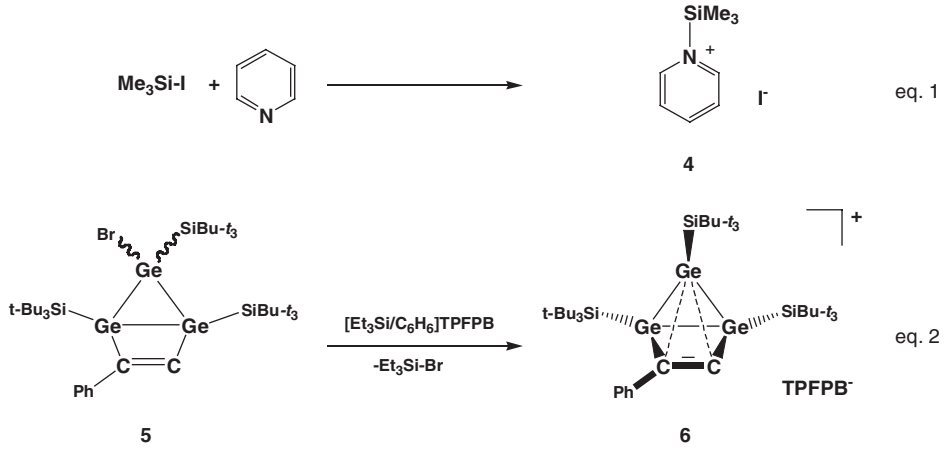

Scheme 1.

of most of the R_3E–X bonds and/or the high reactivity of the incipient element cation toward the leaving group X precludes the use of this synthetically straightforward approach to persistent trivalent organoelement cations. For example, trimethylsilylium Me_3Si^+ cannot be synthesized from the corresponding fluoride in the superacidic HSO_3F/SbF_5 system.[19] Heterolytic E–X bond cleavage can be used, however, if the solvent provides enough stabilization of the transient cation [Scheme 1, Eq. (1)].[20] In this case, solvent complexes of the R_3E^+ cation with the element in a tetrahedral or trigonal–bipyramidal coordination sphere, e.g. the silylated pyridinium cation **4**, are isolated. Similarly, intramolecular interaction can provide enough stabilization of the element cation that it can be generated by dehalogenation, in particular if the halide is efficiently removed from the reaction mixture. A recent example is provided by the dehalogenation of the bicyclic germyl bromide, **5**, to yield the intramolecularly stabilized germyl cation **6**. [Scheme 1, Eq. (2)].[21] As a consequence of the intramolecular interaction of the germyl cation with the remote C=C double bond, the coordination number of the germanium atom in the intramolecularly stabilized element cation is larger than 3.

B. *Hydride Transfer Reaction*

The Bartlett–Condon–Schneider hydride transfer reaction,[22,23] first employed in silicon chemistry by Corey in 1975,[24] developed since then to be the most popular synthetic approach to silylium ions in the condensed phase.[10] Subsequently, it was also used for the generation of germylium[22,56] and stannylium compounds.[4,17,26,29] This method exploits the relative weakness of the E–H bond and involves the transfer of the hydride from the element to a strong Lewis acid, in most cases to trityl cation. The easy access of trityl salts with a wide variety of weakly coordinating counteranions is a clear advantage of this method. The reaction can be applied in polar solvents such as sulfolane, ethers and nitriles but also in chlorinated

or aromatic hydrocarbons. For silicon, careful mechanistic[30] and theoretical[31] studies have shown that the reaction proceeds with the intermediacy of silylium ions and a single electron transfer reaction mechanism that was suggested earlier[32] can be excluded. The hydride transfer method gives access to a wide variety of cationic species of group IV elements, which are either stabilized by intermolecular interaction with solvent molecules and/or with the counterion or by intramolecular interactions. Some recent examples for the application of the hydride transfer reaction in the synthesis of group 14 cationic species are summarized in Scheme 2.[25,33–40] Particularly noteworthy is the synthesis of the silatropylium ion **7** by Komatsu and co-workers from the silepin **8** (see Scheme 3).[33,34]

The major obstacle of the hydride transfer reaction is the steric bulk of the trityl cation as the reagent of choice. Substrates that will allow the isolation of cations R_3E^+, free from intramolecular and/or intermolecular interactions with solvent molecules or anions, need to have bulky substituents and therefore the hydride transfer reaction between the hydride and trityl cation is severely hampered or it is even impossible. Another drawback of this method is the limited availability of the starting hydrido compound, which for example, is not available for lead compounds, due to the high reactivity of lead(IV) hydrides.

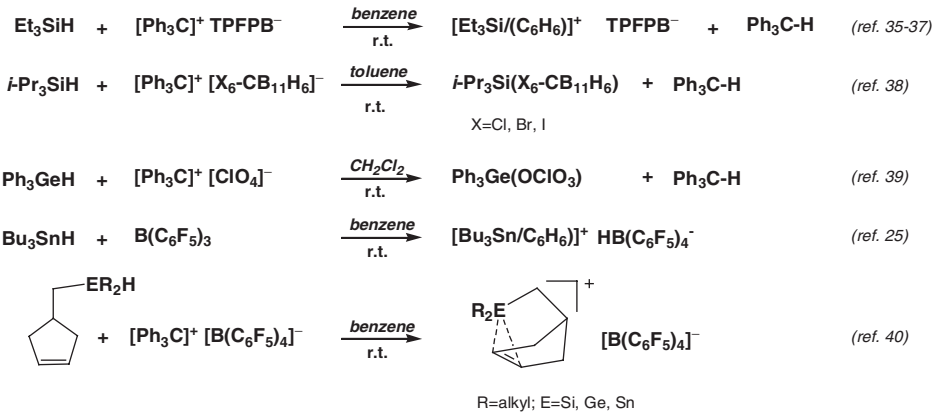

SCHEME 2.

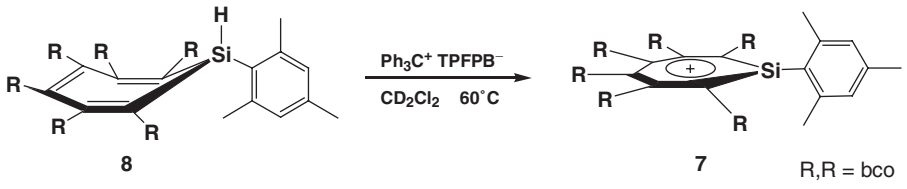

SCHEME 3.

C. *Electrophilic Cleavage of E-Alkyl and E-Silyl Bonds*

The cleavage of an alkyl or silyl group was successfully applied in the synthesis of several R_3E^+ cations. Early attempts were restricted to strongly acidic media. It was shown by Gillespie *et al.*[41,42] and Birchall and co-workers[43–45] that in contrast to silyl or germyl cations, stannyl cations "R_3Sn^+" can be formed by dissolving tetraorganotin compounds in strong acids such as sulfuric acid or fluorosulfonic acid. Similarly, the formation of a Me_3Pb^+ cation in fluorosulfonic acid at low temperatures was reported.[46] Subsequently it was shown by Mössbauer and ^{119}Sn NMR spectroscopy that the generated tin species are five-coordinated complexes of the stannylium ion R_3Sn^+, and two molecules either of the acid or the corresponding anion that adopt the axial positions of the trigonal bipyramidal complete the coordination sphere of tin.[43–45] For the synthesis of R_3E^+ in less nucleophilic organic solvents more moderate reaction conditions and better "leaving groups" had to be found. The use of the allyl moiety as a leaving group was the key for the spectacular synthesis and characterization of silylium, germylium and stannylium ions by Lambert and co-workers.[45,47–49] Reaction of the allyl element compound **9** with the silylated arenium ion $(Et_3Si/C_6H_6)^+$ gives rise to the formation of the β-silyl-substituted carbocation **10,** which undergoes a fragmentation reaction and releases the stable Ar_3E^+ cation (Scheme 4). This allyl fragmentation reaction has some precedence in the reaction of allylsilanes with triflic acid[50] and with trityl cation,[51] and in the fragmentation of β-silyl-substituted vinyl cations, detected in superacidic media at low temperatures.[52]

Similarly, trityl cation in aromatic hydrocarbons initiates the fragmentation of simple tetraalkyl plumbanes and stannanes yielding the plumbyl or stannyl cationic species, e.g. **11**, and alkenes.[40,53,54] The reaction is thought to proceed *via* plumbyl- or stannyl-substituted carbocations **12**, which in a second step eliminate the alkene.[54] This approach was used in the synthesis of norbornyl cations of the elements tin and lead, e.g. **13**, (Scheme 5).[40,53]

The cleavage of a silicon–methyl bond by the silylated benzenium ion $[Et_3Si/C_6H_6]^+$ and formation of the silylium ion **14** is the first step in the unexpected synthesis of the homoaromatic silyl cation **3** from trisilacyclopropene **15** (Scheme 6).[8]

The intermediate formation of the ferrocenyl-substituted silylium ion **16** by protonation of the ansa-ferrocenyl silane **17** can be regarded as a special case of electrophilic cleavage of an activated C–Si bond (see Scheme 7). The driving force for this reaction is the release of a strain by formation of the silyl cation.[55] In a

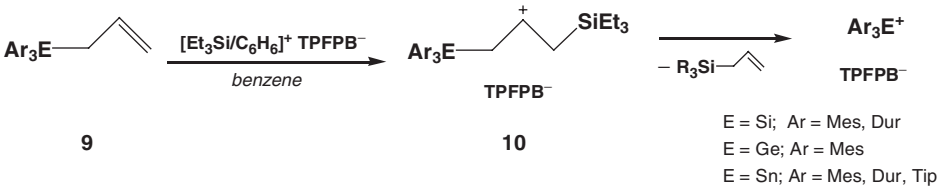

SCHEME 4.

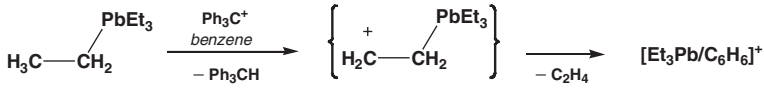

12 11

13

Scheme 5.

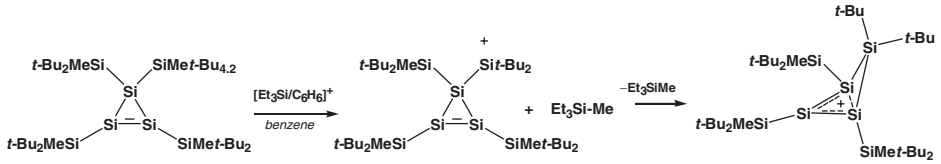

15 14 3

Scheme 6.

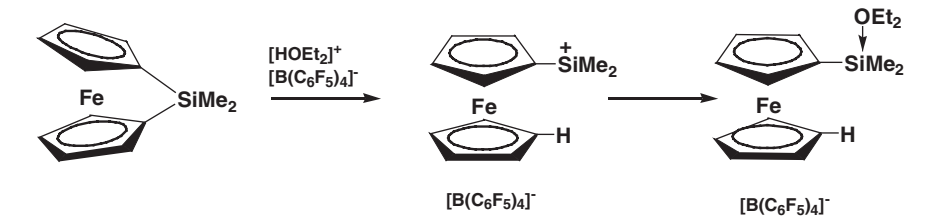

17 16 18

Scheme 7.

spontaneous consecutive reaction the silylium ion **16** forms with ether solvent the oxonium ion **18**.[55]

D. *Oxidative Cleavage of E–E and E–C Bonds*

The early reports on the oxidative generation of R_3E^+ cations are nearly exclusively restricted to the synthesis of R_3Sn^+ cations. Hexamethylditin $Me_3Sn–SnMe_3$ is oxidized in acetonitrile by one-electron oxidants as, for example 10-methacridinium,[56] thianthrene cation radical[57] and $Fe(phen)_3^{3+}$[58] yielding the solvent complexed Me_3Sn^+ cation. Interestingly, the oxidation of the mixed tin element compounds $Me_3Sn–EMe_3$, E = Si, Ge by 10-methacridinium resulted in the

formation of solvated $[Me_3Sn/(N{\equiv}CMe)_n]^+$ and $[Me_3E/(N{\equiv}CMe)_n]^+$ cations ($n = 1, 2$), while the tin-free dielement compounds ($Me_3E–E'Me_3$, E, E′ = Si, Ge) underwent no reaction. This is in line with the lower oxidation potential of the Sn-element bond in tin compounds (see Table I).[56] Mechanistically, these reactions are thought to proceed *via* electron transfer as the rate-determining step. In the case of dielement compounds $R_3E–E'R'_3$ initially the cation radicals $[R_3E–E'R'_3]^{+\bullet}$ are produced, which then decompose by cleavage of the E–E bond to give R_3E^+ and $R_3E^\bullet$. The radical $R_3E^\bullet$ is then further oxidized to the R_3E^+ cation, thus consuming 2 equivalents of the oxidant.[56,57,59,60–62] Oxidation of R_4Sn, Me_3SnR (R = Me, Et, *n*-Bu, Vi, Ph) and Ph_6Sn_2 with thianthrene cation radical was reported to give the solvent complexed stannyl cations.[57] An early communication, reports the preparation of the $[Ph_3Pb/N{\equiv}CMe]^+$ cation by oxidation of the diplumbane Ph_6Pb_2 by $AgNO_3$ in acetonitrile.[63] In all these reactions the need for strongly interacting solvents (in most cases acetonitrile) and the use of chloride or perchlorate as counterion precludes all attempts for the isolation of the generated cationic species. Only with the advent of fluorinated tetraarylborates and carboranes as weakly coordinating anions (WCA^-), did the isolation of the cationic species on a preparative scale become feasible.

The first landmark was the successful synthesis and structural characterization of the cyclotrigermylium cations **2** and **19** by Sekiguchi and co-workers. This was achieved by reaction of trityl cation with the cyclotrigermenes **20** in the presence of weakly coordinating borate anions (Scheme 8). The trityl cation acts here as a one-electron oxidizing reagent and the resulting radical cation of **20** decomposes to the

TABLE I
OXIDATION POTENTIALS (E_P) OF GROUP 14 COMPOUNDS

Compound	E_P(V)
	in MeCN, vs. Ag/AgCl/MeCN
$Me_3Si–SiMe_3$	1.76
$Me_3Ge–GeMe_3$	1.70
$Me_3Sn–SnMe_3$	1.28
$Me_3Si–SnMe_3$	1.60
$Me_3Ge–SnMe_3$	1.44
$Et_3Si–SiEt_3$	1.76
$Et_3Ge–GeEt_3$	1.48
$Et_3Sn–SnEt_3$	1.24
$Et_3Si–GeEt_3$	1.70
$Et_3Si–SnEt_3$	1.56
$Et_3Ge–SnEt_3$	1.40
	in MeCN, vs. Fc/Fc^+
$Ph_3Si–SiMe_3$	1.29
$PhMe_2Si–SiPhMe_2$	1.26
$Me_3Si–SiMe_3$	1.36
$Ph_3Ge–GeMe_3$	1.16
$PhMe_2Ge–GePhMe_2$	1.20
$Me_3Ge–GeMe_3$	1.28

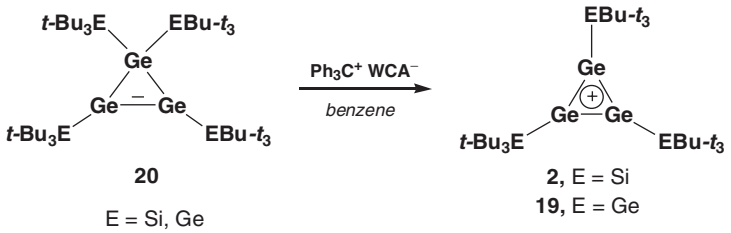

20

E = Si, Ge

2, E = Si
19, E = Ge

$WCA^- = TPB^-, TFPB^-, TPFPB^-, TSFPB^-$

Scheme 8.

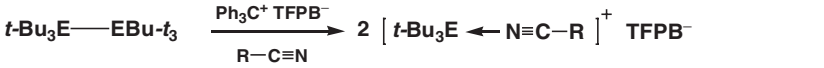

21 E = Si, Ge, Sn, R = *t*-Bu, Me

Scheme 9.

cyclotrigermylium ions, **2**, **19**, by cleavage of a Ge–Si or Ge–Ge bond (Scheme 8).[9,64–66]

Subsequently, the same group demonstrated that the reaction of hexa-*t*-butyldimetallanes *t*-Bu_3E–EBu-t_3; E = Si, Ge, Sn) with two equivalents of trityl $TFPB^-$ in pivaloylnitrile or acetonitrile gave tri-*t*-butylelement cation nitrile complexes, **21**, by oxidative E–E bond cleavage (Scheme 9). The isolated yields of the salts **21** $TFPB^-$ were in the range from 60 to 80%.[67] For silanes, the oxidation only occurs for sterically strongly congested disilanes, having a long central SiSi bond and therefore a low ionization potential. Thus, hexa-*t*-butyl disilane and hexa-iso-propyl disilane gave the corresponding cations, while hexaethyl disilane and hexamethyl disilane are unreactive toward trityl cation in acetonitrile.[67]

A crystalline solvent-free $CB_{11}Me_{12}^-$ salt of the *n*-Bu_3Sn^+ cation with significant anion–cation interaction was prepared by Michl and co-workers by oxidizing *n*-Bu_6Sn_2 with the radical $CB_{11}Me_{12}^{\bullet}$ (Scheme 10).[68] The $CB_{11}Me_{12}^{\bullet}$ radical is a stable and strong one-electron oxidant, comparable in its oxidation power to Ce(IV). It is freely soluble in non-polar solvents as, for example, saturated hydrocarbons and in its reduced form it serves as a WCA^-. Thus, this approach provides the opportunity to generate the group 14 cations in an environment devoid of unsaturated molecules or molecules with lone pairs. This is a clear advantage compared to methods as, for example, the hydride transfer method for which aromatic hydrocarbons as solvents are a prerequisite. Quite recently the solvent-free Me_3E^+ $CB_{11}Me_{12}^-$ salts (E = Ge, Sn, Pb) have been prepared by oxidation of hexamethyldigermane and -distannane and of tetramethyllead, and characterized by NMR and extended X-ray absorption five structure analysis (EXAFS) studies.[69]

The straightforward access to stable radicals[70,71] opened the avenue for the synthesis of the corresponding cations by one-electron oxidations. Thus, the stable radicals $(t\text{-}Bu_2MeSi)_3E^{\bullet}$ (E = Si, Ge, Sn) can be oxidized by trityl cation in benzene, and for germanium and tin the free germylium, **22**, and stannylium ion, **23**, could be

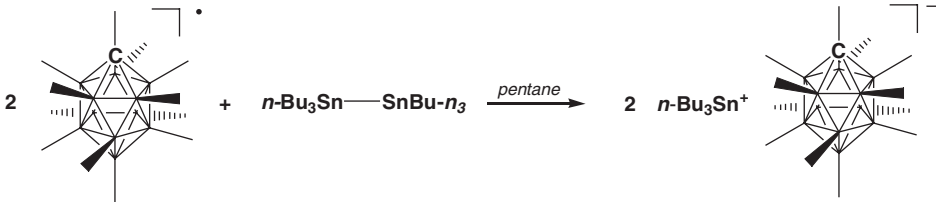

SCHEME 10.

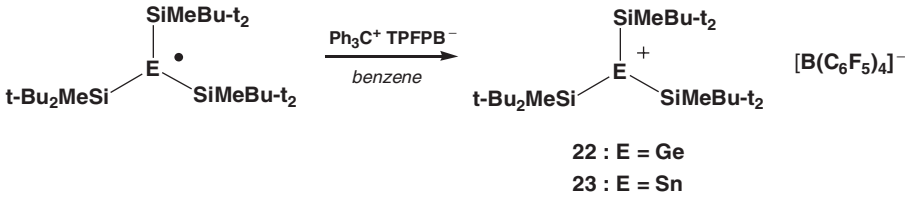

SCHEME 11.

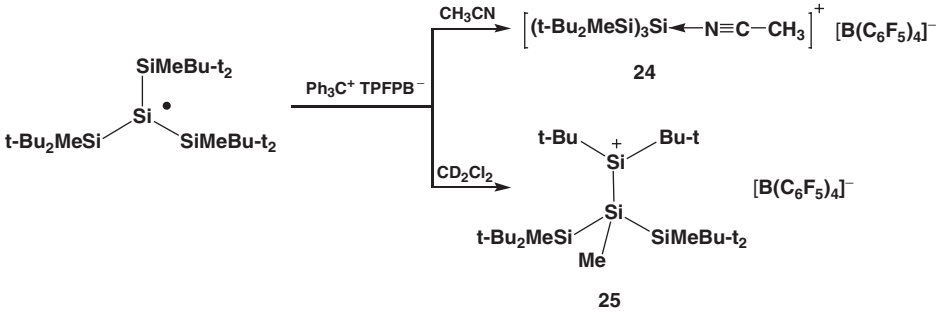

SCHEME 12.

isolated and structurally characterized as tetrakis(pentafluorophenyl)borate ($TPFPB^-$) salts (Scheme 11).[71,72] In the case of the silicon compound the presence of acetonitrile allowed the isolation of the stable nitrilium ion $[(t\text{-}Bu_2MeSi)_3Si/N{\equiv}CMe]^+$, **24**. In the absence of acetonitrile the incipient silylium ion $(t\text{-}Bu_2MeSi)_3Si^+$ undergoes a 1,2-methyl migration yielding the marginally stable silylium ion **25**, which was identified in CD_2Cl_2 solution at low temperatures by NMR spectroscopy (Scheme 12).[73]

In principle, these oxidations are reversible. This was elegantly shown for silenylium ion **3**. Reduction of **3** with *t*-butylsilyl sodium gives the cyclotetrasilenyl radical **26** and one-electron oxidation of **26** by trityl cation results in the back-formation of **3** (Scheme 13).[74] Moreover, **26** can be further reduced giving the corresponding anion **27**. Also the transformation between radical **26** and anion **27** was shown to be reversible. In this case, the silylated benzenium ion $[Et_3Si/C_6H_6]^+$ serves as a one-electron oxidant to give the radical **26** (Scheme 13).[75]

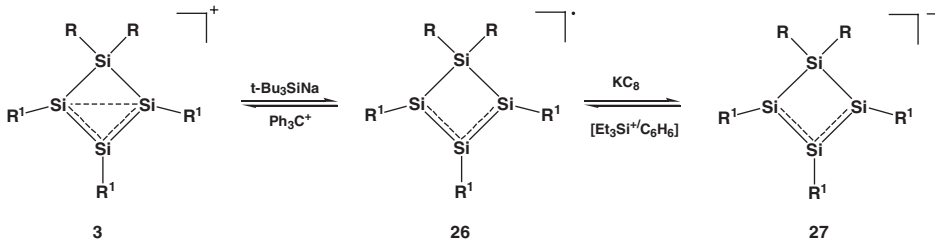

SCHEME 13.

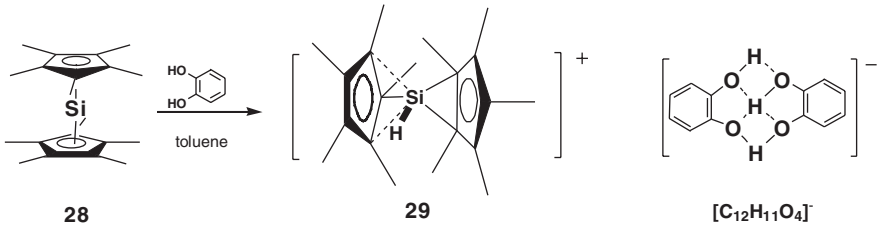

SCHEME 14.

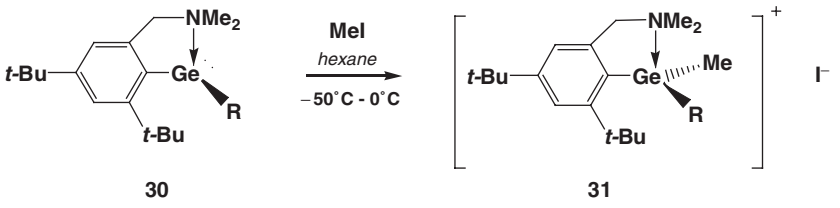

SCHEME 15.

E. *Addition of Electrophiles to Heavy Carbenes*

Alkylation or protonation of neutral, divalent organoelement compounds leads in principle to trivalent cations. There are only a few reports in literature that follow successfully this conceptionally straightforward approach to R_3E^+ cations. In most cases, the resulting cations are strongly stabilized by intramolecular interactions between a remote donor substituent and the electrophilic center. Thus, protonation of decamethylsilicocene **28** by *o*-catechol leads to the unique silyl cation **29** with the unusual hydrogen-bridged bis-catecholate anion, $C_{12}H_{11}O_4^-$ (Scheme 14)[76,77] and the donor-stabilized germylenes **30** reacts with methyliodide to give the four-coordinate germyl cations **31** (Scheme 15) those were isolated as iodide salts.[78,79]

The reaction of the stable germylene **32** with a triarylmethylium ion gave not the expected germylium ion **33**, but in a series of unexpected rearrangements, the germylium ion **34,** which is intramolecularly stabilized by interaction of the electron-deficient germylium center with a remote aryl group (Scheme 16).[80]

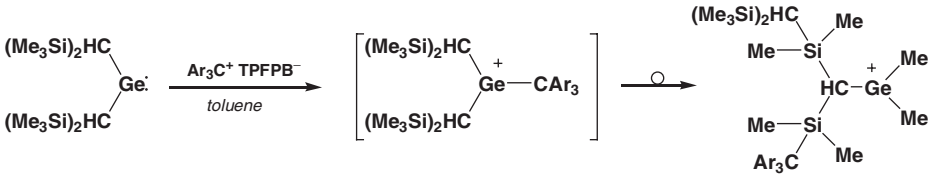

32 33 34

SCHEME 16.

III

STRUCTURE AND PROPERTIES OF R_3E^+ CATIONS

A. *Theoretical Considerations*

1. The EH_3^+ Potential Energy Surface

In agreement with a simple Walsh-type analysis for a AH_3 system with six valence electrons,[81] the planar D_{3h} structure, **35**, is a minimum on the potential energy surface for EH_3^+ cations of all group 14 elements.[82–84] However, a second C_s symmetric minimum, **36**, exists for all cations but the methylium ion CH_3^+.[83,84]

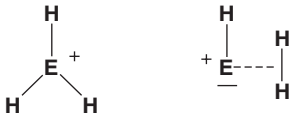

35 **36**

For silylium SiH_3^+ and germylium GeH_3^+ the strongly bonded D_{3h} structures are the global minima, but for Sn and Pb the species **36** are more stable (see Table II). The large preference of the side-on complex **36** for E = Pb by 23.3 kcal mol^{-1} is due to relativistic stabilization of the 6s lone pair in H–Pb$^+$. The EH_3^+-isomers **36** can be described as donor–acceptor complexes between dihydrogen and H–E$^+$, in which the electron density is transferred from the dihydrogen σ-bond to the LUMO of the H–E$^+$ fragment.[83,84] Although the D_{3h} isomers, **35**, of SnH_3^+ and PbH_3^+ are metastable, all D_{3h} EH_3^+ forms should be observable due to the high barriers, which separate **35** from **36** (see Table II). In contrast, the side-on complexes **36** are far less stable toward dissociation into dihydrogen and H–E$^+$. The dissociation energy D_0 for this process is

TABLE II
CALCULATED RELATIVE ENERGIES OF EH_3^+ ISOMERS IN KCAL MOL^{-1} (CALCULATED AT B3LYP/6-311++G(2d,p)(H, C, Si, Ge) SDD (TZ+2p) (Sn, Pb)[83])

Element	E(**35**)	E(**36**)	E(TS(**35**→**36**))	D_0(**36**)
Si	0	27.1	57.8	7.6
Ge	0	10.0	51.3	6.3
Sn	0	–5.2	52.9	2.9
Pb	0	–23.3	54.9	1.1

even for the most strongly bonded complex H_2/SiH^+ merely 7.6 kcal mol^{-1}, this suggests a fast decomposition of the species **36** at elevated temperatures (see Table II).[83]

There is no general theoretical study for trialkyl-substituted cations R_3E^+, which investigates the relationship of the classical planar trigonal structure to isomeric complexes RE^+/R_2 and its relative energy compared to the dissociation products, the singly coordinated four-valence-electron species $R–E^+$ and the hydrocarbon R_2. The only exceptions are 7-norbornadienyl cations **37** for which the germyl and silyl cation has been intensively studied theoretically by Radom and Nicolaides.[85–87] It has been predicted that both cations are unstable toward a facile isomerization to a more stable complex HE^+/C_6H_6, **38**. For the silyl species this was confirmed by fourier transform ion cyclotron resonance (FT-ICR) experiments, which demonstrated that indeed HSi^+/C_6H_6 is formed and not the isomeric trivalent 7-silanorbornadienylium.[88] Similarly, it was shown by our group that the 2,3-benzoannelated 7-silanorbornadienylium **39** undergoes, at ambient temperature in nonpolar solvents, a fast isomerization to the complex $PhSi^+$/tetraphenylnaphthalene (TPN), **40**, which decomposes yielding TPN as the only detectable product.[89]

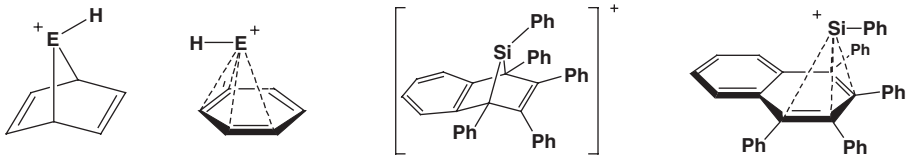

E = Si, Ge

37 **38** **39** **40**

The recent isolation and structural characterization of the toluene complex of the monovalent lead cation **41**[90] in the form of its $[MeB(C_6F_5)_3]^-$ salt is likely to trigger further theoretical work on the intriguing relationship between classical trivalent planar ER_3^+ cations and the monovalent four-valence-electron species ER^+.

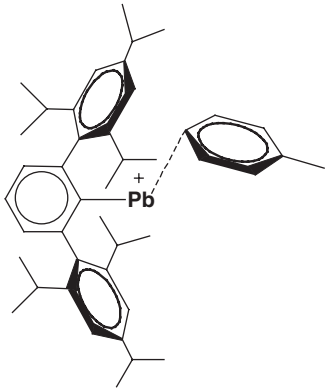

41

2. Thermodynamic Stability of R_3E^+ Cations

The relative thermodynamic stability of R_3E^+ cations as a function of the central element is evaluated by the isodesmic reaction shown in Eq. (3). It increases

TABLE III
STABILIZATION ENERGIES ΔE (KCAL MOL^{-1}) OF R_3E^+, CALCULATED ACCORDING TO ISODESMIC REACTION SHOWN IN EQS. (3) AND (4)

		ΔE, R =							
E	Eq.	H[a]	Me[b]	Ph[c]	SiH_3[d]	F[a]	Cl[a]	Br[a]	I[a]
C	(3)	0.0	0.0	0.0	0.0	0.0	0.0	0.0	0.0
Si	(3)	−58.9	−12.0	2.7	−32.9	−9.1	−9.7	−13.8	−18.4
Ge	(3)	−70.7	−20.6	−2.5	−43.1	−6.1	−9.6	−15.7	−22.4
Sn	(3)	−87.5	−25.6	−3.8	−51.9	−20.8	−15.8	−21.1	−27.4
Pb	(3)	−97.6	−35.2	−10.5	−63.5	−22.1	−19.2	−25.9	−33.6
C	(4)	0.0	−74.8	−111.3	−49.8	−18.8	−42.9	−54.7	−63.1
Si	(4)	0.0	−40.6	−64.5	−26.7	34.9	3.6	−11.5	−25.5
Ge	(4)	0.0	−37.3	−57.4	−28.5	50.8	17.8	0.7	−15.4
Sn	(4)	0.0	−29.9	−45.6	−23.6	50.5	27.1	10.8	−5.1
Pb	(4)	0.0	−29.7	−42.2	−24.9	58.5	35.2	17.6	0.4

[a]From Ref. 93, calculated at MP2/VDZ+P , quasirelativistic ecp for Si, Ge, Sn, Pb, Cl, Br, I.
[b]From Ref. 40, calculated at B3LYP/6-311G(2d,p), SDD for Si, Ge, Sn, Pb // B3LYP/6-31G(d) SDD for Si, Ge, Sn, Pb.
[c]Ref. 92, calculated at B3LYP/6-311G(2d,p), SDD for Si, Ge, Sn, Pb // B3LYP/6-31G(d) SDD for Si, Ge, Sn, Pb.
[d]Ref. 92, calculated at B3LYP/6-31G(d), SDD for Si, Ge, Sn, Pb.

monotonically along the series $R_3C^+ \rightarrow R_3Pb^+$ for most of the substituent listed in Table III, with the exception of the strongly π-donating substituents phenyl, fluorine and chlorine. The increase is most significant for the parent compounds with the plumbylium ion PbH_3^+ being more stable than methylium CH_3^+ by 97.6 kcal mol^{-1}. This marked growth of the thermodynamic stability along the series C→Pb is to be expected on the basis of the known atomic properties of the group 14 elements: the Mulliken electronegativity of the element decreases and the polarizability of the element atom increases steadily for the heavier elements of group 14.[91] The increase of the thermodynamic stability is, however, attenuated for substituted ions. While the electropositive silyl substituent stabilizes the heavier analogues of the trissilyl carbenium ion ($(H_3Si)_3C^+$) still considerably, i.e. the silylium ion ($(H_3Si)_3Si^+$) is more stable than ($(H_3Si)_3C^+$) by −32.9 kcal mol^{-1} and the plumbylium ion ($(H_3Si)_3Pb^+$) by −63.5 kcal mol^{-1}. The effect is, however, markedly smaller for alkyl substituents.[92] In the case of the trimethyl element cations, the plumbylium ion, Me_3Pb^+, is by only 35.2 kcal mol^{-1} more stable than *t*-butyl cation and it diminishes further for the practically very important phenyl substituent. As a consequence Eq. (3) is actually predicted to be slightly endothermic for E = Si, i.e. triphenylsilylium, Ph_3Si^+, is less stable than trityl cation, Ph_3C^+, by 2.7 kcal mol^{-1}. The higher homologues of Ph_3Si^+ are, however, slightly more stable than trityl cation with the plumbylium ion, Ph_3Pb^+, being the most stable cation in this series.[92] For fluorine and chlorine the calculated trend of the thermodynamic stabilization is not so clear, the stabilization of the germylium ions GeF_3^+ and $GeCl_3^+$ being smaller than that of the corresponding silylium ions.[93,94]

$$R_3EH + R_3C^+ \rightarrow R_3E^+ + R_3CH \quad (3)$$

$$R_3EH + H_3E^+ \rightarrow R_3E^+ + EH_4 \quad (4)$$

The substituent effect on the thermodynamic stability of R_3E^+ ion is given by the isodesmic reaction shown in Eq. (4). Carbenium ions are stabilized by each substituent listed in Table III, even by the strongly electronegative fluorine and the effect of many substituents is large, i.e. *t*-butyl cation is more stable than methylium by 74.8 kcal mol^{-1}. The heavier analogues of *t*-butyl cation are also considerably more stable than the hydrogen-substituted cation EH_3^+, the substituent effect is, however, considerably smaller than in the carbon case, i.e. Me_3Si^+ is stabilized by 40.6 kcal mol^{-1} and the plumbylium ion by only 29.7 kcal mol^{-1}.

Similarly, the experimentally important substituents phenyl and silyl are significantly less efficient in stabilizing a silylium or plumbylium ion than a carbenium ion. For example, the stabilization of triphenylsilylium Ph_3Si^+ calculated by using the isodesmic equation (4) is only roughly 58% of that predicted for the trityl cation and it decreases to 38% for the plumbylium ion Ph_3Pb^+. In contrast to the carbon case, plumbylium ions are in general destabilized by halogen substitution, the destabilization increasing with the electronegativity of the halogen atom.[93,94] For a given halogen, there is a constant decrease in their destabilizing effect as E becomes lighter. In consequence, silylium ions are only destabilized by substitution with the most electronegative halogens fluorine and chlorine, while $SiBr_3^+$ and SiI_3^+ are actually more stable than SiH_3^+.[94,95]

The most significant conclusion that can be drawn from the data summarized in Table III is that substituent effects do not exert the same overwhelming importance for the thermodynamic stability of the higher homologues of carbenium ions, thus they do not play the dominant role as in carbocation chemistry. This can be traced back on (i) the inherent higher stability of the trivalent cations of the elements Si→Pb and (ii) the weakness of the stabilizing interaction (in many cases of π-type) of the most common substituents with the central element atom.

One interesting exception is the cyclopentadienyl (Cp) substituent. Density functional calculations at the B3LYP/6-311G(2d,p)//B3LYP/6-31G(d) + ΔZPVE level of theory indicated that the Cp (and likewise the pentamethylcyclopentadienyl (Cp*) substituent) is clearly more efficient in stabilizing a silylium or germylium than a carbenium ion.[77,92] Thus, the isodesmic reaction shown in Eq. (5) is exothermic by −13.8, −18.7 and −25.3 kcal mol^{-1} for E = C, Si, and Ge, respectively. This unusual large substituent effect is explained by the particular bonding situation in the cations **42**–**44**, which is dominated by π-donation to the electron-deficient element atom, which is more efficient for the silylium **43** and in particular for the germylium ion **44**.[77,92]

$$Cp_2EH_2 + Me_3E^+ \rightarrow Cp_2EH^+ + Me_3EH$$

42, E = C

43, E = Si

44, E = Ge (5)

TABLE IV
CALCULATED INTERACTION ENERGIES ΔE_A BETWEEN R_3E^+ CATIONS AND ELECTRON DONORS D[a]

E	C	Si	Ge	Sn	Pb
D = H_2O[a,b]					
R = H	−71.3	−54.7	−44.5	−38.9	−31.4
D = toluene[a,c]					
R = H	−85.1	−53.9	−47.6	−40.3	−44.2
R = Me	−17.8	−28.9	−26.2	−25.7	−30.5
D = RHC=CHR[d,e]					
R = Me	–	−19.5	−17.4	−17.0	−12.5

[a]Calculated as the energy difference between the total energy of the donor acceptor complex $R_3E^+ \leftarrow D$ and the sum of the total energy of D and R_3E^+.
[b]At MP2/VTZ + D + P. Quasi-relativistic pseudopotentials were used for Si, Ge, Sn, Pb, from Ref. 93.
[c]At MP2/CEP. Compact effective core potentials (CEPs) were used for C and Si. Their relativistic counterparts (RCEP) were used for Ge, Sn and Pb. Correction for basis set superposition errors is included, from Ref. 95.
[d]Intramolecular interaction energy calculated for the element norbornyl cations, see Ref. 40.
[e]At B3LYP/6-311G(2d,p), pseudo-relativistic effective core potential and a (31/31/1) valence basis set were used for Si, Ge, Sn, Pb, from Ref. 40.

This particular substituent effect of the Cp ring on the thermodynamic stability gives a rationalization for the exceptionally high stability of protonated decamethyl silicocene **29**, studied by Jutzi and Bunte.[76]

The continuous growth of the thermodynamic stability of the EH_3^+ cations along the series C → Pb is also reflected in the calculated trend of the interaction energies ΔE_A of the EH_3^+ ions with a Lewis base like H_2O (see Table IV).[93] The interaction energy ΔE_A changes from $-71.3\,kcal\,mol^{-1}$ for methylium, H_3C^+, to $-31.4\,kcal\,mol^{-1}$ for plumbylium, H_3Pb^+. A similar trend is computed for the interaction of EH_3^+ ions with the π-electron donating toluene, i.e. the interaction energy for CH_3^+ with toluene is $-85.1\,kcal\,mol^{-1}$, while for silylium H_3Si^+ a significant smaller stabilization energy of $-53.1\,kcal\,mol^{-1}$ is predicted (see Table IV).[95] The trend is reversed for the trimethyl-substituted ions. That is, trimethyl silylium binds much more strongly to toluene than *t*-butyl cation ($-28.9\,kcal\,mol^{-1}$ for Me_3Si^+ compared to $-17.8\,kcal\,mol^{-1}$ for Me_3C^+). This opposite trend in the complexation energies upon substitution at the element reflects a smaller stabilizing interaction between the methyl substituents in Me_3Si^+ compared to Me_3C^+ (see also Table III).[94,95] In the case of the heavier analogues of the norbornyl cations the interaction energy between the remote C=C double bond and the electron-deficient element center decreases steadily from Si → Pb. This indicates less need for additional stabilization in the case of the plumbanorbornyl cation and also suggests that the electrophilicity of the R_3E^+ ions decreases for E = Si → Pb.[40]

B. *NMR Spectroscopic Properties of R_3E^+ Cations*

NMR spectroscopy has, in the last 20 years, become one of the most important analytical tools in the search for R_3E^+ ions in the condensed phases. With only the

exception of germanium, every group 14 element has at least one nucleus of spin 1/2, which is suitable for NMR studies using standard one- and two-dimensional Fourier Transform (FT) NMR techniques. Furthermore, there is a relation between the coordination number of the group 14 element and the NMR chemical shift. The low-frequency limit is defined by compounds with the element in high coordination states. The increasing imbalance of the electron distribution in lower coordination states of the element results in a deshielding of the atom in question. Therefore, cationic species with the charge largely located on the element atom should give a distinctive chemical shift, deshielded with respect to related four-coordinate species, which will allow a straightforward identification of the cationic species and an evaluation of the degree of ionic character indicated by a particular chemical shift. In addition, at least for silicon, reliable NMR chemical shift calculations strongly support the identification and characterization of the cationic species. Therefore, apart from X-ray diffraction, the best criterion for the R_3E^+ species (E = C, Si, Sn, Pb) is the NMR chemical shift of the central element.

1. ^{29}Si NMR Spectroscopic Data of Silylium Ions and Related Species

The presently known silicon chemical shift range is 990 ppm. This includes the D_{5d} form of decamethylsilicocene **28** ($\delta^{29}Si = -423$ (solid state)),[96] which is the most shielded resonance reported to date and the alkyl-substituted silylene **45**, which presently defines the high-frequency end of the spectrum at $\delta^{29}Si = 567$.[97] Most silicon chemical shifts occur, however, in a much smaller range from $\delta^{29}Si = +50$ to -190. This includes hexa-, penta- and tetracoordinated silicon compounds and for trivalent, positively charged silicon a significant low-field shift compared to comparable tetravalent silicon species is expected.

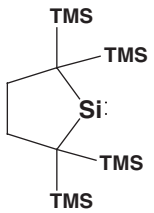

45

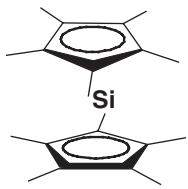

28

a. Si NMR Chemical Shift Calculation for Silylium Ions and Related Species

Early estimates for the ^{29}Si NMR chemical shift of silylium ions were based on an empirical correlation between ^{13}C NMR and ^{29}Si NMR chemical shifts of isostructural silicon and carbon compounds, and predicted for trimethylsilylium a ^{29}Si NMR chemical shift within the range 225–275.[98]

Accurate NMR chemical shift calculations for silicon compounds are available since the early 1990's and these computations played a decisive role in the identification and characterization of silylium ions in the condensed phase. This issue has

been thoroughly reviewed by several authors[10,13,94,99] and we will concentrate here on the pure description of the magnetic properties of silylium ions. Silicon NMR chemical shift calculations for several silylium ions in the gas phase are summarized in Table V. As expected for cationic species with the positive charge mainly localized at the central silicon, all silylium ions are characterized by a distinct chemical shift, significantly deshielded compared to neutral tetravalent compounds. That is, for trialkyl-substituted silylium ions low-field shifts compared to the neutral trialkylsilyl hydride of about 400 ppm are predicted. In addition, the calculations predict also an unusually wide spectral range for the ^{29}Si NMR chemical shift of silylium ions. Silylium ions with π-donating substituents, i.e. amino and phenyl groups have relatively shielded silicon nuclei (app. $\delta^{29}Si = 220$ for Ph_3Si^+ [6] and $\delta^{29}Si = 42$ for $(Me_2N)_3Si^+$),[100] while electropositive trimethylsilyl or dimethylboryl substituents induce a tremendous low-field shift with predicted Si NMR chemical shifts of $\delta^{29}Si = 920$ ($(Me_3Si)_3Si^+$)[101] and $\delta^{29}Si = 572$ ($(Me_2B)_3Si^+$).[102] This huge substituent effect on δ^{29}Si can be easily understood on the basis of the fundamental NMR

TABLE V
CALCULATED ^{29}Si NMR CHEMICAL SHIFTS FOR SILYLIUM IONS USING DIFFERENT METHODS AND BASIS SETS

Compound	Method	δ^{29}Si vs. Me_4Si	Ref.
H_3Si^+	IGLO[a,b]	270.2	106
Me_3Si^+	IGLO[a,b]	355.9	106
	HF/GIAO[c,d]	361.6	6
	B3LYP/GIAO[c,d]	413.0	6
	MP2/GIAO[d,e]	386.2	6
	SOS/DFPT/IGLO[a,b]	382.0	38
Et_3Si^+	IGLO[d,f]	371.3	107
	HF/GIAO[a,b]	371.2	38
	SOS/DFPT/IGLO[a,b]	415.6	38
i-Pr_3Si^+	HF/GIAO[a,b]	342.3	38
	SOS/DFPT/IGLO[a,b]	371.0	38
Ph_3Si^+	HF/GIAO[c,d]	198.8	6
	B3LYP/GIAO[c,d]	205.0	6
Mes_3Si^+	HF/GIAO[c,d]	230.1	6
	B3LYP/GIAO[c,d]	243.9	6
	IGLO	228	7
$(Me_3Si)_3Si^+$	IGLO[b,f]	925.3	108
	IGLO[a,b]	920.4	101
	B3LYP/GIAO[a,d]	1029.1	100
$(Me_2N)_3Si^+$	IGLO[g,h]	42.1	100
$(Me_2B)_3Si^+$	IGLO[a,b]	571.8	102
	B3LYP/GIAO[a,d]	587.3	102

[a]Using Basis II Ref. 109.
[b]Using a HF/6-31G(d) optimized geometry.
[c]Using a 6-311 + G(2df,p) (Si), 6-31G(d) (C,H) basis set.
[d]Using a B3LYP/6-31G(d) optimized geometry.
[e]Using a tz2p (Si), dzp (C,H) basis set.
[f]Using Basis II' Ref. 109.
[g]Using Basis II + sp.
[h]Using a MP2/6-31G(d) optimized geometry.

chemical shift theory. The following discussion can be equally applied for the understanding of the substituent effects on δ^{119}Sn and δ^{207}Pb NMR chemical shifts in stannylium and plumbylium ions. In general, the NMR chemical shift of heteronuclei are dominated by the paramagnetic contributions to the NMR chemical shielding.[101,103–105] This paramagnetic term is, however, directly related to the energy difference ΔE between occupied and unoccupied molecular orbitals with non-vanishing coefficients at the nuclei of interest. The smaller the energy difference ΔE between these magnetically active orbitals the larger is the paramagnetic contribution and in consequence the stronger deshielded is the nuclei. In the case of a trivalent cation R_3E^+ the relevant orbitals are of the R–E σ-bonding type and the formally empty *n*(p) orbital (*n*: principal quantum number) at the central element, the magnetically allowed transition is a $\sigma \leftrightarrow \pi^*$ excitation. Cations R_3E^+ with electropositive substituents in general have high-lying σ-type orbitals and therefore small energy gaps ΔE to the empty *n*(p)-orbital. This results in a strongly deshielding contribution for the nuclei E. On the other hand, electronegative substituents increase ΔE and reduce the paramagnetic contribution. π-Electron-donating substituents R in cations R_3E^+ interact with the p-type orbital at the central element E. This interaction results in destabilization of the *n*(p)E orbital and in a larger energy separation ΔE to the σ-type orbitals. For those cations, R_3E^+, less deshielded nuclei *E* are to be expected. These qualitative arguments give a straightforward interpretation of the computed ^{29}Si NMR data compiled in Table V. The Si NMR chemical shift calculated for the permethylated silaguanidinium ion, $(Me_2N)_3Si^+$,[100] with strongly π-electron-donating dimethylamino substituents marks the high-field end of the expected shift region for trivalent silylium ions, while the substituent effect of the electropositive trimethylsilyl groups of the tris(trimethyl)silylium ion places its predicted Si NMR resonance in the very low-field region. Even more strongly deshielded silicon nuclei are to be expected for germyl and stannyl-substituted silylium ions.

b. Experimental ^{29}Si NMR Data for Silylium Ions and Related Species

The experimental ^{29}Si NMR data on silylium ions are very limited due to the rather small number of examples for truly tricoordinated silylium ions (see Table VI). Trismesityl silylium, **1**, was the first silylium ion to be synthesized in the condensed phase as a long-lived species and it was characterized by its low-field resonance in the ^{29}Si NMR spectra of a solution of the TPFPB salt in benzene at $\delta^{29}Si = 225$.[5] In contrast to all other silyl cationic species previously produced in solution the ^{29}Si NMR chemical shift of **1** was shown to be constant when the solvent was changed from benzene to toluene or other alkylated aromatic hydrocarbons.[4] This indicates negligible interactions between solvent and the cation, characterizing **1** as the first free silylium ion, lacking any coordination to the solvent and the counteranion. NMR chemical shift calculations predict for optimized "gas phase" structures δ^{29}Si between 226 and 230, depending on the method applied.[6,7] Solid state ^{29}Si NMR from the carboranate $[Mes_3Si][HCB_{11}Me_5Br_5]$ obtained by magic angle spinning methods gave an isotropic δ^{29}Si of 226.7.[49] This close congruence suggests that the structure of Mes_3Si^+, **1,** is the same in all phases. The

TABLE VI
^{29}Si NMR CHEMICAL SHIFTS FOR CATIONIC SILICON SPECIES AND RELATED COMPOUNDS

Compound	Solvent	δ^{29}Si vs. Me_4Si	Ref.
1/TPFPB$^-$	C_6D_6	225.5	4, 5
	C_6D_6/C_7H_8 (1/3)	225.7	4, 5
	C_6D_6/*p*-$(D_3C)_2C_6D_4$ (1/1)	225.6	4, 5
	C_6D_6/CH_3CN (1/3)	37.0	4, 5
	C_6D_6/Et_3N (1/1)	47.1	4, 5
1/$HCB_{11}Me_5Br_6^-$	Solid state	226.7	49
46/TPFPB$^-$	C_6D_6	226.8	47
25/TPFPB$^-$	CD_2Cl_2	303.0	73
Me_3Si^+/TPFPB$^-$	C_6D_6	83.6	37
	Solid state	84.8	37
Me_3SiOTf	CD_2Cl_2	43.7	113
$Me_3SiOClO_3$	CD_2Cl_2	46.6	113
Et_3Si^+/TPFPB$^-$	C_6D_6	92.3	37
	C_7D_8	81.8	37
	CD_3CN	36.7	37
	Sulfolane	58.4	37
	Solid state	94.3	37
$Et_3Si^+/[CB_{11}H_6Br_6]^-$	Solid state	111.8/106.2[a]	114
Et_3Si^+/TFPB$^-$	*n*-PrCN	37.0	115
i-Pr_3Si^+/TPFPB$^-$	C_6D_6	107.5	37
	Solid state	107.6	37
i-Bu_3Si^+/TPFPB$^-$	C_6D_6	99.5	37
	Solid state	89.4	37
Me*i*-Pr_2Si^+/TPFPB$^-$	C_6D_6	96.9	37
$Hexyl_3Si^+$/TPFPB$^-$	C_6D_6	90.3	37
$MePh_2Si^+$/TPFPB$^-$	C_6D_6	73.6	37
$(Me_3Si)_3Si^+$/TPFPB$^-$	C_6D_6	111.1	37
55/TPFPB$^-$	C_6D_6	87.2	40
	C_7D_8	87.5	40
	CD_3CN	31.8	40
56/TPFPB$^-$	C_6D_6	82.7	40
57/TPFPB$^-$	C_6D_6	80.2	40
t-Bu_3Si^+/TFPB$^-$	CD_3CN	29.9	67
[*t*-$Bu_3SiOH_2^+$]/$CB_{11}H_6Br_6^-$	Solid state	46.7	116
[(*t*-$Bu_2MeSi)_3SiBu$-t_2]$^+$/TPFPB$^-$	CD_2Cl_2	315.7; 77.3	8
29/$[C_{12}H_{11}O_4]^-$	C_6D_6	−12.1	76
7/TPFPB$^-$	CD_2Cl_2	142.9	33
$(Me_2N)_3Si^+$/TPFPB$^-$	C_6D_6	−30.8	117
	CD_2Cl_2	−39.3	117

[a]Two independent molecules in the unit cell.

determination of the ^{29}Si NMR chemical shift tensor of Mes_3Si^+ provides further important information on the symmetry and electronic situation around the silicon nucleus in **1** (see Table VII).[49] The axially symmetric tensor ($\eta = 0$) is in agreement with a three-fold rotational axis in **1**. The equivalent and strongly deshielded tensor components δ_{11} and δ_{22} lie in the molecular plane and the more shielded δ_{33} component is oriented along the molecular C_3 axis (see Figure 1).

TABLE VII
^{29}Si NMR CHEMICAL SHIFT TENSOR COMPONENTS FOR $Mes_3Si^+/HCB_{11}Me_5Br_6^-$ [49] AND CALCULATED TENSOR COMPONENTS FOR Mes_3Si^+, **1**.[111] THE ORIENTATION OF THE EIGENVECTORS RELATIVE TO THE MOLECULAR FRAME IS GIVEN IN FIG. 1

	Experimental	Theoretical[a]
δ_{11}	319.5	317.6
δ_{22}	319.5	317.6
δ_{33}	41.2	55.3
δ_{iso}	226.7	230.1

[a]At HF/GIAO/Si(6-311 + G(2df,p)//B3LYP/6-31G(d), Ref. 111.

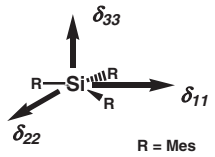

FIG. 1. Orientation of the chemical shift tensor components in trimesityl silylium ion **1**.

The spread of the NMR chemical shift tensor $\Delta\delta$ ($\Delta\delta = \delta_{11} - \delta_{33}$) is 278 ppm, much larger than reported for tetracoordinated silicon compounds ($\Delta\delta = 0-60$)[110]. According to density functional NMR calculations the strong deshielding of the in-plane components δ_{11} and δ_{22} are mainly the result of paramagnetic currents induced by the magnetic field that interrelates the σ-bonding molecular orbitals and the 3(p) Si-type orbital. These currents are very efficient, due the relative small energy gap ΔE between these orbitals in silylium ions.[111]

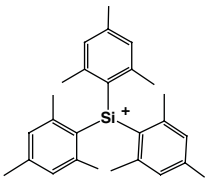

1

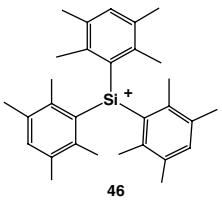

46

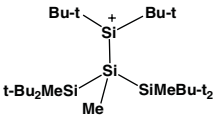

25

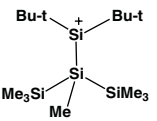

47

There are two other candidates for "free" silylium ions in the condensed phase, the duryl-substituted cation **46**[47] and the silylium ion **25**, which is substituted by two *t*-butyl groups and a bulky silyl group.[73] The situation is clear for the duryl-substituted cation **46**: the ^{29}Si NMR chemical shift of 226.8, very close to that of Mes_3Si^+ and a similar solvent independence of δ^{29}Si strongly suggest that **46** is another example for a silylium ion in the condensed phase.[47] Although for the cation **25** an even more deshielded ^{29}Si NMR resonance is reported ($\delta^{29}Si = 303$),[73] from the theoretical data summarized in Table V, a ^{29}Si resonance at markedly

lower field is expected for silylium ions with the same substitution pattern as **25**. In agreement, silicon NMR chemical shift calculations for **47**,[112] a suitable model for the experimentally investigated silyl cation **25**, predict a ^{29}Si NMR chemical shift of $\delta^{29}Si = 530$, more than 200 ppm to lower field than the signal assigned to the free silylium cation **25**. Thus, some doubts concerning the nature of the observed species in CD_2Cl_2 are warranted.

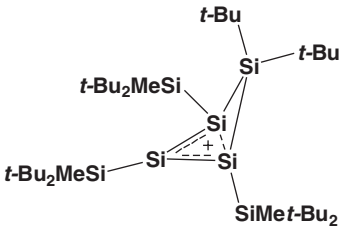

3

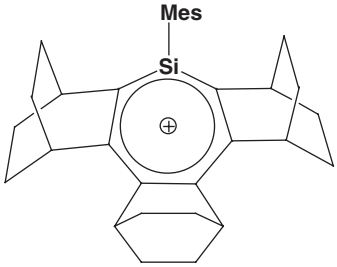

7

Silyl cations like **3** and **7** in which the positively charged silicon is part of a π-conjugated system attracted particular interest. The marginally stable silatropylium ion **7**, is characterized by a ^{29}Si NMR resonance at $\delta^{29}Si = 149$ in CD_2Cl_2 at −50 °C, downfield-shifted by 192 ppm compared to the precursor silane.[33,34] This experimental value is in fair agreement with the calculated silicon NMR chemical shift for the optimized "gas phase" structure of **7** ($\delta^{29}Si = 159.9$, at GIAO/HF/6-311 + G(2df,p)(Si), 6-31G(d) (C,H)).[34] This indicates only small interactions between the cation and dichloromethane, the solvent used for the NMR investigations.[33,34] The reported ^{29}Si NMR data for silyl cation **3** demonstrate its homoaromatic character and characterize **3** as a free silyl cation in solution.[8] The four-membered ring in **3** is identified by three ^{29}Si NMR signals: $\delta^{29}Si = 77.3$ (Si^1, Si^3), 315.7 (Si^2) and 34.3 (Si^2). Remarkably, the most deshielded silicon atom in **3** is the central tricoordinated silicon. This is in agreement with some homoaromatic nature of the cation **3** with charge localization at Si^2 (see Fig. 2a) and it discards the possibility of a classical

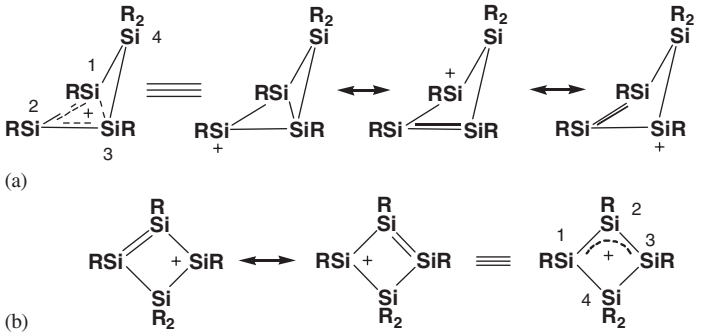

FIG. 2. (a) Homoaromatic conjugation in homocyclotrisilenylium cation **3**. (b) Allylic-type conjugation in a planar tetrasilacyclobutenyl cation.

TABLE VIII
NMR SPECTROSCOPIC DATA FOR SILYL CATIONS HAVING Si–X–Si THREE-CENTER BOND

Compound	X	δ^{29}Si	δX	^{1}J(SiX)	Ref.
48	F	90.6	–	229.2	118
54	F	77.2	−144.2	243.0	119
49	Cl	90.2	–		118
50	Br	90.8	–		118
51	H	99.1	–	26.0	118
52	H	76.7	1.47	39.0	121
53	H	54.4	3.34	45.7	119

allyl-type conjugation in **3**. For a hypothetical trisilaallyl cation the canonical structures imply charge localization at the terminal silicon atoms and therefore strongly deshielded effects for these atoms can be expected (see Fig. 2b). The reported chemical shifts are independent of solvent (dichloromethane, benzene and toluene) implying the lack of any covalent interaction with solvent molecules.[8]

Intramolecular interaction of the positively charged silicon with any remote substituent leads to considerable shielding of the silicon atom. This shielding parallels the extension of the coordination number of silicon from the tricoordinated silylium ion to some intermediate 3 + 1 coordination and, finally, to the regular tetracoordination of neutral silicon(IV) species. Thus, silyl cations stabilized by Si–X–Si three-center bonding with X-groups having lone pair electrons, as for example the halonium ions **48**–**50**, **54** are characterized by ^{29}Si NMR chemical shifts for the positively charged silicon atom between 91 and 77 (see Table VIII).[118,119] The large ^{1}J(SiF) coupling constant found for the fluoronium ions **48** and **54** are in the typical range for the sp^3 silicon–fluorine linkage indicating for the cations **48** and **54** only small silylium ion character.[120]

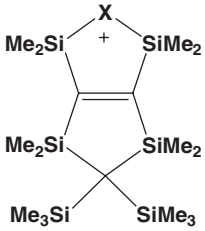

X = F , **48**
X = Cl, **49**
X = Br, **50**
X = H, **51**

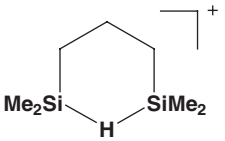

52

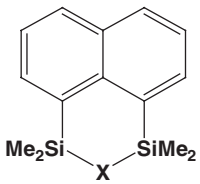

X = H , **53**
X = F, **54**

The situation is different for the silyl cations **51**–**53** having a Si–H–Si 2e-3c-bond.[118,119,121] The ^{29}Si NMR chemical shift of the cationic silicon depends strongly on the system (δ^{29}Si = 99.1, 76.7, 54.4, for **51**, **52**, **53**, respectively) and the ^{1}J(SiH) coupling constant in these cations (^{1}J(SiH) = 26, 39, 46 Hz for **51**, **52**, **53**, respectively) is markedly reduced compared to regular ^{1}J(SiH) coupling constants in

neutral silanes (^{1}J(SiH)~180–200 Hz in R_3SiH).[122] In addition, the central hydrogen of the SiHSi bridge is shielded compared to the precursor silanes. A theoretical analysis of the bonding situation for the silyl cations **52** and **53** suggests that the SiHSi three-center bond results from interaction of orbitals of mostly 3p-character at the silicon atoms with the s-orbital at the hydrogen atom. Due to the mostly complete p-nature of the SiHSi binding orbital at the silicon atoms, the important Fermi contact contribution to the J-coupling is rather small. This explains the very small ^{1}J(SiH) coupling constant in the hydrogen-bridged ions **51**–**53** and suggests that the silylium ion character in these cations is larger than in related halonium ions.[119]

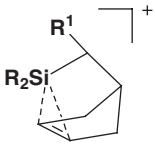

55: R = Me, R^1 = H
56: R = Et, R^1 = H
57: R = n-Bu, R^1 = H
58: R = Me, R^1= C_5H_{11}

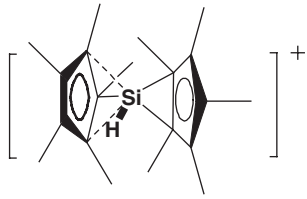

29

The silanorbornyl cations **55**–**58** in which the silicon adopts a formal [3 + 1] coordination, with the extra coordination side occupied by a C═C double bond are characterized by a ^{29}Si resonance between $\delta^{29}Si = 87-80$. The intramolecular interaction between the C═C double bond and the positively charged silicon atom is shown by an appreciable downfield shift of the vinylic carbon atoms by $\Delta\delta^{13}C = 20$ compared to the precursor silanes.[40,123] A quite unusual shielded resonance for a formally three coordinated silyl cation at $\delta^{29}Si = -12.1$ was found for the protonated decamethylsilicocene **29**.[76] The chemical shift reported for **29** is solvent independent, i.e. in benzene the same silicon NMR chemical shift is reported as in THF solution. This high-field resonance clearly mirrors the particular bonding situation in silyl cation **29**. According to a recent computational study silyl cation **29** is a highly fluxional molecule and in the predominant isomer the two Cp* substituents are bonded in an $\eta^2 : \eta^3$-fashion to the positively charged silicon atom.[77]

Silylium ions, which are not protected sterically or are not stabilized either electronically or by intramolecular interaction with a remote substituent do interact strongly with the solvent and/or the counteranion. The reaction of the transient silylium ion with solvents like ethers, nitriles and even aromatic hydrocarbons lead to oxonium, nitrilium and arenium ions with a tetrahedral environment for the silicon atom. These new cationic species can be clearly identified by their characteristic ^{29}Si NMR chemical shifts. That is, the oxonium salt $[Me_3SiOEt_2]^+$ $TFPB^-$ is characterized by $\delta^{29}Si = 66.9$ in CD_2Cl_2 solution at $-70\,^\circ C$.[124] Similar chemical shifts are found for related silylated oxonium ions.[55,116,125,126] Nitrilium ions formed by the reaction of intermediate trialkyl silylium ions with nitriles are identified by Si NMR chemical shifts $\delta^{29}Si = 30-40$[115,127,128–130] (see also Table VI for some examples). Trialkyl-substituted silylium ions generated in benzene solution yield silylated benzenium ions, which can be easily detected by a silicon NMR resonance at $\delta^{29}Si = 90-100$ (see Table VI).[35,36,113,108,131–137] Silyl-substitution

increases the ^{29}Si NMR chemical shift (δ^{29}Si ($[(Me_3Si)_3SiC_6H_6]^+$) = 111), while aryl substitution give smaller δ^{29}Si (δ^{29}Si ($[MePh_2SiC_6H_6]^+$) = 73.6). Therefore, the substituent effects on ^{29}Si NMR chemical shift in silylated arenium ions follows the same pattern as predicted for the free silylium ions (see Table V), however to a less spectacular extent. In general, for toluenium ions ^{29}Si NMR chemical shifts are measured which are by 10 ppm more shielded (see Table VI). More electron-rich arene solvents give an even more shielded ^{29}Si resonance for the silylated arenium ion. That is, the ^{29}Si resonance of the mesitylenium ion $[(cy)_3Si(C_6H_3Me_3)]^+$ ($\delta^{29}Si = 65$), is shifted by 25 ppm to higher field compared to the benzenium ion $[(Cy)_3Si(C_6H_6)]^+$ ($\delta^{29}Si = 90.3$).[37]

The data for *i*-pr_3Si^+ salts, summarized in Table IX, clearly show the influence of the counteranion on the ^{29}Si NMR chemical shift of silyl cationic species. The measured ^{29}Si NMR chemical shift for all *i*-pr_3Si^+ salts deviate considerably from the calculated value ($\delta^{29}Si = 375$, see Table V) being high field shifted by more than 250 ppm. In the absence of solvent/cation interactions, this is a clear indication for ion-pairing in solution and in the solid state. This is further supported by the solid state structure of several trialkylsilylium species with halogenated carborane anions, which show clear indications for interaction between the positively charged silicon center and one of the halogen atoms in the periphery of the carborane anion.[38,114,138] On the other hand, the ^{29}Si NMR chemical shift of the *i*-pr_3Si^+ salts clearly depends on the coordination ability of the counteranion. Therefore, the downfield shift of the ^{29}Si NMR chemical signal of the *i*-pr_3Si^+ X^- species allows a qualitative ranking of WCA^- toward main group Lewis acids.[139,140] By this

TABLE IX
^{29}Si NMR CHEMICAL SHIFTS FOR *i*-Pr_3Si^+/Y^- SALTS AND RELATED SPECIES

Compound	Conditions	δ^{29}Si vs. Me_4Si	Ref.
i-Pr_3SiH	C_7D_8	12	127
i-$Pr_3Si^+/(C_5(CN)_5)^-$	C_7D_8	40	142
i-$Pr_3SiOSO_2CF_3$	C_7D_8	40	143
i-$Pr_3Si(NSO_2CF_3)_2$	C_7D_8	53	144
i-$Pr_3Si^+(AlBr_4)^-$	C_7D_8	56	143
i-Pr_3Si^+(1-H-$CB_{11}H_5I_6)^-$	Solid state	97	143
i-Pr_3Si^+(1-H-$CB_{11}H_5Br_6)^-$	C_6D_6	100	139
	C_7D_8	105	138
	Solid state	110	143
i-Pr_3Si^+(1-H-$CB_{11}H_5Cl_6)^-$	C_6D_6	103	139
	Solid state	115	143
i-Pr_3Si^+(1-H-$CB_{11}Me_5Br_6)^-$	C_6D_6	112	139
i-Pr_3Si^+(1-H-$CB_{11}Me_5Cl_6)^-$	C_6D_6	113	139
i-Pr_3Si^+(1-H-$CB_{11}Cl_5Br_6)^-$	C_6D_6	111	145
i-Pr_3Si^+(1-H-$CB_{11}Br_5Cl_6)^-$	C_6D_6	116	145
i-Pr_3Si^+(1-H-$CB_{11}Cl_{11})^-$	C_6D_6	114	145
i-Pr_3Si^+(1-Me-$CB_{11}F_{11})^-$	C_7D_8	120	141
i-Pr_3Si^+ $TPFPB^-$	C_6D_6	108	37
	C_7D_8	94	127
	Solid state	108	37

criterion, the perfluorinated carborane anion $[1\text{-}MeCB_{11}F_{11}]^-$ is the least coordinating anion, since the salt $[i\text{-}pr_3Si][1\text{-}MeCB_{11}F_{11}]$ has the most deshielded ^{29}Si NMR signal ($\delta^{29}Si = 120$).[141] With anions which have a basicity comparable to that of the arene solvent, competition between solvation and ion-pairing must be considered. For example, according to the ^{29}Si chemical shift criteria in the solid state the interactions between the $TPFPB^-$ anion and the silylium species is stronger than in the case of the chlorinated carborane $[1\text{-}H\text{-}CB_{11}H_5Cl_6]^-$, i.e. the ^{29}Si solid state NMR signal of $[i\text{-}pr_3Si][1\text{-}H\text{-}CB_{11}H_5Cl_6]$ ($\delta^{29}Si = 115$) is at higher frequency than $[i\text{-}pr_3Si][TPFPB]$ ($\delta^{29}Si = 108$, see Table IX). In solution, however the equilibrium shown in Eq. (6) is shifted toward the silylated benzenium ion.[36,37] In the case of the carborane, the ion-pairing prevails also in solution, probably due to the less favored solvation of the anion.[114,140]

$$[R_3Si^+\ X^-] + C_6H_6 \rightarrow [R_3SiC_6H_6]^+ + X^- \qquad (6)$$

c. ^{29}Si NMR Data for Silyl-Substituted Germylium and Stannylium Ions

^{29}Si NMR chemical shifts for several silyl-substituted germylium and stannylium ions were reported. Interestingly, in the case of cyclotrigermylium ions **2** ^{29}Si NMR signals of the α-silicon atom at relatively high frequencies have been found ($\delta^{29}Si = 62-64$).[9,64–66] This is a considerable downfield shift relative to the precursor cyclotrigermene **20** (E = Si) ($\delta^{29}Si = 37.2$ and 50.1). The bishomoaromatic germyl cation **59** is characterized and identified by the two low-field ^{29}Si NMR signals for the SiBu-t_3 groups in the α-position ($\delta^{29}Si = 56.1$ and 67.2).[21] Similarly, for the trissilyl-substituted germylium and stannylium ions **22**, **23** ^{29}Si NMR resonances at $\delta^{29}Si = 50$ and $\delta^{29}Si = 64.9$ were found.[71,72] In the case of the germylium ion, this is about 25 ppm to lower field than in the corresponding germanes ($t\text{-}Bu_2MeSi)_3GeH$.[72] For the germyl cations, this deshielding effect on the silicon atom was rationalized by a significant charge transfer from the positively charged germanium to the more electropositive α-silicon atom.[66,72] It is questionable, however, if arguments based on simple charge delocalization can explain the deshielding effect in the stannylium ion **23**.[71] The influence of energetically high-lying Si–Ge or Si–Sn σ-bonding molecular orbitals on the ^{29}Si NMR chemical shift in the silyl-substituted germyl and stannyl cations should also be taken into account.

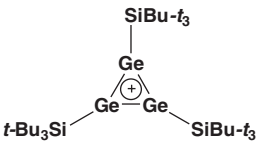

2

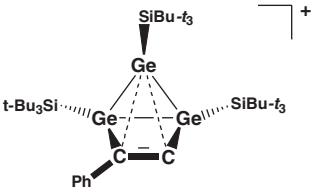

59

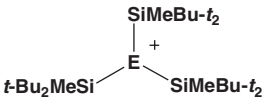

22 : E = Ge
23 : E = Sn

2. ^{119}Sn NMR Spectroscopic Data of Stannylium Ions and Related Species

Sn NMR chemical shifts in organotin compounds cover a range of about 5200 ppm, the current extremes being +2966 ppm in the divalent stannylene

(2,6-$Mes_2C_6H_3$)(GeBu-t_3)Sn:[146] and −2338 ppm in the hypercoordinated (1,3-di(*t*-Bu)C_5H_3)Sn^+ cation.[147] Most tetravalent organotin compounds can be found in a chemical shift range between −200 and +200 ppm and divalent stannylenes are characterized by ^{119}Sn NMR chemical shifts larger than 2000 ppm. These values are the brackets for a rough estimate of ^{119}Sn NMR chemical shift of tricoordinated stannylium ions.

a. Sn NMR Chemical Shift Calculations for Stannylium Ions and Related Species

A number of terms complicate the accurate calculation of Sn NMR chemical shifts, not least the possible importance of spin–orbit coupling and relativistic effects and Sn NMR chemical shift calculations became only feasible quite recently.[48,105,148] Therefore, the early estimates for the ^{119}Sn NMR chemical shift for a trivalent stannylium ion came from empirical correlations between ^{29}Si and ^{119}Sn NMR chemical shift,[46] which has been shown to be a valuable tool for estimating the NMR chemical shifts of structurally related tetravalent silicon and tin compounds.[149,150] Based on these correlations, the ^{119}Sn NMR chemical shift of a trialkylstannylium ion was expected to be around 1770, and for triaryl-substituted cations values around 1250 were predicted.[46] Already early IGLO (individual guage for localized orbitals) calculations of the Sn NMR chemical shift[151] indicated that the empirical correlation between ^{29}Si and ^{119}Sn NMR chemical shift overestimates the deshielding of the tin atom in stannylium ions. That is, for H_3Sn^+ $\delta^{119}Sn = 777$ is calculated and on the basis of methyl increments, the Sn NMR chemical shift for Me_3Sn^+ was estimated to be about 1075,[151] at 700 ppm to higher field of that predicted from the empirical correlation. More recent calculations of ^{119}Sn NMR chemical shift for stannyl cations support this view.[48,105] Computed Sn NMR chemical shifts of various stannylium ions and related species are summarized in Table X. The most striking fact arising from these calculations is the wide spread of the expected ^{119}Sn NMR chemical shift for stannylium ions. That is, for the trisilyl-substituted cation values between $\delta^{119}Sn = 2440$ and 2880 are predicted, depending on the applied method. This is more than 1800 ppm to lower field of that calculated for stannylium ion H_3Sn^+. As already discussed for silylium ions (Section III.B.1.a), this strong deshielding in the silyl-substituted cations is a result from very large paramagnetic (deshielding) contributions to the NMR chemical shift due to the small energy difference ΔE between magnetically active orbitals, here between σ(Sn–Si) bonding orbital and the 5p(Sn) orbital, with large coefficients at the tin atom.

A general comment on the use of the empirical correlation between ^{29}Si and ^{119}Sn NMR (and likewise on ^{13}C/^{29}Si or ^{119}Sn/^{207}Pb NMR) chemical shifts is in order. The basis for this correlation is that the paramagnetic term σ_p dominates the chemical shift. According to Ramsay's theory,[103a,b] σ_p is proportional to the reciprocal energy difference ΔE between the magnetically active orbitals and proportional to the expectation value for the electron radii $\langle r^{-3}\rangle_{np}$. Thus, a linear correlation between the δ^{29}Si and δ^{119}Sn implies that the ratio of *both* determining factors of σ_p is constant for the all compounds of interest. In particular, it is not clear, however, if the ΔE ratio for tetravalent silicon and tin compounds is the same as for trivalent silicon and tin compounds. Therefore, the extension of a correlation based exclusively on the

TABLE X
CALCULATED Sn NMR CHEMICAL SHIFTS FOR CATIONIC TIN SPECIES

Compound	Method	δSn vs. Me_4Sn	Ref.
Mes_3Sn^+, **65**	GIAO/MPW1PW91[a,b]	856	48
Tip_3Sn^+, **68**	GIAO/MPW1PW91[a,c]	763	48
H_3Sn^+	IGLO/HF[d,e]	774	151
	GIAO/HF[a,f]	596	105
	GIAO/MPW1PW91[a,f]	878	105
	GIAO/MP2[a,f]	718	105
Me_3Sn^+	IGLO/HF[d,g,e]	1075	151
	GIAO/HF[a,f]	1166	105
	GIAO/MPW1PW91[a,f]	1466	48, 105
	GIAO/MP2[a,f]	1325	105
$[Me_3Sn/C_6H_6]^+$	GIAO/MPW1PW91[a,f]	482	48
$[Me_3Sn/C_7H_8]^+$	GIAO/MPW1PW91[a,f]	438	48
$Me_3SnOClO_3$	GIAO/MPW1PW91[a,f]	228	48
Me_3SnOTf	GIAO/MPW1PW91[a,f]	229	48
$Me_2Sn^+CH_2C_5H_9$, **62**	GIAO/MPW1PW91[a,h]	406	48
$(H_3Si)_3Sn^+$, **70**	GIAO/MPW1PW91[a,f]	2880	105
	GIAO/HF[a,f]	2440	105
	GIAO/MP2[a,f]	2680	105
	GIAO/B3LYP[i,j]	2841	71
$(Me_3Si)_3Sn^+$, **71**	GIAO/MPW1PW91[a,f]	3450	105

[a]Basis set: 6-31G(d), (Si,C,H,O,S,F) and tzv (19s,15p,9d)[8s,7p,5d] (Sn).
[b]HF/6-31G(d) (Si,C,H,O,S,F) SDD (Sn) optimized geometries has been used.
[c]B3LYP/6-31G(d) (C,H) LACVP** (Sn) optimized geometry has been used.
[d]Basis set: dz(p).
[e]HF/dz(p) optimized geometry has been used.
[f]B3LYP/6-31G(d) (Si,C,H,O,S,F) SDD (Sn) optimized geometries has been used.
[g]Estimated using methyl increments.
[h]MP2/6-311G(d) (Si,C,H,O,S,F) SDD (Sn) optimized geometries has been used.
[i]Basis set: 6-311G(d), (Si,C,H) and [7s,6p,5d] (Sn).
[j]B3LYP/6-31G(d) (Si,C,H) [6s,5p,4d](Sn) optimized geometries has been used.

comparison of tetravalent compounds to trivalent compounds is questionable. Consequently, there are two established correlations between ^{119}Sn and ^{207}Pb NMR chemical shifts, one for divalent[152] and one for tetravalent compounds.[149]

b. Experimental ^{119}Sn NMR Data for Stannylium Ions and Related Species

Early experimental investigations by Birchall and co-workers indicated that tin cations R_3Sn^+ (R = H, Me, Et) are formed from tetracoordinated stannanes $R_{4-n}SnH_n$ ($n = 0-4$) in superacidic media.[43–45] They were identified by ^{119}Sn NMR spectroscopy, and the following shifts in fluorosulfonic acid at low temperatures have been reported: "Me_3Sn^+", $\delta^{119}Sn = 322$ ppm ($T = -60\,^\circ C$), "Et_3Sn^+" $\delta^{119}Sn = 288$ ($T = 20\,^\circ C$) and "H_3Sn^+" $\delta^{119}Sn = -194$.[43] From a careful analysis of the scalar $^1J(SnC)$ coupling and from Mössbauer spectroscopy data, it was concluded that these "R_3Sn^+" cations adopt in fluorosulfonic acid a trigonal-bipyramidal coordination sphere, where the three substituents R form the trigonal basis and two fluorosulfates occupy the apical position.[43,45] The ^{119}Sn NMR

chemical shift depends on the acid and reaction conditions. When 92% sulfuric acid is used for the generation of the "Me_3Sn^+" cation a ^{119}Sn NMR chemical shift of 194 is detected[44] and the ^{119}Sn NMR spectrum of a mixture of Me_4Sn and $SbCl_5$ showed a signal at $\delta^{119}Sn = 208$ attributed to the "Me_3Sn^+" cation.[153]

Various monohalides of triorganotin derivatives have been shown by ^{119}Sn NMR spectroscopy to ionize in polar organic solvents, providing the corresponding coordinated cations.[154–156] The actual ^{119}Sn NMR chemical shift however depends markedly on the solvent, that is for the tin perchlorate, Bu_3SnClO_4, the following ^{119}Sn NMR chemical shifts were reported: $\delta^{119}Sn = 220$ (CH_2Cl_2), 139 (sulfolane), 54 (MeCN), −24 (pyridine), 0 (1,3-dimethyl,2,4,5,6-tetrahydro-2(1 H)-pyrimidone (DMPU)), 12 (dimethyl sulfoxide (DMSO)), −43 (hexamethylphosphoric triamide (HMPA)).[154] This clear dependence of the ^{119}Sn NMR chemical shift on the donicity of the solvent and an analysis of the scalar ^{1}J(SnC) coupling and of the ^{37}Cl NMR linewidths of the perchlorate anion indicate a subtle balance between neutral tetrahedral and cationic trigonal-bipyramidal arrangement of the tin species. Bipyramidal coordination is favored if the solvent donicity is increased. For HMPA as solvent the bipyramidal arrangement is demonstrated by the presence of a ^{119}Sn-^{31}P coupling.[154]

With counteranions of lower nucleophilicity the ^{119}Sn NMR chemical resonance of solutions of tributyl tin salts is further shifted to lower field. Lambert and Kuhlmann reported for the tributylstannyl borate $Bu_3SnB(C_6F_5)_3H$ $\delta^{119}Sn = 360$ in benzene[25] and Kira and co-workers found for the related $Bu_3SnTFPB$ $\delta^{119}Sn = 356$ in CD_2Cl_2.[27] In the latter case, ^{19}F NMR spectroscopy indicates no cation–anion interaction. Finally, for $Bu_3SnTPFPB$ in toluene at −60 °C $\delta^{119}Sn = 434.2$ was reported by Piers *et al.*[28,29] The solvent dependence of the ^{119}Sn NMR chemical shift suggests that in the case of aromatic solvents Wheland-type intermediates are formed.[4,28,29,46] Additional support for the formation of stannylated arenium ions in these experiments[25,28,29] comes from the fair agreement between the calculated ^{119}Sn NMR chemical shift for $[Me_3SnC_6H_6]^+$ ($\delta^{119}Sn = 438$) and $[Me_3SnC_7H_8]^+$ ($\delta^{119}Sn = 482$) compared to the experimental data. The addition of stronger nucleophiles than aromatic hydrocarbons or methylene chloride to the samples has a strong shielding effect on the tin nucleus. That is, addition of excess diethylether to a solution of $Bu_3SnTFPB$ in CD_2Cl_2 yields an oxonium species characterized by a high field shifted ^{119}Sn NMR signal at $\delta^{119}Sn = 165$.[27] Similarly, addition of an equimolar amount of *o*-anisaldehyde to a solution of $Bu_3SnTPFPB$ in C_7D_8 gives a cationic tetracoordinated trialkyltin compound, **60**, identified by a ^{119}Sn NMR chemical shift of $\delta^{119}Sn = 300$. The addition of a second equivalent of anisaldehyde to the reaction mixture leads the formation of the cationic pentacoordinated species, **61**, accompanied by a further decrease of the ^{119}Sn NMR chemical shift ($\delta^{119}Sn = 91$, see Scheme 17).[28]

Recently Michl and co-workers isolated the stannylium ions Bu_3Sn^+ and Me_3Sn^+ with the permethylated carborane anion $[CB_{11}Me_{12}]^-$ as counterion.[68,69] Both cations strongly interact in the solid state with the carborane anion and form infinite one-dimensional columns of alternating R_3Sn^+ and $CB_{11}Me_{12}^-$ ions (see Section III.D.3). In agreement with sizeable cation–anion interactions the solid state NMR chemical shift for both cations ($\delta^{119}Sn = 461$ (Bu_3Sn^+) and $\delta^{119}Sn = 466$ (Me_3Sn^+) are at much higher field than expected for isolated trialkylstannylium ions.[69] Ion aggregation persists in hydrocarbon solution, as the solution ^{119}Sn

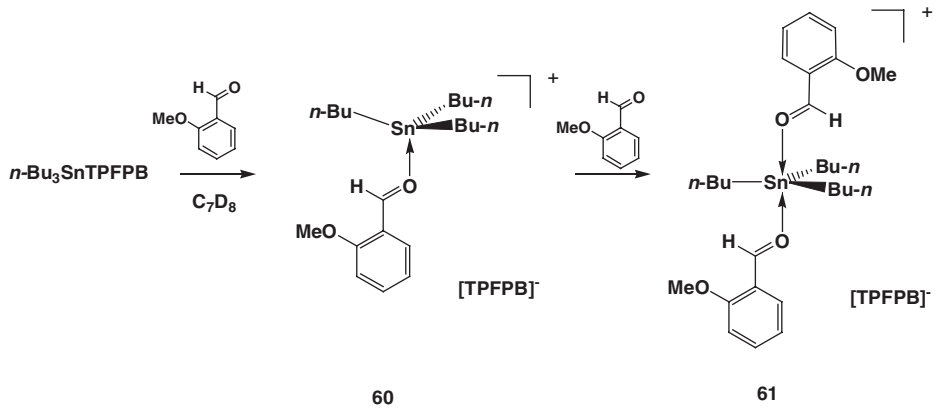

SCHEME 17.

NMR chemical shift in cyclohexane for $[Bu_3Sn^+][CB_{11}Me_{12}^-]$ is only little lower than in the solid state ($\delta^{119}Sn = 454$).[68,69] On the other hand, even in benzene solution, the interaction with the solvent predominates, therefore the ^{119}Sn NMR chemical shift of $[Me_3Sn^+][CB_{11}Me_{12}^-]$ in benzene is 325, indicating formation of stannylated arenium ions. Solutions of these permethylated carborane salts in solvents of higher donicity have ^{119}Sn NMR chemical shifts, which are characteristic for chloronium ions ($\delta^{119}Sn = 336$, $[Me_3Sn^+][CB_{11}Me_{12}^-]$ in CD_2Cl_2), for nitrilium ions ($\delta^{119}Sn = 233$, $[Me_3Sn^+][CB_{11}Me_{12}^-]$ in CDCN) and for oxonium ions ($\delta^{119}Sn = 168$, $[Bu_3Sn^+][CB_{11}Me_{12}^-]$ in Et_2O/CD_2Cl_2).[69]

The intramolecular π-electron donation from the remote double bond to the stannylium ion center in the stannanorbornyl cation, **62** ($\delta^{119}Sn = 336$ in C_6D_6), also leads to a significant shielded tin nucleus compared to what is expected for a free trialkylstannylium ion. As already shown for the sila compounds **55**–**58**, the coordination of the C═C double bond to the electron-deficient tin center in **62** is indicated by a low-field shift of the ^{13}C resonance of the vinylic carbon atoms by 11.1 ppm. Additionally, the small scalar Sn–C coupling constant $^1J(SnC) = 26$ Hz gives clear evidence for the intramolecular π-complexation.[40]

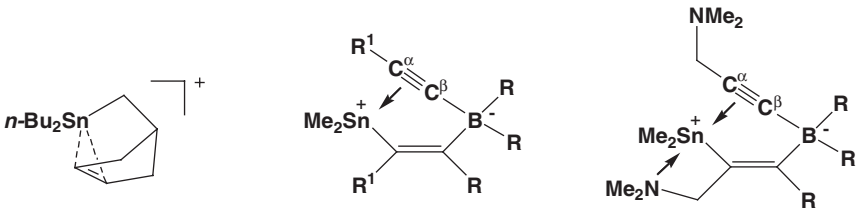

62 **63** **64**

The bonding situation in the stannanorbornyl cation **62** is reminiscent of the intriguing zwitterions of the types **63**[158] and **64**[157] in which triorganotin cations are intramolecularly stabilized by side-on coordination with an alkynyl group. The zwitterions **63** with a [3 + 1] coordination for the tin atom are characterized by a significantly deshielded ^{119}Sn NMR resonance and sizeable ^{1}J(SnC) couplings to the alkynyl carbon atoms (for R^1 = alkyl and R = Et: δ^{119}Sn = 160–215; ^{1}J(SnC^{α}) = 41–48 Hz, ^{1}J(SnC^{β}) = 60–80 Hz).[158] Coordination with the amino group in **64** leads to an additional upfield shift of the ^{119}Sn NMR signal (For R = Et: δ^{119}Sn = 127.7)[157]

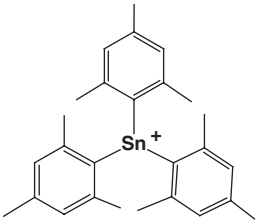

65

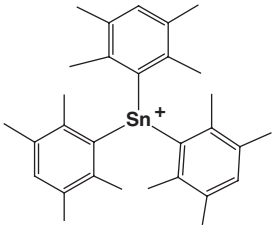

66

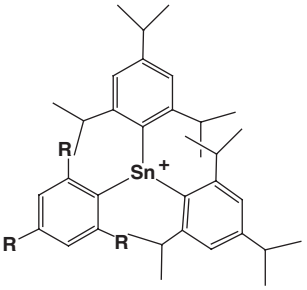

67, R = H
68, R = *i*-Pr

The trimesitylstannylium ion **65**, synthesized in Lambert's group, is characterized by an extremely low-field signal in the ^{119}Sn NMR spectra (δ^{119}Sn = 806 in C_6D_6).[4] This ^{119}Sn NMR chemical shift is unchanged in toluene, mesitylene and *o*-dichlorobenzene, indicating negligible interactions of the cations and aromatic hydrocarbons or their chlorinated derivatives. Similar low-field signals were detected for the tridurylstannylium, **66**, and the di(triisopropylphenyl)-phenylstannylium cation, **67** (δ^{119}Sn (**66**) = 720, δ^{119}Sn (**67**) = 697, see also Table XI).[4,47] These ^{119}Sn NMR chemical shifts are however still at ca 300 ppm at higher field than expected for a *trivalent* triarylstannylium ion based on the empirical correlation between ^{29}Si NMR and ^{119}Sn NMR chemical shifts established for *tetravalent* silicon and tin compounds.[46] For this reason and since cation/anion interaction or intramolecular interactions between the tin center and remote C–H bonds ("agostic interactions") could not be excluded, Lambert and co-workers confined to these cations "only about 75% stannylium ion character".[4,47] The situation changed, however, after the synthesis and structural characterization of the tris(triisopropylphenyl) stannylium ion **68**. Compound **68** was shown to exist as a non-coordinated cation with the TPFPB counteranion (see Section III.D.1). The molecular structure showed no indication for agostic interactions and its δ^{119}Sn NMR chemical shift was 714.[48] Subsequent ^{119}Sn NMR calculations using the MPW1PW91/GIAO density functional method predicted for an optimized structure of cation **68**, a ^{119}Sn NMR chemical shift of 763. A more extensive theoretical study on Sn NMR chemical shift calculations for stannyl cationic species demonstrated that the calculated value (δ^{119}Sn = 763) is fully consistent with the observed value of δ^{119}Sn = 714 (see Tables X and XI).[48,105] On the basis of the experimental results for **68**[24] and

TABLE XI
^{119}Sn NMR CHEMICAL SHIFTS FOR CATIONIC TIN SPECIES

Compound	Solvent	δ^{119}Sn vs. Me_4Sn	Ref.
65/TPFPB$^-$	C_6D_6	806	4
	C_7H_8	806	4
	1,3,5-$(H_3C)_3C_6H_3$	806	4
	1,2-$Cl_2C_6H_4$	806	4
66/TPFPB$^-$	C_6D_6	720	47
67/TPFPB$^-$	C_6D_6	697	4
68/TPFPB$^-$	C_6D_6	714	48
23/TPFPB$^-$	C_6D_6	2653	71
$Me_3Sn^+/CB_{11}Me_{12}^-$	Solid state	466.2	69
	C_6D_6	324.7	69
	CD_2Cl_2	335.9	69
	CD_3CN	233.1	69
Me_3Sn^+/FSO_3^-	FSO_3H	322	43
n-$Bu_3Sn^+/CB_{11}Me_{12}^-$	Solid state	461.2	69
	C_6D_{12}	454.3	68
n-$Bu_3Sn^+/HB(C_6F_5)_3^-$	C_6D_6	360	25
n-Bu_3Sn^+/TFPB$^-$	CD_2Cl_2	356	27
	Et_2O/CD_2Cl_2	165	27
n-Bu_3Sn^+/TPFPB$^-$	C_7D_8	434.2	28
n-$Bu_3SnOClO_3$	CH_2Cl_2	220	154
n-Bu_3SnOTf	CH_2Cl_2	172	154
62/TPFPB$^-$	C_6D_6	334.0	40
	C_7D_8	329.7	40
	CD_3CN	54.4	40
Et_3Sn-O^+(H)-$SnEt_3$/TPFPB$^-$	C_6D_6	250.8	26

supported by the Sn NMR calculations[48,105] it can be concluded that the triarylstannylium ions **65**–**68** all exist as free cations in the condensed phase, unfettered by interaction with solvent, anion or neighboring groups.

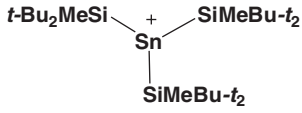

23

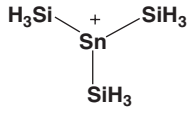

70

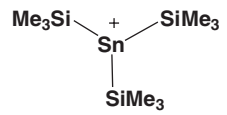

71

The extreme low-field position of the ^{119}Sn resonance of Sekiguchi's trisilyl-substituted stannylium ion **23** ($\delta^{119}Sn = 2653$)[71] is at a first glance surprising, in particular when compared with the ^{119}Sn NMR chemical shifts of the aryl-substituted cations **65**–**68**. The rationalization however, is straightforward on the basis of the discussion in Section III.B.1.a. The occurrence of energetically high-lying SiSn bonding MO's and the relative low-lying p-type orbital at the tin center in stannylium ion **23** leads to large paramagnetic contributions to the Sn NMR chemical shielding and in consequence to the observed absorption at an extraordinarily high frequency.[105] Sn NMR chemical shift calculations at various levels

of theory for stannylium ions **70** and **71**, close models for Sekiguchi's stannylium ion **23**, reproduce qualitatively the tremendous deshielding of the tin nuclei in **23** compared to the triaryl-substituted stannylium ions (see Table X).[71,105]

3. ^{207}Pb NMR Spectroscopic Data of Plumbylium Ions and Related Species

Empirical correlations between δ^{119}Sn and δ^{207}Pb NMR chemical shifts exist for tetravalent[149] and for divalent[152] tin and lead compounds. Keeping in mind the short discussion in Section III.B.2.a, it is clear that both cannot be applied for trivalent cations. Therefore, no empirical estimate for the ^{207}Pb NMR chemical shift of a free plumbylium ion exists. In addition, no reliable NMR chemical shift calculations are available for plumbylium ions.[159] A rough estimate, purely based on the well-established influence of the coordination number on the NMR chemical shift, would place the ^{207}Pb NMR chemical shift for plumbylium ions at higher frequencies than tetravalent organolead compounds ($\delta^{207}\text{Pb} = -1000$ to $+1000$), but shielded compared to divalent diorganoplumbylenes ($\delta^{207}\text{Pb} > 2000$). In agreement with this guideline the formation of triorganoplumbyl cations from tetravalent precursors is always accompanied by a significant low-field shift of the ^{207}Pb NMR chemical signal (see Table XII). The reported ^{207}Pb NMR chemical shift for triorganoplumbyl cationic species depends however, markedly on the actual reaction conditions. That is, while for trimethylplumbyl fluorosulfate in fluorosulfonic acid $\delta^{207}\text{Pb} = 980$ is reported,[48] a solution of the salt $[Me_3Pb^+][CB_{11}Me_{12}^-]$ in C_6D_6 at room temperature is characterized by a ^{207}Pb NMR signal at 1007.[69] In both cases, cation/anion aggregation and/or solvent complexation must be taken into account, since for $[Et_3Pb^+]$TPFPB$^-$ in C_6D_6 a significantly more deshielded lead center is found ($\delta^{207}\text{Pb} = 1432$).[40] The ^{207}Pb NMR chemical shift of $[Et_3Pb^+]$TPFPB$^-$ is relatively insensitive to solvent effects, i.e in toluene solution $\delta^{207}\text{Pb} = 1405$ is found.[160] Therefore, the solvent effect on the ^{207}Pb NMR chemical shift is less than 2%. In the absence of any additional experimental information on the nature of the observed species and in sight of the substantial interaction energy

TABLE XII
^{207}Pb NMR CHEMICAL SHIFTS FOR PLUMBYL CATIONIC COMPOUNDS

Compound	Solvent	δ^{207}Pb vs. Me_4Pb	Ref.
Et_3Pb^+/TPFPB$^-$	C_6D_6	1432	40
	C_7D_8	1405	160
Bu_3Pb^+/TPFPB$^-$	C_6D_6	1309	160
$Me_3Pb^+/CB_{11}Me_{12}^-$	CD_2Cl_2	1007	69
13/TPFPB$^-$	C_6D_6	1049	40
	C_7D_8	1039	40
73/TPFPB$^-$	CH_3CN/C_6D_6	598	40
74/TPFPB$^-$	C_6D_6	807	53
75/TPFPB$^-$	C_6D_6	799	53
72, R = Et		723	161
72, R = *i*-Pr		667	161
Me_3PbOSO_2F		980	46
$Me_3PbOClO_3$		694	46

predicted for Me_3Pb^+ and toluene ($\Delta E_A = 30.5\,kcal\,mol^{-1}$, see Table IV)[94] one cannot exclude the formation and detection of plumbyl arenium ions in these experiments.[40,160]

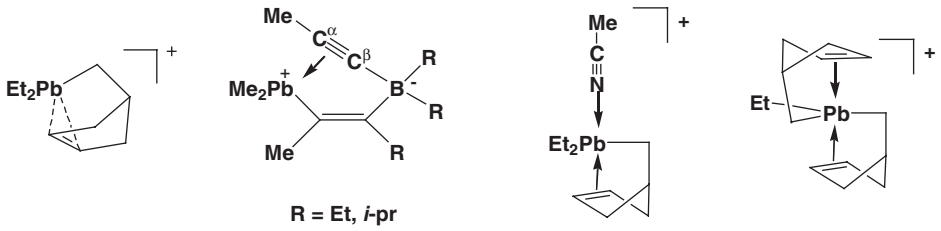

13 72 73 74

Intramolecular π-coordination of the electron-deficient lead center, as for example in the norbornyl cation **13** ($\delta^{207}Pb = 1049$)[40] and in the zwitterions **72** (R = Et : $\delta^{207}Pb = 723$; R = *i*-pr: $\delta^{207}Pb = 667$),[161] leads to a significant high-field shift of the ^{207}Pb NMR resonance when compared to $[Et_3Pb^+]TBFPB^-$. The detection of scalar Pb–C couplings $^1J(CPb)$ between the Pb atom and the vinylic C atoms in **13** or the acetylenic C atoms in **72**, respectively, clearly indicates the intramolecular coordination of the CC multiple bond to the plumbylium ion (**13** : $^1J(CPb) = 16.2$ Hz; **72** : $^1J(CPb) = 11$–30 Hz).[40,161] The significant solvent induced high-field shift detected for **13** when 1 Eq. acetonitrile is added to a benzene solution of [**13** TPFPB] is due to the formation of an acetonitrile complex, **73**, which could also be characterized crystallographically. Similarly, the formation of the bis-alkene complex **74**, in which the Pb atom adopts a trigonal-bipyramidal coordination sphere with the two alkene groups in the apical position, is accompanied by a further decrease of the ^{207}Pb NMR chemical shift ($\delta^{207}Pb = 807$ for **74** in C_6D_6).[53] Nearly the same ^{207}Pb NMR chemical shift as for **74** is measured for the tris-cyclopentenylmethyl-substituted plumbyl cation **75** ($\delta^{207}Pb = 799$ in C_6D_6). ^{13}C NMR data show that all three substituents in the plumbyl cation **75** are equivalent on the NMR time scale at room temperature. This suggests for **75**, a dynamic equilibrium between equivalent bisalkene complexes of trivalent lead, similar to **74** (see Scheme 18).[53]

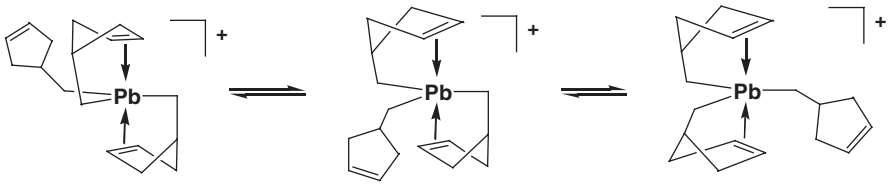

75

SCHEME 18.

4. ^{13}C NMR Spectroscopic Data of Organosubstituted R_3E^+ Cations

^{13}C NMR chemical shifts of organosubstituted R_3E^+ ions are only of small diagnostic value. Several factors such as substitution, charge distribution and small separations of magnetically active molecular orbitals etc. influence the ^{13}C NMR chemical shifts of the C atoms of the organic ligand in R_3E^+ in a not easily predictable manner so that no characteristic pattern is apparent. The only exceptions where ^{13}C NMR chemical shifts are used for the characterization of the R_3E^+ cations are (i) when a series of homologues R_3E^+ cations were investigated and trends in the ^{13}C NMR chemical shifts are discussed and (ii) when intramolecular stabilization of the electron-deficient element atom by CC multiple bonds is important. In these cases, the analysis of ^{13}C NMR chemical shifts played an important role for the characterization of germylium ions, R_3Ge^+, since germanium lacks a sensitive and convenient NMR active nuclide. In the following, examples for both cases are given.

Michl and co-workers recently reported solid state ^{13}C NMR chemical shift of the methyl group in the $Me_3E^+CB_{11}Me_{12}^-$ (E = Ge, Sn, Pb) salts to be 5.6, 10.4 and 31.4 for Me_3Ge^+, Me_3Sn^+ and Me_3Pb^+, respectively.[69] The authors argued that the steady deshielding of the α-carbon atom indicates a continuous increase of positive charge concentration at the central element going from germanium to lead.[69]

Similarly, the cationic character of the germylium ion Mes_3Ge^+, **76**, was estimated by comparison of the low-field shift of the ^{13}C NMR resonances of the aryl carbon atoms upon ionization with those low-field shifts found for the homologous silylium and stannylium ions.[4] The deshielding of the aryl carbon atoms in **76** is comparable to that found for **1** and **65**. This is consistent with charge development on germanium in **76** that is comparable to that on silicon in Mes_3Si^+, **1**, and tin in Mes_3Sn^+, **65**.

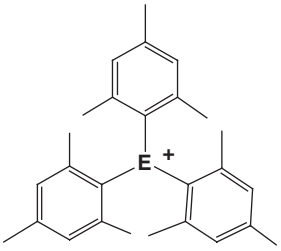

1 E = Si
65 E = Sn
76 E = Ge

55 E = Si, R = Me
56 E = Si, R = Et
57 E = Si, R = *n*-Bu
62 E = Sn, R = *n*-Bu
13 E = Pb, R = Et
77 E = Ge, R = *n*-Bu

The deshielding of the vinylic carbon atoms in the norbornyl cations **13**, **55**–**57**, **62** and **77** compared to the precursor compounds was taken as evidence for the intramolecular coordination of the C=C double bond to the electron-deficient element atom.[40] This high-frequency shift, $\Delta\delta^{13}C$, is largest for the silanorbornyl cations **55**–**57** ($\Delta\delta^{13}C = 20$) and $\Delta\delta^{13}C$ decreases continuously and it reaches for the

plumbanorbornyl cation **13** its minimum value of 8. This implies reduced electron transfer from the C=C double bond to the positively charged element atom in the series C → Pb.[40]

The intramolecular stabilization of germyl cation **34** by a remote aryl substituent was demonstrated by the ^{13}C NMR chemical shifts of the coordinated aryl ring.[80] The chemical shift pattern found for the coordinated arene ring of **34** is characteristic for arenium ions and it closely resembles that found bissilylated arenium ions **78**.[162]

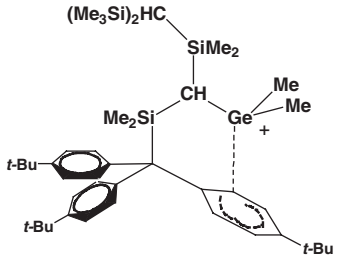

34

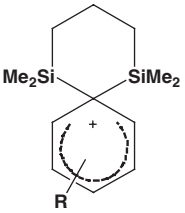

78

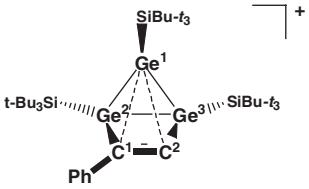

6

One of the most important features of the bicyclic bishomoaromatic germylium ion **6** is the considerably *shielded* ^{13}C NMR chemical shifts of the endocyclic atoms C1 and C2, relative to those of the neutral precursor **5**.[21] Despite the partial delocalization of the positive charge over Ge3, C1 and C2, significant high-field shifts ($\Delta\delta^{13}$C(C1) = −29.8, ($\Delta\delta^{13}$C(C1) = −54.5) are observed and a relatively large ^{1}J(C2H) coupling constant of 165.9 Hz is detected. This counter-intuitive low-frequency shift of the ^{13}C NMR resonance of C1 and C2 as well as the large scalar CH coupling constant was rationalized for similar bishomoaromatic carbon cations like the 7-norbornenyl cation, **79**, by the hypercoordinated nature of the vinylic C atoms and was put forward as spectroscopic evidence for bishomoaromaticity.[163,164]

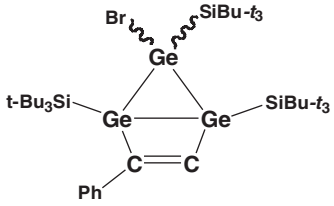

5

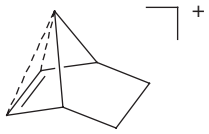

79

C. *Miscellaneous Spectroscopic Data of R_3E^+ Cations*

Spectroscopic information on R_3E^+ other than NMR chemical shifts and coupling constant are hardly available. Some UV data are reported for Mes_3E^+ cations (E = Si, Sn) in benzene solution.[4] The UV absorption in these aryl-substituted

cations was taken as measure for the conjugation between the central element atom and the π-system of the aryl ligand. Two absorptions were observed for the silylium ion Mes_3Si^+, **1**, a maximum at 304 nm and a shoulder at 370 nm. The tailing of the 370 nm absorption into the visible region causes the dark yellow color of the solutions and of the salts of the Mes_3Si^+ cation.[4,49] The silylium cation absorbs at shorter wavelength than triphenylmethylium Ph_3C^+, which exhibits two peaks at 409 and 428 nm in conc. sulfuric acid.[165] The ultraviolet spectrum of trimesitylstannylium TPFPB, (**65**/TPFPB), in benzene showed clear maxima at 286 and 398 nm.[4] The latter is at slightly longer wavelength than the longest wavelength silylium absorption (370 nm). These UV data suggest that the conjugation is slightly more efficient in Mes_3Sn^+ than in Mes_3Si^+ most probably due to the better alignment of the mesityl substituents with the empty π-orbital at the central element in the stannylium ion.[4]

The stannylium ion Tip_3Sn^+, **68**, was investigated by Mössbauer spectroscopy.[166] The resonance spectra consist of a doublet indicating the axial symmetry of the stannylium ion. The quadropole coupling (QS) for **68** of $5.534 \pm 0.011\ mm\ s^{-1}$ is among the largest such values yet reported for an organotin complex and can be compared with the QS values for Me_3Sn^+ in HSO_3F (QS = 4.95) for which a trigonal-bipyramidal coordination is established.[43,45] The isomer shift (IS) is $1.875 \pm 0.011\ mm\ s^{-1}$, at the higher end of the shift range for Sn(IV) compounds [IS(Sn(IV)) = −0.5–2.5 $mm\ s^{-1}$]. This value is consistent with the presence of one 5s electron, expected for a Sn atom with sp^2 hybridization and predominant covalent metal–ligand bonding interaction. The metal atom motion in a temperature range between 90 and 170 K is isotropic within experimental error of the Mössbauer data, which is surprising in regard of the highly anisotropic bonding situation in the trigonal planar coordination environment of the Sn atom in $Tips_3Sn^+$, **68**.[166]

D. *Solid State Structure of R_3E^+ Cations and Related Species*

1. Solid State Structure of R_3E^+ Cations

Until the year 2002 no experimental data existed on the structures of unperturbed R_3E^+ cations, the exact analogues of the carbenium ions. Computational data combined with NMR chemical shift calculations, which could be compared to experiment, were the only source of reliable structural information for silylium ions[6,7,13,77,121] while for germylium, stannylium and plumbylium ions this combined approach was not attractive due to either the non-existence of the experimental data (Ge) or the complexity of the computational problem (Sn, Pb). On the other hand, a series of excellent experimental studies demonstrated, for example, the high coordination tendency of small trialkylsilylium ions either toward the counteranion[38,114,127,138] or toward the solvent.[36,37,67,116,127] The solid state structures of these silyl cation salts showed clear indications either of cation/anion or cation/solvent coordination. Thus, the nature of the observed cation, i.e. the degree of silylium ion character remained disputable.[10,11,13]

One strategy to overcome these problems is to increase the steric bulk around the cationic center in order to minimize intermolecular interactions. However, the

classical hydride transfer reaction also is severely hampered when the steric congestion of the substrate is increased. Therefore, novel synthetic strategies had to be found, which shifts the reactive side from the center of the incipient cation to the periphery of the molecule.

These requirements were perfectly met for the first time by the synthesis of trimesitylsilylium Mes_3Si^+, **1**, by the allyl fragmentation reaction by Lambert and coworkers (see Section II.C).[4,5] Their NMR characterization of the silylium ion and consecutive computational studies indicated that Mes_3Si^+ is the first example for a silylium ion unfettered by any interaction with neighbouring groups solvents or counteranions. In the NMR work the $TPFPB^-$ anion was used, well known for its inertness but also well known for its tendency to form oils intractable to crystallization. In contrast, with the brominated carboranate anion $[HCB_{11}Me_5Br_6]^-$ as counteranion the groups of Reed and Lambert obtained yellow crystals of the benzene solvate of the salt $[Mes_3Si][HCB_{11}Me_5Br_6]$.[49] The crystal structure revealed well separated molecules. No atoms of the carboranate or benzene approach the Si atom closer than 600 pm. The closest approaches to the Mes_3Si^+ cation arise from methyl–methyl group non-bonded interactions rather than from the more electron-rich bromine atoms of the carborane anion or the π-system of benzene. The mesityl groups in Mes_3Si^+ have a propeller-like arrangement around the trigonal planar Si center with twist angles of 51.3, 54.5 and 41.9° relative to the coordinate plane (see Fig. 3). The planar coordination geometry is indicated by summation of the three C–Si–C angles to 359.9°, within experimental error (0.2°) of 360°. As expected, the Si–C bonds (average, 181.7 pm) are significantly shorter than those observed in the neutral tetrahedral trimesitylallylsilane precursor (average, 191 pm).[5] Despite the large twist angles, the aryl rings show a marked dactylic bond length alternation, typical for conjugating interactions between the aryl substituent and the electron-deficient silicon atom (see Fig. 3). The solid state ^{29}Si NMR chemical shift of $[Mes_3Si]$ $[HCB_{11}Me_5Br_6]$ agrees well with the solution value for the TPFPB salt ($\delta^{29}Si = 226.7$ vs $\delta^{29}Si = 225.5$). This demonstrates that in solution as well as in the solid state the structure of Mes_3Si^+ is the same. No structural indication for internal solvation or agostic interaction is found in the experimental geometry of the Mes_3Si^+ cation,[49] in agreement with the conclusions from a previous theoretical study.[6] In general, the previously calculated structures at the density functional level

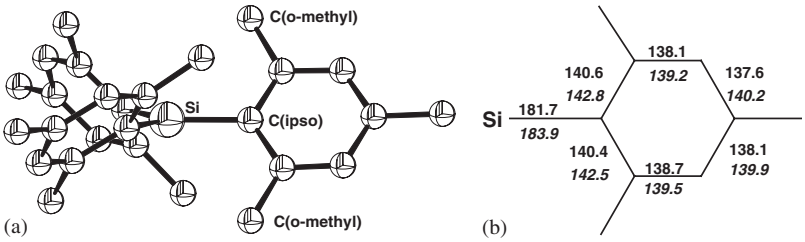

FIG. 3. (a) Perspective view of the Mes_3Si^+ cation. Thermal ellipsoids are drawn at the 50% probability level, for further details see text and Table XIII. (Reprinted with permission from Ref. 49. Copyright 2002, AAAS.) (b) Comparison between experimental and calculated (italic, at the B3LYP/6-31G(d) level of theory) bond lengths [pm] in Mes_3Si^+ (from Refs. 49 and 6).

of theory[6,7] match well the experimental solid state structure of Mes_3Si^+, the differences between the calculated and experimental bond lengths being smaller than 1.2%.[6,7,49] This good agreement between experimental and theoretical structure is reflected also by the correspondence between the ^{29}Si NMR chemical shifts measured in solution and in the solid state and the computed ^{29}Si NMR chemical shift ($\delta^{29}Si = 226-230$).[6,7]

Trismesitylgermanium, **76**, and trismesitylstannylium, **65**, have been prepared as their TPFPB salts however, no experimental structure is reported.[4] For the TPFPB salt of the related stannylium ion Tip_3Sn^+, **68**, suitable crystals for X-ray analysis were obtained and the crystal structure was solved.[48] The stannylium ion and the TPFPB anion are well separated, no atom of the anion approaches the cation to within 400 pm. The molecular structure of the stannylium ion Tip_3Sn^+ parallels in many features closely that of Mes_3Si^+. That is, the aryl groups are twisted in the usual propeller fashion from the plane of the tin atom and its three attached carbon atoms. The twist angle is 61.1°, larger than found for Mes_3Si^+ due to the larger *ortho* substituent in Tip_3Sn^+ (*i*-pr vs. Me) being 61.1°. The sum of the C–Sn–C angles is 359.9(2), which indicates planarity of the central SnC_3 group (Fig. 4). No structural evidence for interaction between the isopropyl-H atoms and the tin center is found.[48] The average Sn–C bond length in Tip_3Sn^+ is 211.1 pm, somewhat shorter than found for the Sn–C bonds in $(o\text{-tol})_4Sn$ (215.2 pm).[167]

The next landmark was the synthesis of the germylium, **22**, and the stannylium ion, **23**, by one-electron oxidations from the corresponding stable radicals with trityl TPFPB by Sekiguchi and co-workers. As in the case of the allyl cleavage to generate the mesityl-substituted cations, the reaction, in this case the oxidation, occurs at the periphery of the molecule and gives the possibility for efficient steric protection of the incipient cation. Both trivalent cations were obtained as their TPFBP salts and the crystal structure show well separated anions and cations.

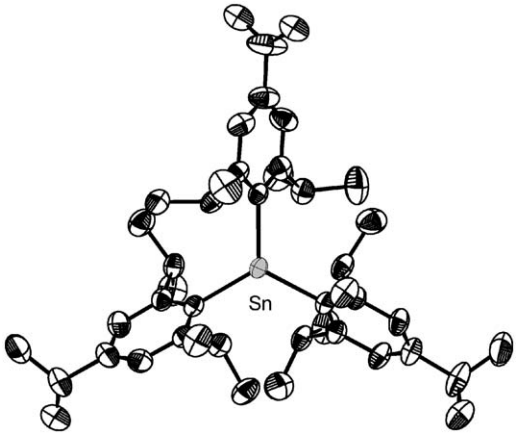

FIG. 4. Molecular structure of Tip_3Sn^+. Thermal ellipsoids are drawn at the 50% probability level, for details see text and Table XIII.[48]

In both structures the element atom has an essentially planar environment, which indicates for the cations **22** and **23** perfect trigonality (see Fig. 5). The average Ge^+–Si bond in **22** is longer [251.95(10) pm] than a regular Ge–Si bond (238.4–246.2)[168] and it is also longer than in the radical $(t\text{-Bu}_2\text{MeSi})_3\text{Ge}^\bullet$ [245.35(4) pm] and the anion $(t\text{-Bu}_2\text{MeSi})_3\text{Ge}^-$ [243.32(10) pm]. This unexpected decrease of the Ge–Si bond length in the cation/radical/anion triple was explained by negative [Ge(4p)→σ*(Si–C)] hyperconjugation in the anion and the radical, which cannot be active in the cation **22**.[72] In contrast, the average Sn^+–Si bond in **23** is in the usual range [268.63(8) pm] for Si–Sn bonds (256.1–278.9 pm)[71,167] although also the Si–Sn bonds in the radical $(t\text{-Bu}_2\text{MeSi})_3\text{Sn}^\bullet$ are shorter [261.76(5) pm].

Historically, the first solid state structure of a truly tricoordinated cation of the heavier group 14 elements (Si–Pb) was that of the cyclotrigermenium cation $[((t\text{-Bu}_3\text{Si})\text{Ge})_3]^+$, **2** published in 1997.[9] Cation **2** was prepared by one-electron oxidation of the cyclotrigermene **20** (E = Si) with trityl cation (see Scheme 8).[9,64–67]

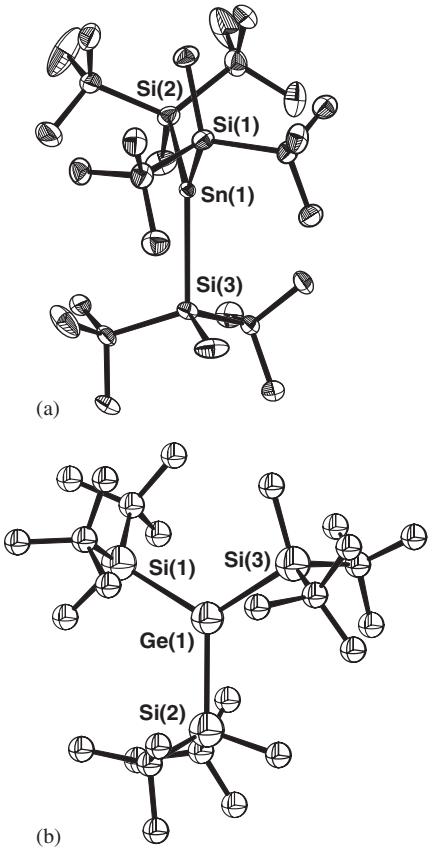

FIG. 5. Molecular structures of (a) $(t\text{-Bu}_2\text{MeSi})_3\text{Sn}^+$, **23**, and (b) of $(t\text{-Bu}_2\text{MeSi})_3\text{Ge}^+$, **22**. Thermal ellipsoids are drawn at the 30% probability level, for details see text and Table XIII. (Reprinted from Ref. 71. Copyright 2003, American Chemical Society and reprinted from Ref. 72. Copyright 2003, Wiley-VCH.)

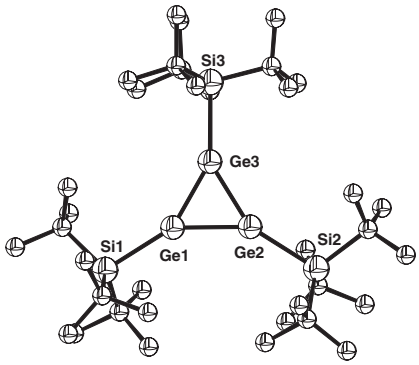

FIG. 6. Molecular structure of tris(tri-*t*-butylsilyl)cyclotrigermenium [*t*-$Bu_3SiGe)_3^+$], **2**. Hydrogen atoms are omitted for clarity. Mean innercyclic bond angle Ge–Ge–Ge: 60.01°, for more data see Table XIII. (Reprinted with permission from Ref. 9. Copyright 1997, AAAS.)

The originally used TPB^- counteranion proved to be unstable in the presence of the cation in methylene chloride solutions at temperatures above −78 °C.[65,66] Therefore, salts with different fluorinated borate counteranions were prepared and crystal structures are reported for the TPB^{-9} (see Fig. 6), $TFPB^{-}$[64–66] and $TSFPB^{-}$[66] salts.

All crystal structures of the cyclotrigermenium cation **2** reveal a free germyl cation with a two π-electron system. The three germanium atoms form an equilateral triangle (mean Ge–Ge distance 233.1 pm, mean innercyclic bond angle GeGeGe : 60.0°). The Ge–Ge bond length observed for **2** is intermediate between the Ge═Ge double bond and the Ge–Ge single bond of the cyclotrigermene **20** (E = Si). The sum of the bond angles around the ring germanium atoms is 359.9°, which indicates planarity of the $(SiGe)_3$ moiety in **2**. These structural features indicate delocalization of the positive charge over the three-membered germanium cycle similar to its carbon analog, the cyclopropenium ion. In agreement, quantum mechanical calculations indicate for the parent cation [$(HGe)_3^+$] a very similar structure [r(GeGe) = 236.1 pm using a B3LYP hybrid density functional and basis sets of triple zeta quality] and a stabilization energy which is ~50% of that of the cyclopropenium ion.[169] Recently, a preliminary communication appeared, which reports the preparation of the analogous cyclotrisilenium cation [((*t*-$Bu_3Si)Si)_2$(*t*-$BuMe_2Si)^+$] which is characterized by an average innercyclic Si–Si bond length of 221.7(3) pm.[170]

The reaction of cyclotrisilene **15** with the silylated benzenium ion $[Et_3Si/C_6H_6]^+$ results in the formation of the cyclotetrasilenylium ion **3** (see Scheme 6). The solid state structure of silyl cation **3** indicates its homoconjugative nature (see Fig. 7 and Table XIII).[8]

The central four-membered ring of cation **3** is folded and the dihedral angle between the Si1–Si2–Si3 and Si1–Si4–Si3 planes is 46.6°. The bond angles at the silicon atoms in the four-membered ring suggest that the silicon atoms Si1, Si2 and Si3 (mean Σ°Si = 359.8, see Table XIII) have a completely planar trigonal geometry and Si4 has a distorted tetrahedral environment. The Si–Si bonds of the cationic

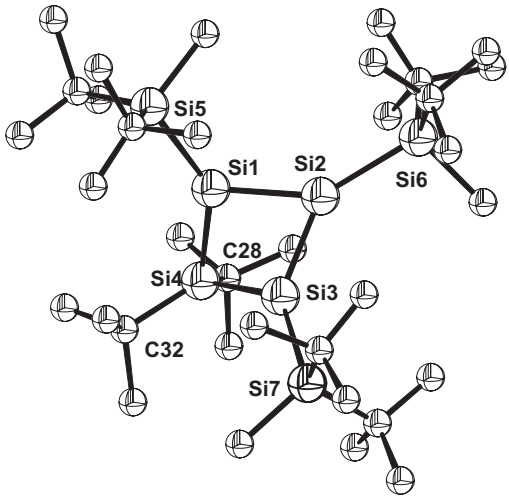

FIG. 7. ORTEP drawing of cyclotetrasilenium **3**. Hydrogen atoms are omitted for clarity. Selected bond lengths (pm) (see also text and Table XIII): Si1–Si4 = 2.336 (2), Si3–Si4 = 2.325 (2). (Reprinted with permission from Ref. 8. Copyright 2000, American Chemical Society.)

TABLE XIII
STRUCTURAL DATA FOR R_3E^+ CATIONS[a]

Compound	d(R–E) (pm)	$\Sigma\alpha$(RER)[b] (deg)	Coordination number	Ref.
$[Mes_3Si^+][HCMe_5Br_6^-]$	181.7	359.9	3	49
$[Tip_3Sn^+][TPFPB^-]$	211.1(4)	359.9(2)	3	48
$[(t\text{-}Bu_2MeSi)_3Ge^+][TPFPB^-]$	251.95(10)	359.9	3	72
$[(t\text{-}Bu_2MeSi)_3Sn^+][TPFPB^-]$	268.63(8)	360.0	3	71
$[(t\text{-}Bu_3SiGe)_3^+][TBP^-]$	232.6(4)[c] 244.3(9)[d]	359.8(2)	3	9
$[(t\text{-}Bu_3SiGe)_3^+][TFPB^-]$	233.5(2)[c] 243.8(3)[d]	358.9(1)	3	64–66
$[(t\text{-}Bu_3SiGe)_3^+][TSFPB^-]$	233.25(8)[c] 243.7(1)[d]	359.94(4)	3	66
$[(t\text{-}Bu_2MeSi)_3^+SiBu\text{-}t_2]$ $[TPFPB^-]$	224.2, 233.1	359.72(8)	3	8

[a]Structural data from X-ray analysis.
[b]Sum of the three bond angles of the element and its three nearest substituents, tetrahedral: $\Sigma = 328.5^\circ$ trigonal planar: $\Sigma = 360^\circ$.
[c]Innercyclic Ge–Ge distance.
[d]Exocyclic Ge–Si distance.

part [Si1–Si2 = 224.0(2) pm and Si2–Si3 = 224.4(2) pm] are intermediate between the Si═Si double bond [213.8(2) pm] and the Si–Si single bond [236.4(3) and 235.2(3) pm] of the precursor **15**.[171] The interatomic distance between Si1 and Si3 is relatively short, 269.2(2) pm, only 15% longer than a normal Si–Si single bond (236 pm).[172] This indicates a possible 1,3-orbital interaction in cation **3**, which is

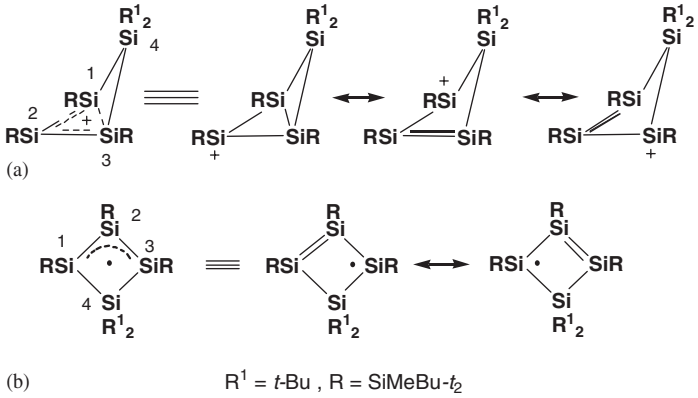

FIG. 8. (a) Homoaromatic 2π-electron conjugation in silyl cation **3**. (b) Allyl-type resonance in 3π-electron radical **26**.[8,74]

supported by the ^{29}Si NMR spectroscopic data (see Section III.B.1.b). Upon reduction of cation **3** to the cyclotetrasilenyl radical **26**, the central Si1/Si3 distance increases (Si1/Si3 322.5(2) pm) and the four-membered ring becomes almost planar with a folding angle of 4.7°.[74] This comparison indicates that homoconjugative effects determine the structure of the 2π-electron cation **3**, while allylic conjugation is important for the 3π-electron radical **26** (see Fig. 8).

2. Solid State Structure of Intramolecularly Stabilized R_3E^+ Cations

The high electrophilicity of the positively charged element can be modified by intramolecular donation from remote donor substituents. This interaction leads to solvent-free cations with coordination numbers for the positively charged element >3 and to a considerable electron transfer from the donor group to the element. Frequently used donor substituents utilize heteroatoms with lone pairs (e.g. amino, hydrazino, methoxy, carboxy, phosphino, etc.), in many cases in combination with pincer-type topology of the ligand, for the stabilization of the cationic center.[173] These strongly stabilized cations are beyond the scope of this review and instead we will concentrate on few examples where we have weak donors such as CC multiple bonds, which stabilize the electron-deficient element atom.

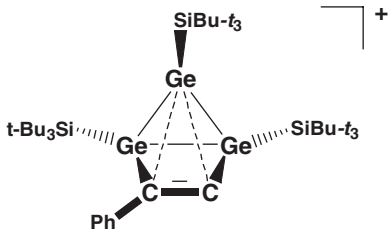

6

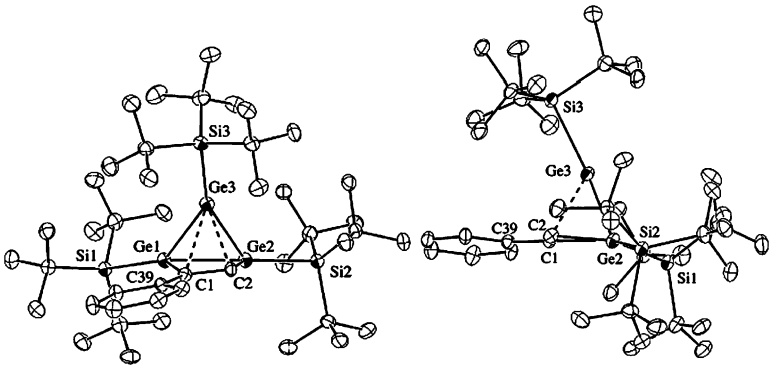

FIG. 9. ORTEP drawing of **6**, left front view on the Ge_3 cycle, right side view. Hydrogen atoms are omitted for clarity. Selected bond lengths (Å): Ge1–Ge2 = 247.65(10), Ge1–Ge3 = 246.71(10), Ge2–Ge3 = 247.40(10), Ge3–C1 = 241.5(7), Ge3–C2 = 225.4(7), C1–C2 = 141.1(9). Selected bond angles (deg): Ge1–Ge2–Ge3 = 59.78(3), Ge2–Ge3–Ge1 = 60.16(3), Ge3–Ge1–Ge2 = 60.06(3). (Reprinted with permission from Ref. 21. Copyright 2003, American Chemical Society.)

A intriguing example for the intramolecular interaction between an germylium ion and a remote C═C double bond was recently provided by Sekiguchi and coworkers.[21] The bishomocyclopropenylium-type cation **6** was synthesized by halogen abstraction from the corresponding germyl bromide **5** (see Scheme 1) and the crystal structure of the TPFPB salt of **6** was determined by X-ray crystallographic analysis (Fig. 9). The germyl cation **6** has a highly strained "housene"-type skeleton, which consists of a Ge_3 equilateral triangle and a Ge_2C_2 four-membered ring. The ridge Ge3 atom is strongly bended towards the C1═C2 double bond with a folding angle between the Ge_3 plane and the mean Ge_2C_2 plane of 67°. This folding results in short Ge3–C1 [241.5(7) pm] and Ge3–C2 [225.4(7) pm] interatomic distances, clearly below the sum of the van der Waals radii of Ge and C(sp^2). In addition, the C1═C2 bond [141.1(9) pm] is considerably longer than a regular C═C double bond in related compounds (135.7 pm[174]). These structural particularities of cation **6** indicate the effective interaction between the empty 4p-orbital on the Ge atom and the π-orbital of the C═C double bond. A natural bond analysis based on a structure of the silyl-substituted model compound for cation **6**, which was optimized at the density functional B3LYP/dzp level of theory, indicates appreciable electron transfer from the C1═C2 double bond to the formally empty 4p orbital at Ge3 (occupancy 0.42 electrons) and predict Wiberg bond orders for the Ge3–C1, Ge3–C2 and C1–C2 bonds of 0.37, 0.46 and 1.39, respectively. In addition, nucleus independent chemical shift calculations [NICS(1)] for the silyl-substituted model compound indicate a diatropic ring current in **6**. Thus, structural as well as theoretical evidence is provided for the 2π-bishomoconjugative nature of cation **6**. Additional support comes from the ^{13}C NMR spectroscopic data (see Section III.B.4).

The stannyl cation in zwitterion **80** is only stabilized by side-on coordination with the remote C≡C triple bond. The crystal structure of **80** revealed a pyramidalized tin center with the sum of valence angles of 351.1° (see Table XIV). The coordination of the tin atom to the C≡C triple bond is unsymmetrical and the SnC distances

TABLE XIV
STRUCTURAL DATA OF INTRAMOLECULAR COORDINATED R_3E^{+} [a]

Compound	d(R–E) (pm)	Σα(RER)[b] (deg)	d(E–X)[c] (pm)	Coordination number	Ref.
74[TPFPB]	221.1(15), 227(2) 231.0(19)	360.0	293.4(14), 285.5(14) 288.9(17), 287.5(15)	3 + 2	53
73[TPFPB]	221.4(4), 221.9(5) 222.3(4)	359.97(16)	296.9(5),298.9(4) 250.6(5)	3 + 2	40
81	220.3(3), 222.2(7) 220.6(7)	355.7(3)	264.8(6), 246.7(6)	3 + 1	161
80	211.6(4), 212.8(5) 213.6(5)	351.1	233.9(4), 252.3(5)	3 + 1	158
6[TPFPB][e]	247.65(10), 247.40(10)[d], 247.2(2)[f]	359.2(5)	225.4(7), 241.5(7)	3 + 1	21
	246.81(10), 247.54(10)[d], 247.1(2)[f]	359.2(5)	225.0(7), 239.6(6)	3 + 1	21

[a]Structural data from X-ray analysis.
[b]Sum of the three bond angles of the element and its three nearest substituents, tetrahedral: $\Sigma = 328.5^{\circ}$, trigonal planar: $\Sigma = 360^{\circ}$.
[c]Distances to the fourth and fifth substituent, in the case of multiple bonds both centers are given.
[d]Innercyclic Ge–Ge distance.
[e]Two independent molecules in the unit cell.
[f]Exocyclic Ge–Si distance.

(264.8, 246.7 pm) are too long for a regular SnC bond [210 pm for SnC(sp)], but are well below the sum of the van der Waals radii of Sn and C(sp). The direct bonding relation between the cationic tin and the C≡C triple bond is also apparent from the sizeable ^{1}J(SnC) couplings detected by NMR spectroscopy.[158]

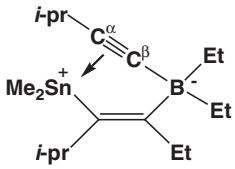

80

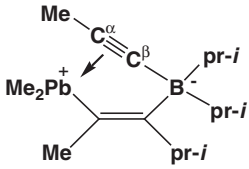

81

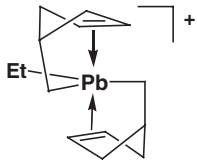

74

The closely related lead analogue **81** shows essentially the same structural features, but the lead atom in **81** is less pyramidalized (355.7°, see Table XIV), which indicates weaker coordination. The NMR spectroscopic parameters for **81**, such as ^{207}Pb NMR chemical shift and scalar Pb–C(sp) coupling constants (see Section III.B.3) clearly demonstrate however the side-on complexation of the plumbyl cation by the C≡C triple bond in zwitterions **81**.[161]

The ''spironorbornyl cation'' **74** is best described as an intramolecular bisalkene complex of a plumbylium ion (see Fig. 10 and Table XIV).[53] The Pb atom in cation **74** has a distorted trigonal–bipyramidal coordination geometry (Fig. 10b). The planarity of the trigonal base is indicated by summation of the three C–Pb–C angles

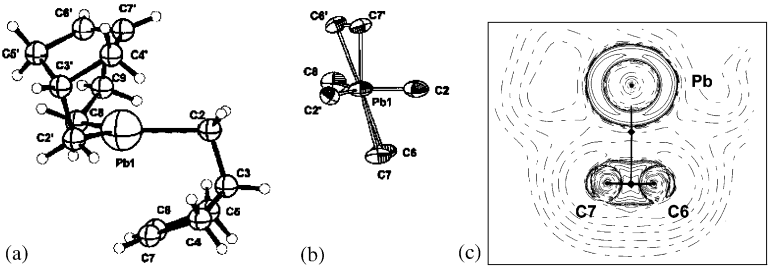

FIG. 10. Molecular and electronic structure of cation **74**. (a) Perspective view on the cation **74**. (b) Coordination sphere of the Pb atom, selected interatomic distances (pm) and angles (deg): Pb–(center C6′, C7), 281.7; Pb–(center C6; C7′), 280.7; Pb1–C2, 227(2); Pb1–C2; 221.1(15); Pb1–C8, 231.0(19); C6–C7, 133(2); C6′–C7′; 132(2); (center C6, C7)–Pb–(center C6′, C7′), 163.6. (c) Contour plots of the Laplacian distribution $[\nabla^2\rho(r)]$ in the plane containing the atoms Pb, C6 and C7. Solid and dotted lines designate regions of local charge concentration and depletion, respectively. The bond paths are indicated by the solid back lines, bond critical points are marked with a black square. (Reprinted with permission from Ref. 53. Copyright 2003, Wiely-VCH.)

to 360.0°. The coordination sphere of lead is completed by the C═C double bonds of the two cyclopentenemethyl substituents, which take up the apical positions. The steric requirements of this intramolecular interaction enforce the deviations from the ideal trigonal–bipyramidal coordination. This spatial arrangement places seven carbon atoms at distances less than 290 pm around the positively charged Pb atom. A topological "atoms in molecules" analysis of the electron density for cation **74** (see Fig. 10c) reveals a T-shaped electron density distribution between the Pb atom and the C═C double bond, typical for π-type complexes between strong Lewis acids and C═C multiple bonds.[53]

The related intramolecular monoalkene complexes of R_3E^+ cations, the norbornyl cations of group 14 elements (Si → Pb), have been synthesized with TPFPB as counteranion and characterized by NMR spectroscopy in solution supported by quantum mechanical calculations.[40] Only the acetonitrile complex, **73**, of the plumbanorbornyl cation **13** could be characterized by X-ray crystallography. Similar to the structure of the plumbyl cation **74**, the Pb atom in the acetonitrile complex **73** adopts a trigonal–bipyramidal coordination sphere with the C═C double bond and the acetonitrile in the apical positions and the Pb atom in the center of the trigonal plane (see Fig. 11 and Table XIV, for details).[40]

3. Solid State Structure of Cation/Anion Aggregates of R_3E^+ Cations

The solid state structure of most carborane salts deriving from hydrocarbon solutions is dominated by cation/anion interactions. For example the *n*-Bu_3Sn^+ salt of the permethylated carborane $[CB_{11}Me_{12}]^-$ forms infinite columns of alternating *n*-Bu_3Sn^+ and $[CB_{11}Me_{12}]^-$ ions,[68] similar to those of covalent R_3SnX compounds. This alignment which results in a trigonal–bipyramidal coordination sphere for the Sn atom with two apical positions occupied by methyl groups of the anion (see Fig. 12 and Table XV). In contrast to the neutral tin(IV) compounds where strong covalent interactions give short SnX bonds, the average axial distance between the

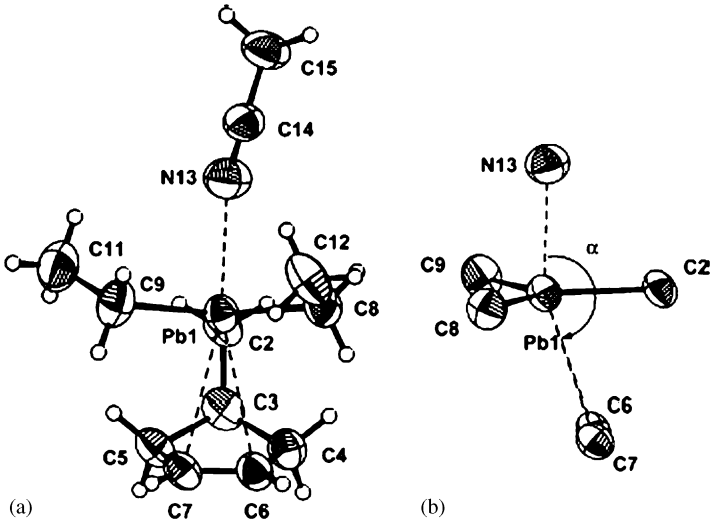

FIG. 11. (a) Molecular structure of cation **73** in the crystal. (b) Coordination sphere of the Pb atom in cation **73**. Selected bond lengths (pm) and bond angles (deg): Pb1–C2, 222.3(4); Pb1–C8, 221.9(5); Pb1–C9, 221.4(4); Pb–(center C6, C7), 290.4; Pb1–N13, 250.6(5); C6–C7, 132.7(5); (center C6, C7)–Pb–N13, 159.0; N13–Pb–C2, 86.80(14). (Reprinted with permission from Ref. 40. Copyright 2003, American Chemical Society.)

Sn atom and the methyl carbon atoms of the anion are large (281 pm), clearly longer than a covalent Sn–C bond (214 pm) but much shorter than the sum (417 pm) of the van der Waals radii of a methyl (200 pm) and tin (217 pm).[175]

The tin atom in $[n\text{-}Bu_3Sn^+][CB_{11}Me_{12}^-]$ is displaced from the center of the trigonal plane toward one of the anions by 3.2 pm, which results in a pyramidalization of the $n\text{-}Bu_3Sn^+$ cation. This is also indicated by the sum of the C–Sn–C angles, which is clearly smaller than the 360° expected for planarity of the $n\text{-}Bu_3Sn^+$ cation.[68] Similar structures have been recently found for the $[CB_{11}Me_{12}^-]$ salts of the most simple organometallic cations of germanium, tin and lead, Me_3E^+ (E = Ge, Sn, Pb). The cations were synthesized from the hexamethyldielement compounds (Ge, Sn) or from Me_4Pb by reaction with the one-electron oxidant $[CB_{11}Me_{12}]^\bullet$ in pentane.[69] The obtained amorphous white solids, insoluble in hydrocarbons, were investigated by trapping experiments and by NMR spectroscopy. Significant structural information was obtained from an EXAFS study. Two sets of E–C distances, a short one and a long one, were found by EXAFS of the salts $[Me_3E^+][CB_{11}Me_{12}^-]$ (E = Ge, Sn, Pb). The first-shell peak is assigned to the methyl carbon directly attached to the metal. As expected, it moves progressively to longer distance on going from Ge to Sn and to Pb (194, 212 and 217 pm, respectively; see Fig. 13 and Table XV). This M–C^α-(sp^3) distance is for Sn and in particular for Pb shorter than a normal M–C^α-(sp^3) bond (194.5 (Ge–C), 214 (Sn–C) and 225 pm (Pb–C)[151]). The precision of EXAFS is typically 0.4 pm,[176] therefore this small difference is significant. For all three cations, the longer E–C distances (250–300 pm) can only be interpreted as the distance between the Me_3E^+ cation and the carbon atom of a

FIG. 12. Part of an infinite column of alternating cations and anions as a detail of the crystal structure of [*n*-Bu_3Sn^+][$CB_{11}Me_{12}$]. Thermal ellipsoids are drawn at 50% probability level. Hydrogen atoms and one component of the disordered butyl groups are omitted for clarity, Sn and B atoms are gray and C atoms are black. (Reprinted with permission from Ref. 68. Copyright 2000, American Chemical Society.)

methyl group of the $CB_{11}Me_{12}^-$ anion with which the cation interacts. These distances are longer than the normal M–C bond lengths but are much shorter than the sum of van der Waals radii of Ge (200 pm), Sn (217 pm) or Pb (220 pm) and of a methyl group (200 pm).[175] The cation/anion interaction energy decreases from Ge to Pb and as a consequence different structures are adopted. In Fig. 13 possible structures on the basis of the EXAFS analysis for all three salts are shown.

For [Me_3Pb^+] [$CB_{11}Me_{12}^-$] a nearly symmetric, trigonal–bipyramidal arrangement for the Me_3Pb^+ cation with rather weak coordination to the two axial methyl groups provided by the $CB_{11}Me_{12}^-$ anions is suggested. In contrast, for the tin compound a clearly unsymmetrical coordination sphere with the Sn atom displaced from the center of the trigonal plane along the central axis, which leads to two different Sn–Me(anion) distances is proposed. The EXAFS analysis for the germanium compound indicates the formation of discrete anion/cation aggregates and the most likely coordination sphere for the germanium is a distorted tetrahedral environment (see Fig. 13).

In a series of papers Reed and colleagues present the solid state structures of a series of simple trialkyl-substituted silyl cations with halogenated carborane anions

TABLE XV
STRUCTURAL DATA FOR COMPOUNDS OF THE TYPE $[R_3E^+]$ [ANION] AND OF $Ph_3SiOClO_3$ FOR COMPARISON[a]

Compound	D(R–E) (pm)	Σα(RER)[b] (deg)	d(E/3R)[c] (pm)	d(E–X)[d] (pm)	Coordination number	Ref.
$[Me_3Ge][CB_{11}Me_{12}]$[e]	194			249	4	69
$[Me_3Sn][CB_{11}Me_{12}]$[e]	212			277, 302	3+2	69
$[Me_3Pb][CB_{11}Me_{12}]$[e]	217			290	3+2	69
$[Bu_3Sn][CB_{11}Me_{12}]$[f]	207	353	3.2	281	3+2	68
$[Bu_3Sn][CB_{11}Me_{12}]$[e]	216			276	3+2	69
$[(i\text{-}pr_3Si)][Cl_6CB_{11}H_6]$	184.8(9)	351.8(4)	3.07	232.3(3)	4	38
$[(i\text{-}pr_3Si)][Br_6CB_{11}H_6]$	186(2)	351.0(13)	3.00	247.9(9)	4	114, 138
$[(i\text{-}pr_3Si)][I_6CB_{11}H_6]$	188.3(21)	346.8(9)	4.00	266.1(6)	4	38
$[Et_3Si][Br_6CB_{11}H_6]$[g]	183(2)	345.0(10)	4.19	244.4(7)	4	114
	184(2)	349.0(9)	3.48	243.0(6)	4	114
$[(t\text{-}Bu_3Si)][Br_6CB_{11}H_6]$	189(2)	348.7(7)	3.71	246.5(5)	4	114
$[(t\text{-}Bu_2MeSi)][Br_6CB_{11}H_6]$	186(4)	345.8(7)	4.08	246.6(12)	4	114
$[i\text{-}pr_3Si][Br_5CB_9H_5]$	347.4(20)		4.0	182(2)	4	127
$Ph_3SiOClO_3$	184.6(5)	340.5(2)	4.79	174.5(5)	4	177

[a]Structural data from X-ray analysis if not indicated otherwise.
[b]Sum of the three bond angles of the element and its three nearest substituents, tetrahedral: $\Sigma = 328.5^\circ$, trigonal planar: $\Sigma = 360^\circ$.
[c]Distance of the element and the plane spanned by the atoms in α-position.
[d]Distance to the fourth substituent.
[e]EXAFS data.
[f]X-ray data, disordered crystal.
[g]Two independent molecules in the unit cell.

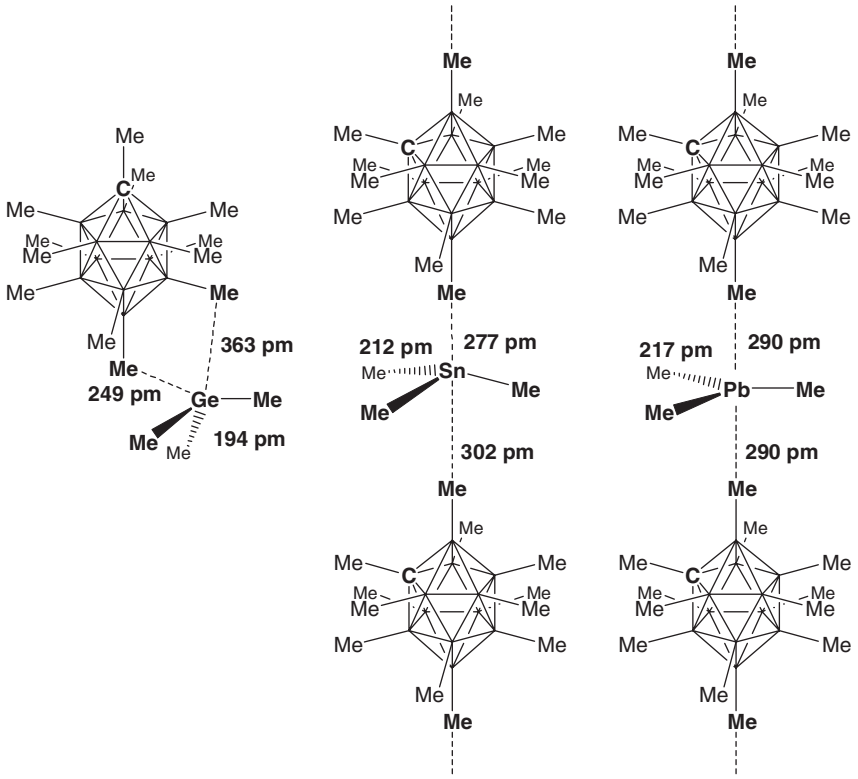

FIG. 13. Possible structures of $[Me_3E]$ $[CB_{11}Me_{12}]$ proposed on the basis of EXAFS results. (a) $[Me_3Ge]$ $[CB_{11}Me_{12}]$, (b) $[Me_3Sn]$ $[CB_{11}Me_{12}]$, (c) $[Me_3Pb]$ $[CB_{11}Me_{12}]$.[69]

(see Table XV and Fig. 14).[11,38,114,127,138] All structures show clear indications of cation/anion interactions, which result in discernible distortions of the R_3Si^+ group from planarity and an effective $3+1$ coordination for the silicon atom. The sum of the bond angles around the silicon atom $\Sigma\alpha$(RSiR) was used to estimate the degree of interaction between silyl cation and the carborane anion. According to this measure, the closest approach to a silylium ion devoid of any distortions was achieved for the *i*-pr_3Si^+ cation and the $[CB_{11}H_6Cl_6^-]$ anion, see Table XV.[38]

4. Solid State Structure of Cation/Solvent Complexes of R_3E^+ Cations

Several solid state structures of R_3E^+(solvent) complexes are known and structural data of significant examples are given in Table XVI. Considerable attention was paid to the structure of the TPFPB salt of the silylated toluenium ion **82** and its interpretation.[36,37,108,126,131,133,135,136] The molecular structure of cation **82** is characterized by a significantly pyramidalized Et_3Si group (sum of the bond angles around Si, $\Sigma\alpha$(Si): 341–342°) and the fourth-coordination side of the silicon atom is occupied by a toluene molecule. The Si–C^{ipso} (toluene) is 217–219 pm, clearly longer

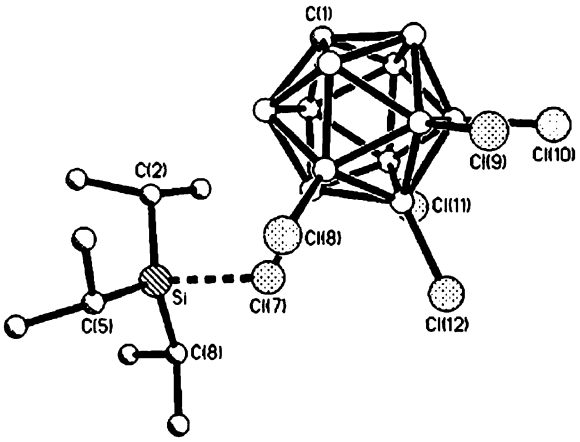

FIG. 14. Perspective view of $[ipr_3Si][CB_{11}H_6Cl_6]$. (Reprinted with permission from Ref. 38. Copyright 1996, American Chemical Society.)

than regular Si–C(aryl bonds (187.9 pm[172]), but also significant smaller than the sum of the van der Waals radii.[36,37]

These features of **82** are typical for many cation/solvent complexes of silylium and germylium ions and they change gradually with the nature of the coordinating solvent and with the cationic group. Hensen's silylated pyridinium iodide **4** with a strongly pyriamidalized trimethylsilyl group and a relatively short Si–N separation marks the strongly coordinating end of this spectrum[20] and the germylated acetonitrilium ion **83**, is, according to the structural data, an example for a more loosely bonded complex.[72] In the nitrilium ion **83**, synthesized by reaction of germylium ion **22** with acetonitrile, the germanium atom is only slightly pyramidalized [$\Sigma\alpha$(Ge): 358.3°] and the Ge/N separation is comparatively large (see Table XVI and Fig. 15).

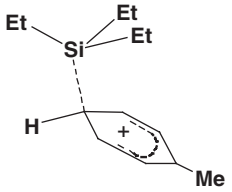

82

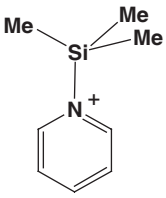

4

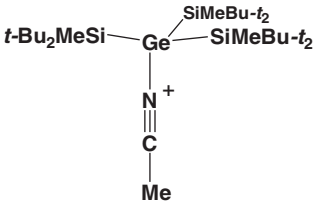

83

While for silyl and germyl cation complexes tetracoordination of the element prevails, stannyl cations favor pentacoordination. That is, the trigonal–bipyramidal environment of the Sn atom in the diwater complex of the stannylium ion Me_3Sn^+ $[Me_3Sn(H_2O)_2]^+$ **84**[178] has its counterpart in the tetrahedral structure of the protonated silanol **85**.[116] The structure of the bis(acetonitrile)tricyclohexyltin hexafluoroantimonate **86** SbF_6[179] reveals pentacoordination for the tin atom,[180] while all

TABLE XVI
STRUCTURAL DATA FOR COMPOUNDS OF THE TYPE $[R_3E^+(\text{solvent})][\text{anion}]$[a]

Compound	d(R–E) (pm)	$\Sigma\alpha$(RER)[b] (deg)	D(E–X)[c] (pm)	Coordination number	Ref.
82 [$TPFPB^-$][d]	185(1)	341.4(5)	219(1)	4	36, 37
	185(1)	342.5(6)	217(1)	4	36, 37
83 [$TPFPB^-$]	252.70(6); 252.10(6)	358.3	201.99(17)	4	72
	256.14(6)				
[(*t*-Bu_3Si)(*t*-BuCN)][$TFPB^-$]	190.1(6)	347.7	182.2(5)	4	67
[(*t*-Bu_3Ge)(*t*-BuCN)][$TFPB^-$]		350.7	197.5(7)	4	67
[(*i*-pr_3Si)(MeCN)][$Br_5CB_9H_5^-$]		346.7(13)	182(2)	4	127
85 [$Br_6CB_{11}H_6^-$]	189.2(15)	348.0(6)	177.9(9)	4	116
[Me_3SiOEt_2][$TFPB^-$]	183.6(5)		177.7(3)	4	126
4 [I^-]	186.7(9)	340.4(5)	185.8(9)	4	20
86 [SbF_6^-]	215.9(3)	359.7(1)	237.4(3), 247.2(3)	5	179
84 [$C_5(CO_2Me)_5^-$]	217.8(12)		229.5(4), 232.6(5)	5	178

[a]Structural data from X-ray analysis.
[b]Sum of the three bond angles of the element and its three nearest substituents, tetrahedral: $\Sigma = 328.5^\circ$, trigonal planar: $\Sigma = 360^\circ$.
[c]Distances to the fourth and fifth substituent.
[d]Two independent molecules in the unit cell.

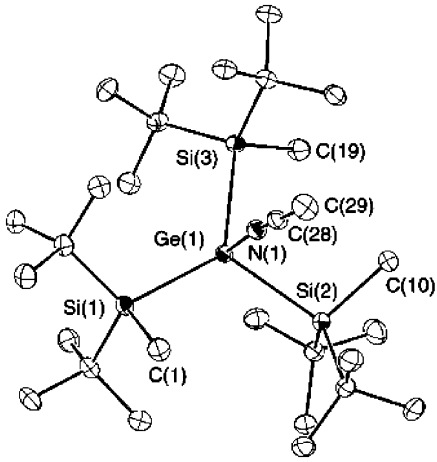

FIG. 15. Molecular structure of nitrilium ion **83** (ORTEP plot, thermal ellipsoids set at 30% probability; hydrogen atoms omitted for clarity). Selected bond lengths (pm) and angles (deg): Ge(1)–N(1), 201.99(17); C(28)–C(29), 144.7(3); Si(3)–Ge(1)–Si(1), 128.682(19); Si(3)–Ge(1)–Si(2) 110.562(19); Si(1)–Ge(1)–Si(2), 119.11(2); N(1)–Ge(1)–Si(1), 92.14(5); N(1)–Ge(1)–Si(2), 92.20(5); N(1)–Ge(1)–Si(3), 98.27(5). (Reprinted with permission from Ref. 72. Copyright 2003, Wiley-VCH.)

structurally characterized germyl and silyl cation complexes with nitriles indicate a tetrahedral coordination of the germanium and silicon atom.

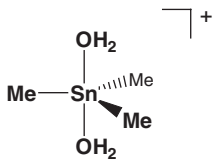

84

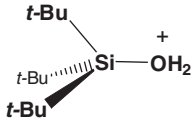

85

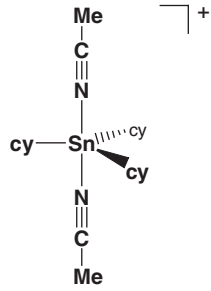

86

IV
A CHEMISTRY OF R_3E^+ CATIONS

The isolation and characterization of stable trivalent cations of the group 14 elements Si, Ge, Sn, which are free of any interaction with solvent, counteranion or neighboring groups, are milestones in organoelement chemistry. These results finally answer the question for the pure existence of these species in the condensed phase. The quest for a chemistry of these highly reactive cations, however remains. Clearly to explore the chemistry of organometallic group 14 cations it is necessary

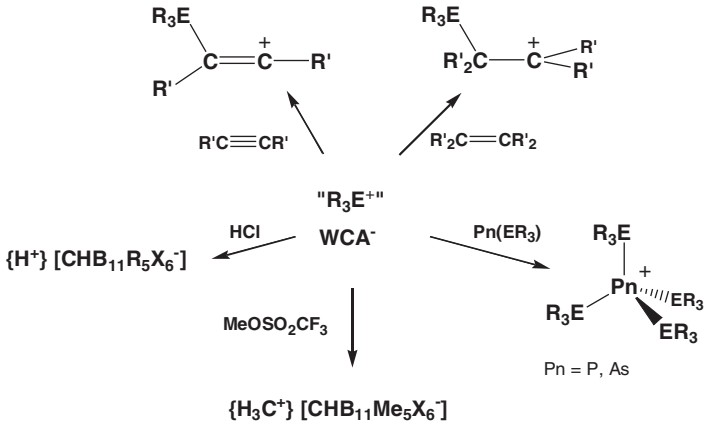

SCHEME 19. Some recent application of organometallic group 14 cations.

to reduce the steric bulk, which was an indispensable prerequisite for the kinetic stabilization and finally isolation of tricoordinated group 14 cations. Consequently, intra- or intermolecular interactions of the cations with electron-donating groups or molecules will be important and a chemistry of cationic R_3E^+ species of group 14 elements will be dominated by either intra- or intermolecular stabilized cations. The electron-donating group or molecule modifies the electron deficiency of the cationic element center and lowers the reactivity. The synthetic challenge is, to find suitable sytems, which allow to control and to exploit the enormous electrophilicity of these cations. Although this chemistry is at its infancy there are already quite spectacular results in various fields. For example, it has been shown that trialkylsilyl arenium ions [R_3Si^+/arene] may react as a synthetic equivalent of trialkylsilylium ions and can be used as highly active silylating agents (Scheme 19). The trialkylsilylium ion adds instantaneously to CC multiple bonds to yield silylated carbenium ions **87**[181] and vinyl cations **88**.[182] Similarly, persilylated onium ions of phosphorus and arsenic **89** are formed by transfer of the trimethylsilyl group from trimethylsilyl arenium to the corresponding phosphanes and arsanes, a reaction which is not possible using conventional trimethylsilylating agents.[126,183] The synthesis of the stable secondary β-trimethyltin-substituted carbocation **90** is thought to proceed by addition of transient trimethylstannylium to the C═C double bond of the propene $(Me_3Si)CH{=}CHCH(SiMe_3)SnMe_3$.[184]

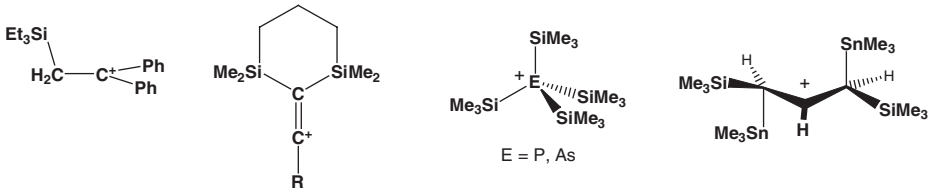

87 88 89 90

Reed and co-workers utilized the silylium carboranate salts to generate novel Brønstedt superacids based on carborane anions as conjugate bases by reaction of the salts with liquid HCl [Eq. (7)].[185] These carborane superacids are able to cleanly protonate C_{60} and benzene at room temperature to yield HC_{60}^{+}[185] and benzenium $C_6H_7^{+}$[186] and are the strongest isolable Brønstedt acids presently known.[187] Similarly, the same group developed the most potent electrophilic methyl transfer agent by reaction of the silyl cation salt $[ipr_3Si^{+}][HCB_{11}Me_5Br_6^{-}]$ with methyltriflate [Eq. (8)].[188] The product $H_3C(HCB_{11}Me_5Br_6)$ abstracts hydride from simple branched alkanes and forms at room temperature the corresponding tertiary carbocations as isolable carborane salts.[189]

$$[Et_3Si]CHB_{11}R_5X_6](s) + HCl(1) \rightarrow Et_3SiCl(g) + H(CHB_{11}R_5X_6)(s) \qquad R = H,\ Me;\ X = Cl,\ Br,\ I \tag{7}$$

$$[i\text{-}pr_3Si][CHB_{11}Me_5Br_6](s) + H_3COSO_2CF_3 \rightarrow i\text{-}pr_3SiOSO_2CF_3 + H_3C(CHB_{11}Me_5Br_6) \tag{8}$$

Owing to the high Lewis acidity the group 14 organometallic cations are polymerization catalysts par excellence.[184,190] Silanorbonyl cations[191] and triethylsilyl arenium[181] have been shown to be efficient catalysts for metal-free hydrosilylation reactions. Chiral silyl cation complexes with acetonitrile have been applied as cata - lysts in Diels Alder-type cyclization reactions[130,192] and intramolecularly stabilized tetracoordinated silyl cations have been successfully used as efficient catalysts in Mukaiyama-type aldol reactions.[193]

The reactions quoted in the last paragraph and partly summarized in Scheme 19, all exploit the high electrophilicity of organometallic group 14 cations, and the reactivity follows conventional routes. Quite recently, however, a novel-type of chemistry for R_3E^{+} cations came into attention. The decisive step in Jutzi's synthesis of η^5-Cp*Si^{+}, **91**, by protonation of decamethylsilicocene, Cp^*_2Si, **28**,[194] is most likely the fragmentation of the intermediate $Cp^*_2Si^{+}$-H cation **29** into the neutral Me_5C_5H and the cation η^5-Cp*Si^{+} (see Scheme 20). The cation **91** can be regarded as synthetic equivalent for the singly coordinated silylidynium η^1-Cp*Si, **92**.

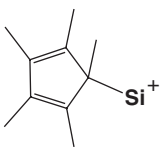

92

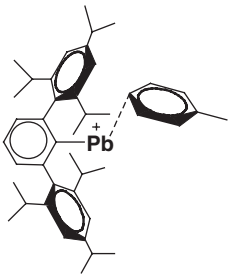

41

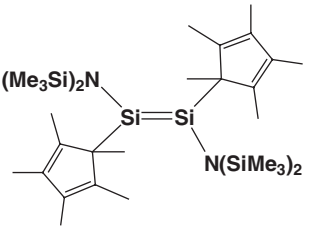

93

This type of α-elimination with the generation of a singly coordinated four-valence-electron compound is rather unusual in silylium ion chemistry, only two

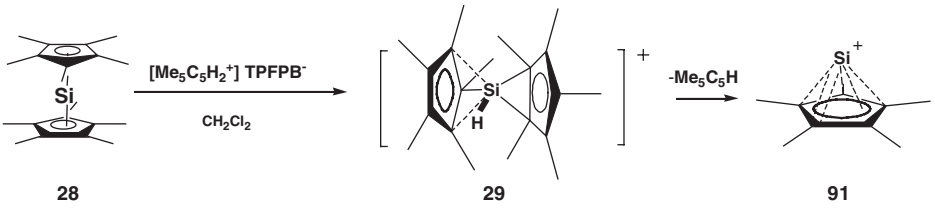

SCHEME 20. Synthesis of η^5-Cp*Si$^+$.[194]

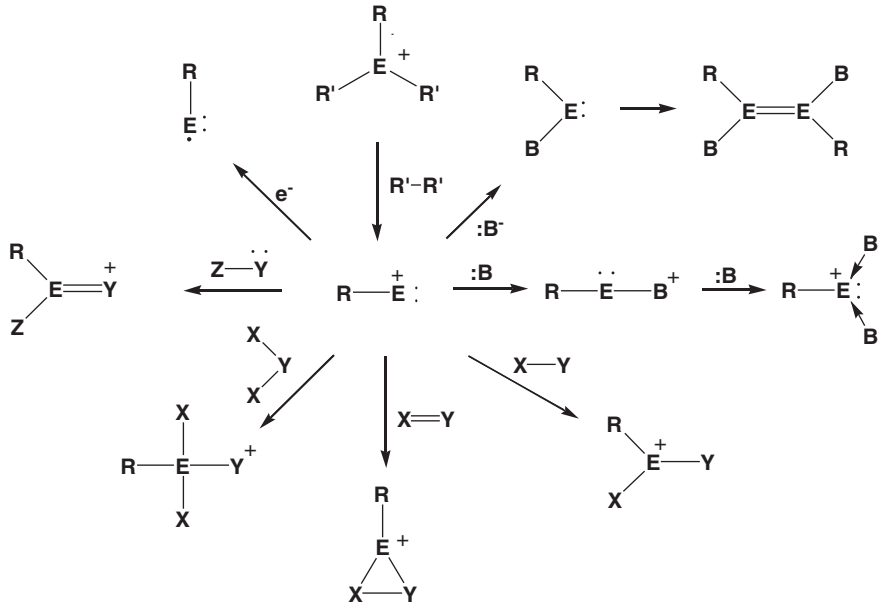

SCHEME 21. Generation of four-valence-electron, singly coordinated organometallic group 14 cations by a 1,1-elimination reaction from R_3E^+ cations and its potential reaction scheme.[195,196]

other examples have been reported so far (see Section III.A.1).[88,89,195,196] Computations[82,83] propose that this type of fragmentation of trivalent group 14 organometallic cations is preferred for the heavier elements of group 14 and with the toluene complex of the terphenyl-substituted plumbylidynium **41** the first example of this type of compounds has been recently synthesized.[90] Gaspar recently pointed out the synthetic potential of these novel low-valent reactive intermediates, which is summarized in Scheme 21.[195,196] The intermediate formation of these species gives access to novel highly intriguing compounds and opens new synthetic approaches to heavy carbene analogues, to E=E unsaturated compounds, to trivalent R_3E^+ cations and to neutral element(I) compounds. The synthesis of the disilene **93** from reaction of the cation η^5-Cp*Si$^+$, **91**, with bis(trimethylsilyl)amide shows in principle the applicability of the suggested reactivity scheme.[194] Clearly, the chemistry of organometallic group 14 cations is only at its beginning and there is still much to investigate!

LIST OF ABBREVIATIONS

bco	bicyclooctyl
Cp	cyclopentadienyl
Cp*	pentamethylcyclopentadienyl
Cy	cyclohexyl
Dur	2, 3, 5, 6 tetramethylphenyl
DMPU	1,3-dimethyl,2-4,5,6-tetrahydro-2(1H)-pyrimidone
DMSO	dimethyl sulfoxide
FT ICR	Fourier Transform Ion Cyclotron Resonance
FT NMR	Fourier Transform Nuclear Magnetic Resonance
HMPA	hexamethylphosphoric triamide
IGLO	Individual Guage for Localized Orbitals
Mes	2, 4, 6-trimethylphenyl
Tip	2, 4, 6-triisopropylphenyl
TPN	1, 2, 3, 4-tetraphenylnaphthalene
$TPFPB^-$	tetrakis(pentafluorophenyl)borate
$TFPB^-$	tetrakis[3, 5-bis(trifluoromethyl)phenyl]borate
$TSFPB^-$	tetrakis[4-{tert-butyl(dimethyl)silyl}-2,3,5,6-tetrafluorophenyl]borate
TPB^-	Tetraphenylborate
Tol	Tolyl
WCA^-	weakly coordinating anion

Acknowledgements

Our contributions to the chemistry of organometallic cations of group 14 chemistry were supported by the Deutsche Forschungsgemeinschaft (DFG) and the German Israeli Foundation for Scientific Research and Development (GIF). The author wishes to thank the Professors C. A. Reed, A. Sekiguchi, J. Michl and K. Jurkschat for kindly supplying information prior to publication.

References

(1) (a) Sekiguchi, A.; Kinjo, R.; Ichinohe, M. *Science* **2004**, *305*, 1755. (b) Wiberg, N.; Niedermayer, W.; Fischer, G.; Nöth, H.; Suter, M. *Eur. J. Inorg. Chem.* **2002**, 1066. (c) Wiberg, N.; Vasisht, S. K.; Fischer, G.; Mayer, P. *Z. Anorg. Allg. Chem.* **2004**, *630*, 1823. (d) Stender, M.; Phillips, A. D.; Wright, R. J.; Power, P. P. *Angew Chem. Int. Ed.* **2002**, *41*, 1785. (e) Phillips, A. D.; Wright, R. J.; Olmstead, M. M.; Power, P. P. *J. Am. Chem. Soc.* **2002**, *124*, 5930. (f) Pu, L.; Twamley, B.; Power, P. P. *J. Am. Chem. Soc.* **2000**, *122*, 3524. (g) Power, P. P. *J. Chem. Soc. Chem. Commun.* **2003**, 2091.
(2) Olah, G. A. *J. Org. Chem.* **2001**, *66*, 5943.
(3) (a) Norris, J. F. *Am. Chem. J.* **1901**, *25*, 117. (b) Kehrmann, F.; Wentzel, F. *Chem. Ber.* **1901**, *34*, 3815.
(4) Lambert, J. B.; Zhao, Y.; Wu, H.; Tse, W. C.; Kuhlmann, B. *J. Am. Chem. Soc.* **1999**, *121*, 5001.
(5) Lambert, J. B.; Zhao, Y. *Angew. Chem. Int. Edit. Engl.* **1997**, *36*, 400.
(6) Müller, T.; Lambert, J. B.; Zhao, Y. *Organometallics* **1998**, *17*, 278.
(7) Kraka, E.; Sosa, C. P.; Gräfenstein, J.; Cremer, D. *Chem. Phys. Lett.* **1997**, *279*, 9.
(8) Sekiguchi, A.; Matsuno, T.; Ichinohe, M. *J. Am. Chem. Soc.* **2000**, *122*, 11250.
(9) Sekiguchi, A.; Tsukamoto, M.; Ichinohe, M. *Science* **1997**, *275*, 60.

(10) Lickiss, P. D. (Z. Rappoport, Y. Apeloig, Eds.), *The Chemistry of Organic Silicon Compounds* Vol. 2, **1998**, Wiley & Sons, Chichester, p. 557.
(11) Reed, C. A. *Acc. Chem. Res.* **1998**, *31*, 325.
(12) Lambert, J. B.; Kania, L.; Zhang, S. *Chem. Rev.* **1998**, *95*, 1191.
(13) Maerker, C.; Schleyer, P. v. R. (Z. Rappoport, Y. Apeloig, Eds.), *The Chemistry of Organic Silicon Compounds* Vol. 2, **1998**, Wiley & Sons, Chichester, p. 513.
(14) Houk, K. N. *Chemtracts Org. Chem.* **1993**, *6*, 360.
(15) Schleyer, P. v. R. *Science* **1997**, *275*, 39.
(16) Belzner, J. *Angew. Chem. Int. Edit.* **1997**, *36*, 1277.
(17) Zharov, I.; Michl, J. (Z. Rappoport, Y. Apeloig, Eds.), *The Chemistry of Organic Germanium, Tin, and Lead Compounds* Vol. 2, **2002**, Wiley & Sons, Chichester, p. 633.
(18) Prakash, G. K. S., Schleyer, P. v. R., Eds., *Stable Carbocation Chemistry*, Wiley, New York, 1997.
(19) Olah, G. A.; Mo, Y. K. *J. Am. Chem. Soc.* **1971**, *93*, 4942.
(20) (a) Hensen, K.; Zengerley, T.; Pickel, P.; Klebe, G. *Angew. Chem. Int. Edit. Engl.* **1983**, *32*, 725. (b) Hensen, K.; Zengerley, T.; Pickel, P.; Klebe, G. *Angew. Chem. Suppl.* **1983**, 973.
(21) Ishida, Y.; Sekiguchi, A.; Kabe, Y. *J. Am. Chem. Soc.* **2003**, *125*, 11468.
(22) Bartlett, P. D.; Condon, F. E.; Schneider, A. *J. Am. Chem. Soc.* **1944**, *66*, 1531.
(23) Deno, N. C.; Peterson, H. J.; Gaines, G. S. *Chem. Rev.* **1960**, *60*, 7.
(24) Corey, J. Y. *J. Am. Chem. Soc.* **1975**, *97*, 3237.
(25) Lambert, J. B.; Kuhlmann, B. *J. Chem. Soc. Chem. Commun.* **1992**, 931.
(26) Lambert, J. B.; Ciro, S. M.; Stern, C. L. *J. Organomet. Chem.* **1995**, *499*, 49.
(27) Kira, M.; Oyamada, T.; Sakurai, H. *J. Organomet. Chem.* **1994**, *471*, C4.
(28) Blackwell, J. M.; Piers, W. E.; McDonald, R. *J. Am. Chem. Soc.* **2002**, *124*, 1295.
(29) Henderson, L. D.; Piers, W. E.; Irvine, G. J.; McDonald, R. *Organometallics* **2002**, *21*, 340.
(30) Mayr, H.; Basso, N.; Hagen, G. *J. Am. Chem. Soc.* **1992**, *114*, 3060.
(31) Apeloig, Y.; Merin-Aharoni, O.; Danovich, D.; Ioffe, A.; Shaik, S. *Isr. J. Chem.* **1993**, *33*, 387.
(32) Chojnowski, J.; Fortuniak, W.; Stanczyk, W. A. *J. Am. Chem. Soc.* **1987**, *101*, 7776.
(33) Nishinaga, T.; Izukawa, Y.; Komatsu, K. *J. Am. Chem. Soc.* **2000**, *122*, 9312.
(34) Nishinaga, T.; Izukawa, Y.; Komatsu, K. *Tetrahedron* **2001**, *57*, 3645.
(35) Lambert, J. B.; Zhang, S. *J. Chem. Soc. Chem. Commun.* **1993**, 383.
(36) Lambert, J. B.; Zhang, S.; Stern, C. L.; Huffman, J. C. *Science* **1993**, *260*, 1917.
(37) Lambert, J. B.; Zhang, S.; Ciro, S. M. *Organometallics* **1994**, *13*, 2430.
(38) Xie, Z.; Manning, J.; Reed, R. W.; Mathur, R.; Boyd, P. D. W.; Benesi, A.; Reed, C. A. *J. Am. Chem. Soc.* **1996**, *118*, 2922.
(39) Lambert, J. B.; Schilf, W. *Organometallics* **1988**, *7*, 1659.
(40) Müller, T.; Bauch, C.; Ostermeier, M.; Bolte, M.; Auner, N. *J. Am. Chem. Soc.* **2003**, *125*, 2158.
(41) Gillespie, R. J.; Robinson, E. A. *Proc. Chem. Soc.* **1957**, 147.
(42) Gillespie, R. J.; Kapoor, R.; Robinson, E. A. *Can. J. Chem.* **1966**, *44*, 1197.
(43) Birchall, T.; Manivannan, V. *J. Chem. Soc. Dalton Trans.* **1985**, 2671.
(44) Birchall, T.; Manivannan, V. *Can. J. Chem.* **1985**, *63*, 2211.
(45) Birchall, T.; Chan, P. K. H.; Pereira, A. R. *J. Chem. Soc. Dalton Trans.* **1974**, 2157.
(46) Arshadi, M.; Johnels, D.; Edlund, U. *J. Chem. Soc. Chem. Commun.* **1996**, 1279.
(47) Lambert, J. B.; Lin, L. *J. Org. Chem.* **2001**, *66*, 8537.
(48) Lambert, J. B.; Lin, L.; Keinan, S.; Müller, T. *J. Am. Chem. Soc.* **2003**, *125*, 6022.
(49) Kim, K.-C.; Reed, C. A.; Elliot, D. W.; Mueller, L. J.; Tham, F.; Lin, L.; Lambert, J. B. *Science* **2002**, *297*, 825.
(50) Uhlig, W. (N. Auner, J. Weis, Eds.), *Organosilicon Chemistry*, **1994**, VCH, Weinheim, Germany, p. 21.
(51) Shade, L.; Mayr, H. *Makromol. Chem. Rapid Commun.* **1988**, *9*, 477.
(52) Siehl, H.-U.; Kaufmann, F.-P. *J. Am. Chem. Soc.* **1992**, *114*, 4937. Siehl, H.-U.; Kaufmann, F.-P.; Hori, K. *J. Am. Chem. Soc.* **1992**, *114*, 9343.
(53) Müller, T.; Bauch, C.; Bolte, M.; Auner, N. *Chem. Eur. J.* **2003**, *9*, 1746.
(54) Jerkunica, J. M.; Traylor, T. G. *J. Am. Chem. Soc.* **1971**, *93*, 6278.
(55) MacLachlan, M. J.; Bourke, S. C.; Lough, A. J.; Manners, I. *J. Am. Chem. Soc.* **2000**, *122*, 2126.
(56) Fukuzumi, S.; Kitano, T.; Mochida, K. *J. Am. Chem. Soc.* **1990**, *112*, 3246.

(57) Lochynski, S.; Boduszek, B.; Shine, H. J. *J. Org. Chem.* **1991**, *56*, 914.
(58) Peloso, A. *J. Organomet. Chem.* **1974**, *67*, 423.
(59) Kochi, J. K. *Angew. Chem. Int. Edit. Engl.* **1988**, *27*, 1227.
(60) Mochida, K.; Itani, A.; Yokoyama, M.; Tsuchiya, T.; Worley, S.; Kochi, J. K. *Bull. Chem. Soc. Jpn.* **1985**, *58*, 2149.
(61) Tanaka, H.; Ogawa, H.; Suga, H.; Torii, S.; Jutand, A.; Aziz, S.; Suarez, A. G.; Armatore, C. *J. Org. Chem.* **1996**, *61*, 9402.
(62) Okano, M.; Mochida, K. *Chem. Lett.* **1991**, 819.
(63) Doretti, L.; Faleschini, S. *Gazz. Chim. Ital.* **1970**, *100*, 819.
(64) Ichinohe, M.; Fukaya, N.; Sekiguchi, A. *Chem. Lett.* **1998**, 1045.
(65) Sekiguchi, A.; Fukaya, N.; Ichinohe, M. *Phosphorous Sulfur Silicon* **1999**, *150–151*, 59.
(66) Sekiguchi, A.; Fukaya, N.; Ichinohe, M.; Ispida, Y. *Eur. J. Inorg. Chem.* **2000**, 1155.
(67) Ichinohe, M.; Fukui, H.; Sekiguchi, A. *Chem. Lett.* **2000**, 600.
(68) Zharov, I.; King, B. T.; Havlas, Z.; Pardi, A.; Michl, J. *J. Am. Chem. Soc.* **2000**, *122*, 10253.
(69) Zharov, I.; Weng, T.-C.; Orendt, A. M.; Barich, D. H.; Penner-Hahn, J.; Grant, D. M.; Havlas, Z.; Michl, J. *J. Am. Chem. Soc.* **2004**, *126*, 12033.
(70) Sekiguchi, A.; Fukawa, T.; Nakamoto, M.; Ya Lee, V.; Ichinohe, M. *J. Am. Chem. Soc.* **2002**, *124*, 9865.
(71) Sekiguchi, A.; Fukawa, T.; Ya Lee, V.; Nakamoto, M. *J. Am. Chem. Soc.* **2003**, *124*, 9250.
(72) Sekiguchi, A.; Fukawa, T.; Nakamoto, M.; Ya Lee, V.; Ichinohe, M. *Angew. Chem. Int. Edit. Engl.* **2003**, *42*, 1143.
(73) Nakamoto, M.; Fukawa, T.; Sekiguchi, A. *Chem. Lett.* **2004**, *33*, 38.
(74) Sekiguchi, A.; Matsuno, T.; Ichinohe, M. *J. Am. Chem. Soc.* **2001**, *123*, 12436.
(75) Matsuno, T.; Ichinohe, M.; Sekiguchi, A. *Angew. Chem. Int. Edit. Engl.* **2002**, *41*, 1575.
(76) Jutzi, P.; Bunte, A. E. *Angew. Chem. Int. Edit.* **1992**, *31*, 1605.
(77) Müller, T.; Jutzi, P.; Kühler, T. *Organometallics* **2001**, *20*, 5619.
(78) Schmidt, H.; Keitemeyer, S.; Neumann, B.; Stammler, H.-G.; Schoeller, W. W.; Jutzi, P. *Organometallics* **1998**, *17*, 2149.
(79) Jutzi, P.; Keitemeyer, S.; Neumann, B.; Stammler, H.-G. *Organometallics* **1999**, *18*, 4778.
(80) Ichinohe, M.; Hayata, Y.; Sekiguchi, A. *Chem. Lett.* **2002**, 1054.
(81) Walsh, A. D. *J. Chem. Soc.* **1953**, 2260, 2266, 2288, 2296, 2301, 2306.
(82) Das, K. K.; Balasubramanian, K. *J. Chem. Phys.* **1990**, *93*, 5883.
(83) Kapp, J.; Schreiner, P.; Schleyer, P. v. R. *J. Am. Chem. Soc.* **1996**, *118*, 12154.
(84) del Rio, E.; Menandez, M. I.; Lopez, R.; Sordo, T. L. *J. Chem. Soc. Chem. Comm.* **1997**, 1779.
(85) Nicolaides, A.; Radom, L. *J. Am. Chem. Soc.* **1996**, *118*, 10561.
(86) Nicolaides, A.; Radom, L. *J. Am. Chem. Soc.* **1997**, *119*, 11933.
(87) Nicolaides, A.; Radom, L. *J. Am. Chem. Soc.* **1994**, *116*, 9769.
(88) Jarek, R. L.; Shin, S. K. *J. Am. Chem. Soc.* **1997**, *119*, 6376.
(89) Schuppan, J.; Herrschaft, B.; Müller, T. *Organometallics* **2001**, *20*, 4584.
(90) Hino, S.; Brynda, M.; Phillips, A. D.; Power, P. P. *Angew. Chem.* **2004**, *116*, 2709.
(91) Basch, H.; Hoz, T. (S. Patai, Z. Rappoport, Eds.), *The Chemistry of Organic Germanium Tin and Lead Compounds* Vol. 1, **1995**, Wiley & Sons, Chichester, p. 1.
(92) Müller, T. Unpublished results.
(93) Frenking, G.; Fau, S.; Marchand, M.; Grützmacher, H. *J. Am. Chem. Soc.* **1997**, *119*, 6648.
(94) Karni, M.; Apeloig, Y.; Kapp, J.; Schleyer, P. v. R. (Z. Rappoport, Y. Apeloig, Eds.), *The Chemistry of Organic Silicon Compounds* Vol. 3, **2001**, Wiley & Sons, Chichester, p. 1.
(95) Basch, H. *Inorg. Chim. Acta* **1996**, *242*, 191.
(96) Kühler, T.; Jutzi, P. *Adv. Organomet. Chem.* **2003**, *49*, 1.
(97) Kira, M.; Ishida, S.; Iwamoto, T.; Kabuto, C. *J. Am. Chem. Soc.* **1999**, *212*, 9722.
(98) Olah, G. A.; Field, L. *Organometallics* **1982**, *1*, 1485.
(99) Maerker, C.; Kapp, J.; Schleyer, P. v. R. (N. Auner, J. Weis, Eds.), *Organosilicon Chemistry II*, Wiley-VCH, Weinheim, **1996**, p. 329.
(100) Pidun, U.; Stahl, M.; Frenking, G. *Chem. Eur. J.* **1996**, *2*, 869.
(101) Ottosson, C.-H.; Cremer, D. *Organometallics* **1996**, *15*, 5495.
(102) Ottoson, C.-H.; Szabó, K.; Cremer, D. *Organometallics* **1997**, *16*, 2377.

(103) (a) Atkins, P. W.; Friedman, R. S. *Molecular Quantum Mechanics*, 3rd Ed., Oxford University Press, Oxford, 1997. (b) Mason, J. (Ed.) *Multinuclear NMR*, Plenum Press, New York, 1987. (c) Kaupp, M.; Bühl, M.; Malkin, V. G. *Calculations of NMR and EPR Parameters*, Wiley-VCH, Weinheim, 2004.
(104) Müller, T. *J. Organomet. Chem.* **2003**, *686*, 251.
(105) Müller, T.; Hennegriff, T. *Organometallics* **2004** (submitted).
(106) Olsson, L.; Ottosson, C.-H.; Cremer, D. *J. Am. Chem. Soc.* **1995**, *117*, 7460.
(107) Olah, G. A.; Rasul, G.; Prakash, G. K. S. *J. Organomet. Chem.* **1996**, *521*, 271.
(108) Olah, G. A.; Rasul, G.; Buchholz, H. A.; Li, X.-Y.; Prakash, G. K. S. *Bull. Soc. Chim. Fr.* **1995**, *132*, 569.
(109) Kutzelnigg, W.; Fleischer, U.; Schindler, M. *NMR Basic Principles and Progress*, Vol. 23, Springer, Berlin, Heidelberg, **1990**, p. 165.
(110) Duncan, T. M. *A Compilation of Chemical Shift Anisotropies*, Farragut Press, Farragut, TN.
(111) Müller, T. Presented in part at the XXth North American Organosilicon Symposium, London, Ontario, May 1997 and at the 13th International Symposium on Organosilicon Chemistry, Guanojuato, GTO, Mexico, September 2002.
(112) Calculated at GIAO/B3LYP/6-311G(2d,p)//B3LYP/6-31G(d). (Me3Si)2(Me)Si-Si$^+$tBu2; E(B3LYP/6-31G(d) = −1752.92353H; r(Si$^+$Si) = 236.2 pm; r(Si$^+$C) = 191.8 pm, Σ°(Si+) = 360°. [92]
(113) Arshadi, M.; Johnels, D.; Edlund, U.; Ottoson, C.-H.; Cremer, D. *J. Am. Chem. Soc.* **1996**, *118*, 5120.
(114) Xie, Z.; Bau, R.; Benesi, A.; Reed, C. A. *Organometallics* **1995**, *14*, 3933.
(115) Bahr, S.; Boudjouk, P. *J. Am. Chem. Soc.* **1993**, *115*, 4514.
(116) Xie, Z.; Bau, R.; Reed, C. A. *J. Chem. Soc. Chem. Commun.* **1994**, 2519.
(117) Lambert, J. B. Personal communication to Frenking G. reported in ref.100. Chicago, 1990.
(118) Sekiguchi, A.; Muratami, A.; Fukaya, N.; Kabe, Y. *Chem. Lett.* **2004**, *33*, 530.
(119) (a) Panisch R. Diploma Thesis, University Frankurt, **2004**. (b) Panisch, R.; Müller, T. submitted for publication.
(120) Berger, S.; Braun, S.; Kalinowski, H.-O. NMR –Spektroskopie von Nichtmetallen, Stuttgart; New York Thieme: Bd. 4 ^{19}F NMR Spektroskopie.
(121) Müller, T. *Angew. Chem. Int. Edit. Engl.* **2001**, *40*, 3033.
(122) Takeuchi, Y.; Takayama, T. (Z. Rappoport, Y. Apeloig, Eds.), *The Chemistry of Organic Silicon Compounds* Vol. 2, **1998**, Wiley & Sons, Chichester, p. 267.
(123) Steinberger, H.-U.; Müller, T.; Auner, N.; Maerker, C.; Schleyer, P. v. R. *Angew. Chem. Int. Edit. Engl.* **1997**, *36*, 626.
(124) Kira, M.; Hino, T.; Sakurai, H. *J. Am. Chem. Soc.* **1992**, *114*, 6697.
(125) Olah, G. A.; Li, X.-Y.; Wang, Q.; Rasul, G.; Prakash, G. K. S. *J. Am. Chem. Soc.* **1995**, *117*, 8962.
(126) Driess, M.; Barmeyer, R.; Monsé, C.; Merz, K. *Angew. Chem. Int. Edit.* **2001**, *40*, 2308.
(127) Xie, Z.; Liston, D. L.; Jelinek, T.; Mitro, V.; Bau, R.; Reed, C. A. *J. Chem. Soc. Chem. Commun.* **1993**, 384.
(128) Olah, G. A.; Narang, S. C.; Gupta, B. G. B.; Malhotra, R. *J. Org. Chem.* **1979**, *44*, 1247.
(129) Kira, M.; Hino, T.; Sakurai, H. *Chem. Lett.* **1993**, 555.
(130) Johannsen, M.; Jørgensen, K. A.; Helmchen, G. *J. Am. Chem. Soc.* **1998**, *120*, 7637.
(131) Schleyer, P. v. R.; Buzek, P.; Müller, T.; Apeloig, Y.; Siehl, H.-U. *Angew. Chem. Int. Edit. Engl.* **1993**, *32*, 1471.
(132) Lambert, J. B.; Zhang, S. *Science* **1994**, *263*, 984.
(133) Reed, C. A.; Xie, Z. *Science* **1994**, *263*, 985.
(134) Olsson, L.; Cremer, D. *Chem. Phys. Lett.* **1993**, *6*, 360.
(135) Olah, G. A.; Rasul, G.; Buchholz, H. A.; Li, X. Y.; Sandford, G.; Prakash, G. K. S. *Science* **1994**, *263*, 983.
(136) Pauling, L. *Science* **1994**, *263*, 983.
(137) Ottosson, C.-H.; Cremer, D. *Organometallics* **1996**, *15*, 5495.
(138) Reed, C. A.; Xie, Z.; Bau, R.; Benesi, A. *Science* **1993**, *262*, 402.
(139) Stasko, D.; Reed, C. A. *J. Am. Chem. Soc.* **2002**, *124*, 1148.
(140) Reed, C. A. *Acc. Chem. Res.* **1998**, *31*, 133.

(141) Ivanov, S. I.; Rockwell, J. J.; Polykov, O. G.; Gaudinski, C. M.; Anderson, O. P.; Solntsev, K. A.; Strauss, S. H. *J. Am. Chem. Soc.* **1998**, *120*, 4224.
(142) Richardson, C.; Reed, C. A. *J. Chem. Soc. Chem. Commun.* **2004**, 706.
(143) Xie, Z.; Manning, J.; Reed, R. W.; Mathur, R.; Boyd, P. D. W.; Benesi, A.; Reed, C. A. *J. Am. Chem. Soc.* **1996**, *118*, 2922.
(144) Mathieu, B.; de Fays, L.; Ghosez, L. *Tetrahedron Lett.* **2000**, *41*, 9561.
(145) Tsang, C.-W.; Yang, Q.; Tung-Po, E.; Mak, T. C. W.; Chan, D. T. W.; Xie, Z. *Inorg. Chem.* **2000**, *39*, 5851.
(146) Setaka, W.; Sakamoto, K.; Kira, M.; Power, P. P. *Organometallics* **2001**, *20*, 4460.
(147) Jutzi, P.; Dickbreder, R. *J. Organomet. Chem.* **1989**, *373*, 301.
(148) (a) Nakatsuji, H.; Inoue, T.; Nakao, T. *Chem. Phys. Lett.* **1990**, *167*, 111. (b) Nakatsuji, H.; Inoue, T.; Nakao, T. *J. Phys. Chem.* **1992**, *96*, 7953. (c) Kaneko, H.; Hada, M.; Nakajiama, T.; Nakatsuji, H. *Chem. Phys. Lett.* **1996**, *261*, 1. (d) de Dios, A. C. *Magn. Res. Chem.* **1996**, *34*, 773. (e) Avalle, P.; Harris, R. K.; Karadakov, P. B.; Wilson, P. J. *Phys. Chem. Chem. Phys.* **2002**, *4*, 5925. (f) Vivas-Reyes, R.; De Proft, F.; Biesemans, M.; Willem, R.; Geerlings, P. *J. Phys. Chem. A.* **2002**, *106*, 2753. (g) Avalle, P.; Harris, R. K.; Fischer, R. D. *Phys. Chem. Chem. Phys.* **2002**, *4*, 3558.
(149) Mitchell, T. N. *J. Organomet. Chem.* **1983**, *255*, 279.
(150) Watkinson, P. J.; Mackay, K. M. *J. Organomet. Chem.* **1984**, *275*, 39.
(151) Cremer, D.; Olsson, L.; Reichel, F.; Kraka, E. *Isr. J. Chem.* **1994**, *33*, 369.
(152) Wrackmeyer, B.; Stader, C.; Horchler, K. *J. Magn. Reson.* **1989**, *83*, 601.
(153) Dillon, K. B.; Hewitson, G. F. *Polyhedron* **1984**, *3*, 957.
(154) Edlund, U.; Arshadi, M.; Johnels, D. *J. Organomet. Chem.* **1993**, *456*, 57.
(155) Nádvorník, M.; Holeček, J.; Handlíř, K.; Lička, A. *J. Organomet. Chem.* **1984**, *275*, 43.
(156) Holeček, J.; Nádvorník, M.; Handlíř, K.; Lička, A. *J. Organomet. Chem.* **1983**, *241*, 177.
(157) Wrackmeyer, B.; Kundler, S.; Milius, W.; Boese, R. *Chem. Ber.* **1994**, *127*, 333.
(158) Wrackmeyer, B.; Kundler, S.; Boese, R. *Chem. Ber.* **1993**, *126*, 1361.
(159) Rodriguez-Fortea, A.; Alemany, P.; Ziegler, T. *J. Phys. Chem. A* **1999**, *103*, 8244.
(160) Bauch, C. Ph. D. Thesis, Frankfurt/Main, FRG, **2003**.
(161) Wrackmeyer, B.; Horchler, K.; Boese, R. *Angew. Chem. Int. Edit. Engl.* **1989**, *28*, 1500.
(162) Meyer, R.; Werner, K.; Müller, T. *Chem. Eur. J.* **2002**, *8*, 1163.
(163) Olah, G. A.; Liang, G. *J. Am. Chem. Soc.* **1975**, *97*, 6803.
(164) Prakash, G. K. S.; Farnia, M.; Keyanian, S.; Olah, G. A.; Kuhn, H. J.; Schaffner, K. *J. Am. Chem. Soc.* **1987**, *109*, 911.
(165) Branch, G.; Walba, H. *J. Am. Chem. Soc.* **1954**, *76*, 1564.
(166) Lambert, J. B.; Lin, L.; Nowik, I.; Herber, R. H. *Inorg. Chem.* **2004**, *43*, 405.
(167) Mackay, K. M. (Z. Rappoport, Y. Apeloig, Eds.), *The Chemistry of Organic Germanium, Tin, and Lead Compounds* Vol. 1, **1995**, Wiley & Sons, Chichester, p. 97.
(168) Baines, K. M.; Stibbs, W. G. *Coord. Chem. Rev.* **1995**, *145*, 157.
(169) Jemmis, E. D.; Srinivas, G. N.; Leszczynski, J.; Kapp, J.; Korkin, A. A.; Schleyer, P. v. R. *J. Am. Chem. Soc.* **1995**, *117*, 11361.
(170) Ichinohe, M.; Igarashi, M.; Sauuki, K.; Sekiguchi, A. *J. Am. Chem. Soc.,* **2005**, ASAP, published on web 25.06.05.
(171) Ichinohe, M.; Matsuno, T.; Sekiguchi, A. *Angew. Chem. Int. Edit.* **1999**, *38*, 2194.
(172) Kaftory, M.; Kapon, M.; Botoshansky, M. (Z. Rappoport, Y. Apeloig, Eds.), *The Chemistry of Organic Silicon Compounds* Vol. 2, **1998**, Wiley & Sons, Chichester, p. 181.
(173) (a) Chuit, C.; Corriu, R. J. P.; Mehdi, A.; Reyé, C. *Angew. Chem. Int. Edit. Engl.* **1993**, *32*, 1311. (b) Belzner, J.; Schär, D.; Kneisel, B. O.; Herbst-Irmer, R. *Organometallics* **1995**, *14*, 1840. (c) Berlekamp, U.-H.; Jutzi, P.; Mix, A.; Neumann, B.; Stammler, H.-G.; Schoeller, W. W. *Angew. Chem. Int. Edit.* **1999**, *38*, 2048. (d) Schmidt, H.; Keitemeyer, S.; Neumann, B.; Stammler, H.-G.; Schoeller, W. W.; Jutzi, P. *Organometallics* **1998**, *17*, 2149. (e) Kalikhman, I.; Krivonos, S.; Lameyer, L.; Stalke, D.; Kost, D. *Organometallics* **2001**, *20*, 1053. (f) Kingston, V.; Gostevskii, B.; Kalikhman, I.; Kost, D. *Chem. Commun.* **2001**, 1272. (g) Kost, D.; Kingston, V.; Gostevskii, B.; Ellern, A.; Stalke, D.; Walfort, B.; Kalikhman, I. *Organometallics* **2002**, *21*, 2293. (h) Kalikhman, I.; Gostevskii, B.; Girshberg, O.; Krivonos, S.; Kost, D. *Organometallics* **2002**, *21*, 2551.

(i) Jurkschat, K.; Pieper, N.; Seemeyer, S.; Schürmann, M.; Biesemanns, M.; Verbruggen, I.; Willem, R. *Organometallics* **2001**, *20*, 868. (k) Ruzicka, A.; Jambor, R.; Cisarova, I.; Holecek, J. *Chem. Eur. J.* **2003**, *9*, 2411. (l) Mehring, M.; Löw, C.; Schürmann, M.; Jurkschat, K. *Eur. J. Inorg. Chem.* **1999**, 887. (m) Mehring, M.; Vrasidas, I.; Horn, D.; Schürmann, M.; Jurkschat, K. *Organometallics* **2001**, *20*, 4647. (n) Peveling, K.; Schürmann, M.; Ludwig, R.; Jurkschat, K. *Organometallics* **2001**, *20*, 4654. (o) Peveling, K.; Schürmann, M.; Jurkschat, K. Z. *Anorg. Allg. Chem.* **2002**, *628*, 2435. (p) Kasna, B.; Jambor, R.; Dostal, L.; Ruzicka, A.; Cisarova, I.; Holecek, J. *Organometallics* **2004**, *23*, 5300.

(174) Fukaya, N.; Ichinohe, M.; Sekiguchi, A. *Angew. Chem. Int. Edit.* **2000**, *39*, 3881.

(175) (a) Bondi, A. *J. Phys. Chem.* **1964**, *68*, 441. (b) Davies, A. G. *Organotin Chemistry*, VCH, Weinheim, 2003. (c) Batsanov, S. S. *Russ. J. Gen. Chem.* **1998**, *68*, 495.

(176) Riggs-Gelasco, P. J.; Mei, R.; Ghanotakis, D. F.; Yocum, C. F.; Penner-Hahn, J. E. *J. Am. Chem. Soc.* **1996**, *118*, 2400.

(177) Prakash, G. K. S.; Keyaniyan, S.; Aniszfeld, R.; Heiliger, L.; Olah, G. A.; Stevens, R. C.; Choi, H.-K.; Bau, R. *J. Am. Chem. Soc.* **1987**, *109*, 5123.

(178) Davies, A. G.; Goddard, J. P.; Hursthouse, M. B.; Walker, N. P. C. *J. Chem. Soc. Chem. Commun.* **1983**, 597.

(179) Nugent, W. A.; McKinney, R. J.; Harlow, R. L. *Organometallics* **1984**, *3*, 1315.

(180) Nitrile complexes of stannyl cations with a stoichiometry of stannyl cation/nitrile = 1:1 are described in the literature;[67] however no structural or spectroscopic data are given.

(181) (a) Lambert, J. B.; Zhao, Y. *J. Am. Chem. Soc.* **1996**, *118*, 7867. (b) Lambert, J. B.; Zhao, Y.; Wu, H. *J. Org. Chem.* **1999**, *64*, 2729. (c) Lambert, J. B.; Liu, C.; Kouliev, T. *J. Phys. Org. Chem.* **2002**, *15*, 667.

(182) (a) Müller, T.; Meyer, R.; Lennartz, D.; Siehl, H. U. *Angew. Chem. Int. Edit.* **2000**, *39*, 3074. (b) Müller, T.; Juhasz, M.; Reed, C. A. *Angew. Chem. Int. Edit.* **2004**, *43*, 1543.

(183) Driess, M.; Monsé, C.; Merz, K.; van Wüllen, C. *Angew. Chem. Int. Edit.* **2000**, *39*, 3684.

(184) Schormann, M.; Garratt, S.; Hughes, D. L.; Green, J. C.; Bochmann, M. *J. Am. Chem. Soc.* **2002**, *124*, 11266.

(185) Reed, C. A.; Kim, K.-C.; Bolskar, R. D.; Mueller, L. *Science* **2000**, *289*, 101.

(186) (a) Reed, C. A.; Fackler, N. L. P.; Kim, K.-C.; Stasko, D.; Evans, D. R.; Boyd, P. D. W.; Rickard, C. E. F. *J. Am. Chem. Soc.* **1999**, *121*, 6314. (b) Reed, C. A.; Kim, K.-C.; Stoyanov, E. S.; Stasko, D.; Tham, F. S.; Mueller, L. J.; Boyd, P. D. W. *J. Am. Chem. Soc.* **2003**, *125*, 1796.

(187) Juhasz, M.; Hoffmann, S.; Stoyanov, E.; Kim, K.-C.; Reed, C. A. *Angew. Chem. Int. Edit.* **2004**, *43*, 5352.

(188) Stasko, D.; Reed, C. A. *J. Am. Chem. Soc.* **2002**, *124*, 1148.

(189) Kato, T.; Reed, C. A. *Angew. Chem. Int. Edit.* **2004**, *43*, 2907.

(190) Auner, N. *Eur. Pat. Appl.* **1998**, EP 97-306480 19970826 .

(191) Steinberger, H.-U.; Bauch, C.; Müller, T.; Auner, N. *Can. J. Chem.* **2003**, *11*, 1223.

(192) Olah, G. A.; Rasul, G.; Prakash, G. K. S. *J. Am. Chem. Soc.* **1999**, *121*, 9615.

(193) Tanaka, M.; Hatanaka, Y. Presented at the XIIIth International Symposium on Organosilicon Chemistry, Guanajuato, GTO Mexico, Aug 2002, *Book of Abstracts C06*, p. 28.

(194) Jutzi, P.; Mix, A.; Rummel, B.; Schoeller, W. W.; Neumann, B.; Stammler, H. G. *Science* **2004**, *305*, 849.

(195) (a) Gaspar, P. P. Presented at the 2nd European Silicon Days, Munich, Germany, Sep 2003. (b) Gaspar, P. P. (N. Auner; J. Weis, Eds.), *Organosilicon Chemistry VI*, Wiley–VCH, Weinheim, 2005.

(196) Gaspar, P. P.; Read, D. Presented at the XIIIth International Symposium on Organosilicon Chemistry, Guanajuato, GTO Mexico, August 2002.

Recent Advances in Nonclassical Interligand Si···H Interactions

GEORGII I. NIKONOV*

Department of Chemistry, Brock University, St. Catharines ON, Canada L2S 3A1

I. Introduction . . . 217
II. Silane σ-Complexes and Si–H···M Agostic Complexes . . . 219
A. Silane σ-Complexes. A Short Historical Overview of Benchmark Results . . . 219
B. Dewar–Chatt–Duncanson Scheme – A Simple Model for Electron-Deficient Three-Center Interactions . . . 220
C. Structural Features of Silane σ-Complexes . . . 222
D. Spectroscopic Features of Silane σ-Complexes . . . 225
E. Recent Results on Silane σ-Complexes . . . 229
F. Si···H···M Agostic Bonding . . . 247
III. Silylhydride Complexes with Interligand Hypervalent Interactions M–H···SiX . . . 270
A. A Short Remark on the Heuristic Aspect . . . 270
B. IHI MH···SiX in Metallocene and Related Ligand Environments . . . 272
C. β-IHI . . . 288
D. IHI MH···SiX in Complexes not Isolobal with Metallocenes . . . 289
E. Comparison of IHI with Residual σ Interactions in Silane Complexes . . . 290
IV. Multicenter H···Si Interactions in Polyhydridesilyl Complexes . . . 291
A. Evidence for Multicenter H···Si Interactions . . . 291
B. Comparison of Multicenter H···Si Interactions with IHI and Residual σ-Interactions in Silane Complexes . . . 301
C. A Comment on the Terminology . . . 301
V. Conclusions and Outlook . . . 303
Acknowledgments . . . 304
References . . . 304

I
INTRODUCTION

The discovery by Kubas *et al.*[1] of the coordination of an intact dihydrogen molecule to transition metals to form a dihydrogen σ-complex **1** was one of the most exciting and important discoveries of the late 20th century.[2–4] This discovery had a significant influence on the study of activation of small molecules by metal centers and led to an impressive development of the general field of nonclassical complexes.[5] Neglecting the vast class of compounds with delocalized π-bonds, by nonclassical we understand a compound in which bonding between elements X and Y cannot be presented by a single Lewis structure. Broadly speaking, a *nonclassical bond* is one that includes a significant delocalization of σ-bonds over three or more centers. The concept of 3 center–2 electron (3c–2e) bonds developed for the earlier examples of trihydrogen cation H_3^+ (**2**), methonium cation CH_5^+ (**3**) (observed in the gas phase in mass-spectral experiments), and polyboranes **4** serves well to illustrate this point. In nonclassical complexes, one or several metal–ligand and/or ligand–ligand bonds are involved in nonclassical bonding. The terms *secondary*

*Corresponding author. Tel.: (905) 688-5550; fax: (905) 682-9020.
E-mail: gnikonov@brocku.ca (G.I. Nikonov).

ADVANCES IN ORGANOMETALLIC CHEMISTRY
VOLUME 53 ISSN 0065-3055/DOI 10.1016/S0065-3055(05)53006-5

interactions and *weak interactions* are also used occasionally to describe this phenomenon.[5] Apart from its obvious aesthetic beauty, the discovery of H–H σ-bond coordination to metals[1] and the almost simultaneous formulation of C–H–M agostic bonding (as schematically shown in **5**)[6,7] were quickly realized to be highly relevant to transition metal activation of inert bonds, with all the important implications for catalysis.[3,4,6–9]

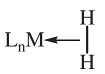

1

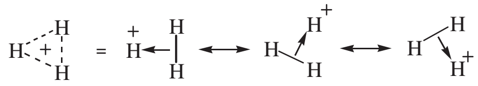

2

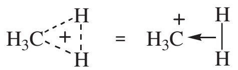

3

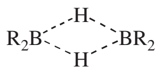

4

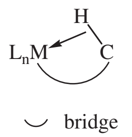

5

Curiously enough, although the element silicon is only second to hydrogen in the number of known nonclassical complexes, it was the first one for which the idea of nonclassical Si···H interaction was clearly put forward for the binuclear silane σ-complex **6** almost 35 years ago.[10,11] The resurgence of interest in silane σ-complexes **7** in the early 1980s resulted in a significant advance in our understanding of the Si–H bond activation, which is important for the investigation of various hydrosilation reactions. Although silicon is a heavier analog of carbon, the Si–H bond complexation to metals has a much closer resemblance to H–H bond coordination rather than to C–H bond complexation.[2] However, the presence of substituents at silicon with different electronic and steric properties, a feature absent for hydrogen, has a significant impact not only on the strength of Si–H interaction but also on the type of nonclassical complex formed. Thus, a class of agostic Si–H···M complexes **8**, which is related to **7** but differs from it in the presence of an additional bridge between the metal and interacting silicon atom, has been discovered. The earlier work and subsequent development of this field have been well summarized in a monograph[2] and a series of review articles.[3,4,8,11–15]

More recently, several new families of compounds have been found that exhibit bonding features different from what is normally observed in complexes **7** and **8**.[16,17] These new classes can be classified as compounds with interligand hypervalent interactions (IHI) Si–H, as schematically shown in **9**, and complexes with multiple hydride–silicon interactions like in **10**, where the dotted line represents a nonclassical interaction between the silicon atoms and hydride ligands.[16–20] In contrast to σ-complexes **7** with three-center bonds, in compounds **9** and **10** the nonclassical bonding is essentially delocalized over four and more centers. Bonding such as in **9** and **10** requires a specific conformation of the complex and exhibits very different dependence of bond lengths and spectroscopic features on the nature of substituents at silicon than in silane σ-complexes **7**. That is, groups X and H should be *trans*, the M–Si bond is shortened, and the electron-withdrawing groups

X on silicon strengthen the interaction. This work and some new findings in the field of agostic complexes **8** led to the refinement of the original bonding schemes developed for nonclassical complexes with Si–H interaction. The intent of the current account is to discuss the general features and ideas of nonclassical Si–H interactions in transition metal complexes and to review the recent experimental and theoretical achievements of this field. Some earlier work is included and discussed if there is new relevant experimental and/or theoretical information, or to illustrate the discussion of general aspects. Different types of nonclassical bonding are treated separately. Section II highlights the basic features of the chemistry of silane σ-complexes **7** and the related agostic complexes **8**, and discusses the recent advances in this field. Next, Section III is dedicated to compounds with interligand hypervalent Si–H interactions **9**, finally, Section IV describes the chemistry of polyhydride compounds like **10** with multiple hydride–silicon interactions.

In this review, as is common in the literature, the nonclassical compounds are often written in the η^m-form ($m \geqslant 2$), i.e. $[M(\eta^2\text{-}HSiR_3)L_n]$ ($m = 2$). Such an η^2-designation is based on the important phenomenological feature that both the hydrogen and silicon atoms, albeit still bound to each other, have some kind of a bond to the metal. As such, this designation does not tell us anything about the origin of the interaction and is entirely ambiguous. However, the absence, until recently, of any kind of interligand Si–H bonding different from the complexation of silane σ-bonds to metals, leads sometimes to incorrect mixing up of the general η^2-form with σ-complexes, which constitute only one type of nonclassical complexes.

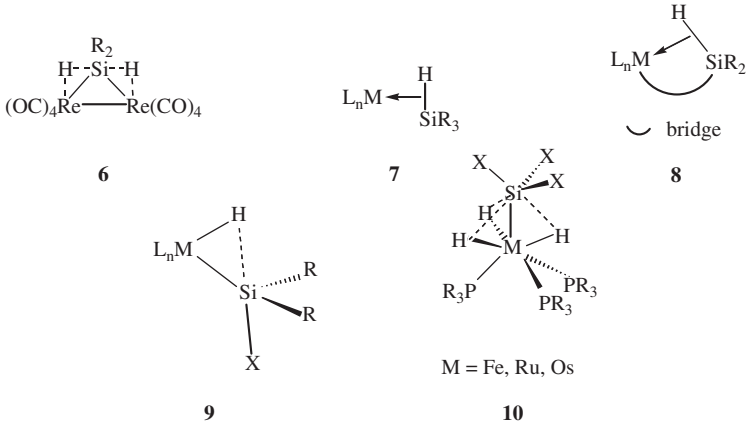

II

SILANE σ-COMPLEXES AND SI–H···M AGOSTIC COMPLEXES

A. *Silane σ-Complexes. A Short Historical Overview of Benchmark Results*

The formation of a silane σ-complex **7** can be viewed as the result of incomplete Si–H bond activation ("arrested" oxidative addition[21]) by an electrophilic metal

center[4] and, indeed, many of the compounds **7** are formed by the addition of hydrosilanes to unsaturated metal fragments.[13] The formation of a structure of this type was first proposed by Graham *et al.* for the rhenium compound **6**,[10,11] which is a prototype of many bridging silane σ-complexes.[13,22] Although the hydrides were not found from the X-ray experiment for **6**, the geometrical restrictions imposed by the positions of heavy elements led to a short estimated Si–H contact of 1.57 Å, compared with the normal Si–H bond of 1.48 Å in silanes. The observation of a coupling between the methyl group and two "hydrides" ($J(H-H) = 1.5$ Hz compared to 4.2 Hz in Me_2SiH_2) in the ^1H NMR spectrum of the related methyl-substituted complex $[Re_2(\mu\text{-}H_2SiMe_2)(CO)_8]$ was interpreted as additional, although still indirect, evidence for the presence of nonclassical interactions. Similar arguments were used to assign a nonclassical structure to the analogous ditungsten complex $[W_2(\mu\text{-}H_2SiMe_2)(CO)_8]$.[23] Subsequent X-ray studies of some related molecules, however, did find the hydride atom in close proximity to the silicon atom,[24,25] but reliable structural and spectroscopic evidence for interligand Si–H bonding was still absent at this earlier stage of research, which can, at least in part, account for the slow development of this field. A significant advance was made just shortly before Kubas' original report[1] on the dihydrogen σ-complex **1**. Corriu *et al.*[26] suggested an effective test for the presence of nonclassical Si–H bonding, based on the measurements of silicon–hydrogen coupling constants $J(^{29}Si\text{-}^1H)$ (65 Hz in $[Mn(\eta^2\text{-H-}SiPh_3)(CO)_2Cp']$ compared with >180 Hz in silanes and 3–10 Hz in classical silylhydrides, *vide infra*), and Schubert *et al.* reported neutron diffraction (ND) study of the compound $[Mn(\eta^2\text{-H-}SiFPh_2)(CO)_2Cp']$ exhibiting a short Si–H distance of 1.802(5) Å compared with 1.48 Å in hydrosilanes.[27] Following Kaesz's suggestion, it became common to think of silane σ-complexes as "arrested" intermediates on the way to Si–H bond oxidative addition[21] – a view that still appears to dominate the chemical thinking even when applied to other types of nonclassical Si–H interactions. The earlier work was reviewed by Graham[11] and its subsequent development until 1990 was thoroughly discussed by Schubert.[12]

B. *Dewar–Chatt–Duncanson Scheme – A Simple Model for Electron-Deficient Three-Center Interactions*

The three-center–two-electron bond description (3c–2e, like that on the left-hand side of Fig. 1) designed originally for the compounds **2**–**4** is electron-deficient[2,8] in that less than two electrons are used for the bond between any two atoms. The 3c–2e bond is formed by mixing a vacant orbital on one of the centers with a 2e σ-bond of two other. In the case of silane complexes, if the vacant center is considered to be the metal, this corresponds to the complexation of the Si–H bond. If the incoming particle is a proton, this corresponds to the protonation of the M–Si bond, which is indeed another practical way of preparing silane σ-complexes.[13] Whatever the origin of the resultant compound, the theoretical description will be the same. This bonding picture can be correctly applied to σ-complexes only if the electron count of the metal is zero (d^0 configuration) and the metal center acts as a pure electrophile. The essential feature of complexes with the configuration d^n ($n \geqslant 1$) is that backdonation

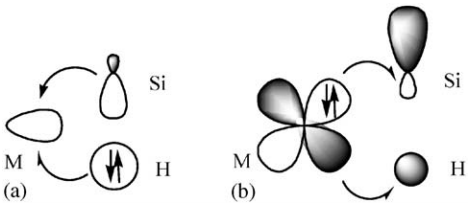

FIG. 1. Dewar–Chatt–Duncanson model for the Si···H···M bonding.

from an occupied metal d-orbital on the σ*(Si–H) antibonding orbital becomes feasible (right-hand side of Fig. 1). The resultant bonding scheme, shown in Fig. 1, bears a close resemblance to the well-known Dewar–Chatt–Duncanson (DCD) diagram originally designed to describe bonding in olefin complexes.[15]

The DCD scheme forms the basis for discussion of chemical bonding in all σ-complexes and conveys the key features of silane σ-complexation. Compared to dihydrogen H_2, silanes $HSiR_3$ have a weaker Si–H bond, with higher lying Si–H bonding orbital and lower lying σ*(Si–H) antibonding orbital.[2,4,14] Thus, silanes are both better σ-donors to metals and better π-acids, able to accept electrons from the metal d-orbitals (right-hand part of Fig. 1). The strength of backdonation is thought to be the key factor controlling the extent of the Si–H bond oxidative addition.[2–4,15] The important difference between silicon and hydrogen, not explicitly shown in Fig. 1, is that silicon has up to three more substituents, R, that also crucially effect the steric and electronic situation around the silicon center. Electron-donating groups R drive both the σ(Si–H) and σ*(Si–H) orbitals higher in energy[28] thus increasing the donation component in Fig. 1, but decreasing the backdonation. In the majority of compounds with the configuration d^n ($n \geqslant 1$) this leads to a weakening of the Si–H bond complexation to metals. In contrast, electron-withdrawing substituents on silicon push both the bonding and antibonding orbitals of the Si–H bond down in energy, decreasing the donation and increasing the backdonation components. The latter leads to weakening of the Si–H interaction, and in the limit of a very strong backdonation, results in complete Si–H bond addition to the metal. The exception is compounds with several strong π-acidic ligands, usually carbonyls such as $[M(CO)_5]$ (M = Cr, Mo, W),[29] where the d-orbitals are effectively delocalized on supporting ligands and are not amenable to bonding with silanes. In these highly unstable compounds with negligible backdonation, the electron-donating groups R on silicon favor stronger interaction of the Si–H bonds with the metal.[2]

The DCD scheme allows us to understand the conditions required to stabilize a σ-complex. Since backdonation from metal is the crucial factor controlling the Si–H bond interaction with a metal, any factor that reduces this component will lead to the strengthening of the residual Si–H σ bonding. These factors are[2]

1. the presence of a metal from the first transition series. These metals have rather contracted (core-like) d-orbitals that do not provide a sufficient overlap with the ligand orbitals;

2. the presence of π-acidic ancillary ligands (such as CO and PF_3), effectively delocalizing the metal-centered electrons, and/or strongly electron-withdrawing σ-ligands at the metal (such as halogens) that push the d level down in energy;
3. the high oxidation state of the metal and/or the presence of a positive charge, which contracts the d-orbitals.

C. *Structural Features of Silane σ-Complexes*

The presence of a chemical bond between fragments X and Y has its manifestation in structural and spectroscopic features and in chemical reactivity. It is rather obvious to deduce the presence of a direct X–Y bonding when both fragments X and Y can be brought into an infinite separation, like in donor-accepting complexes, but this can be rather problematic for the rather weak intramolecular interactions such as interligand bonding in nonclassical complexes. In this case, changing the characteristics of bonding between X and Y can be masked by the variation of bonding of X and Y to other parts of the molecule.

By analogy with the η^2-H_2 complexes, it is tempting to assume that in silane σ-complexes **7** and Si–H···M agostic species **8**, a more advanced oxidative addition of the Si–H bond to a metal will result in shorter M–H and M–Si bonds and longer Si–H separation. However, recent results show that a straightforward comparison with dihydrogen complexes is not valid because of the special role of substituents at silicon and the difference in electronegativity of hydrogen and silicon atoms.

The Si–H distance appears to be the parameter of choice to assign the presence or absence of a Si–H interaction. It is very tempting to have a simple threshold value serving as a criterion for the bond. However, this assumption can be incorrect if one takes into account that there is no obvious reason for an abrupt change of the backdonation component in the DCD scheme. Thus, in the ideal case of smooth tuning of the electronegativity of substituents either on metal and/or silicon, a continuum of structures ranging from a pure 3c–2e bond to a product of complete Si–H bond addition to metal (two separate 2c–2e bonds) can be imagined. Indeed, complexes with rather long Si–H separations of about 2.0–2.2 Å have been recently observed and are in the focus of current debate (*vide infra*). These compounds with *elongated Si–H bonds* (or short nonbonding Si–H contacts if the opposite view is accepted) correspond to the case of stretched dihydrogen complexes (H–H distance of up to 1.3–1.4 Å)[30], bonding in which is equally poorly understood.

In an earlier review article Schubert suggested that the shortest nonbonding Si–H contact can be estimated as 2.0 Å,[12] with the inexplicit assumption that any distance above this value is nonbonding, whereas shorter contacts correspond to the presence of some kind of Si–H bond. Schubert's structural criterion has been widely used in the 1990s to identify silane σ-complexes both in experimental and theoretical studies.[13,14] This criterion was obtained by summing up half of the nonbonding Si–Si distance in 1,3-cyclodisiloxanes (2.3–2.4 Å)[31,32] with half of the H–H distance of 1.85 Å, at which the H–H interaction is supposed to be weak.[12] Therefore, this

estimation is clearly based on the concept of atomic radii, which implies the transferability of a value of an atomic radius obtained from one class of compound to another.[33] Such a concept serves rather well for the elements of the two first periods of the Periodic Table that form rather rigid bonds but may encounter problems when applied to heavier elements generally exhibiting rather soft potentials for interatomic interactions. For example, the known Si–Si bonds span the wide range of 2.33–2.70 Å,[34–36] the upper value well exceeding the nonbonding Si–Si distance[32] in 1,3-cyclodisiloxanes. The Si–H potential curve is also very soft, so that half of the bonding energy corresponds to a rather long separation of 2.2 Å,[37] about 0.7 Å apart from the equilibrium value of 1.48 Å. Another problem is that a short distance between X and Y may not necessarily mean the presence of a bond, but rather be the result of sterically forced closeness (see, for example, the above-cited case of 1,3-cyclodisiloxanes[32]). In this case the interaction can be even repulsive. All together these arguments suggest that caution should be exercised in the application of a structural criterion such as Schubert's criterion of 2 Å.

The influence of substituents on the magnitude of H–Si contacts is also not straightforward. Thus, the thoroughly studied series of complexes $[Mn(\eta^2\text{-}HSiR_3)(CO)LCp'']$ (**11**, L = CO or another two-electron ligand; Cp″ = Cp, Cp′, or Cp*) has the X-ray determined H–Si distances in a rather narrow range of 1.75(4)–1.802(5) Å (the upper limit comes from the sole available ND study). Contrary to expectations based on the DCD scheme, the electron-withdrawing groups on silicon do not have any significant effect on this parameter (see Table II in Ref. 12). And while the X-ray value may be not very reliable, the recent computational study shows the same situation.[38]

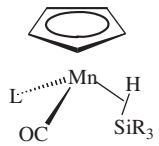

11

Given the DCD scheme, one may expect the M–H bond in silane σ-complexes to be longer than normal due to its inherent electron-deficiency.[27] Indeed, the elongation of the M–H bond in σ-complexes of molecular dihydrogen is a well-defined parameter determined by several structural and spectroscopic methods.[1,2,30,39] In the field of silane σ-complexes, as with the Si–H distances, the situation is much less straightforward. There is only one ND study of the compound $[Mn(\eta^2\text{-}HSiFPh_2)(CO)_2Cp']$ mentioned above and the rest of structural information is provided by X-ray diffraction studies only[2,13] that suffer from the well-known inaccuracy in locating hydrogen atoms in the vicinity of heavy elements.[40] Nevertheless, both the ND work on $[Mn(\eta^2\text{-}HSiFPh_2)(CO)_2Cp']$[27] and the available X-ray data show that, contrary to expectations, the M–H bond is not elongated, being quite comparable to the normal M–H bond.[12,41] In the thoroughly studied series of complexes $[Mn(\eta^2\text{-}HSiR_3)(CO)LCp']$ (**11**) and $[Mo(\eta^2\text{-}HSiR_3)\{(PR'_2CH_2\text{-})_2\}_2(CO)]$ (**12**) the M–H bonds are in the range

1.47(3)–1.569(4) Å (seven compounds with $\Delta = 0.11(3)$ Å) and range 1.70–2.04 (5) Å (two compounds with $\Delta = 0.34(7)$ Å), respectively.[2,12,13] Thus, even neglecting the inaccuracy of hydride positions determined from X-ray studies, the difference in the M–H bond is very close to three esd's, which does not allow for accurate conclusions to be drawn on how the variation of substituents either at silicon or metal effects this bond. In the latter example of complexes [Mo(η^2-HSiR$_3$)(CO)(depe)$_2$] the marginal difference between the Mo–H bond in [Mo(η^2-H$_3$SiPh)(CO)(depe)$_2$] (1.70(5) Å) and [Mo(η^2-H$_2$SiPh$_2$)(CO)(depe)$_2$] (2.04(5) Å, $\Delta = 0.34(7)$ Å), however, does correlate with the somewhat longer Si–H bond in the first complex (1.78(6) Å vs. 1.66(6) Å, $\Delta = 0.12(8)$ Å) and the decreased J(H–Si) (39 Hz vs. 50 Hz), which suggests that a more advanced oxidative addition of the Si–H bond is accompanied by a decrease of the M–H distance (see, however, the discussion below). However, recent theoretical investigation of the silane σ-complexes **11** shows the absence of any significant elongation of the M–H bond.[38]

In contrast, the experimental M–Si bonds span a wide range depending, for a given M, on the nature of substituents on silicon. To understand why this happens, we have to take into account the difference in the electronegativity of H and Si. Since hydrogen is more electronegative, the bonding σ(Si–H) orbital is more localized on the hydrogen end of the bond, the negative charge is also accumulated there.[28] On the other hand, the antibonding orbital is more localized on the silicon atom. When a silane approaches a metal, the initial interaction is formed *via* the hydrogen atom to form an M–H distance not very different from the normal M–H bond.[12,42] Then the Si–H bond pivots around H to bring the silicon atom in a closer proximity with the metal.[12] As discussed above, the nature of substituents R's on silicon controls the position of the σ*(Si–H) antibonding orbital and hence the extent of backdonation from metal to the silane. Increasing electronegativity of R's increases the population of σ*(Si–H) with the predominant effect on the M–Si distance. If one imagines a smooth increase of the electronegativity of R's, this process defines a trajectory of silicon addition to metal.[12] The increased backdonation from metal should be accompanied by the decreased direct donation from the Si–H bond because the σ(Si–H) bonding orbital lowers in energy. This should compensate the weakening of the Si–H interaction and strengthening of the M–H interaction upon the population of σ*(Si–H) with the result that, in the first approximation, both the M–H and Si–H distances do not change significantly. Thus, the M–Si distance is the sole parameter that exhibits a significant change and thus may serve as a structural criterion for the extent of Si–H addition to metal, with the advantage of being the most reliable one determined by X-ray crystallography. This picture is, however, complicated by the fact that the M–Si bonds in classical transition metal silyl complexes also depend on the substitution at silicon and steric factors, and therefore a proper choice of a reference classical silyl system is required to make the structural assignment for a given silane σ-complex. For example, the Mn–Si distance of 2.254(1) Å in the compound [Mn(η^2-HSiCl$_3$)(CO)$_2$Cp′], which according to recent results has some weak residual Si–H σ-bonding (*vide infra*), is even shorter than the Mn–Si bonds in the related classical bis(silyl) complex [Mn(SiCl$_3$)$_2$(CO)$_2$Cp′] (2.320(2) and 2.326(2) Å).[43] In the latter compound the silyls are mutually *trans* and their Mn–Si bonds are, no doubt, true 2c–2e bonds.

Finally, a word of caution should be offered against making a straightforward comparison of the M–Si bonds in complexes of different metals, since this parameter is strongly affected by the size of the metal. The latter tends to decrease from left to right in a given row of the Periodic Table due to the d-contraction, but increases down the Group (particularly between the first and second transition series).

To summarize, the Si–H distance can serve as a criterion of the Si–H interaction when it does not differ much from the normal Si–H bond and is determined by an accurate method such as ND and high-level quantum mechanic calculations. The discussion of other structural parameters requires the proper choice of a reference system. In systems with elongated Si–H interactions a justified conclusion can be made only on the basis of a combined application of several independent structural, spectroscopic, and computational methods.

D. *Spectroscopic Features of Silane σ-Complexes*

1. NMR Spectroscopy. The Saga of Silicon–Proton Coupling Constant

Given the inaccuracy of X-ray crystallography in finding hydrogen atoms and the scarcity of ND data on silane σ-complexes (and the cost and complexity of the ND experiment), the development of a cheap, quick, and reliable method to identify the presence of nonclassical Si–H interactions is required. In the field of dihydrogen σ-complexes, several spectroscopic NMR techniques have been developed, based on the measurements of spin–spin coupling constants in labeled HD complexes and the measurement of minimal T_1 relaxation times.[2,3] As mentioned above, Corriu *et al*. were the first to discover that the silicon–hydride coupling constant J(Si–H) in a silane σ-complex is significantly increased (65 Hz)[26] compared with classical hydridosilyl complexes, where a J(Si–H) of 3–10 Hz is usually observed.[12] To use J(Si–H) as an indicator of nonclassical Si–H bonding, one may wish to estimate the minimal value corresponding to the presence of a significant Si–H interaction. In an earlier review article, Schubert arbitrarily suggested that the values of 10–20 Hz define an approximate borderline so that lower values correspond to a nonbonding situation. The vast majority of known σ-complexes have been characterized by means of this spectroscopic criterion[13] with the assumption (in analogy with dihydrogen complexes) that the decrease of J(Si–H) upon variation of substituents either on metal or silicon corresponds to the decrease of Si–H bonding.[12] In some cases this criterion was applied rather incautiously, and values as low as 22–27 Hz were used for structural assignments. Unfortunately, as in the case of the M–H and Si–H distances discussed above, the presence of substituents on silicon severely complicates the picture.

The complex $[Mn(\eta^2\text{-}HSiCl_3)(CO)_2Cp']$ is an illuminating example to illustrate the complexity of the application of the J(Si–H) for the assignment of Si–H interactions. This compound, a member of the series **11** of silane σ-complexes thoroughly studied by a combination of several independent methods, was discovered early on to be an exception from the general trend. Detailed PES (PES = photoelectron spectroscopy) studies by Lichtenberger *et al*. showed that while complexes

11 with L = CO and R's on silicon equal to H, Ph, or alkyl are in the earlier stages of oxidative addition of the Si–H bond and can be formulated as Mn(I) complexes,[44,45] the compound $[Mn(HSiCl_3)(CO)_2Cp]$ is in a very advanced stage of oxidative addition, closer to the Mn(III) state.[46,47] Earlier extended Hückel calculations on the model compound $[Mn(HSiH_3)(CO)_2Cp]$ revealed donation from the Si–H bond to the metal as the main bonding component, supported by a much weaker backdonation from the metal to the silane.[48] In contrast, Fenske–Hall calculations of $[Mn(HSiCl_3)(CO)_2Cp]$ showed very strong donation from the metal into the σ*(Si–H) antibonding orbital to give an almost complete rupture of the Si–H bond in accord with the PES studies.[46] In spite of this, the observed J(Si–H) of 54.8 ± 0.6 Hz in the closely related compound $[Mn(HSiCl_3)(CO)_2Cp']$[49] is very close to the range 63.5–69 Hz observed in the nonclassical compounds **11**[12,13] and is much larger than the 20 Hz proposed to be the boundary value for any significant Si–H interaction.[12] To account for this discrepancy, Lichtenberger *et al.* suggested that the large J(Si–H) in $[Mn(HSiCl_3)(CO)_2Cp']$ could be due to nonbonded NMR coupling.[46] Surprisingly enough, the latter apparently is not the case for the closely related compound $[FeH(SiCl_3)_2(CO)Cp]$ that was found to have a much lower J(H–Si) of only 20 Hz.[50]

Further contributing to the intrigue, more recent calculations at the MP2 and B3LYP levels provided a short Si–H contact in $[Mn(HSiCl_3)(CO)_2Cp]$ (1.806 Å at the MP2 level and 1.732 Å for the B3LYP calculations), in good accord with the X-ray distance of 1.785 Å and very close to the Si–H distances in other complexes **11**.[38] These apparently contradictory results of the NMR, PES, and computational studies have been explained by *the revised DCD scheme*[52] that takes into account the difference in the electronegativity between the hydrogen and silicon atoms, expressed in terms of a Bent's rule[51] effect. Bent's rule states that if the electronegativity of the central atom E is intermediate between those of its substituents, the bonds to the more electropositive substituents receive more s character of E, making these bonds shorter, whereas the p character goes mainly to the bonds to more electronegative substituents, resulting in their elongation. As discussed above, in silanes $HSiR_3$ the bonding σ(Si–H) orbital is more localized on hydrogen, whereas silicon atom contributes mostly to the antibonding σ*(Si–H) orbital. The substitution at silicon for more electron-withdrawing chlorine groups brings about a rehybridization of the silicon center, namely, more Si 3s character goes to the bond with the hydride and more 3p character goes to the bond with the chlorine atoms in accordance with Bent's rule. As has been already discussed, such a replacement lowers the energy of *both* the σ(Si–H) bonding and σ*(Si–H) antibonding orbitals, with the effect that the M–H and Si–H distances do not change significantly, whereas the M–Si bond decreases. Stabilization of the σ(Si–H) bonding orbital results in *a decreased direct donation from the Si–H bond* to the metal, whereas the stabilization of σ*(Si–H) leads to *an effective electron density transfer* from the metal onto silane, as observed by the PES study.[46] The decreased Si–H donation to metal should partially compensate the increased backdonation and thus lead to some residual Si–H bonding and formation of the nonclassical silane complex $[Mn(\eta^2\text{-}HSiCl_3)(CO)_2Cp]$, as observed in the calculations. Since the J(Si–H) of 370 Hz in free $HSiCl_3$ is significantly larger than in silanes $HSiR_3$ (R = alkyl, aryl;

J(Si–H) < 200 Hz) one can expect that, if any bonding between H and Si in a complex of $HSiCl_3$ is retained, the J(Si–H) for the *same degree of oxidative addition* of the Si–H bond to metal should be higher than the coupling constant in a related complex of $HSiR_3$ (R = alkyl, aryl) owing to a larger s character of Si in the residual Si···H σ-bond in [Mn(η^2-$HSiCl_3$)$(CO)_2$Cp]. This mseans that comparable values of coupling constants can be found for both the [Mn(η^2-$HSiCl_3$)$(CO)_2$Cp] and [Mn(η^2-$HSiR_3$)$(CO)_2$Cp] (R = alkyl, aryl) complexes, even though the former can have a *greater degree of Si–H oxidative addition.* This bonding situation can be schematically described as shown in **13**, where dotted line represents *weak residual Si–H σ-bonding.* A similar structure without the dotted line was written for the hypothetical case of a classical complex [Mn(H)(SiR_3)$(CO)_2$Cp].[12] Thus, the rather large *one-bond* J(Si–H) in [Mn(η^2-$HSiCl_3$)$(CO)_2$Cp] is the result of a relatively large Si 3s character in the residual Si–H bond, rather than strong Si–H interaction.

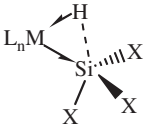

13

More recent DFT (Density Functional Theory) calculations of [Mn($HSiCl_3$)$(CO)_2$Cp′] by Lichtenberger[53] are in accord with the work of Lin *et al.* in finding a short Si–H contact of 1.823 Å and the observation of a normal Mn–H bond of 1.570 Å. In spite of the proximity of the Si and H atoms, the calculated and observed (by PES) parameters are in very good accord and confirm the earlier suggestion that this compound is very close to complete Si–H bond rupture. Interestingly, a very recent atom-in-molecule (AIM) study of this complex revealed the bond critical points for all the Mn–H, Mn–Si, and Si–H bonds under discussion,[54] thus further providing evidence for its nonclassical nature. Also noteworthy is that not only the Si–H interaction but also the Mn–Si bonds were found to be topologically unstable, whereas the M–H bond exhibited features of a normal bond.* This result is unexpected because this compound was used to be thought of as containing an almost-formed Mn–Si bond.[12,46,53] Both the Si–H and Mn–H bonds exhibit large bond ellipticities (0.722 and 1.079, respectively), indicating that the bond path is susceptible to rupture by a change in geometry. For comparison,

*Ref. 54 erroneously states that Nikonov's view given in Ref. 52 of this review is opposed to the view that in [Mn($HSiCl_3$)$(CO)_2$Cp′] the formation of the Mn–H interaction occurs at the expense of a weakening of the Si–H interactions. A careful reader can see that Ref. 52 does not contain this *ascribed* opposite statement. Apart from this, I think that the results of Ref. 54 are consistent with and complement my views expressed in Ref. 52 and in the current review. I also think that my work (Ref. 52) complements the *main* conclusions of D. L. Lichtenberger given in Ref. 53, although some *details* and in particular *drawings* (**3** in Ref. 52 vs. **5** and **6** in Ref. 52) differ. I think that [Mn($HSiCl_3$)$(CO)_2$Cp′] is indeed close to the Si–H bond rupture, but cannot give a degree of the oxidative addition. I think that such a degree (80% in Ref. 53) cannot be estimated from the decrease of the silicon–hydride coupling constant because the addition is accompanied by a rehybridization of silicon center in accordance with Bent's rule, which effects the J(H–Si).

the ellipticity of the Mn–H bond is 0.158. The delocalization indices (the parameter resembling the conventional bond order) for the Mn–H, Mn–Si, and Si–H bonds are 0.650, 0.575, and 0.311, respectively. The latter value indicates a degree of electron exchange characteristic of a polar interaction, which is further consistent with the calculated charges for the H and Si atoms of −0.284e and +2.091e, respectively.[54]

Important also is that the calculated J^{calcd}(H–Si) of −38 Hz at the optimized Mn–Si distance, although less in absolute value than the experimental one,† was found to be negative,[53] which suggests that there is a direct Si–H interaction. A negative J(H–Si) is also found even for the compound [$Mn(HSiCl_3)(CO)(PMe_3)Cp'$] (−22 Hz vs. the experimental absolute value of 22 Hz)[53] which, according to PES, is a classical Mn(III) complex.[45] Finally, the composition of localized bond orbitals in [$Mn(HSiCl_3)(CO)_2Cp'$] does confirm that some weak Si···H interaction is present.[53]

In this regard, the following general comment on the silicon–hydride coupling constants is pertinent.[55] Since the scalar coupling constant is primarily a through-bond interaction, the observed coupling constant can be thought of as the sum of a one-bond (H–Si) and a two-bond (H–M–Si) interactions:

$$J^{obs}(H-Si) = {}^1J(H-Si) + {}^2J(H-Si) \quad (1)$$

The relative signs and magnitudes of two coupling constants will determine the magnitude and sign of the observed coupling constant. ^1J(Si–H) is known to be negative[56] and in many cases two-bond silicon coupling constants are positive.[56] Because variation of the substituents at silicon can change the percentage of silicon 3s and 3p orbitals participating in the Si–M and Si–H bonds,[51,52] they can, in theory, alter *both the magnitude and the sign* of the observed J(Si–H). This might, in turn, result in an irregular change in the magnitude of the observable coupling constant,$|J^{obs}$(Si–H)|, as the electronegativity of the substituents at silicon is varied. Another problem can arise if the magnitudes of ^1J(Si–H) and ^2J(Si–H) are comparable. In this case it is possible that a large negative value of ^1J(Si–H), indicative of the presence of a direct Si–H interaction, could be compensated for by a large positive value of ^2J(Si–H). This might happen, for example, when an increase in the electronegativity of the substituents at silicon increases the two-bond component ^2J(Si–H) owing to an increase of Si 3s character in the M–Si bond.[52] In this case, a small value of$|J^{obs}$(Si–H)|would be highly misleading if taken as the sole indicator of the absence of Si–H interactions. It appears that the *sign* of J^{obs}(Si–H) might at least provide an additional and meaningful indicator because, if negative, it shows at least the dominance of ^1J(Si–H) over ^2J(Si–H). Therefore, the calculated negative J(Si–H) in [$Mn(HSiCl_3)(CO)(PMe_3)Cp'$],[53] having the absolute value of 22 Hz compared with the experimental value of 20 Hz, provides an additional argument against the application of Schubert's criterion of 20 Hz (see above) to the identification of nonclassical Si–H interactions. It would be very interesting to carry out a similar theoretical study on compounds [$FeH(SiCl_3)_2(CO)Cp$], which has the J^{obs}(Si–H) of 20 Hz,[50] and [$FeH(SiPh_3)(SnPh_3)(CO)Cp$] ($J^{obs}$(Si–H) of 23 Hz),[57]

†The experimental J^{obs}(H–Si) of 54.8 Hz is close in absolute value to the J^{calcd}(H–Si) of −46 Hz calculated at the experimentally observed Mn–Si distance.

among which the first one was stated to be clearly classical, while the second was suggested to have very little, if any Si–H interaction.[12,57]

From the previous discussion, we can conclude that when the observed value of J(H–Si) is relatively large, say, in the range 70–160 Hz, it is safe to think that the Si–H bond is involved in nonclassical bonding with metal. In contrast, any conclusion on the presence or absence of a Si–H interaction on the basis of a small value of silicon–proton coupling constant *in the absence of an independent evidence* can be erroneous. In this case, the measurement or calculation of the sign of J(Si–H) can help to identify a direct Si–H interaction.

2. NMR Spectroscopy. The ^{1}H NMR Spectra

Many complexes with nonclassical H···Si interaction discussed below exhibit a characteristic high-field shift of the hydride signal in the ^{1}H NMR spectra. This high-field shift of the resonance can be relative to the typical Si–H region if the Si–H interaction is strong (for example, in agostic complexes **8** with d^0 metals), or relative to the typical M–H region if the Si···H bond is stretched. Such a high-field shift appears to be a general feature of three-center interactions involving hydrogen atoms, but its origin has not been clearly established. Analogous shifts of ^{1}H NMR signals of bridging hydrides relative to the terminal ones were long known for bridging hydride complexes.

3. IR Spectroscopy

IR spectroscopy has been less popular than NMR spectroscopy for the identification of silane σ-complexes. Nevertheless, analysis of the available literature data shows that there is a clear shift of the Si–H stretch to longer wavelengths upon the formation of a σ-complex or agostic complex, which can be used for the identification of these compounds. In the case of significant Si–H bond activation it becomes increasingly senseless to talk about a pure Si–H band since the Si–H and M–H vibrations are strongly coupled. At least in one example, when a theoretical study was conducted, the main contribution to the observed hydride-related band came from the M–H stretch. However, the exact origin of the red shift has not been clearly established and in some case the band is observed well below the usual M–H region. Such a red shift appears to be an intrinsic feature of three-center interactions involving a hydrogen atom, since analogous shifts of M–H stretches are found for compounds with *dihydrogen bonding* M–H···HA.[58]

E. *Recent Results on Silane σ-Complexes*

Excellent compilations of silane σ-complexes can be found in Refs. 2 and 13, particularly in the latter. Therefore, this review is mainly focused on the recent results, and the discussion below is far from being comprehensive. Earlier results are touched when there is new relevant work and for the purpose of comparison only.

1. Group 3 and 4 Metals

To the best of my knowledge the only relevant report on Si···H···M interactions for Group 3 elements is the unique Si–H–B bridge in the compounds **14**.[59] This bonding is reminiscent of the one in diboranes and, since a boron atom is unable to backdonate, serves as an example of a pure 3c–2e bond including a silicon atom. The presence of a Si···H···B interaction was unequivocally established by the ^{1}H, ^{11}B and ^{29}Si NMR and IR spectroscopic data. As is common in σ-complexes and agostic complexes, the ^{1}H NMR signal of the bridging hydrogen atom is high-field shifted by 1.5 ppm relative to the "normal" Si–H group position, and this shift increases when the temperature is lowered. The magnitude of J(Si–H) is reduced by ca. 40–55 to 131–146 Hz and there is an unprecedented isotope-induced shift $^{2}\Delta^{10/11}B(^{29}Si)$ in the ^{29}Si NMR, transmitted through the Si–H–B bridge. Also as typical for σ-complexes and agostic compounds, the Si–H stretch is markedly (by about 250 cm^{-1}) shifted to lower wave numbers. Interestingly, the related tin compounds indicate a negligible Sn–H···B interaction.

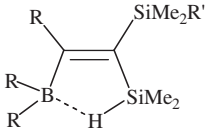

R = $CH_2CH{=}CH_2$ $CH_2CH{=}CH_2$ Et
R' = Me H Me

14

A related situation occurs in the disilyl cation **15**, which has a pure 3c–2e Si···H···Si bond. This compound was prepared by a hydride transfer from 1,3-disilylpropane to a trityl borate reagent and characterized by NMR spectroscopy and DFT calculations.[60] The observed coupling constant J(Si–H) of 39 Hz is unexpectedly low in spite of the absence of backdonation from silicon, emphasizing again the point that relatively weak coupling constants can be observed even for rather strong Si–H interactions. The calculated structure of **15** reveals elongated Si–H bonds (1.646 Å at the B3LYP/6-311G(d,p) level and 1.623 Å at the MP2/6-311G(d,p) level of theory) and an open Si–H–Si bond angle (140.3 and 136.6°, respectively). Both silicon centers bear a large positive charge (1.80), whereas the bridging hydrogen is negatively charged (−0.35), reflecting the high concentration of the bonding orbital on this H atom. Both silyl fragments $SiMe_2R$ are close to planarity, leading to the large Si p character in the Si–H bonding, which accounts for the small J(H–Si).

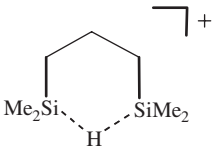

15

Only few examples of silane σ-complexes are known for the titanium triad and most of the work has been done on titanium itself. The first examples were

discovered by Harrod *et al.* during their work on the titanocene catalyzed dehydrogenative coupling of primary silanes. The reaction of $[TiMe_2Cp_2]$ with $PhSiH_3$ in the ratio 1:3 affords a dimeric titanocene complex **16** with two Ti···H···Si interactions:[61]

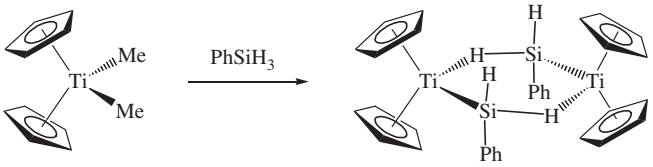

(2)

16

On keeping, this product converted *via* formal silylene extrusion reaction into the hydride bridged complex **17**:

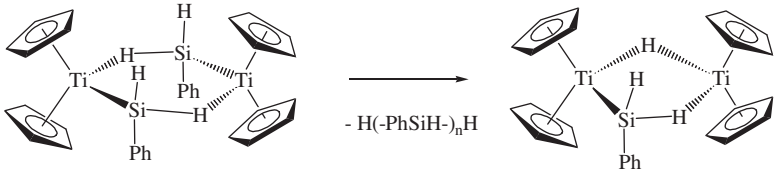

(3)

17

Both products are diamagnetic and were characterized by ^1H NMR spectroscopy and X-ray structure determinations. In addition, the ^{29}Si NMR spectrum of **17** revealed a coupling of the silicon atom with two nonequivalent geminal protons (148 Hz to the terminal proton‡ and 58 Hz to the proton in the Ti–H–Si bridge) along with a weaker coupling (14 Hz) to the bridging hydride. The Si–H bonds to the nonclassical hydrides in **16** and **17** were slightly elongated, 1.58(3) and 1.56(3) Å, respectively. In a similar reaction of a zirconocene derivative the product was the hydride-bridged dimer **18**.[62,63] However, the dimeric cationic nonclassical zirconocene complexes **19**, thoroughly studied by NMR techniques, have been reported by Dioumaev and Harrod:[64,65]

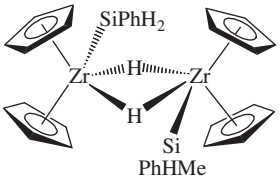

18

‡This value of silicon–hydride coupling constant is less than the arbitrary upper limit of bonding Si–H interactions (70–160 Hz) given on page 229 because of the rehybridization effect caused by the complexation of the Si–H bond to metal. Such a complexation leads to relatively large Si p character in the $Si–H_{term}$ bond, and hence the reduced J(Si–H) for an ordinary Si–H bond.

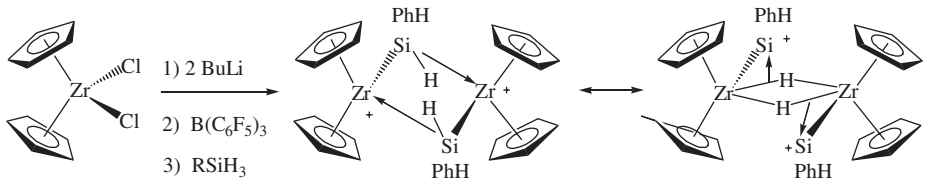

19

(4)

Buchwald *et al.* reported that addition of H_2SiPh_2 to the titanocene complex $[Ti(PMe_3)_2Cp_2]$ affords a silane σ-complex $[Ti(\eta^2\text{-}H_2SiPh_2)(PMe_3)Cp_2]$ (**20**) having an electronic structure intermediate between a Ti(IV) and a Ti(II) compound,[66] or in other words, it is a stretched silane σ-complex.[2] An analogous silane σ-complex $[Ti(\eta^2\text{-}H_3SiPh)(PMe_3)Cp_2]$ is found in the reaction of $[Ti(PMe_3)_2Cp_2]$ with $PhSiH_3$.[67] A somewhat related compound $[Ti(\eta^2 - HBcat')(\eta^2\text{-}H_3SiPh)Cp_2]$ (cat′ = catechol) was reported by Hartwig *et al.*[68] but a more recent theoretical study revealed this compound to be a silylborato complex $[Ti(\eta^2\text{-}H_2Bcat')(SiH_2Ph)Cp_2]$.[69] Interestingly, the zirconium and hafnium analogs have been found to be classical.[70,71] Thus, the addition of H_2SiPh_2 and $HSiPh_3$ to the olefin–phosphine precursors affords the M(IV) complexes, as shown in the equation.

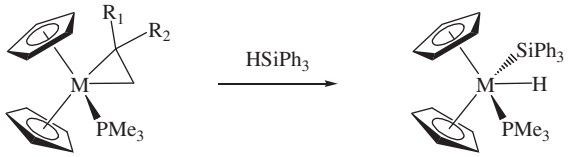

21

M = Zr, R_1=H, R_2 = Et; 48%

M = Hf, R_1=Me, R_2 = Me; 66%

(5)

The interesting feature of **20** is that the Si–H interaction occurs for the set of electron-donating ancillary ligands Cp_2/PMe_3. Thus, the only factor that can, in principle, account for the different behavior of titanium and its heavier analogs in these reactions is the contracted nature of the titanium d-orbitals and hence the less effective backdonation from metal as discussed in Section II.B. The nonclassical nature of the zirconium complex **19** compared with neutral **18** can be then attributed to the presence of a positive charge.

Nevertheless, a neutral zirconium complex with nonclassical Si···H···Zr bonding has been reported for the much less donating ligand set Cp/Cl_3.[72] The compound $[ZrCl_3(\eta^5\text{-}C_5H_4SiMe_2H)]$ (**22**) was found by X-ray crystallography to form a dichloride-bridged dimer with two additional SiH–M contacts (Fig. 2) that are close to linearity (158.3°). The Si–H bond was normal (1.47(2) Å) and the H···Zr contact was rather long (2.28(3) Å), signifying the initial stage of the Si–H bond activation.

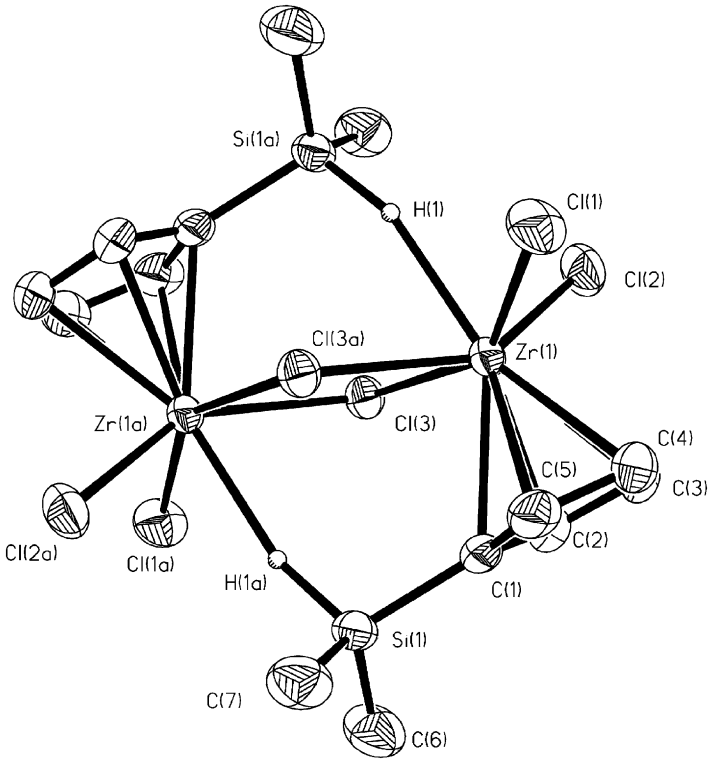

FIG. 2. Molecular geometry of the compound **22**. (Reproduced from Ref. 72, with permission from The Royal Society of Chemistry.)

The weak shift of the Si–H bond stretching mode from 2117 cm^{-1} in the free silane $HSiMe_2(C_5H_6)$ to 2066 cm^{-1} in the complex confirmed some weakening of this bond. The ^1H NMR spectrum, however, showed the Si–H proton signal in its normal place with unperturbed coupling to the Me group (3.6 Hz), which can be accounted for by facile dissociation of the compound in solution. No ^{29}Si NMR data were reported to verify the presence of the Si···H···Zr bonding.

The presence of nonclassical Si···H···Ti bonding in the compound $[Ti(\eta^2\text{-}H_2SiPh_2)(PMe_3)Cp_2]$ (**20**) was inferred from a set of spectroscopic and structural data.[66] The X-ray determined hydride forms a short Si–H contact of 1.69(5) Å, compared with the Si–H bond of 1.56(5) Å to the terminal hydrogen ($\Delta = 0.13(7)$ Å), and is somewhat below the range normally observed in nonclassical complexes **11**. Nevertheless, the Si–H (hydride) coupling constant of 28 Hz, although above 20 Hz, was much less than the J(Si–H(terminal)) of 161 Hz. Indirect evidence was also provided by the observation of increased H–H coupling (11 Hz) compared with 3 Hz in the classical **21**. The observed short Si–H contact in **20** stems from the small Si–Ti–H bond angle of 44(2)°, as compared with the H–Ti–P bond angle of 68(2)° (the Si–Ti–P bond angle was 111.78(7)°). Putting the hydride at the observed Ti–H distance of 1.81(5) Å but making the Si–Ti–H and H–Ti–P bond angles equal (55.89°) would give a much longer Si–H contact of 2.18 Å. To verify

the nature of the Si–H interaction in these titanocene silylhydride complexes, DFT calculations (with the BP86 potential) have been performed on the model compound [Ti(η^2-HSiMe$_2$)(PMe$_3$)Cp$_2$] (**23**).[55] The optimized structure of **23** shows a longer Ti–Si bond of 2.658 Å (cf. 2.597 Å in **20**) but a shorter Ti–H bond (1.742 Å) than the experimental structure. The short Si–H contact (1.840 Å) establishes the nonclassical nature of this compound, which was further confirmed by the calculation of a large Wiberg bond index (WI) of 0.3210 for the Si–H bond (for comparison the WI for the Ti–Si bond was 0.4915) and the observation of a bond critical point for the Si–H(hydride) bond in an AIM study. Analysis of the Laplacian contour map of **23** shows that the Ti–Si bond critical point is close to the ring critical point (0.3600 and 0.3621e Å^{-3}, respectively), i.e. a situation emerges where the Ti–Si bond is about to vanish, which means that the observed topological structure of [Ti(η^2-H-SiMe$_3$)(PMe$_3$)Cp$_2$] is very close to the structure [Ti(η^1-H-SiMe$_3$)(PMe$_3$)Cp$_2$]. Optimization of the compound [Ti(HSiMeCl$_2$)(PMe$_3$)Cp$_2$] (**24**), having two electron-withdrawing Cl substituents at silicon and the Me group *trans* to the hydride, gave, as expected, a structure with a more advanced Si–H addition to metal but still with a significant Si–H interaction (the Ti–Si and Si–H bond lengths were 2.551 and 1.862 Å, respectively; the WI for the Si–H bond equals 0.2815 and the bond critical point was found), which allows for its formulation as a stretched silane σ-complex. It is essential that the optimization was carried out with the restriction that the Me group on silicon was forced to be *trans* to the hydride. When this restriction is lifted, the structure relaxes to a rotamer of **24** having one of the chlorine groups *trans* to the hydride and exhibiting a different type of nonclassical bonding – IHI (see Section III.B.2).

2. Group 5 Metals

The authentic silane σ-complex of the Group 5 metals has been documented only for a vanadium carbonyl complex. The highly unstable compound [V(η^2-HSiEt$_3$)(CO)$_3$Cp] was generated in xenon matrix at −80 °C upon photolytic reaction of [V(CO)$_4$Cp] with HSiEt$_3$ and studied by IR spectroscopy. Similar reactions with chlorosilanes HSiEt$_{3-n}$Cl$_n$ ($n = 2$, 3) afforded products of complete oxidative addition of the H–Si bond, [V(H)(SiEt$_{3-n}$Cl$_n$)(CO)$_3$Cp].[73] This effect of the substitution at silicon on the extent of Si–H interaction mirrors that discussed above for the related manganese system **11**.

Most of the d^0 silylhydride complexes of niobo- and tantalocenes without strong electron-withdrawing substituents at silicon are classical[13] in spite of the presence of a metal in its highest oxidation state (V). The ND structure of [TaH(SiMe$_2$H)$_2$Cp$_2$] establishes the equidistant hydride position from both silicon atoms with two Si–H distances of 2.189(18) and 2.190(18) Å, ruling out its nonclassical formulation suggested by an earlier X-ray study.[74] The protonation of [TaH$_2$(SiMe$_2$Ph)Cp$_2$] does not afford the anticipated cationic silane σ-complex ([TaH$_2$(η^2-HSiMe$_2$Ph)Cp$_2$]$^+$) or ([Ta(η^2-H$_2$)(η^2-HSiMe$_2$Ph)Cp$_2$]$^+$), but rather is accompanied by the loss of silane and the formation of a binuclear hydride-bridged structure [Ta$_2$H$_2$(μ-H)Cp$_4$]$^+$.[75]

However, Tilley *et al.* reported an unusual d^0 silylhydride ate-complex **25** that was suggested to have an interligand interaction Si–H.[76] The 18e compound **25**

exhibits an increased Si–H coupling constant of 31 Hz and a Ta–H stretch at 1805 cm^{-1} *somewhat shifted toward the Si–H region* (about 2100 cm^{-1}) compared with the Ta–H vibration (1785 cm^{-1}) observed in the classical 16e complex [Ta(H)(Si{$SiMe_3$}$_3$)(= NAr)(Cp*)] (Ar = 2, 6-$Pr^i_2C_6H_3$).[76] In the related classical 18e d^0 complex [Ta(H)(SiHMePh)(= NAr)(PMe_3)(Cp)] **26**,[77] isolobal with **25**, the *J*(Si–H) equals 14 Hz and the Ta–H stretch is at 1674 cm^{-1}. In contrast, red shift is usually observed in complexes with three-center M···H···E interactions. The X-ray diffraction study of **25** reveals an elongated Ta–Si bond of 2.722(3) Å as compared with 2.689(1) Å in [Ta(H)(Si{$SiMe_3$}$_3$)(= NAr)(Cp*)], 2.624(2) and 2.633(2) Å in [$TaH(SiHMe_2)_2Cp_2$],[74] and 2.651(4) Å in [$Ta(H)_2(SiMe_2Ph)Cp_2$].[78] Such an elongation could manifest the presence of a Si–H bond σ-complexation but can also reflect the increased steric strain in **25**. The observed Si–H distance of 2.51 Å is definitely too long to correspond to any significant interaction, but the X-ray determined hydrogen position could be inaccurate. The observed Ta–Si–Si bond angles (range 107.7–117.4(2)°) are normal and reflect the absence of any structural distortion of the silyl ligand. Comparing with neutral **26**, one can expect that the presence of a negative charge in **25** would result in the increased backdonation from tantalum on the σ*(Si–H) and hence, since **26** is classical, would lead to complete Si–H bond oxidative addition and formation of a d^0 silylhydride. Also, the electron-releasing $SiMe_3$ substituents at silicon atom should decrease the magnitude of *J*(Si–H) (see Section II.D). In this regard, the origin of the high Si–H coupling constant in **25** is enigmatic and definitely deserves a computational study to resolve the question of the presence and nature of any Si–H interaction. The reason why the hydride atom in **25** occupies the position between nitrogen and silicon, whereas in all other structures of type [M(H)(SiR_3)(X)(= NR′)(Cp)] (M = Nb, Ta) it lies between groups SiR_3 and X (see **26** and *vide infra*), is also unclear.

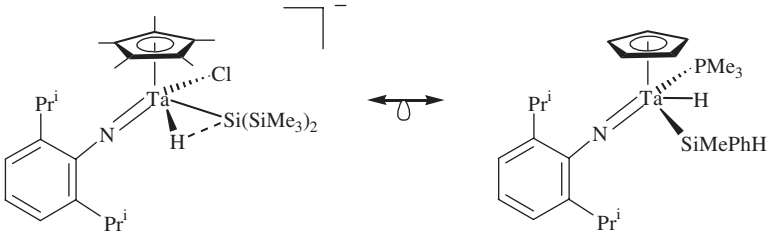

25 **26**

3. Group 6 Metals

Silane σ-complexes of the Group 6 metals are among the best studied.[13] Three families of compounds are particularly noteworthy. These are the half-sandwich arene complexes [Cr(η^2-$HSiMe_2H$)$(CO)_2(C_6Me_6)$] (**27**),[79,80] the above-mentioned Kubas's complexes **12**,[2,81,82] and the pentacarbonyl derivatives [M(η^2-$HSiR_3$)$(CO)_5$].[29,83] Complex **27** is an isolobal analog of the manganese system **11** and like the latter exhibits rather large Si–H coupling constant of 80 Hz compared with the range

54.8–65.4 Hz found for **11**. These values correlate well with the X-ray determined Si–H distance of 1.61(4) Å in **27**, which is shorter than the range 1.75(4)–1.802(5) Å determined in **11**. The stronger Si–H interaction in **27** is apparently the result of a weaker donor ability of the arene ligand compared with the cyclopentadienyl ligand, which leads to a weaker backdonation from the chromium center. A similar correlation between the r(Si–H) and the *J*(Si–H) in complexes **12** has been discussed above.

Representatives of family **12**, the compounds $[Mo(\eta^2\text{-}HSiH_3)(CO)(\{R_2PCH_2\text{-}\}_2)_2]$ (R = Ph, Et, Bu^i),[82] are particularly interesting because (i) these are the first examples of a silane σ-complex of the prototypical silane SiH_4, and (ii) because it is the first system where an equilibrium is observed between the η^2-form and the silylhydride product of complete Si–H oxidative addition to metal, for the case of R = Et [Eq. (6)]. The structure of the compound $[Mo(\eta^2\text{-}HSiH_3)(CO)(\{Bu^i_2PCH_2\text{-}\}_2)_2]$ has been determined but suffers from a disorder of the CO and SiH_4 groups. However, it is clear from the X-ray structure that this compound, like the analogous complexes $[Mo(\eta^2\text{-}HSiPhH_2)(CO)(\{Et_2PCH_2\text{-}\}_2)_2]$ and $[Mo(\eta^2\text{-}HSiPh_2H)(CO)(\{Et_2PCH_2\text{-}\}_2)_2]$, has the *cis*-orientation of the CO and SiH_4 ligands.[2,81] This structural aspect has recently received a theoretical treatment in a study aimed to elucidate the factors controlling the formation of the *cis*- vs. *trans*-forms.[84] This difference between the silane and η^2-H_2 σ-complexes has been attributed to a better ability of the Si–H bond to serve as an acceptor of the electron density from metal through the backdonation component so that the observed structure of **12** is the result of avoided competition between the σ*(Si–H) and π*(C–O) antibonding orbitals:

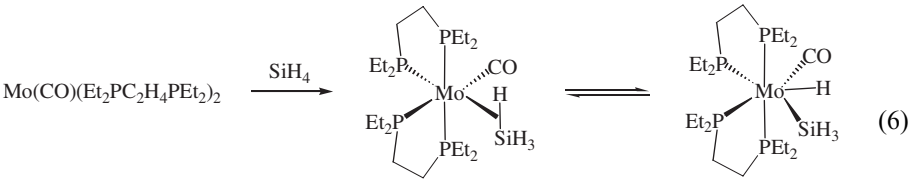

(6)

12

Silane σ-complexes $[M(\eta^2\text{-}HSiR_3)(CO)_5]$[29,83] are interesting in that here the electron density of metal is effectively delocalized over five electron-accepting carbonyl ligands so that a situation of almost negligible backdonation is modeled well. Therefore, the M···H···Si interaction in this system is very close to the 3c–2e limit; thus, it is not surprising that these complexes are highly unstable.

4. Group 7 Metals

The silane σ-complexes **11** have been intensively studied as discussed above and in Refs. 2, 4, and 12–14. No examples of such complexes are known for technetium, whereas the related rhenium complex $[Re(H)(SiR_3)(CO)_2Cp]$ has been concluded to be classical on the grounds of a long-estimated Si–H distance of 2.2 Å.[85] Schubert favors a classical description of the latter compound,[12] whereas Kubas noted that this distance may correspond to a stretched σ-complex on the verge of oxidative

addition.[2] Complexes $[M(\eta^2\text{-H-SiH}_{3-n}Cl_n)(CO)_2Cp]$ (M = Mn, Tc, Re; $n = 1-3$) have been studied computationally at the MP2 and B3LYP levels and showed short Si–H distances (B3LYP: range 1.728–1.732 Å for M = Mn, range 1.879–1.881 Å for M = Tc, range 2.011–2.018 Å for M = Re), indicating the presence of nonclassical Si–H interaction.[38] The length of the Si–H contact increases from $n = 1$ to 3 and down Group 7 in accord with the previous conclusion that heavier transition metals and electron-withdrawing groups on silicon atom favor a deeper degree of the Si–H bond oxidative addition. The rhenium complexes were concluded to be closer to the classical end, attributed to their greater reducing ability and more diffuse d-orbitals. It was established that for a given metal, the silane dissociation energies increase as the number of chlorine substituents at silicon increases, in accord with the kinetic studies of Graham[11,12] and the theoretical predictions (Section II.B and Ref. 13). As discussed above (Section II.C), the variation of the M–H and Si–H distances upon changing n is minimal, whereas the M–Si bond contracts noticeably when n increases. It was therefore concluded that the increase of dissociation energies with increasing of numbers of chlorine substituents at silicon is the result of strengthening of the M–Si interaction, and this is not accompanied by weakening of the Si–H interaction.[38]

Taking into account that a set of *fac*-$(CO)_3$ ligands is isolobal to a Cp^- ligand,[86] the cationic rhenium compounds $[Re(HSiR_3)(CO)_4(PR'_3)]^+$ (**28**) are isolobal analogs of the half-sandwich complex $[Re(HSiR_3)(CO)_2Cp]$. However, the presence of four π-accepting carbonyl ligands and a positive charge makes the fragment $[Re(CO)_4(PR'_3)]^+$ highly electrophilic[87,88] with the effect that the backdonation from metal is reduced significantly, leading to a strong Si–H interaction characterized by increased J(Si–H) (60.9 Hz for R′ = Ph and 61.6 Hz for R′ = Cy) and small J(P–H) (10.5 and 9.3 Hz, respectively).[87,88] The compounds **28** were prepared by the reaction of a rhenium alkyl precursor with $HSiEt_3$ in the presence of a Lewis acid:

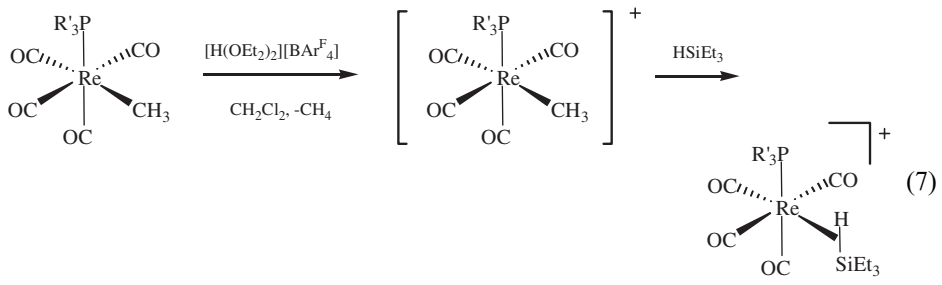

(7)

28

Complexes **28** are thermally unstable and decompose above 0 °C.[87] The very related unstable mono(phosphite) derivative $[Re(\eta^2\text{-HSiEt}_3)(CO)_4(P\{OCH_2\}_3CMe)]^+$ was characterized only by ^1H NMR,[89] whereas the bis(phosphite) derivative $[Re(\eta^2\text{-HSiR}_3)(CO)_3(P\{OCH_2\}_3CMe)_2]^+$ is more stable than **28** but exhibits a similar J(Si–H) of 66 Hz.[88] Analogous manganese complexes $[Mn(\eta^2\text{-HSiR}_3)(CO)_3(P\{OCH_2\}_3CMe)_2]^+$ ($R_3 = Et_3$; PhH_2) were generated in a similar fashion at low temperatures but the J(Si–H) could not be measured due to

Mn quadrupolar broadening.[89] On heating these compounds decompose *via* heterolytic cleavage of the η^2-H–Si bond, typical behavior for a cationic silane complex because the silicon center becomes electron deficient upon coordination of the H–Si bond to metal and thus activated toward nucleophilic attack.

The σ-coordination of a silane has been proposed for the tripodal tren complex [Re(η^2-HSiHR$_2$)(tren)] (**29**) on the basis of increased *J*(Si–H) observed for two examples (R = Et: 44 Hz; R = Ph: 38 Hz) and by analogy with the related dihydrogen complex [Re(η^2-HD)(tren)] having the *J*(H–D) of 17 Hz (compared to 43 Hz in the free HD and 30 Hz usually observed in dihydrogen complexes).[90] This compound should be classified as having the rhenium center in an oxidation state intermediate between (III) and (V), corresponding to the ideal cases of a 3c–2e bond and complete oxidation addition of silane, respectively. Since such an oxidation state is not exceptionally high for rhenium, the only factor that seems to contribute to the formation of a σ-complex is the low donating ability of the rigid tren ligand, which may be due to the electron-withdrawing substituents on the nitrogen atoms. It has been suggested that steric pressure to maintain the trigonal coordination pocket may be the factor controlling the preference for the formal Re(III) state over Re(V).[90]

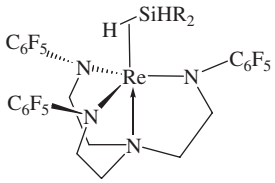

R =	Et	Ph
J(Si-H), Hz =	44	38

29

5. Group 8 Metals

The iron subgroup exhibits a plethora of nonclassical M···H···Si interactions both for mono- and dinuclear complexes.[13] Iron in the high formal oxidation states IV and ruthenium in the high formal oxidation states IV–VI are particularly prone to form such species. Some of them having three or more hydrides will be discussed in Section IV.

The iron complexes [Fe(η^2-HSiR$_3$)(CO(PR$'_3$)Cp]$^+$ (**30**, R$_3$ = Et$_3$, HPh$_2$, MeHPh, H$_2$Ph; R$'_3$ = Et$_3$, Ph$_3$)[91] are isolobal analogs of the manganese system **11** and chromium complexes **27** and are interesting in that they are rare examples of cationic silane complexes. These species were generated upon protonation of [Fe(SiR$_3$)(CO)(PR$'_3$)Cp] by HBAr$^F_4$ (Ar^F = 3,5-(CF$_3$)$_2$C$_6$H$_3$) at low temperature and by dihydrogen displacement by silane in [Fe(η^2-H$_2$)(CO)(PR$'_3$)Cp]$^+$ (Scheme 1). The complexes **30** are stable at room temperature in the presence of excess silane. The occurrence of nonclassical Si–H bonding was inferred from the observation of increased *J*(Si–H) of 58–67.3 Hz, which is about 30 Hz larger than in the related neutral complexes [Mn(η^2-HSiR$_3$)(CO)(PR$'_3$)Cp]. Obviously, such an increase in *J*(Si–H) is a combined effect of the smaller metal and the presence of a positive

charge, which leads to the decreased backdonation from the metal (see Section II.B). These two factors are compensated for by the presence of a donating phosphine ligand in place of carbonyl, so that the observed coupling constants are comparable to the J(Si–H) in the dicarbonyl derivatives [Mn(η^2-HSiR$_3$)(CO)$_2$Cp] (for instance, 63.5 Hz in [Mn(η^2-HSiHPh$_2$)(CO)$_2$Cp′]).[12]

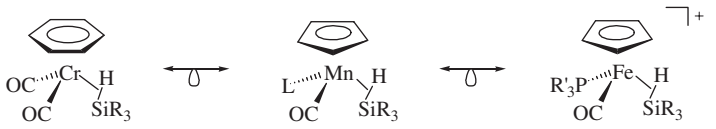

27 **11** **30**

J(Si-H) = 80 Hz J(Si-H) = 54.8-65.4 Hz J(Si-H) = 58 - 67.3 Hz

Analogous protonation of [Ru(SiCl$_3$)(PMe$_3$)$_2$Cp] (**31**) by (H*OEt$_2$)BAr$^F_4$ afforded a cationic silane σ-complex [Ru(η^2-HSiCl$_3$)(PMe$_3$)$_2$Cp]$^+$ (**32**) characterized by NMR spectroscopy and X-ray analysis.[92] The increased coupling constant J(Si–H) of 48 Hz suggests the presence of a Si–H interaction. The J(Si–H) shows small temperature dependence, increasing to 51 Hz at −65 °C. Such behavior can be attributed to the anharmonicity of the Si–H potential, leading to a shorter average Si–H distance at lower temperatures. The crucial hydride ligand found from the X-ray experiment is only 1.77(5) Å from the silicon atom, but the Ru–H distance of 1.60(5) Å is normal.[92] A comparison between [Ru(η^2-HSiCl$_3$)(PMe$_3$)$_2$Cp]$^+$ and the parent complex **31**[93] reveals the elongation of the Ru–Si bond upon the formation of a σ-complex from 2.265(2) to 2.329(1) Å and the decrease of the average Si–Cl bond length from 2.119 to 2.043 Å. It should, however, be taken into account that **31** has abnormally short Ru–Si and long Si–Cl bonds due to the negative hyperconjugation of the metal d-electrons with the antibonding orbital σ*(Si–Cl), as schematically shown below. For comparison, the related neutral complexes [Ru(H)(SiCl$_3$)(Cl)(PR$_3$)Cp*] have only marginally shorter Ru–Si bonds (range 2.3107(7)–2.3153(8) Å) than **32**.[94]

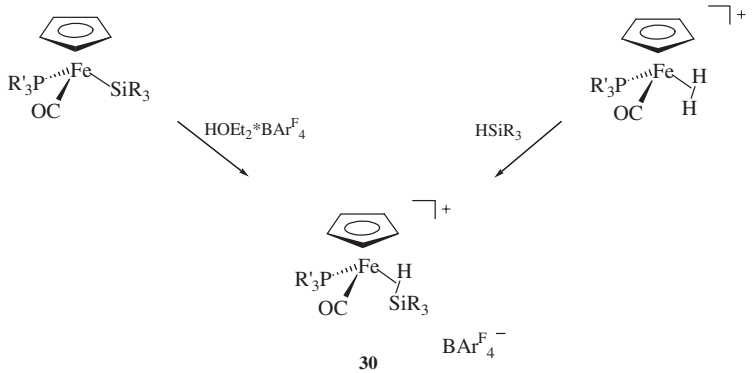

30

SCHEME 1.

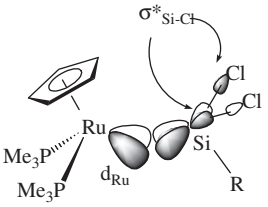

31

Chirik *et al*. have recently shown that the neutral high spin diiminepyridine iron fragment [Fe({(2,6-$Pr^i_2C_6H_3$)N═C(Me)}$_2$)(2,6-NC_5H_3)] can stabilize two η^2 Si–H silane bonds in the coordination sphere of iron.[95] The bis(silane) adduct **33** was prepared by dinitrogen substitution [Eq. (8)] and characterized by multinuclear NMR spectroscopy in solution and X-ray structure determination. The compound is fluxional at room temperature, but on cooling, a static structure with the C_s molecular symmetry and two nonequivalent silane ligands was observed. The Si–H bonds complexed to iron give rise to two high-field signals at −0.02 and −7.02 ppm, assigned on the basis of NOESY and ROESY NMR experiments to the apical and basal silanes, respectively. The ^{29}Si NMR spectra at −80 °C revealed two silicon signals having the Si–H coupling constants (to the proton in the Si–H–Fe bridge) of 54 and 119 Hz, among which the larger *J*(Si–H) of 119 Hz corresponds to a shorter Si–H bond of 1.59(2) Å in the basal silane. To date, this is the largest *J*(Si–H) observed in an isolated silane σ-complex. The smaller *J*(Si–H) of 54 Hz was found for the apical silane, which has a longer Si–H bond of 1.82(3) Å, both these parameters fall in the range normally observed in silane σ-complexes.[12,13] The basal Si–H bond is *trans* to the pyridine ligand and forms a much longer Fe–Si bond of 2.4733(7) Å, compared to 2.3266(8) Å found for the Fe–Si bond of the apical silane that is *trans* to a vacant site and exhibits a stronger coordination to the metal. A noteworthy finding is that the stronger coordination results in a reduced Si–H coupling to both the bridging and terminal hydrogen atoms (54 and 196 Hz vs. 119 and 220 Hz, respectively), which suggests a rehybridization at silicon upon the Si–H bond addition to metal. That is, more Si s character goes to the Si···H···M bonding but the Si–H coupling diminishes as the M–Si bond builds up. As has been discussed in Section II.D, such a rehybridization can lead to a significant Si–H coupling even when the Si–H bond is essentially reduced:

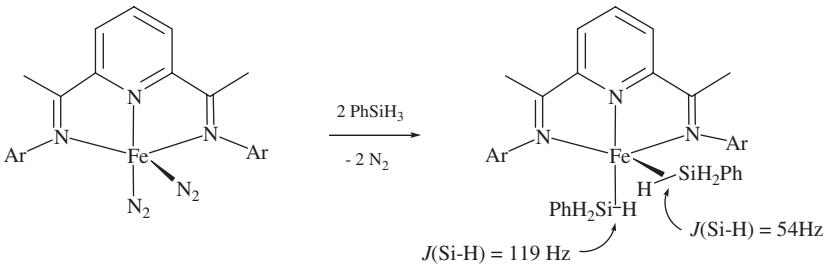

(8)

33

The first dinuclear μ-silane σ-complex of iron $[Fe_2(\mu\text{-}H)_2(\mu\text{-}H_2SiBu^t_2)Cp^*_2]$ (**34**) has been prepared by the reaction of silane $H_2SiBu^t_2$ with the dinuclear compound $[Fe_2(\mu\text{-}H)_4Cp^*_2]$, and the related compound $[Fe_2(\mu\text{-}H)_2(\mu\text{-}H_2SiPh_2)Cp^*_2]$ was obtained by silane exchange reaction.[96] A ruthenium analog, the complex $[Ru_2(\mu\text{-}H)_2(\mu\text{-}H_2SiBu^t_2)Cp^*_2]$, is also known.[97] These compounds resemble the historic Graham's complex $[Re_2(\mu\text{-}H_2SiMe_2)(CO)_8]$ (**6**) in having two Si–H bonds complexed to two different metal centers. A broad band at 1790 cm^{-1} in the IR spectrum was assigned to the Si–H–Fe vibration, and the metal-silicon bridging hydrides were found by an X-ray study at short Si–H distances of 1.60(5) and 1.64(5) Å. The Fe–Si bond of 2.376(1) Å is longer than the usual σ-bond, and although it is known that groups in a bridging position often have longer bonds than the terminal ones, the comparison with the μ-silylene derivative $[Fe_2(\mu\text{-}H)_2(\mu\text{-}SiPh_2)Cp^*_2]$ (Fe–Si bonds of 2.2582(8) and 2.2549(8) Å)[98] allows one to rule out an alternative μ-silylene formulation $[Fe_2(\mu\text{-}H)_2(H_2)(\mu\text{-}SiR_2)Cp^*_2]$ for **34**. The relatively low value for $\delta(^{29}Si)$ of 71 ppm is also more consistent with the nonclassical structure than with a dihydride-μ-silylene formulation. No data on the Si–H coupling have been given to verify the extent of Si–H bonding.

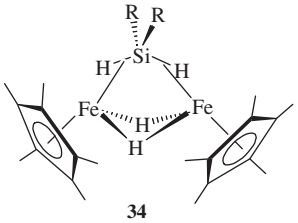

34

There is a problem on how the presence of a small iron center in the high formal oxidation state IV can effect the formation of a silane σ-complex. In this regard, two iron families, $[Fe(H)(SiR_3)_2(CO)Cp]$ and $[Fe(H)_2(SiR_3)_2(arene)]$, are worth discussing. Three crystal structures are known for the complexes $[Fe(H)(SiR_3)_2(CO)Cp]$ ($R_3 = F_2CH_3$,[99] Cl_3,[100] and $Ph(CH_3)_2$[101]), among which the hydride was found directly from an X-ray diffraction study only in the structure of $[Fe(H)(SiF_2CH_3)_2(CO)Cp]$. The observed Si–H distance of 2.06(7) Å is independent of the variation of the Fe–H distance (changing the Fe–H distance in the range 1.4–1.6 Å gives the Si–H distance range of 2.04–2.09 Å) and of the X–Fe–H bond angle (where X is the centroid of the Cp ring). Varying the latter angle from 117.5 to 127.5° corresponds to changing the Si–H distance in the range 2.02–2.11 Å, and therefore this value of the Si–H distance is mainly the result of the small Si–Fe–Si bond angle. This suggests that similar Si–H contacts can be expected for the other two compounds too. Schubert suggested that these species may contain a classically bonded SiR_3 group and a σ-complexed H–SiR_3 ligand,[12] which would make them isoelectronic and isostructural analogs of the manganese complexes $[Mn(\eta^2\text{-}HSiR_3)(PR'_3)(CO)Cp]$ (the anion SiR_3^- is isolobal with PR'_3) and of the iron complex **30** discussed above, but this contradicts the similarity of geometrical parameters of both silyls. A coupling constant J(H–Si) of 20 Hz was measured for the compound $[FeH(SiCl_3)_2(CO)Cp]$,[50] which, although slightly larger than the

normally observed one in classical silylhydride derivatives,[13] was rationalized as indicative of the classical nature. Alternatively, these compounds may contain two simultaneous Si–H interactions similar to the multiple H···Si···H interactions discussed in Section IV. A computational study on the electron density distribution and the sign of J(H–Si) is required to resolve this bonding dilemma.

The formal Fe(IV) complexes [Fe(H)$_2$(SiR$_3$)$_2$(η^6-arene)] do not have a π-accepting ligand such as carbonyl but contain a combination of a small metal from the first transition series in a high formal oxidation state and a weakly donating arene ligand, all three factors being good for the formation of a σ-complex.[2] The crystal structures of [Fe(H)$_2$(SiCl$_3$)$_2$(η^6-arene)] (arene = C_6H_6, toluene, and *p*-xylene) and of [Fe(H)$_2$(SiF$_3$)$_2$(η^6-toluene)] are available and show slightly longer Fe–Si bonds in the SiF$_3$ derivative (2.251(5) and 2.261(5) Å) compared with the SiCl$_3$ derivative (range 2.207(3)–2.226(2) Å).[102,103] Such a trend is unusual since the electron-withdrawing groups on silicon are expected to render the Si–M bond shorter in accordance with Bent's rule. These values can be compared with what is seen forthe four-leg piano-stool complexes [Fe(H)(SiCl$_3$)$_2$(CO)Cp] (2.252(3) Å) and [Fe(H)(SiMeF$_2$)$_2$(CO)Cp] (2.249(1) Å) which may be nonclassical (see above). However, a set of arguments exists for the classical description of the complexes [Fe(H)$_2$(SiR$_3$)$_2$(η^6-arene)]. Thus, the Mössbauer spectrum of [Fe(H)$_2$(SiCl$_3$)$_2$(η^6-toluene)] is in accord with the Fe(IV) oxidation state and the measured J(Si–H) of 15 Hz was interpreted to signal the absence of a Si–H interaction in accordance with Schubert's criterion of 20 Hz. It is however noteworthy that the longer Fe–Si bond in the SiF$_3$ derivative corresponds to the higher field shift of the hydride resonance (−19.0 ppm vs. −17.07 ppm), which may indicate the presence of some Si–H bonding in the former. A computational study may help to elucidate the bonding situation in these compounds.

The addition of silanes HSiR$_3$ (R$_3$ = MeCl$_2$, Cl$_3$, PhH$_2$ or PhHSiPhH$_2$) to the unsaturated species [RuCl(R$_3$P)Cp*] affords the adducts [Ru(H)(SiR$_3$)(Cl)(PPr$^i_3$)Cp*], which were originally described as classical according to the low Si–H coupling constants (<20 Hz[12]), measured at room temperature.[94,104,105] In contrast, the silane HSiMe$_2$Cl reacts at room temperature to afford the dihydride derivative [Ru(H)$_2$(SiClMe$_2$)(PPr$^i_3$)Cp*], but an intermediate [Ru(η^2-HSiClMe$_2$)(Cl)(PPr$^i_3$)Cp*] (**35**) can be trapped below −10 °C.[106] The ^{1}H NMR spectrum at −40 °C reveals a hydride signal at −9.65 ppm flanked by the ^{29}Si satellites with the J(H–Si) = 33.5 Hz, suggesting the presence of a Si–H σ-interaction. The adduct [Ru(η^2-HSiPhMe$_2$)(Cl)(PPr$^i_3$)Cp*] (**36**), exhibiting a similar J(H–Si) of 32 Hz, is even less stable and is observed only at −90 °C. No silicon–hydride coupling can be resolved in the hydride region of [Ru(HSiH$_2$Ph)(Cl)(PPr$^i_3$)Cp*] (**37**),[104,106] but cooling to −10 °C affords a J(H–Si) of 30 Hz, suggesting a structure similar to that of **35** and **36**. The formulation of **35**–**37** as σ-complexes is in accord with the high formal oxidation state IV of the metal and the presence of an electron-withdrawing chloride ligand on ruthenium.[2] Taking into account the isolobal relationship of the silyl and phosphine ligands, the complexes **35**–**37** can be considered as isolobal analogs of the σ-complexes [Ru(η^2-HSiCl$_3$)(Me$_3$P)$_2$Cp*]$^+$ [92] and [Ru(η^2-H$_2$)(Cl)(PPhPr$^i_2$)Cp*].[107] A weak Si–H interaction may be present in the compound [Ru(η^2-HSiMeCl$_2$)(Cl)(PPr$^i_3$)Cp*] too, since this easily eliminates the

silane upon reduced pressure or addition of a phosphine.[94] The remarkable feature of **35** is that according to the X-ray structure and DFT calculations it has simultaneously a residual σ-Si–H interaction and the stabilizing RuCl···Si–Cl hypervalent interaction, stemming from the donation of the Ru-bound chloride lone pair to the σ*(Si–Cl) antibonding orbital of the silane. The latter bonding results in the elongation of the Si–Cl bond to 2.155(1) Å, a value beyond the range 2.094–2.149 Å found for classical chlorosilyl complexes.[106] The Si–H coupling constant, calculated for the series of model complexes $[Ru(H)(SiMe_{3-n}Cl_n)(Cl)(PMe_3)Cp]$ $(n = 0-3)$ is *negative* and increases from −23.0 to −0.4 Hz as n rises from 0 to 3, corresponding to a decrease of the Si–H σ-interaction. The RuCl···Si hypervalent interaction is absent in $[Ru(\eta^2\text{-}HSiMe_3)(Cl)(PMe_3)Cp]$ and decreases from $[Ru(\eta^2\text{-}HSiMe_2Cl)(Cl)(PMe_3)Cp]$ to $[Ru(H)(SiCl_3)(Cl)(PMe_3)Cp]$. The rotation of the silyl group in $[Ru(\eta^2\text{-}HSiMe_2Cl)(Cl)(PMe_3)Cp]$ was also found to weaken the RuCl···Si interaction because it breaks the favorable *trans* position of the chloride on ruthenium and the silicon-bound chlorine, but does not affect the Si–H σ-interaction much:[106]

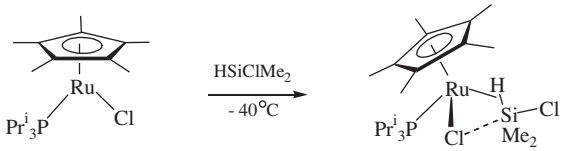

(9)

35

The unsaturated complex [Ru(Cl)(SiL$_2$)Cp*] of a stable West–Denk-type silylene is an analog of the compound [Ru(Cl)(PPr$^i_3$)Cp*] through the isolobal relationship between the silylene SiL$_2$ and phosphine. However, in contrast to the formation of the phosphine species **35**–**37**, the addition of H_3SiR to [Ru(Cl)(SiL$_2$)Cp*] does not give a hydride silyl(silylene) derivative but rather a bimetallic species **38** having the Ru–H–Ru, Si–H–Ru, and Si–Cl–Ru bridges [Eq. (10)].[108] The structure of **38** was assigned on the basis of ^{1}H and ^{29}Si NMR data, and confirmed by an X-ray study of one of the complexes (R = *n*-hexyl). The hydride atoms were not found but the presence of a Si···H···Ru interaction was derived from the observation of $J(Si-H) = 42$ Hz and a broad band at 1869 cm^{-1} assigned to the η^2-Si–H bond:

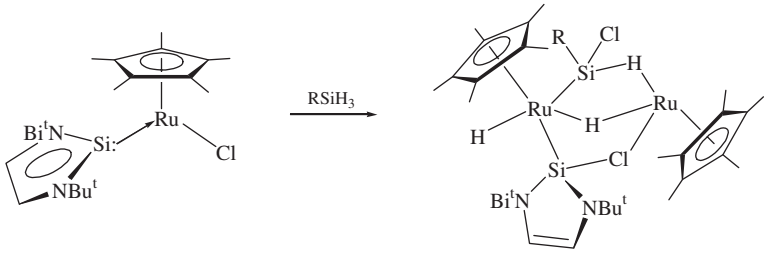

(10)

38

No well-defined silane σ-complexes are known for osmium. The compound $[OsH_2(SiEt_3)Cl(CO)(PPr^i_3)_2]$ has been found in equilibrium with the dihydrogen species $[Os(\eta^2\text{-}H_2)(SiEt_3)Cl(CO)(PPr^i_3)_2]$, rather than with $[OsH(\eta^2\text{-}HSiEt_3)Cl(CO)(PPr^i_3)_2]$, as judged by the measurement of short relaxation time $T_1 = 17$ ms for the hydride signals,[109] but the related compound with phenyl groups on silicon could be the silane σ-complex $[OsH(\eta^2\text{-}HSiPh_3)Cl(CO)(PPr^i_3)_2]$.[109] The calculations at the MP2 and MP4 levels of a model system $[OsH_2(SiH_3)Cl(CO)(PH_3)_2]$ reveal that both the η^2-H_2 and η^2-$HSiH_3$ forms are close in energy[110] so that the preference of one form vs. another can be the result of subtle factors such as different substitution at silicon or phosphorus atoms.

6. Groups 9–10 Metals

At the moment there are no experimentally characterized silane σ-complexes of cobalt and nickel, but several mononuclear species are known for their heavier analogs.[13] Crabtree's iridium complex $[IrH_2(\eta^2\text{-}HSiEt_3)_2(PPh_3)_2]^+$ is noteworthy in that it was proposed to contain two η^2-coordinated silane groups and also as an example of a cationic silane σ-complex,[111] which would be the first representative of this kind. No doubt, the reason for the incomplete addition of the Si–H bond is the presence of a positive charge and the high formal oxidation state of the metal in the otherwise Ir(VII) tetrahydride bis(silyl) species. The structure of this and the related complex $[IrH_2(\eta^2\text{-}HSiEt_3)(MeOH)(PPh_3)_2]^+$ was deduced on the basis of kinetic data on the catalytic silane alcoholysis and by analogy to other σ-complexes. Some stereochemical information for these complexes was derived from ^{1}H NMR, which was consistent with the *cis* position of the two phosphine ligands, each of which was *trans* to a silane ligand and also consistent with the trans positions of two classical hydride ligands. However, no data on the J(Si–H) or solid state structure of these highly fluxional and unstable compounds are available.

The Rh(V) half-sandwich complex $[RhH_2(SiEt_3)_2Cp^*]$ has been found by ND to possess isolated silyl and hydride ligands with long Si–H contacts of 2.212(2) Å thought to be nonbonding and corresponding to low J(Si–H) of 7.9 Hz.[112] The related iridium complex $[IrH_2(SiEt_3)_2Cp^*]$ exhibits even longer Si–H distances (2.272(2) and 2.384(2) Å).[113] All experimental data point to the classical nature of these compounds, which should be considered as remarkable taking into account that other Rh(V) and Ir(V) compounds are strong oxidants[112,113] and therefore, *an intramolecular oxidation* of the H^- and $SiEt_3^-$ ligands to give a η^2-$HSiEt_3$ ligand may have seemed plausible. It was noted that $[RhH_2(SiEt_3)_2Cp^*]$ was sterically strained due to the repulsion of the bulky Cp* and $SiEt_3$ ligands.[112]

Steric strain appears to be the main factor leading to the formation of a nonclassical structure for the closely related trisilyl complex $[RhH(SiEt_3)(SiMe_3)_2Cp]$.[114] The hydride exhibits a J(Si–H) of 24.3 Hz to the $SiEt_3$ ligand and J(Si–H) of 6 Hz to the $SiMe_3$ groups, leading on the basis of Schubert's criterion of 20 Hz to the formulation of a silane σ-complex $[Rh(\eta^2\text{-}HSiEt_3)(SiMe_3)_2Cp]$ (**39**). If this formulation is correct, the σ-complex is formed from the bulkiest silyl $SiEt_3$, which should provide the greatest relief of interligand repulsions through the

elongation of the Rh–$SiEt_3$ bond. And indeed, the lower rhodium–silicon coupling constant for the $SiEt_3$ group (19.2 Hz) corresponds well to the larger J(Si–H) (compare with J(Rh–Si) of 33.3 Hz for the $SiMe_3$ group), suggesting weaker Ru–$SiEt_3$ bonding. The related complexes [Rh(H)($SiEt_3$)$_3$Cp], [RhH($SiEt_3$)$_2$($SiMe_3$)Cp], and [Rh(H)($SiMe_3$)$_3$Cp] all have J(H–Si) values <20 Hz (12.8, 19.3 Hz (SiEt) and <3 (SiMe), 13.5 Hz, respectively) but a dynamic process that places different silyl groups in the η^2-position has been proposed.[114] One should take into account that the metal–ligand and ligand–ligand potentials in these silylhydride systems can be rather soft and highly influenced by the solvation and crystal-packing effects, which may at least partly account for the observed discrepancy between the solution and solid state experiments. These polysilyl complexes appear to be good candidates for a theoretical study of the Si–H bonding in highly stretched silane σ-complexes. This conclusion is further supported by the recent observation that the complex [RhH$_2$($SiEt_3$)(Bpin)Cp] (Bpin = (pinacolato)boryl) has some degree of B–H interaction.[115] Since the vacant orbital on boron is effectively involved in conjugation with the oxygen p-orbitals, such a "p-saturated" boryl can be considered as an analog of a silyl ligand,[16] and thus the complex [RhH$_2$($SiEt_3$)(Bpin)Cp] is related to [MH$_2$($SiEt_3$)$_2$Cp*] (M = Rh, Ir).

The Rh(III) complexes [Rh(H)(SiR_3)(*t*-butylacrylate)Cp] (**40**) exist in two isomeric forms of comparable energy, interconverting through an intramolecular process that does not involve a reversible [1,3] hydride or [1,3] silyl migration.[116] The formation of a silane σ-complex intermediate, [Rh(η^2-HSiR_3) (*t*-butylacrylate)Cp], was invoked to account for the dynamic ^{1}H NMR data. In the case R = OMe, the silane σ-complex was estimated from kinetic data to lie 10 kJ mol^{-1} higher in energy than the silylhydrido form. The H–Si coupling constants in **40** for R = Me or Et are in the range 15–19 Hz but increase to 38 Hz for R = OMe. Such a large value, significantly exceeding Schubert's criterion of 20 Hz, was attributed to a two-bond coupling, increased by the presence of three electron-accepting groups at silicon due to the Bent's rule effect. This conclusion is further substantiated by the observation of a much larger rhodium–silicon coupling (39 Hz) in comparison with the J(Rh–Si) of 18–30 Hz observed for other R's on silicon. With only one electron-accepting group at silicon present, i.e. $R_3 = ClMe_2$, the J(Si–H) is also small (15 Hz). If such a large silicon–hydride coupling in [Rh(H)(Si(OMe)$_3$)(*t*-butylacrylate)Cp] is indeed *via* two bonds, a critical revision of the assignment of nonclassical structures on the basis of J(H–Si) > 20 Hz will be required. This is particularly relevant to the compounds like the tantalum complex **25** and the rhodium complex **39**, where the presence of a nonclassical Si–H interaction is not supported by independent evidence.

Reaction of the compound [Rh(Me)(ClCD_2Cl)(PMe_3)Cp*]$^+$ with 3–5 equiv. of $HSiR_3$ (R = Me, Et) at −60 °C gives a silyl (η^2-silane) complex [Rh(η^2-HSiR_3)(SiR_3)(PMe_3)Cp*]$^+$ [**41**, Eq. (11)] characterized by the observed coupling constant J^{obs}(H–Si) measured from the ^{29}Si satellites in the ^{1}H NMR spectrum (28.5 Hz for R = Me and 27.8 Hz for R = Et).[117] Since these compounds are highly fluxional, exchanging the hydride between the silyl and silane sites, these values of J^{obs} correspond to the genuine ^1J(H–Si) of 57 Hz for R = Me and 56 Hz for R = Et. An exchange between the η^2-silane and free silane $HSiEt_3$ was observed in the

case R = Et. In solution **41** eliminates the disilane $R_3Si–SiR_3$ and, after addition of an equivalent of $HSiR_3$, rearranges into a species with the possible formulation $[Rh(H)(\eta^2\text{-}HSiR_3)(PMe_3)Cp^*]^+$ or $[Rh(H)_2(SiR_3)(PMe_3)Cp^*]^+$. No ^{29}Si satellites were observed, which either indicates a classical structure or is due to a rapid exchange of the hydride and the Si–H sites and the loss of thus diminished J^{obs} ($J^{obs}={}^1J(Si-H_{term})+{}^2J(Si-H_{Ru})$) in the signal width ($v_{1/2}\approx 50$ Hz)[116] (see, however, the discussion of the relative signs and magnitudes of ^1J(Si–H) and ^2J(Si–H) in Section II.D). A similar result was obtained for the reaction of $[Rh(Me)(ClCD_2Cl)(PMe_3)Cp^*]^+$ with excess $HSiPh_3$, whereas a reaction with 1 equiv. of the silane affords the agostic complex $[Rh(\eta^2\text{-}HSiPh_2\text{-}C_6H_4\text{-})(PMe_3)Cp^*]^+$ discussed in Section II.F.2. In analogous iridium chemistry the product was formulated as an Ir(V) compound $[Ir(H)_2(SiMe_3)(PMe_3)Cp^*]^+$ on the basis of NMR data:[118]

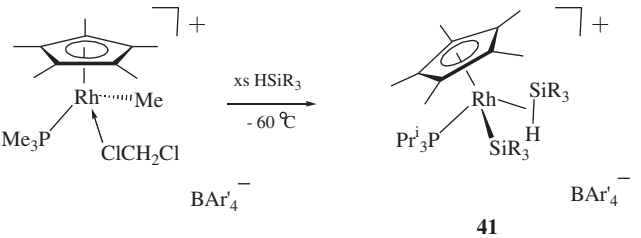

(11)

41

Ar'= 3,5-$(CF_3)_2C_6H_3$)

The only example of a monomeric silane σ-complex of palladium was suggested to arise from the reaction of a cationic diimine complex $[Pd(Me)(N(OCH_2CH_2CH_2O\text{-}Me)=CMe)_2]^+[B\{C_6H_3(CF_3)_2\text{-}1,2\}_4]^-$ with the silane $HSiEt_3$ at −78 °C, but the product was characterized only by ^1H NMR. On warming to room temperature it decomposes, giving the products of Si–H cleavage, a behavior typical for cationic η^2-silane complexes. In the analogous platinum chemistry the product is the corresponding cationic silyl hydride complex.[119]

However, many bimetallic species of Pt and Pd with nonclassical Si···H···M interactions have been discovered and are thoroughly described in the previous reviews.[13,14,22] Some related recently studied complexes of this type are $[Pd_2(\mu,\eta^2\text{-}H\text{-}SiPh_2)_2(PMe_3)_3]$,[120] $[PtRh(\mu\text{-}H)(\mu,\eta^2\text{-}H\text{-}Si\{C_6H_4F\text{-}p\}_2)(SiCl\{C_6H_4F\text{-}p\}_2)(PMe_3)_4]$,[121] $[Pd_2(\mu,\eta^2\text{-}H\text{-}SiH\{2\text{-}Pr^i\text{-}6\text{-}MeC_6H_4\})_2(PMe_{3-n}Ph_n)_2]$,[122] $[Pd_2(\mu,\eta^2\text{-}H\text{-}SiPh_2)_2(PCy_3)_2]$,[123] and $[PdPt(\mu,\eta^2\text{-}H\text{-}SiPh_2)_2(PCy_3)_2]$.[123]

The gas-phase interaction of $H_3C–CH_2–SiH_3$ and its analogs $H_3C–CH_2–XH_3$ (X = C, Ge) with Ni^+ has been studied computationally by means of B3LYP calculations and AIM study.[124] Several σ-complexes have been found on the potential energy surface for all the (hetero)propanes, but the structure of the global minimum crucially depends on the nature of the element X. For X = Si and Ge a η^2-complex **42** is the most stable species, whereas for propane a 1,3-chelate system **43** with two η^1-C–H···M interactions lies lower in energy. NBO (Natural Bond Orbital) analysis of the electron density of **42** revealed the existence of two dative interactions from the X–H σ bond supported by backdonation from nickel in accord with the conventional DCD scheme (see Section II.B). The high value of electron density in the bond critical points ($0.096e^*\,au^{-3}$ for Si and $0.101e^*\,au^{-3}$ for

Ge), revealed by the AIM study for the X–H–Ni interactions, and the negative sign of the energy density establish the covalent nature of these interactions. These nonclassical species **42** and **43** are particularly stable for X = Si, Ge, which has been attributed to the higher electron-donor ability of these XH_3 groups.

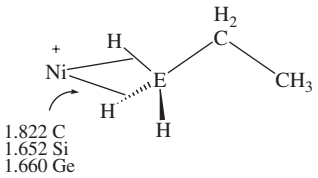

42

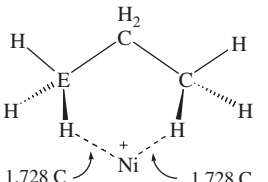

43

7. Group 11 Metals

No experimental data exist for the silane complexes of copper and its analogs but the complexation of $H_3C–CH_2–XH_3$ (X = C, Si, Ge) to Cu^+ has been studied computationally by means of B3LYP method supplemented by AIM analysis.[125] Structures similar to **42** and **43** with the corresponding bond critical points have been found. The comparison of propane with ethylsilane and ethylgermane shows that the XH bonds, where X = Si or Ge, are both better electron donors and electron density acceptors than the C–H bond, but in all cases the donation component predominates. For example, the calculated second-order NBO orbital interactions have the following ratios of donation/backdonation energies (in kcal mol^{-1}) for the copper analog of **42**: 14/4.7 for C, 45.1/11.5 for Si and 53.9/13.7 for Ge. Comparing different metal ions, the coordination of the species $H_3C–CH_2–XH_3$ to Cu^+ is weaker than Ni^+, which is due to the more efficient donation and backdonation interactions in the case of nickel. This difference was ascribed to the nickel monocation being an open-shell system.[125]

F. *Si···H···M Agostic Bonding*

Si···H···M agostic bonding is usually described in terms of the DCD scheme discussed in Section II.B and is experimentally identified by means of the same structural and spectroscopic criteria used for silane σ-complexes. The difference between the agostic bond **8** and σ-bond complexation, as in **7**, is the presence of a supportive link to the metal in the former, which can be either a sequence of atoms, as in the case of β- (one atom), γ- (two atoms), δ- (three atoms), and so on agostic species, or just a chemical bond between M and Si (classified as α-agostic interaction). Formally speaking, the bimetallic complexes **16**, **17**, **22**, **34**, and **38** and related compounds should also be regarded as agostic, although sometimes their classification in terms of β, γ, δ etc. species can be dubious (see, for example, structures **16** and **22**). Agostic interaction is often considered as an intramolecular

version of **7**, which is a quite correct description in the case of long-chain agostic species having flexible bridges. However, as we shall see below, short and rigid chains may impose essential restrictions on the interaction of the Si–H bond with a metal. The Si···H···M α-agostic interaction is particularly a recently discovered phenomenon and its theoretical description is still in its infancy. The following discussion will be systematized according to the length of the link and the nature of bridging atoms.

1. δ- and Other High-Order Si···H···M Agostics

Relatively little work has been done on high-order Si···H···M agostic interactions and, no species of an order higher than δ-agostics have been reported, which might be due to entropic effects.

Addition of the silylphosphines $H\text{-}SiR_2CH_2CH_2PPh_2$ (R = Me, Ph) to $[Mn(CO)_3Cp']$ under photolytic conditions affords the δ-agostic product $[Mn(\eta^3\text{-}H\text{-}SiR_2CH_2CH_2PPh_2)(CO)Cp']$, characterized by spectroscopic methods and X-ray study of one of the products (R = Me).[126] The spectral and structural properties of these derivatives are very similar to those of other manganese compounds of the family **11**, showing no specific effect of the long-chain agostic bonding on the extent of the Si–H complexation to metal.

The related family of tungsten compounds $[W(\eta^3\text{-}H\text{-}SiR_2CH_2CH_2PPh_2)(CO)_4]$ (**44**) was prepared analogously by a photochemical reaction of $[W(CO)_3]$ with $HSiR_2CH_2CH_2PPh_2$:[127]

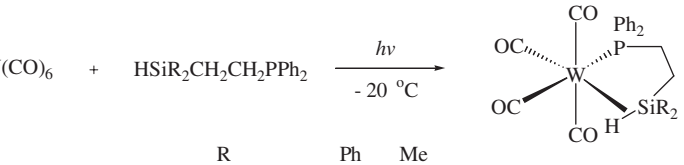

(12)

R	Ph	Me
J(Si-H), Hz	98.1	95.2

44

IR data for the CO region of **44** are consistent with the octahedral geometry of these complexes, whereas the large Si–H coupling constants indicate the presence of strong Si–H bonding. The values of 98.1 (R = Ph) and 95.2 Hz (R = Me) come at the upper end of *J*(Si–H) usually observed in silane σ-complexes (40–80 Hz);[12,13] thus, in **44**, the Si–H bond is not very stretched. Schubert suggested that this can be a feature of the agostic interaction, so that "incorporating Si–H bonds into a chelate system allows one to arrest the oxidative addition of the Si–H bonds at an earlier stage than in corresponding nonchelated complexes."[127] Relatively large *J*(Si–H) are indeed often observed in other Si···H···M agostic systems, but the related unchelated $[W(\eta^2\text{-}H\text{-}SiR_3)(PR'_3)(CO)_4]$ is not available for direct comparison with **44**. It is still unclear whether the large *J*(Si–H) in **44** is the result of the presence of four electron withdrawing carbonyl ligands or is due to a specific chelate effect, but there is no doubt that the latter does help to stabilize the system. The compound $[W(\eta^2\text{-}H\text{-}SiPh_3)(PPh_3)(CO)_4]$ is too unstable,[127] whereas the coordination of silanes to the less electrophilic fragments $[M(PR_3)_2(CO)_3]$, as in Kubas's complexes **12** and their tungsten analogs, results in smaller *J*(Si–H) of 30–60 Hz^2,

and some of them, such as $[W(H)(SiH_2Ph)(PR_3)_2(CO)_3]$ (R = Cy, Pr^i), are classical silylhydrides. A related dimeric species **45** also has a reduced *J*(Si–H) of 52 Hz, which probably corresponds to a more stretched Si–H interaction.[128]

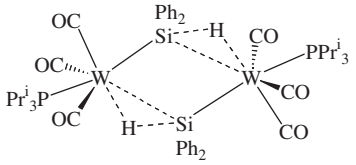

45

2. γ-Agostic Si···H···M Interaction

The first example of a γ-agostic Si···H···M interaction was reported for the compound **46** obtained *via* unusual thermal rearrangement of the silylhydride precursor $[Ta(H)(Si\{SiMe_3\}_3)(=N\{2,6\text{-}Pr^i_2C_6H_3\})(Cp^*)]$.[76]

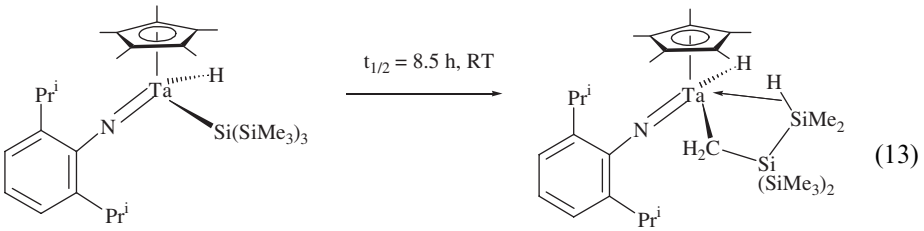

(13)

46

The connectivity of **46** was inferred from spectroscopic data that show (^{1}H NMR) the presence of diastereotopic methylene hydrogens, a hydrogen substituent at silicon and a Ta-bound hydride. The Si–H signal (2.57 ppm) was found ca. 2 ppm in a higher field than expected for a typical Si–H group, which suggests that this group is involved in nonclassical bonding. An exceptionally large coupling constant of 9 Hz between the Ta–H and Si–H hydrogens was observed, which cannot be due to a 5-bond coupling. The ^{29}Si NMR spectrum revealed a large *J*(Si–H) of 78 Hz that is slightly temperature dependent, whereas the IR spectrum shows the Si–H stretch at 1726 cm^{-1}, well below the typical values found for the Si–H bond (usually around 2150 cm^{-1}). The connectivity of **46** was further confirmed by the hydrolysis with H_2O or D_2O, which gave the silane product $Me_2HSi\text{-}Si(SiMe_3)_2\text{-}CH_2\text{-}H(D)$. Altogether, these data establish that the Si–H hydrogen is involved in a nonclassical interaction. The value of *J*(Si–H) of 78 Hz is interesting in that it is noticeably lower than the values observed in other formally d^0 Si···H···M agostic complexes (usually about 150 Hz), in which backdonation is absent. The reason for such a low coupling is not quite clear, although the presence of a donating silyl substituent at the γ-silicon atom could be a possibility. In the nonclassical disilyl cation **15**, however, the value of *J*(Si–H) is only 39 Hz.[60]

Rhodium complex $[Rh(SiPh_3)(ClCD_2Cl)(PMe_3)Cp^*]^+$, prepared by the C/Si exchange between $[Rh(Me)(ClCD_2Cl)(PMe_3)Cp^*]^+$ and an equivalent of $HSiPh_3$ at −80 °C, rearranges above −40 °C to the agostic compound **47** [Eq. (14)].[117] The J(H–Si) of 84 Hz determined from the ^{29}Si satellites suggests the presence of a H–Si bond coordinated to the Rh(III) center. In the related iridium chemistry the activation of the Si–H bond proceeds further to give an Ir(V) derivative $[Ir(H)(\text{-}SiPh_2\text{-}C_6H_4\text{-})(PMe_3)Cp^*]^+$:[129]

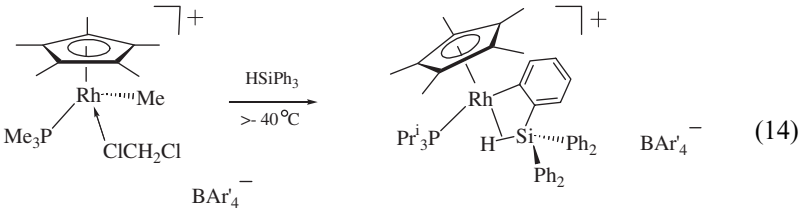

(14)

Another example of γ-agostic Si···H···M interaction has been recently reported for the platinum complex **48** obtained by the insertion of dimethyl acetylenedicarboxylate into the Pt–Si bond of $[Pt(SiHPh_2)_2(PMe_3)_2]$ [Eq. (15)]. **48** was characterized by a Pt–H coupling constant of 14 Hz and a J(Si–H) of 196 Hz, the latter value being slightly reduced compared with 206 Hz in the free $Ph_2SiH(CH{=}CH_2)$. These data and a small red shift of the Si–H vibration vs. free silane (2078 cm^{-1} vs. 2124 cm^{-1}) were interpreted to signal the occurrence of agostic bonding.[130] Similar features were observed for the *cis*-isomer of **48** and the related dmpe derivative. The X-ray structure of **48** revealed that the Si–H bond was directed toward the platinum atom to give a long Pt–H contact of 2.93 Å and a long Pt–Si distance (3.657(2) Å). This structural feature strongly resembles the coordination of the Si–H bond to the zirconium atom in **22**. In both cases, the interaction between the metal and the Si-bound hydrogen is rather weak; it is tempting to speculate that, at least in the former case, this is due to the rigidity of the alkenyl bridge, which prevents a closer approach of the Si–H bond to the metal from the vertex of a square pyramid. Although γ-agostic bond in **48** is weak, it is apparently related to the reversible silane elimination from *cis*-**48** to give a silametalacyclobutene derivative $[Pt\{\text{-}SiPh_2C(CO_2Me){=}C(CO_2Me)\text{-}\}(PMe_3)_2]$.

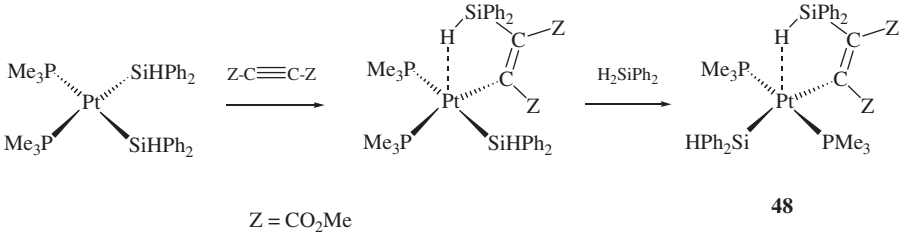

(15)

3. β-Agostic Si···H···M Interaction

β-Agostic Si···H···M bonding is the oldest and best studied type of agostic interactions involving silicon atoms. Such interactions are known for carbon (7 classes of complexes), phosphorus (1 example), and nitrogen (5 examples) bridging atoms. With few exceptions, the known β-agostic Si···H···M interactions have the $J(\text{Si–H}) > 100$ Hz, i.e. are intermediate between those normally observed in silane σ-complexes (range 40–80 Hz) and free silanes (180–200 Hz). Such large values suggest a strong Si–H interaction and hence a weak complexation of the Si–H bond to metal. The reason for this appears to be the additional stabilization provided by the atom in the α-position holding the Si–H bond in close proximity to metal, so that a stable structure can be achieved for a rather early stage of the Si–H bond oxidative addition. The silane σ-complexes with a comparable degree of Si–H activation are probably too unstable toward silane elimination to permit their isolation and characterization by common techniques (see, however, the compound **33** as an exception). In spite of this, many X-ray characterized structures have the M–Si and M–H distances close to the values found in classical silyl and hydride complexes, whereas the Si–H bonds appear to be somewhat shorter than in silane σ-complexes. The following discussion is systematized according to the type of bridge.

a. Carbon Bridges

An interesting feature of the β-agostic Si···H···M interactions with carbon bridges is that with one exception, all known complexes contain an unsaturated carbon center forming multiple bonds either to metal or other substituents at carbon. Thus, most of them are observed for silyl-substituted alkene or alkyne ligands coordinated to metal through their π-system (beside the Si–H bond). This feature appears to be merely a coincidence because the theory does not require any unsaturation at the bridging atom for the agostic interaction to occur. The first agostic compound from this series, **49**, was generated by photolysis of the 18e Fischer carbene complex $[W(=C\{NMe_2\}SiHMes_2)(CO)_5]$ [Eq. (16)].[131] The Si–H bond coordination to metal stabilizes this otherwise unsaturated 16e complex formed upon CO extrusion:

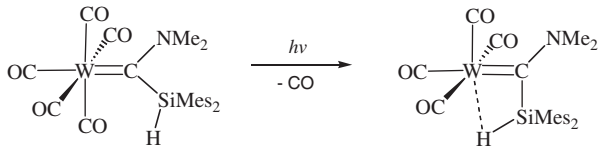

(16)

49

In **49**, the ^{1}H NMR signal of the Si–H group at −2.40 ppm is shifted to higher field relative to the Si–H signal of the starting compound (6.56 ppm), indicative of the participation of the hydrogen atom in the formation of a bridge. The strongest piece of evidence for the W···H···Si bond comes from the observation of a large J(Si–H) of 109 Hz. This is about twice as large as normally observed in silane σ-complexes but lower than in other carbon-bridged β-agostic complexes discussed below. The

X-ray structure analysis of **49** revealed that agostic bonding causes a severe distortion of the carbene ligand, so that the W–C–Si bond angle is reduced to 87.8(6)°, compared with 113.1(4)° in the starting complex. The hydride atom was, however, found closer to the silicon atom, the W–H and Si–H distances being 2.1(1) and 1.5(1) Å, respectively.[131]

The magnesium reduction of titanocene dichloride in the presence of alkynylsilanes affords a family of agostic complexes **50** (Scheme 2).[132] The same compounds can be obtained by the acetylene exchange reaction starting from $[Ti(\eta^2\text{-}Me_3SiC_2SiMe_3)Cp_2]$.[133] The analogous zirconocene complexes were prepared by acetylene exchange/THF extrusion reaction between $[Zr(\eta^2\text{-}Me_3SiC_2SiMe_3)(THF)Cp_2]$ and the alkynylsilane $RC{\equiv}CSiMe_2H$.[132]

The X-ray structure determination of complex $[Ti(\eta^4\text{-}H\text{-}SiMe_2C{\equiv}CBu^t)Cp_2]$ reveals the Si–H bond coordinated to titanium to form a Ti–H bond of 1.82(5) Å and the Si–H bond of 1.42(6) Å, both in the normal ranges for these bonds.[133] The X-ray structure of the related complex $[Zr(\eta^4\text{-}H\text{-}SiMe_2C{\equiv}CBu^t)Cp_2]$ (Fig. 3) shows a normal Zr–H bond (2.042(4) Å) and elongated Si–H bond (1.634(4) Å), which nicely corresponds to a smaller *J*(Si–H) (*vide infra*).[132] The salient feature of both structures is the *trans*-conformation of the alkyne ligand, which is in contrast to the parent compounds $[Ti(\eta^2\text{-}RC{\equiv}CR)Cp_2]$ where only *cis*-conformation is found. It is this distortion which allows for the close proximity of the Si–H bond and the metal. Another interesting feature is the somewhat contracted Si–C bonds (1.787(3) and 1.766(6) Å), which implies a partial multiple character and suggests that these species can be considered as intermediates toward the hydride(silaallene) complexes (ordinary Si–C bonds are found in the range 1.87–1.97, whereas the Si=C bond in a silaallene is 1.04 Å).[132] Complexes **50** and their zirconium analogs exhibit Si–H coupling constants in the range 68–123 Hz (Table I),[132] which is significantly less than a one-bond Si–H coupling in free silanes but exceeds the values

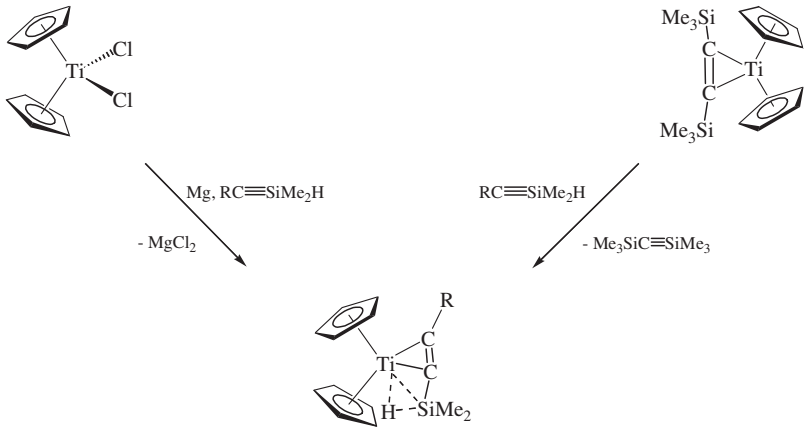

50

SCHEME 2.

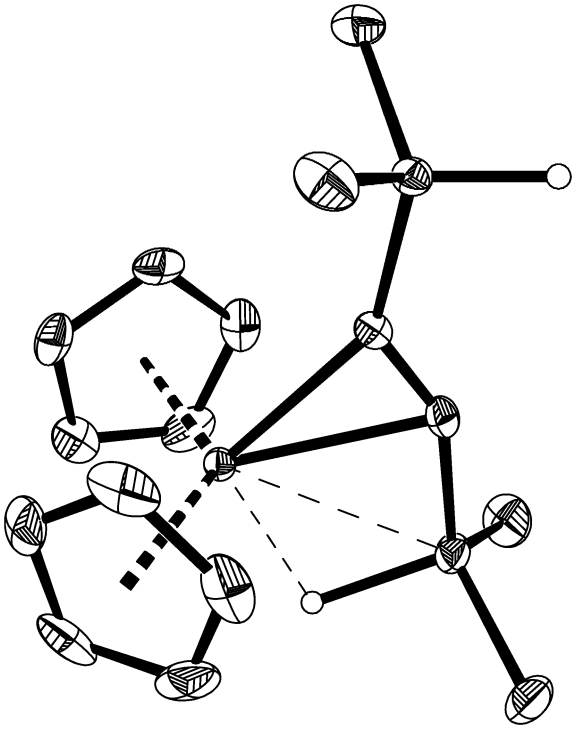

FIG. 3. The molecular structure of complex [Zr(η^4-H-SiMe$_2$C$\equiv$CSiMe$_3$)Cp$_2$]. (Reproduced from Ref. 132, with permission from Wiley-VCH.)

TABLE I
SELECTED SPECTROSCOPIC DATA[a] FOR COMPLEXES **50** AND THEIR ZIRCONIUM ANALOGS

Compound	IR ν(SiH), ν(C$\equiv$C) (cm^{-1})	NMR δ (^{1}H) (ppm)	NMR J(Si–H) (Hz)
[Ti(η^4-H-SiMe$_2$C$\equiv$CBu^t)Cp$_2$]	1747, 1685	−3.74	123
[Ti(η^4-H-SiMe$_2$C$\equiv$CPh)Cp$_2$]	1752, 1737	−5.96	99
[Ti(η^4-H-SiMe$_2$C$\equiv$CsiMe$_3$)Cp$_2$]	1766, 1685	−5.24	117
[Ti(η^4-H-SiMe$_2$C$\equiv$CBu^t)Cp$_2$*]	2081, 1614	4.47	183
[Ti(η^4-H-SiMe$_2$C$\equiv$CBu^t)THI$_2$][b]	2090	3.97	185
[Ti(η^4-H-SiMe$_2$C$\equiv$CBu^t)(η^5–C$_5$H$_4$)$_2$(SiMe$_2$)]	1753	−6.54	100
[Ti(η^4-H-SiMe$_2$C$\equiv$CBu^t)Cp$_2$]	1689	−3.74	72
[Zr(η^4-H-SiMe$_2$C$\equiv$CPh)Cp$_2$]	1688, 1617	−3.55	88
[Zr(η^4-H-SiMe$_2$C$\equiv$CsiMe$_3$)Cp$_2$]	1700(br)	−4.29	68

[a]The data in the temperature range 297–303 K.
[b]THI, tetrahydroindenyl.

normally found for silane σ-complexes. The Si–H stretches in the IR spectra are shifted to lower wave numbers and are found in the range more typical for the C≡C triple bonds than for the Si–H vibrations.

The data for the sterically hindered compound [Ti(η^4-H-SiMe$_2$C≡CBu^t)Cp$^*_2$] show that steric factors can prevent the coordination of the Si–H bond to metal. For this reason, the zirconium complexes, which have a more open space around the metal, tend to exhibit stronger complexion of the Si–H bond. In both the titanium and zirconium series, the Si–H coupling constants decrease on lowering the temperature (for [Ti(η^4-H-SiMe$_2$C≡CBu^t)Cp$_2$] from 123 Hz at 303 K to 93 Hz at 193 K), accompanied by a high-field shift of the hydride resonance (from −3.74 to −7.32 ppm). This behavior was rationalized in terms of the contribution of a Si–H uncomplexed form at higher temperature rather than as a decrease of the Si–H interaction. The alkynes having two Si–H groups exhibit an additional "flip-flop" dynamic behavior [Eq. (17)], which can be frozen out at low temperature:[132]

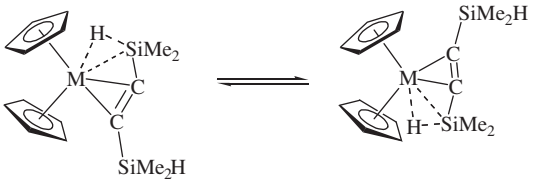

M = Ti, Zr (17)

The electronic structure of complexes **50** has been elucidated by means of DFT and MP2 calculations of the model complex [Ti(η^4-H-SiH$_2$C≡CH)Cp$_2$], supplemented by the analysis of the Laplacian of electron density.[134] The calculated Si–H bond is longer than the X-ray value and implies a significant backdonation from metal to the σ*(Si–H) antibonding orbital. An inward bent Si–H bond path, which is a typical feature of agostic complexes, was revealed in the Laplacian plot. The overall structure was rationalized in terms of a d^2 complex with the competition between the π* orbital of the acetylene moiety and the σ* orbital of the Si–H bond for the metal-centered electron pair. The observed *trans*-structure was calculated to be about 33 kJ mol^{-1} more stable than the uncomplexed *cis*-form,[134] which correlates well with the experimentally estimated barrier ($\Delta G^{\neq}_{190}$ = 37 kJ mol^{-1}) for the flip-flop exchange in the compound [Ti(η^4-H-SiMe$_2$C≡CSiMe$_2$H)Cp$_2$].[132]

A similar bonding situation is found in the ruthenium silylalkene complex **51** formed quantitatively upon the addition of 3 equiv. of the terminal alkene CH$_2$=CHCH$_2$SiMe$_2$H to the precursor [RuH$_2$(η^2-H)$_2$(PCy$_3$)$_2$] [Eq. (18)].[135] The complexation of the alkene is accompanied by a double-bond isomerization and formation of 2 equiv. of the hydrogenation product PrSiMe$_2$H. Complex **51** is an intermediate on the way to the dihydridesilyl product [RuH$_2$(SiMe$_2$Pr){(η^3-C$_6$H$_8$)PCy$_2$}(PCy$_3$)] with a dehydrogenated cyclohexyl group at phosphorus:

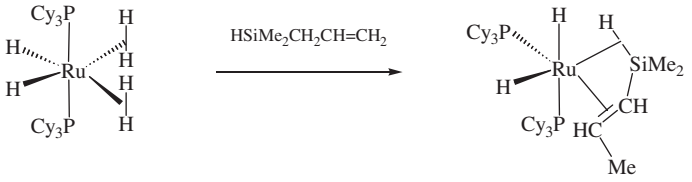

(18)

51

Spectroscopic and structural data for **51** establish its agostic structure. The Si–H coupling constant of 105 Hz is larger than normally observed in silane σ-complexes (see Section II.D) and is indicative of an earlier stage of the Si–H bond activation. The high-field shift of the Si-bound hydrogen (−8.77 ppm) in the ^{1}H NMR spectrum is in accord with its involvement in a nonclassical bonding. The Si–H stretch in the IR spectrum is found at 1945 cm^{-1} when compared with 2121 cm^{-1} in free allylsilane, thus further supporting the Si–H bond coordination to the ruthenium center. The X-ray structure of **51** reveals a normal (within the experimental error) Si–H bond of 1.59(8) Å and the Ru–H distance of 1.74(7) Å comparable (again within the experimental error) to the Ru–H bonds to the genuine hydrides (1.61(7) and 1.64(9) Å). Like in **50**, the Ru–Si bond (2.498(2) Å) is elongated, whereas the Si–C bond (1.820(6) Å) is somewhat shortened, reflecting some partial multiple character.

The theoretical study of complexation of silylalkenes and silylalkynes and their Ge- and C-analogs to metal cations by means of B3LYP calculations revealed a somewhat different picture.[124,125,136,137] The gas-phase interaction of $H_2C{=}C(H)EH_3$ (E = C, Si, Ge) with Ni^+ has been calculated to give agostic species **52**, with the hydrogen atoms of the EH_3 group interacting with the metal.[124] But contrary to conventional π-complexes, the double bond of vinylsilane and vinylgermane coordinates to metal not symmetrically but *via* the C_α atom only. NBO analysis shows that the loss of interaction with the C_β is profitably compensated for by donation from the EH_3 group. The conventional π-complex is the global minimum of the potential energy surface only for propene; for E = Si or Ge, this classical species lies 28–34 kJ mol^{-1} above the agostic complexes. The complexation to Cu^+ is qualitatively similar but systematically weaker than in the case of nickel[125] because the Ni^+ is both a better electron donor and electron acceptor, which leads to stronger donation and backdonation components.[124]

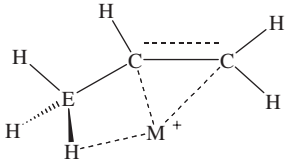

52

M = Ni,	E = Si	Ge
H···M distance, A:	1.684	1.686

M = Cu,	E = Si	Ge
H···M distance, A:	1.754	1.717

Complexation of $HC{\equiv}C{-}EH_3$ (E is C, Si, or Ge) to Ni^+ and Cu^+ differs from the alkene complexation in that conventional π-complexes are the global minima for all the elements E.[136,137] However, when E = Si or Ge, the agostic complexes analogous to **52** were found to be only 2.9 and 10.1 kJ mol^{-1} less stable.[136] As in **52**, only one carbon atom of the acetylene moiety interacts with the metal. The lower stability of these nonconventional π-complexes was attributed to the higher electronegativity of the C≡C moiety compared with the C=C group, which results in a lower polarity of the E–H bond and renders the neighboring EH_3 group a weaker donor to metal. The methyl substitution at the carbon end increases the stability of conventional π-complexes but has little influence on the agostic component. In contrast, substitution at silicon enhances the donor ability of the Si–H bond. A similar picture was found for the complexation of alkynes to Cu^+.[137]

Probably the most stretched Si–H bonding in β-agostic (C)Si–H–M species is found in the silylvinyl compounds **53** and **54**, thoroughly characterized by spectroscopic methods and X-ray structure determination.[138] The large coupling constant (66 Hz in **53** and 57 Hz in **54**), although smaller than in some agostic complexes discussed above, shows that the residual Si–H interaction is still significant. The molecular structure of **53** has an elongated Si–H bond of 1.70(3) Å, whereas the Ru–H bond is normal (1.58(5) Å). The Si–Ru bond (2.507(2) Å) is about 0.1 Å longer than normal 2c–2e bonds and can stem not only from the electron-deficiency of the Si···H···Ru interaction but also from the strained nature of the silylvinyl ligand. Indeed, the observed Si–C–Ru bond angle of 79.1(2)° is much smaller than the ideal one of 120° and can hardly be further reduced to allow for a closer approach of the Si atom to metal. In fact, such a small bond angle suggests that it may be more convenient to consider **53** and **54** as silaallene complexes with a π-coordinated Si=C bond to metal and additional interligand Si–H interaction rather than agostic silylvinyl compounds. Backdonation in metal-silene complexes $[M(\eta^2\text{-}CR_2{=}SiR_2')L_n]$ is known to be strong, so that they are close to the metalasilacyclopropane extreme. In **53**, this is seen from the sp^2 hybridization of the α-C center (the angle C–C–Si is 128.6(4)°). Apart from this, the observed Si–C bond length of 1.805(6) Å in **53** is equal to the values found in metal-silene complexes (range 1.78(2)–1.810(6) Å) and is between the values observed in free 1-silaallene (1.704(4) Å) and normal Si–C(sp^2) single bonds (range 1.85–1.90 Å).[138] Both the β-agostic Si···H···M interaction in a silylvinyl complex and the interaction of a hydride with a π-complexed silaallene ligand are alternative and equivalent views of the same bonding situation. The same may occur in Wrighton's silene hydride complex $[FeH(\eta^2\text{-}CH_2{=}SiMe_2)(CO)Cp^*]$ (**55**)[139] and Tilley's $[RuH(\eta^2\text{-}CH_2{=}SiMe_2)(PR_3)Cp^*]$ (**56**),[140] since both complexes show no M–H absorption in the IR spectra. As Jones *et al.* pointed out, this could be interpreted as the result of a Si–H interaction;[138] however, no significant Si–H coupling (i.e. according to Schubert >20 Hz)[12] has been determined in **56**.[140] The observed Ru–Si bond length in **56** (for R = Pr^i, the Ru–Si distance is 2.382(4) Å) compares well with the data in classical silyl derivatives, which also suggests the absence of significant Si–H interactions. The hydride atom has not been found.[140] Like **53**, complexes **56** can be prepared by chloride substitution in the unsaturated complexes $[Ru(Cl)(PR_3)Cp^*]$ by silylcarboanion $(CH_2-SiR_2'H)^-$, followed by the Si–H bond activation, which

appears to be complete in the case of **56**. Although **56** is regarded as classical, it exhibits a facile, reversible hydrogen transfer to silicon, in contrast to the nonclassical **53**, which already has a partial Si–H interaction but shows no dynamics. The thermal stability of **56** and **53** is also very different: whereas the former decomposes at room temperature, the latter survives heating to 45 °C. Given the DCD scheme, it is quite easy to explain the reason for the possible nonclassical nature of **55** (the small metal from the first transition series +π- accepting carbonyl ligand) but overall, the tiny difference in the electronic structure of **53**–**56** appears to be an interesting problem for theoretical chemists.

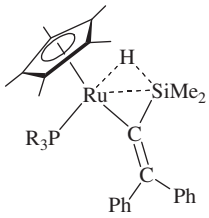

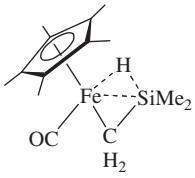

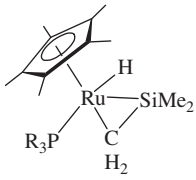

55 **56**

R_3 =	Cy_3	$PhMe_2$
J(Si-H), Hz =	66	57
	53	**54**

The silanol complex **57** exhibits a Si···H···M agostic interaction characterized by a J(Si–H) of 41 Hz and a Si–H distance of 1.70(7) Å.[141] It would be incautious to interpret such a low value of the Si–H coupling in terms of a significant Si–H bond activation, because the Si–H bond forms rather acute angles with the Si–C and Si–Si bonds (about 82 and 101°, respectively) and thus must have a considerable p character on silicon, which should contribute to the decrease of J(Si–H). The silanol ligand is η^5-coordinate to ruthenium and the Ru–Si bond of 2.441(3) Å is not exceptional, but the $Si(SiMe_3)_3$ deviates from the silanol plane by 19.0°, probably as a result of the Si–H interaction. Deprotonation of **57** by strong bases affords a neutral ruthenocene-like product.

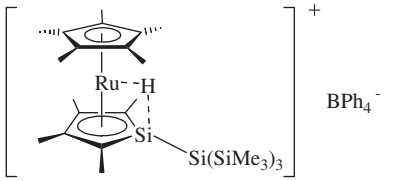

J(Si-H) = 41 Hz

57

So far, the only example of a saturated carbon bridge in a Si–H–M β-agostic complex is found in the Ru complex **58**, prepared by an interesting reaction of

$[Ru(H)(SiMe_3)(PMe_3)_4]$ with $HSiMe_2CH_2Cl$ [Eq. (19)] or, alternatively, by chlorination of the Ru–H bond in the silene complex $[Ru(H)_2(\eta^2\text{-}CH_2SiMe_2)(PMe_3)_3]$.[142]

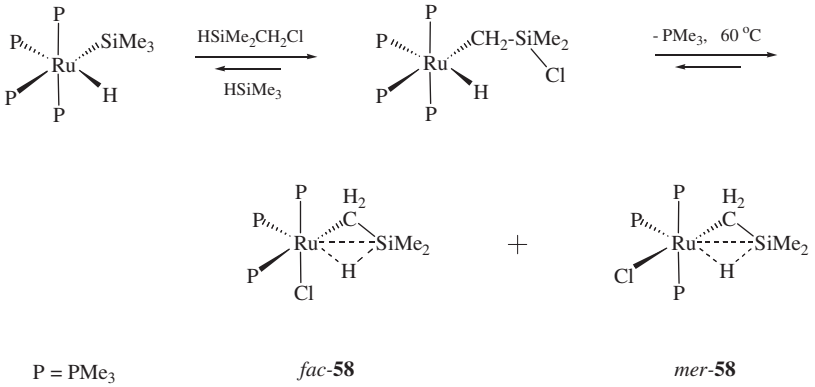

(19)

The presence of direct Si–H bonding is evident from strong Si–H coupling ($J(Si-dH) = 75$ Hz) in *fac*-**58**, which is between the values found for other ruthenium agostic complexes **51** and **53**. The Si–H stretch was found to be red-shifted (1615 cm^{-1}), which is also characteristic of agostic bonding, but the very low intensity of this band makes the assignment less reliable. X-ray structure determinations of the *fac* and *mer* isomers of **58** revealed the hydride in a bridging position between the Ru and Si atoms. In *fac*-**58** the Ru–H and Si–H distances are 1.550 and 1.664 Å, respectively, whereas the Ru–Si bond length of 2.526(2) Å was at the long end for the Ru–Si single bonds (range 2.3–2.58 Å), further supporting the presence of an agostic interaction. The *mer* isomer has a longer Ru–H bond (1.732 Å) and a shorter Si–H bond (1.557 Å), but the Ru–Si distance (2.468(2) Å) is also shorter. This apparent discrepancy can be the result of uncertainty in locating hydride atoms by X-ray diffraction. As in agostic complexes **51** and **53** discussed above, in *fac*-**58** and *mer*-**58**, the C–Si bonds to the bridging carbon are shortened (1.788(11) and 1.790(6) Å, respectively) compared with normal Si–C single bonds, and are close to the values observed in silene complexes (1.78–1.81 Å), suggesting a partial multiple character of this bond.

b. Phosphorus Bridge

The only example of Si···H···M agostic interaction supported by a phosphorus bridge was discovered by Driess *et al.* in the complexation of a silylated triphosphine ligand to a chromium tricarbonyl complex [Eq. (20)].[143,144] A bigger metal (M = Mo) or smaller substituent at silicon (R = Ph) leads to the normal triphosphine complexes. The presence of a Si···H···M interaction in **59** is deduced from the lack of C_3 symmetry (evident from NMR), the red shift of the IR band for the coordinated Si–H bond (1994 cm^{-1} vs. 2142 cm^{-1}), and the observation of a reduced Si–H coupling (135.7 Hz for the coordinated Si–H bond vs. 210.9 and 228.6 Hz for the free Si–H bonds). The X-ray structure determination of **59** shows that one of the phosphine ligands is tilted away from the chromium atom so that the

freed coordination site can be occupied by the Si–H ligand. The resultant Si–H bond is only marginally elongated (1.52(4) Å), whereas both the Cr–Si and Cr–H bonds (2.616(1) and 1.75(5) Å, respectively) are long. This and the large value of J(Si–H) suggest an early stage of Si–H bond activation. Comparison of a series of chromium complexes with different aryl groups at silicon shows that the formation of agostic structure **59** is the result of avoided steric strain that would be imposed by the second *ortho*-substituent in the mesityl group of the third phosphine coordinated to a small chromium center:[144]

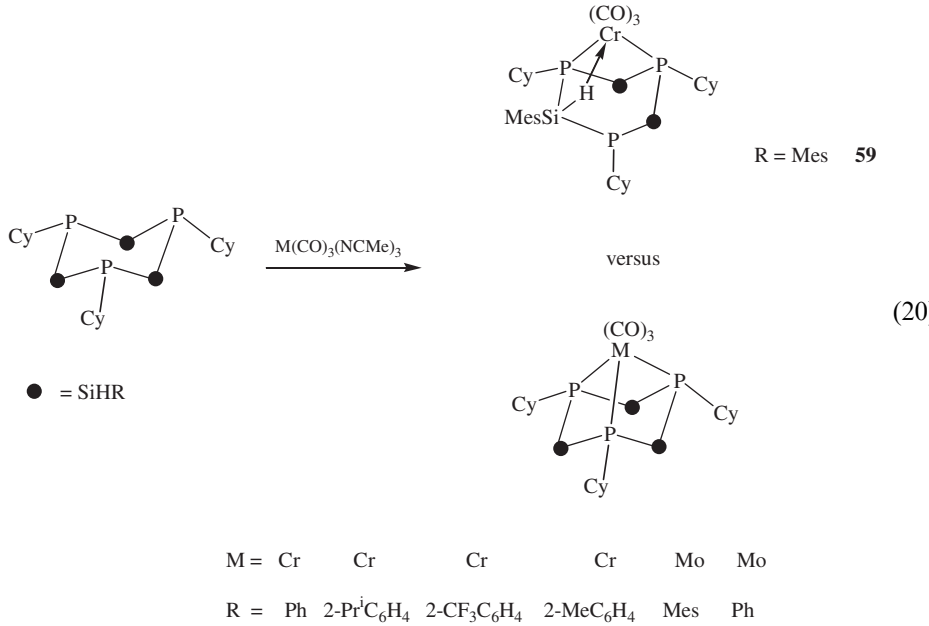

(20)

M =	Cr	Cr	Cr	Cr	Mo	Mo
R =	Ph	2-Pr^{i}C$_6$H$_4$	2-CF$_3$C$_6$H$_4$	2-MeC$_6$H$_4$	Mes	Ph

c. Nitrogen Bridge

Si···H···M agostic interactions in silylamido complexes have been extensively studied to date. The earlier examples were prepared by halide displacement in the coordination sphere of a metal by a silylated amide, which puts severe limitations on the nature of the substituents at silicon (usually, robust methyl groups are used). More recently, a new route to β-agostic silylamides based on the direct coupling of silanes with imido ligands was discovered that allows one to trace the effect of substitution at silicon on the extent of the Si–H bond complexation (*vide infra*).

For the first time, agostic interactions were found in the d^0 bimetallic zirconium complex **60** bearing two silylamido groups at each zirconium center with essentially different structural parameters.[145] Namely, one of the amido groups has a Zr–N–Si bond angle of 102.8(2)° that is noticeably smaller than another Zr–N–Si bond angle at the same nitrogen (129.5(1)°) and the Zr–N–Si angles in the second amide (117.2(2) and 126.9(2)°). Such a tilt of the amido ligand brings the Si–H bond in to

close proximity with the metal so that the resulting Zr–Si distance is not very much longer than an ordinary Zr–Si bond (2.943(1) Å vs. the range 2.654(1)–2.815(1) Å) and can thus compensate the electron-deficiency of metal *via* ligation. However, the observed Zr–H contact (2.40(3) Å) is rather long, whereas the Si–H bond is normal (1.45(2) Å), indicating insignificant activation of the Si–H bond. This is a result of missing backdonation from the d^0 metal center. Another support for the presence of a Si···H···Zr agostic bonding comes from the red shift of the Si–H absorbance in the IR spectrum (1948 cm^{-1} vs. the normal range 2080–2280 cm^{-1}).

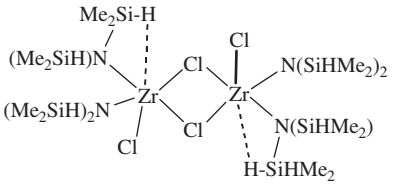

60

Berry *et al.* prepared a series of d^0 zirconocene silylamides [Zr(HSiMe$_2$NBu)(X)Cp$_2$] (**61**), which allowed for the systematic investigation of the effect of ligand X on the extent of Si···H···M bonding.[146] The spectroscopic features (Table II) and X-ray study of [Zr(HSiMe$_2$NBu^t)(Cl)Cp$_2$] suggest the presence of significant Si···H···M agostic interaction, which appears to be surprisingly strong, considering the fact that no electron density on metal is available for backdonation. As typical for agostic species, the Si-bound hydride exhibits a high-field shift, which parallels the red shift of the Si–H band in the IR spectrum. Most notable are the values of the Si–H coupling constants found in the range 113.2–135.4 Hz and much reduced compared to the parent silane HSiMe$_2$NBu^t (192.6 Hz). The lowest value of 113.2 Hz is comparable to the J(Si–H) observed in d^n ($n>0$) agostic species (see **49**–**51** and *vide infra*) and suggests a significant degree of Si–H bond activation. In contrast, the structure of [Zr(HSiMe$_2$NBu^t)(Cl)Cp$_2$] shows virtually an unperturbed Si–H bond (1.416(3)) and a long Zr–H contact (2.27(3) Å), which can certainly reflect the low accuracy of finding a hydride in the heavy element environment. The amide ligand shows the same type of distortion as the related complex **60** in that the Zr–N–Si angle is acute (99.1(1)°), whereas the Zr–N–C bond angle of 137.3(2)° is much larger than the ideal 120°. The structure of [Zr(HSiMe$_2$NBu^t)(H)Cp$_2$] was

TABLE II
SELECTED SPECTROSCOPIC DATA FOR COMPLEXES **61**

Compound	IR ν(SiH) (cm^{-1})	NMR δ ^{1}H (ppm)	NMR J(Si–H) (Hz)
[Zr(H)(HSiMe$_2$NBu^t)Cp$_2$]	1912	1.21	113.2
[Zr(HSiMe$_2$NBu^t)(I)Cp2]	1960	1.69	118.7
[Zr(HSiMe$_2$NBu^t)(Br)Cp$_2$]	1975	2.24	123.2
[Zr(HSiMe$_2$NBu^t)(Cl)Cp$_2$]	1981	2.58	126.5
[Zr(HSiMe$_2$NBu^t)(F)Cp$_2$]	1998	2.84	135.4
HSiMe$_2$NHBu^t	2107	4.83	192.6

also determined, but a detailed analysis is complicated by the disorder of the crucial amido ligand. Nevertheless, the characteristic tilt of the amido ligand, bringing the silyl group to the coordination sphere of zirconium, was clearly observed. The different spectroscopic data in Table II correlate well and define a clear trend in that the complexation of the Si–H bond to Zr decreases in the order H > I > Cl > Br > F. This was rationalized in terms of decreased electrophilicity of the metal due to partial donation of a halogen lone pair that becomes more important as the size of the halide decreases. This π-donation, competing with the Si–H bond for a vacant orbital of Zr, can be presented by the resonance form **62**, which corresponds to a formally saturated 18e species.

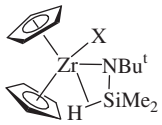

61

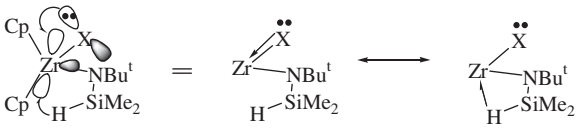

62

Very similar Si···H···M agostic interactions, characterized by a red shift of the Si–H absorption (IR), a high-field shift of the Si–H resonance (^{1}H NMR), reduced Si–H coupling constants, and acute M–N–Si bond angles, were thoroughly studied by Anwander *et al.*[147–150] for a range of d^0 lanthanide complexes. In particular, the series of metallocene complexes [(Ln((η^2-HSiMe$_2$)$_2$N)(Cp$'_2$)], where Ln is a lanthanide metal and Cp$'_2$ denotes ring-substituted cyclopentadienyl and ansa-fluorenyl and indenyl ligands, exhibits peculiar *di-agostic* Si···H···Ln interactions schematically shown in **63**.[147,149] The Si–H stretches were found at lower energies by 200–300 cm^{-1}, and the Si–H coupling constants were observed in the range 133–155 Hz, suggesting weaker metal–hydride interactions than in the β-agostic Si···H···M interactions discussed above. Very acute Ln–N–Si bond angles (down to 98(1)°) and large Si–N–Si angles (as large as 160.1(2)°) signify the simultaneous approach of two silyl groups to the metal. Smaller metals were shown to have a stronger interaction with the Si–H bond.[149] An eterbium trisamido complex with three β-agostic Si···H···Er interactions was described by Schumann *et al.* on the basis of X-ray and IR evidence.[151]

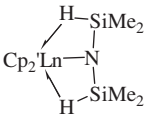

63

The first example of stretched β-agostic Si···H···M interactions in a silylamido complex, the compound [Nb(η^3-H-SiMe$_2$-NAr)(Cl)(PMe$_3$)Cp] (**64**, Ar = 2,6-Pr$^i_2$C$_6$H$_3$), was prepared by the reaction of HSiMe$_2$Cl with [Nb(PMe$_3$)$_2$(NAr)Cp] (Scheme 3).[152] Two isomers (**a** and **b**), differing in the position of the ligand *trans* to the hydride (Cl or PMe$_3$), have been identified in the solution by ^{1}H NMR with the ratio 10:1. In contrast, only one isomer, **65** (PMe$_3$ *trans* to hydride), analogous to **64b**, was formed in the reaction of the less-encumbered compound [Nb(PMe$_3$)$_2$(NAr′)Cp] (Ar′ = 2,6-Me$_2$C$_6$H$_3$) with HSiMe$_2$Cl. The presence of agostic Si···H···M bonding follows from the spectroscopic features of **64a**, **64b** and **65**, X-ray structure determinations of **64a** (Fig. 4) and **65**, and DFT calculations of model complexes.[152] All these complexes exhibit a characteristic red shift of the Si–H bond and reduced Si–H coupling constants. These are less than normally observed in the d^0 agostic silylamido complexes **60**–**63** owing to a partial backdonation from the d^2 level of niobium on the σ*(Si–H) antibonding orbital in **64a** and **65**. The *J*(Si–H) coupling constant is smaller in **64a** (97 Hz) than in **65** (113 Hz), in accord with a longer Si–H bond in the former (DFT calculated 1.73 Å vs. 1.57 Å, respectively). As in **61**, a stronger Si–H bond interaction with the metal in **64a** corresponds to a greater high-field shift of the hydride resonance (−5.67 ppm vs. −3.76 ppm in **65b** and −3.41 ppm in **65**). Reactions of compound **63** with the silanes Me$_3$SiX (X = Br, I, OTfl) allow for the syntheses of functionalized agostic compounds [Nb(η^3-H-SiMe$_2$-NAr)(X)(PMe$_3$)Cp].[152] Reactions of the tantalum analog [Ta(PMe$_3$)$_2$(NAr)Cp] with silanes HSiMe$_n$Cl$_{3-n}$ (n = 0−2) lead to silylhydride derivatives with IHI, which will be discussed in Section III. The formation of the isomer **64a** vs. **64b**, and the extent of the Si–H bond activation, are determined by the repulsion of the group *trans* to the hydride from the

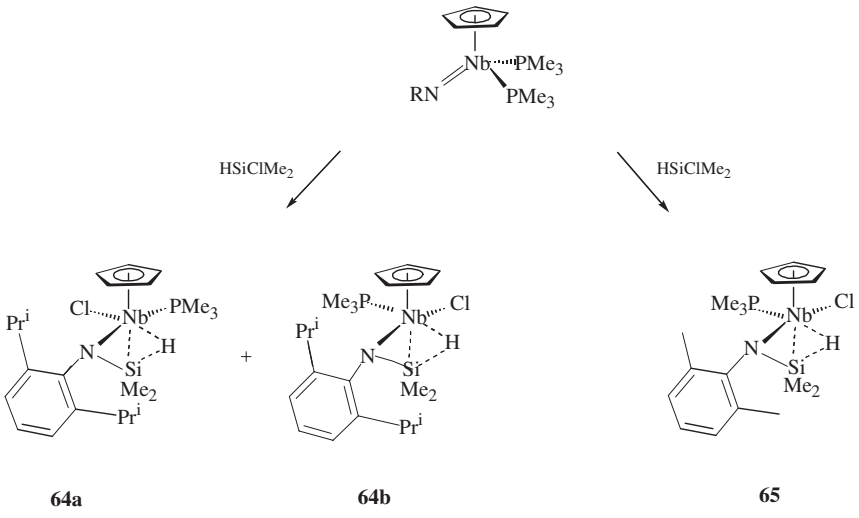

SCHEME 3.

ortho-substituent in the arene group at nitrogen. For Ar′ the repulsion is small, and PMe_3 can be accommodated *trans* to the Si–H bond, leading to weaker Si–H bond activation. For Ar, a smaller chloride ligand is preferred for steric reasons, and since this is a ligand with weaker *trans* effect than phosphine, the Si–H bond is more activated.

Reactions of the bis(imido) complexes $[M(NR)_2(PMe_3)_3]$ (M = Mo, W; R = Ar, Ar′, Bu^t) with $HSiMe_2Cl$ and $HSiMeCl_2$ give the agostic complexes $[M(\eta^3\text{-H-SiMeX-NR})(Cl)(NR)(PMe_3)_2]$ (M = Mo, W; X = Me or Cl) [Eq. (21)] related to **64** and **65** through the isolobal relationship between the Cp^- and $(RN)^{2-}$ ligands.[153,154] This formulation follows from the observation of high H–Si coupling constants (range 81–130 Hz) and is supported by X-ray structure analysis of $[Mo(\eta^3\text{-H-SiMe}_2\text{-NAr}')(Cl)(NAr')(PMe_3)_2]$ (**66**, Fig. 5) and $[Mo(\eta^3\text{-H-SiMeCl-NAr}')(Cl)(NAr')(PMe_3)_2]$ (**67**, Fig. 6). The analogous reaction of $[M(=NR)_2(PMe_3)_3]$ with $HSiCl_3$ leads to formation of $[M(=NR)(Cl)_2(PMe_3)_3]$ and the silanimine dimer $(RN\text{-SiHCl})_2$. In good accord with the isolobal relationship between **64a** and **65**, both complexes have very close *J*(Si–H) (97 Hz in **64a** and 96 Hz in **66**). The *J*(Si–H) of 129 Hz in **67** is *larger* than in **66**, which contradicts the common assumption that more electron-withdrawing substituents at silicon favor more advanced Si–H bond oxidative addition, thereby leading to reduced H–Si coupling constants.[12] However, the Mo–Si bond (2.657(1) Å) in **67** is in fact *marginally shorter* than in **66** (2.668(1) Å), whereas the M–H and Si–H distances do not change significantly upon substitution of Me for Cl. DFT calculations of a series of model complexes $[Mo(\eta^3\text{-H-SiMe}_n\text{Cl}_{2-n}\text{-NMe})(Cl)(NMe)(PMe_3)_2]$ $(n = 0-2)$

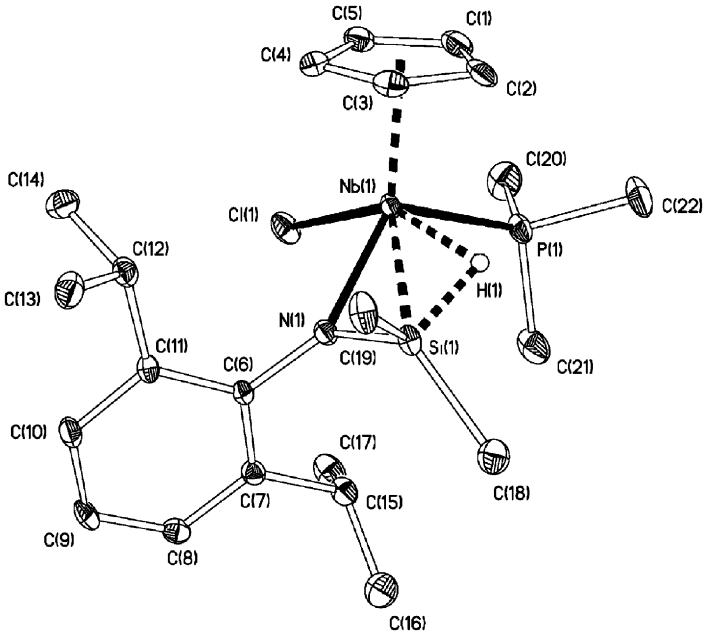

FIG. 4. Molecular structure of complex **64a**. (Reproduced from Ref. 152, with permission from The Royal Society of Chemistry.)

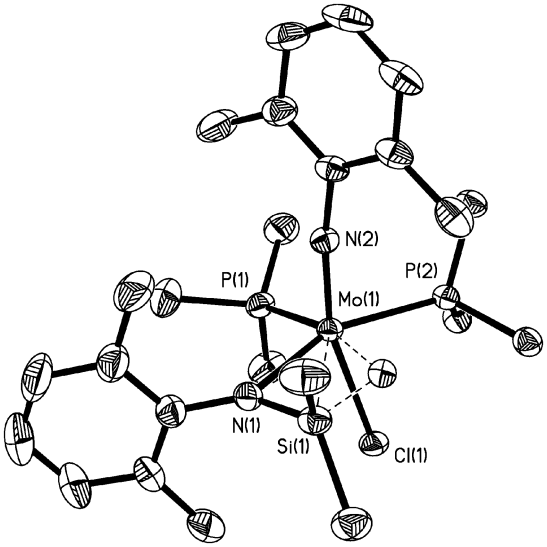

FIG. 5. Molecular structure of the complex **66**. (Reproduced from Ref. 153, with permission from The Royal Society of Chemistry.)

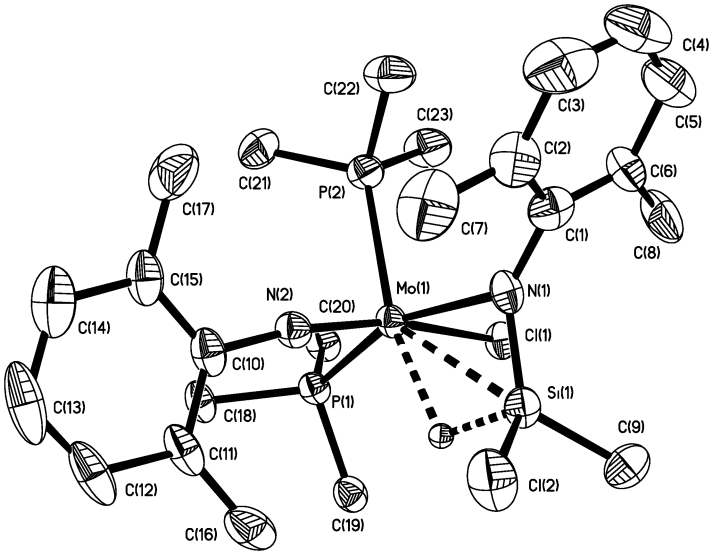

FIG. 6. Molecular structure of the complex **67**. (Reproduced from Ref. 153, with permission from The Royal Society of Chemistry.)

showed that, unexpectedly, this shorter Mo–Si distance in **67** corresponds to a weaker bond, whereas the M–H bond elongates and weakens and the Si–H bond shortens and strengthens when more Cl groups are put on silicon, thus indicating the decrease of the Si–H bond oxidative addition. These surprising results were

rationalized in terms of a revised DCD diagram taking into account the substituent effects (Section II.B). Namely, the sequential substitution of the Me groups on Si for an electron-withdrawing Cl group provides more Si 3s character in the Si–H bond in accord with Bent's rule, leading to the contraction of this bond and making it a worse σ-donor, which decreases the donation component in the DCD scheme. This, and the increased Si 3s character, account for the increase of the Si–H coupling constant from **61** to **67**. On the other hand, the introduction of Cl groups on silicon makes the Si atom more Lewis acidic, thus increasing the Mo → σ^*(H–Si) backdonation as normally discussed for σ-complexes.[2] These changes affect the Mo–Si and Mo–H interactions unevenly, since the Si–H bonding orbital is more localized on the H atom, whereas the σ*(Si–H) orbital has a bigger contribution from Si, with the effect that the M–H bond elongates and the M–Si bond shortens.[153] As a result, the M–Si bond contracts whereas the M–H bond elongates:

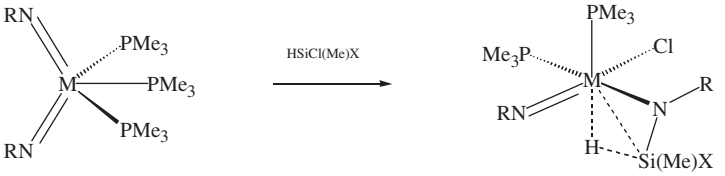

(21)

M = Mo, W;
X = Me (**66**), Cl (**67**)

4. α-Agostic Si···H···M Interaction

α-Agostic Si···H···M interaction (see **68**) is the most recent phenomenon[155–160] and its adequate description has yet to be developed. The case of d^n ($n > 2$) complexes is particularly difficult because for these compounds an alternative rationalization in terms of an interaction between a hydride ligand and an electrophilic silylene ligand is, in principle, possible (see **69**).[158] The first authentic example of an α-agostic Si–H–M bond was found in a cationic hafnocene complex **70** prepared by methyl group abstraction from [Hf(Me)(SiHMes$_2$)Cp$_2$] by B(C$_6$F$_5$)$_3$.[155] This compound is able to activate the C–H bonds of arenes by an apparent σ-bond metathesis mechanism, producing the silane H_2SiMes_2 and cationic aryl derivatives. The presence of agostic bonding was inferred from the observation of a decreased H–Si coupling constant (57 Hz), downfield-shifted ^{29}Si signal, and a red-shifted Si–H stretch (1414, 1015 cm^{-1} in the D-labeled derivative). The DFT-calculated structures of model complexes [Hf(η^2-HSiH$_2$)Cp$_2$]$^+$ and [Hf(η^2-HSiMes$_2$)Cp$_2$]$^+$ also exhibit a strong interaction between the Si–H bond and the Hf center. Thus, the calculated Hf–Si–H$_{bridge}$ bond angles are acute (52.3 and 50.4°) to provide short Hf–H$_{bridge}$ distances (2.05 and 2.02 Å, respectively). The calculated Si–H stretching vibration (1475 cm^{-1}) was close to the experimental value.

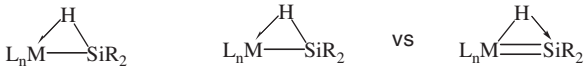

68 **69**

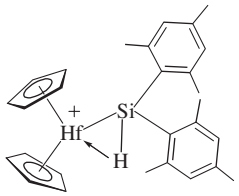

70

Addition of secondary silanes H_2SiR_2 (R = Me_2, Et_2, MePh, Ph_2, HPh, HMes, H(CH_2Ph), ClMes) to the η^3-benzyl complex [Mo(η^3-$CH_2C_6H_5$)(dmpe)Cp*] affords formal 16e silyl complexes **71** with significant α-agostic Si···H···M interactions [Eq. (22)].[156,157] Alternatively, complexes **71** can be viewed as Mo(IV) hydridesilylenes with interligand interactions H···Si(= Mo). Complexes **71** exhibit nonequivalent Me resonances for the dmpe ligand, upfield-shifted ^{29}Si signals, indicative of a substantial silylene character, downfield hydride resonances, and decreased[¶] H–Si coupling constants (Table III) supporting their nonclassical formulation. An ND study of the compound [Mo(η^2-H-$SiEt_2$)(dmpe)Cp*] unequivocally establishes the presence of direct Mo–H (1.847(12) Å) and Si–H (1.683(13) Å) bonds. Judged by its length, the activation of the H–Si bond in **71** is less than normally observed in silane σ-complexes (Section II.C), suggesting that the α-agostic silyl description is more appropriate:

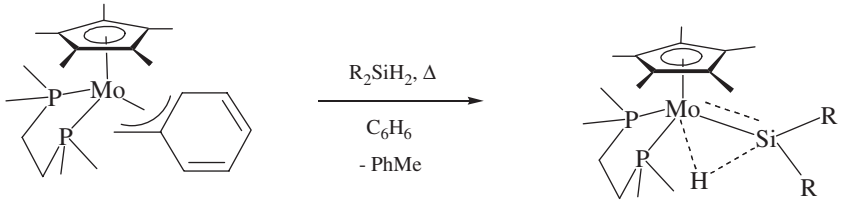

(22)

71

Interestingly, the protonated form of the tungsten analog of **71**, the compound $[W(H)_2(SiR_2)(dmpe)Cp^*]^+$ (**72**), is a dihydridesilylene complex without H–Si interactions.[158] This compound was prepared by silane addition to a cationic, doubly tucked, Cp* precursor according to Eq. (23). If one considers the silylene SiR_2 as a two-electron ligand, analogous to phosphine, the complex **72** is a tungsten (IV)

[¶]These coupling constants are highly decreased if one considers **71** as a silyl compound with an agostic bond. Alternatively, if the hydride silylene description is chosen, the value of *J*(Si–H) is increased in comparison with usually observed nonbonding values.

TABLE III
SELECTED SPECTROSCOPIC DATA FOR COMPLEXES **71**

Compound	NMR δ ^{1}H (ppm)	NMR J(Si–H) (Hz)	NMR δ ^{29}Si (ppm)
[Mo(η^2-H-SiMe$_2$)(dmpe)Cp*]	−14.06	30	263
[Mo(η^2-H-SiEt$_2$)(dmpe)Cp*]	−13.91	44	273
[Mo(η^2-H-SiMePh)(dmpe)Cp*]	−13.10	46	214
[Mo(η^2-H-SiPh$_2$)(dmpe)Cp*]	−11.36	37	242
[Mo(η^2-H-SiHPh)(dmpe)Cp*]	−9.96	30	250
[Mo(η^2-H-SiHMes)(dmpe)Cp*]	−13.08	48	214
[Mo(η^2-H-SiHCH$_2$Ph)(dmpe)Cp*]	−13.29	42	239
[Mo(η^2-H-SiClMes)(dmpe)Cp*] [a]	−12.50	38	182

[a]This compound exhibits a C_s symmetry in the NMR.[157]

derivative. If a W–Si double bond is implied, the W center achieves the highest oxidation state VI. An alternative formulation of **72** as a dihydrogen complex was excluded on the basis of T_1 measurements ($T_1 = 600-800$ ms). The H–Si coupling constants determined for R = Me$_2$, MePh, and Ph$_2$ were 7, 17, and 17 Hz, respectively, more consistent with the classical formulation of this compound on the basis of 20 Hz criterion (Section II.D). DFT calculations of a model complex [W(H$_2$SiMe$_2$)(PH$_3$)$_2$Cp]$^+$ optimized with a C_s symmetry constraint afforded a classical structure with the d^2 configuration (i.e. no backdonation from metal onto the silylene ligand) and without significant Si–H interactions, according to the charge decomposition analysis.[159] However, four more structures with one or two Si–H–M bridges were found to lie only <5 kcal mol^{-1} higher in energy, indicating a very fluxional coordination sphere of the transition metal. It is not quite clear yet whether the difference between complexes **71** and **72** is due mainly to the difference in metal (Mo vs. W) or charge (neutral vs. cationic), but it is apparent that the classical and nonclassical forms are close in energy, and their relative stability may be subject to steric and electronic effects of substituents:

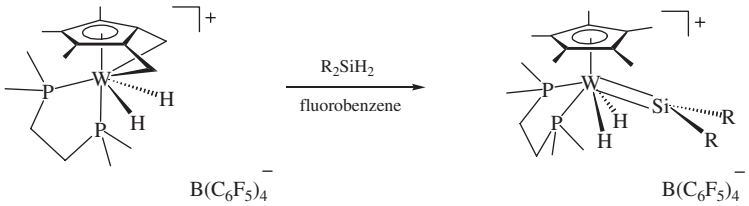

(23)

72

Photoinduced oxidative addition of primary silane H$_3$SiC(SiMe$_3$)$_3$ to [WMe(CO)$_3$Cp*] [Eq. (24)] produced a hydridesilylene complex [W(H){ = SiH(C(SiMe$_3$)$_3$)}(CO)$_2$Cp*] (**73**) in 62% yield in a reaction similar to that shown in Eq. (23).[160] An analog with the C$_5$Me$_4$Et ligand has been prepared similarly:

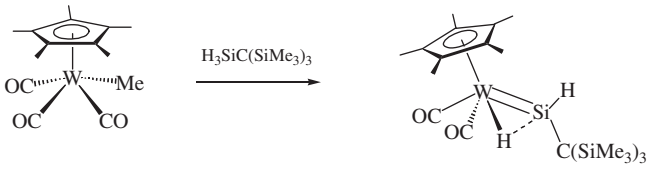

(24)

73

The silylene center in **73** gives rise to a downfield ^{29}Si signal at 275.3 ppm, consistent with the formally sp^2 hybridized silicon atom. In accordance with this, the Si-bound proton is downfield-shifted to 10.39 ppm. Importantly, the increased H–Si coupling constant of 28.6 Hz observed for the hydride signal suggests the presence of some Si–H interaction, which is further supported by the observation of a characteristic red-shifted W–H band at 1589 cm^{-1} (the Si–H band is at 2052 cm^{-1}). The X-ray study of **73** shows a short Si–H(W) distance of 1.71(6) Å, which is in good accord with the DFT value of 1.71 Å. The NBO bond orders were 0.511 for the W–H bond, 0.476 for the Si–H bond, and 1.518 for W–Si bonds. In other words, this compound can be considered either as a silyl complex with a stretched α-agostic Si···H···W bond, or as a nonclassical silylene complex with interligand bonding H···Si(= W), in which the W–H bond serves as an internal base stabilizing the unsaturated silylene center. The analogous base-stabilized silylenehydride derivative [W(H){ = SiR_2←py}$(CO)_2$Cp*] lacks any interaction between the hydride and silicon atoms.[161] Complex **73** reacts with CO to give the silyl derivative [W{SiH_2(C($SiMe_3$)$_3$)}$(CO)_3$Cp*], but inserts acetone across the Si–H bond, affording an alkoxy-substituted silylene complex.[160]

The related cationic hydrido(hydrosilylene) complex of Ru, [Ru(H)$_2$(= SiPhH)(Pr^i_3)Cp*]$^+$, has been prepared by chloride abstraction from the precursor [Ru(H)(SiH_2Ph)(Cl)(Pr^i_3)Cp*] and characterized by spectroscopic methods.[162] The X-ray structure and H(Si–H) coupling constants are not available, but DFT calculations of a model complex [Ru(H)$_2$(SiH_2)(PH_3)Cp]$^+$ show double $RuH_2^{\cdot\cdot}SiH_2$ interactions similar to those in **71** and **73**.[163] The unique property of these cationic silylene complexes of ruthenium is their ability to catalyze the hydrosilation of 1-hexane[162] by a mechanism involving olefin coordination to the highly electrophilic silicon center, which is followed by insertion into the Si–H bond.[163] Weak coordination of olefin to silicon in the form of a π-complex does not break the $RuH_2^{\cdot\cdot}SiH_2$ interactions (the RuH–Si distances are 1.68 and 1.72 Å), but more advanced coordination to give the olefin σ-complex results in a dihydride silylene structure without H···Si interactions. The H···Si interactions are, however, restored when the insertion is complete. Other known hydrido(hydrosilylene) complexes, [Ir(H)$_2$(= SiH{2,6-$Mes_2C_6H_3$})(PEt_3)$_3$]B(C_6F_5)$_4$ [164] and [Ir(H)$_2$(= SiH{2,4,6-$Pr^i_3C_6H_2$})({PPh_2CH_2}$_3$BPh)][165], like **72**, exhibit no significant Si–H coupling and are regarded as classical. Their structures are, however, unknown.

The reaction of the compound [Mo(H)(= SiClMes)(dmpe)Cp*] with LiB(C_6F_5)$_4$ affords an unusual, formal, hydridosilylyne complex [MoH(= SiMes)(dmpe)Cp*][B(C_6F_5)$_4$] [**73**, Eq. (25)] exhibiting a downfield-shifted ^{29}Si NMR signal at 289 ppm and a low H–Si coupling constant of 15 Hz.[157] Although

the latter fact speaks against the presence of significant H–Si interaction, the X-ray structure analysis and preliminary DFT calculations at the B3LYP/LACVP** level are consistent with the hydride bridging the Mo and Si atoms. The experimental values for the Mo–H and Si–H bond lengths are 1.85(5) and 1.39(5) Å, respectively. Apart from this, the silylyne ligand exhibits an approximately linear geometry (the M–Si–C bond angle is 170.9(2)°), and the Mo–Si bond of 2.219(2) Å is the shortest of this kind. The observation by NMR of an effective C_s symmetry at room temperature (at −30 °C the C_1 symmetry is found) is further consistent with the facile migration of the hydrogen atom between the silicon and metal centers.

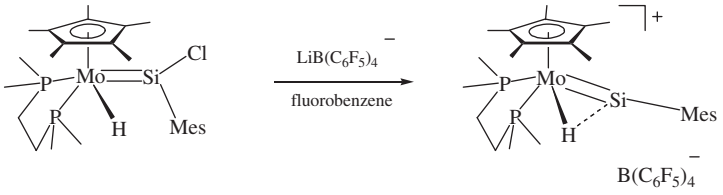

(25)

74

It should be noted that structural distortions with short M–HC contacts, very similar to those in **71**, **73**, and possibly in **74**, were previously observed in some Schrock's alkylidene complexes, which was theoretically rationalized in terms of electronic rearrangements of the carbene center.[166]

The structure of the cationic silyl platinum complexes $[Pt(SiHR_2)(dhpe)]^+$ ($dhpe = H_2PCH_2CH_2PH_2$) were studied by DFT (B3LYP) calculations.[167] For R = H, an α-agostic Si···H···Pt structure **75** with a Pt–H distance of 1.747 Å and Si–H bond of 1.772 Å was found to be the global minimum. A classical silyl derivative and another agostic structure with a weaker H–Pt bond (2.414 Å) lie by 3–4 kcal mol^{-1} higher. The substitution of two hydrogen atoms at silicon for methyl groups or strong π-donors (R = Cl, OMe, SMe, NMe_2) stabilizes the isomeric silylenehydride form **76**. With $R = SiH_3$, the α-agostic Si···H···Pt complex is by 10.22 kcal mol^{-1} less stable than the β-agostic Si···H···Pt complex $[Pt(\eta^2\text{-H-}SiH_2SiH(SiH_3))(dhpe)]^+$. These finding were rationalized in terms of a better stabilization of the silylene ligand in **76** when either σ-donating (Me) or π- donating substituents are present.

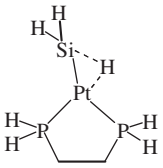

75

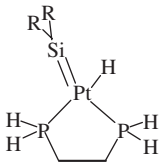

76

R = Me, OMe, SMe, NMe_2

The IR study of the reaction of titanium atom with SiH_4 at 12 K in argon matrices revealed, among other products, the hydridesilyl complexes **77** and **78** with two and three agostic Ti···H···Si interactions, respectively.[168] The reaction occurs

spontaneously upon deposition of the titanium atom together with SiH_4 to give four products, which were differentiated according to their response to selective photolysis at different wavelengths and by means of using the deuterated silane SiD_4. To identify the nature of these products, quantum-chemical calculations were carried out, which established the species **78** to be the global minimum. The *cis*- and *trans*- forms of **77** are by 24.3 and 24.7 kJ mol^{-1}, respectively, less stable and can be converted to **78** upon photolysis at $\lambda_{max} = 410$ nm. The monoagostic adduct **79** was calculated to be a minimum too, but lies about 3 kJ mol^{-1} higher than **77**. Similar conclusions have been reached on the analogous reaction with SnH_4, whereas the addition of CH_4 is much more sluggish and gives a different product, the hydridomethyl complex $[Ti(H)(CH_3)]$.[168] In contrast to titanium, the reaction of nickel atoms with SiH_4 gives the product of complete oxidative addition of the Si–H bond, the compound $[Ni(H)(SiH_3)]$, which, however, may also show a weak attractive interaction between the hydrido and silyl ligands.[169] The reactions of metal cations M^+ (M = Fe, Co, Ni) with SiH_4 were found to give species of the general formula $[Ni(SiH_x)]^+$ ($x = 0-3$), but their exact structure remains unknown.[170]

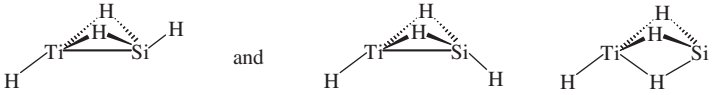

trans **cis**

77 **78**

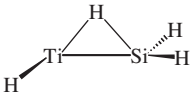

79

III

SILYLHYDRIDE COMPLEXES WITH INTERLIGAND HYPERVALENT INTERACTIONS M–H···SIX

A. *A Short Remark on the Heuristic Aspect*

The development of chemistry is often based on analogy, which although not necessarily always exact, may lead to surprising results. Below is given a short account on how the chemical analogy led to the discovery of IHI of type M–H···SiR_2X. In the early 1990s our attention was attracted by the report by Berry *et al.* that a silylhydride complex of molybdenum **80** has an unusually elongated Si–Cl bond of 2.158(1) Å and a shortened Mo–Si bond (2.513(1) Å).[171] These structural features were rationalized in terms of hyperconjugation between the

metal-centered lone pair and the σ∗(Si–Cl) antibonding orbital as shown in **80**, which can be reformulated in terms of a resonance between a hydridesilyl and a hydridesilylene (**81**) structure.[171]

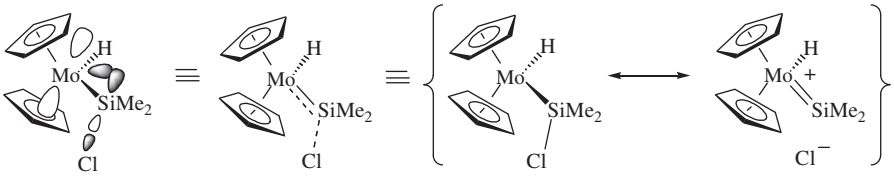

80 **81**

This result suggested a ''mental experiment'' shown in Scheme 4. If one substitutes a lone pair on the metal for a metal–hydride bond but keeps the electron count constant, a positively charged structure like **82** would emerge. This procedure corresponds simply to the protonation of the metal lone pair. To get rid of the charge, one has then to shift to the Group 5 metals to obtain the isoelectronic structure **83**. Since many metal–hydride bonds are rather high-lying in energy, electron density transfer from the M–H bond (M = Group 5 metal) on the σ∗(Si–Cl) antibonding orbital could be anticipated in analogy with **80**. This would lead to the same structural distortions as had been previously observed for **80**, namely, the elongation of the Si–Cl bond and the contraction of the M–Si bond. At that time, the trisubstituted vanadocenes were not available (and still are not) owing to their extreme instability, whereas the chemistry of tantalocene silylhydrides related to **83** had already been developed; however, the crucial structural information of the halosilyl-substituted complexes was not available then. This prompted us to investigate the chemistry of niobocene silylhydrides, which had been developed by that time, but to a much lesser extent.

Some years later, when presenting our first results on IHI in a talk at the Technical University of Munich, a colleague from TUM drew my attention to an earlier review by Hamilton and Crabtree on the H–H and other σ-complexes where a very similar idea, presented in the form of structure **84**, had been suggested to account for the bonding in Schubert's complex $[Mn(HSiFPh_2)(CO)_2Cp']$.[3] There was no explanation of how this bonding could account for the observed structural and spectroscopic properties of this molecule and, in fact, this bonding idea was not

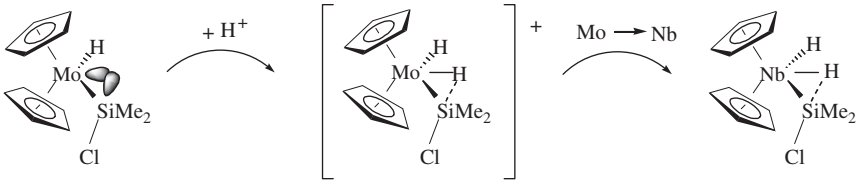

82 **83**

SCHEME 4.

developed further in the subsequent work of these authors. The later review by Robert Crabtree on σ-complexes,[4] which appeared in 1993, described the bonding in compounds like **84** on the basis of the conventional DCD scheme as discussed in Section II.B. Below, it will be shown in more detail that the IHI and the residual Si–H interactions in silane σ-complexes occur for different types of compounds and are characterized by very different structural and spectroscopic features.

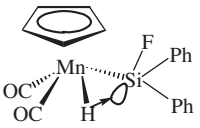

84

B. *IHI MH···SiX in Metallocene and Related Ligand Environments*

1. IHI in Niobocene Complexes

a. Monosilyl and Symmetric bis(silyl) Derivatives

Earlier work on IHI was focused on niobocene derivatives.[172,173] The monosilyl complex **83** was prepared in a mixture with its central isomer **85** by heating niobocene trihydride $[Nb(H)_3Cp_2]$ with $HSiMe_2Cl$ at 50 °C [Eq. (26)].[173] In spite of increased steric strain due to the close proximity of the $SiMe_2Cl$ ligand to the Cp ring, **83** was found to be a thermodynamically more preferable form than **85** up to 100 °C, when both complexes decompose to give the bis(silyl) derivative $[Nb(H)(SiMe_2Cl)_2Cp_2]$ (**86**). This observation suggested the presence of an electronic factor, overcoming the increased interligand repulsion in **83**. Further, although indirect, support for the presence of an interligand interaction between the central hydride and the *cis* silyl in **83** comes from the ^1H NMR upfield shift of the central hydride signal relative to the lateral hydride, a feature different from what is found for $[Nb(H)_3Cp_2]$:

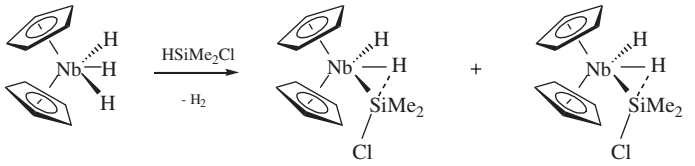

(26)

83 **85**

The X-ray structure of **83** was in accord with the prediction of Scheme 4 in that the Si–Cl bond lies in the niobocene bisecting plane *trans* to the hydride and is elongated compared with classical complexes of the type $[M(SiR_2Cl)L_n]$.[173] There was, however, no good reference system that would allow for the comparison of the Nb–Si bond lengths. The metal-silyl bond lengths are strongly affected by Bent's

rule effect, and all the structurally characterized niobo- and tantalocene silylhydrides available by that time had only electron-releasing substituents at silicon and, hence, longer M–Si bonds. Therefore, they were not useful for spoting the relative shortening of the Nb–Si bond in **83** due to IHI. This problem was partially resolved by analyzing the structures of a series of bis(silyl) complexes $[Nb(H)(SiMe_2X)_2Cp_2]$ (**87**, X = F, Cl, Br, I) prepared from **86** and the compound $[Nb(H)(SiMe_2H)_2Cp_2]$ by electrophilic and/or nucleophilic substitution at silicon.[173,174] Complexes **87** were found to have even more delocalized IHI Si–H, stemming from the donation of the Nb–H bonding density on two neighboring Si–X bonds and spread over five atoms in three ligands (one hydride, two X's, two silicons). This five-center interligand interaction occurs in the coordination sphere of the metal (the sixth center) and involves six electrons (two Si–X bonds and the Nb–H bond each provide an electron pair).

The MO diagrams describing the 3c–4e interligand interaction in **83** and the 5c–6e interligand interaction in **87** are given in Figs. 7 and 8, respectively.[173] Since these are very similar to the MO diagrams for the hypervalent organosilicon compounds, the term *interligand hypervalent interactions* (IHI) was coined.[172,173] On the basis of the analogy with hypervalent organosilicon compounds it was anticipated that the structural distortions due to IHI would increase down the halogen group. In contrast, the electronic effects due to Bent's rule operates in the opposite way, so that summation of two opposite trends produces an extremum. And indeed, the Nb–Si bond in **86** (2.597(1) Å) is shorter than in the then available $[Nb(H)(SiMe_2F)_2Cp_2]$ (average 2.620(1) Å) and $[Nb(H)(SiMe_2Br)_2Cp_2]$ (2.604(2) Å), whereas the relative elongation of the Si–X bond against the classical halosilyls XSiR3 shows an inverted V-type curve with the maximum value again at **86** (Fig. 9). The later determined structure of $[Nb(H)(SiMe_2I)_2Cp_2]$ exhibits a marginal elongation of the Si–I bond relative to organoidosilanes but a somewhat shorter Nb–Si bond compared with $[Nb(H)(SiMe_2Br)_2Cp_2]$ (Fig. 10).[174] This discrepancy is explained in terms of increased crystal-packing effects due to the large size of the iodine substituent at silicon.[174] Complexes with IHI have relatively shorter Nb–Si bond length because of the rehybridization of the silicon center upon the formation of a pentacoordinate geometry. In other words, more Si p character goes to bonding with the apical groups (the hydride and the group X), leaving relatively more Si s character for bonding with the equatorial groups (the M and two R's). Thus, the origins for

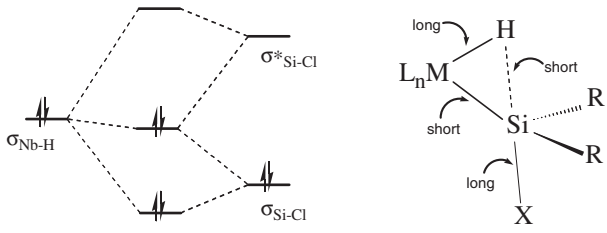

FIG. 7. The MO diagram for the IHI MH···SiCl in mono(silyl) systems (left) and the key structural features of IHI (right).

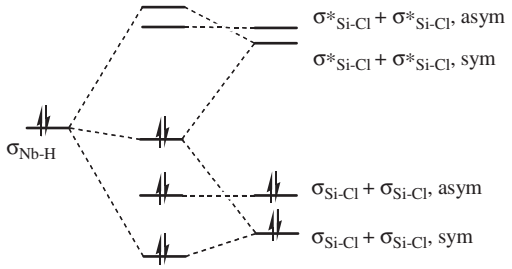

FIG. 8. The MO diagram for the IHI MH···SiCl in the bis(silyl) systems **87**.

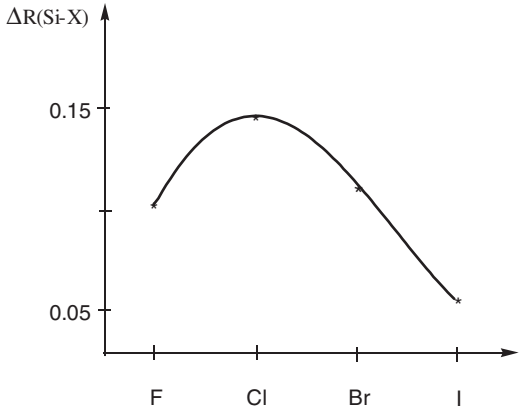

FIG. 9. Dependence of the relative lengthening of the Si–X bond in **87** in comparison with organosilanes X-SiR_3 on the halogen X. (Reproduced from Ref. 174, with permission from The Royal Society of Chemistry.)

the short M–Si bond in **80** (M–Si multiple bond) and **83** (rehybridization of Si) are different.

The attraction of two lateral silyls to the central hydride is clearly seen from the decrease of the Si–Nb–Si bond angles in **87** (range 103.37(7)–105.57(4)°) compared with the classical compounds [Nb(H)($SiMe_2Ph$)$_2Cp_2$] (110.81(5)°)[173] and [Ta(H)($SiMe_2H$)$_2Cp_2$] (109.90(7)°).[175] The comparison of the X-ray structures of [Nb(H)($SiMe_2Ph$)$_2Cp_2$] with [Nb(H)($SiMe_2F$)$_2Cp_2$] is particularly persuasive, taking into account that the former has bulkier silyl groups and hence experiences a greater steric interaction between the Cp and silyl ligands, which might have been relieved by the decrease of the Si–Nb–Si bond angle.[173,174] Therefore, the smaller Si–Nb–Si bond angle in [Nb(H)($SiMe_2F$)$_2Cp_2$] manifests the presence of an electronic factor, namely, the attraction of lateral silyls to the central hydride. The related compound [Nb(H)($SiMe_2OMe$)$_2Cp_2$] turned out to be classical, as judged from the lack of significant structural distortion, such as the shortening of the Nb–Si bond, the elongation of the Si–O bond, and the decrease of the Si–Nb–Si bond angle,[174] which is in accord with the general observation that in hypervalent compounds, significant structural distortions are observed only when the apical

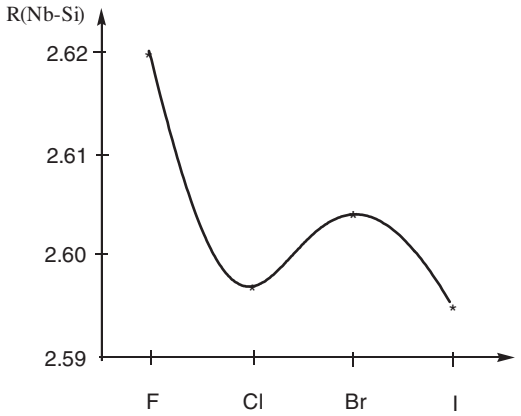

FIG. 10. Variation of the Nb–Si bond length in **87** with X. (Reproduced from Ref. 174, with permission from The Royal Society of Chemistry.)

substituent is both a good electron-withdrawing and good leaving group. The latter condition does not hold for the OMe^- group.

Combined ND study of the bis(silyl) complex **86** and an NMR study of hydride relaxations in **83** and **86** allowed for the accurate determination of the Nb–H bond lengths in **83** and **86** and also of the H–H distance in **83**.[176] Importantly, the ND study of **86** not only unequivocally established the central position of the hydride, equidistant from the silyls, but also, in a very good accord with the NMR relaxation study and the DFT calculations of model complexes $[Nb(H)(SiH_2Cl)_2Cp_2]$ (Table IV), allows one to underpin the theoretical prediction that IHI causes the elongation of interacting M–H bond.[176] However, it turns out that the X-ray determined Si–H distances in **83** and **87** (range 1.86–2.08 Å) are rather invariable for the hydride position. Since the valent orbitals of the fragment $[NbCp_2]$ lie in the bisecting plane of niobocene moiety, the hydrides are restricted to lie in this plane too, which puts certain constraints on the possible length of the Si–H contact in **83** and **87**.

The DFT calculations at the BP86 level of model complexes $[NbH_2(SiH_2Cl)Cp_2]$, $[NbH(SiH_2Cl)_2Cp_2]$, $[NbH_2(SiH_3)Cp_2]$, and $[NbH(SiH_3)_2Cp_2]$ confirmed the main structural trends observed experimentally in **83** and **86** and also, through the use of NBO analysis, allowed for the identification of the proposed electron density transfer from the Nb–H bonding orbital to the $\sigma*$(Si–Cl) antibonding orbital.[173] The symmetrical monosilyls like **85** were found to have IHI too, although this was weaker,[173] possibly owing to the different basicity of the lateral hydride vs. the central one.[177] An AIM study revealed a strongly inwardly curved bond path for the Si–H interaction in $[NbH_2(SiH_2Cl)Cp_2]$ but not in $[NbH(SiH_2Cl)_2Cp_2]$ or their SiH_3 derivatives. While the latter were found to have only very weak IHI of type $NbH\cdots SiH$, the $[NbH(SiH_2Cl)_2Cp_2]$ has a very shallow variation of the electronic density in the interatomic region between the hydride and silicon atoms owing to a greater degree of electron delocalization.

TABLE IV
THE M–H, H–H AND Si–H DISTANCES (Å) IN **83**, **85**, AND **86** FROM EXPERIMENTAL METHODS AND DFT CALCULATIONS

Compound	Parameter	X-ray	NMR relax. At 210 K	ND at 100 K	DFT[2]
83	$Nb–H^X$	1.76(6)[a]	1.68(1)		1.745
	$Nb–H^A$	1.67(9)[a]	1.74(1)		1.793
	$H^X–H^A$	1.92[a]	1.97(1)		1.688
	$Si–H^A$	1.860	1.86[b]		2.043
85	$Nb–H^X$		1.71(1)		1.739, 1.774[c]
	$Si–H^X$				2.097
86	$Nb–H^A$	1.74(7)[d]	1.78(1)	1.816(8)	1.811[e]
	Si–H	2.056	2.076(3)		2.134

[a]At 193 K.
[b]Estimated with the X-ray value for the $Si–Nb–H^{lat}$ bond angle of 114.1°.
[c]Two nonequivalent bond lengths calculated for the model complex $[NbH_2(SiH_2Cl)Cp_2]$.
[d]At 173 K.
[e]Calculated for the model complex $[NbH(SiH_2Cl)_2Cp_2]$.

The presence of IHI in niobocene silylhydrides was discussed from a different point of view on the basis of MP2 calculations of the model complexes $[M(H)(SiH_nCl_{3-n})(X)Cp_2]$ (M = Nb, Ta; X = H, Me, SiH_nCl_{3-n}, Cl; $n = 0-3$) and qualitative analysis of Laplacian maps.[178] The spherical appearance of the Laplacian of electron density around the metal center was interpreted as an indication of d^0 configuration, consistent with the silylhydride description of these complexes. The H···Si bond paths were observed only for the compounds $[M(H)(SiH_nCl_{3-n})(X)Cp_2]$, where X = Cl or Me, but the presence of hypervalent interactions H···Si and the special role of the in-plane chlorine substituent at silicon in all three classes (with different X) of complexes was recognized.[178] It was suggested that the H···Si interaction stems from the polarization of the central hydride by the silyl ligand enhanced by the chlorine groups on silicon. The related compounds $[M(H)(SiH_nCl_{3-n})(Cl)Cp_2]$ (M = Nb, Ta; $n = 0-3$) were rationalized to be the usual silane σ-complexes due to the presence of an electron-withdrawing chlorine on metal. Interestingly, in all the complexes under discussion, the increasing chlorine substitution at silicon strengthens the Si···H interaction so that the strongest bond is observed for the compounds with the $SiCl_3$ group,[178] which is the opposite trend to what is normally observed in silane σ-complexes. However, the X-ray structure of complex $[Nb(H)(SiCl_3)_2Cp_2]$ (**88**), which became available more recently,[179] does not support this theoretical prediction. In fact, the molecular parameters for **88** are more consistent with its classical description and the absence of any significant interactions, in contrast to the (monochloro)silyl complexes **83** and **86**. This is seen from the absence of any significant difference in the Si–Cl bond lengths between the in-plane and out-of-plane chlorines (a narrow range 2.0835–2.0989(7) Å is observed) and from the increased value of the Si–Nb–Si bond angle of 109.61(2)°, which is about 5° larger than in complexes with IHI and very close to the values in classical Group 5 bis(silyl) metallocenes. The experimentally observed Si–H contacts of 2.14(3) and 2.11(3) Å were about 0.1 Å longer than in

complexes **83** and **86** with IHI. The lack of Si–H interactions in **88** can be attributed either to the low basicity of the Nb–H bond stemming from the presence of a large number of electron-withdrawing chlorine substituents on both silyl centers, or to hyperconjugation between the in-plane antibonding orbital (Si–Cl)* and the out-of-plane chlorine lone pairs of electrons. It should be noted that investigations of related chlorosilyl systems discussed below lead to the same conclusion: the strength of IHI decreases on going from monochloro- to trichlorosubstituted silyl complexes.

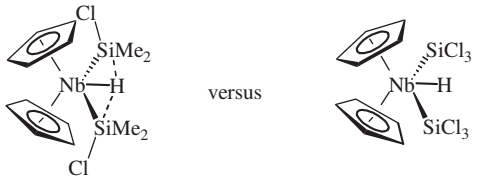

86 nonclassical with IHI

88 classical

b. Asymmetric bis(Silyl) Niobocene Derivatives

A series of asymmetric complexes $[Nb(H)(SiHMe_2)(SiXMe_2)Cp_2]$ (X = F (**89**), Cl (**90**), Br (**91**), I (**92**)) was studied assuming that the interaction of the silyls $SiMe_2X$ and $SiMe_2Y$ with the central hydride H would be different.[180,181] An ND study of $[Nb(H)(SiHMe_2)(SiClMe_2)Cp_2]$ (**90**) reveals the symmetrical position of the hydride in the bisecting plane of niobocene. However, owing to the shorter $ClMe_2Si$–Nb bond length, the $ClMe_2Si$–H distance is shorter than the HMe_2Si–H distance (2.085(17) Å vs. 2.126(17) Å), resulting in a stronger interaction of the hydride with the chlorosilyl center.[180] Comparison with the symmetrical complexes **86** shows that in the asymmetric compounds **89**–**92**, the Si–X bonds are longer (Table V),

TABLE V
THE COMPARISON OF SELECTED MOLECULAR PARAMETERS IN THE SYMMETRICAL BIS(SILYL) COMPLEXES **87**[163,164] WITH THE ASYMMETRICAL DERIVATIVES **89**–**92**[180,181]

Compound	Nb–Si (Å)	Si–X (Å)	Si–Nb–Si (°)	XSi···H (Å)
$[Nb(H)(SiFMe_2)_2Cp_2]$	2.618(1)	1.652(3)	105.57(4)	1.98
	2.622(1)	1.644(3)		
89[a]	2.6167(8)	1.614(3)	106.31(3)	2.02(4)
	2.6411(8)	1.581(5)		2.20(4)
$[Nb(H)(SiClMe_2)_2Cp_2]$	2.597(1)	2.163(1)	104.27(5)	2.06
90	2.5969(6)	2.1829(7)	105.85(2)	2.06(3)
$[Nb(H)(SiBrMe_2)_2Cp_2]$	2.604(2)	2.349(2)	103.37(7)	2.05
91	2.586(2)	2.377(2)	107.27(8)	2.07(3)
$[Nb(H)(SiIMe_2)_2Cp_2]$	2.595(3)	2.590(3)	104.4(1)	2.07
92	2.5782(8)	2.6287(8)	107.99(2)	1.99(4)

[a]The $SiMe_2F$ and $SiMe_2H$ groups are disordered in the positions of H and F.

suggesting stronger IHI. It should be noted that the Si–Nb–Si bond angle in **90–92** opens upon descending Group 7, whereas in **87** the bond angle shortens owing to the increased attraction of *both silyls* to the central hydride. Such an increase in the Si–Nb–Si bond angle in **90–92**, contradicting the increase of the size of the silyl ligand $SiMe_2X$, can be rationalized in terms of a stronger interaction of the $SiMe_2X$ groups with the hydride relative to the H–$SiMe_2H$ interaction, with the difference increasing down the halogen group. Therefore, the opening of the Si–Nb–Si bond angle is achieved at the expense of decreased NbH···$SiMe_2H$ interaction. The DFT studies of **90–92** confirmed that the strength of IHI (covalent term) increases from Cl to I but, unexpectedly, the longest Si–H contact is seen in the chloro derivative **90**, rather than in **89**. This irregularity was attributed to the contribution of an electrostatic dipole–dipole attraction Si···H, which is expected to be the strongest in the fluoro derivative **89** and to decrease down the halogen group. Such a polar interaction can contribute to an additional shortening of the Si–H contact in **89** compared with **90**. To conclude, since the difference in the Si···H interactions was found to be rather small in **89–92**, it appears rather unlikely to determine any difference in the interaction of different silyl groups with the central hydride H in the asymmetrically disubstituted complexes **93**.

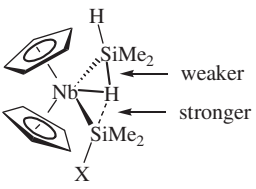

X = F, Cl, Br, I
89, 90, 91, 92

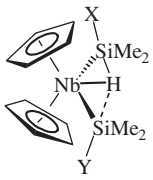

93
compatitive IHI

c. The Dependence of IHI MH···EX on the Nature of Group 4 Element E

The disubstituted complexes $[NbH(GeMe_3)(GeMe_2Cl \rightarrow SnMe_2Cl_2)Cp_2]$ (**94**)[172] and $[NbH(SnMe_2Cl)_2Cp_2]$ (**95**)[183] were prepared according to Eqs. (27) and (28) by the H/E (E = Ge, Sn) exchange and chlorodealkylation reactions:

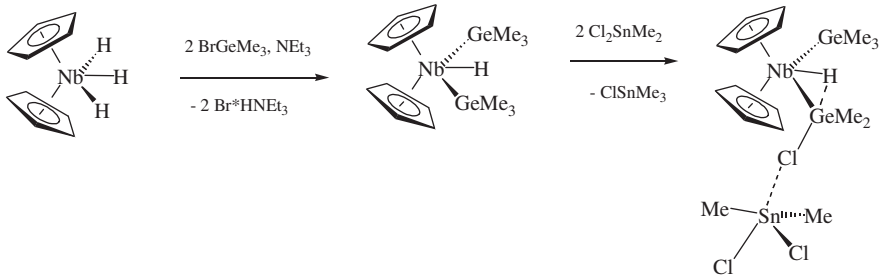

(27)

94

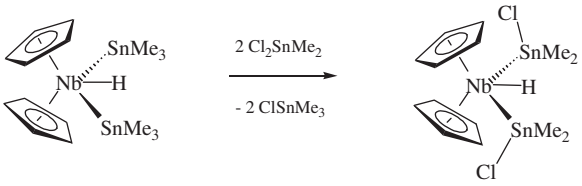

(28)

95

The X-ray structure[172] of **94** (Fig. 11) reveals two different germyl centers, with the $GeMe_2Cl$ group being coordinated to the Cl_2SnMe_2 group and interacting with the hydride. This conclusion follows from the elongation of the Ge–Cl bond (2.358(3) Å) in comparison with other derivatives of type $L_nM–GeR_2Cl$ (range 2.215–2.270(3) Å, R = alkyl, aryl). This Ge–Cl bond is comparable in length to the Ge–Cl bond of $Cp_2W(SiMe_3)(GeMe_2Cl)$ (2.3541(4) Å), which is already elongated owing to the conjugation of the σ∗(Ge–Cl) antibonding orbital with the tungsten lone pair.[184] The Ge(1)–Nb–Ge(2) bond angle of 108.31(4)° in **94** is between the values for the Si–Nb–Si bond angles observed for the bis(silyl) niobocene with IHI (about 105°) and the related classical bis(silyls) niobocenes (about 110°). These features were interpreted in terms of an IHI between the central hydride and *only one lateral group*, namely, the $GeMe_2Cl$ group. The question as to how the coordination of a Lewis acid, Cl_2SnMe_2, to the chlorine of $GeMe_2Cl$ increases the electrophilicity of the germanium center and thus promotes the IHI remained open. Nevertheless, it was noted that the monogermyl complex $[NbH_2(GeMe_2Cl)Cp_2]$, like the related monosilyl **83**, exists in the form of two isomers, and it is tempting to speculate that the sterically disfavored lateral isomer (**96**) can be stabilized by the IHI NbH···GeCl with the central hydride.[182]

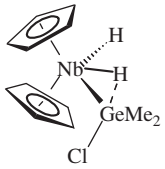

96

nonclassical with IHI

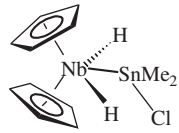

97

classical

In contrast, the lateral isomer is absent in the case of mono(tin) compound **97**, whereas the X-ray structure of the bis(tin) complex **95** is consistent with the lack of any significant Sn···H interactions, although the Cl group is in the *trans* position to the hydride.[183] The X-ray structure of **97** (central isomer) is also classical, with the Sn–Cl rotated out of the bisecting plane, so that IHI is not possible.[185]

The fact that the silyl and germyl compounds have IHI, whereas the tin derivatives do not, seems surprising, considering the greater tendency of heavier main group elements to form hypervalent structures.[186] This discrepancy can be explained considering the mechanism of IHI. Because IHI stems from the electron

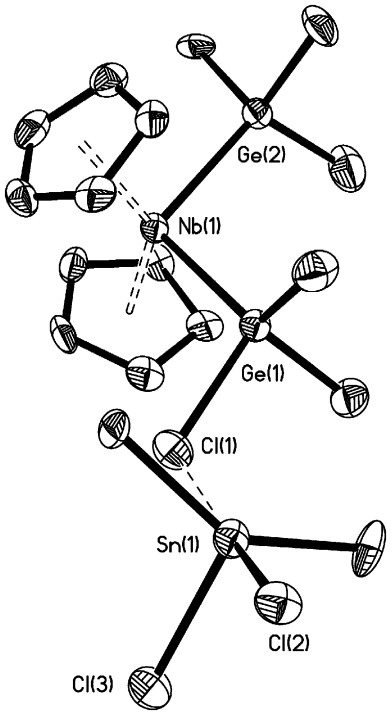

FIG. 11. Molecular structure of complex **94**.

density transfer from the M–H bonding orbital to the σ*(E–X) antibonding orbital, it requires a significant orbital overlap. Since the covalent radii of the heavier Group 4 elements follow the order Si (1.17 Å) > Ge (1.22 Å), Sn (1.40 Å),[187] the direction of the (E–X)* antibonding orbital moves away from the M–H bonding region as E descends Group 4, as is schematically shown in **98**. It should be noted that it is the difference in covalent radii of E and H that prevents the M–E–X bond angle from adopting the ideal value of 90°, required by the trigonal bipyramidal geometry. It can be seen from **98** that such an acute angle will bring the lobe of the σ*(E–X) antibonding orbital away from the M–H bonding orbital. In the main group element compounds the M–E–R angles deviate significantly from the ideal tetrahedral value of 109° because of the increased p character in the E–R bonds due to the operation of the Bent's rule effect. For example, in the classical compound **88**, the six Nb–Si–Cl bond angles fall within the range 116.17–116.67(3)°.[180] In the compounds with IHI this angle is reduced by a few degrees to 113–115°, which thus appears to be a compromise between the Bent's rule effect and the rehybridization of the center E caused by IHI. In the classical compound **97** the bond angles are 108.895(14)° for the Nb–Sn–Cl bond angle and 121.15(7) and 122.21(7)° for the Nb–Sn–C bond angles,[185] because the Sn–Cl bond has a larger tin p character, whereas bonding to Nb and two methyl groups can be described by the sp^2 set. It follows, therefore, that (i) it is incorrect to infer the presence of IHI from the

deviation of the M–E–X bond angles from the tetrahedral value (as some authors do); and (ii) the largest IHI could be expected for a compound with the carbon center, i.e. MH···CX. The problem in obtaining such a species can lie in the possibility of a facile H/X exchange, induced by electronegative group X.

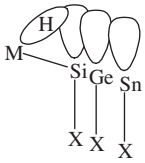

98

The importance of proximity of the hydride and silyl ligands to "switch on" the IHI is also nicely seen from the structure of the molybdenum complex **80**. This compound has both a basic hydride and a functionalized silyl in the *cis*-position. But the bond angle H–Mo–Si, determined by the valence orbitals of the fragment [$MoCp_2$], is 64.9(12)°,[171] which does not allow for any significant interaction between the hydride and silyl ligands (in **83** and **87**, the H–Nb–Si bond angles are 46–52°). The presence of d^n ($n>0$) electron density can be another reason for the absence of IHI, since the negative hyperconjugation of the lone pair on metal with the $SiClR_2$ ligand[171] can be energetically more favorable than IHI. It is reasonable to conclude that in d^n systems the IHI can be possible only if the special arrangement of the metal lone pair and the silyl ligand does not allow for their hyperconjugation. Such a situation occurs, for example, in half-sandwich ruthenium complexes discussed below.

2. IHI in Titanocene Silylhydrides

The compound [$Ti(H)(SiXR_2)(PMe_3)Cp_2$] (**99**) is an isolobal analog of the niobocene compounds **83** with IHI, and is therefore expected to have the IHI too. By contrast, the compound [$Ti(\eta^2\text{-}H_2SiPh_2)(PMe_3)Cp_2$] (**20**) discussed above is a stretched silane σ-complex, i.e. it has an electronic structure intermediate between Ti(IV) and Ti(II).[66]

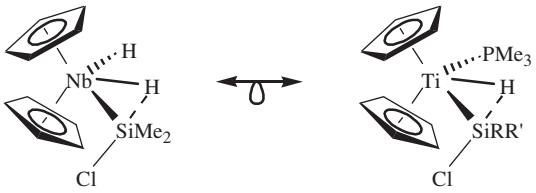

83 **99**

A series of titanocene complexes **100**–**104** has been prepared according to Eq. (29).[55] Complex **100** turned out to be highly unstable and readily decomposes in

solutions into $[Ti(PMe_3)(Cl)Cp_2]$, but the stability of **101**–**104** increases markedly with the number of chlorines on the silicon atom to permit their investigation. Spectroscopic (NMR and IR), structural data (X-ray diffraction studies for **101**, **103**, **104**), and DFT calculations establish that these titanocene silylhydride complexes have IHI Ti–H···Si–Cl. Complexes **101**–**104** exhibit increased silicon–hydride coupling constants in the range 22–40 Hz that change rather irregularly with the nature of the substituents at silicon. Importantly, the signs of the J(Si–H) measured experimentally in **103** and **104** were found to be negative, thus providing conclusive evidence of the presence of direct Si–H bonding. Both **103** and **104** have markedly different Si–Cl bond length for the in-plane and out-of-plane chlorines, the former being elongated because of IHI (Table VI). This allows for the direct comparison at the same silicon center of two different types of Si–Cl bonds, one of which is involved in the interligand hypervalent interaction with the hydride while the other is not. This feature is significant, since in the only σ-complex of a dichlorosilane, the compound $[Mn(\eta^2\text{-H-SiCl}_2Ph)(CO)_2Cp]$, the two Si–Cl bonds are almost identical (2.098(3) Å vs. 2.103(3) Å, $\Delta = 0.005(4)$ Å).[101] Large WI and NBO bond orders support the presence of significant direct Si–H interaction, which is further seen from the observation of corresponding bond critical points in an AIM study. Notably, the X-ray studies and DFT calculations show that *the strength of IHI decreases with increasing chlorine substitution at silicon*. It is interesting that in the absence of a Si-bound electron-withdrawing group lying *trans* to the Si···H moiety, the compound adopts a silane σ-complex form. Thus, the DFT calculations of $[Ti(H)(SiMe_3)(PMe_3)Cp_2]$ and a rotamer of **103**, the compound $[Ti(H)(SiMeCl_2)(PMe_3)Cp_2]$ (**24**) having the Me group *trans* to hydride, revealed significant σ-interactions between the silicon and hydride atoms as discussed in Section II.E.1. Attempts to prepare a classical titanocene silylhydride by reacting $[Ti(PMe_3)_2Cp_2]$ with $HSi(OEt)_3$ did not afford the compound $[Ti(H)(Si(OEt)_3)(PMe_3)Cp_2]$, but rather led to NMR silent titanium (apparently Ti(III)) complex(es) and the silane redistribution product $Si(OEt)_4$. To date, a classical titanocene–phosphine silylhydride derivative without *any* Si–H interaction has not been observed. It was concluded that the titanocene fragment $[Ti(PMe_3)Cp_2]$ is unique in supporting two different types of nonclassical Si–H interaction. Depending on the nature of the R groups on Si, these are either silane σ-complexes or compounds with an IHI.

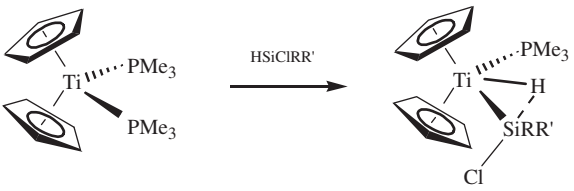

(29)

R, R'	MeMe	MePh	PhPh	MeCl	ClCl
|J(H-Si)|, Hz	-	31	40	22	34
	100	**101**	**102**	**103**	**104**

TABLE VI
SELECTED CALCULATED BOND LENGTHS (Å) FOR $[Ti(H)(SiMe_{3-n}Cl_n)(PMe_3)Cp_2]$ ($n = 0-3$) AND 24[a,b]

	$SiMe_3$[c]	$SiMe_2Cl$[d](**100**)	$SiMeCl_2$[e] (**103**)	$SiCl_3$[f](**104**)	$SiMeCl_2$[a](**24**)
Ti–Si	2.658	2.581	2.535	2.520	2.551
	(2.597)	(2.546)	(2.517)	(2.492)	
Ti–P	2.541	2.555	2.559	2.557	2.557
	(2.550)	(2.557)	(2.554)	(2.556)	
Ti–H	1.742	1.759	1.755	1.754	1.745
	(1.81)		(1.733)	(1.751)	
Si–H	1.840	1.805	1.822	1.847	1.862
	(1.69)		(1.749)	(1.751)	
Si–Cl	–	2.292[g]	2.259[g]	2.225[g]	
		(2.222)	(2.192)	(2.161)	
	–	–	2.216[h]	2.190[h]	2.218[h]
			(2.133)	(2.107 av.)	

[a]Experimental X-Ray Values are in Brackets. **24** is a rotomer of **103** with the Me *trans* to hydride.
[b]X-ray data in parentheses for comparison, in **103** and **104** the hydride atoms were located from the difference map and refined.
[c]X-ray data for $[Ti(\eta^2\text{-}H_2SiPh_2)(PMe_3)Cp_2]$ (**20**).
[d]X-ray data for $[Ti(H)(SiMePhCl)(PMe_3)Cp_2]$.
[e]X-ray data for **103**.
[f]X-ray data for **104**.
[g]Cl *trans* to hydride.
[h]Out-of-plane Cl.

3. IHI in Group 5 Cp-Imido Complexes

The isolobal analogy between the imido and Cp ligands[188] makes the Cp/imido ancillary a potential platform to study the IHI (see **105** and Scheme 5).

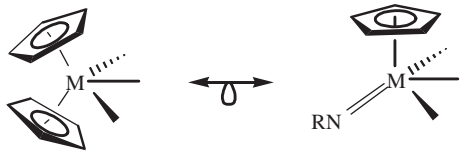

105

a. Cp/Imido Complexes of Tantalum with IHI

The chlorosilyl derivatives $[Ta(H)(SiCl_nMe_{3-n})(=NAr)(PMe_3)Cp]$ ($n = 0-3$), prepared at room temperature according to Eq. (30), have IHI whose strength, according to X-ray and DFT evidence, decreases from $n = 0$ to 3, as was found for the related titanocene derivatives **101**–**104**.[152,77] The similar compound [Ta(H)(SiHPhMe)(=NAr)(PMe_3)Cp] (**106**) is classical, whereas the analogous addition of $HSiPhMe_2$ does not occur even under forcing conditions.[152] The X-ray structure determinations of **107** and **108** revealed the same structural features as in other

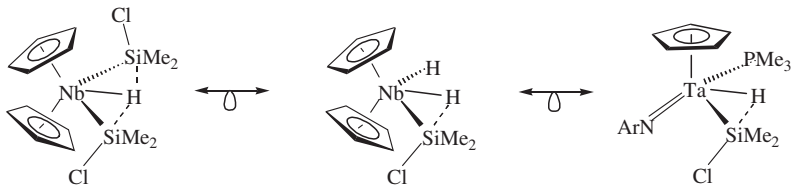

Scheme 5.

compounds with IHI, namely, the shortened Ta–Si and elongated Si–Cl bonds. The Si–Cl bond in **107** of 2.177(2) Å is longer than in the related niobocene complex **83**, whereas **108**, like titanocenes **103** and **104**, contains two types of Si–Cl bonds, with the bond to the "in-plane" chlorine lying *trans* to the hydride (2.117(2) Å) being significantly longer ($\Delta = 0.053(4)$ Å) than the bond to the "out-of-plane" chlorine (2.064(3) Å). It is interesting that that there is no significant difference in the Ta–Si bond lengths in **107** (2.574(1) Å) and **108** (2.569(2) Å, $\Delta = 0.005(2)$ Å), although the latter contains two electron-withdrawing substituents at silicon. This unusual trend was explained in terms of a compensation of the shortening of the Ta–Si bond in **108** relative to **107** (in accordance with Bent's rule) by the diminished contribution of IHI:

(30)

X	H	Cl	Cl	Cl
R,R'	Ph,Me	Me,Me	Me,Cl	Cl,Cl
	106	**107**	**108**	**109**

The measurement of the Si–H coupling constants in **106**–**109** revealed an unexpected trend in that the magnitude of the *J*(H–Si) coupling constant increases from 14 in **106** to 50 Hz in **109** as the number of chlorine groups on silicon increases.[77] This trend is opposite to what is observed for normal silane σ-complexes.[12,13] Surprisingly, the *J*(H–Si) in **106**–**109** does not correlate well with the strength of the Si–H interaction.[77] The structural trends discussed above, and the results of DFT calculations supported by the NBO analysis and the calculation of WI, show that IHI is "switched on" on going from the classical compound [Ta(H)(SiHPhMe)(= NAr)(PMe_3)Cp] (**106**) to the (monochloro)substituted complex [Ta(H)($SiClMe_2$)(= NAr)(PMe_3)Cp] (**107**) and then decreases from **107** to **109**. This can be seen from Fig. 12, showing the variation of the Si–H and Ta–H bond lengths (in Å) and the corresponding bond strengths in complexes [Ta(H)($SiCl_nH_{3-n}$)(= NMe)(PMe_3)Cp] ($n = 0-3$) on *n*. The shortest and strongest Si–H interaction in **107** ($n = 1$) corresponds to the longest and weakest Ta–H interactions,

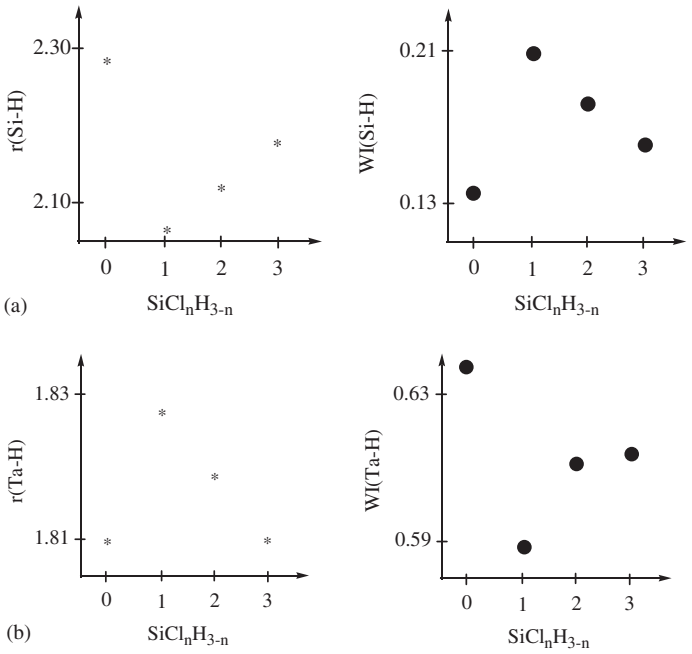

FIG. 12. The variation of bond lengths (in Å) and bond strengths on n, expressed in Wieberg bond indices in complexes [Ta(H)(SiCl$_n$H$_{3-n}$)(= NMe)(PMe$_3$)Cp] ($n = 0-3$): (a) the variation of the *Si···H* interaction, (b) the variation of the Ta–H bond.

in accordance with the theoretical description that IHI is due to the donation of the electron density from the M–H bond into the σ*(Si–X) antibonding orbital.

Thus, the common assumption made in the identification and characterization of silane σ-complexes that a larger H–Si coupling constant corresponds to a stronger interligand interaction (Section II.D) is not valid for the compounds with IHI. This unexpected result can be explained in the same way as it was in Section II.D for the compound [Mn(η^2-HSiCl$_3$)(CO)$_2$Cp]. That is, although the increased chlorine substitution in **107**–**109** results in the decreased IHI, the relative contribution of silicon's character in the Si···H bond increases, which leads to the increase of Si–H coupling.

The weakening of IHI upon progressive chlorine substitution at silicon in **107**–**109** is not *a priori* obvious. Since the increasing n in SiR$_{3-n}$Cl$_n$ decreases the Ta–Si bond, the silicon and hydride atoms can be expected to come into closer contact and thus interact more strongly. On the other hand, the introduction of additional Cl groups on silicon results in several electronic effects that lead to the decrease of orbital overlap between the silicon and hydride atoms. These effects are (i) the contraction of the orbitals on silicon with increasing n; (ii) the decrease of the basicity of the hydride owing to the increasing electron-withdrawing ability of the SiR$_{3-n}$Cl$_n$ group; and (iii) the possibility of conjugation between the p-electrons of the "out-of-plane" chlorine with the σ* (Si–Cl). Although it is difficult to estimate which effect dominates, they can all decrease the Si–H interaction.

It should be noted that the silylhydrides **106 109** were the only products of the reaction shown in Eq. (30). The isomeric agostic species, related to the niobium species **64** and **65** were not identified, and all attempts to convert **106–109** into these or other rearranged species at elevated temperatures resulted in decomposition.

b. Silylhydride Derivatives of Niobium Supported by the Cp/Imido Ligand Set

In contrast to the formation of the agostic complexes **64**, the reactions of $[Nb(PMe_3)_2(NAr)Cp]$ with the silanes $H_2SiPhMe$, $HSiClPh_2$, and $HSiCl_nMe_{3-n}$ $(n = 2, 3)$ afford exclusively the hydridosilyl derivatives $[Nb(H)(SiR_3)(=NAr)(PMe_3)Cp]$ (Scheme 6).[152,189,190] The analogous reaction with $HSiPhMe_2$ does not proceed. The X-ray structures of $[Nb(H)(SiClPh_2)(PMe_3)(NAr)Cp]$ (**111**)[189] and $[Nb(H)(SiCl_3)(PMe_3)(NAr)Cp]$ (**113**)[190] suggest the absence of any significant Si–H interaction. This is particularly surprising in light of the close analogy between **111** and the tantalum complex **107** with IHI. It may be argued that a conjugation between the p-electrons of the phenyl rings with the σ∗ (Si–Cl) orbital in **111** (or analogous conjugation between the p-electrons of the "out-of-plane" chlorine atoms and the $\sigma^*(Si–Cl_{inplane})$ orbital) saturates the silicon center, thus preventing its interaction with the hydride. It is interesting that according to recent NMR studies, the compound $[Nb(H)(SiClMe_2)(PMe_3)(NAr)Cp]$ (**114**), isostructural with **107** and **111**, is formed as a kinetic product in the reaction of $[Nb(PMe_3)_2(NAr)Cp]$ with $HSiClMe_2$, but readily converts into the agostic species **64** at room temperature. According to DFT calculations the molecular parameters of **114** are very close to those of the tantalum analog **107**, and as the latter **114** has IHI of type $NbH\cdots SiCl$.[190] However, the DFT calculations show that **114** is

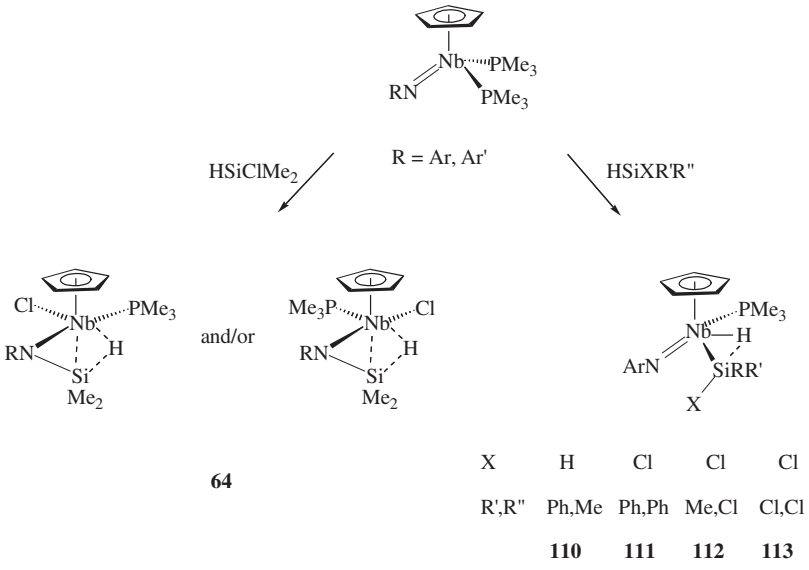

SCHEME 6.

1.4 kcal mol^{-1} less stable than its agostic isomer **64**. It appears, therefore, that niobium shows a greater tendency than tantalum to stabilize formal M(III) structures such as **64**, which is a general trend in the chemistry of these two analogs of the Periodic Table.

4. The IHI MH···SiX in Half-Sandwich Complexes of Ruthenium

Some ruthenium complexes such as **32** and **35**, in the formal oxidation state of Ru(IV), are silane σ-complexes. On the other hand, the Group 8 fragment $[Ru(R_3P)Cp]$ (**115**) is isolobal to the Group 5 metallocene moiety $[MCp_2]$ (**116**), thus giving rise to the question of the occurrence of IHI in the Ru(IV) compounds $[RuH_2(SiR'_2X)(PR_3)Cp]$.[94] The properties of the fragment $[M(R_3P)Cp]$ can be tuned by varying the properties of the Cp and PR_3 ligands.

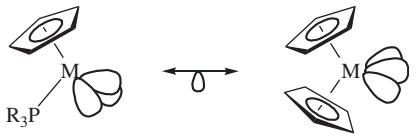

Group 8 Group 5

115 **116**

The structural features of complexes $[RuH_2(SiR_2Cl)(PR_3)Cp^*]$ (**117**)[94,191,192] and $[RuH_2(SiMeCl_2)(PR_3)Cp^*]$ (**118**)[94] are consistent with the presence of interligand interactions similar to those found in metallocene complexes **83**, **87**, **101**–**104** and isolobal Cp/imido complexes **107**–**109**. In **117** the Si–Cl bond is comparable in length to those in **83** and **107** (for instance, in $[RuH_2(SiMe_2Cl)(PMePr^i_2)Cp^*]$: 2.170(1) Å). The novel feature observed in **118** is that the silyl group appears to interact simultaneously with two hydrides (compare with **87** where two silyls interact with one hydride) since each chlorine atom at silicon finds a hydride partner in the approximate *trans* position (both bond angles Cl–Si–H are 154(2)° for the case $[RuH_2(SiMe_2Cl)(PPr^i_3)Cp^*]$). This leads to the somewhat elongated Si–Cl bonds (2.1271(7) and 2.1170(7) Å) which, however, are shorter than in **117** because the p character of Si is distributed over two chlorine atoms in accordance with Bent's rule. The strength of IHI can be tuned by changing the basicity of the phosphine, which in turn affects the basicity of the hydride ligands. Thus, there is no Si–H interaction in the compound $[RuH_2(SiMe_2Cl)(PPh_3)Cp^*]$ with the poorly donating PPh_3 ligand.[192] As expected, more electron-releasing groups at silicon break the IHI, so that the compounds $[RuH_2(SiR_3)(PMePr^i_2)Cp^*]$ (R = alkyl, aryl or H) are classical. This unique dependence of the interligand interactions in the compounds **117** and **118** on the nature of the substituents at phosphorus and silicon atoms allows one to differentiate them from the phosphine polyhydride complexes with multicenter H···Si interligand interactions discussed in Section IV. Although complexes **117** and **118** are Ru(IV) species with the d^4 configuration, negative hyperconjugation with the σ*(Si–Cl) antibonding orbital is not possible because the

metal lone pairs derived from the dz^2 and dxy orbitals (the z-axis is assumed to be directed toward the center of the Cp* ligand) are directed *trans* to the Cp* and hydride ligands, respectively, and thus cannot overlap with the σ*(Si–Cl).

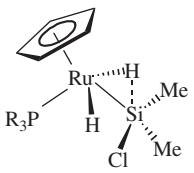

117

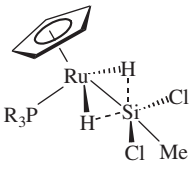

118

C. *β-IHI*

The IHI discussed so far occur between a functionalized silyl ligand (i.e. in the α-position relative to a metal) and a *cis* hydride and thus, in analogy with the agostic complexes, can be classified as α-IHI. Gountchev and Tilley reported the unique example of compound **119**, in which the silyl group in the β-position to metal interacts with the hydride.[193] Complex **119** was obtained according to Eq. (31) apparently *via* a sophisticated mechanism including the Si–H addition across the Ta = N double bond followed by the rearrangements of the substituents at silicon. The key structural and spectroscopic features of this complex are similar to what is found in the compounds **83**, **87**, **101**–**104**, and **107**–**109** with α-IHI. A *trans* arrangement of the chloride and hydride atoms (the Cl–Si–H bond angle equals 174(1)°) with an elongated Si–Cl bond of 2.149(2) Å was observed. Although the elongation of this bond may seem not to be as significant as in compounds with α-IHI, it is not influenced by the presence of an M–Si bond (which is absent in **119**), and thus, the elongation due to the Bent's rule effect is absent. In fact, this Si–Cl bond is rather long when compared with organochlorosilanes and approaches the values observed for an axial chlorine in hypervalent silicon compounds. The silicon atom adopts a distorted trigonal bipyramidal geometry, with the hydride and chloride occupying the apical sites and the sum of the N–Si–H, H–Si–C, and C–Si–N bond angles (351(2)°) close to 360°. The Ta–N–Si bond angle of 108.8(2)° is diminished in comparison with related systems (bond angles > 120°), which allows for the close approach of the SiClHPh group to the hydride to form a short Si···H contact of 1.67(3) Å. Simultaneously, as in complexes with α-IHI, the Ta–H bond is elongated to 1.83(4) Å. Although the Si–hydride coupling was not observed, several spectroscopic features suggest the presence of a direct Si···H interaction. First, the Ta–H stretching frequency is low (1678 cm^{-1} vs. 1779–1790 cm^{-1} in related compounds). Second, there is a large coupling constant of 6 Hz between the hydride and silicon-bound hydrogen, which is too large a value for a formal ^4J(H–H) between these four-bond separated nuclei. The Si···H bonding in **119** can be described in terms of resonance structures **120** and **121**,[193] or alternatively by an MO interaction diagram, which is very similar to that written to describe bonding in **83** (Fig. 7).[16]

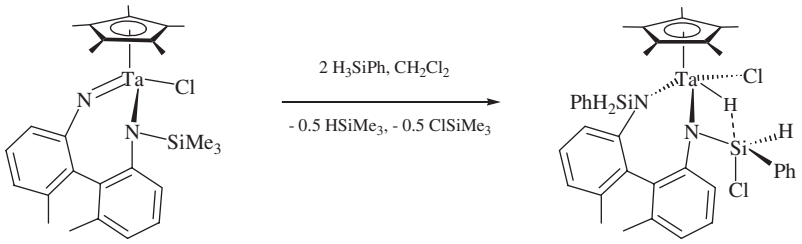

119

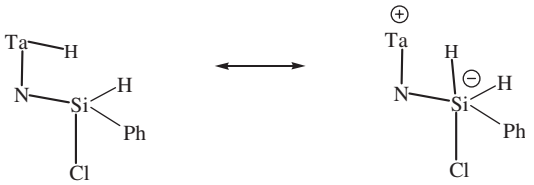

(31)

120 **121**

D. *IHI MH···SiX in Complexes not Isolobal with Metallocenes*

Metallocene or metallocene–isolobal ligation is not a prerequisite of IHI. IHI can be expected for any supporting ligand set, provided it ensures *cis* disposition of the hydride and functionalized silyl groups and sufficient basicity of the hydride ligands.

IHI does not occur in the nonmetallocene tungsten complex $[W(H)_2(SiPh_2Cl)(CO)_2Cp^*]$ (**122**) owing to the presence of two electron-withdrawing carbonyl ligands.[194] Although the *trans* orientation of the hydride and the Si–Cl bond is seen in **122**, the Si–Cl bond length (2.135(1) Å) falls within the range (2.094–2.148 Å) found for classical chlorosilyl complexes, and the W–Si bond is not contracted either. The H–Si coupling constant of 18.3 Hz is somewhat increased, but the hydride atoms remain equivalent on the NMR timescale down to −80 °C.[194] The negative hyperconjugation of the metal lone pair and the σ*(Si–Cl) does not occur either, because the metal electron density is effectively delocalized on the carbonyl ligands. It would be interesting to explore the possible competition of IHI with negative hyperconjugation in the so-far unknown diphosphine analogs of **122**, $[M(H)_2(SiR_2X)(PR_3)_2Cp^*]$ (M = Mo, W).

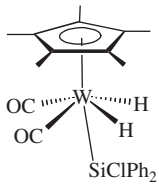

122

TABLE VII
THE SUMMARY OF STRUCTURAL TRENDS IN COMPLEXES WITH IHI AND IN σ-COMPLEXES

IHI	σ-Complexes
Shortened M–Si bonds	Elongated M–Si bonds
Long Si–X bonds	Normal Si–X bonds
Si–H contacts of 1.8–2.1 Å	Si–H contacts of 1.7–1.8 Å
Small Si–M–Si angles in bis(silyl)hydride systems	No regulations
X and H substituents in the apical positions in respect to silicon atom	No regulations
Elongated M–H bonds	Normal M–H bonds

E. *Comparison of IHI with Residual σ Interactions in Silane Complexes*

The main structural trends for σ-complexes and compounds with IHI are compared in Table VII. As can be seen, the key structural parameters differ markedly in these two types of nonclassical complexes, and can be used for their differentiation. This is not surprising, taking into account that these Si···H interactions differ electronically and occur for different types of complexes. Thus, σ-complexes are formed for electron-deficient metal centers with electron-accepting ligands, whereas IHI is formed for metal fragments supported by donating ligand sets. The ''hydrides'' in σ-complexes are often acidic, whereas in complexes with IHI the high basicity of the hydride is a prerequisite for the interaction.

The comparison of spectral parameters is less straightforward. Large silicon–proton coupling constants are expected for the compounds with significant residual σ interactions, while the *J*(H–Si) should be small in the case of an *ideal IHI* when the hydride and the functionalized group X on silicon are mutually *trans* and a pure p orbital of silicon is used for bonding. As has been discussed above, none of these premises is purely realized in practice. *J*(H–Si) can be rather high in silane complexes with even weak interaction of silicon atom with hydride because of rehybridization of silicon owing to the presence of electron-withdrawing substituents.[52] On the other hand, in the compounds with α-IHI, the hydride and group X at silicon are never perfectly *trans* (i.e. the angle H–Si–X $< 180^\circ$) owing to the small size of the hydride and, hence, a short M–H distance. For this reason, there is always some contribution of silicon s character in bonding with the hydride and a fairly large *J*(H–Si) can be observed, which does not necessarily correspond to strong bonding.

To summarize, the following conditions for the occurrence of IHI can be deduced:

1. A basic hydride ligand should be present. This is usually realized for electropositive early transition metals or late transition metals in low oxidation states supported by electron-donating ligands. The metals are preferably from the second and third transition series to ensure strong covalent bonding.

2. A functionalized silyl ligand with an electron-withdrawing group X should be located *cis* to the hydride. The IHI is stronger when X is a good leaving group and when only one such group is present.
3. The bond angle between the H and SiR_2X ligands should not be large (about 50°) to ensure significant overlap of the σ(M–H) bonding orbital and the σ*(Si–X) antibonding orbital.
4. *Trans* orientation of the H and X group should be accessible.
5. If an electron pair is present on metal, its direction should be such that a negative hyperconjugation of this lone pair with the σ*(Si–X) antibonding orbitals is not possible.

IV
MULTICENTER H···SI INTERACTIONS IN POLYHYDRIDESILYL COMPLEXES

A. *Evidence for Multicenter H···Si Interactions*

There is mounting evidence that polyhydride complexes substituted by a main group element ligand ER_n can have multiple interligand E···H interactions. The unusual properties of the rhenium polyhydride silyl complexes $[Re(H)_6(SiR_3)(PPh_3)_2]$ (**123**, $R_3 = Ph_3$, Et_3, HEt_2) and $[Re(H)_2(SiPh_3)(CO)(PPh_3)_3]$ (**124**) were found as early as 1990.[195,196] Complexes **123** are highly fluxional, but on cooling to 193 K, a tricapped trigonal prism geometry was determined by NMR and confirmed by an X-ray diffraction study of $[Re(H)_6(SiPh_3)(PPh_3)_2]$. Although the $T_{1\,min}$ measurements for the hydride ligands gave rather small values of 76–79 ms (for 259 MHz at 209 K), the dihydrogen σ-complex alternative was rejected on the basis of very small isotopic perturbation of resonance. And indeed, Hartree–Fock calculations of a model complex $[Re(H)_6(SiH_3)(PH_3)_2]$ found all the H–H distances between any pair of *cis*-hydrides to fall in nonbonding range 2.083–3.157 Å. The most striking structural feature of $[Re(H)_6(SiPh_3)(PPh_3)_2]$ is the Re–Si bond length of 2.474(4) Å, which is much shorter than the sum of covalent radii (2.65 Å), unusual for a formal d^0 complex. This and the observation of two short Si–H contacts of 1.76 and 1.92 Å led to the suggestion of a possible $M(\eta^3\text{-}H_2SiR_3)$ ligation in **123**. A similar structural motif with a short Re–Si bond of (2.451(3) Å) and two close Si–H distances was observed for **124**, which, unlike many seven-coordinate complexes, is a stereochemically rigid molecule. While the spectroscopic data for **123** and **124** do not support the presence of any Si–H or H–H interactions, calculations of model complexes $[Re(H)_6(SiH_3)(PH_3)_2]$ and $[Re(H)_2(SiH_3)(CO)(PH_3)_3]$ do show somewhat shortened Si–H distances (2.247–2.322 Å and 2.28 Å, respectively).[197] Moreover, the features of the Laplacian of electron density were interpreted to support the presence of four weak, attractive Si–H interactions in **123** and two similar interactions in **124**.

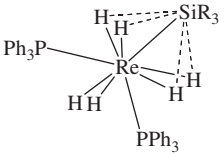

123

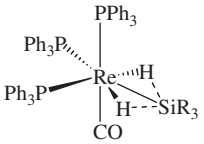

124

The reason why the idea of multiple $H^{\cdots}SiR_3$ interactions did not receive much attention in the early work was, possibly, the absence of a simple bonding scheme that would allow one to conceive of this type of bonding. While a σ-bond coordinated to a metal can be considered as a two-electron donor like phosphine, the perception of multiple $H^{\cdots}SiR_3$ interactions awaited both more conclusive evidence and the development of an adequate theoretical description.

The investigation of iron complexes $[Fe(H)_3(SiMePh_2)(PBuPh_2)_3]$ (**125**) and $[Fe(H)_3(SiR_3)(CO)(dppe)]$ (**126**, $SiR_3 = Si(OMe)_3$, $Si(OEt)_3$, $SiMe_3$, $SiPhMe_2$, $SiPh_3$) approached but did not achieve these goals.[20,198] The compound **125** was prepared by silane addition to the dihydrogen complex $[Fe(H)_2(\eta\text{-}H_2)(PBuPh_2)_3]$:

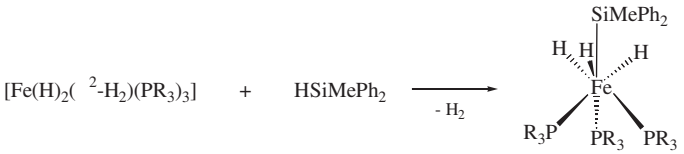

(32)

125

In **125** the hydrides are equivalent at room temperature, but cooling to −60 °C gives two broad singlets in the ratio 1:2, which indicates a restricted rotation of the $SiMePh_2$ group around the Fe–Si single bond. These data were interpreted in terms of the formation of only one 3c–2e Fe–H–Si bond on a three-minima potential energy surface. For the related tin complexes $[Fe(H)_3(SnPh_3)(PRPh_2)_3]$ (R = Bu, Et), the increased value of J(Sn–H) (174.2 Hz for R = Bu), measured from the *tin satellites in the* ^{1}*HNMR spectrum*, did suggest the presence of a Fe–H–Sn bond, but the X-ray structure was in accord with three hydrides interacting with one tin center, which was accounted for by packing forces in the solid state. The low-temperature proton-coupled ^{29}Si NMR spectrum (or the ^{119}Sn NMR spectra for the tin analogs), which might have established the number of hydrides interacting with the silyl (or stannyl) ligand, was not determined for any of these complexes.

The compound $[Fe(H)_3(SiR_3)(CO)(dppe)]$ (**126**) features a π-accepting ligand (CO), a metal from the first transition series (Fe) with contracted 3d shell, and a high formal oxidation state (IV); all these factors promote the formation of σ-complexes.[2] In view of this and the nonclassical nature of $[Fe(H)_2(\eta\text{-}H_2)(PBuPh_2)_3]$, the occurrence of a Si–H σ-bonding seems very likely. As in **125**, equivalent hydrides were observed in the room temperature NMR spectra of **126**, with the J(P–H)

coupling constant increasing from 18.9 to 20.9 Hz as *the electronegativity of the R groups at silicon decreases* (in the related classical compound $[Fe(H)_2(CO)_2(dppe)]$ the $J(P–H) = 30.4$ Hz).[198] This trend is opposite to what would be expected if these compounds were the usual silane σ-complexes that have a smaller $J(P–H)$ for the stronger Si–H interaction promoted by donating groups at silicon. X-ray structure of the compound $[Fe(H)_3(Si\{OEt\}_3)(CO)(dppe)]$ is consistent with the three hydrides lying *cis* to the silicon atom, but the hydrides were not observed. Again, the ^{29}Si NMR data were not determined for any of these complexes.

The structure of the di-iron complex $[Fe_2(\mu, \eta^3, \eta^3\text{-}BH_6)(PEt_3)_6]$ (**127**) contains a boron atom in the octahedral environment of 6 equiv. hydrides capped on the opposite facets by two iron atoms.[199] Thus, neglecting the second iron center, the geometry is very reminiscent of the complex **125**. DFT calculations supplemented by an AIM study confirmed the presence of six H–B interactions and direct Fe–B bonds. The structure was considered as containing a boron trication B^{3+} sandwiched between two anions $[Fe(H)_3(PEt_3)_3]^-$.

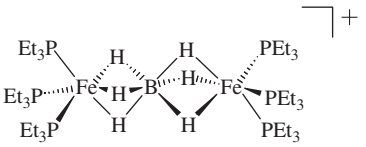

127

Finally, the presence of three Si–H interactions was found in a series of structurally analogous triphosphine ruthenium and osmium complexes of the type $[M(H)_3(SiX_3)(PR_3)_3]$[18,19] (**10**), and ruthenium diphosphine–hydrogen complexes $[M(H)_3(\eta^2\text{-}H_2)(SiX_3)(PR_3)_2]$, having a dihydrogen ligand in place of a phosphine as a two-electron ligand.[200–202] Similar to the iron complexes discussed above, the compounds $[Ru(H)_3(Sipyr_3)(PPh_3)_3]$ (**128**, pyr = pyrrolyl) and $[Os(H)_3(SiR_3)(PPh_3)_3]$ (R = pyr, Et, Ph) exhibit equivalent hydride ligands, which remain indistinguishable down to −85 °C.[18] An octahedral arrangement of the hydride and phosphine ligands was established by NMR in accord with DFT calculations of model systems. The possibility of a nonclassical dihydrogen ligand ($\eta^2\text{-}H_2$) was ruled out on the basis of large T_1. Unlike many seven-coordinate polyhydride compounds, including the relevant complex $[Os(H)_3(PPh_3)_4]^+$, these trihydridosilyl derivatives are rigid, attributed to the presence of stabilizing Si–H interactions. And indeed, the coupling of the silyl to 3 equiv. hydrides with a large $J(Si–H) = 47.4$ Hz for the ruthenium compound **128** was observed in the proton-coupled ^{29}Si NMR spectrum. (A quartet of quartets due to the coupling to 3 equiv. phosphorus and 3 *equiv. hydride nuclei* was observed.) The same pattern was found for the osmium derivatives too, but the coupling is weaker and *reduces on going to more electron-donating groups on silicon* (29.2 Hz for R = pyr vs. 17.9 Hz for R = Et). It should be noted again that, as in the related iron complex **126**, this trend is opposite to what is usually observed in silane σ-complexes.

The X-ray structure of the osmium complex $[Os(H)_3(SiR_3)(PPh_3)_3]$ (**129**) was determined but the hydride ligands were not observed. Nevertheless, the structure is consistent with three hydrides being *cis* to the silyl, capping the three SiP_2 facets of the distorted tetrahedron formed by the heavy atoms. The remarkable feature of $[Os(H)_3(SiR_3)(PPh_3)_3]$ is the very short Os–Si bond (2.293(3) Å), which speaks against the presence of an (η^2-H-SiR_3) ligand. Another noteworthy feature is the elongated Si–N bond of 1.782(10) Å compared to 1.729 Å in the parent silane $HSipyr_3$. The capped octahedral geometry of **129** and its main structural features were well reproduced by DFT calculations of a model complex $[Os(H)_3(Si-pyr_3)(PH_3)_3]$. Short Si–H contacts of 2.10 Å were calculated. Rotation of the silyl group, breaking the favorable *trans* arrangement of the substituent R at silicon and the hydride, was found to destabilize the system, leading to the elongation of the Os–Si bond and increase of the Si–H contacts.

Three bonding schemes were invoked to account for the properties of **128** and **129**. The NBO analysis of $[Os(H)_3(SiX_3)(PH_3)_3]$ led Hübler and Roper *et al.* to propose that the Si···H interactions stem from the delocalization of hydride electrons to the σ*(Os–Si) (see **130** in Fig. 13) and, to a lesser extent, to the σ*(Si–X) orbital (**131**, Fig. 13).[18] Surprisingly enough, it was suggested that donation to the σ*(Os–Si) orbital diminishes the antibonding between osmium and silicon, which was used to account for the very short Os–Si distances in **129**. Alternatively, the peculiar structural and spectroscopic features of **128** and **129** are reminiscent of what was observed in the compounds with IHI, thus a triple IHI Os–H···SiX can account, in principle, for all the observed properties, including the short Os–Si bond and elongated Si–N bond.[17] However, this view is not entirely consistent with the high formal oxidation state IV of ruthenium. A more general description, applicable to all complexes of the type $[M(H)_3(SiX_3)L_3]$, where L is a two-electron donor including the (η^2-H_2) ligand, is shown on the right side of Fig. 13 and implies a σ-coordination of the Si–H bonds of a hypervalent ligand $(H_3SiX_3)^{2-}$.[16] This means that the Si–H bonding is, in a sense, hypervalent, but that the M–(H–Si) bonding is similar to that in σ-complexes.

Several other complexes, structurally related to **125**, **128**, and **129**, have been described. Like **128**, the compound $[Ru(H)_3(SiMeCl_2)(PPh_3)_3]$ (**133**) exhibits a

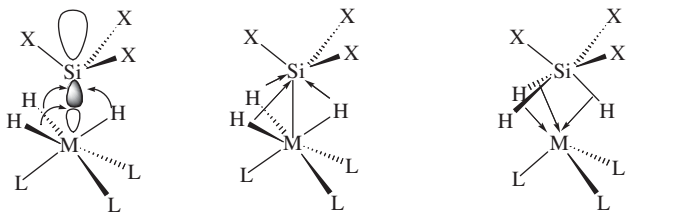

FIG. 13. Possible theoretical descriptions of the bonding in complexes $[M(H)_3(SiR_3)L_3]$.

single hydride resonance in the ^{1}H NMR spectrum and increased J(Si–H) of 39.7 Hz. The X-ray structure reveals three short Si–H distances in a narrow range 1.86(2)–1.94(3) Å with the interesting feature that the shortest Si–H distance of 1.86(2) Å corresponds to the longest *trans* Si–Cl bond (2.130(1) Å, compared with 2.075(1) Å for the Si–Cl bond *trans* to the Si–H bond of 1.94(3) Å), as would be expected for a hypervalent silicon center.[19] The related compound **134** was formulated as a $[Ru(H)_2(\eta^2\text{-}SiPh_2\{OSiR_3\})(PPh_3)_3]$ species, but again, a single hydride resonance with J(Si–H) = 34 Hz is seen at room temperature.[201] Two signals for the nonequivalent hydride ligands (*trans* to the Ph and $OSiR_3$ groups at silicon) with the relative intensities 1:2 are resolved in the ^{1}H NMR spectrum at 213 K. The low-temperature proton-coupled ^{29}Si NMR spectrum that may, in principle, differentiate between the silicon coupling to two types of nonequivalent hydrides has not been reported. The Si–H distances observed by an X-ray study at 140(2) K were in the range 1.97(5)–2.07(5) Å, with the shortest Si–H bond lying *trans* to the most electron-withdrawing substituent $OSiR_3$. The common feature of complexes **129**, **133**, and **134** are the short M–Si bonds of 2.293(3), 2.2760(4), and 2.3539(15) Å, respectively, which allow one to distinguish them from silane σ-complexes, where elongated M–Si bonds are observed.[12,13]

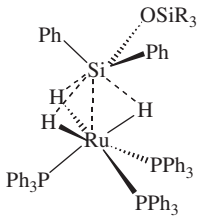

134

An Os–Si bond of 2.3442(8) Å, which is longer than in **129**, and longer Si–H contacts of 1.93930–2.06(4) Å have been found for the silatranyl derivative $[Os(H)_3(Si\{OCH_2CH_2\}_3N)(PPh_3)_3]$ (**135**), which was rationalized to have very weak Si–H interactions.[203] The related compounds $[Os(H)_3(SiR_3)(CO)(PR'_3)_2]$ ($R_3 = H_2Ph$, HPh_2, Ph_3 with $R' = Pr^i$ (**136**)[204] and R = Me with R′ = Ph (**137**)[205]) were regarded as classical on the basis of large J(H–P),[205] presumed to be small in a nonclassical compound, and on the basis of calculations of a model complex $[Os(H)_3(SiH_3)(CO)(PH_3)_2]$.[204] The complex **137** was found to belong to the same type as **125**, **128**, **129**, and **134**, whereas the X-ray structure determination of $[Os(H)_3(SiHPh_2)(CO)(PPr^i_3)_2]$ did not reveal the hydrides,[204] although a different structure with three hydrides *cis* to one of the phosphorus center was found to be the minimum for $[Os(H)_3(SiH_3)(CO)(PH_3)_2]$. A shorter Si–H bond of 1.869 Å to one of the hydrides suggests that a silane σ-complex can be present.[204] Neither for **136** nor for **137** were the H–Si coupling constants measured.

Since the DCD scheme consists of donation and backdonation components, the σ-complexation of the Si–H bond to metals depends both on the π-acidity of the *trans* ligand and its donor ability, as related to the *trans* effect. The structure **132**

suggests that if the ligand L is a π-acid, such as carbonyl, the H–Si bond should strengthen for the same reasons, as π-acidic ligands promote the formation of σ-complexes. However, the essential difference with the conventional silane σ-complexes is that electron-withdrawing groups on silicon will strengthen the Si–H bond in **132** and thus cause a less-advanced S–H bond addition to metal, because such groups promote the formation of a hypervalent silicon species. On the contrary, the Si–H bond *trans* to the most electron-donating group at Si will be more activated. This effect is reflected, for instance, in the smaller J(Si–H) in the ethyl-substituted complex $[Os(H)_3(SiEt_3)(PPh_3)_3]$ (17.9 Hz) compared with 29.2 Hz in the pyrrolyl derivative $[Os(H)_3(Sipyr_3)(PPh_3)_3]$,[18] and in the decrease of Si–H bonding in **135**, which has an electron-rich silatranyl center because of the intramolecular Si←N dative bond. The compound $[Ru(H)_3(SiMe_3)(PMe_3)_3]$, having donor groups at both the silicon and phosphorus atoms, is classical according to a ND study.[206] The case of carbonyl complexes **136** and **137** suggests that substitution at silicon is more important than the π-acidity of ligands *trans* to the hydrides, but the evidence against the nonclassical structure is inconclusive. The ^{29}Si NMR data and more sophisticated quantum-mechanical calculations are required to test this hypothesis.

If the bonding scheme **132** is valid, it can be expected that ligands with weak π-acidity will provide the advanced Si–H bond oxidative addition. Such a situation is observed, for instance, in the compound $[Ru(H)_2(\eta^2\text{-}H_2)(\eta^2\text{-}HSiPh_3)(PCy_3)]$ (**138**, the original formula of the authors is given) that was rationalized to simultaneously contain a η^2-dihydrogen and a η^2-silane coordination[202] with additional stabilizing *secondary interactions between the silicon and hydride atoms* (SISHA).[200–202,207] Changing the phosphine in **132** for a dihydrogen ligand to give **138** causes the rupture of the H–Si bond *trans* to the η^2-H_2 and yields a hydride ligand, owing to the weak *trans* effect and weak π-acidity of the η^2-H_2 ligand. The hydride ligand possibly still has some weak residual interaction with the silicon atom,[202] while the two remaining phosphines on **138**, which are bulky, occupy the sterically unfavorable but electronically advantageous *cis* positions that are *trans* to two H–Si bonds of what is left of the $(\eta^4\text{-}H_3SiX_3)^{2-}$ ligand, the $(\eta^3\text{-}H_2SiX_3)^-$ ligand.[16] The two Si–H bond lengths observed by X-ray in **138** (1.72(3) and 1.83(3) Å with $\Delta = 0.11(4)$ Å) and calculated for its model $[Ru(H)_2(\eta^2\text{-}H_2)(\eta^2\text{-}HSiH_3)(PH_3)]$ (1.946 and 2.071 Å with $\Delta = 0.135$ Å) *do not show any significant difference*, although one of them was considered as a residual σ Si–H interaction in the η^2-silane ligand $HSiR_3$ and the other was proposed to be a SISHA between the silicon atom and the putative hydride. Such close Si–H distances suggest the presence of a $(\eta^3\text{-}H_2SiX_3)^-$ ligand, whose slight asymmetry can be then explained by a second-order Jahn–Teller distortion.[16]

Very similar Si–H interactions are seen in the compound $[Ru(H)(\eta^2\text{-}HSiClMe_2)(\eta^3\text{-}C_6H_8PCy_2)(PCy_3)]$ (**139**, the original formula of the authors is given), which relates to **138** in that the hydride and the dihydrogen ligands are substituted by the η^3-allylic ligand derived from a dehydrogenated cyclohexyl ligand. Again, very close values for the Si–H bonds are found in this compound (originally rationalized to be a silane σ-complex with additional SISHA) by an X-ray study (1.91(2) and 1.99(2) Å, $\Delta = 0.08(3)$ Å).[200]

The predicted free ligand $(H_2SiPh_3)^-$, isolated in the form of its potassium salt, has been recently prepared and studied by X-ray analysis.[208] A D_{3h} geometry with

the hydrides in the apical sites was observed in the solid state and calculated by DFT to be the minimum. However, a second conformer with one axial and one equatorial hydride was found to be another local minimum, lying only 8.6 kcal mol^{-1} higher than the *trans*-form. Therefore, the energy cost of the distortion of *trans* $(H_2SiPh_3)^-$ to give the *cis*-form can be easily compensated for by the double ligation of both Si–H bonds to a metal. *Cis* hydrides were also proposed for the compounds $(H_2Si\{OPr^i\}_3)^-$ and $(H_2Si\{OBu^{sec}\}_3)^-$ on the basis of NMR evidence, but no structural information is available.[209]

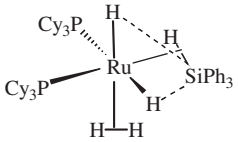

138

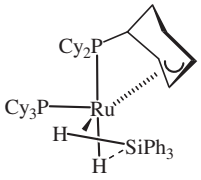

139

Whereas the complexes $[Ru(H)_2(SiR_3)(PR'_3)Cp^*]$ with electron-donating groups R (R = alkyl, aryl) are classical,[94] the isolobal tris(pyrazolyl)borate complexes **140** (Cp* is isolobal with Tp) were formulated as silane σ-complexes of type $[Ru(H)(\eta^2\text{-}HSiR_3)(PPh_3)Tp]$.[210] The compounds **140** were prepared by silane addition to $[Ru(H)(NCCH_3)(PPh_3)Tp]$ according to Eq. (32). Similar to the related complex $[Ru(H)(\eta^2\text{-}H_2)(PPh_3)Tp]$,[211] complexes **140** are highly fluxional, exhibiting 2 equiv. hydride signals in the ^{1}H NMR spectra even down to −100 °C, but the η^2-H_2 form is absent since the T_1 values are large (436–690 ms), well outside the usual range of T_1 values for dihydrogen complexes. The presence of a H–Si interaction in **140** is evident from the large observed J(H–Si) in the range 23.3–52.8 Hz, and since the hydrides are fluxional, even higher values for the J(H–Si) could be expected if complexes **140** contained a separate η^2-silane ligand.[210] As in **129**, the highest J(Si–H) is seen for the silyl group bearing the most electron-withdrawing groups, a feature not compatible with the presence of a conventional σ-complex. It is obvious that the occurrence of interligand interactions in the $[Ru(PR_3)Tp]$ system compared with the isolobal $[Ru(PR_3)Cp]$ fragment is due to a weaker donation ability of the rigid Tp^- ligand and, hence, a diminished backdonation from the metal:

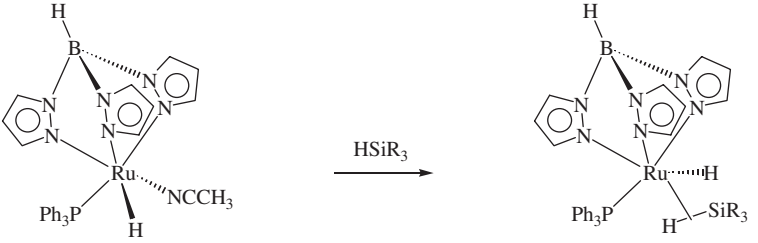

(33)

R_3 =	Et_3	$(OEt)_3$	Ph_3	HEt_2	HPh_2	H_2Ph
J(H-Si), Hz =	23.3	52.8	28.4	23.5	23.5	27.4

140

The J(H–Si) in **140** were measured from the ^{29}Si satellites in the ^{1}H NMR spectrum and, therefore, do not tell us how many hydrogen atoms are bound to the silicon. This problem was solved by a B3LYP calculation of a model of **140** (Tp was a modeled by $(H_2C=NNH)_3BH$, PPh_3 by PH_3, and SiR_3 by SiH_3), which shows that among several possible representations **140a**–**140d**, the most stable one is **140a**.[210] The optimized structure exhibits a Si–H distance of 1.823 Å and a longer Ru–H distance to the Si-bound hydrogen than the Ru–H(hydride) bond (1.629 Å vs. 1.610 Å). The Si–H(hydride) distance is longer (2.108 Å) and was considered as nonbonding,[210] although it should be noted that similar values are found in complexes with SISHA.[200–202,207] The occurrence of the interaction Si–H(hydride) may account for the very low calculated barrier (0.5 kcal mol^{-1}, structure **140b**) of silicon swinging between the different hydrogen centers, which explains the extreme fluxionality of the complex **140**. This bonding picture (one stronger Si–H and one weaker Si–H interaction) is very reminiscent of the *cis*-effect well described in a range of hydride(dihydrogen) complexes, which are often very fluxional.[2] The isomeric form **140d** was found to have even stronger Si–H interaction (1.765 Å), whereas the *cis*-effect was absent (the H–H distance is 1.765 Å), apparently owing to the difference in the electronegativity of the silicon and central hydrogen atom, leading to the polarization H^{-}–Si^{+}. The interconversion of **140a** and **140d** requires a much higher barrier of 7.5 kcal mol^{-1}.

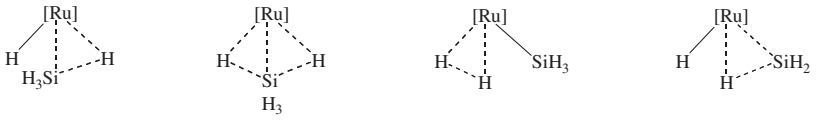

140a **140b** **140c** **140d**

[Ru] = TpRu(PH_3)

The observation of a much larger Si–H coupling (52.8 Hz) for the triethoxy derivative [Ru(H)(η^2-HSi(OEt)$_3$)(PPh_3)Tp] compared with other complexes **140** (range 23.3–27.4 Hz) contradicts the usual trend that electron-donating groups on silicon favor stronger Si–H interaction. Interestingly, B3LYP calculation of the model [Ru($H_2Si(OH)_3$)(PH_3)Tp] shows a stronger Si–H interaction for both the Si-bound hydrogen and the Ru-bound hydride (the Si–H distances are 1.787 and 1.985 Å). Therefore, it is tempting to postulate that the actual form of **140** is intermediate between **140a** and **140b** and that the overall bonding picture is different from what is observed in normal silane σ-complexes. That is, the structure of **140** can be rationalized as containing a $(H_2SiR_3)^{-}$ ligand distorted due to the second-order Jahn–Teller effect, as is discussed above.[16] The transition state **140b** then corresponds to a complex of symmetrical $(H_2SiR_3)^{-}$. Such a "breathing" $(H_2SiR_3)^{-}$ ligand may be alternatively applied to explain the fluxionality of complexes **140**.

Stabilizing SISHA interactions were invoked to account for the unusual properties of the chelate complexes [Ru(H)$_2${(η^2-HSiR$_2$)$_2$X}(PCy_3)$_2$] (**141**).[212] These compounds were prepared by disilane additions to [Ru(H)$_2$(η^2-H$_2$)$_2$(PCy_3)$_2$]

[Eq. (34)] and thoroughly studied by IR and multinuclear NMR spectroscopy, X-ray analyses, and DFT calculations. Two very different Si–H distances (range 1.73(3)–1.84(3) Å vs. range 2.21(2)–2.27(2) Å) have been observed, which allows the authors to differentiate between two types of nonclassical bonding in **141**: the η^2-coordination of H–Si bonds to metal and the H···Si secondary interactions. Complexes **141** have symmetry C_2 or C_{2v} and, as in **138**, the two bulky phosphine ligands are in the sterically disfavored *cis* positions. The hydrides are *trans* to the phosphines rather than to the ligands with the weakest *trans* influence, the η^2-H-Si bonds, which was attributed to the presence of stabilizing SISHA interactions between these hydrides and the silicon atoms. The two η^2-H-Si bonds are mutually *trans* and thus compete for the backdonation from the same d-orbital on metal, according to a B3LYP study.[213] Moving the two η^2-H-Si bonds away from the phosphines weakens this competition and stabilizes the structure. The compounds $[Ru(H)_2\{(\eta^2\text{-}HSiR_2)_2O\}(PCy_3)_2]$ (R = Me, Ph) have a structure of type **142** with C_1 symmetry, with one η^2-H-Si bond lying *trans* to a hydride and the other η^2-H-Si bond *trans* to a phosphine ligand, so that the H–Si bonds do not compete and are activated more strongly through enhanced backdonation.[213] Interestingly, the theoretical work by Lin *et al.* did recognize the unusual geometry of **141** (the $\eta^2 - H{-}Si$ bonds are *trans*, making the ligands with strongest *trans* influence mutually *trans*) but provided no rationale for this, because the stabilizing secondary interactions between the silicon and hydride atoms were not identified. Instead, it was stated that "the *trans* bis($\eta^2 - H{\cdots}Si$)) structure reflects the inherent stabilization of the complex through a particular distorted coordination of the two *trans*-(H···Si) units":[213]

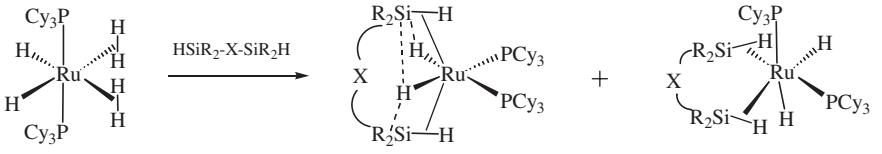

(34)

141 **142**

X = O, 1,2-C_6H_4, C_2H_4, C_3H_6, $OSiMe_2O$
R = Ph, Me, Me, Me, Me

X = O, O
R = Ph, Me

In $[Ru(H)_2\{(\eta^2\text{-}HSiR_2)_2X\}(PCy_3)_2]$, the H–Si coupling constants depend on the nature of other R groups at silicon in a way different from the normal silane σ-complexes. Thus, in $[Ru(H)_2\{(\eta^2\text{-}HSiR_2)_2O\}(PCy_3)_2]$ (**142**) J(H–Si) rises from 22 Hz for R = Me to 41 Hz for R = Ph, although phenyl is a weaker electron donor than methyl. In the symmetrical **141** the J(H–Si) increases with the length of the bridge (65 Hz for X = 1,2-C_6H_4 to 75 Hz for X = $(CH_2)_3$) and also increases for electron-withdrawing substituents at silicon (75 Hz for X = $(CH_2)_3$ vs. 82 Hz for X = $OSiMe_2O$). Further support for the presence of H–Si interactions comes from the low-frequency shifted (by 350–450 cm^{-1}) stretching bands (range 1985–2045 cm^{-1}). Theoretical studies show that the Si–H and Ru–H vibrations

are strongly coupled and the low-frequency bands are better described as Ru–H^b stretchings (H^b – the hydrogen bridging the ruthenium and silicon atoms). Complexes analogous to **141** with more electron-withdrawing phosphines PPh_3 and $Ppyr_3$ (pyr = pyrrolyl) have been also prepared, but the observed H–Si coupling constants are very close to those in **141**, and no definite conclusion about the dependence of the H–Si bonding on the nature of phosphine can be made.[212]

Complexes **141** are fluxional at or above room temperature, exchanging the "hydrides" and the protons of the η^2-H-Si bond.[202,212] Analysis of different exchange mechanisms supported by DFT calculations favors the exchange to occur *via* an asymmetric structure of type **142**, which is followed by the silane-dihydrogen and bis(dihydrogen) structures **143** and **144** (Scheme 7).[212] The formation of **142** from the symmetrical **141** is the most energy-demanding step ($\Delta E = 30.9\,kJ\,mol^{-1}$ with the barrier of $42.8\,kJ\,mol^{-1}$), which was attributed to the loss of stabilizing SISHA interaction. A mechanism analogous to that for **140** and involving a $[M(\eta^3\text{-}H_2SiR_3)L_n]$ structure has not been discussed, although this is also compatible with the low entropy of activation of the exchange determined by NMR studies (Scheme 7).

The compound $[Ru_2(H)_4(\mu\text{-}\eta^2 : \eta^2 : \eta^2 : \eta^2\text{-}H_4Si)(PR_3)_4]$ (**145**, R = Cy, Pr^i) prepared according to Eq. (35) is a unique example of a complex of the simplest silane SiH_4, in which all four Si–H bonds are coordinated to metal.[212,214] All the eight hydrogen atoms present in the molecule are in fast exchange with $\Delta G^{\neq} = 36\,kJ\,mol^{-1}$ and are coupled to the silicon atom with J(H–Si) of 36 Hz. The structure of **145** resembles that of **127** in that the central (silicon) atom is sandwiched between two metal polyhydride fragments. The Si–H bonds (1.69(3) and 1.73(3) Å) observed by an X-ray study for the compound $[Ru_2(H)_4(\mu\text{-}\eta^2 : \eta^2 : \eta^2 : \eta^2\text{-}H_4Si)(PPr^i_3)_4]$ correspond well to the value (1.685 Å) calculated for the model complex $[Ru_2(H)_4(\mu\text{-}\eta^2 : \eta^2 : \eta^2 : \eta^2\text{-}H_4Si)(PH_3)_4]$ and are of the order of magnitude usually observed for silane σ-complexes. The remarkably short Ru–Si bond (2.1956(9) Å), although close to the values observed in ruthenium silylene complexes, does not mean the presence of a Ru=Si double bond, but is rather a compromise of η^3-H_2Si coordination to each of the ruthenium centers. The bonding of H_4Si to each of the metals occurs through the donation of electron density from a pair of Si–H bonds. A novel feature of the H–Si bond coordination in **145**, identified through DFT calculations, is that the backdonation on the σ*(Si–H) orbital occurs from the opposite ruthenium center with which the antibonding orbital finds a better match:

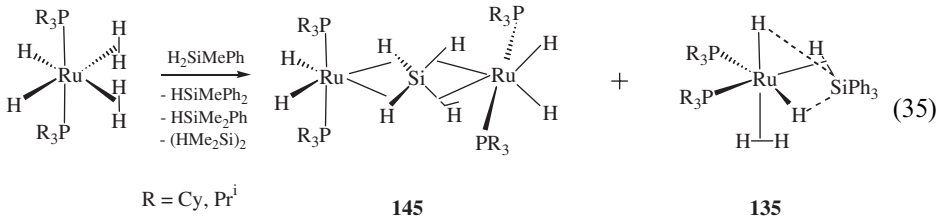

(35)

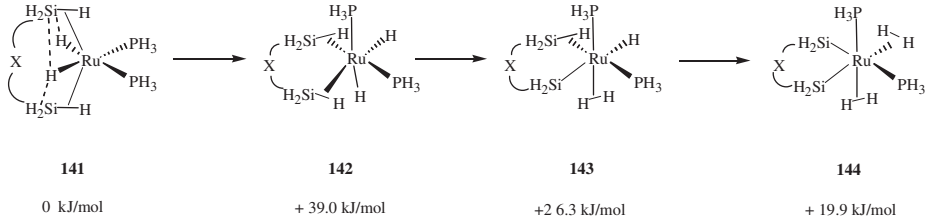

SCHEME 7.

B. *Comparison of Multicenter H···Si Interactions with IHI and Residual σ-Interactions in Silane Complexes*

While the last class of complexes considered in this section, the compounds **145**, closely resemble the usual silane σ-complexes, other multicenter H···Si interactions discussed above have spectroscopic and structural features common to both the IHI and σ-complexes. This enigmatic situation can be explained well by the structure **132** in terms of a σ-coordination of the Si–H bonds of the hypervalent ligand $(H_{n+1}SiX_3)^{n-}$ $(n \geqslant 1)$ to metal, which thus includes both the hypervalent interaction of the silicon with the hydride atoms and the σ-complexation of the Si–H bonds to metals. The key features of complexes with multicenter H···Si interactions are summarized in Table VIII, where a comparison with the IHI and the residual H–Si interactions in silane σ-complexes is given.

The case of ruthenium complex $[Ru(H)_3(SiMe_3)(PMe_3)_3]$ and osmium complexes **135**–**137** clearly shows that donor groups at silicon atoms break the Si–H interaction. The effect of the donor ability of phosphine ligands is less defined and deserves further studies. On the one hand, highly donating phosphines make the metal more electron-rich, which stabilizes the high oxidation state and promotes advanced Si–H bond addition. On the other hand, strongly donating phosphines have strong *trans* influence, destabilizing the *trans* hydrides. Such an unfavorable situation can be avoided by the formation of a Si–H bond, which transforms the ligand with a strong *trans* influence into the ligand with a weak *trans* influence. The formation of multicenter H···Si interactions allows the compound to avoid the undesirably high formal oxidation state of the middle/late transition metals (such as state IV for Group 8 metals) and/or a situation that ligands with strong *trans* influence, such as hydride and phosphines), are forced to be *trans*. Thus, the multicenter interligand H···Si interactions allow the compound to optimize its metal–ligand bonding. The short M–Si bond observed in such compounds is not an indicator of strong M–Si bonding, but the inevitable consequence of the coordination of several Si–H bonds, all stemming from the same silicon center.

C. *A Comment on the Terminology*

The term *secondary interactions* was introduced in chemistry by Alcock to describe all types of interactions not explainable by conventional theories, i.e. for *nonclassical* interactions.[5,215] As has been recently discussed, the term *secondary*

TABLE VIII
COMPARISON OF STRUCTURAL AND SPECTROSCOPIC FEATURES OF MULTICENTER H···Si INTERACTIONS IN COMPLEXES $[MH_N(SiX_3)L_M]$ WITH THE IHI AND σ-COMPLEXES[a]

Feature of multicenter H···Si interactions	IHI	σ-Complex
Electron-withdrawing groups X on Si favor the Si–H interaction	+	−
The metal is in a high formal oxidation state	+/−	+
The X and H are in the approximate *trans* positions	+	−[b]
The M–Si bond is shortened	+	−
The *J*(H–Si) coupling constant is large	+/−	−
J(H–Si) increases with the rise of the electronegativity of groups X on silicon	+	+
The supporting ligands L on metal are poorly donating or electron-withdrawing	−	+

[a] + Indicates that the feature is also typical for the other type of Si–H interaction, +/− means that both situations are possible.
[b] Although a halogen X *trans* to H was observed in some silane σ-complexes this is not a prerequisite of the theory (Section II.B).

interaction covers a wide range of different types of nonclassical interatomic interactions.[5] The term *secondary interactions between the silicon and hydride atoms* (SISHA) was introduced by Sabo–Etienne *et al.*[200–202,207] to describe the simultaneous interaction of a silicon center with several hydride atoms, among which one is considered to be part of a η^2-silane ligand, whereas others are considered to be hydrides interacting with the silicon atom *via secondary interactions.* While the nature of these *secondary interactions* has not been explicitly defined, in the systems in which they were discovered, it closely resembles the so-called *cis*-effect, which is an interaction of a hydride with a *cis*-located dihydrogen molecule.[2,216] Therefore, it should be clearly realized that SISHA is not *a special type* of interligand Si–H interaction, but rather an alternative way of saying that *some nonclassical* Si–H bond is present, thus masking the concrete nature of the Si–H interaction. The term *weak interaction*, used by some authors and implying that the strength of nonclassical bonding is different from the conventional covalent bonding, is even less accurate, because in some molecules a genuine covalent bond can be as weak as a few kcal mol^{-1}, comparable to the strength of nonclassical bonding. It should be the difference in the electronic structure of the compound that provides a justified classification of chemical bonds.[217] In this regard, the classification of nonclassical H–Si complexes as σ-complexes (**1**), agostic complexes (**5**), complexes with IHI (**9**), and polyhydridesilyl complexes with the σ-coordination of hypervalent silyl anions (such as **132**) proposed in this review appears to be advantageous because it is based on clearly defined MO pictures of bonding in these compounds that have predictable structural and spectroscopic features, allowing for their verification by experimental and theoretical methods. The theory of multicenter H···Si interactions is still in its infancy and further work is required to clarify their nature. The bonding mode proposed for **132** can be verified by synthesizing polyhydride complexes in high formal oxidation state of the metal, bearing electron-withdrawing groups on both the metal and silicon atom. Carbonyl analogs of complexes **128**–**129** substituted by halosilyl ligands are promising candidates for such a study.

V
CONCLUSIONS AND OUTLOOK

It is obvious that studying interligand Si–H interactions has reached a great extent of sophistication. At least three classes of nonclassical Si–H bonding can be identified. These are the electron-deficient residual Si–H interactions in silane σ-complexes and agostic complexes, electron-rich IHI MH···SiX, and the more recent multicenter H···Si interactions, which are the subject of current debate and have features common to both IHI and σ-complexes. This surprising diversity stems from the special role the substituent at silicon can play in tuning the extent of Si–H interaction, and from the propensity of silicon to be hypervalent.

The silane ligand, η^2-$HSiR_3$, is both a better σ-donor and π-acceptor than the η^2-H_2 ligand, and thus undergoes a deeper Si–H bond activation by a metal center. The effect of substitution at silicon on the extent of Si–H oxidative addition has received a great deal of attention. It appears that electron-withdrawing groups promote the Si–H bond activation in silane σ-complexes through increased back-donation from metal, but as the recent example of complex **67** shows, the opposite can be the case for agostic complexes. Here, decreased Si–H donation to metal may be the key bonding factor, and the presence of a link between the metal and silicon centers (the NAr group) may impose restrictions on the optimal orientation of the group relative to the rest of complex, thus decreasing the backdonation.

Substituent effects opposite to those found for silane σ-complexes were observed for the complexes with IHI, where the presence of one electron-withdrawing group *trans* to the hydride "switches" the IHI on in comparison with a silyl SiR_3 with the donating R's only. However, the IHI weakens with the further increase of the number of electron-withdrawing substituents at silicon. It also appears that electron-donating groups on silicon decrease the extent of H···Si interactions in the recently discovered class of polyhydride complexes with multicenter H···Si interactions.

The measurements of silicon–hydride coupling constants have been commonly considered as the main method for identification of nonclassical Si–H interactions on the basis of "20 Hz" criterion. But as more and more nonclassical complexes appear, it becomes clear that the original assumptions and analogies with the η^2-H_2 complexes were far too oversimplified. Quite significant coupling can be found in systems with rather weak Si–H bonding and, vice versa, strong Si–H interactions may correspond to small J(H–Si). It appears reasonable to infer the presence of M···H···Si three-center interaction if the coupling constant is rather large, more than, say, the arbitrary value of 70 Hz. Lower values of 15–40 Hz suggest that some H–Si interaction may be present, but a reliable, independent, spectroscopic, structural, or computational evidence is required. The observation of even lower values, however, does not rule out the existence of a Si–H bonding. In this case, when the *absolute value* of the J(H–Si) is small, the measurement (or calculation) of the *sign of silicon–hydride coupling constant* can be a more reliable signature for the presence of a nonclassical interaction. The case of complex [Rh(H)(Si$(OMe)_3$)(*t*-butylacrylate)Cp] being an apparent Rh(III) silyl hydride compound, but exhibiting a large J(Si–H) of 38 Hz, deserves intense scrutiny, because this can be

the first example of a classical compound with an unusually large hydride–silicon coupling constant. If this is indeed the case, a critical revision of the assignment of nonclassical structures on the basis of $J(\mathrm{H–Si}) > 20$ Hz will be required for compounds characterized by relatively small J(H–Si), in the absence of a independent evidence for the Si–H bonding. Finally, it is rather incautious to estimate the extent of the Si–H bond oxidative addition to a metal on the basis of the decrease of J(H–Si) relative to the value found for the parent silane $HSiR_3$, since the Si–H bond oxidative addition is accompanied by a significant rehybridization of the silicon atom, and relatively large Si s character in the residual Si–H bonding can lead to misleadingly large coupling even for weak Si–H interactions.

A significant advance in studying Si···H···M agostic interactions has been achieved with the discovery of α-agostic silyls and silylene complexes. Another recently discovered class of compounds are the complexes with multicenter H···Si interactions, in which the silicon atom interacts simultaneously with two, three, or four hydrogen atoms. Such a situation is found for several complexes of metals from the middle of the Periodic Table in rather high formal oxidation states. The nature of such multicenter H···Si interactions has not been conclusively established and more experimental and computational work is required. Some of their features are akin to complexes with IHI, others resemble σ-complexes. At least some of them can be considered as containing hypervalent silyl ligands $(H_{n+1}SiX_3)^{n-}$ $(n \geqslant 1)$. It can be predicted that similar multicenter interactions of one hydride with several silicon centers will be discovered in the near future. A prospective system, which is long known but deserves reinvestigation, are the complexes of type $[Fe(H)(SiR_3)_2(L)(Cp)]$, where L is a π-accepting ligand. Another potential system, analogous to the previously discussed polyhydrides $[M(H)_3(SiR_3)L_3]$ (M = Fe, Ru, Os), are the so-far unknown complexes $[M(H)(SiR_3)_3L_3]$ (M = Group 8 metal).

Acknowledgments

I am indebted to my co-workers K. Dorogov, A. Osipov, A. Khalimon, and A. Merkoulov for their enthusiasm and dedication to studying nonclassical Si–H interactions. My contribution to this area would not be possible without a long-lasting collaboration with Prof. L. Kuzmina, Dr. P. Mountford, Dr. S. Vyboishchikov, Prof. J. Howard, Dr. S. Ignatov, Prof. A. Lledós, Prof. R. Bau, and Dr. S. Duckett, to whom I am very grateful. I thank Prof. D. A. Lemenovskii for helpful advice and the unstinting support of my work. Our work was supported by grants from Russian Fund for Basic Research, Royal Society (London), Royal Society of Chemistry, and INTAS. I thank Prof. T. Cuenca for providing me with Fig. 2, and also thank Prof. Dr. U. Rosenthal and Dr. A. Spannenberg for sending me Fig. 3. I am grateful to Prof. R. Graham for providing me with the information from the Ph.D. Thesis of K. A. Simpson. I extend my thanks to the Royal Society of Chemistry for the permission to reproduce Figs. 2,4–6,9–10 and to Wiley-VCH for the permission to reproduce Fig. 3. Finally, I would like to express my gratitude to Profs. G. Kubas, R. Crabtree, J. Corey, J. Braddock-Wilking, who read the manuscript and made many valuable comments.

References

(1) Kubas, G. J.; Ryan, R. R.; Swanson, B. I.; Vergamini, P. J.; Wasserman, H. J. *J. Am. Chem. Soc.* **1984**, *100*, 451.
(2) Kubas, G. J. *Metal Dihydrogen and σ-Bond Complexes*, Kluwer Academic Publishers, Plenum Press, New York, 2001.
(3) Crabtree, R. H.; Hamilton, D. G. *Adv. Organomet. Chem.* **1988**, *28*, 299.

(4) Crabtree, R. H. *Angew. Chem. Int. Ed. Engl.* **1993**, *32*, 789.
(5) Kuzmina, L. G. *Koord. Khimia* **1999**, *25*, 643.
(6) Brookhardt, M.; Green, M. L. H. *J. Organomet. Chem.* **1983**, *250*, 395.
(7) Brookhardt, M.; Green, M. L. H.; Wong, L. L. *Prog. Inorg. Chem.* **1988**, *36*, 1.
(8) Schneider, J. *Angew. Chem. Int. Ed. Engl.* **1996**, *35*, 1068.
(9) Hall, C.; Perutz, R. N. *Chem. Rev.* **1996**, *96*, 3125.
(10) Hoyano, J. K.; Elder, M.; Graham, W. A. G. *J. Am. Chem. Soc.* **1969**, *91*, 4568.
(11) Graham, W. A. G. *J. Organomet. Chem.* **1986**, *300*, 81.
(12) Schubert, U. *Adv. Organomet. Chem.* **1990**, *30*, 151.
(13) Corey, J. Y.; Braddock-Wilking, J. *Chem. Rev.* **1999**, *99*, 175.
(14) Lin, Z. *Chem. Soc. Rev.* **2002**, *31*, 239.
(15) Kubas, G. J. *J. Organomet. Chem.* **2001**, *635*, 37.
(16) Nikonov, G. I. *J. Organomet. Chem.* **2001**, *635*, 24.
(17) Nikonov, G. I. *Angew. Chem. Int. Ed. Engl.* **2001**, *40*, 3353.
(18) Hübler, K.; Hübler, U.; Roper, W. R.; Schwerdtfeger, P.; Write, L. J. *Chem.- Eur. J.* **1997**, *3*, 1608.
(19) Yardy, N. M.; Lemke, F. R.; Brammer, L. *Organometallics* **2001**, *20*, 5670.
(20) Schubert, U.; Gilbert, S.; Mock, S. *Chem. Ber.* **1992**, *125*, 835.
(21) Andrews, M. A.; Kirtley, S. W.; Kaez, H. D. (R. Bau, Ed.) *Transition Metal Hydrides*, American Chemical Society, Washington, 1978. p. 215.
(22) Choi, S.-H.; Lin, Z. *J. Organomet. Chem.* **2000**, *608*, 42.
(23) Bennett, M. J.; Simpson, K. A. *J. Am. Chem. Soc.* **1971**, *93*, 7156.
(24) Hutcheon, W. L. Ph.D. Thesis, University of Alberta, **1971**.
(25) Auburn, M.; Ciriano, M.; Howard, J. A. K.; Murray, M.; Pugh, N. J.; Spencer, J. L.; Stone, F. G. A.; Woodward, P. *J. Chem. Soc., Dalton Trans.* **1980**, 659.
(26) Colomer, E.; Corriu, R. J. P.; Marzin, C.; Vioux, A. *Inorg. Chem.* **1982**, *21*, 368.
(27) Schubert, U.; Ackermann, K.; Wörle, B. *J. Am. Chem. Soc.* **1982**, *104*, 7378.
(28) Albright, T. A.; Burdett, J. K.; Whangbo, M.-H. *Orbital Interactions in Chemistry*, Wiley, New York, 1985, p. 36.
(29) Burkey, T. J. *J. Am. Chem. Soc.* **1990**, *112*, 8329.
(30) Heinekey, D. M.; Lledós, A.; Lluch, J. M. *Chem. Soc. Rev.* **2004**, *33*, 175.
(31) Michalczyk, M. J.; Kink, M. J.; Haller, K. J.; West, R.; Michl, J. *Organometallics* **1986**, *5*, 531.
(32) Kapp, J.; Remko, M.; Schleyer, P. *Inorg. Chem.* **1997**, *36*, 4241.
(33) Pauling, L. P. *The Nature of Chemical Bond and the Structure of Molecules and Crystals*, Cornell University Press, Ithaca, 1945.
(34) Wiberg, N.; Schuster, H.; Simon, A.; Peters, K. *Angew. Chem. Int. Ed. Engl.* **1986**, *25*, 79.
(35) Watanabe, H.; Kato, M.; Okawa, T.; Nagai, Y.; Goto, M. *J. Organomet. Chem.* **1984**, *271*, 225.
(36) Weidenbruch, M. *Comm. Inorg. Chem.* **1986**, *5*, 247.
(37) Mavridis, A.; Harrison, J. F. *J. Phys. Chem.* **1982**, *86*, 1979.
(38) Choi, S.-H.; Feng, J.; Lin, Z. *Organometallics* **2000**, *19*, 2051.
(39) Maseras, F.; Lledós, A.; Clot, E.; Eisenstein, O. *Chem. Rev.* **2000**, *100*, 601.
(40) Koetzle, T. F. *Trans. Am. Crystallogr. Assoc.* **1997**, *31*, 57.
(41) Bau, R.; Drabnis, M. H. *Inorg. Chim. Acta* **1997**, *259*, 27.
(42) Demianov, P. I., personal communication.
(43) Schubert, U.; Ackermann, K.; Kraft, G.; Wörle, B. *Z. Naturforsch.* **1983**, *38b*, 1488.
(44) Lichtenberger, D. L.; Rai-Chaudhuri, A. *Organometallics* **1990**, *9*, 1686.
(45) Lichtenberger, D. L.; Rai-Chaudhuri, A. *J. Am. Chem. Soc.* **1990**, *112*, 2492.
(46) Lichtenberger, D. L.; Rai-Chaudhuri, A. *J. Am. Chem. Soc.* **1989**, *111*, 3583.
(47) Complexes $[Mn(HSiR_3)(CO)(L)Cp]$ with an additional donor ligand are also in the oxidation state III: Lichtenberger, D. L.; Rai-Chaudhuri, A. *Inorg. Chem.* **1990**, *29*, 975.
(48) Rabaa, H.; Saillard, J.-Y.; Schubert, U. *J. Organomet. Chem.* **1987**, *330*, 397.
(49) Schubert, U.; Scholz, G.; Müller, J.; Ackermann, K.; Wörle, B. *J. Organomet. Chem.* **1986**, *306*, 303.
(50) Jetz, W.; Graham, W. A. G. *Inorg. Chem.* **1971**, *10*, 1159.
(51) Bent, H. A. *Chem. Rev.* **1961**, *61*, 275.
(52) Nikonov, G. I. *Organometallics* **2003**, *22*, 1597.

(53) Lichtenberger, D. L. *Organometallics* **2003**, *22*, 1599.
(54) Bader, R. F. W.; Matta, C. F.; Cortés-Guzmán, F. *Organometallics* **2004**, *23*, 66253.
(55) Ignatov, S. K.; Rees, N. H.; Tyrrell, B. R.; Dubberley, S. R.; Razuvaev, A. G.; Mountford, P.; Nikonov, G. I. *Chem. Eur. J.* **2004**, *10*, 4991.
(56) Harris, R. K.; Mann, B. E. (Eds.), *NMR and the Periodic Table*, Academic Press, London, 1978.
(57) Gordon, C.; Schubert, U. *J. Organomet. Chem.* **1994**, *224*, 177.
(58) Alkorta, I.; Elguero, J.; Mó, O.; Yáñez, M.; Del Bene, J. E. *J. Phys. Chem. A* **2002**, *106*, 9325.
(59) Wrackmeyer, B.; Tok, O. L.; Bubnov, Y. N. *Angew. Chem. Int. Ed. Engl.* **1999**, *38*, 124.
(60) Muller, T. *Angew. Chem.* **2001**, *113*, 3124.
(61) Aitken, C.; Harrod, J. F.; Samuel, E. *J. Am. Chem. Soc.* **1986**, *108*, 4059.
(62) Aitken, C.; Harrod, J. F.; Samuel, E. *Can. J. Chem.* **1986**, *64*, 1677.
(63) Mu, Y.; Aitken, C.; Cote, B.; Harrod, J. F.; Samuel, E. *Can. J. Chem.* **1991**, *69*, 264.
(64) Dioumaev, V. K.; Harrod, J. F. *Organometallics* **1996**, *15*, 3859.
(65) Dioumaev, V. K.; Harrod, J. F. *Organometallics* **1997**, *16*, 2798.
(66) Spaltenstein, E.; Palma, P.; Kreutzer, K. A.; Willoughby, C. A.; Davis, W. M.; Buchwald, S. L. *J. Am. Chem. Soc.* **1994**, *116*, 10308.
(67) Shu, R.; Hao, L.; Harrod, J. F.; Woo, H.-G.; Samuel, E. *J. Am. Chem. Soc.* **1998**, *120*, 12988.
(68) Muhoro, N.; He, X. M.; Hartwig, J. F. *J. Am. Chem. Soc.* **1999**, *121*, 5033.
(69) Liu, D.; Lam, K. C.; Lin, Z. *Organometallics* **2003**, *22*, 2827.
(70) Kreutzer, K. A.; Fisher, R. A.; Davis, W. M.; Spaltenstein, E.; Buchwald, S. L. *Organometallics* **1991**, *10*, 4031.
(71) Takahashi, T.; Hasegawa, M.; Suzuki, N.; Saburi, M.; Rousset, C. J.; Fanwick, P. E.; Negishi, E. *J. Am. Chem. Soc.* **1991**, *113*, 8564.
(72) Ciruelo, G.; Cuenca, T.; Gómez, R.; Gomez-Sal, R.; Martín, A. *J. Chem. Soc., Dalton Trans.* **2001**, 1657.
(73) George, M. W.; Howard, M. T.; Hamley, P. A.; Hughes, C.; Johnson, F. P. A.; Popov, V. K.; Poliakoff, M. *J. Am. Chem. Soc.* **1993**, *115*, 2286.
(74) Tanaka, I.; Ohhara, T.; Niimura, N.; Ohashi, Y.; Jiang, Q.; Berry, D. H.; Bau, R. *J. Chem. Res.* **1999**, 14.
(75) Sabo-Etienne, S.; Rodrigez, V.; Donnadieu, B.; Chaudret, B.; al Makarim, H. A.; Barthelat, J.-C.; Ulrich, S.; Limbach, H.-H. *New J. Chem.* **2001**, 55.
(76) Burckhardt, U.; Casty, G. L.; Gavenonis, J.; Tilley, T. D. *Organometallics* **2002**, *21*, 3108.
(77) Dubberley, S. R.; Ignatov, S. K.; Rees, N. H.; Razuvaev, A. G.; Mountford, P.; Nikonov, G. I. *J. Am. Chem. Soc.* **2003**, *125*, 642.
(78) Curtis, M. D.; Bell, L. G.; Buter, N. M. *Organometallics* **1985**, *4*, 701.
(79) Schubert, U.; Müller, J.; Alt, H. G. *Organometallics* **1987**, *6*, 469.
(80) Matarasso-Tchiroukhine, E.; Jaoune, G. *Can. J. Chem.* **1988**, *66*, 2157.
(81) Luo, X. L.; Kubas, G. J.; Burns, C. J.; Bryan, J. C.; Unkefer, C. J. *J. Am. Chem. Soc.* **1994**, *116*, 10312.
(82) Luo, X. L.; Kubas, G. J.; Burns, C. J.; Bryan, J. C.; Unkefer, C. J. *J. Am. Chem. Soc.* **1995**, *117*, 1159.
(83) Zhang, S.; Dobson, G. R.; Brown, T. L. *J. Am. Chem. Soc.* **1991**, *113*, 6908.
(84) Fan, M.-F.; Jia, G.; Lin, Z. *J. Am. Chem. Soc.* **1996**, *118*, 9915.
(85) Smith, R. A.; Bennett, M. J. *Acta Cryst*. **1977**, *B33*, 1113.
(86) Albright, T. *Tetrahedron* **1982**, *38*, 1339.
(87) Huhmann-Vincent, J.; Scott, B. L.; Kubas, G. J. *Inorg. Chim. Acta.* **1999**, *294*, 240.
(88) Fang, X.; Scott, B. L.; John, K. D.; Kubas, G. J. *Organometallics* **2000**, *19*, 4141.
(89) Fang, X.; Huhmann-Vincent, J.; Scott, B. L.; Kubas, G. J. *J. Organomet. Chem.* **2000**, *609*, 95.
(90) Reid, S. M.; Neuner, B.; Schrock, R.; Davis, W. M. *Organometallics* **1998**, *17*, 4077.
(91) Scharrer, E.; Chang, S.; Brookhart, M. *Organometallics* **1995**, *14*, 5686.
(92) Freeman, S. T. N.; Lemke, F. R.; Brammer, L. *Organometallics* **2002**, *21*, 2030.
(93) Lemke, F. R.; Galat, K. J.; Youngs, W. J. *Organometallics* **1999**, *18*, 1419.
(94) Osipov, A. L.; Gerdov, S. M.; Kuzmina, L. G.; Howard, J. A. K.; Nikonov, G. I. *Organometallics* **2005**, *24*, 587.
(95) Bart, S. C.; Lobkovsky, E.; Chirik, P. J. *J. Am. Chem. Soc.* **2004**, *126*, 13794.

(96) Ohki, Y.; Kojima, T.; Oshima, M.; Suzuki, H. *Organometallics* **2001**, *20*, 2654.
(97) Takao, T.; Yoshida, S.; Suzuki, H.; Tanaka, M. *Organometallics* **1995**, *14*, 3855.
(98) Ohki, Y.; Suzuki, H. *Angew. Chem. Int. Ed. Engl.* **2000**, *39*, 3120.
(99) Smith, R. A.; Bennett, M. J. *Acta. Crystallogr*. **1977**, *B33*, 1118.
(100) Manojlovich-Muir, L.; Muir, K. W.; Ibers, J. A.; Bennett, M. J. *Inorg. Chem.* **1970**, *9*, 447.
(101) Simpson, K. A. Ph.D. Thesis, University of Alberta, **1973**.
(102) Yao, Z.; Klabunde, K. J.; Asirvatham, A. S. *Inorg. Chem.* **1995**, *34*, 5289.
(103) Asirvatham, A. S.; Yao, Z.; Klabunde, K. J. *J. Am. Chem. Soc.* **1994**, *116*, 5493.
(104) Campion, B. K.; Heyn, R. H.; Tilley, T. D. *Chem. Commun.* **1988**, 278.
(105) Campion, B. K.; Heyn, R. H.; Tilley, T. D. *Chem. Commun.* **1992**, 1201.
(106) Osipov, A. L.; Vyboishchikov, S. F.; Dorogov, K. Y.; Kuzmina, L. G.; Howard, J. A. K.; Lemenovskii, D. A.; Nikonov, G. I. *Chem. Commun.* **2005**, 3349.
(107) Johnson, T. J.; Coan, P. S.; Caulton, K. *Inorg. Chem.* **1993**, *32*, 4594.
(108) Dysard, J.; Tilley, T. D. *Organometallics* **2000**, *19*, 4726.
(109) Esterueleas, M. A.; Oro, L. A.; Valero, C. *Organometallics* **1991**, *10*, 462.
(110) Maseras, F.; Lledos, A. *Organometallics* **1996**, *15*, 1218.
(111) Luo, X.-L.; Crabtree, R. H. *J. Am. Chem. Soc.* **1989**, *111*, 2527.
(112) Fernandez, M. J.; Bailey, P. M.; Bentz, P. O.; Ricci, J. S.; Koetzle, T. F.; Maitlis, P. M. *J. Am. Chem. Soc.* **1984**, *106*, 5458.
(113) Ricci, J. S.; Koetzle, T. F.; Fernandez, M. J.; Maitlis, P. M.; Green, J. C. *J. Organomet. Chem.* **1986**, *299*, 383.
(114) Duckett, S. B.; Perutz, R. N. *Chem. Commun.* **1991**, 28.
(115) Cook, K. S.; Incarvito, A.; Webster, C. E.; Fan, Y.; Hall, M. B.; Hartwig, J. F. *Angew. Chem. Int. Ed. Engl.* **2004**, *43*, 5474.
(116) Ampt, K. A. M.; Duckett, S. B.; Perutz, R. N. *Chem. Soc., Dalton* **2004**, 3331.
(117) Taw, F. L.; Bergman, R. G.; Brookhart, M. *Organometallics* **2004**, *23*, 886.
(118) Golden, J. T.; Andersen, R. A.; Bergman, R. G. *J. Am. Chem. Soc.* **2001**, *123*, 5837.
(119) Fang, X.; Scott, B. L.; Watkin, J. G.; Kubas, G. J. *Organometallics* **2000**, *19*, 4193.
(120) Kim, Y.-J.; Lee, S.-C.; Park, J.-I.; Osakada, K.; Choi, J.-C.; Yamamoto, T. *Organometallics* **1998**, *17*, 4929.
(121) Osakada, K.; Tanabe, M. *Chem. Lett* **2001**, *30*, 962.
(122) Braddock-Wilking, J.; Levchinsky, Y.; Rath, N. P. *Organometallics* **2001**, *20*, 474.
(123) Tanabe, M.; Yamada, T.; Osakada, K. *Organometallics* **2003**, *22*, 2190.
(124) Corral, I.; Mó, O.; Yáñez, M. *New J. Chem.* **2003**, *27*, 1657.
(125) Corral, I.; Mó, O.; Yáñez, M. *Int. J. Mass. Spect.* **2003**, *227*, 401.
(126) Schubert, U.; Bahr, K.; Muller, J. *J. Organomet. Chem.* **1987**, *327*, 357.
(127) Schubert, U.; Gilges, H. *Organometallics* **1996**, *15*, 2373.
(128) Butts, M. D.; Bryan, J. C.; Luo, X.-L.; Kubas, G. J. *Inorg. Chem.* **1997**, *36*, 3341.
(129) Klei, S. R.; Tilley, T. D.; Bergman, R. G. *J. Am. Chem. Soc.* **2000**, *122*, 1816.
(130) Tanabe, M.; Osakada, K. *Chem.-Eur. J.* **2004**, *10*, 416.
(131) Schubert, U.; Schwartz, M.; Möller, F. *Organometallics* **1994**, *13*, 1554.
(132) Peulecke, N.; Ohff, A.; Kosse, P.; Tillack, A.; Spannenberg, A.; Kempe, R.; Baumann, W.; Burlakov, V. V.; Rosenthal, U. *Chem.-Eur. J.* **1998**, *4*, 1852.
(133) Ohff, A.; Kosse, P.; Baumann, W.; Tillack, A.; Kempe, R.; Görls, H.; Burlakov, V. V.; Rosenthal, U. *J. Am. Chem. Soc.* **1995**, *117*, 10399.
(134) Fan, M.-F.; Lin, Z. *Organometallics* **1997**, *16*, 494.
(135) Delpech, F.; Sabo-Etienne, S.; Donnadieu, B.; Chaudret, B. *Organometallics* **1998**, *17*, 4926.
(136) Corral, I.; Mó, O.; Yáñez, M. *Theor. Chem. Acc.* **2004**, *112*, 298.
(137) Corral, I.; Mó, O.; Yáñez, M. *J. Phys. Chem. A* **2003**, *107*, 1370.
(138) Yin, J.; Klozin, J.; Abboud, K.; Jones, W. M. *J. Am. Chem. Soc.* **1995**, *117*, 3298.
(139) Randolph, C. L.; Wrighton, M. S. *Organometallics* **1987**, *6*, 365.
(140) Campion, B. K.; Heyn, R. H.; Tilley, T. D.; Rheingold, A. L. *J. Am. Chem. Soc.* **1993**, *115*, 5527.
(141) Freeman, W.; Tilley, T. D.; Rheingold, A. L. *J. Am. Chem. Soc.* **1994**, *116*, 8428.
(142) Dioumaev, V. K.; Carroll, P. J.; Berry, D. H. *Angew. Chem. Int. Ed. Engl.* **2003**, *42*, 3947.
(143) Driess, M.; Pritzkow, H.; Reisgys, M. *Angew. Chem. Int. Ed. Engl.* **1992**, *31*, 1510.

(144) Driess, M.; Pritzkow, H.; Reisgys, M. *Chem. Ber.* **1996**, *129*, 247.
(145) Herrmann, W. A.; Huber, N. W.; Behm, J. *Chem. Ber.* **1992**, *125*, 1405.
(146) Procopio, L. J.; Carroll, P. J.; Berry, D. H. *J. Am. Chem. Soc.* **1994**, *116*, 177.
(147) Herrmann, W. A.; Eppinger, J.; Spiegler, M.; Runte, O.; Anwander, R. *Organometallics* **1997**, *16*, 1813.
(148) Nagl, I.; Scherer, W.; Tafipolsky, M.; Anwander, R. *Eur. J. Inorg. Chem.* **1999**, 1405.
(149) Eppinger, J.; Spiegler, M.; Hieringer, W.; Herrmann, W. A.; Anwander, R. *J. Am. Chem. Soc.* **2000**, *122*, 3080.
(150) Klimpel, M. G.; Görlitzer, H. W.; Tafipolsky, M.; Spiegler, M.; Scherer, W.; Anwander, R. *J. Organomet. Chem.* **2002**, *647*, 236.
(151) Rees, W. S.; Just, O.; Schumann, H.; Weimann, R. *Angew. Chem. Int. Ed. Engl.* **1996**, *35*, 419.
(152) Nikonov, G. I.; Mountford, P.; Ignatov, S. K.; Green, J. C.; Cooke, P. A.; Leech, M. A.; Kuzmina, L. G.; Razuvaev, A. G.; Rees, N. H.; Blake, A. J.; Howard, J. A. K.; Lemenovskii, D. A. *Dalton Trans.* **2001**, 2903.
(153) Ignatov, S. K.; Rees, N. H.; Dubberley, S. R.; Razuvaev, A. G.; Mountford, P.; Nikonov, G. I. *Chem. Commun.* **2004**, 952.
(154) Ignatov, S. K.; Rees, N. H.; Dubberley, S. R.; Razuvaev, A. G.; Mountford, P.; Nikonov, G. I., in preparation.
(155) Sadow, A. D.; Tilley, T. D. *J. Am. Chem. Soc.* **2003**, *125*, 9462.
(156) Mork, B. V.; Tilley, T. D.; Schultz, A. J.; Cowan, J. A. *J. Am. Chem. Soc.* **2004**, *126*, 10428.
(157) Mork, B. V.; Tilley, T. D. *Angew. Chem. Int. Ed. Engl.* **2003**, *42*, 357.
(158) Mork, B. V.; Tilley, T. D. *J. Am. Chem. Soc.* **2001**, *123*, 9702.
(159) Pandey, K. K.; Lein, M.; Frenking, G. *Organometallics* **2004**, *23*, 2944.
(160) Watanabe, T.; Hashimoto, H.; Tobita, H. *Angew. Chem. Int. Ed. Engl.* **2004**, *43*, 218.
(161) Sakaba, H.; Tsukamoto, M.; Hirata, T.; Kabuto, C.; Horino, H. *J. Am. Chem. Soc.* **2000**, *122*, 11511.
(162) Glaser, P. B.; Tilley, T. D. *J. Am. Chem. Soc.* **2003**, *125*, 13640.
(163) Beddie, C.; Hall, M. B. *J. Am. Chem. Soc.* **2004**, *126*, 13564.
(164) Simons, R. S.; Gallucci, J. C.; Tessier, C. A.; Youngs, W. J. *J. Organomet. Chem.* **2002**, *654*, 224.
(165) Felman, J. D.; Peters, J. C.; Tilley, T. D. *Organometallics* **2002**, *21*, 4065.
(166) Goddard, R. J.; Hoffmann, R.; Jemmis, E. D. *J. Am. Chem. Soc.* **1980**, *102*, 7667.
(167) Besora, M.; Maseras, F.; Lledos, A.; Eisenstein, O. *Inorg. Chem.* **2002**, *26*, 7105.
(168) Bihlmeier, A.; Greene, T. M.; Himmel, H.-J. *Organometallics* **2004**, *23*, 2350.
(169) Himmel, H.-J. *Chem.-Eur. J.* **1997**, *3*, 1608.
(170) Kickel, B. L.; Armentrout, P. B. *J. Am. Chem. Soc.* **1995**, *117*, 764.
(171) Koloski, T. S.; Pestana, D. C.; Carroll, P. J.; Berry, D. H. *Organometallics* **1994**, *13*, 489.
(172) Nikonov, G. I.; Kuzmina, L. G.; Lemenovskii, D. A.; Kotov, V. V. *J. Am. Chem. Soc.* **1995**, *117*, 10133.
(173) Nikonov, G. I.; Kuzmina, L. G.; Vyboishchikov, S. F.; Lemenovskii, D. A.; Howard, J. A. K. *Chem.-Eur. J.* **1999**, *5*, 2497.
(174) Nikonov, G. I.; Kuzmina, L. G.; Howard, J. A. K. *J. Chem. Soc., Dalton Trans.* **2002**, 3037.
(175) Jiang, Q.; Carroll, P. J.; Berry, D. H. *Organometallics* **1991**, *10*, 3648.
(176) Bakhmutov, V. I.; Howard, J. A. K.; Keen, D. A.; Kuzmina, L. G.; Leech, M. A.; Nikonov, G. I.; Vorontsov, E. V.; Wilson, C. C. *J. Chem. Soc., Dalton Trans.* **2000**, 1631.
(177) Bakhmutova, E. V.; Bakhmutov, V. I.; Belkova, N. V.; Besora, M.; Epstein, L. M.; Lledós, A.; Nikonov, G. I.; Shubina, E. S.; Tomàs, J.; Vorontsov, E. V. *Chem.-Eur. J.* **2004**, *10*, 661.
(178) Fan, M.-F.; Lin, Z. *Organometallics* **1998**, *18*, 1092.
(179) Dorogov, K. Yu.; Churakov, A. V.; Kuzmina, L. G.; Howard, J. A. K.; Nikonov, G. I. *Eur. J. Inorg. Chem.* **2004**, 771.
(180) Dorogov, K. Y.; Dumont, E.; Ho, N. N.; Kuzmina, L. G.; Poblet, J. M.; Schultz, A. J.; Howard, J. A. K.; Bau, R.; Lledos, A.; Nikonov, G. I. *Organometallics* **2004**, *23*, 2845.
(181) Dorogov K. Y.; Kuzmina, L. G.; Nikonov, G. I., unpublished.
(182) Nikonov, G. I.; Churakov, A. V.; Antipin, M. Y. *Organometallics* **2003**, *22*, 2178.
(183) Nikonov, G. I.; Kuzmina, L. G.; Lorberth, J.; Howard, J. A. K. *Eur. J. Inorg. Chem.* **1999**, 825.
(184) Figge, L. K.; Carroll, P. J.; Berry, D. H. *Organometallics* **1996**, *15*, 209.

(185) Nikonov, G. I.; Kuzmina, L. G.; Howard, J. A. K., unpublished results.
(186) Wilkinson, G.; Stone, F. G. A.; Abel, E. W. (Eds.), *Comprehensive Organometallic Chemistry*, Vol. 2, Pergamon Press, Oxford, 1982.
(187) Emsley, J. *The Elements*, Clarendon Press, Oxford, 1991.
(188) For example: Williams, D. S.; Schofield, M. H.; Schrock, R. R. *Organometallics* **1993**, *12*, 4560.
(189) Nikonov, G. I.; Mountford, P.; Dubberley, S. R. *Inorg. Chem.* **2003**, *42*, 258.
(190) Ignatov, S. K.; Rees, N. H.; Merkoulov, A.A.; Dubberley, S. R.; Razuvaev, A. G.; Mountford, P.; Nikonov, G. I., in preparation.
(191) Campion, B. K.; Heyn, R. H.; Tilley, T. D. *Chem. Commun.* **1992**, 1201.
(192) Duckett, S. B.; Kuzmina, L. G.; Nikonov, G. I. *Inorg. Chem. Comm.* **2000**, *3/3*, 126.
(193) Gountchev, T. I.; Tilley, T. D. *J. Am. Chem. Soc.* **1997**, *119*, 12831.
(194) Sakaba, H.; Hirata, T.; Kabuto, C.; Horino, H. *Chem. Lett.* **2001**, *30*, 1078.
(195) Luo, X.-L.; Baudry, D.; Boydel, P.; Charpin, P.; Nierlich, M.; Ephritikhine, M.; Crabtree, R. H. *Inorg. Chem.* **1990**, *29*, 1511.
(196) Luo, X.-L.; Schulte, G. K.; Demou, P.; Crabtree, R. H. *Inorg. Chem.* **1990**, *29*, 4268.
(197) Lin, Z.; Hall, M. *Inorg. Chem.* **1991**, *30*, 2569.
(198) Knorr, M.; Gilbert, S.; Schubert, U. *J. Organomet. Chem.* **1988**, *347*, C17–C20.
(199) Hillier, A. C.; Jacobsen, H.; Gusev, D.; Schmalle, H. W.; Berke, H. *Inorg. Chem.* **2001**, *40*, 6334.
(200) Lachaize, S.; Sabo-Etienne, S.; Donnadieu, B.; Chaudret, B. *Chem. Commun.* **2003**, 214.
(201) Atheaux, I.; Delpech, F.; Donnadieu, B.; Sabo-Etienne, S.; Chaudret, B.; Hussein, K.; Barthelat, J. C.; Braun, T.; Duckett, S. B.; Perutz, R. N. *Organometallics* **2002**, *21*, 5347.
(202) Hussein, K.; Marsden, C. J.; Barthelat, J. C.; Rodriguesz, V.; Coneiro, S.; Sabo-Etienne, S.; Donnadieu, B.; Chaudret, B. *Chem. Commun.* **1999**, 1315.
(203) Rickard, C. E. F.; Roper, W. R.; Woodgate, S. D.; Write, L. J. *J. Organomet. Chem.* **2000**, *609*, 177.
(204) Biul, M.; Espinet, P.; Esteruelas, M. A.; Lahoz, F. J.; Lledós, A.; Martínez-Ilarduya, J. M.; Maseras, F.; Modrego, J.; Oñate, E.; Oro, L. A.; Sola, E.; Valero, C. *Inorg. Chem.* **1996**, *35*, 1250.
(205) Mohlen, M.; Rickard, C. E. F.; Roper, W. R.; Salter, D. M.; Write, L. J. *J. Organomet. Chem.* **2000**, *593*, 458.
(206) Berry, D. H., personal communication.
(207) Said, R. H.; Hussein, K.; Barthelat, J.-C.; Atheaux, I. S.; Sabo-Etienne, S.; Grellier, M.; Donnadieu, B.; Chaudret, B. *Dalton Trans.* **2003**, 4139.
(208) Bearpark, M. J.; McGrady, G. S.; Prince, P. D.; Steed, J. W. *J. Am. Chem. Soc.* **2001**, *123*, 7736.
(209) Corriu, R. J. P.; Guerin, C.; Henner, B.; Wang, Q. *Organometallics* **1991**, *10*, 3574.
(210) Ng, S. M.; Lau, C. P.; Fan, M.-F.; Lin, Z. *Organometallics* **1999**, *18*, 2484.
(211) Chen, Y.-Z.; Chan, W. C.; Lau, C. P.; Chu, H. S.; Lee, H. L.; Jia, G. *Organometallics* **1997**, *16*, 1241.
(212) Delpech, F.; Sabo-Etienne, S.; Daran, J.-C.; Chaudret, B.; Hussein, K.; Marsden, C. J.; Barthelat, J.-C. *J. Am. Chem. Soc.* **1999**, *121*, 6668.
(213) Fan, M. F.; Lin, Z. *Organometallics* **1999**, *18*, 286.
(214) Atheaux, I.; Donnadieu, B.; Rodriguez, V.; Sabo-Etienne, S.; Chaudret, B.; Hussein, K.; Barthelat, J.-C. *J. Am. Chem. Soc.* **2000**, *122*, 5664.
(215) Alcock, N. W. *Adv. Inorg. Radiochem.* **1972**, *15*, 1.
(216) Maseras, F.; Lledós, A.; Clot, E.; Eisenstein, O. *Chem. Rev.* **2000**, *100*, 601.
(217) Bersuker, I. B. *The Electronic Structure and Properties of Transition Metal Compounds. Introduction to the Theory*, Wiley, New York, 1996, Chapter I.

Index

A

A WCA, 162
Acidity, 61
Actinide, 125
Agostic interactions, 22, 24–28, 32–33, 35, 184, 248, 251, 259, 261, 304
Alkali metal derivatives, 106
Alkali metal silsesquioxanes, 107
Allyl fragmentation reaction, 159
Allyl(chloromethyl)silanes, 49
Allylic inversion, 43–44, 48
Allylsilanes, 41–42, 50, 52–53
Allylsilylation, 41–49, 52, 59
Aluminasilsesquioxane, 111
Aluminosilsesquioxane, 134
Aluminum chloride, 42–43, 45–47, 49–56, 58
Amide route, 137
Aminoboron, 67
Anionic ferrasilsesquioxane complexes, 144
Antipodal, 26
Arenium, 177–178, 183
Arenium ions, 159, 187, 207
"ate"-complex, 125
Au55 clusters, 148

B

B3LYP, 67, 71
Beryllium and magnesium, 108
Bidentate, 98
Bimetal compounds, 25
Bimetallic complexes, 22, 27, 32
1,2-bis(alumino)tetrafluorobenzene, 75
1,2-bis(chloro(methyl)aluminum)phenylene, 74
1,2-bis(dichloroaluminum)phenylene, 74
1,2-bis(dichloroboryl)tetrafluorobenzene, 64
1,2-bis(dimethylaluminum)phenylene, 74
Bis(silsesquioxane) "sandwich" complex, 139
Bis(silsesquioxane) titanium complex, 127
Bishomoaromatic, 179
Bishomoaromaticity, 189
Bishomocyclopropenylium, 197
3c–2e bond, 89
Boracycle, 68
Borafluorene, 70
9-borafluorenyl, 71
Boranes, 62
Borata-benzo[de]anthracene, 68
Boratalkene, 68
Borepin, 70
Boron, 63–65, 67, 70–71, 81, 85, 89, 91
Boron substitution, 9–19, 29–37
Boron/tin, 72
Brønsted acidic aluminasilsesquioxanes, 113
Brellochs reaction, 28
Bridging iodide, 16
Bridging iodine, 20
Butterfly complexes, 36

C

Cage expansion reactions, 38
Cage-promoted hydroboration, 38
Carboranate, 208
Carboranate anion, 191
Carboranes, 1, 161, 178–179, 199, 201, 208
Catalysis, 94
Catalysts, 85, 149
Cation–anion interactions, 182, 186, 199, 203
Charge-Compensated Complexes, 9, 12, 23
Chelates, 86, 93
Chemical shift tensor, 173
Chlorogallium, 81
Chloroindium, 82
(chloromercurio), 62
Chloronium, 183
Chromium(VI) derivative, 140
Chromophore, 90
Chromophoric properties, 97
Closo-silsesquioxane monosilanol ligand, 133

Cluster contraction, 31
CO scavenging, 34
Cobalt complexes, 7, 21–23
Completely condensed oligomeric silsesquioxanes, 102
Complexes, 16, 85, 89, 94, 96
Computational chemistry, 156
Computationally, 71
Cooperative, 85
Cooperative effects, 67
Coordinated, 90
-coordination, 187
Copper complexes, 21–23, 27, 31–36
Copper(I) silsesquioxane complex, 148
Cr silsesquioxane complexes, 140
Crystallography, 75
[3 + 2] cycloaddition, 46–47
Cyclopropenium, 194
Cyclotetrasilenyl radical, 163, 196
Cyclotetrasilenylium, 194
Cyclotrigermenium, 193–194
Cyclotrigermylium, 161, 179
Cyclotrisilenium, 194

D

DFT, 67, 71–72
Di- and triorganotin(IV) silsesquioxane, 118
Dialaanthracene, 74
Dialuminum, 94
Diastereomers, 43
Diazine, 86
Diboraanthracene, 96
Diboranes, 65, 67, 91, 94, 96–97
9,10-diboraoctafluoroanthracene, 76
1,8-Diborylnaphthalenes, 66
Diborylnaphthalene, 90
(dibromoboryl), 64
(dichloroboryl), 62
(dichlorogallium)-8, 72
(dichloroindium)-8, 72
Diels Alder-type cyclization reactions, 208
Digallacycle, 81
Diindaanthracene, 78, 85
Diindacycles, 79–80, 83, 88
Diindacyclic, 87
Diindium, 83
1,8-(diindium)naphthalenediyl, 82
Dimeric vanadium(III) complex, 137
Dimesitylboron, 72
(dimesitylboryl)-8, 68
Dimetallacycle, 81
Dimethylboron, 67–68
Dimethylboryl)naphthalene, 89
Dimethylpyranone, 85
Dimethyltin, 65
Dinuclear metallasilsesquioxane, 129
Diphenylboron, 67–68
(diphenylboryl), 66
Diplatinum complex, 20
Distannane, 63
Dynamic exchange processes, 27

E

Electron counting, 29
Electron-donating effects, 42
Electronic effect, 51
Electrophilic Cleavage, 158–159
Epoxidation, 127
Ethylene polymerization, 135, 140
Ethylene polymerization, olefin epoxidation, 136
EXAFS, 162, 200–201
Exo-polyhedral metal fragment, 23
Experimental, 172, 181

F

Ferrasilsesquioxanes, 143, 144
Ferrocene, 50, 52–53, 59
Fluoride sensor, 90
Fluorobenzene, 79
Fluoronium ions, 176
Friedel–Crafts alkylation, 41, 50–51, 53, 55–56
"fulvene route", 131–132
Fulvene titanium complex, 131
Functionalization of cage boron atoms, 12

G

6-31 + G*, 67, 71
6-31G, 72
Gallasilsesquioxane, 116
Gallium, 81, 92
Gallium-containing metallasilsesquioxanes, 115
Gallium/tin, 97
Germanium silsesquioxane complex, 118

Germylium, 165
Gold complexes, 21–23, 31–36

H

Hafnium-containing metallasilsesquioxanes, 135
Hafnium, 136
Half-sandwich titanium complexes, 133
Halogenation, 11
Halonium ions, 176
Hammet equation, 51
Heterobimetallic Li/Sm silsesquioxane complex, 123
Heterobimetallic Li/Yb silsesquioxane complex, 122
Heterobimetallic Pt/Tl silsesquioxane complex, 147
Heterolytic Cleavage, 156
Heterotrimetallic complexes, 34–37
Homoaromatic, 175, 196
Homoconjugation, 155, 194, 196
1,5-hydride shift, 43, 45
Hydride abstraction, 9–12, 16–19, 29
Hydride anion, 89
Hydride ligands, 218, 244, 287–289, 291, 293–295
Hydride transfer method, 158
Hydride Transfer Reaction, 157
Hydrido complex, 20
Hydrido compounds, 7
Hydrido species, 20
Hydrogen bonding, 133
Hydrosilylation, 41, 57–58, 136
Hyperconjugation, 193

I

IGLO, 180
Imine, 30
Imine formation, 8–10, 16–17
Incompletely condensed oligomeric silsesquioxanes, 103
Indium, 78–80
Indium(I), 77, 83
Insertion of an alkyne molecule into a cage B–H bond, 10
Interaction energy, 169
Interactions, 22
Intermolecular interaction, 158
Intramolecular, 187
Intramolecular allyl-migration, 41, 49
Intramolecular interaction, 158, 164, 176
Intramolecularly Stabilized, 196
Ion-pairing, 178–179
Iridium complexes, 25–28, 33–36
Iron complexes, 5, 22–26
Iron(II)-silsesquioxane complexes, 144
Iron(III), 143
Iron(III) silsesquioxane complexes, 144
Isodesmic reaction, 166, 168
Isolobal relationship, 1, 2

L

Lanthanide silsesquioxanes, 121
Lanthanide tris(silylamides), 121
Lanthanides and Actinides, 120
Lewis acid, 62, 64, 98
Lewis Acid-Catalyzed Reactions, 41, 43, 45, 47, 49, 51, 53, 55, 57, 59
Lewis acids, 85
Lewis basic, 62

M

Mössbauer spectroscopy, 181, 190
Manganese complexes, 28–37
Mercuraindacycles, 97
Mercury, 61, 78
Metal boride clusters, 36
Metal dicarbollides, 1
Metal oxide particles, 150
Metal–metal bond, 22–23, 29–34, 36
Metallacarboranes, 1–37
Metallasilsesquioxanes, 106, 108, 141, 142, 149
Metallosilicates, 109
Metathesis, 83
Methylium, 165, 167, 169
Methyltin-chlorogallium, 92
"mixed-sandwich" complex, 139
Model system, 133
Molybdate ester, 140
Molybdenum carbene complex, 141, 144
Molybdenum complexes, 5, 23–25, 35–37
Mono(pentamethylcyclopentadienyl) titanium(IV) silsesquioxane complex, 132
Monocarbon metallacarboranes, 1–37

Monocarboranes, 28
Monosilylated precursor, 144
Monosilylated silsesquioxane precursor, 132
Mukaiyama-type aldol reactions, 208

N

Naphthalenediyl, 72, 92
1,8-naphthalenediboronic, 66
1,8-naphthalenediyl, 81
Naphthalenes, 62, 67–68, 70, 83
Nickel complex, 6, 21–23, 29–31
Niobium-containing metallasilsesquioxane complex, 137
Nitrile complexes, 162
Nitrilium, 177, 183, 204
Nitrosyl molybdenum silsesquioxane complex, 142
NMR, 70, 75, 82–83, 85–86, 172–173, 191
NMR Chemical Shift Calculation, 170, 175, 180
NMR chemical shift tensor, 174
NMR, 73, 170, 179, 181, 185, 186
Non-spectator behaviour, 2
Nonclassical complexes, 217–219, 222, 233, 290, 303
Norbornyl cation, 187–188, 199

O

Octameric silsesquioxane ligand, 113
Of Cobalt, 16
Of Iron, 9–12
Of Molybdenum, 12
Of Nickel, 16
Of Tungsten, 12
Olefin, 94
Olefin polymerizations, 127
One-electron oxidation, 29, 192, 200
Oppenauer oxidation, 136
Organoindium, 82
Organomercurial, 64, 82–83
Ortho-dilithiobenzene, 77
Ortho-phenylene, 65, 97
Ortho-phenylene diboranes, 93
Ortho-phenylene-diindium, 76
Ortho-phenylene-mercury, 77
Ortho-phenylenemagnesium, 77
Ortho-phenylenezinc, 77
Osmasilsesquioxane complex, 145
Osmium, 144
Osmium cluster complex, 145
Osmium Cluster Compounds, 7–10
Oxidation catalysts, 127
Oxidation of methane, 140
Oxidative Cleavage, 160
Oxidative-substitution reaction, 16
Oxidizing agents, 29
(-oxo-bridged dianionic complex, 144
(-oxo-dititanium complex, 129
Oxonium, 177, 182–183
Oxo species, 128

P

Palladium complexes, 29–31
Peralkylation, 54–55
Peri-naphthalenediyl, 97
Phenylene, 62
Phenylenemercury, 64
Phenylzinc, 64
Phthalazine, 86
Piano-stool complexes, 2, 7
Platinasilsesquioxane, 147
Platinum complexes, 6–7, 18–23, 25–26, 29–31
Platinum(II) complexes, 147
Platinum-selenium complexex, 21
Platinum-tellurium complexes, 21
Plumbanorbornyl, 189
Plumbanorbornyl cation, 199
Plumbylidynium, 209
Plumbylium, 167, 169
Polydentate Lewis acids, 61
Polyhedral oligosilsesquioxanes, 101
Polymerization, 94
Protonation, 20, 37
Protonation reactions, 7, 16, 19
Pyrazine, 86–88
Pyrimidine, 86

R

Radicals, 29, 161–162, 193, 196
Ramsay's theory, 180
Rare earth metals, 120
"realistic" molecular models of silica-supported metal catalysts, 149
Resonance, 91
Resonance effect, 51
Rhenium complexes, 5, 25–34

Rhodium complexes, 25–28, 33–36
Ruthenium, 144–145
Ruthenium carbene complex, 144
Ruthenium Cluster Compounds, 7–10

S

Samarium, 125
Scandium, 125
Scandium silsesquioxane complex, 125
Si, 176
Si NMR Data, 172
Silanorbornyl cations, 177, 188, 208
Silatropylium, 158, 175
Silenylium ion, 163
Silsesquioxane derivative of copper, 148
Silsesquioxane lithium salt, 133
Silsesquioxane Precursors, 105
Silsesquioxane–borato complexes, 110
Silsesquioxane-tethered fluorene, 135
Silver complexes, 21–23
Silyl ligands, 270, 274, 281, 302, 304
Silylidynium, 208
Silylium, 165, 169
Solid state NMR, 182
Solid state structure, 178, 190, 196, 199, 203
"spironorbornyl cation", 198
Stability constants, 86
β-stabilization, 41–42, 45
Stannanorbornyl, 184
Stannanorbornyl cation, 183
Stannasilsesquioxanes, 119

T

Tantalacarborane species, 139
Tantalasilsesquioxanes, 140
Tantalum silsesquioxanes, 137
Tetraarylborates, 161
Tetrachlorodiborane, 85
Tetrafluorobenzene, 65
Tetrafluorophenylene dialuminum, 80
Thallium intermediate, 140
Thallium silsesquioxane complexes, 117
The first boron-containing silsesquioxane, 110
Thermodynamic Stability, 166–169
Thioethers, 14, 16
Thiol-functionalized silsesquioxane ligands, 148
Three-center bonding, 176
Three-center two-electron bonds, 31
Ti(III) silsesquioxane complex, 131
Ti(III)67,68
Ti(IV) silsesquioxanes, 125
Tin, 61, 93
Tip3Sn+, 192
Titanasilsesquioxane alkoxides, 127
Titanasilsesquioxane phenoxide derivatives, 127
Titanasilsesquioxanes, 127
Trans addition, 44
Transmetalation, 72, 77–78
Transmetallation, 82–83
Triarylmethylium ion, 164
(triisopropylphenyl) stannylium, 184
Trimesitylsilylium, 155, 191
Trimesitylstannylium, 184
Trimetallic complexes, 32, 34
Trimetallic species, 28
Trimethylgallium, 117
Trimethylsilylium, 157
Trimethylstannyl, 68
Triosmium Complexes, 3–4, 7–10
Triphenylsilylium, 167, 168
Triruthenium Complexes, 3–5, 7–10
Trismesityl silylium, 172
1,3,5-trititana-2,4,6-trioxane derivative, 130
Trityl cation, 157, 159, 161–163, 167
Tungsten complexes, 5, 35–37
Two-electron oxidation, 29

U

Uranium(VI) complex, 142
Uranium(VI) compound, 125
Uranium(VI) species, 139
UV data, 189
UV–Vis, 72, 91

V

V-shaped trimetal unit, 35
V-shaped trimetallic unit, 33
Vanadyl silsesquioxane, 137
Vertex extrusion, 32, 34

W

WCA, 178
Weakly coordinating anions, 25

Weakly coordinating anions (WCA), 161
Weakly coordinating counteranions, 157
Wheland-type intermediates, 182

X

X-ray diffraction, 34, 67, 70–71, 73, 75, 91

Y

Ytterbium, 122–123

Z

Zinc, 65
Zirconium, 136
Zirconium silsesquioxane complexes, 134
zirconocenes, 134, 135, 136
zwitterionic, 2
zwitterionic complexes, 10, 16, 17, 22, 27, 30
zwitterions, 184, 187, 197

Cumulative List of Contributors for Volumes 1–36

Abel, E. W., **5**, 1; **8**, 117
Aguiló, A., **5**, 321
Akkerman, O. S., **32**, 147
Albano, V. G., **14**, 285
Alper, H., **19**, 183
Anderson. G. K., **20**, 39; **35**, 1
Angelici, R. J., **27**, 51
Aradi, A. A., **30**, 189
Armitage, D. A., **5**, 1
Armor, J. N., **19**, 1
Ash, C. E., **27**, 1
Ashe, A. J., III., **30**, 77
Atwell, W. H., **4**, 1
Baines, K. M., **25**, 1
Barone, R., **26**, 165
Bassner, S. L., **28**, 1
Behrens, H., **18**, 1
Bennett, M. A., **4**, 353
Bickelhaupt, F., **32**, 147
Binningham, J., **2**, 365
Blinka, T. A., **23**, 193
Bockman, T. M., **33**, 51
Bogdanović, B., **17**, 105
Bottomley, F., **28**, 339
Bradley, J. S., **22**, 1
Brew, S. A., **35**, 135
Brinckman, F. E., **20**, 313
Brook, A. G., **7**, 95; **25**, 1
Bowser, J. R., **36**, 57
Brown, H. C., **11**, 1
Brmon, T. L., **3**, 365
Bruce, M. I., **6**, 273; **10**, 273; **11**, 447; **12**, 379; **22**, 59
Brunner, H., **18**, 151
Buhro, W. E., **27**, 311
Byers, P. K., **34**, 1
Cais, M., **8**, 211
Calderon, N., **17**, 449
Callahan, K. P., **14**, 145
Canty, A. J., **34**, 1
Cartledge, F. K., **4**, 1
Chalk, A. J., **6**, 119
Chanon, M., **26**, 165
Chatt, J., **12**, 1
Chini, P., **14**, 285
Chisholm, M. H., **26**, 97; **27**, 311
Chiusoli, G. P., **17**, 195
Chojinowski, J., **30**, 243
Churchill, M. R., **5**, 93
Coates, G. E., **9**, 195
Collman, J. P., **7**, 53
Compton, N. A., **31**, 91
Connelly, N. G., **23**, 1; **24**, 87
Connolly, J. W., **19**, 123
Corey, J. Y., **13**, 139
Corriu, R. J. P., **20**, 265
Courtney, A., **16**, 241
Coutts, R. S. P., **9**, 135
Coville, N. J., **36**, 95
Coyle, T. D., **10**, 237
Crabtree, R. H., **28**, 299
Craig, P. J., **11**, 331
Csuk, R., **28**, 85
Cullen, W. R., **4**, 145
Cundy, C. S., **11**, 253
Curtis, M. D., **19**, 213
Darensbourg, D. J., **21**, 113; **22**, 129
Darensbourg, M. Y., **27**, 1
Davies, S. G., **30**, 1
Deacon, G. B., **25**, 337
de Boer, E., **2**, 115
Deeming, A. J., **26**, 1
Dessy, R. E., **4**, 267
Dickson, R. S., **12**, 323
Dixneuf, P. H., **29**, 163
Eisch, J. J., **16**, 67
Ellis, J. E., **31**, 1
Emerson, G. F., **1**, 1
Epstein, P. S., **19**, 213
Erker, G., **24**, 1
Ernst, C. R., **10**, 79
Errington, R, J., **31**, 91
Evans, J., **16**, 319
Evan, W. J., **24**, 131
Faller, J. W., **16**, 211
Farrugia, L. J., **31**, 301
Faulks, S. J., **25**, 237
Fehlner, T. P., **21**, 57; **30**, 189
Fessenden, J. S., **18**, 275
Fessenden, R. J., **18**, 275
Fischer, E. O., **14**, 1
Ford, P. C., **28**, 139
Forniés, J., **28**, 219
Forster, D., **17**, 255
Fraser, P. J., **12**, 323
Friedrich, H., **36**, 229

Friedrich, H. B., **33**, 235
Fritz, H. P., **1**, 239
Fürstner, A., **28**, 85
Furukawa, J., **12**, 83
Fuson, R. C., **1**, 221
Gallop, M. A., **25**, 121
Garrou, P. E., **23**, 95
Geiger, W. E., **23**, 1; **24**, 87
Geoffroy, G. L., **18**, 207; **24**, 249; **28**, 1
Gilman, H., **1**, 89; **4**, 1; **7**, 1
Gl̆adfelter, W. L., **18**, 207; **24**, 41
Gladysz, J. A., **20**, 1
Glänzer, B. I., **28**, 85
Green, M. L. H., **2**, 325
Grey, R. S., **33**, 125
Griffith, W. P., **7**, 211
Grovenstein, E., Jr., **16**, 167
Gubin, S. P., **10**, 347
Guerin, C., **20**, 265
Gysling, H., **9**, 361
Haiduc, I., **15**, 113
Halasa, A. F., **18**, 55
Hamilton, D. G., **28**, 299
Handwerker, H., **36**, 229
Harrod, J. F., **6**, 119
Hart, W. P., **21**, 1
Hartley, F. H., **15**, 189
Hawthorne, M. R., **14**, 145
Heck, R. F., **4**, 243
Heimbach, P., **8**, 29
Helmer, B. J., **23**, 193
Henry, P. M., **13**, 363
Heppert, J. A., **26**, 97
Herberich, G. E., **25**, 199
Herrmann, W. A., **20**, 159
Hieber, W., **8**, 1
Hill, A. F., **36**, 131
Hill, E. A., **16**, 131
Hoff, C., **19**, 123
Hoffmeister, H., **32**, 227
Holzmeier, P., **34**, 67
Honeyman, R. T., **34**, 1
Horwitz, C. P., **23**, 219
Hosmane, N. S., **30**, 99
Housecroft, C. E., **21**, 57; **33**, 1
Huang, Y. Z., **20**, 115
Hughes, R. P., **31**, 183
Ibers, J. A., **14**, 33
Ishikawa, M., **19**, 51
Ittel, S. D., **14**, 33
Jain, L., **27**, 113
Jain, V. K., **27**, 113
James, B. R., **17**, 319
Janiak, C., **33**, 291
Jastrzebski, J. T. B. H., **35**, 241
Jenck, J., **32**, 121
Jolly, P. W., **8**, 29; **19**, 257
Jonas, K., **19**, 97
Jones, M. D., **27**, 279
Jones, P. R., **15**, 273
Jordan, R. F., **32**, 325
Jukes, A. E., **12**, 215
Jutzi, P., **26**, 217
Kaesz, H. D., **3**, 1
Kalck, P., **32**, 121; **34**, 219
Kaminsky, W., **18**, 99
Katz, T. J., **16**, 283
Kawabata, N., **12**, 83
Kemmitt, R. D. W., **27**, 279
Kettle, S. F. A., **10**, 199
Kilner, M., **10**, 115
Kim, H. P., **27**, 51
King, R. B., **2**, 157
Kingston, B. M., **11**, 253
Kisch, H., **34**, 67
Kitching, W., **4**, 267
Kochi, J. K., **33**, 51
Köster, R., **2**, 257
Kreiter, C. G., **26**, 297
Krüger, G., **24**, 1
Kudaroski, R. A., **22**, 129
Kühlein, K., **7**, 241
Kuivila, H. G., **1**, 47
Kumada, M., **6**, 19; **19**, 51
Lappert, M. F., **5**, 225; **9**, 397; **11**, 253; **14**, 345
Lawrence, J. P., **17**, 449
Le Bozec, H., **29**, 163
Lendor, P. W., **14**, 345
Linford, L., **32**, 1
Longoni, G., **14**, 285
Luijten, J. G. A., **3**, 397
Lukehart, C. M., **25**, 45
Lupin, M. S., **8**, 211
McGlinchey, M. J., **34**, 285
McKillop, A., **11**, 147
McNally, J. P., **30**, 1
Macomber, D. W., **21**, 1; **25**, 317
Maddox, M. L., **3**, 1
Maguire, J. A., **30**, 99
Maitlis, P. M., **4**, 95
Mann, B. E., **12**, 135; **28**, 397
Manuel, T. A., **3**, 181
Markies, P. R., **32**, 147
Mason, R., **5**, 93
Masters, C., **17**, 61
Matsumura, Y., **14**, 187
Mayr, A., **32**, 227
Meister, G., **35**, 41
Mingos, D. M. P., **15**, 1

Mochel, V. D., **18**, 55
Moedritzer, K., **6**, 171
Molloy, K. C., **33**, 171
Monteil, F., **34**, 219
Morgan, G. L., **9**, 195
Morrison, J. A., **35**, 211
Moss, J. R., **33**, 235
Mrowca, J. J., **7**, 157
Müller, G., **24**, 1
Mynott, R., **19**, 257
Nagy, P. L. I., **2**, 325
Nakamura, A., **14**, 245
Nesmeyanov, A. N., **10**, 1
Neumann, W. P., **7**, 241
Norman, N. C., **31**, 91
Ofstead, E. A., **17**, 449
Ohst, H., **25**, 199
Okawara, R., **5**, 137; **14**, 187
Oliver, J. P., **8**, 167; **15**, 235; **16**, 111
Onak, T., **3**, 263
Oosthuizen, H. E., **22**, 209
Otsuka, S., **14**, 245
Pain, G. N., **25**, 237
Parshall, G. W., **7**, 157
Paul, I., **10**, 199
Peres, Y., **32**, 121
Petrosyan, W. S., **14**, 63
Pettit, R., **1**, 1
Pez, G. P., **19**, 1
Poland, J. S., **9**, 397
Poliakoff, M., **25**, 277
Popa, V., **15**, 113
Pourrean, D. B., **24**, 249
Powell, P., **26**, 125
Pratt, J. M., **11**, 331
Prokai, B., **5**, 225
Pruett, R. L., **17**, 1
Rao, G. S., **27**, 113
Raubenheimer, H. G., **32**, 1
Rausch, M. D., **21**, 1; **25**, 317
Reetz, M. T., **16**, 33
Reutov, O. A., **14**, 63
Rijkens, F., **3**, 397
Ritter, J. J., **10**, 237
Rochow, E. G., **9**, 1
Rokicki, A., **28**, 139
Roper, W. R., **7**, 53; **25**, 121
Roundhill, D. M., **13**, 273
Rubezhoc, A. Z., **10**, 347
Salerno, G., **17**, 195
Salter, I. D., **29**, 249
Satgé, J., **21**, 241
Schade, C., **27**, 169
Schaverien, C. J., **36**, 283
Schmidbaur, H., **9**, 259; **14**, 205
Schrauzer, G. N., **2**, 1
Schubert, U., **30**, 151
Schultz, D. N., **18**, 55
Schurnann, H., **33**, 291
Schwebke, G. L., **1**, 89
Seppelt, K., **34**, 207
Setzer, W. N., **24**, 353
Seyferth, D., **14**, 97
Shapakin, S. Yu., **34**, 149
Shen, Y. C., **20**, 115
Shriver, D. F., **23**, 219
Siebert, W., **18**, 301; **35**, 187
Sikora, D. J., **25**, 317
Silverthorn, W. E., **13**, 47
Singleton, E., **22**, 209
Sinn, H., **18**, 99
Skinner, H. A., **2**, 49
Slocum, D. W., **10**, 79
Smallridge, A. J., **30**, 1
Smeets, W. J. J., **32**, 147
Smith, J. D., **13**, 453
Speier, J. L., **17**, 407
Spek, A. L., **32**, 147
Stafford, S. L., **3**, 1
Stańczyk, W., **30**, 243
Stone, F. G. A., **1**, 143; **31**, 53; **35**, 135
Su, A. C. L., **17**, 269
Suslick, K. M., **25**, 73
Süss-Fink, G., **35**, 41
Sutin, L., **28**, 339
Swincer, A. G., **22**, 59
Tamao, K., **6**, 19
Tate, D. P., **18**, 55
Taylor, E. C., **11**, 147
Templeton, J. L., **29**, 1
Thayer, J. S., **5**, 169; **13**, 1; **20**, 313
Theodosiou, I., **26**, 165
Timms, P. L., **15**, 53
Todd, L. J., **8**, 87
Touchard, D., **29**, 163
Traven, V. F., **34**, 149
Treichel, P. M., **1**, 143; **11**, 21
Tsuji, J., **17**, 141
Tsutsui, M., **9**, 361; **16**, 241
Turney, T. W., **15**, 53
Tyfield, S. P., **8**, 117
Usón, R., **28**, 219
Vahrenkamp, H., **22**, 169
van der Kerk, G. J. M., **3**, 397
van Koten, G., **21**, 151; **35**, 241
Veith, M., **31**, 269
Vezey, P. N., **15**, 189
von Ragué Schleyer, P., **24**, 353; **27**, 169

Vrieze, K., **21**, 151
Wada, M., **5**, 137
Walton, D. R. M., **13**, 453
Wailes, P. C., **9**, 135
Webster, D. E., **15**, 147
Weitz, E., **25**, 277
West, R., **5**, 169; **16**, 1; **23**, 193
Werner, H., **19**, 155
White, D., **36**, 95
Wiberg, N., **23**, 131; **24**, 179
Wiles, D. R., **11**, 207
Wilke, G., **8**, 29
Williams, R. E., **36**, 1
Winter, M. J., **29**, 101
Wojcicki, A., **11**, 87; **12**, 31
Yamamoto, A., **34**. 111
Yashina, N. S., **14**, 63
Ziegler, K., **6**, 1
Zuckerman, J. J., **9**, 21
Zybill, C., **36**, 229

Cumulative Index for Volumes 37–53

	VOL.	PAGE
Abu Ali, Hijazi, *see* Dembitsky, Valery M,		
Al-Ahmad, Saleem, *see* Ashe, Arthur J., III		
Andersen, Jo-Ann M., and Moss, John R., *Alkyl (pentacarbonyl) Compounds of the Manganese Group Revisited*	37	169
Ashe, Arthur J., III, and Al-Ahmad, Saleem, *Diheteroferrocenes and Related Derivatives of the Group 15 Elements: Arsenic, Antimony, and Bismuth*	39	325
Aumann, Rudolf, *(l-Alkynyl)carbene Complexes (= 1-Metalla-1-buten-3-ynes): Tools for Synthesis*	41	165
Baines, K. M., and Stibbs, W, G., *Stable Doubly Bonded Compounds of Germanium and Tin*	39	275
Baker, Paul K., *The Organometallic Chemistry of Halocarbonyl Complexes of Molybdenum (II) and Tungsten (II)*	40	45
Belzner, Johannes, and Ihmels, Heiko, *Silylenes Coordinated to Lewis Bases*	43	1
Berry, Donald H., *see* Reichl, Jennifer A.	43	197
Bertrand, Guy, *see* Bourissou, Didier		
Bode, Katrin, and Klingebiel, Uwe, *Silylhydrazines; Lithium Derivatives, Isomerism, and Rings*	40	1
Bo-Hye Kim and Hee-Gweon Woo, *Dehydrocoupling, Redistribute Coupling, and Addition of Main Group 4 Hydrides*	52	143
Bok Ryul Yoo, *see* Il Nam Jung		
Bourissou, Didier, and Bertrand, Guy, *The Chemistry of Phosphinocarbenes*	44	175
Braunschweig, Holger, *Borylenes as Ligands to Transition Metals*	51	163
Breunig Hans Joachim and Ghesner Ioan, *Coordination Compounds with Organoantimony and Sb_n Ligands*	49	95
Brook, Adrian, G., and Brook, Michael, A., *The Chemistry of Silenes*	39	71
Brook, Michael A., *see* Brook, Adrian G.		
Brothers, Penelope J., and Power, Philip P., *Multiple Bonding Involving Heavier Main Group 3 Elements Al, Ga, In, and Tl*	39	1
Brothers, Penelope J., *Organometallic Chemistry of Transition Metal Porphyrin Complexes*	46	223
Brothers, Penelope J., *Organoelement Chemistry of Main Group Porphyrin Complexes*	48	289
Bruce, Michael I., and Low, Paul J., *Transition Metal Complexes Containing All-Carbon Ligands*	50	179
Carty, Arthur J., *see* Doherty, Simon		
Chatgilialoglu, Chryssostomos, and Newcomb, Martin, *Hydrogen Donor Abilities of the Group 14 Hybrides*	44	67
Corey, Joyce Y., *Dehydrocoupling of Hydrosilanes to Polysilanes and Silicon Oligomers: A 30 Year Overview*	51	1
Corrigan, John R, *see* Doherty, Simon		
Cumulative Subject Index for Volumes 1–44	45	1
Dembitsky, Valery M., Abu Ali, Hijazi, and Stebnik, Morris, *Recent Chemistry of the Diboron Compounds*	51	193
Doherty, Simon, Corrigan, John P., Carty, Arthur J., and Sappa, Enrico, *Homometallic and Heterometallic Transition Metal Allenyl Complexes: Synthesis, Structure, and Reactivity*	37	39

Driess, Matthias, *Silicon-Phosphorus and Silicon-Arsenic Multiple Bonds*	39	193
Dyson, Paul J., *Chemistry of Ruthenium–Carbide Clusters $Ru_5C(CO)_{15}$ and $Ru_6C(CO)_{17}$*	43	43
Eduardo J. Fernández, Antonio Laguna, and M. Elena Olmos, *Recent Developments in Arylgold(I) Chemistry*	52	77
Eichler, Barrett, and West, Robert, *Chemistry of Group 14 Heteroallenes*	46	1
Eisch, John J., *Boron–Carbon Multiple Bonds*	39	355
Erker, Gerhard, Kehr, Gerald, and Fröhlich, Roland, *The (Butadiene) zirconocenes and Related Compounds*	51	109
Escudie, Jean, and Ranaivonjatovo, Henri, *Doubly Bonded Derivatives of Germanium*	44	113
Esteruelas, Miguel A. *The Chemical and Catalytic Reactions of Hydrido-chloro-carbonylbis (triisopropylphosphine) osmium and its Major Derivatives.*	47	1
F. Gordon A. Stone, *see* Thomas D. McGrath		
Fleig, Patrick R, *see* Wojtczak, William A.		
François P. Gabbai, *see* Mohand Melaimi		
Frank T. Edelmann, *see* Volker Lorenz		
Gable, Kevin P., *Rhenium and Technetium Oxo Complexes in the Study of Organic Oxidation Mechanisms*	41	127
Gauvin, François, Harrod, John F., and Woo, Hee Gweon, *Catalytic Dehydrocoupling: A General Strategy for the Formation of Element–Element Bonds*	42	363
Georgii I. Nikonov, *Recent Advances in Nonclassical Interligand Si···H Interactions*	53	217
Gibson, Susan E., and Peplow, Mark A., *Transition Metal Complexes of Vinylketenes*	44	275
Hampden-Smith, Mark J., *see* Wojtczak, William A.		
Hanusa, Timothy P., *see* Hays, Melanie L.		
Harrod, John K., *see* Gauvin, François		
Haubrich, Scott, Power, Philip, and Twamley, Brendan, *Element Derivatives of Sterically Encumbering Terphenyl Ligands*	44	1
Hays, Melanie L., and Hanusa, Timothy, P., *Substituent Effects as Probes of Structure and Bonding in Mononuclear Metallocenes*	40	117
Hemme, Ina, *see* Klingebiel, Uwe		
Hopkins, Michael D., *see* Manna, Joseph		
Humphrey, Mark G., *see* Whittall, Ian R.		
Humphrey, Mark G., *see* Waterman, Susan M.		
Herrmann, Wolfgang A., Weskamp, Thomas, and Böhm, Volker P. W., *Metal Complexes of Stable Carbenes*	48	1
Ihmels, Heiko, *see* Belzner, Johannes	43	1
Il Nam Jung and Bok Ryul Yoo, *Synthesis of Novel Silicon-Containing Compounds via Lewis Acid Catalyzed Reactions*	53	41
Jafarpour, Laleh, and Nolan, Steven P., *Transition-Metal Systems Bearing a Nucleophilic Carbene Ancillary Ligand: from Thermochemistry to Catalysis*	46	181
Jean-Paul Picard, *Silylmethylamines and Their Derivatives: Chemistry and Biological Activities*	52	175
John, Kevin D., *see* Manna, Joseph		
Jones, William M., and Klosin, Jerzy, *Transition-Metal Complexes of Arynes, Strained Cyclic Alkynes, and Strained Cyclic Cumulenes*	42	147
Jung, IL Nam, *see* Yoo, Bok Ryul		
Jung, II Nam, and Yoo, Bok Ryul, *Friedel-Crafts Alkylations with Silicon Compounds*	46	145
Kalikhman, Inna, *see* Kost, Daniel		

Kawachi, Atsushi, *see* Tamao, Kohei
Kehr, Gerald, *see* Erker, Gerhard
Klingebiel, Uwe, and Hemme, Ina, *Iminosilanes and Related Compounds: Synthesis and Reactions* 39 159
Klingebiel, Uwe, *see* Bode, Katrin
Klosin, Jerzy, *see* Jones, William M.
Kost, Daniel, and Kalikhman, Inna, *Hydrazide-Based Hypercoordinate Silicon Compounds* 50 1
Kühler Thorsten and Jutzi Peter, *Decamethylsilicocene: Synthesis, Structure, Bonding and Chemistry* 49 1
Kyushin Soichiro and Matsumoto Hideyuki. *Ladder Polysilanes* 49 133
Lotz, Simon, Van Rooyen, Pertrus H., and Meyer, Rita, *σ, π-Bridging Ligands in Bimetallic and Trimetallic Complexes* 37 219
Low, Paul J., *see* Bruce, Michael I.
Low, Paul J., and Bruce, Michael I., *Transition Metal Chemistry of 1,3-Diynes, Poly-ynes, and Related Compounds* 48 71
Lucas, Nigel T., *see* Waterman, Susan M.
Manna, Joseph, John, Kevin D., and Hopkins, Michael, D., *The Bonding of Metal-Alkynyl Complexes* 38 79
Manners, Ian, *Ring-Opening Polymerization of Metallocenophanes: A New Route to Transition Metal-Based Polymers* 37 131
Mathur, Pradeep, *Chalcogen-Bridged Metal–Carbonyl Complexes* 41 243
McDonagh, Andrew M., *see* Whittall, Ian R.
Meyer, Rita, *see* Lotz, Simon
Mohand Melaimi and François P. Gabbai, *Bidentate Group 13 Lewis Acids with ortho-Phenylene and peri-Naphthalenediyl Backbones* 53 61
Moss, John R., *see* Andersen, Jo-Ann M.
Nakazawa, Hiroshi, *Transition Metal Complexes Bearing a Phosphenium Ligand* 50 107
Newcomb, Martin, *see* Chatgilialoglu, Chryssostomos
Nienaber, Hubert, *see* Aumann, Rudolf
Nolan, Steven P., *see* Jafarpour, Laleh
Ogino, Hiroshi, and Tobita, Hiromi, *Bridged Silylene and Germylene Complexes* 42 223
Okazaki, Renji, and West, Robert, *Chemistry of Stable Disilenes* 39 231
Oro, Luis A. *see* Esteruelas, Miguel A.
Peplow, Mark A., *see* Gibson, Susan E.
Power, Philip P., *see* Brothers, Penelope J.
Power, Philip, *see* Haubrich, Scott
Ranaivonjatovo, Henri, *see* Escudie, Jean
Pülm, Melanie, *see* Tacke, Reinhold
Reichl, Jenifer A., and Berry, Donald H., Recent Progress in Transition Metal-Catalyzed Reactions of Silicon, Germanium, and Tin 43 197
Roland, Fröhlich, *see* Gerhard, Erker
Roth, Gerhard, *see* Fischer, Helmut 43 125
Roundhill, D. M., *Organotransition-Metal Chemistry and Homogeneous Catalysis in Aqueous Solution* 38 155
Sakurai, Hideki, *see* Sakiguchi, Akira
Samoc, Marek, *see* Whittall, Ian R.
Sappa, Enrico, *see* Doherty, Simon
Sekiguchi, Akira, and Sakurai, Hideki, *Cage and Cluster Compounds of Silicon, Germanium, and Tin* 37 1
Schulz Stephan. *Group 13/15 Organometallic Compounds-Synthesis, Structure, Reactivity and Potential Applications* 49 225
Sita, Lawrence R., *Structure/Property Relationships of Polystannanes* . . 38 189

Smith, David J., *Organometallic Compounds of the Heavier Alkali Metals* 43 267
Smith, Paul J., *see* Welton, Tom
Srebnik, Morris, *see* Dembitsky, Valery M.
Stibbs, W. G., *see* Baines, K. M.
Stumpf, Rüdiger, *see* Fisher, Helmut 43 125
Sun, Shouheng, and Swelgart, Dwight A., *Reactions of 17- and 19-Electron Organometallic Complexes* 40 171
Sweigart, Dwight A., *see* Sun, Shouheng
Tacke, Reinhold, Pülm, Melanie, and Wagner, Brigitte, *Zwitterionic Penta-coordinate Silicon Compounds* 44 221
Tamao, Kohei, Kawachi, Atsushi, *Silyl Anions*. 38 1
Thayer, John S., *Not for Synthesis Only: The Reactions of Organic Halides with Metal Surfaces*. 38 59
Thomas D. McGrath and F. Gordon A. Stone, *Metal Complexes of Monocarbon Carboranes: A Neglected Area of Study?*. 53 1
Thomas Müller, *Cations of Group 14 Organometallics* 53 155
Tobisch Sven. *Structure-Reactivity Relationships in the Cyclo-Oligomerization of 1,3-Butadiene Catalyzed by Zerovalent Nickel Complexes* . 49 168
Tobita, Hiromi, *see* Ogino, Hiroshi
Twarnley, Brendan, *see* Haubrich, Scott
Uhl, Werner, *Organoelement Compounds Possessing Al–Al, Ga–Ga, In–In, and Tl–Tl Single Bonds*. 51 53
Van Rooyen, Petrus H., *see* Lotz, Simon
Volker Lorenz and Frank T. Edelmann, *Metallasilsesquioxanes* 53 101
Wagner, Brigitte, *see* Tacke, Reinhold
Warren E. Piers, *The Chemistry of Perfluoroaryl Boranes*. 52 1
Waterman, Susan M., Lucas, Nigel T., and Humphrey, Mark G., *"Very-Mixed" Metal Carbonyl Clusters* 46 47
Weber, Lothar, *Transition-Metal Assisted Syntheses of Rings and Cages from Phosphaalkenes and Phosphaalkynes* 41 1
Welton, Tom, and Smith, Paid J., *Palladium Catalyzed Reactions in Ionic Liquids* 51 251
Went, Michael J., *Synthesis and Reactions of Polynuclear Cobalt-Alkyne Complexes*. 41 69
West, Robert, *see* Eichler, Barrett
West, Robert, *see* Okazaki, Renji
Whitmire, Kenton H., *Main Group-Transition Metal Cluster Compounds of the group 15 Elements* 42 1
Whittall, Ian R., McDonagh, Andrew M., Humphrey, Mark G., *Organometallic Complexes in Nonlinear Optics II: Third-Order Nonlinearities and Optical Limiting Studies* 43 349
Whittall, Ian, R., McDonagh, Andrew M., Humphrey, Mark G., and Samoc, Marek, *Organometallic Complexes in Nonlinear Optics I: Second-Order Nonlinearities*. 42 291
Wojtczak, William A., Fleig, Patrick F., and Hampden-Smith, Mark J., *A Review of Group 2 (Ca, Sr, Ba) Metal-Organic Compounds as Precursors for Chemical Vapor Deposition* 40 215
Woo, Hee Gweon, *see* Gauvin François
Yoo, Bok Ryul, *see* Jung, II Nam
Yoo, Bok Ryul, and Jung, II Nam, *Synthesis of Organosilicon Compounds by New Direct Reactions* 50 145
Zemlyansky Nikolai N., Borisova, Irina V., and Ustynyuk, Yuri A. *Organometallic Phosphorous and Arsenic Betaines*. 49 35